

Arkady E. Glikin

# Polyminerals- Metasomatic Crystallogenesis

 Springer

# Polymineral-Metasomatic Crystallogenesi

Arkady E. Glikin

# Polym mineral-Metasomatic Crystallogenesis

 Springer

Arkady E. Glikin  
Crystallography Department  
Geological Faculty  
Saint Petersburg State University  
University Embankment 7/9  
199034 St. Petersburg  
Russia  
glikin@ag2460.spb.edu

ISBN 978-1-4020-8982-4 e-ISBN 978-1-4020-8983-1

Library of Congress Control Number: 2008933944

© 2009 Springer Science+Business Media B.V.

No part of this work may be reproduced, stored in a retrieval system, or transmitted in any form or by any means, electronic, mechanical, photocopying, microfilming, recording or otherwise, without written permission from the Publisher, with the exception of any material supplied specifically for the purpose of being entered and executed on a computer system, for exclusive use by the purchaser of the work.

Printed on acid-free paper

springer.com

# Acknowledgments

I'd like to express my sincere gratitude to the fate that ensured my successful work and happy human relations at the Crystallography Department of St Petersburg State University and Russian Mineralogical Society. I express my gratefulness to my teacher, Thomas G. Petrov, whose guiding influence has been invaluable for my scientific outlook formation. With deepest appreciation for the school of thought I treasure recollections about my late professors: Vitalii B. Tatarskii, Victor A. Frank-Kamenetskii, Alexander A. Kukhareenko, Alexey A. Shternberg, and Vladimir V. Nardov.

I feel myself deeply indebted to my most devoted collaborators: Sergey N. Bocharov, Valeria D. Franke, Elena V. Kiryanova, Vladimir G. Krivovichev, Lyudmila Yu. Kruchkova, Julia V. Plotkina, Marina Yu. Sinai, and Alexei E. Voloshin. I also thank students, postgraduate students, and researchers of Department of Crystallography of St Petersburg University, who took part in the research works and became coauthors of the cited publications.

My particular gratitude should be addressed to Prof. Vladimir V. Dolivo-Dobrovol'skii, whose valuable remarks greatly helped me in preparation of Russian version of the present monograph.

A considerable part of the investigations and preparation and publication of the book itself were supported by the Russian Fund for Basic Research (projects 03-05-78003, 07-05-00380, and others), programs "Russia's Universities" of Ministry of Education and Science of the Russian Federation, State Contract 02.523.12.3004 (project DN 08/07-03). Grants of DAAD (Germany), NWO-NATO (Netherlands), and INTAS (EC) allowed me to present the results of the investigations to International Society of Mineralogists and Crystallographers and to develop some aspects of the problem in close collaboration with my foreign colleagues Profs. Valter A. Franke, Peter Gille, Helmut Klapper, Andrew Putnis, and Cornelis F. Woensdregt and Drs. Christine Putnis, Julius Schneider, and Robert Stark.

I am greatly thankful to the editors of both the versions. The Russian version of the book was issued by Anton V. Voznesenskii, Svetlana A. Bulacheva, and Nina R. Liberman (the company "Kolo," formerly "Zhurnal Neva"). The primary translation into English was carried out by Tatyana Yu. Nikolaenko and the figures for the English version were edited by Olga A. Temezhnikova. These preparations were sponsored by the Geological Faculty of St Petersburg University under its Dean

Igor V. Buldakov's initiation. The agreement of Springer to publish the book is of a great honor for me.

I am particularly obliged to my wife Elena N. Kotel'nikova, mother Sofia E. Glikina, and son Anton A. Glikin for long-standing and invaluable assistance.

I dedicate my work to the memory of my grandparents Cecil A. Glikina and Karp F. Dvornikov.

# Contents

<b>Foreword</b> .....	xi
<b>Introduction</b> On the Concept of Polymineral-Metasomatic Crystallogenesis.....	1
<b>1 Replacement of Monocrystals</b> .....	7
1.1 Natural and Experimental Products of Replacement.....	7
1.2 Technique, Terminology, and Experimental Results .....	12
1.3 Metasomatic Transformations in Polymorphic Pair Retgersite– Nickelhexahydrite ( $\alpha$ – $\beta$ -NiSO <sub>4</sub> ·6H <sub>2</sub> O).....	25
1.4 Structural-Morphological Classification of Replacement Products.....	28
1.5 Genetic Nature of Replacement Products.....	30
1.5.1 Types of Physicochemical Systems and Structure of Replacement Products .....	30
1.5.2 Volume Effect of the Reactions .....	34
1.5.3 Kinetic Factors and Shape of Replacement Products .....	36
1.5.4 Imperfection of Protocrystals as a Factor of Replacement Process .....	40
1.6 Mineralogical Aspects of the Problem of Crystal Replacement.....	45
References.....	53
<b>2 Joint Growth of Crystals of Different Phases</b> .....	61
2.1 Growth and Dissolving in Supercooled Solutions.....	61
2.1.1 Technique.....	61
2.1.2 Crystal Morphology.....	64
2.1.3 Kinetics .....	66
2.2 Physicochemical Model.....	72
2.2.1 Phase Equilibria in KCl–NaCl–MgCl <sub>2</sub> –H <sub>2</sub> O System.....	72
2.2.2 Kinetic Effects and Peculiarities of Phase Equilibria .....	76
References.....	82

<b>3</b>	<b>Formation of Mixed Crystals in Solutions</b> .....	85
3.1	Particular Characteristics of the Process and Historical Survey .....	85
3.2	Material Balance and Mechanisms of Replacement.....	88
3.3	Physicochemical Model .....	96
3.3.1	Modified Concentration Diagrams.....	96
3.3.2	Formation of Crystals Under Equilibrium, Quasi-equilibrium, and Non-equilibrium Conditions .....	100
3.3.3	Heterogeneous Metastable Equilibrium Between Crystals and Solutions.....	107
3.4	Morphological and Kinetic Behavior of Monocrystals .....	115
3.4.1	Tutton Salt Series $(\text{Co,Ni})(\text{NH}_4)_2(\text{SO}_4)_2 \cdot 6\text{H}_2\text{O}$ .....	115
3.4.2	Series of Potassium–Rubidium Acidic Phthalates $(\text{K,Rb})\text{HC}_8\text{H}_4\text{O}_4$ .....	128
3.4.3	Arcanite-Tarapacaite $\text{K}_2(\text{S,Cr})\text{O}_4$ Series .....	137
3.5	Inhomogeneity of Crystals.....	141
3.6	Mass Precipitation of Mixed Crystals: Distribution by Compositions and Sizes .....	145
3.7	On the Mechanism of Isomorphic Component Selection during the Crystal Formation .....	147
	References.....	149
<b>4</b>	<b>Physicochemical Analysis of Metasomatic Crystallogensis</b> .....	153
4.1	Brief Overview.....	153
4.2	Isothermal Replacement in Ternary Systems.....	157
4.3	Isothermal Replacement in Complex Systems and Formation of Poikilitic Crystals .....	162
4.4	Polythermal Processes .....	164
4.5	Common and Different Features of the Processes Proceeding in Systems Containing either Isomorphic or Non-isomorphic Components .....	167
4.6	Some Methods of Estimation of Reaction Volume Effect .....	170
	References.....	173
<b>5</b>	<b>Metasomatic Transformation of Aggregates</b> .....	177
5.1	On Replacement and Growth of Monocrystals in the Course of Transformation of Aggregates .....	177
5.2	A Model of Formation of Rapakivi-Type Structures .....	182
5.3	Recrystallization of Polymineral Aggregates .....	195
5.3.1	Natural and Experimental Products of Recrystallization.....	195
5.3.2	Technique and Experimental Results.....	197
5.3.3	General Regularities and Possible Mechanisms .....	212
	References.....	223



<b>6 Epitaxy and Quasiepitaxy in Solutions .....</b>	<b>229</b>
6.1 Principle Phenomena .....	229
6.2 Technique.....	231
6.3 Epitaxial Regularities on a Growing or Dissolving Substrate .....	235
6.4 Regularities of Orientation of CaCO <sub>3</sub> Microcrystals Adhered to a Substrate.....	240
6.5 Model of Formation of Epitaxial and Quasiepitaxial Textures.....	241
References.....	245
<b>7 Crystal Faceting .....</b>	<b>249</b>
7.1 Stationary Forms of Faceting.....	249
7.2 Crystal Habit under Nonstationary Growth Conditions.....	260
7.3 Regularities of Fluorite Faceting.....	266
7.4 Structure-Chemical Model of Crystal Faceting .....	275
7.5 Effect of Infrared Radiation on Crystal Growth Kinetics in Solutions .....	279
7.6 Kinetic Anomalies of Crystal Growth in Solutions .....	282
7.7 Nature of Kinetic Anomalies and Crystal Growth Mechanisms.....	284
References.....	294
<b>Conclusion</b> On Interrelation between Crystallogenesi and Geological and Mineralogical Sciences.....	301
<b>Index</b> .....	305

# Foreword

A vast list of publications concerning the influence of formation conditions upon the process of crystal growth begins with the work concerning the supposed relationship between the shape of natural galenite and its silver content published by Abraham G. Werner (1774) and with experimental findings of Jean-Baptiste L. Romé de l'Isle and Sieffert, who observed in 1780 the effects of impurities on sodium chloride and alum crystal shape.

Crystallogenesis as a term to denote a branch of science dealing with correlations between conditions of crystal formation and its properties was introduced as early as in the beginning of the nineteenth century by an outstanding American mineralogist James D. Dana. It was he who outlined the main tasks of crystallogenesis in his famous book *A System of Mineralogy*. Intensive development of crystallogenesis started from the beginning of the twentieth century. At present, crystallogenesis (crystallogenesis, crystallogeny, crystal genesis) is a subject of official activities of the International Union of Crystallography, although the use of the term is comparatively infrequent and predominately used in Russian publications.

In Russia, in the 1910s, there were organized two scientific institutions for studying crystallogenesis, which have been developing in parallel ever since.

The first institution was founded in St. Petersburg University by the Head of its Mineralogical Department Piotr A. Zemyatchenskii who from 1909 to 1914 carried out the first object-oriented observations of crystal growth. His investigations of influence of solution impurities upon crystals of alum and sodium chlorate were summarized in the first specialized monograph concerning this field *Crystallogenesis Essays*. For many years, this work had served as a tabletop manual for everyone who dealt with growing crystals.

Development of crystallogenic school of St. Petersburg University was mainly influenced by geologists, who, nevertheless, paid great attention to the physical aspect of the art. The founder of Crystallography Department in Leningrad/St. Petersburg University Osip M. Ansheles was taught by the famous crystallographer Evgraf S. Fedorov, who, of course, influenced his ideas. In particular, he was probably the first to observe in situ a macrostepwise growth of crystals (in hyposulfite). That allowed him and his followers and colleagues Vitalii B. Tatarskii and Alexei A. Shternberg to pioneer development of a fast method for growing single crystals of Seignette salt, which was successfully applied in the defense

industry during World War II in besieged Leningrad. Just before World War II, A. A. Shternberg organized Laboratory of Crystallogenesi, but his scientific plans were disrupted by the war (later, he moved to Moscow and became a foremost authority in the art of hydrothermal crystal growing and one of the creators of synthetic quartz). The postwar period started for St. Petersburg crystallogenic school with morphological-kinetic investigations of macrocrystals of magnesium sulfate heptahydrate conducted by Vladimir A. Mokievskii. In the mid-1950s, Thomas G. Petrov refounded the laboratory, which has been successfully functioning ever since, where experimental and theoretical investigations of growth kinetics, crystal morphology, and crystal imperfection, and simulations of mineral formation processes have been carried out. This book presents results, which have been obtained by the author and his research team in this laboratory since 1965, after the author's graduation from the Crystallography Department.

The other institution was established at the Academy of Sciences by Alexey V. Shubnikov, who afterwards headed this branch of science in the Soviet Union. Some particular applied investigations (elaboration of static method of growing sucrose and Seignette salt with N. N. Sheftal and growing corundum S. K. Popov) were carried out first in Leningrad Physical and Engineering Institute, and later in the Institute of Geochemistry, Crystallography, and Mineralogy named after M. V. Lomonosov (Leningrad and Moscow). After the Academy of Science was moved to Moscow he organized the Laboratory of Crystallography, which was afterwards reorganized into the Institute of Crystallography. The greatest contribution to development of the academic school was made by physicists, who considerably enriched crystallogenic science. Observation of growth phenomena in situ and their interpretation from the points of view of natural sciences – chemistry and physics – served as a basis for experimental and theoretical investigations that, in turn, made it possible to develop reliable experimental approaches and discover some important crystallogenic processes. The Institute of Crystallography contains a net of departments solving a wide spectrum of problems in crystal growth.

An outstanding contribution to crystallogenesi of that period was made by Shubnikov's follower and colleague George G. Laemmlein. Thus, in 1945 (4 years before the famous publication by F. C. Frank), he published the discovery of layered-spiral growth mechanism. He stated regularities of zonal-sectorial crystal structure, and principles of inclusion formation. Moreover, his follower Alexander A. Chernov made a world-renowned contribution to the modern theory of elementary processes of crystal growth.

Russian history of crystallogenesi was substantially enriched by the works of Professor of Mineralogy of Moscow University, Mikhail A. Tolstopyatov. He pioneered systematic investigations of phenomenological and genetic aspects of imperfection of natural crystals and summarized them in his doctoral thesis "General tasks of crystallogenesi theory," which appeared as early as in 1869. His monograph *To the Subject of Crystallogenesi*, was published in 1916 posthumously. It should be noted that A. A. Shubnikov experimented first on growing the crystals of potassium dichromate and alum and investigated their morphology as a student of the Institute of Mineralogy at Moscow University in 1911–1913 under

the guidance of George V. Wulff. A laboratory on crystal growth is functioning now at the Geological Faculty of Moscow University headed by Nikolai I. Leonyuk.

In 1970s a versatile laboratory on crystallogenesis was organized by Nikolai P. Yushkin in Syktyvkar Institute of Geology of the Academy of Sciences. Its director Askhab M. Askhabov forwarded principal concepts of media structure in relations with crystal formation. Also, several other scientific centers for crystal growth investigations successfully operate in different regions of Russia.

As a whole, the tasks of crystallogenesis were unified by a general formula suggested by G. G. Laemmlein half a century ago: "finding the correlative signs between internal and external morphology of a crystal, its physical and chemical properties and conditions of its formation in the broadest aspect."

Last decades of the twentieth century were marked by considerable progress made in the field of crystallogenesis. Nevertheless, complexity of the problems involved is still increasing and the branch itself is still developing. It can be expected that crystallogenic study enters a new stage of its development, which consists in combining physicochemical, experimental-methodological and mineralogical aspects to create a general problem-theoretical concept. Extremely important for development of the art is interpretation of phenomena observed during crystal nucleation, growth, and dissolution, which form the basis for the great majority of important crystallochemical regularities, minerogenetic, petrologic, and lithogenic processes, as well as for industrial processes, etc. However, common approaches do not generally take into consideration the theory of crystallogenesis. Partly, this is caused by impossibility to supply a clear, obvious, and thorough explanation for complex phenomena of crystal formation, and partly this is reasoned by the fact that the theory has not been developed sufficiently to elucidate natural phenomena of the utmost complexity.

Since 1980s the author of the present monograph together with coworkers, students, and postgraduate students has been conducting systematical investigations, which have shown that polymineral crystallogenesis is characterized by a number of characteristic features that cannot be explained within the limits of classical theory. The processes of polymineral crystallogenesis are complicated by various forms of synchronized growth and dissolution, interaction between crystals of different phases, and peculiarities of phase equilibria that have not been taken into account until now. Naturally, elementary processes forming the basis of polymineral crystallogenesis are similar to those extensively studied in simple and binary systems. The difference consists in greater diversity and singularity of their combinations.

In the present monograph attention is paid to crystallogenesis in polymineral media, which is the most complicated process typically occurring in natural environments. Previously, the concepts involved in this problem have not been fully developed and that has naturally led to various misunderstandings. First, there are some terminological problems, since conventional vocabulary does not cover the terms invented for all new phenomena. This prompts using mineralogical, crystallogenic, and physicochemical terminology, inventing hybrids and also absolutely new terms. Probably, some of them are not quite justified, and in future something

more suitable will be found for the corresponding terms, if the concept proposed turns out to be viable.

The references cited in the monograph undoubtedly do not cover wholly and consistently every aspect of crystallogenesis. On the other hand, presenting a whole and consistent review of such an immense subject seems to be impossible. The cited works serve as a basis for an overview of the problem, which is, hopefully, quite objective. Some repetitions proved inevitable, mostly due to relative independence of the chapters. It is also clear that degree of sketchiness varies depending on the tasks set forth by a particular chapter. For example, detailed description and discussion of crystal faceting requires at least a special book; therefore, the monograph presents only briefly outlined information.

The author sincerely hopes that his monograph will give an impulse to new ideas and further development of theoretical concepts of crystallogenesis and the use of these concepts in numerous genetic interpretations, as well as for improvement of academic educational programs.

# Introduction

## On the Concept of Polymineral-Metasomatic Crystallogenesis

*Rigorous and quite accurate analysis of the surrounding phenomena in a certain field of science is possible only when elementary structural units and elementary phenomena are singled out in the subject of analysis. ... [T]he absence of unambiguous distinguishing and accurate formulae for such elementary structures and phenomena produce two essential negative consequences, viz.: impossibility of accurate analysis of the processes proceeding because of its “pointlessness,” and inevitable confusion in the terminology.*

N. V. Timofeev-Resovskii, N. N. Vorontsov, A. V. Yablokov (1969)

Fundamental crystallogenesis can be divided into three stages of development differing in the extent of theoretical generalization. Qualitative theories providing a basis for the first stage, comprising processes of crystallization in single-component gaseous or melt systems, have been already developed. The second stage, which encompasses processes of crystal formation in binary systems and also those in aqueous solutions, is based on satisfactory developed qualitative notions also including some quantitative concepts. The third stage should be distinguished as encompassing processes occurring in multicomponent and polymineral media, where crystallization is complicated by a metasomatic constituent, i.e., chemical reactions of salting-in and salting-out, which manifest themselves in a correlated combination of growth and dissolution processes. According to their main distinctive features, here such processes are referred to as “polymineral-metasomatic crystallogenesis.”

Interaction of crystals and aggregates with solutions must be primarily regarded as a physicochemical process. Crystal growth, which is unaffected by dissolution of another substance and caused by a change in temperature, pressure, and solution concentration, is referred to as “ordinary” or “direct” growth. “Ordinary” or “direct” dissolution should be defined analogously. Metasomatic substitution means a process consisting in spatiotemporally correlated stages of dissolution of a protocystal and precipitation of a new formation having a composition differing from that of the protocystal.

In natural polymineral environments these processes are unlikely to proceed unaccompanied by other phenomena. Temperature fluctuations and various heterogeneities of the natural systems influence crystal formation, which, as a result,

becomes a combination of salting-in/salting-out processes (metasomatic component) and growth/dissolution induced by supercooling/overheating (“direct” components). Moreover, direct growth and dissolution processes can be accompanied by metastable salting-in/salting-out reactions, i.e., include a metasomatic component. Furthermore, metasomatic replacement is a result of local growth/dissolution processes, which are separated by a certain spatiotemporal interval, which can vary within a wide range.

All the above-stated processes allow to consider polymineral-metasomatic crystallogensis at three different levels of generalization: elementary, subelementary, and overelementary.

*Elementary level* involves crystal dissolution and growth and equilibrium states of crystals regarded as physicochemical processes. These generalized concepts define the main constituents of crystallogensis and are used throughout the whole monograph.

*Subelementary level* involves processes and phenomena limited only or predominantly by either growth or dissolution or equilibrium space, which do not depend or essentially do not depend upon a method of setting a driving force (metasomatic or direct). This level comprises nucleation of individuals, faceting, formation of surface relief and other macrodefects, capture of impurities, separation of a solution into layers, diffusion and convective mass transfer, and some phenomena of joint crystal growth (epitaxy, crystallization pressure, etc.). Detailed interpretation of these processes showed a vast diversity and ambiguousness of their combinations occurring in direct growth. Two types of the above process are briefly outlined in the present monograph – oriented overgrowth (Chapter 6) and crystal faceting (Chapter 7).

A model proposed for oriented growth of crystals explains epitaxy and a number of similar “quasiepitaxial” phenomena on the basis of data on orientation mechanisms, which are defined by the following processes: heterogeneous and homogeneous nucleation, turn of the precipitated crystals from the epitaxial position to acquire another direction in respect to substrate, turning the crystals to take an oriented position under the action of long-range forces, and, of course, crystallochemical similarity between crystals. General cases of epitaxy on growing or dissolving substrates are discussed. Understanding these phenomena widens the scope of mineral origin analysis and allows to obtain information about relative growth rates and nucleation of epitaxial crystals.

A structural-chemical model of crystal faceting is also proposed. It is based on the concept of adsorption film of solvent, which defines morphogenesis of crystals. This concept has been elaborated and proved experimentally, as it is possible to predict some experimental phenomena on its basis and to explain influence of a number of factors upon the crystal faceting. Experimental and theoretical data prompt a conclusion about a low information value of faceting in genetic analysis. Nevertheless, some suitable criteria can be formulated on the basis of correlations between specific growth conditions and formation of some details of the surface relief that are unusual for a particular substance, as well as formation of curved, multi-edged and multiheaded forms.

*Ovelementary level* includes metasomatic processes. Dissolution of a protocrystal is a basic initial stage for any reaction of solid phase replacement taking place

in interacting solutions. Dissolution of a protocystal results in supersaturation of solution in respect to the other substance that results in growth of new phases (salting-out). Some other reactions, which are referred to as metasomatic, are induced by the reverse effect, i.e., salting-in, that is caused, on the contrary, by undersaturation of the solution with one component during dissolution of the other. A metasomatic process can be a priori supposed to encompass (similar to the processes of direct growth) a wide variety of phenomena, which arise from a vast diversity of combinations of subelementary processes.

It is suggested that polymineral-metasomatic processes should be classified according to their degree of spatiotemporal correlation between growth and dissolution. Qualitative attributes of the correlation make it possible to single out four overelementary classes; correlation in the first class is maximal, while in the fourth one it is minimal.

1. Dissolution and growth occur within a single crystal grain and take place synchronously. Secondary formations preserve a considerable part of structural-morphological information about a protocystal. Characteristic features of the secondary crystals indicating cause-effect relationships between growth and dissolution are concealed by inherited attributes of the initial crystals. This class also includes a unique process of monocrystal isomorphic replacement. Every moment in the course of this replacement, growth, and dissolution microsites covering the protocystal relic and the relic itself form a mosaic-heterogeneous monocrystal. The problem of structure and genesis of isomorphic monocrystal-line pseudomorphs was solved for the first time ever. The mechanism of isomorphic component selection by a growing crystal is established as a consequence of action of metasomatic component during a mixed crystal formation.
2. Crystals undergoing dissolution and growth are separated from each other by some volumes of solution, but dissolution and growth are unambiguously coordinated with each other in space and proceed almost simultaneously. Secondary formations preserve sufficient structural-morphological information about a protocystal. Characteristic features of the secondary crystals and aggregates indicating cause-effect relationships between growth and dissolution are extremely distinct. This class comprises a majority of polycrystalline and negative products of replacement of monocrystals (see Sect. 1.2). We observed formation of both pseudomorphs and new replacement products, e.g., "automorphs," which to a high degree lose attributes of the protocystal. Our genetic classification is based on the principle of disappearance of information about a protocystal and encompasses known and possibly existing structural-morphological types. There were synthesized case-like aggregates and combined products, i.e., poikilite crystals, polymineral pseudomorphs, and overlapping polycrystalline and negative automorphs. All main types and factors of replacement were provided with reliable genetic interpretations. Structure of replacement products is defined by a physicochemical type of a system. Degree of the product inheriting the protocystal contours depends upon the nature of kinetic constituents of replacement process. Ratio of component solubilities calculated from the phase diagrams defines a volume effect of the replacement, which is one of the most



important kinetic factors. Quantitative ratios between dissolving and precipitating components are defined by salting-in and salting-out mechanisms.

3. Dissolution and growth are not coordinated with each other in space, but proceed more or less simultaneously. Secondary formations lose a sufficient part of structural-morphological information about a protocystal or initial structure of aggregate. Characteristic features of secondary crystals and aggregates characterizing cause–effect relationships between growth and dissolution are dissipated. This class includes such type of monocystal replacement as formation of dissipated automorphs (see Sect. 1.2). However, the most numerous group includes replacements of aggregates. Naturally occurring aggregates and rocks are highly diversified in their mineral compositions and primary structures that make the number of their possible forms and combinations practically uncountable. The present monograph discusses some principal attributes of interaction between the products obtained via replacement of an ensemble of individuals (see Sect. 5.1). A model for formation of rapakivi granites, which are considered here as products of replacement of feldspar rocks (see Sect. 5.2), is proposed.
4. Dissolution and growth are not spatially coordinated and are asynchronous. Secondary formations lose any information about a protocystal or initial structure of aggregate or acquire false information. Characteristic features of secondary crystals and aggregates characterizing cause–effect relationships between growth and dissolution are absent. This class includes such type of monocystal replacement as formation of “translocated” replacement products localized at random in respect to initial crystals (see Sect. 1.2). The most numerous group includes processes of recrystallizations in solutions. Our experimental investigations revealed principle regularities of layering and transformation of grain sizes in polymineral aggregates in fluctuating temperature modes or at temperature gradients (see Sect. 5.3). Under temperature fluctuation conditions, two main factors acting simultaneously define the process: the first factor is temperature fluctuations (or fluctuations of other intensive parameters), while the second factor is heterogeneity of an aggregate caused by structural differences of its composing individuals and their various degrees of imperfection. Aggregates can be divided into passive and active depending upon the properties of the physicochemical systems, i.e., salting-in or salting-out. The process becomes stationary at its final stage and the aggregate structure does not undergo any changes. A particular case of the suggested model is recrystallization of monomineral aggregates proceeding as a sequence of alternating acts of growth and dissolution of crystals having various degrees of imperfection.

It should be noted that only a borderline between the first and second classes is definite enough, while the other boundary criteria are not too distinct. Outer boundaries of the first class and the fourth class, which define distinctions between metasomatic processes and the processes of direct growth/dissolution, are also imprecise. Imprecision of the outer border of the first class is a result of concealing attributes of isomorphic monocrystalline replacement by full information about the protocystal, which is inherited by the replacement products. On the contrary, imprecision

of boundaries of the third and fourth classes is a result of dissipating the information inherited from a protocystal. Therefore, classification of any particular phenomenon can be changed after the phenomenon has been thoroughly investigated. Thus, direct growth of isomorphic-mixed crystals was previously referred to as a subelementary process; later it was found to involve a metasomatic component and consequently regarded as a first overelementary class phenomenon.

Mixed processes mentioned above, which are some combinations of direct growth (or direct dissolution) and metasomatic replacement, also affect the whole crystallogenesis picture. Moreover, complex equilibria in multicomponent systems cause a nonmonotonous character of the phase diagrams and in an inadequacy of supersaturation and supercooling (or undersaturation and overheating). It means that crystals can dissolve in supercooled, and grow in overheated, media, while functions of kinetics versus supercooling/overheating of the medium can be nonmonotonous.

As a whole, all observed overelementary-level effects, as well as subelementary phenomena including oriented growth and faceting of crystals, can be interpreted from a conventional crystallogenic point of view, which should be widened to include all necessary concepts concerning physicochemical nature of the process and combinations of growth and dissolution.

It should be emphasized that for many decades numerous investigators have accumulated vast experimental and naturally obtained data concerning compositions, crystal structures, morphology, and spatiotemporal correlations between synthesized and natural products. Nevertheless, those vast data do not include all possible products and they lack any unifying systematization or generalized genetic scheme. Classification criterion of synchronous–asynchronous growth and dissolution was introduced by A. G. Zhabin and V. L. Rusinov in 1973, but it has not been modified to suit various types of replacement products and does not take into account spatial correlations of elementary processes. Diffusion–infiltration theory of matter redistribution in metasomatic columns, which has been developed by D. S. Korzhinskii and his scientific group since 1950s, does not take into consideration behavior of primary and secondary crystalline material. Numerous mismatching interpretations of metasomatic phenomena result in conclusion about its totally paradoxical nature made by G. L. Pospelov in 1973. To resolve the contradictions an unrealistic assumption has been introduced about the particular nature of chemical reactions taking place in the earth crust expressed from time to time by some scientists (for instance by N. I. Nakovnik in 1949, D. P. Grigor'ev in 1961, and E. K. Lazarenko in 1979).

Poorly developed basis of physicochemical and crystallogenic concepts describing processes proceeding in polymineral media determines preference of intuition genetic interpretations of morphological-crystallochemical properties of minerals and structure–texture peculiarities of aggregates that results in ambiguous or false conclusions. The purpose of the presented monograph is to facilitate development of fundamental crystallogenesis and improve efficiency of studying the natural mineral formation.

# Chapter 1

## Replacement of Monocrystals

### 1.1 Natural and Experimental Products of Replacement

Numerous descriptions of natural products of metasomatic replacement and their interactions with initial minerals (“protocrystals”; they can be also referred to as “educts” – Nakovnik 1964) cannot provide a consistent overview of regularities and mechanisms of the process. However, they do allow to state that no prior limitations could be imposed upon the product composition and structure and extent of its inheriting the educt form.

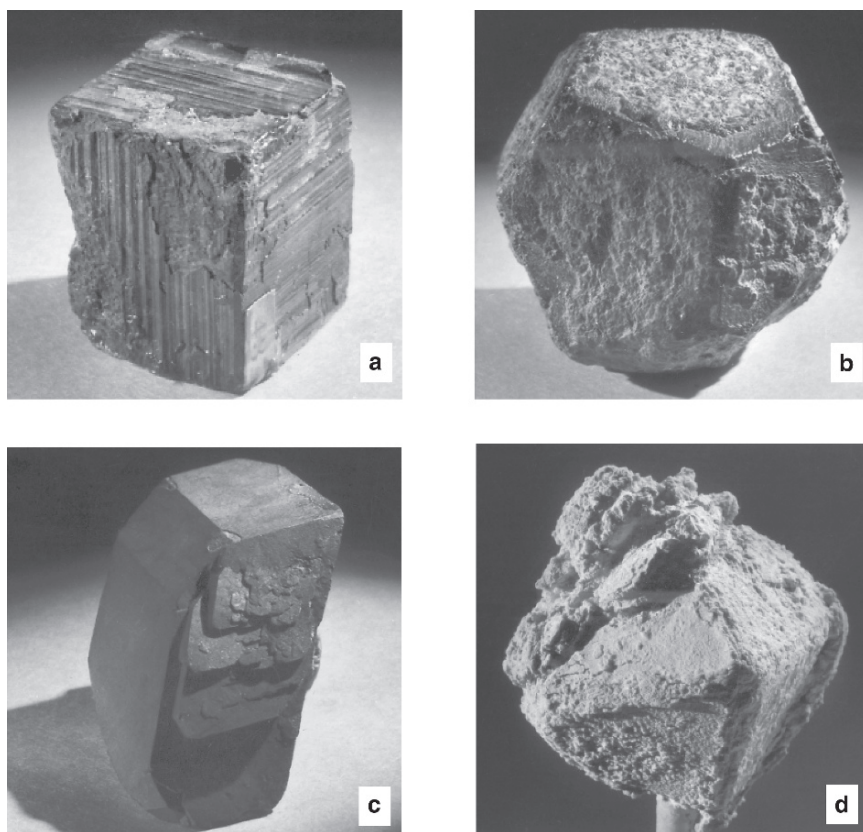
Apparently, a majority of minerals can be exposed to replacement. Certain pairs “educt → product” are widely distributed (pyrite → ferrous hydroxides, orthoclase → kaolinite, calcite → quartz). However, even more diversified kinds of replacements were observed, which included such exotic examples as magnetite → talc (Dr. V. I. Levitskii’s collection, private communication, 1996) and aragonite → copper (Amstutz 1981a). Analysis of crystal grain replacement products shows that they can be both monomineral, such as malachite pseudomorphs formed after azurite (Amstutz 1981b), which is in good agreement with the concept of simplifying a mineral composition of the rock under metasomatic conditions (Korzhinskii 1970, 1993, and others), and polymineral, such as achtarandite (Lyakhovich 1954; Kleber and Pascal 1960; Galuskin et al. 1995, 1998, 2001).

Most natural formations unambiguously identified as products of metasomatic replacement are polycrystalline pseudomorphs of mineral individuals. The first description of pseudomorphs and the term itself belonged to R.-J. Haüy (1801). The first register of different pseudomorphs occurring in the mineral environment was issued as early as in the middle of the nineteenth century (Blüm 1843), and this work has not lost its significance until now. Various facts concerning pseudomorphs are reported in treatises dealing with descriptions and classifications of rocks and ores (Ramdohr 1955; Betekhtin et al. 1958; Polovinkina 1966; Atlas... 1976; Yardley et al. 1990; Barker 1994, and others), in numerous special studies of specific pseudomorph products (e.g., Pelican 1902; Krotov 1925; Plotnikov and Tatarskii 1946; Pidjian 1950; Kostov 1956; Zhabin 1960; Yakshin 1962; Lyakhovich 1954; Brodin and Dymkova 1966; Chesnokov and Yakshin 1969; Shergin 1970; Zhabin and Samsonova 1975; Amstutz 1981a, b, c, d; Fontbole and Rastad 1981;

Strunz 1982; Rudashevskii 1984; Yushkin 1990), and the data are also scattered in the published literature concerning different aspects of mineralogy and petrology.

Extent of pseudomorph inheriting the shape of a protocrystal may vary even for the same educt/product pairs obtained from different deposits, as can be seen, for example, in replacing pyrite with limonite (Figs. 1.1*a, b*).

In addition to pseudomorphs of uniform polycrystalline structure, a variety of pseudomorphs having some specific features have been also described (Betekhtin 1961; Kostov 1968; Chesnokov 1974; Strunz 1982; Lutz 1989, and others). They are found to comprise perimorphs (substituted external zones of individuals), epimorphs (formations enveloping individuals), and elongated case-like, box-like, profiled and



**Fig. 1.1** Natural (*a, b*) and synthetic (*c, d*) pseudomorphs preserving (*a, c*) and losing (*b, d*) the primary face texture (actual size) *a, b* goethite after pyrite (Mining Museum, St. Petersburg), *c* copper chromates after copper vitriol, *d* potassium chromates after Al-k-alum

hollow pseudomorphs (synonyms having a clear sense), negative pseudomorphs (rock cavities with contours preserving the shapes of initial crystals), and shadow pseudomorphs (naturally delineated zones of mineral inclusions occurring in aggregations).

Also known are monocrystalline pseudomorphs (“homoaxial” – Nakovnik 1949; Polovinkina 1966; Chesnokov 1974, and others), which are the products of spatial superposition of primary and secondary monocrystals. Structural types of these pseudomorphs are generally identical to those of initial crystals; these products are identified according to a few structural-morphological signs indicating a possibility of isomorphic replacement that include, for instance, a monocrystal rim or perthitic intergrowth of a mineral grain having composition differing from that of the relic component (Ramdohr 1955; Betekhtin et al. 1958; Polovinkina 1966; Chesnokov 1974; Atlas... 1976; Galuskin and Golovanova 1987, and others). In some cases structural types of educt and product differ, for example uralite (amphibole after pyroxene) and bastite (serpentine after enstatite) (Strunz 1957; Betekhtin 1961; Popov 1984). This type of replacement is practically unexplored as identification of pseudomorphs in monocrystals, if the products are structurally and morphologically similar to the educts, is usually rather complicated (Chesnokov 1974). Nevertheless, monocrystalline replacement in isomorphic series should evoke a certain interest, since minerals having variable composition are widely distributed in nature and are paramount objects of crystal-chemical and genetic analyses.

Moreover, shapes of replacement products can be profoundly different from those of protocrystals (Chesnokov 1974). Primary and secondary minerals can be spatially isolated from each other, examples comprising variable replacement veins and numerous metasomatic ores; however, this fact has not been discussed in published literature.

Metasomatic origin has also been suggested for aggregates showing no outward pseudomorph attributes, but such assumption is still open to doubt. These aggregates include such reaction forms produced within the rocks as corona and coronite structures and drusites (Levinson-Lessing and Struve 1963; Drüppel et al. 2001), concentric aggregations of crystals, forming Liesegang rings (Chukhrov 1955; Carl and Amstutz 1958; Betekhtin 1961; Krasnova and Petrov 1997), myrmekite formations in granitoids (Collins 1988), sphalerite crystals and other crystalline minerals containing both solid and liquid inclusions (Rudenko 1951, 1966; Sinai and Shakhmuradyan 1995; Zaitsev et al. 1998; Zaitsev and Sinai 2001), various types of ovoids (orbiculars) in rapakivi granites (Levinson-Lessing and Vorobyova 1929; Velikoslavinskii 1953; Sudovikov 1967; Velikoslavinskii et al. 1978) and other formations.

It is evident that data derived from natural formations cannot furnish a basis for a general concept of structural and morphological variety of replacement products. The above classification attributes take into account the most evident peculiarities of pseudomorphs, but do not cover the pseudomorphs as a whole. Other products, including formations losing the shape of the initial grain, remain far beyond any systematization.

Conventional genetic schemas of replacement process proposed on the basis of data obtained in experiments and derived from natural sources also present a poor foundation for the general concept. They can explain some specific behavior of crystals undergoing replacement, but cannot provide a solid background for discussing known phenomena of metasomatism in an integrated way, therefore resulting in rather discrepant (paradoxical – Pospelov 1973) models.

Pseudomorphs are usually divided into the following groups: products that replace the protocystals and expel some part of the secondary material outside the initial volume; synchronous and asynchronous, ion-exchanging pseudomorphs; and transformation, displacement, and filling-up pseudomorphs (Grigor'ev 1961; Zhabin and Rusinov 1973; Grigor'ev and Zhabin 1975). Basis of this phenomenological model of spatiotemporal relationship between educts and products does not comprise any concepts of regularity, factors, and mechanisms of the process, and, therefore, the list of the potential variants cannot be considered as complete and the conditions of their existence are still undefined. This approach sometimes leads to rather unrealistic conclusions, such as generation of pseudomorphs as a result of substitution of a crystal from within, while the crystal faceting serves as a barrier for reprecipitation of matter (V. F. Barbanov, private communication, 1996). A theory was proposed (Korzhiinskii 1952, 1955, 1970, 1993; Zaraiskii 1991, 1993, and others) to explain the time series and zoning of the new formations obtained in polymineral-metasomatic processes as a function of thermodynamic potentials of the compounds, which is now generally accepted; however, it never considered the shapes of the products and the mechanism of their formation.

A fundamental breakthrough in describing mechanisms of substantial interchange occurring during replacement processes was made by introducing a three-zone model interconnecting dissolution of the educt, diffusion transfer of the matter in the solution, and precipitation of the product (Beus 1961; Bogolepov 1965; Pospelov 1973). Quantitative aspects of diffusion stage were studied (Fisher 1973), and it was demonstrated that the product precipitation consisted in a simple crystal growth (Pospelov et al. 1961; Pospelov 1973; Chekin and Samotoin 1983). Monocrystalline replacement was, according to the three-zone model, assumed to proceed via epitaxial growth of newly formed crystals with gradual coalescence to form a secondary monocrystal (Grigor'ev 1961). It is worth noting that so far the popular idea of crystal-solution interaction proceeding as an equimolecular exchange of "particle-for-particle" type with preservation of general components (Lindgren 1918; Nakovnik 1949; Grigor'ev 1961; Bogolepov 1965; Chelishchev 1973; Zhabin and Samsonova 1975; Frank-Kamenetskii et al. 1983, and others) does not agree with the three-zone model, which assumes the total dissolution of the initial crystal.

It is a priori considered that propagation of exchange processes in the rocks proceeds via their natural porosity, and isomorphic replacement of the internal zones of a crystal proceeds through its interstitial spaces (Fisher 1973).

Volume ratio of educt and product, being an important thermodynamic parameter, has been under discussion for decades and is considered the most important factor of metasomatic processes in geological objects (Lindgren 1918, 1925, 1933;

Currier 1937; Grigor'ev 1948, 1961; Grogan 1949; Nakovnik 1949; Korzhinskii 1955, 1993; Ames 1961a; Rudnik 1962, 1978; Zhabin and Samsonova 1975; Pospelov 1976; Kazitsyn 1979; Landa 1979; Lazarenko 1979; Collins 1988, and others). The concept of equal volumes known as Lindgren's law is stated to be a necessary criterion creating a basis for computation of chemical reaction balances (Nakovnik 1949, 1958, 1964; Rudnik 1962, 1978; Kazitsyn and Rudnik 1968; Kazitsyn 1979; Grant 1986; Gordienko et al. 1987; Collins 1988, and others).

The above views became conventional and have migrated unchanged from one geological publication to another until now. However, this theory contains an unsolvable contradiction as it assumes not only conformability of physical volumes, but also matching the molar ratios, i.e. the criterion which was rather vaguely expressed in presumption of "ion-for-ion," "molecule-for-molecule," or "particle-for-particle" exchange. The contradiction has been compensated by an arbitrary assumption of natural regulation of a proportion between physical volumes owing to changeable rock porosity, with the total volume remaining constant. Moreover, it was arbitrarily assumed that chemical reactions in the earth crust are of specific nature and thus cannot meet the usual calculation formulae (Nakovnik 1949; Grigor'ev 1961; Lazarenko 1979), which, of course, cannot be true.

Model experiments on replacement of monocrystals produced morphology-structural analogs of natural pseudomorphs reported in literature, and also various products, which did not replicate the shapes of the initial crystals. Pseudomorphs identical to naturally occurring pairs were synthesized, including the following couples: calcite  $\rightarrow$  scheelite, calcite  $\rightarrow$  fluorite, pyrite  $\rightarrow$  hydrogoethite, labradorite  $\rightarrow$  montmorillonite (Ames 1960, 1961b; Glover and Sippel 1962; Balitskii 1966; Balitskii and Komova 1968; Karpov 1970; Dobrovolskii 1975; Egorov 1982, 1983, and others). Some artificial pseudomorphs were mentioned in connection with results of experimental study of acidic metasomatism in rocks; the synthesized formations comprised polymineral aggregates on plagioclase, chlorite, and biotite; carbonates after plagioclase and hornblende; chlorite and pyrite after biotite, etc. (Zaraiskii et al. 1981). Also sporadic reports of obtaining some products, which, according to their morphological characterization, can be classified as monocrystalline pseudomorphs, were found in series of amphiboles (Zaraiskii et al. 1981), plagioclases (Tsuchiyama 1985; Wark and Stimac 1992; Johannes et al. 1994), and zircons (Geisler et al. 2001).

However, most of the experimental data have been obtained for pairs produced in low-temperature modeling under conditions differing from the natural environment.

The low-temperature simulation of the crystal replacement processes was commenced more than 40 years ago. The examples of investigated pairs include  $\text{CuSO}_4 \cdot 5\text{H}_2\text{O} \rightarrow \text{K}_2\text{Cu}(\text{SO}_4)_2 \cdot 6\text{H}_2\text{O}$  (Dr. E. B. Treivus and Mr. D. P. Sipovskii 1962, unpublished data),  $\text{NiSO}_4 \cdot 7\text{H}_2\text{O} \rightarrow \text{NiSO}_4 \cdot 6\text{H}_2\text{O}$  (Kukui 1969),  $\text{NaCl} \rightarrow \text{AgCl}$  (Strunz 1982),  $\text{Al}(\text{OH})_3 \rightarrow \text{AlOHF}_2$ ,  $\text{CaF}_2 \rightarrow \text{Ca}(\text{OH})_2$  (Egorov 1983). Replacement processes also comprise topochemical interactions on crystal surfaces occurring in dehydration and thermal decomposition reactions, which were studied in detail for the following pairs:  $\text{Na}_3\text{P}_3\text{O}_9 \cdot 6\text{H}_2\text{O} \rightarrow \text{Na}_3\text{P}_3\text{O}_9$ ,  $\text{CaSO}_4 \cdot 2\text{H}_2\text{O} \rightarrow \text{CaSO}_4$ ,  $\text{CuSO}_4 \cdot 5\text{H}_2\text{O} \rightarrow \text{CuSO}_4$ ,  $\text{Li}_2\text{SO}_4 \cdot \text{H}_2\text{O} \rightarrow \text{LiSO}_4$ ,  $\text{CdCO}_3 \rightarrow \text{CdO}$ ,  $\text{FeCO}_3 \rightarrow \text{FeO}$ ,  $\text{Ba}_2\text{P}_4\text{O}_8\text{S}_4 \cdot 10\text{H}_2\text{O}$

$\rightarrow \text{Ba}_2\text{P}_4\text{O}_8\text{S}_4 \cdot 6\text{H}_2\text{O}$ ,  $\text{Sr}_2\text{P}_4\text{O}_8\text{S}_4 \cdot 10\text{H}_2\text{O} \rightarrow \text{Sr}_2\text{P}_4\text{O}_8\text{S}_4 \cdot 6\text{H}_2\text{O}$ , etc. (Prodan 1990), and numerous microchemical reactions, which were earlier assumed to be important for diagnostics (Ansheles and Burakova 1948; Tananaev 1954).

Our systematic experiments considerably extended the above studies and, as a whole, resulted in development of a general concept of replacement mechanisms and regularities including cause–effect relationships, physicochemical correlations, and volume effects (Glikin and Sinai 1983, 1988, 1991; Sinai and Glikin 1989; Glikin et al. 1994a, b, 2003, 2007; Glikin 1995, 1996a, b, 2004, 2007; Sinai and Shakhmuradyan 1995; Voloshin et al. 2001, 2004; Kryuchkova et al. 2002; Woensdregt and Glikin 2005; Franke et al. 2007; Kulkov and Glikin 2007). A substantial part of our investigations comprises the study of isomorphic monocrystal-line replacement staying apart in the series of other metasomatic reactions and processes of crystal formation. Our experimental and theoretical data are summarized in the following sections.

## 1.2 Technique, Terminology, and Experimental Results

Our experiments were carried out using water-soluble salts, mainly at ambient temperature, and consisted in inserting crystals of one component in the solution of the other, with retention time varying from several hours to several months.

The most significant reactions and key salt components are presented in Table 1.1. Some reactions were conducted in the presence of salt admixtures added into the solution, or with variation of pH, and with elevation of temperature up to 60°C. It should be noted that some of the above crystalline products are analogs of natural minerals (epsomite, morenosite, sylvite, halite, lopezite, barite, etc.); therefore, some of the reactions can simulate certain natural processes.

Flat thin sections (Fig. 1.2a) of the sort used in petrography investigations were used for microscopic studies (up to 20-fold magnification of objectives) of the processes in progress at the replacement front and in the other parts of the systems (Glikin and Sinai 1983). Protocrystal sections with a width of 3–5 mm and thickness of 0.2–0.5 mm were prepared; volumes of the solutions were usually 0.5–1.5 ml. Some results (see examples in Figs. 1.1c, d) were obtained using massive samples and relatively great solution volumes (Fig. 1.2b); similar objects were used by Prodan (1990) in the experimental substitutions of large, up to several centimeters, individuals conducted in crystallizers of 1 liter. Simplicity of the experimental techniques and generally rapid reactions ensured reproducibility and easiness of the experiments. In each case, combination of solid (initial crystal, primary crystal, or protocrystal) and dissolved reactants was selected on the basis of reference data of their mutual solubility in water, or it was selected empirically as to provide the desired phase ratios in the system (see Sect. 1.5.1).

More than 150 reactions were studied, which were divided into three types indicated in Table 1.1. Reactions of Type I were conducted at constant temperature in



**Table 1.1** Representative examples of some model reactions of replacement of monocrystals

Type of reaction	Salt components			
	No	Proto-crystal	Initial solution	Main products
<i>Ia</i> (systems with salting-out containing non-isomorphic components conducted at a constant temperature or temperature varying within a certain range)	1	NaCl	NaNO <sub>3</sub>	NaNO <sub>3</sub>
	2	NaNO <sub>3</sub>	NaCl	NaCl
	3	NaNO <sub>3</sub>	(NH <sub>4</sub> ) <sub>2</sub> SO <sub>4</sub>	(NH <sub>4</sub> ) <sub>2</sub> SO <sub>4</sub>
	4	(NH <sub>4</sub> ) <sub>2</sub> SO <sub>4</sub>	NaNO <sub>3</sub>	NaNO <sub>3</sub>
	5	KAl(SO <sub>4</sub> ) <sub>2</sub> ·12H <sub>2</sub> O	K <sub>2</sub> CrO <sub>4</sub>	K <sub>2</sub> CrO <sub>4</sub> + K <sub>2</sub> Cr <sub>2</sub> O <sub>7</sub>
	6	K <sub>2</sub> CrO <sub>4</sub>	KAl(SO <sub>4</sub> ) <sub>2</sub>	KAl(SO <sub>4</sub> ) <sub>2</sub> ·12H <sub>2</sub> O + K <sub>2</sub> (Cr <sub>2</sub> SO <sub>4</sub> ) <sub>4</sub>
	7	NH <sub>4</sub> Cl	MgSO <sub>4</sub>	MgSO <sub>4</sub> ·7H <sub>2</sub> O
	8	NH <sub>4</sub> Cl	(NH <sub>4</sub> ) <sub>2</sub> CrO <sub>4</sub>	(NH <sub>4</sub> ) <sub>2</sub> CrO <sub>4</sub>
	9	NH <sub>4</sub> Cl	(NH <sub>4</sub> ) <sub>2</sub> Cr <sub>2</sub> O <sub>7</sub>	(NH <sub>4</sub> ) <sub>2</sub> Cr <sub>2</sub> O <sub>7</sub>
	10	KCl	MgCl <sub>2</sub>	KMgCl <sub>3</sub> ·6H <sub>2</sub> O
	11	KCl	K <sub>2</sub> Cr <sub>2</sub> O <sub>7</sub>	K <sub>2</sub> Cr <sub>2</sub> O <sub>7</sub>
	12	KBr	(NH <sub>4</sub> ) <sub>2</sub> SO <sub>4</sub>	(NH <sub>4</sub> ) <sub>2</sub> SO <sub>4</sub>
	13	KBr	(NH <sub>4</sub> ) <sub>2</sub> Cr <sub>2</sub> O <sub>7</sub>	(NH <sub>4</sub> ) <sub>2</sub> Cr <sub>2</sub> O <sub>7</sub>
	14	KBr	K <sub>2</sub> Cr <sub>2</sub> O <sub>7</sub>	K <sub>2</sub> Cr <sub>2</sub> O <sub>7</sub>
	15	KNO <sub>3</sub>	(NH <sub>4</sub> ) <sub>2</sub> SO <sub>4</sub>	(NH <sub>4</sub> ) <sub>2</sub> SO <sub>4</sub>
	16	KH <sub>2</sub> PO <sub>4</sub>	(NH <sub>4</sub> ) <sub>2</sub> SO <sub>4</sub>	(NH <sub>4</sub> ) <sub>2</sub> SO <sub>4</sub>
	17	CoSO <sub>4</sub> ·7H <sub>2</sub> O	KCl	KCl
	18	CoSO <sub>4</sub> ·7H <sub>2</sub> O	MgSO <sub>4</sub>	MgSO <sub>4</sub> ·7H <sub>2</sub> O
	19	NiSO <sub>4</sub> ·7H <sub>2</sub> O	KCl	NiK <sub>2</sub> (SO <sub>4</sub> ) <sub>2</sub> ·6H <sub>2</sub> O
	20	Ni(NH <sub>4</sub> ) <sub>2</sub> (SO <sub>4</sub> ) <sub>2</sub> ·6H <sub>2</sub> O	NaBrO <sub>3</sub>	NaBrO <sub>3</sub>
	21	CuSO <sub>4</sub> ·5H <sub>2</sub> O	KCl	KCl
	22	CuSO <sub>4</sub> ·5H <sub>2</sub> O	K <sub>2</sub> Cu(SO <sub>4</sub> ) <sub>2</sub>	K <sub>2</sub> Cu(SO <sub>4</sub> ) <sub>2</sub> ·6H <sub>2</sub> O
	23	KC <sub>8</sub> H <sub>3</sub> O <sub>4</sub>	C <sub>8</sub> H <sub>3</sub> O <sub>4</sub>	K <sub>2</sub> C <sub>8</sub> H <sub>3</sub> O <sub>4</sub> ·4C <sub>8</sub> H <sub>3</sub> O <sub>4</sub> ·4H <sub>2</sub> O
	24	NiSO <sub>4</sub> ·7H <sub>2</sub> O	MgSO <sub>4</sub>	(Ni <sub>1</sub> Mg)SO <sub>4</sub> ·7H <sub>2</sub> O
	25	MgSO <sub>4</sub> ·7H <sub>2</sub> O	NiSO <sub>4</sub>	(Ni <sub>1</sub> Mg)SO <sub>4</sub> ·7H <sub>2</sub> O

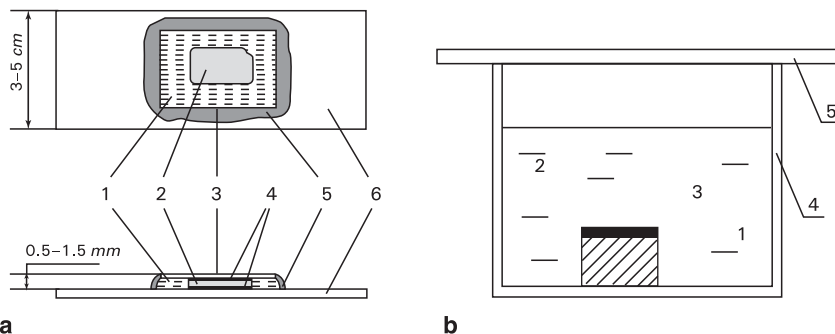
*Ib* (systems with salting-out containing isomorphic components conducted at a constant temperature or temperature varying within a certain range)

(continued)

**Table 1.1** (continued)

Type of reaction	Salt components				
	No	Protocrystal	Initial solution	Main products	
<i>II</i> (systems with salting-in, lowering temperature)	26	FeSO <sub>4</sub> ·7H <sub>2</sub> O	CoSO <sub>4</sub>	(Fe,Co)SO <sub>4</sub> ·7H <sub>2</sub> O	
	27	CoSO <sub>4</sub> ·7H <sub>2</sub> O	FeSO <sub>4</sub>	(Fe,Co)SO <sub>4</sub> ·7H <sub>2</sub> O	
	28	KAl(SO <sub>4</sub> ) <sub>2</sub> ·12H <sub>2</sub> O	KCr(SO <sub>4</sub> ) <sub>2</sub>	K(Al,Cr)(SO <sub>4</sub> ) <sub>2</sub> ·12H <sub>2</sub> O	
	29	KCr(SO <sub>4</sub> ) <sub>2</sub> ·12H <sub>2</sub> O	KAl(SO <sub>4</sub> ) <sub>2</sub>	K(Al,Cr)(SO <sub>4</sub> ) <sub>2</sub> ·12H <sub>2</sub> O	
	30	Ni(NH <sub>4</sub> ) <sub>2</sub> (SO <sub>4</sub> ) <sub>2</sub> ·6H <sub>2</sub> O	Co(NH <sub>4</sub> ) <sub>2</sub> (SO <sub>4</sub> ) <sub>2</sub>	(Ni,Co)(NH <sub>4</sub> ) <sub>2</sub> (SO <sub>4</sub> ) <sub>2</sub> ·6H <sub>2</sub> O	
	31	Co(NH <sub>4</sub> ) <sub>2</sub> (SO <sub>4</sub> ) <sub>2</sub> ·6H <sub>2</sub> O	Ni(NH <sub>4</sub> ) <sub>2</sub> (SO <sub>4</sub> ) <sub>2</sub>	(Ni,Co)(NH <sub>4</sub> ) <sub>2</sub> (SO <sub>4</sub> ) <sub>2</sub> ·6H <sub>2</sub> O	
	32	Ni(NH <sub>4</sub> ) <sub>2</sub> (SO <sub>4</sub> ) <sub>2</sub> ·6H <sub>2</sub> O	NiK <sub>2</sub> (SO <sub>4</sub> ) <sub>2</sub>	Ni(K,NH <sub>4</sub> ) <sub>2</sub> (SO <sub>4</sub> ) <sub>2</sub> ·6H <sub>2</sub> O	
	33	NiK <sub>2</sub> (SO <sub>4</sub> ) <sub>2</sub> ·6H <sub>2</sub> O	Ni(NH <sub>4</sub> ) <sub>2</sub> (SO <sub>4</sub> ) <sub>2</sub>	Ni(K,NH <sub>4</sub> ) <sub>2</sub> (SO <sub>4</sub> ) <sub>2</sub> ·6H <sub>2</sub> O	
	34	K <sub>2</sub> SO <sub>4</sub>	K <sub>2</sub> CrO <sub>4</sub>	K <sub>2</sub> (CrO <sub>4</sub> ) <sub>2</sub> SO <sub>4</sub>	
	35	K <sub>2</sub> CrO <sub>4</sub>	K <sub>2</sub> SO <sub>4</sub>	K <sub>2</sub> (CrO <sub>4</sub> ) <sub>2</sub> SO <sub>4</sub>	
	36	NaCl	NiSO <sub>4</sub>	NiSO <sub>4</sub> ·7H <sub>2</sub> O	
	37	KBr	NaNO <sub>3</sub>	NaNO <sub>3</sub>	
	38	NaNO <sub>3</sub>	(NH <sub>4</sub> ) <sub>2</sub> Cr <sub>2</sub> O <sub>7</sub>	(NH <sub>4</sub> ) <sub>2</sub> Cr <sub>2</sub> O <sub>7</sub>	
	39	NaNO <sub>3</sub>	K <sub>2</sub> Cr <sub>2</sub> O <sub>7</sub>	K <sub>2</sub> Cr <sub>2</sub> O <sub>7</sub>	
	40	KNO <sub>3</sub>	NaNO <sub>3</sub>	NaNO <sub>3</sub>	
	41	CuSO <sub>4</sub> ·5H <sub>2</sub> O	KAl(SO <sub>4</sub> ) <sub>2</sub>	KAl(SO <sub>4</sub> ) <sub>2</sub> ·12H <sub>2</sub> O	
	<i>III</i> (exchange reactions with precipitation of the insoluble product conducted at a constant temperature or temperature varying within a wide range)	42	CuSO <sub>4</sub> ·5H <sub>2</sub> O	K <sub>2</sub> CrO <sub>4</sub>	Copper chromates
		43	K <sub>2</sub> CrO <sub>4</sub>	CuSO <sub>4</sub>	Copper chromates
		44	KAl(SO <sub>4</sub> ) <sub>2</sub> ·12H <sub>2</sub> O	Ba(NO <sub>3</sub> ) <sub>2</sub>	BaSO <sub>4</sub>
		45	Ba(NO <sub>3</sub> ) <sub>2</sub>	KAl(SO <sub>4</sub> ) <sub>2</sub>	BaSO <sub>4</sub>
		46	K <sub>2</sub> SO <sub>4</sub>	CaCl <sub>2</sub>	CaSO <sub>4</sub> ·2H <sub>2</sub> O
		47	BaCl <sub>2</sub> ·2H <sub>2</sub> O	KAl(SO <sub>4</sub> ) <sub>2</sub>	BaSO <sub>4</sub>
		48	BaCl <sub>2</sub> ·2H <sub>2</sub> O	(NH <sub>4</sub> ) <sub>2</sub> CrO <sub>4</sub>	BaCrO <sub>4</sub>
		49	CoSO <sub>4</sub> ·7H <sub>2</sub> O	BaCl <sub>2</sub>	BaSO <sub>4</sub>
		50	CoSO <sub>4</sub> ·7H <sub>2</sub> O	(NH <sub>4</sub> ) <sub>2</sub> CrO <sub>4</sub>	Cobalt chromates
		51	NiSO <sub>4</sub> ·7H <sub>2</sub> O	BaCl <sub>2</sub>	BaSO <sub>4</sub>
		52	NiSO <sub>4</sub> ·7H <sub>2</sub> O	(NH <sub>4</sub> ) <sub>2</sub> CrO <sub>4</sub>	Nickel chromates
		53	NiSO <sub>4</sub> ·7H <sub>2</sub> O	K <sub>2</sub> CrO <sub>4</sub>	Nickel chromates + K <sub>2</sub> CrO <sub>4</sub>

**Note:** Systems 5, 6, 42, 43, 50, 52 and 53 were observed to form several precipitating phases.



**Fig. 1.2** A flat thin section (**a**) and a massive sample (**b**) used for replacement experiments **a**: 1 – solution, 2 – crystal, 3 – glass-cover slip, 4 – glue, 5 – sealant, 6 – object glass; **b**: 1 – solution, 2 – crystal, 3 – film of glue, 4 – cell, 5 – lid

the “systems with salting-out,” which means that addition of one substance into the system resulted in decrease in solubility of the other (Anosov et al. 1976; Kirgintsev 1976). This type of reactions was further divided into two subtypes: reactions between non-isomorphic (*Ia*) and reactions between isomorphic (*Ib*) components. Reactions of Type *II* were conducted with lowering the temperature in the “systems with salting-in,” which means that addition of one substance into the system resulted in enhanced solubility of the other (Anosov et al. 1976; Kirgintsev 1976).

Reactions of Type *III* were exchange interactions between the protocystal matter and dissolved substances resulting in precipitation of an insoluble product; they were conducted at constant temperature.

The products of replacements are described below. They are quite diversified in their structures and shapes. Hereinafter, several terms are used, both conventional and some of our invention (Glikin and Sinai 1983, 1988, 1991; Glikin et al. 1988; Sinai and Glikin 1989), that need special explanations, which are also given below.

Our classification includes monocrystalline,<sup>1</sup> polycrystalline, and amorphous products. The first two terms do not require any explanation. The term “amorphous products” means cavities occurring in a former site of protocystal that contain (or contained) solution, which are considered as an amorphous substance.<sup>2</sup>

<sup>1</sup>The term “homoaxial pseudomorphs” (Nakovnik 1949, Polovinkina 1966, Chesnokov 1974, et al.) used as a synonym for “monocrystal pseudomorphs” seems inappropriate, since directions of the protocystal axes and the axes of pseudomorphous crystal do not generally coincide.

<sup>2</sup>Introduction of the term “amorphous products” is required for uniformity of the taxonomic units in this series. This term is similar to “negative pseudomorphs” (Betekhtin et al. 1958, p. 223; Kostov 1968) applied to faceted cavities, and thus it is logical to classify mono- and polycrystalline products as “positive” pseudomorphs.

According to their shapes, the products are divided into pseudomorphs and “automorphs” and their modifications.

As usual, pseudomorphs are referred to as products of replacement replicating the shape of the protocystal. We divide them into embossed, i.e., preserving details of the protocystal surface relief; faceted, i.e., preserving the faces but losing the relief; and blurred, which preserve only the principal features of protocystal morphology like elongation, flattening, etc.

Automorphs<sup>3</sup> are the products which do not replicate the elements of the protocystal shape. They can be divided into localized automorphs, if it is possible to define the former location of the substituted protocystal at the site of the secondary crystal aggregation, and dissipated<sup>4</sup> automorphs, free of any morphological information about the protocystal when the area covered with uniformly scattering secondary crystals exceeds considerably, and theoretically infinitely, the protocystal size. Translocated automorphs, located far away from the site of the initial crystal, should also be included into the classification.

While illustrating the above, it is necessary to describe some other important complementary effects we observed, which can promote our understanding of naturally proceeding processes. More detailed description of replacement products is presented in Sinai's thesis (1991).

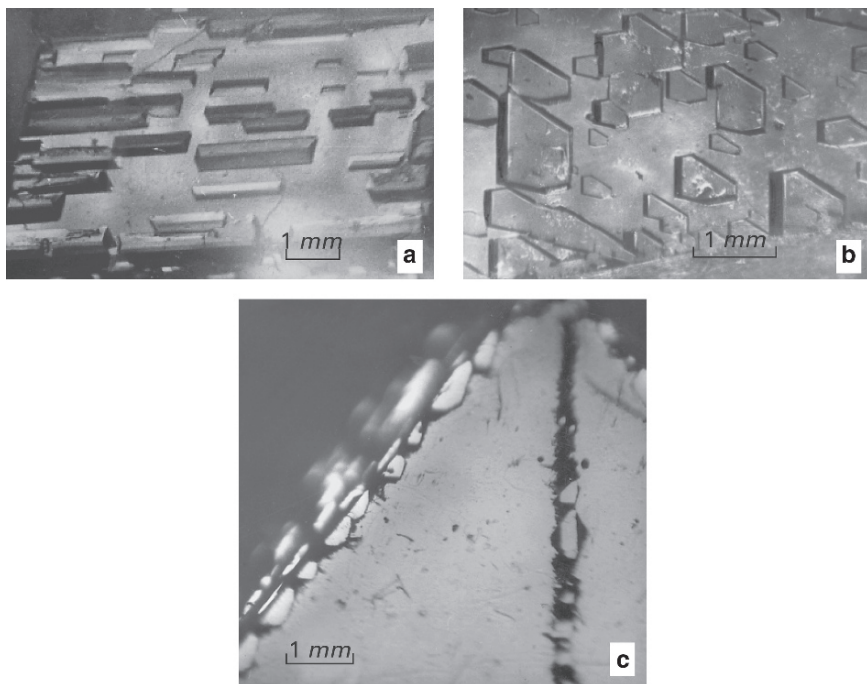
**Monocrystal products** were obtained mainly in isomorphic replacement experiments (Type *Ib* reactions), and they took pseudomorphic forms (Glikin and Sinai 1983; Glikin et al. 1994a, b, and others). The rare effect of non-isomorphic replacement of monocrystals was observed under special conditions of metasomatic transformation of monoclinic nickelhexahydrate  $\beta$ -NiSO<sub>4</sub>·6H<sub>2</sub>O into tetragonal retgersite  $\alpha$ -NiSO<sub>4</sub>·6H<sub>2</sub>O (see Sect. 1.3 and 1.5.1). The distinguishing features of replacement of monocrystals have not been discussed previously.

*Embossed and faceted pseudomorphs (continuous)* were obtained in reactions *Ib/24, 26, 28, 30, 32–34* (hereinafter Roman and Arabic numerals are the types and numbers, respectively, of reactions cited in Table 1.1). The faces of the pseudomorphs bear autoepitaxial excrescences (Fig. 1.3). They are observed to grow in sectors containing imperfections, i.e., outcroppings of dislocations on the faces, their agglomerations on the edges, scratches, etc., which can be clearly seen in Fig. 1.3c. Figure 1.3a also shows accumulation of outgrowing formations near the edges. When a pseudomorph hosts only a few excrescences, they only insignificantly shield the primary surface relief and the pseudomorph type is close to embossed (reactions 30, 32, 33). Pseudomorphs of this type grow very slowly: it takes about 1–2 months to replace a peripheral zone of a crystal having thickness varying from some hundredths of a millimeter to 1–1.5 mm (reactions 26 and 30, respectively).

---

<sup>3</sup>The term is suggested on the assumption that these formations, unlike the pseudomorphs, possess their own shapes. We also mean certain analogies when using prefixes “auto-” (e.g., “autogenesis” – *Geologic Dictionary* 1973).

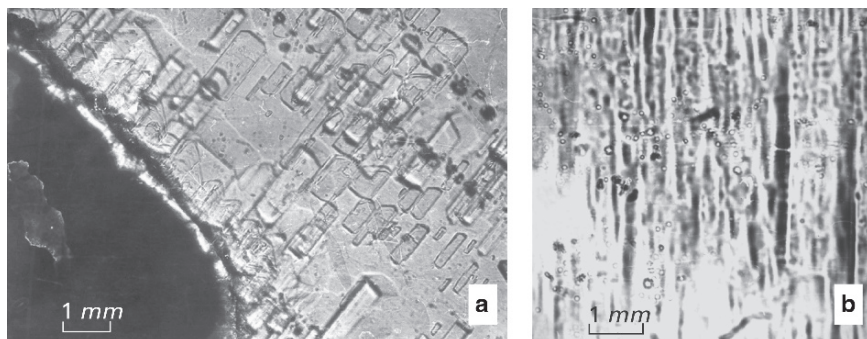
<sup>4</sup>The term was proposed by Prof. A. P. Khomyakov.



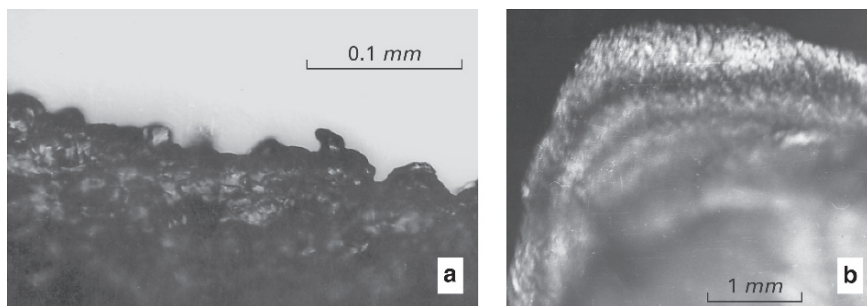
**Fig. 1.3** Autoepitaxial excrescences on the faces of solid monocrystalline pseudomorphs. Isomorphic replacement of  $\text{Ni}(\text{NH}_4)_2(\text{SO}_4)_2 \cdot 6\text{H}_2\text{O}$  crystals with  $(\text{Ni},\text{Co})(\text{NH}_4)_2 \cdot 6\text{H}_2\text{O}$  phase (reaction *Ib/30*) **a** – {010} face; **b** – {110} face; **c** – localization of excrescences in areas of the {111} face containing imperfections, i.e., along the edge and the scratch

Cracks including those formed during the replacement process make way for the replacement to penetrate deeper inside the crystal that results in formation of replacement structures of perthite type (reaction 24, Fig. 1.4).

*Faceted and blurred pseudomorphs (spongy)* were obtained in reactions *Ib/25*, 27, 29, 31, and 35. They can be distinguished due to their uneven surfaces. At the initial stage of replacement, a pseudomorph surface is scalloped with chaotically alternating protuberances having sometimes evident faceting and pits (Fig. 1.5a). The relief changes gradually including formation of pockets in the places of protuberances and vice versa. The change is quite rapid and can be easily detected in the course of 1–2 h of continuous observation of the edge of a flat sample. As the time passes, the deepest pits initiate development of channels (Fig. 1.5b), which at subsequent stages pierce the whole bulk of the crystal. Development of such relief and formation of the channels do not affect the average position of the crystal boundary, and, in some cases, it can shift to the center of the protocystal due to its dissolving as replacement progresses. This can lead, for instance, to formation of blurred

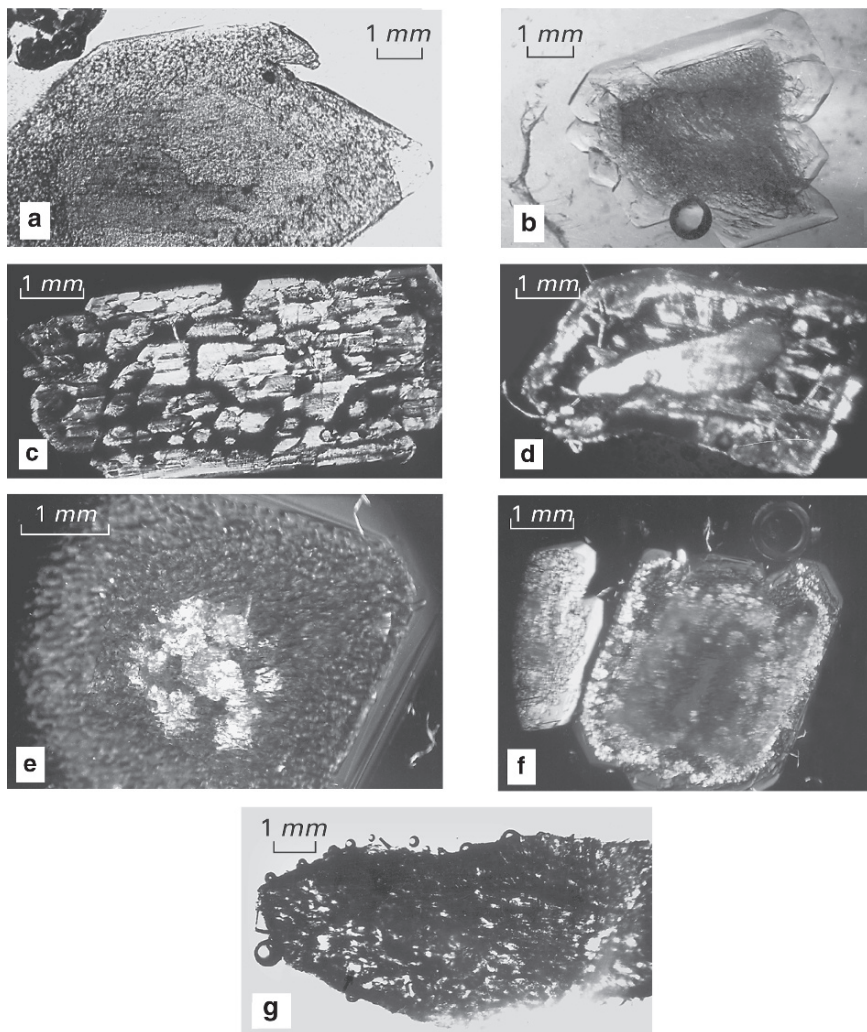


**Fig. 1.4** Monocrystalline isomorphic replacement of  $\text{Ni}(\text{SO}_4)_2 \cdot 7\text{H}_2\text{O}$  with  $(\text{Ni},\text{Mg})\text{SO}_4 \cdot 7\text{H}_2\text{O}$  (reaction *Ib/24*) with formation of cracks and perthite structure **a** – surface; **b** – section



**Fig. 1.5** Changes in a surface relief observed in situ in a crystal undergoing replacement with formation of spongy pseudomorphs (flat section, the reaction takes place on the crystal border) **a** – scalloped profile formed at the first stage of  $\text{MgSO}_4 \cdot 7\text{H}_2\text{O}$  replacement with  $(\text{Mg},\text{Ni})\text{SO}_4 \cdot 7\text{H}_2\text{O}$  (reaction *Ib/25*); **b** – channels formed at the second stage of  $\text{CoSO}_4 \cdot 7\text{H}_2\text{O}$  replacement with  $(\text{Co},\text{Fe})\text{SO}_4 \cdot 7\text{H}_2\text{O}$  accompanied by dissolving (reaction *Ib/27*)

pseudomorphs with rounded near-edge sections (Fig. 1.5*b*). The end product of the process is a monocrystalline “sponge,” i.e., a monocrystal of intermediate isomorphic composition permeated with randomly oriented tortuous channels and inclusions. A section of such a product can look like a section of a porous body (Figs. 1.6*a, b*) or like a graphic crystalline aggregation (Fig. 1.6*b*). Extremely high porosity causes separation of newly formed blocks, their parallelism breaking, and formation of a localized automorph (Fig. 1.6*d*). Saturation of the initial solution with an additional non-isomorphic salt can result in filling up the newly formed inclusions with the salt crystals, i.e., with solid intrusions, and formation of poikilite structure (Figs. 1.6*e–g*).



**Fig. 1.6** Spongy monocrystalline pseudomorphs **a–d** – monocrystalline pseudomorphs with implanted pores filled up with solution: **a** –  $(\text{Mg,Ni})\text{SO}_4 \cdot 7\text{H}_2\text{O}$  after  $\text{MgSO}_4 \cdot 7\text{H}_2\text{O}$  with spongy frontier zone and relic of protocrystal (reaction *Ib/25*); **b** –  $(\text{Co,Fe})\text{SO}_4 \cdot 7\text{H}_2\text{O}$  after  $\text{CoSO}_4 \cdot 7\text{H}_2\text{O}$ , in which a spongy pseudomorph (reaction *Ib/27*) becomes surrounded with a monocrystalline rim at lowering temperature; **c** –  $(\text{Ni,Mg})\text{SO}_4 \cdot 7\text{H}_2\text{O}$  after  $\text{MgSO}_4 \cdot 7\text{H}_2\text{O}$  with graphical structure of the pseudomorph formed owing to implantation of large inclusions (reaction *Ib/25*); **d** –  $\text{K}_2(\text{S,Cr})\text{O}_4$  after  $\text{K}_2\text{CrO}_4$ , in which separated and disoriented blocks of new formation make up a new polycrystalline localized automorph (reaction *Ib/35*); **e–g** – monocrystalline pseudomorphs having pores filled up with implanted crystalline inclusions (poikilitic crystals; matrix and inclusions are depicted as dark and light areas, respectively): **e**, **f** – pseudomorphs  $(\text{Co,Fe})\text{SO}_4 \cdot 7\text{H}_2\text{O}$  after  $\text{CoSO}_4 \cdot 7\text{H}_2\text{O}$  containing inclusions of  $(\text{NH}_4)_2(\text{Co,Fe})\text{SO}_4 \cdot 6\text{H}_2\text{O}$  permeating the core (**e**) and the periphery (**f**) of the pseudomorph; **g** – pseudomorph of  $\text{K}_2(\text{S,Cr})\text{O}_4$  after  $\text{K}_2\text{CrO}_4$  containing implanted inclusions of KCl

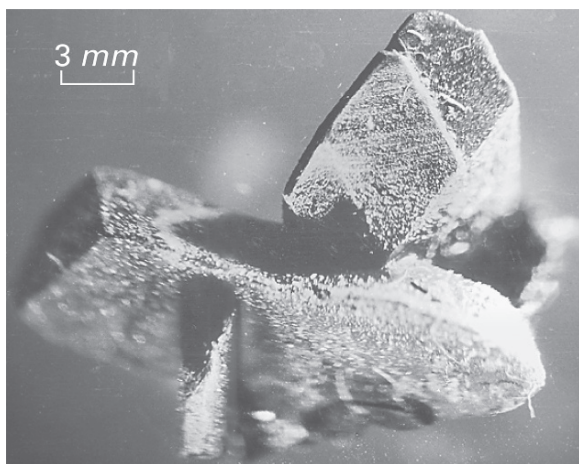
*Localized automorphs.* When using a considerably large amount of the initial solution, replacement of protocystal (e.g., reaction *Ib/35*) can be preceded and accompanied by its intensive dissolution. The monocrystal produced occupies the place of the initial protocystal and can be about ten times smaller in linear size and totally free of information about its initial shape.

*Translocated automorphs.* Total dissolving of the initial crystal was observed in reaction *Ib/31*; in this case, the initial crystal of  $\text{Co}(\text{NH}_4)_2(\text{SO}_4)_2 \cdot 6\text{H}_2\text{O}$  disappeared completely and a new monocrystal of  $(\text{Ni},\text{Co})(\text{NH}_4)_2(\text{SO}_4)_2 \cdot 6\text{H}_2\text{O}$  was formed in a different part of the system. This was likely to be initiated by temporary elevation of the ambient temperature.

Polycrystalline products of replacement precipitate in reactions of Type *I* (mainly *Ia*) and *III* and are represented by all morphological varieties.

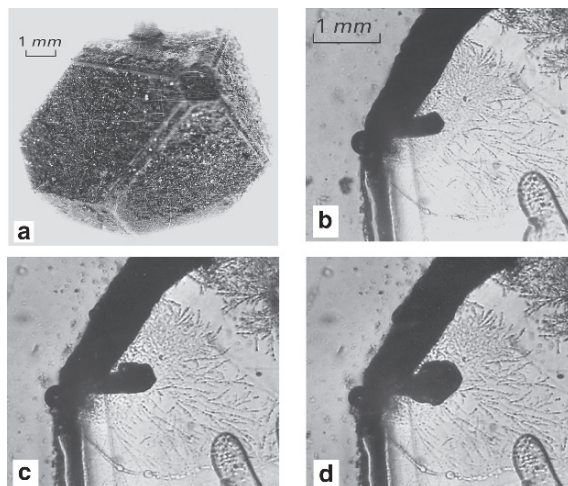
*Embossed pseudomorphs* were obtained in reaction *III/42* (Figs. 1.1c and 1.7). The products comprised solid aggregations of dark-brown copper chromates. The replacement front was smooth and uninterrupted. Continuous addition of KOH into the solution caused pseudomorphs to transform into faceted, and then into blurred, forms, which had loose structures and modified phase compositions. Alteration of composition was easily discernible as initial color changed to black.

*Faceted pseudomorphs* were formed in reactions *Ia/5*, 8, 10, 15, 16 and *III/42* (with addition of KOH), 53. They were located within the slightly diffused contours of the protocrystals, and, as a rule, they had a dense structure and were made up of individuals having sizes up to tenths of a millimeter. Products obtained in reaction *Ia/5* (Figs. 1.1d and 1.8) were composed of fine grains of relatively densely packed  $\text{K}_2\text{CrO}_4$  crystals and isometric mono- and polycrystalline inclusions of  $\text{K}_2\text{Cr}_2\text{O}_7$ , which sometimes reached 1 mm in size (this is an example of polymineral pseudomorph). Such inclusions



**Fig. 1.7** Embossed polycrystalline pseudomorphs of copper chromates after  $\text{CuSO}_4 \cdot 5\text{H}_2\text{O}$  crystals (reaction *III/42*)





**Fig. 1.8** Faceted polycrystalline pseudomorph of potassium chromates after potassium alum crystal (reaction *Ia/5*) **a** – general view of a large crystal; **b–d** – stages of ingrowth of  $K_2Cr_2O_7$  crystals into the potassium alum substrate (flat section)

located in parallel to the replacement front were observed to have stratified distribution. The replacement front was uninterrupted, but not smooth: its individual sectors contained relatively big crystals of  $K_2CrO_4$ , which grew into the alum crystal undergoing substitution (Figs. 1.8 *b–d*) at the rate of about 0.1 mm/s for the thinnest individuals. The in-growing crystals were well faceted, the process was accompanied by skeletal growth and splitting of crystals. The gap between the in-growing newly formed crystal and the protocystal was not discernible under microscope. Elevation of temperature to 50–60°C or addition of  $H_2SO_4$  into the solution resulted in significant fuzziness of the contours and loosening the structure of pseudomorphs with increase of  $K_2Cr_2O_7$  content in them. Addition of alkali did not change the morphology in comparison with that observed in a stoichiometric solution, but led to disappearance of  $K_2Cr_2O_7$ .

Reaction *III/53* is notable by the fact that in some experiments it led to formation of hollow pseudomorphs composed of fine-grained aggregates of black nickel chromates and  $K_2Cr_2O_7$  (one more example of polymineral pseudomorphs). Fractures of the pseudomorphs bore visible cyclic lamination formed owing to variations in the component ratio (the layer thickness was up to 0.1 mm). The fractures also hosted isometric isolated formations having sizes of up to 1 mm and a similar phase composition, but differing in granularity; they were produced in an interaction between solution contained in protocystal inclusions and the surrounding solution.

*Blurred pseudomorphs* were formed in reactions *Ia/2*, 3, 5 (with addition of  $H_2SO_4$  or at elevated temperature), 7, 9, 11, 12, 14, 19, 22, *III/42* (with addition of KOH), 46, 50, 52. Their contours exceeded significantly the bounds of the protocystal.

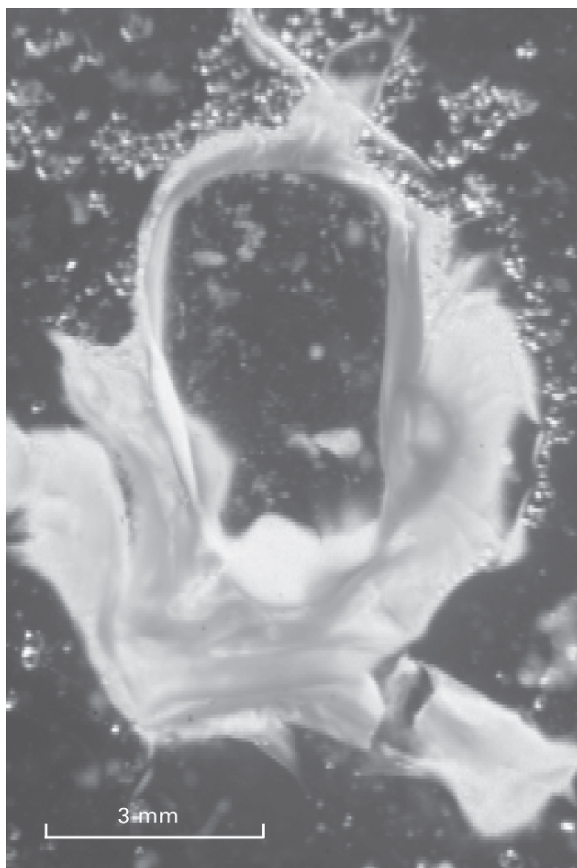
They were relatively loose, fine-grained, or coarse-grained (up to 0.5–1 mm; reaction 46). Pseudomorphs obtained in reaction 9 can be referred to as intermediate, faceted–blurred-type formations.

Hollow (case-like) pseudomorphs produced in reactions 11, 14, 22 and sometimes in reactions 50 and 52 (Fig. 1.9) are of special interest. Their formation was observed in system 22 as early as in 1962 (Dr. E. B. Treivus and Mr. D. P. Sipovskii, unpublished data). Our observations demonstrated the process as follows. First, replacement of peripheral parts of the protocrystal results in formation of a faceted fine-grained crystalline pseudomorph. As the time passes, the progress of the replacement front stops, but relic of the protocrystal continues to dissolve until it totally disappears. Precipitated individuals grow larger, and, so, the pseudomorph loses its well-defined contours, transforming into a blurred pseudomorph. If the initial solutions contained an excessive, in comparison with its eutonic content, concentration of  $K_2SO_4$ , the pseudomorph's initial outline became diffused and the size of the newly formed crystals increased. Similar hollow pseudomorphs were produced in reactions 11 and 14; they were mainly composed of new needle-like crystals. Illustrative examples of  $K_2Cr_2O_7$  replacement with KBr and KBr with  $K_2Cr_2O_7$  demonstrated (Sect. 6.3) that the process can be accompanied by phase epitaxy determined by the rate of protocrystal dissolution and growth rate of the new formations (Glikin and Kaulina 1988).

*Localized automorphs* were obtained in reactions 1a/1, 4, 6, 13, 17, 18, 20, 21, 22 (the latter with excess of  $CuSO_4$  in the solution), 1b/35, III/43, 44, 45, 47, 48, 49, and 51. Automorphs of this type are aggregates of secondary crystals varying from fine-grained (reactions 44, 49, and 51) to submillimeter-sized (reactions 17, 18, and 21). The automorphs can be considerably bigger than protocrystals (e.g., 1.5 times greater in system 22) or smaller (3 times less in system 20). Certain reactions produce hollow automorphs, forming circular zones (6, 45, and 47) or “bags” (43, 48).



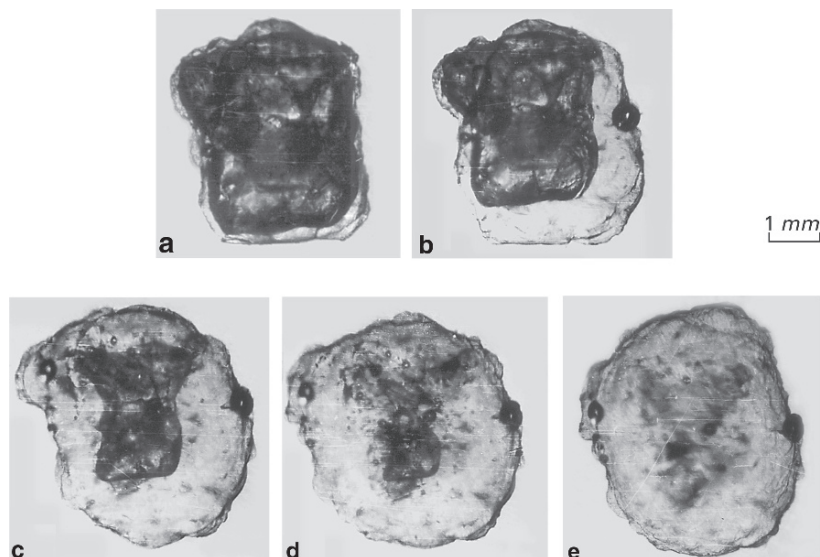
**Fig. 1.9** Hollow (box-like, case-like) blurred pseudomorph of  $K_2Cu(SO_4)_2 \cdot 6H_2O$  after  $CuSO_4 \cdot 5H_2O$  crystals (reaction 1a/22)



**Fig. 1.10** Circular localized automorph formed during replacement of  $K_2CrO_4$  crystal in solution of potassium alum (reaction 1a/6).

Thus, a circular loose fine-grained new formation (the central hole is of  $3 \times 5$  mm) (Fig. 1.10) was formed in reaction 6 around a protocystal with the size of  $2 \times 3$  mm. Circular zones formed in reactions 44, 45, and 47 were complicated with thin tubular radial aggregates of  $BaSO_4$  (see section 1.5.4, Fig. 1.18) produced due to interaction between surrounding solution and a matter coming out of bursting inclusions of the protocystal (Glikin and Sinai 1988).

The best-defined “bags” were obtained in reaction 43 (Fig. 1.11). They were formed by a very thin transparent film of copper chromates enveloping the protocystal at the initial stage of the reaction (Fig. 1.11a). Within 10–15 min a constantly growing gap between the film and the crystal filled up with  $K_2CrO_4$  solution became visible under microscope (Figs. 1.11b–d), as solutions outside and inside the bag were easily distinguished by their blue and yellow colors, respectively. The bag was continuously expanding due to constantly appearing small ruptures, which instantly healed, that could be



**Fig. 1.11** Stages of formation of a copper chromate bag-shaped automorph after  $K_2CrO_4$  crystal (reaction III/43)

noticed as small jerks of the bag. This process, accompanied by protocystal dissolution, enlarged the gap between the bag and the protocystal. The bag could remain intact for an undefined period of time even after complete dissolving of the protocystal (Fig. 1.11e); after its mechanical, or sometimes spontaneous, rupture, the solutions intermixed causing spontaneous and instant mass precipitation of copper chromate microcrystals to form a localized automorph, which did not contain any cavity.

*Dissipated automorphs* were obtained in reactions Ia/13, 23. They formed an array of fine (up to 1 mm) separated crystals uniformly dispersed on the bottom of a crystallizer. Using reaction 23 as an example, it should be noted that the nature of the replacement products remained unchanged even when the initial crystal was encapsulated into a low-penetrable glue capsule, or clay or sand mass; this could not help to confine the new formation within the borders of a protocystal and, thus, to produce a pseudomorph.

**Amorphous products** were formed in reactions of Type II. We observed formation of both pseudomorphs (faceted and blurred pseudomorphs) and automorphs (localized and dissipated automorphs; see Fig. 1.12).

*Faceted pseudomorphs* were found in reactions III/37, 41. They were cavities preserving the shape of protocystals and taking their place, surrounded by a fine crystalline mass of initially dissolved substance precipitating when the system was cooled.

*Blurred pseudomorphs* or *localized automorphs* were obtained in reactions III/38–40. They were cavities with fuzzy outlines. Extent of fuzziness depends upon the rate of cooling.



**Fig. 1.12** Amorphous (negative) localized automorph after  $\text{NaNO}_3$  formed in a mass of newly produced  $\text{K}_2\text{Cr}_2\text{O}_7$  (reaction *II/39*). Glue film fixes the initial size of protocrystal

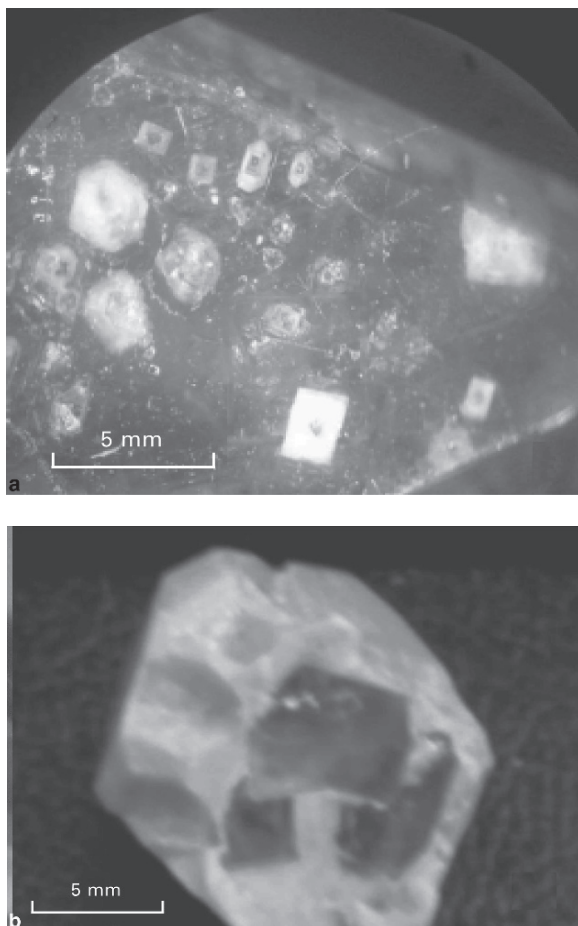
*Dissipated automorphs* were formed in reaction *III/36*. Loose fine-crystalline products of the reaction did not contain any cavities in places formerly occupied by the protocrystals, while additional free volume caused by salting-in effect was evenly distributed in the interspaces between the precipitated crystals.

To complete the description we should note that reactions of Types *I* and *III* can be relatively fast or slow. Most of the described reactions were fast; total replacement of crystals having thickness of 0.3–0.5 cm took from 1–2 h to 5–7 days. The minimal observed time for total replacement of such crystals in slow reactions was 2–3 months (reactions *Ia/10*, *III/46*). In some cases replacement practically stopped after progressing to the depth of several millimeters in peripheral sectors and areas located near the cracks. This was the case for reactions *Ib/24*, *26*, *28*, *30* and *34*; known reactions producing passivating films on metals should be also mentioned (e.g.,  $\text{Al}_2\text{O}_3$  on Al).

### 1.3 Metasomatic Transformations in Polymorphic Pair Retgersite–Nickelhexahydrite ( $\alpha$ – $\beta$ - $\text{NiSO}_4 \cdot 6\text{H}_2\text{O}$ )

Mutual equilibrium of tetragonal crystals of retgersite, monoclinic crystals of nickelhexahydrite, and aqueous solution of  $\text{NiSO}_4$  exists in the eutonic point at  $\approx 53^\circ\text{C}$  (with addition of sulfuric acid so that the solution pH is about 1), and the crystals undergo reciprocal replacements in the neighborhood of the eutonic point. Replacement does not occur in the absence of solution medium, thus indicating occurrence of a metasomatic process instead of polymorphic solid-phase transition.

Nickelhexahydrite replacement with retgersite (Kulkov and Glikin 2007) takes place in solution, which has been saturated at a temperature below the eutonic point;



**Fig. 1.13** Metasomatic replacement of nickelhexahydrite  $\beta\text{-NiSO}_4\cdot 7\text{H}_2\text{O}$  with retgersite  $\alpha\text{-NiSO}_4\cdot 7\text{H}_2\text{O}$  **a** – retgersite crystals (light) growing within a periphery zone of transparent nickelhexahydrite crystal (dark); **b** – pseudomorph of retgersite formed as monocrystals (dark) and fine-grain mass (light) after nickelhexahydrite crystal

replacement occurs either in solution bulk or within a solution film, if it is present on the surface of the crystals. The initial stage of the process, which usually takes from about 10 to 15 min, consists in nucleation of faceted monocrystals or aggregations of retgersite on the surface of a crystal undergoing replacement. As replacement progresses, it can result in the formation of the following three texture types of faceted pseudomorphs.

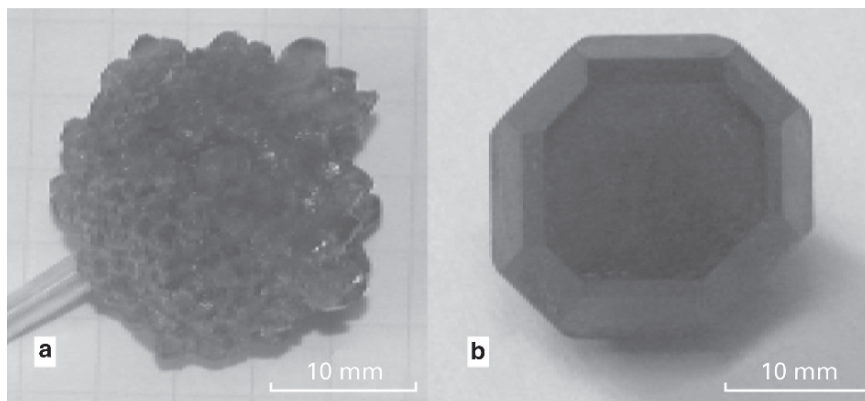
1. If deviation of the solution composition from the eutonic point is not significant, the retgersite crystals formed grow into the initial crystal (Fig. 1.13a), thus completely consuming it. Nucleation of a single replacing individual results in formation of a monocrystalline paramorph oriented at a random direction in respect to that of the protocystal. Image in crossed nicols shows strong tension patterns arising at the

phase interface, which result in formation of cracks that subsequently disappear, being consumed by a growing retgersite crystal. This pattern is typical for a transparent initial crystal of nickelhexahydrite, having no apparent defects. Complete replacement of a crystal the size of about 1.5–2 cm takes approximately 5 days.

2. If deviation of the solution composition from the eutonic point is considerable, the mass crystallization of retgersite takes place, occupying the whole volume of the crystal undergoing replacement. As a result, an opaque fine-grained mass of fibrovesicular or radiate-veined retgersite aggregations is formed. This pattern is typical for replacement of a nickelhexahydrite crystal containing a great number of macrodefects (cracks, growth regions, cleaved blocks, etc.). Complete replacement of a crystal the size of about 1.5–2 cm takes approximately 1 day.
3. Replacement progressing in a solution having an intermediate composition results in formation of a combined texture made up of large retgersite crystals in a fine-grained formation of the same phase (Fig. 1.13*b*). First, large faceted crystals of retgersite start growing in a manner similar to that described in point 1. Then their growth abruptly slows down, and the relic part of nickelhexahydrite is gradually replaced by a fine-grained aggregation in a way similar to the process described in point 2. If the size of the initial crystal is about 1.5–2 cm, it takes approximately 1–1.5 days to complete the growth of the large crystals and about 2–5 days to form the fine aggregations.

Replacement of retgersite with nickelhexahydrite (A. M. Kulkov, unpublished data of 2007) takes place in solutions, which have been saturated at temperatures exceeding the eutonic point. The reaction proceeds regardless of deviation of the solution composition from that of the eutonic one, and results in formation of blurred pseudomorphs or localized automorphs, which are aggregation of relatively big joint nickelhexahydrite crystals (Fig. 1.14).

It is to be noted that the above reactions proceed via metasomatic replacement involving dissolution of the initial crystal and depositing the formerly dissolved



**Fig. 1.14** Blurred pseudomorph–localized automorph of nickelhexahydrite  $\beta\text{-NiSO}_4\cdot 6\text{H}_2\text{O}$  (a) after retgersite  $\alpha\text{-NiSO}_4\cdot 6\text{H}_2\text{O}$  (b)

matter. The reactants are a pair of polymorphic modifications, but the reaction itself is not a solid-phase transformation despite the fact that the phase ratio between the educts and the products is similar to that observed for polymorphic transformations. Also, it should be pointed out that replacement processes in the system under discussion are unsymmetrical in respect to the eutonic point, i.e., substitution of nickelhexahydrate results in formation of faceted pseudomorphs, while replacement of retgersite leads to morphologically diffused formations.

## 1.4 Structural-Morphological Classification of Replacement Products

The above morphological correlations between protocrytals and their replacement products are shown in Fig. 1.15. It can be seen that new formations may have monocrystalline, polycrystalline, and amorphous structure.

In other words, our systematic description of the results includes a basic two-coordinate classification of replacement products (Table 1.2) according to the extent to which a new formation loses the shape and details of the corresponding protocrytals structure.

Preservation of *shape details* of the protocrytals deteriorates in downward direction of Table 1.2, from embossed pseudomorphs to dissipated and translocated automorphs. Dissipated automorphs can be considered to contain a little more information about the protocrytals compared to translocated automorphs: the former have real finite dimensions limiting to some extent the potential location of the protocrytals, while the latter, on the contrary, can provide false information about the protocrytals location.

In general, preservation of *structural details* of the protocrytals regresses when moving from left to right in Table 1.2, from monocrystalline products to amorphous ones.

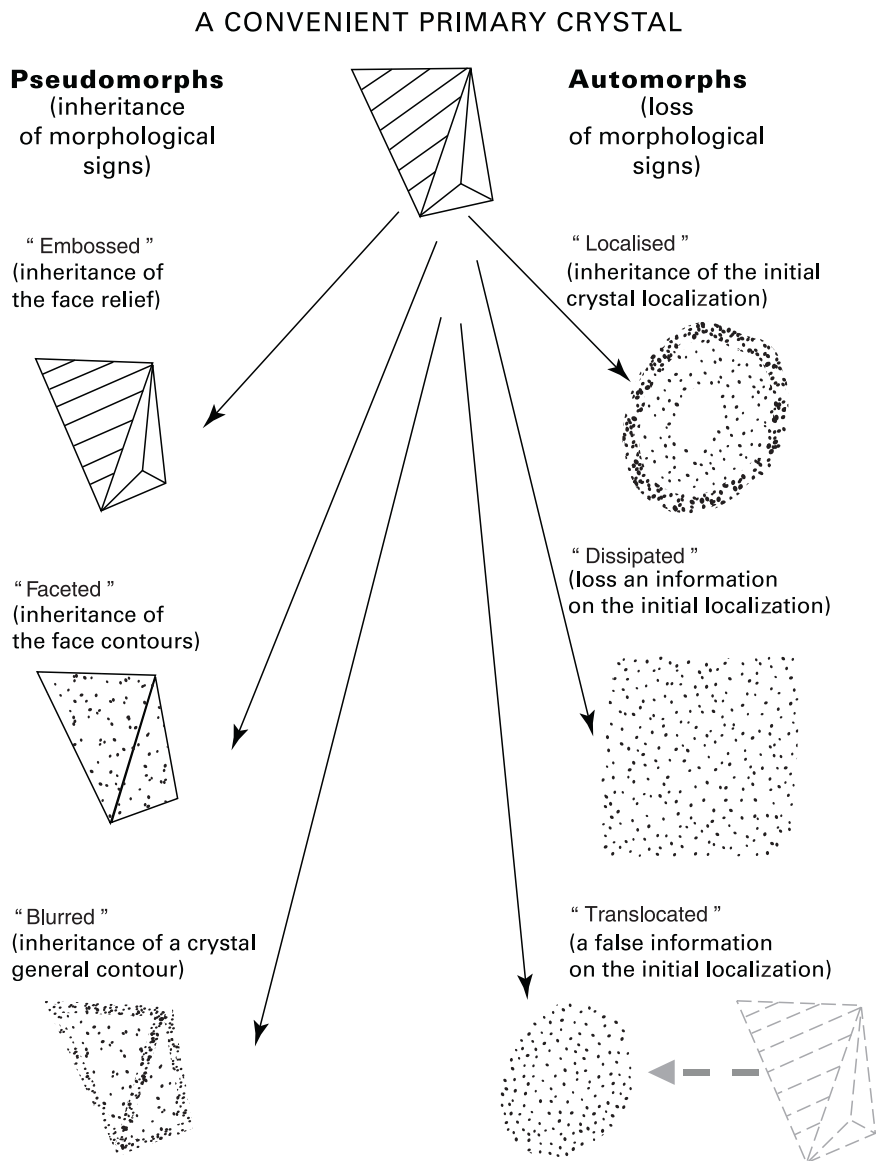
*Monocrystalline products* are isomorphic to their protocrytals, i.e., they directly and to the maximum extent inherit and preserve integrity of the initial atomic structure, its pattern, and orientation (Glikin and Sinai 1983, 1991).

*Polycrystalline products* may indirectly reflect certain peculiarities of the protocrytals atomic structure. If they are isostructural to the primary crystal, the inherited information is mediated by epitaxial metasomatic textures (Glikin and Kaulina 1988). If the protocrytals has nonuniform distribution of impurities, some part of this information may be preserved in the product in a similar way of distribution of initial inclusions (Chesnokov 1974, p. 67; Sinai and Glikin 1989). Non-isomorphic monocrystal products (Kulkov and Glikin 2007; see Sects. 1.3 and 4.2 of the present monograph) are of spontaneous origin and should be included in this category.

*Amorphous products* are cavities filled up with a solution (Sinai and Glikin 1989). They do not practically preserve any peculiarities of the protocrytals structure apart from insoluble solid inclusions, which should be accumulated in the bottom parts of the cavities formed at the sites of the protocrytals.

It is interesting to point out a nonuniform distribution of new formations according to taxons of the classification (Table 1.2), considering that the systems had been





**Fig. 1.15** Schematic representation of morphology correlation between a symbolic protocrystal and possible products of its replacement

selected stochastically. It can be seen that polycrystalline formations (the most representative part of the selection) are most likely to form localized automorphs and blurred pseudomorphs. Faceted pseudomorphs make up a majority of monocrystalline products, while most of the amorphous products are blurred pseudomorphs and localized automorphs.

**Table 1.2** Classification of crystal replacement products with references to the products and reactions listed in Table 1.1

Shape	Structure		
	Positive products		Negative products (amorphous)
	Monocrystalline	Polycrystalline	
<u>Pseudomorphs</u>			
Embossed	<b>3</b> ( <i>Ib/31–33</i> )	<b>5</b> ( <i>III/42</i> )	<b>0</b>
Faceted	<b>12</b> ( <i>Ib/24–35</i> )	<b>18</b> ( <i>Ia/5, 8, 10, 15, 16;</i> <i>III/42, 53</i> )	<b>3</b> ( <i>III/37, 41</i> )
Blurred	<b>8</b> ( <i>Ib/25, 27, 29, 31–33,</i> <i>35</i> )	<b>30</b> ( <i>Ia/2–5, 7, 9, 11, 12, 19,</i> <i>22; III/42, 46, 50, 52</i> )	<b>8</b> ( <i>III/38–40</i> )
<u>Automorphs</u>			
Localized	<b>2</b> ( <i>Ib/35</i> )	<b>37</b> ( <i>Ia/1, 4, 6, 13, 17, 18, 20,</i> <i>21, 22; Ib/35; III/43–45,</i> <i>47–49, 51</i> )	<b>8</b> ( <i>III/39, 40</i> )
Dissipated	<b>0</b>	<b>3</b> ( <i>Ia/13, 23</i> )	<b>1</b> ( <i>III/36</i> )
Translocated	<b>1</b> ( <i>Ib/31</i> )	<b>0</b>	<b>0</b>

**Note:** The numbers of systems where the corresponding products were observed are printed in bold; examples of the systems are given in brackets.

Some of the products were not studied at all, apparently due to impossibility to cover the whole vast variety of possibly existing systems and experimental conditions. Existence of some formations is highly improbable; nevertheless, its complete disregard could be erroneous: even such presumably impossible formation as a monocrystalline dissipated automorph can take a shape of lace skeleton, considerably (up to infinitely) exceeding the size of protocystal.

Of course, taxons selected above do not cover the entirety of the real replacement products, and numerous structural and shape peculiarities of the natural and experimental product (loose structures, case-like shapes, polymineralogical and textural properties, etc.) can considerably widen the classification characteristics. The proposed classification provides a basis, which can be specified and developed further. For the purposes of the present monograph it is more important that it comprises essential structural and morphological properties of replacement products closely related to their genetic basis that will be discussed below.

## 1.5 Genetic Nature of Replacement Products

### 1.5.1 Types of Physicochemical Systems and Structure of Replacement Products

Structure of replacement products obtained from monocrystals (Table 1.2) complies with the following principal physicochemical types of metasomatic reactions (Table 1.1):

- (a) Monocrystalline products formed in systems containing isomorphic components (reactions of Type *Ib*)
- (b) Polycrystalline products formed in systems comprising non-isomorphic components with mutual salting-out effect (reduced solubility of one component under the action of another component introduced into the system; reactions of Types *Ia* and *III*)
- (c) Amorphous products formed in systems containing non-isomorphic components with mutual salting-in effect (increased solubility of one component under the action of another component introduced into the system; reactions of Type *II*)

Essential aspects of replacement processes are discussed below with reference to the Schreinemakers concentration diagrams characterizing systems of the above types and schematically shown in Fig. 1.15 (elementary processes for some types of the systems are analyzed in Chapter 4).

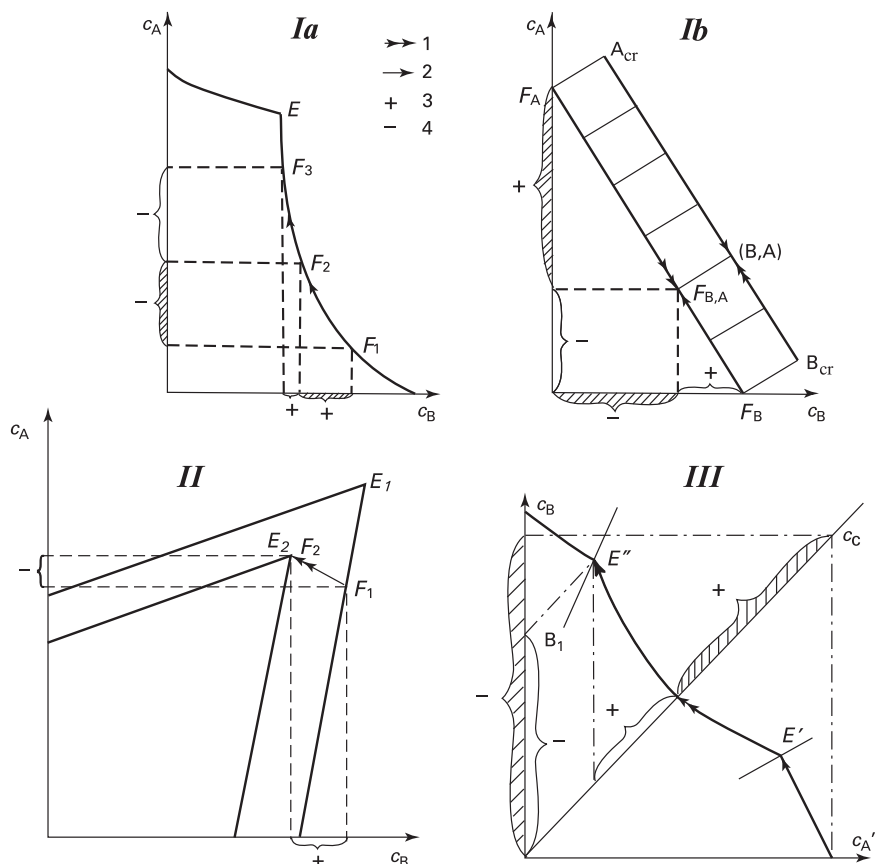
The Schreinemakers diagrams have been used to discuss phase associations in experimental metasomatic columns (Treivus and Rozhnova 1962; Korzhinskii 1970); however, they have not been widely accepted for mineralogical and petrological studies, and the author of the present monograph is not aware of their being used for genetic analysis of structure and morphology of replacement products. At the same time these diagrams are the most informative tools for metasomatic process analysis, since the shapes of isotherms can facilitate unambiguous identification of systems with salting-in and salting-out and determining the reactant quantitative ratios and predicting some other properties of reactions.

It is useful to remember that the Schreinemakers diagrams (Anosov et al. 1976) are composed of liquidus isotherms plotted in the component concentration coordinates, with absolute values of concentrations obtained in a predetermined amount of a solvent. When composing a diagram for a system containing isomorphic components, it is necessary to match curves of the solution compositions with the scale of the solid-phase composition using conodes, as shown in Fig. 1.16*b*, or using some other method (see Sect. 3.3). Systems comprising non-isomorphic components (Figs. 1.16*a*, *II*, and *III*) have constant compositions of the solid phases and, thus, do not require representation of the solid-phase figurative points.

Reactions *Ia*, *Ib*, and *III* occur in the systems with salting-out and, so, result in formation of positive products (Tables 1.1, 1.2).

As a matter of fact, the process known in mineralogy as synchronized metasomatic replacement (Pospelov 1973, 1976; Zhabin and Rusinov 1973) is identical to the process known as “salting-out” in chemistry (Anosov et al. 1976; Kirgintsev 1976). It starts from transferring the protocystal components into a saturated solution of the other product. As a result, the initial dissolved matter occurs in supersaturated state and crystallizes out forming the products of metasomatic replacement (Treivus and Rozhnova 1962; Korzhinskii 1970; Glikin and Sinai 1991; Glikin 1996a) and similar topochemical reactions (Prodan 1990).

In the course of the process, solution composition deviates from the initial figurative point and proceeds along the isotherm toward the dissolving component point (Fig. 1.16). The rate of the composition evolution depends upon a quantitative ratio between the solution and protocystal components. When the solution volume



**Fig. 1.16** Schematic representation of the Schreinemakers diagrams plotted for the principal types of physicochemical systems *I* – types of systems containing non-isomorphic (*Ia*) and isomorphic (*Ib*) components A and B having mutual salting-out effect. *II* – type of systems containing non-isomorphic components having mutual salting-in effect. *III* – systems with an exchange reaction resulting in formation of an intermediate compound C. **Bold lines** – solubility isotherms  $c_A$  and  $c_B$  of components A and B; (B, A) – compositions of isomorphic-mixed crystals In Fig. *Ib*:  $A_{cr}$ – $B_{cr}$  line – solidus line, perpendicular lines ( $F_A$ – $A_{cr}$  etc.) – conodes In Figs. *Ia* and *II*:  $E$  – eutonic points (in Fig. *II*  $E_1$  isotherm corresponds to a higher temperature than  $E_2$  isotherm) 1 and 2 – directions of changes in solution compositions from figurative points  $F_i$  (for systems *Ib* these are also directions of changes in protocrystral compositions) in metasomatic replacements proceeding with volume excess (1) or deficit (2); 3 – amounts of new formations, and 4 – amounts of dissolved phases (designated with filled and empty curly brackets)

decreases, the composition varies within certain limits: for systems of Types *Ia* and *III* the limit is a eutonic point, while for systems of Type *Ib* this is a saturated solution of the protocrystral matter. Composition of the newly formed crystals in systems *Ia* and *III* does not vary with time, while in system *Ib* it moves toward the composition of the dissolved matter.

Replacement in systems *Ia* and *Ib* proceeds at constant temperature or at temperature varying within a certain permissible range (see Sect. 4.4). Some reactions of Type *III* (like  $\text{Ba}^{2+} + \text{SO}_4^{2-} \rightarrow \text{BaSO}_4$ ) stay apart as resulting in formation of a practically insoluble substance and, therefore, they can occur in solutions having any concentration and at temperatures varying from boiling to freezing points of the solution.

Reactions of Type *II* occur in salting-in systems and result in formation of negative products. This process differs from the above reactions in being initiated only by changes in solution temperature (usually lowering the temperature) and resulting in mass crystallization of the substance within. The protocystal dissolving simultaneously with precipitation of the dissolved substance causes decrease of its concentration in the layer surrounding the protocystal due to salting-in effect and, thus, hampers precipitation of the dissolved substance or terminates it completely. This results in formation of “amorphous” products, i.e., cavities containing solutions, or aggregations with increased porosity (Sinai and Glikin 1989; Glikin and Sinai 1991).

Essential distinctions in processes within systems of certain type define structural peculiarities of the replacement products, summarized in Table 1.2. The above discussion clearly shows that positive new formations are obtained in system of Types *Ia*, *Ib*, and *III*, while the negative ones are formed in systems of Type *II*.

*Monocrystalline products* inheriting protocystal structure and orientation are formed only in systems *Ib* owing to isomorphism existing between the substances. In such systems precipitation of a new formation proceeds via its autoepitaxial growth on the surface of a protocystal (Glikin and Sinai 1983, 1991; Glikin 1996a). Such systems differ from the others in requiring no nucleation for individuals of the new formation (in systems in question this is the substance with modified isomorphic composition).

*Polycrystalline products* are obtained in systems of Types *Ia* and *III*. They can be formed via nucleation of new individuals, which is necessary to take place due to the lack of isomorphism between the reactants. Experiments demonstrated (reaction *Ib/35*, Fig. 1.6*d*) some of the systems containing isomorphic components that form polycrystalline products; in this case high reaction rates can cause some regions with high local supersaturations to occur that result in mass nucleation in proximity of a protocystal.

In systems containing non-isomorphic components formation of monocrystalline products is considered highly improbable. Replacements in some systems having characteristic peculiarities discussed in Sect. 1.3 can cause formation of disoriented monocrystal pseudomorphs in narrow condition ranges, when low supersaturation assures formation of only one nucleus (Kulkov and Glikin 2007). Also, there is a possibility of nucleation of a single secondary monocrystal, which is likely to form a translocated automorph. Theoretically, good epitaxy conditions are expected to facilitate formation of sub-monocrystalline pseudomorphs via coalescence of the oriented nuclei (Grigor'ev 1961); however, actual possibility for such a phenomenon to take place is negligible due to kinetic effects of disorientation (Glikin and Kaulina 1988) and incoherence of mosaic borders.

Systems of Type *II* have specific properties showing in formation of *negative*, “*amorphous*” products. In this case, precipitation of substance from the solution inevitably proceeds via a nucleation stage; however, the negative products have neither nucleation nor growth stages.

So, physicochemical analysis of metasomatic replacement processes allows to define all the main structural types of replacement products and basis for their genesis.

It is clear that systems with more complex compositions would present more complicated process schemes, including formation of polymineral products (see Sect. 4.3). Such processes would have needed the reaction analysis in the multicomponent systems using three-dimensional phase diagrams and other methods to display equilibria. However, the above generalized classification is fundamental for all possible systems.

### 1.5.2 Volume Effect of the Reactions

Volume effects in the crystal replacement reactions described herein are discussed on the basis of physicochemical concepts of salting-out (Gerasimov et al. 1970; Anosov et al. 1976). This concept allows removing the existing contradictions between the formula and volume representations of metasomatic reactions and also revealing some important conclusions demonstrating the key significance of volume effect for genetic issues of metasomatism.

Review of the diagram represented in Fig. 1.16 obviously demonstrates that the quantitative ratio between educts and products (sectors “-” and “+”, respectively) is unambiguously reflected in positions of figurative points corresponding to a start and completion of the reaction. This ratio is clearly represented by the decline in solubility isotherms. If solution composition varies in the course of isothermal reactions *Ia* and *Ib* with the corresponding dot moving from the abscissa to the ordinate, and the angle formed between the abscissa and the line exceeds  $45^\circ$ , the replacement is a volume-deficit reaction, but when this angle is less than  $45^\circ$ , the replacement is a volume-excess reaction. In other words, the more soluble product is substituted by the less soluble educt with deficit of volume, and, on the contrary, the less soluble product is substituted by the more soluble educt with excess of volume.

If coordinates are expressed in volumetric concentrations (for instance in  $\text{cm}^3/100\text{ml}$  of solvent), the ratio between dissolved (“-”) and precipitated (“+”) volumes can be easily derived from the lengths of the sections located between the projections of the figurative points on the axes. For systems *Ia* and *II* direct measurement of the sections is sufficient, while computation taking into account a variable composition of the new formation is required for system *Ib*. The volume effect for systems of Type *III* is calculated using the same approach as for *Ia*, and if the product solubility is negligible, it is estimated from the balance of chemical-exchange reaction. More detailed schemes of calculations are presented in Sect. 4.6.

The most important output of this approach is a qualitative division of all metasomatic reactions into two types: proceeding with an excess or deficit of volume of the new formation in comparison with that of the protocystal.<sup>5</sup> Reactions of these types differ in mechanisms. The volume effect is of principal importance for

---

<sup>5</sup>The equal-volume replacement represents a special case, which is unlikely to occur in reality.

morphology of the products and rate of their formation, especially in the course of pseudomorph replacements.

At the initial stage of volume-excess replacements, a new formation tightly envelops the protocystal, and thereafter reactions *Ia/10*, *Ib/24*, *26*, *28*, *30* (Fig. 1.3), and *34*, *III/46* proceed very slowly or terminate. As a result, the process appears uncompleted and the system remains in nonequilibrium but in a stable state for an indefinite period of time; the size of the blocked relic can vary up to the initial size of protocystal enveloped with very fine (tenths and hundredths of a millimeter) tight rim of the reaction products. Volume-excess automorph replacement produces products formed some way apart from the protocystal, leaving it free for the access of the solution. However, even in this case the replacement may slow down, like in system *III/43*, where a very thin dense bag of copper chromates is formed (Fig. 1.11), the process accelerating abruptly after the bag breaks. On the contrary, the new formation obtained via replacements with volume deficit always has considerable friability, and solution, penetrating through the pores, rapidly and freely reacts with the protocystal causing its complete replacement as, for example, in systems *Ia/22* (Fig. 1.9) and *Ib/25*, *27* (Figs. 1.5 and 1.6).

The sharpest difference in the replacement mechanisms with volume excess and deficit was observed in monocrystalline isomorphic replacements in system of Type *Ib* (Glikin and Sinai 1983; Glikin et al. 1994a, 2003; Glikin 1996a, 2007) accompanied by totally new effects, which appeared to be beyond traditional concepts of crystallization. Detailed analysis is given in the following sections, but the essence of the process is briefly stated below.

Monocrystalline pseudomorphs are divided into two modifications corresponding to reactions proceeding with excess and deficit of volume.

Pseudomorphs of the first type were observed to be formed in the reactions *Ib/24*, *26*, *28*, *30*, *32*, *33*, and *34* (Fig. 1.3). In this case, a continuous envelope of the new formation forms a permanent autoepitaxial prolongation of the relic, therefore shielding the relic completely. Reactions of this type are very slow; for example, it took about 2–3 months to replace the entire volume of a crystal with the size up to 0.3–0.5 mm, while the large crystals were observed to be surrounded only by a thin autoepitaxial rim.

The second modification was found in corresponding reversed reactions *Ib/25*, *27*, *29*, *31*, *32*, *33*, and *35*. The new formations also grew autoepitaxially on the initial crystal, but they did not cover its whole surface. The volume deficit was compensated by inclusions formed in the protocystal that allowed easy detection of the effect (Fig. 1.6). The reactions were very fast and the total volume of 4–5 mm crystal was replaced within 2–7 days.

It should be noted that nonlinear isotherms occur more frequently, and due to this fact the volume effect of the reaction, as a rule, varies with time. This variation is a reason for the cavities to occur in pseudomorphs obtained in reactions *Ia/11*, *14*, *22* (Fig. 1.9) and some other effects discussed in Chapters 3–5. Thus, Fig. 1.16 (diagram *Ia*) shows that dissolving the peripheral zones of the protocystal makes the reaction proceed at the relatively flat bottom sector of isotherm  $F_1-F_2$  and, therefore, the volume of the new formation is relatively

large (the periphery part of the pseudomorph structure is formed). Steep top section of isotherm  $F_2-F_3$  means that dissolving the remaining mass of the protocrystal is accompanied by insignificant growth of crystals composing the already-formed case-like structure (Sinai and Glikin 1989).

Concluding the present section, it should be noted that visual assessment of volume effects is not always possible for polycrystalline replacements. However, in certain cases the effect can be detected, at least approximately, in thin sections, but this opportunity has hardly ever been realized (e.g., Brodin and Dymkova 1966).<sup>6</sup>

### 1.5.3 Kinetic Factors and Shape of Replacement Products

As indicated above, kinetic processes of metasomatic crystallogensis include the following stages corresponding to the three-zone model: dissolving the protocrystal, new crystalline phase nucleation (excepting reactions of isomorphic monocrystalline replacement), growth of the new crystalline phase, and diffusion (and/or convective) mass transfer. Comparison of replacement products obtained in different systems shows combination of the above-mentioned stages to define the product shapes in the “pseudomorphs–automorphs” series.

Below is a review of inverted pairs composed of “direct” and “inverse” reactions, i.e., reactions occurring in the same physicochemical system, but with inverted state of salts, which can be either solid or dissolved reactants. Pairs of reactions 1 and 2, 3 and 4, 5 and 6 (Type *Ia*), as well as 42 and 43, 44 and 45 (Type *III*), are taken for comparison.

1. Extent of differences observed in replacement products obtained in various inverted reaction pairs is not the same. The sharpest shape difference was observed for the pair 42–43 in the absence of additives (embossed pseudomorphs and bag-shaped automorphs, respectively – Figs. 1.7 and 1.11), and to a lesser extent – in reaction pair 5–6 (faceted pseudomorphs and circular automorphs – Figs. 1.8a and 1.10); the difference was gradually lessening for each successive case, culminating in imperceptible difference in pair 44–45 (localized automorphs). The conclusion which can be drawn from such regularity is: the greater the extent of preserving the shape patterns in a course of a direct reaction, the lesser it is in a reversed reaction. This effect is considered to be related to the rate of delivering the reactants to the reaction zone and can be easily explained by assuming reactions of Types *Ia* and *III* to be crystallizations proceeding under conditions of counterdiffusion of the reactants. In this case, as it was suggested (Petrov et al. 1983), delivering the reactants to the reaction zone

---

<sup>6</sup>Estimation of porosity is possible using measurement of a gas volume trapped in cavities of random configuration (Kasatkin and Glikin 1974, Glikin and Kasatkin 1976); but the method has not been properly developed.



is determined by diffusion rates and solubilities of the substances involved and, thus, localization of the reaction products can be represented as follows.

The rates of protocrystal dissolution ( $v_p$ ) and the growth of the new formation ( $v_n$ ) affect the distribution of the component concentrations around the protocrystal. In one extreme case, when the reaction is taking place directly on the surface of the slowly dissolving protocrystal and resulting in formation of a pseudomorph, the necessary and sufficient condition of the process to occur is providing the following ratios between the protocrystal dissolution rate ( $v_p$ ), the diffusion coefficient of the dissolved component ( $D$ ), and the growth rate of the new formation ( $v_n$ ):  $v_p < kD < v_n$  ( $k$  is a proportionality constant), or  $v_p \ll v_n$ . In the other extreme case, when the reaction is taking place at a considerable distance from the protocrystal and resulting in formation of an automorph, the ratio is to be inverted:  $v_n < kD < v_p$ , or  $v_n \ll v_p$ .

The new formations abut on the protocrystal when the substance making up the protocrystal has a considerably lower diffusion ratio or solubility in the system in comparison with those of the dissolved compound (when they have close values of solubility or diffusion ratio, respectively). This is a case of pseudomorph formation. If the ratios are inverted, the new formation occurs far away from the protocrystal; in this case automorphs are formed. It is obvious that a whole range of intermediate formations can exist.

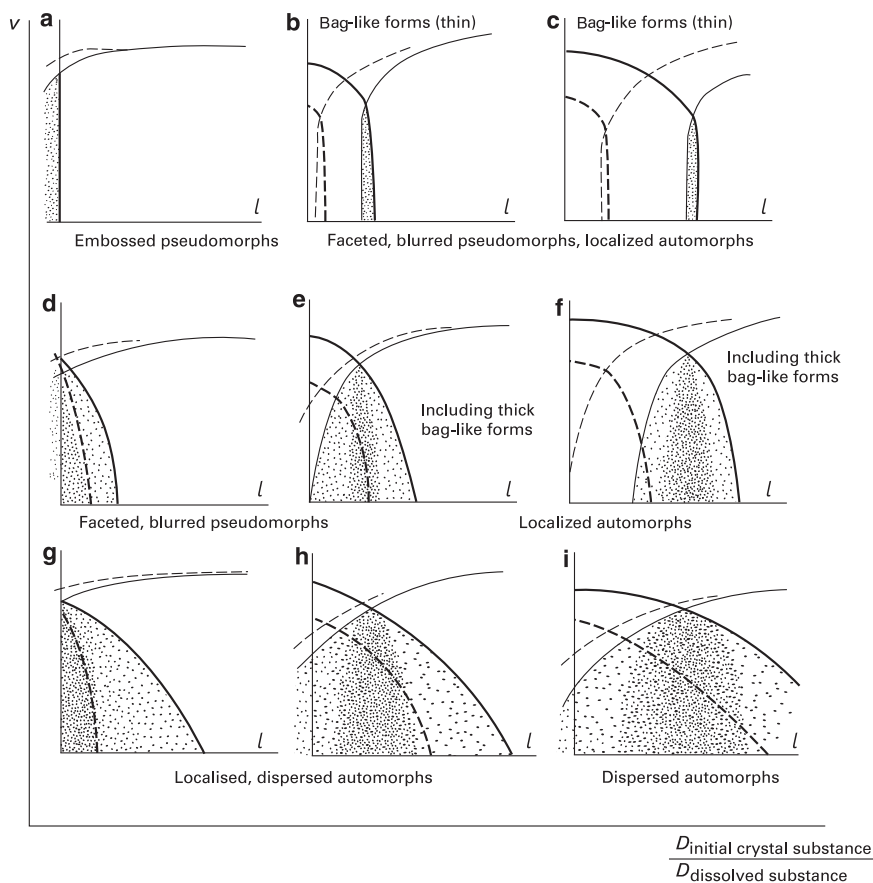
Quantitative analysis of different factors and identification of a limiting stage of the general process are rather complicated, first, due to a small size of the protocrystal surface in comparison with surface area of the new polycrystalline formations, whose number and sizes cannot be predicted beforehand, and, second, due to shielding effect exerted by the new formation upon the diffusion flows, which cannot be determined, and it is this process that defines the replacement kinetics, especially in volume-excess interactions.

2. Comparison of results obtained for the same reactions, but with different pair combinations (42–43 and 5–6), shows that transition from embossed to faceted pseudomorphs observed in direct reactions 42 and 5 (Figs. 1.7 and 1.8a) agrees with transition from thin bag-shaped automorphs to thicker circular ones obtained in inverted reactions 43 and 6 (Figs. 1.11 and 1.10).

It is understandable that the extent of such transition corresponds to linear dimensions of the reaction zone, which depend upon the rates of nucleation and growth of the new formation. When the rates are high and diffusion-limited, the reaction zone is narrow, and collision of diffusion fronts causes an immediate precipitation. At the same time, rapidly growing nuclei completely envelop the substance delivered into the reaction zone and prevent further nucleation and expansion of the zone. When the rates of the nucleation and growth of a new formation are low and limit the process, the reaction zone is wide, and in some cases initiates formation of a dissipated automorph; nucleation starts long after merging the diffusion fronts and their penetration into “foreign” diffusion areas, and so, slowly proceeding precipitation promotes formation of a wide nucleation area.

It is the width of the reaction zone which limits the minimum height of the protocrystral face relief preserved in a pseudomorph. Therefore, high growth and nucleation rates and ratio  $v_p < kD < v_n$  facilitate formation of embossed pseudomorphs (according to Grigor'ev 1961, "precipitation in situ"). Low growth and nucleation rates and ratio  $v_n < kD < v_p$  facilitate formation of the faceted and blurred pseudomorphs and automorphs (according to Grigor'ev 1961, "precipitation with transportation").

Generally, higher relative rates of diffusion of protocrystral matter and increased rate of its dissolution make the external borders of the new formation expand, while increased rates of nucleation and growth of the new formation cause its precipitation zone to reduce (Fig. 1.17).



**Fig. 1.17** Relationship between the shape of replacement products and kinetic factors  $v$  – rate of the new formation precipitation;  $D_{\text{protocrystral}}$  – rate of diffusion of protocrystral matter;  $D_{\text{solute}}$  – rate of the solute diffusion;  $l$  – distance from the protocrystral;  $c$  – concentration of dissolved substances. **Bold lines** – concentration of protocrystral matter; **thin lines** – solute concentration; **dash lines** – the same characteristics at lower rate of protocrystral dissolution; dots show nucleation intensity

This scheme can lead to an assumption that automorphs should have had a wider range of formation conditions and, consequently, a more frequent occurrence in comparison with pseudomorphs, but this conclusion is not confirmed by the data shown in Table 1.2. The most frequently occurring are shown to be blurred pseudomorphs and localized automorphs that is likely to be explained by relatively close rates of the reactant counterdiffusion and similar rates of precipitation of new formations.

Kinetic analysis in systems *Ib* and *II* requires a different approach.

Monocrystalline pseudomorphs (systems *Ib*) also have different morphology, practically, in all the investigated pairs of direct and reversed reactions of Type *Ib*: reactions 24, 26, 28, 30, 34 form only embossed and faceted pseudomorphs, while reactions 25, 27, 29, 31, 35 produce spongy faceted and blurred pseudomorphs; products in reaction pair 32–33 are indistinguishable by the shape from each other, as are the products of pair *Ia*/44–45. In general, these phenomena can be formally explained by similar distribution and interaction of the diffusion fields as described above. However, such explanations are not illustrative, and in Type *Ib* systems other effects must be given a priority, with volume effect defining differences in the mechanisms of direct and inverse reactions being the major one (see Sect. 3.2).

When the negative products are formed in systems of Type *II*, diffusing the borders of the cavities is defined by the rate of lowering the temperature and by the positions of figurative dots versus the eutonic point. In general, it can be stated that diffusing the contours depends to somewhat extent upon the followings: protocrysal dissolution rate, diffusion of its matter into the solution, crystal precipitation from the solution, temperature gradient of solubility of precipitating substance, and salting-in effect of the protocrysal matter. The highest degree of preserving the protocrysal shape is achievable only either by means of extremely slow dissolution of the protocrysal and fast crystallization of the surrounding precipitating matter, regardless the salting-in effect, or by means of fast dissolving the protocrysal and a very slow diffusion of its matter under the action of a strong salting-in effect.

The easiest way to obtain the negative pseudomorphs with maximum preservation of the shape is abrupt and deep supercooling with slow dissolution of the protocrysal tightly enveloped by the precipitate; in this case the salting-in effect of the protocrysal matter should be weak, limiting the growth of the precipitating crystals, which border the cavity. The process is similar to a conventional crystal encrustation followed by its dissolution, i.e., the formation of asynchronous negative pseudomorphs.

Translocated automorphs can be formed in all types of the systems following two varying pathways having different kinetic nature (for corresponding negative products under conditions of undersaturation cavities are formed instead of growing solid phase). The first pathway is as follows: a portion of the solution that surrounds the protocrysal and is supersaturated with the newly forming phase is transferred (translocated) by convective streams from the protocrysal to a deposition area. Following the second pathway, a temporary elevation of temperature reduces supersaturation in the portion of the solution that surrounds the protocrysal and prevents precipitation of a new formation, which, after cooling, crystallizes independently, far from the former location of dissolved protocrysal. Our methods

make realization of this pathway possible, and, accidentally, a monocrystalline translocated automorph was produced in replacement experiment conducted in isomorphous  $(\text{Co,Ni})\text{SO}_4 \cdot 7\text{H}_2\text{O}$  series.

Thus, the list of taxons, which specifies the forms of replacement products (Table 1.2) is considered to be comprehensive in accordance with the above analysis of the replacement kinetic effects.

In addition to the relationships between the process kinetics and structural-morphological characteristics of the products discussed above, the following should be noted.

First, the process kinetics defines a rhythmical zonal distribution of the secondary mineral phases forming polycrystalline polymineral pseudomorphs (reaction *III/53*).

Apparently, such zoning is formed in a self-oscillating diffusion mode defining crystallization process, which is similar to formation of Liesegang rings (Liesegang 1913; Stern 1954; Carl and Amstutz 1958; Krasnova and Petrov 1997), or cyclic capture of inclusions by a crystal (Treivus 1979; Petrov et al. 1983, and others). It is interesting to note that in the above case *III/53* the diffusion front was expanding from a protocystal periphery to its center.

Second, microimpurities, which can be present in the solution (including acidic-alkaline admixtures: reaction *Ia/5*, *III/42*), and the process temperature (*Ia/5*) have different effects upon morphology of the new formations due to their unequal influence upon the diffusion ratios of different reactants and also due to variation of the adsorptive effects, which, by modification of the growth and dissolution kinetics (Treivus 1979; Petrov et al. 1983, and others), may totally alter distribution of diffusion fields and, consequently, location and width of the reaction zone.

Third, metasomatic crystallogenesis differs from conventional crystallization occurring at lowering temperature, pressure drop, etc., as it always proceeds under profoundly nonstationary conditions determined by variations in solution composition (Dolivo-Dobrovolskii 1967, and others). It was already mentioned (Glikin and Sinai 1991; Glikin 1996a) that this is the reason of formation of case-like pseudomorphs and occurrence of protocystal relics in replacement products. Nevertheless, this fact has not been properly investigated yet, and so discussion of some effects demonstrating its significance is presented in Chapter 4.

#### ***1.5.4 Imperfection of Protocrystals as a Factor of Replacement Process***

Influence of defects present in protocystals upon replacement process has already been mentioned in the previous sections, but it deserves a thorough and careful study. Growth and dissolution of crystals is generally known to depend to a considerable extent upon the crystal defects (Petrov et al. 1983; Chernov 1984, and others). Genetic role of inclusions, twins, dislocations, etc. is being extensively studied. It is obvious that imperfection of a protocystal affects the product morphology and replacement kinetics, its influence upon morphology being dual.

On one hand, imperfection is inherited and can be seen in some features of the new formations. They include such well-known phenomena as inheritance of polytypic motives during transformations of layered silicates in hydrothermal solutions (Frank-Kamenetskii et al. 1981), and retention of solid inclusions in the form of shade pseudomorphs at their initial places in protocrytals (Chesnokov 1974, p. 67). This list can be extended by addition of the above-mentioned examples of autoepitaxial excrescences formed on fractures and outcrops of dislocations in the course of monocrystal replacement: see reactions *Ib/24* (Fig. 1.4), *26*, *28*, *30* (Fig. 1.3), *32*, *33* (Glikin and Sinai 1983, 1991), of replacement product inheriting inclusions localized in a protocrytal: see reactions *III/44*, *45*, *47* (Fig. 1.18 *a-c*) (Sinai and Glikin 1989; Glikin and Sinai 1991), of pseudomorph inheriting the attributes of the initial twin structure (Glikin and Sinai 1983): see reactions *Ib/35* (Fig. 1.19).

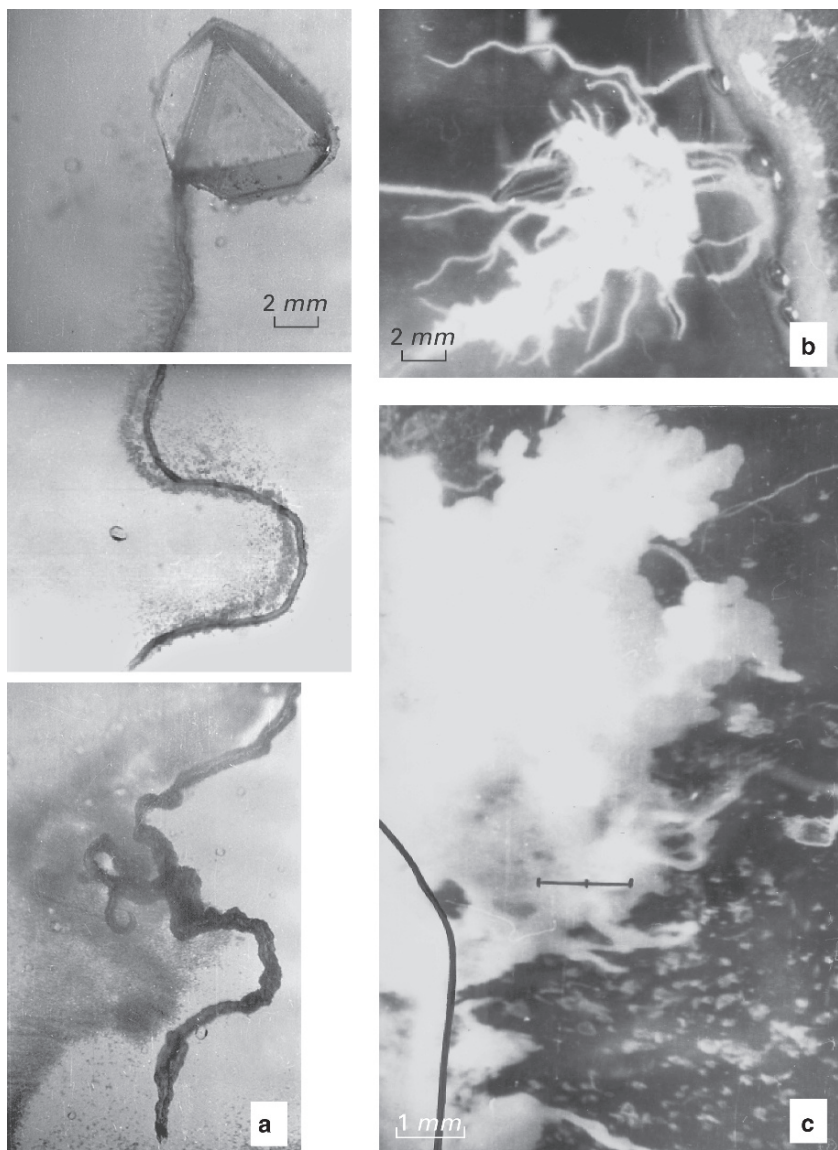
On the other hand, under replacement conditions imperfection of a protocrytal promotes loss of information about the protocrytal. For example, monocrystalline pseudomorphs formed under volume-excess conditions and bearing a large number of autoepitaxial excrescences (Fig. 1.4) lose the initial face relief (reactions *Ib/26*, *28*, *30*, *32*, *33*), while the products of interaction between the surrounding solution and liquid inclusions of protocrytal may completely overlap and hide the new formation, which replaces a solid matter of the protocrytal (reaction *III/47* – Fig. 1.18*c*).

Our experimental results are represented below.

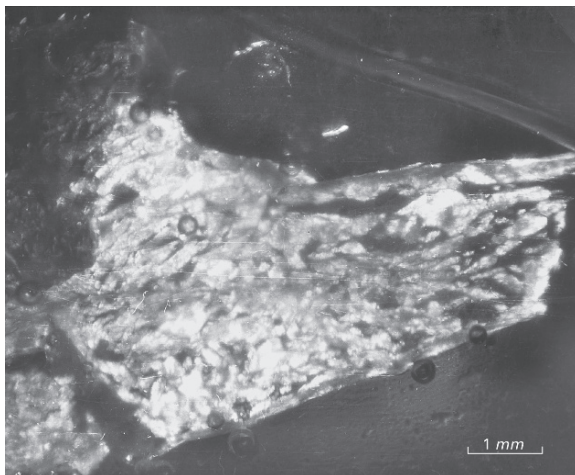
Interaction of the substances contained in the protocrytal fluid inclusions with a metasomatic solution takes place after opening the inclusions as the protocrytal dissolves. Under these conditions precipitation of new formations is facilitated by salting-out or ion-exchange reactions (reactions of Types *Ia* and *III*). This results in formation of solid products of inclusion replacement, which are genetically and morphologically similar to the crystal replacement products (Glikin and Sinai 1988, 1991; Sinai and Glikin 1989). This analogy is supported by a well-known opinion of the fluid inclusions being regarded as negative crystals (Laemmlein 1929, 1973).

Some examples of the reactions shown in Table 1.1 are given below.

Reaction *III/53* (replacement of  $\text{NiSO}_4 \cdot 7\text{H}_2\text{O}$  crystals by nickel chromates in  $\text{K}_2\text{CrO}_4$  solution). The protocrytals possess prismatic shapes having tetrahedral heads and the sizes of about 1 cm. They contain dissipated isolated inclusions with the size of about 1 mm or less having isometric shapes or slightly elongated along the longest dimension of the crystal. The products of replacement of such crystals are represented by faceted or faceted-embossed polycrystalline pseudomorphs, composed of fine-grain aggregates of nickel chromates and  $\text{K}_2\text{CrO}_4$ . The products of the inclusion replacement are visible on the pseudomorph fractures. They are isolated fragments having similar phase composition, but differing in grain size; generally their sizes and shapes correspond to those of initial inclusions, but precise definition has not been carried out. These products crystallize directly in the volume of the inclusions, either at the moment of their opening, when the front of crystal replacement touches the inclusion, or in advance owing to solution penetrating the crystal through the microcracks and reaching the inclusions in accordance with the mechanism defined formerly (Grigor'ev 1961, p. 173). Reaction *Ia/5*



**Fig. 1.18** Fine-grained aggregates of  $\text{BaSO}_4$  – products of replacing the inclusions contained in the initial crystals **a**, **b** – tubular shapes (localized automorphs): replacement of potassium alum in  $\text{Ba}(\text{NO}_3)_2$  solution (**a** – tube and a circular automorph, reaction III/44) and replacement of  $\text{Ba}(\text{NO}_3)_2$  in potassium alum solution (**b** – a tube cluster, reaction III/45; photo by N.I. Krasnova); **c** – dense precipitate (dissipated automorph): tube coalescence during replacement of  $\text{BaCl}_2 \cdot 2\text{H}_2\text{O}$  in potassium alum solution (the upper part contains the protocystal contour, reaction III/47)



**Fig. 1.19** Preservation of initial boundaries between the individuals of the triplet during volume-deficit monocystal replacement of  $K_2CrO_4$  with  $K_2(Cr,S)O_4$  (reaction *Ib/35*). Crossed nicols. Absent and bloomed individuals are visible

(replacing  $KAl(SO_4)_2 \cdot 12H_2O$  crystals predominately with nickel chromates in  $K_2CrO_4$  solution) is analogous to the previous one. Pseudomorphs formed on the inclusions have radiate-fibrous or laminated structures, and, in contrast to the previous case, it is difficult to find a unique correspondence between their shapes and the shapes of the initial inclusions.

Reaction *III/44* (replacement of  $KAl(SO_4)_2 \cdot 12H_2O$  crystals with barite in  $Ba(NO_3)_2$  solution). The protocystals have octahedral shapes with weakly developed cubic faces and the size of about 1 cm. Inclusions are confined within the sectors of the cube growth.

Reaction *III/45* (replacement of  $Ba(NO_3)_2$  crystals with barite in  $KAl(SO_4)_2$  solution). The protocystals having the size of about 1 cm are faceted by positive and negative tetrahedrons and cube and flattened along the  $\{111\}$  axis. Multiple point-like inclusions are confined within the cube sectors. Both above reactions result in gradual development of the localized  $BaSO_4$  automorphs containing weakly bonded grains with the size up to 0.1 mm. This process is accompanied by much faster growth of tubular barite aggregates having complex shapes, which start developing from the tetrahedron sectors saturated with inclusions (the crystal size up to 0.1 mm) (Figs. 1.18*a, b*). The tubes have diameter of about 0.5–1 mm and length up to several centimeters; they are composed of the liquid contents of opened inclusions, which has already reacted with the solution medium, and the rate of their elongation is about 0.5–1 mm/s.

The tubes define localization of inclusions in protocystals. Successive opening the inclusions, which are frequently arranged in chains directed from the crystal periphery to its center, results in formation of the tubes. The tubes promote diffusive transportation of the inclusion solution to the solution surrounding the crystal

and, thus, facilitate growth of the tube end faces. Breaking an inclusion chain stops growth of the tube. Several tubes can grow simultaneously, being initiated at different time. The growth is fast as the both reactants are in dissolved state.

Reaction *III/47* (replacement of  $\text{BaCl}_2 \cdot 2\text{H}_2\text{O}$  crystals with barites in  $\text{KAl}(\text{SO}_4)_2$  solution) is partially similar to the previous one. The protocrystals having the sizes of about 1 cm are impregnated with multiple point-like and relatively large (up to 0.5 mm) inclusions, which do not group in any obvious arrangement. In contrast to the previous case, the tubes are quickly merged to form a dense precipitate, which overlaps the automorph replacing the solid part of the crystal (Fig. 1.18c).

Such new formations comply with suggested basic classification of replacement products of monocrystals (Sect. 1.4): the above products of the inclusion replacement are similar to the pseudomorphs deposited within the contours of the initial inclusions (reactions *III/53* and *Ia/5*), and to localized automorphs, if the products indicate location of the inclusions (reactions *III/44*, *45*), and to dissipated automorphs, when this location cannot be determined (reaction *III/47*). It should be noted that both pseudomorphic and automorphic replacements of the solid part of the crystals are accompanied by the same type of inclusion replacement. This is to be expected as morphology of the products is defined by the ratio of reactant diffusion rates in the solution (Sect. 1.5.3). However, it should be kept in mind that replacement of the crystal matter is complicated by crystal dissolution and the above regularity may not hold true for all reactions.

Unfortunately, scarcity of the investigated products does not allow us to draw a complete analogy between the classification of the crystal replacement products and that of inclusion replacement products, since it is difficult to estimate a probability of the other structural (monocrystalline and amorphous) and morphological types to occur in the process concerned. In any case, there is no a priori prohibition for the majority of taxons of the basic classification. However, classification of pseudomorphs according to their inclusions into “embossed,” “faceted” and “blurred” pseudomorphs is hardly appropriate, since regarding the inclusion as negative crystals cannot be universal, and lack of the faces and microreliefs in majority of inclusions cannot promote their division into corresponding morphological types.

Therefore, structural-morphological classification of the replacement products may be represented in the form of Table 1.3. Outward similarity between classification of replacements of monocrystals and that of inclusion replacements does not mean genetic resemblance of all the corresponding processes. Of course, polycrystalline replacement of the inclusions is certainly quite similar to replacement of monocrystals of Types *Ia* or *III*. However, a hypothetic monocrystalline replacement of inclusions normally reflects the natural growth of individual, which totally or partially fills up the inclusion volume, and monocrystalline isomorphic replacement (Type *Ib*) is absolutely impossible in this case. It should be noted, however, that formation of automorphs on inclusions (reactions *III/44*, *45* and *47*) was observed in clusters of inclusions, but not on individual inclusions; i.e. such automorphs can be closer related to some products of replacement of certain crystalline aggregates, although this phenomenon has not been thoroughly studied.

During monocrystalline *replacement of a twin*, the individuals preserve their initial borders (Fig. 1.19), but monoclinic and triclinic crystals change orientation



**Table 1.3** Classification of the inclusion replacement products

Shape	Structure		
	Monocrystalline	Polycrystalline	Amorphous
Pseudomorphs	Hypothetic	<b>2</b> ( <i>Ia/5, III/53</i> )	Hypothetic
<u>Automorphs</u>			
Localized	Hypothetic	<b>2</b> ( <i>III/44, 45</i> )	Hypothetic
Dissipated	Hypothetic	<b>1</b> ( <i>III/47</i> )	Hypothetic

**Note:** The number of systems where the corresponding products were observed is printed in bold; examples of the systems are given in brackets.

of the optical indicatrix. In those cases there must exist a discrepancy between the twinning angles and the composition, which either can be a sign of isomorphic replacement process (for instance, for plagioclases) or the source of errors when optical methods are used for isomorphic analysis of mineral composition.

Influence of *protocrystal imperfection* upon the reaction kinetics was not thoroughly investigated; however, some specific phenomena have been observed in direct and inversed monocrystalline replacements in isomorphic  $\text{K(Al,Cr)(SO}_4)_2 \cdot 12\text{H}_2\text{O}$  alum series (reactions *Ib/28* and *29*).

Replacement rates observed for protocrytals having similar appearance (4–5 mm), which have been grown together, differ significantly in spite of location near each other in the same reacting solution. For instance, spongy pseudomorphs containing at intermediate stages various ratios of isomorphic components are produced under volume-deficit conditions (*Ib/29*). On the contrary, under volume-excess conditions (*Ib/28*) the replacement front is very uneven with threefold to fourfold variation in the thickness of the newly forming rim. Both phenomena can be easily distinguished as new formations differ in color. The protocrytals and/or their sectors are likely to contain different amount of defects. Clusters of fluid inclusions should effectively influence these processes owing to accelerated transportation of the substances by means of the liquid phase; under conditions of sponge replacement dislocation clusters should accelerate dissolution and growth of the new formation, while under conditions of continuous replacement they should accelerate the solid phase diffusion (see Sect. 3.2).

## 1.6 Mineralogical Aspects of the Problem of Crystal Replacement

The proposed replacement concept based on experimental data includes known mineralogical classifications of the numerous natural replacement forms and defines genetic position of the products (Blüm 1843; Strunz 1957; Betekhtin et al. 1958; Grigor'ev 1961; Polovinkina 1966; Kostov 1968; Zhabin and Rusinov 1973; Amstutz 1981c, and others). Moreover, the concept includes the forms, which are

not normally paid attention to, and, by doing this, extends the list of products of potentially metasomatic genesis.

Conventional types of replacement products, normally described in published literature, are arranged according to the taxons of our classification represented in Table 1.4. It is remarkable that despite a certain conditional character of such distribution it has been possible not only to represent pseudomorphs as a whole, but also to correlate many products with the new taxons, which include modifications of both pseudomorphs and automorphs. The list of pseudomorphs indicates that polycrystalline replacement products are described more frequently and in more details. However, their generalized list has been considerably extended by including some new formations, which were put into the table on the basis of developed genetic concepts. The debatable cases are reviewed below.

The crystal ensembles of metasomatic veins represent the products of transformations of minerals, which were located outside those veins. The educts and the products are spatially separated and degree of this separation is not particularly limited. All this corresponds to a definition of translocated automorphs. The crystal ensembles of metasomatic rocks are the products of transformation of minerals, which were located within a massif. In this case the educts and the products are also spatially separated; however, if they are at least uniformly distributed in the initial and transformed massifs, the areas of their distribution overlap and the products can be regarded as dissipated automorphs. Secondary porosity in metasomatic rocks

**Table 1.4** Some traditional types of natural replacement products within the new classification scope (Table 1.2)

Shape	Structure		
	Monocrystalline	Polycrystalline	Amorphous
<b>Pseudomorphs</b>			
In general	Monocrystalline	Continuous	Hollow
	Homoaxial	Box-shaped (case-like, enveloping, hollow)	Replica
	Ion-exchanging	Shadowed	
	Rims Borders		
Embossed and faceted		Formed in situ	
		Formed with filling up Perimorphs	
Blurred		Epimorphs	
		Formed with transportation (displacement)	
<b>Automorphs</b>			
Localized		Rims, borders, coronas, coronites, drusites	
		Crystal clusters in a uniform matrix	
		Liesengang rings	
		Orbiculars	
Dissipated		Ensembles of crystals in metasomatic rocks	Secondary porosity
Translocated		Ensemble of crystals in metasomatic veins	

can be regarded similarly. This approach can be supported by reliable observation of diffusing the pseudomorphs by means of product transfer beyond the boundaries of the initial monocrystal (Grigor'ev 1961). We propose a combined approach to all the above phenomena, taking into account that the distance of the matter transfer may be great enough. Of course, metasomatic nature of the process is defined by cause–effect relationships, which control dissolution of the educt, transfer of the matter, and deposition of the product; however, correlation between the above processes cannot be proved in each particular case even for ordinary pseudomorphs.

Analysis of data on replacement of monocrystals demonstrates that metasomatic crystallogeneses can be applied to a significantly greater phenomenological range in comparison with the diapason limited by traditional views adopted in mineralogy, especially considering the absence of the term “automorph” in mineralogical methodology. In other words, mineralogical definition of metasomatic replacement consists in simultaneous dissolving the protocystal and growing the new formation, which does not permit essential deviations from the simultaneous proceedings of elementary processes and significant outgrowing the boundaries of the initial crystal.

We think that the concept of space-time superposition of dissolution and growth processes should be extended. The data shown in Table 1.2 and analysis of the respective cause–effect relationships (Sects. 1.4–1.5) demonstrate that complete superposition was observed only during volume-deficit formation of embossed pseudomorphs and also during formation of products, in which deficiency of physical volume was accompanied by the total volume compression. At the same time, the borders in the series of taxons ranging from embossed pseudomorphs to translocated automorphs are rather conventional and changes from one taxon to another are stipulated by monotonous alteration of some kinetic parameters of physicochemical systems. Alterations in volume effect are also determined by arbitrary variations in relative solubility of components in various systems. The essential conclusion is that all these products are of common nature depending upon a similar driving force (salting-out for reactions of Types *I* and *III* or salting-in for reactions of Type *II*).

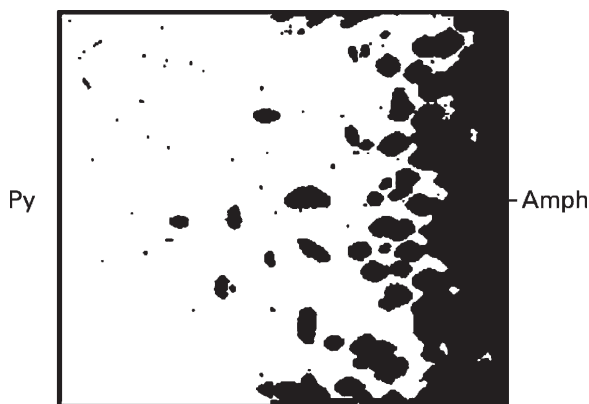
Therefore, in general, an extent of time-space superposition of elementary processes of growth and dissolving is very important. It has a maximum in processes of monocrystalline isomorphic replacement. This maximum is likely to have a physical meaning defined by the sizes of diffusion fields surrounding adjacent points of growth and dissolution. The extent of time-space superposition is gradually reducing (both in time and space) when transferring to the processes of formation of other products, and completely absent in the case of translocated automorph formation. Obviously, such transition causes the products to gradually lose the metasomatic attributes, and in the cases of translocated automorphs they cannot be distinguished from the products of conventional direct growth. This fact probably explains a conventional understanding of metasomatism as a process proceeding within a limited volume.

Classical division of replacement products into various types of pseudomorphs seems to be insufficient, as the products are divided into the groups according to their structural-morphological attributes regardless to their genesis. The commonly used genetic definitions (pseudomorphs of displacement and pseudomorphs of mixing, synchronous and asynchronous pseudomorph types, ion-exchange types, etc.) are incomplete and are not related to morphological attributes or physicochemical factors.

Our classification do not contradict the classical one, but makes it more detailed, streamlined, and elaborated, since it takes into consideration genetic peculiarities of the taxons. It seems convenient and easy to visualize, because taxons are defined in accordance with known hierarchy of discrete and readily detected structural and morphological signs. Therefore, our classification can be recommended as a basis for description and genetic analysis of natural products.

The classification can be modified for numerous individual peculiarities of the products to be taken into consideration. On one hand, it can include additional taxons. For example, intermediate (faceted-blurred pseudomorphs etc.) or combined (various extent of preserving different protocystal faces) morphological modifications can be added. Structural species can include intermediate products, transitional from mono- to polycrystalline and comprising graphical (Figs. 1.6*c, d*) or epitaxial (Glikin and Kaulina 1988) textures. It might have been appropriate to divide polycrystalline products into twins, textured, and irregular formations, and classify amorphous formations into dispersed, glass, and fluid structures. It could be interesting to use the same approach to review metasomatic replacements of liquid phases in fluid systems and glasses. On the other hand, the basic classification can be elaborated to include additional attributes, such as volume ratio between a protocystal and a new formation (and related dividing the products into continuous, loose, sponge and hollow ones), the number and space distribution of the newly formed phases, overlapping the protocystal replacement products and inside inclusions. Those attributes can be considered as additional coordinates of the classification transforming it into a multi-dimensional concept.

An example of classification modified to comprise products of inclusion replacement in crystals is presented in Sect. 1.5.4. We succeeded in finding the only analogous result in published mineralogical literature describing some synthesized products. It shows a schematic representation of replacement front containing “advancing sites” (Fig. 1.20) corresponding to pseudomorphs formed on inclusions described by us.



**Fig. 1.20** Replacement front containing “advancing sites” for pyroxene replacement with amphibole (According to data obtained by Grigor’ev 1961)

**Table 1.5** Some natural morphological analogs of synthetic replacement products

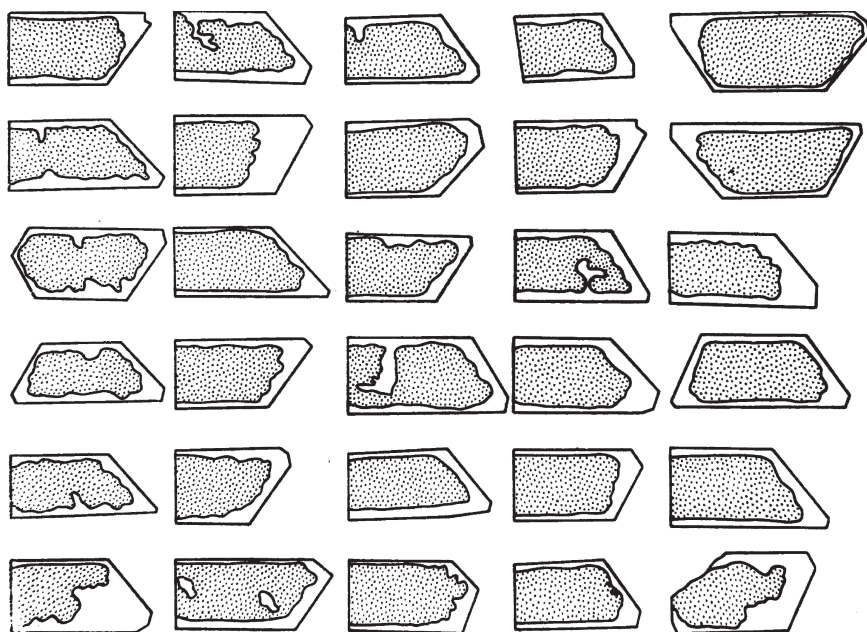
Shape	Example	Reference
<b>Monocrystalline products</b>		
<u>Pseudomorphs</u>		
Embossed	Zeolite → zeolite $\alpha$ -sulfur → $\beta$ -sulfur Nepheline → cancrinite	Fersman 1952 Strunz 1982 Chesnokov 1974
Faceted (continuous)	Augite → uralite Enstatite → bastite tremolite → actinolite Plagioclase → plagioclase*	Betekhtin 1961 Betekhtin 1961 Goldschmidt 1913 Saranchina and Shinkarev 1973
Faceted (spongy)	Feldspar → feldspar* Beryl → beryl* Mica → biotite* Amphibole → amphibole* Topaz → topaz* Pyrrhotite → pyrite Zircon → zircon*	Shinkarev and Rundkvist 1986 Fersman 1960 Galdin 1968 Galdin 1968 Barabanov 1977 Zhabin and Samsonova 1975 Rudenko 1966
Blurred	Hornblende → actinolite Feldspar → feldspar* Feldspar → feldspar*	Polovinkina 1966 Sudovikov 1967 Shinkarev and Rundkvist 1986
<b>Polycrystalline products</b>		
<u>Pseudomorphs</u>		
Embossed	Pyrite → limonite	Betekhtin 1961, Kostov 1968
Faceted (continuous)	Calcite → actinolite Hematite → magnetite Azurite → malachite Calcite → calamine Gaylussite → calcite Zeolite → chlorite + vermiculite + montmorillonite + hydromica	Zhabin 1960 Betekhtin 1961 Betekhtin 1961 Betekhtin 1961 Plotnikov and Tatarskii 1946 Makhmudov and Babaev 1972
Faceted (hollow)	Halite → dolomite + gypsum	Krotov 1925
Blurred	Garnet → plagioclase + zoisite	Chesnokov and Yakshin 1969
<u>Automorphs</u>		
Localized	Chromite → magnetite (rims) Cu-platinum → platinum Chalcopyrite → bornite + goethite Feldspar → feldspar*	Nazimova 1984 Betekhtin et al. 1958 Betekhtin et al. 1958 Sudovikov 1967
<b>Amorphous products</b>		
<u>Pseudomorphs</u>		
Embossed	$\alpha$ -Quartz → cavities	Balitskii and Komova 1968

**Note:** Asterisk is used to denote formations, which according to our experimental data are supposed to have metasomatic genesis.

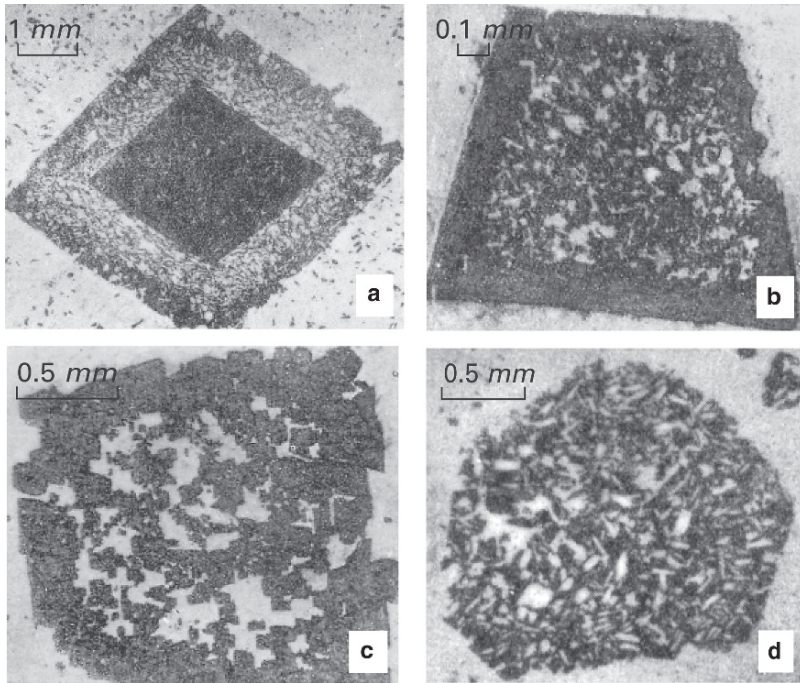
Nevertheless, it should be taken into consideration that fluid inclusions in natural crystals may contain negligible concentrations of the crystal matter, and, so, the solid products can have an extremely small volume. Moreover, precipitation of some specific products may be caused by the action of mineralizers dissolved in the inclusions.

Considering the resources of our elaborated classification, it will be possible to cover all known synthetic and overwhelming majority of natural products of replacement of monocrystals in solutions. Crystallogenic concept of replacement of monocrystals appears to be completed at a qualitative level. It can be applied as a basis for classifying and discovering some natural replacement products and for development of genetic analysis including a number of details, presented in the next sections. The classification can be applied for products obtained in the other processes of crystal modification, e.g., polymorphism, metamict decomposition, mechanical and thermal destructions, etc. Of course, for those cases some modifications of the classification will be certainly required.

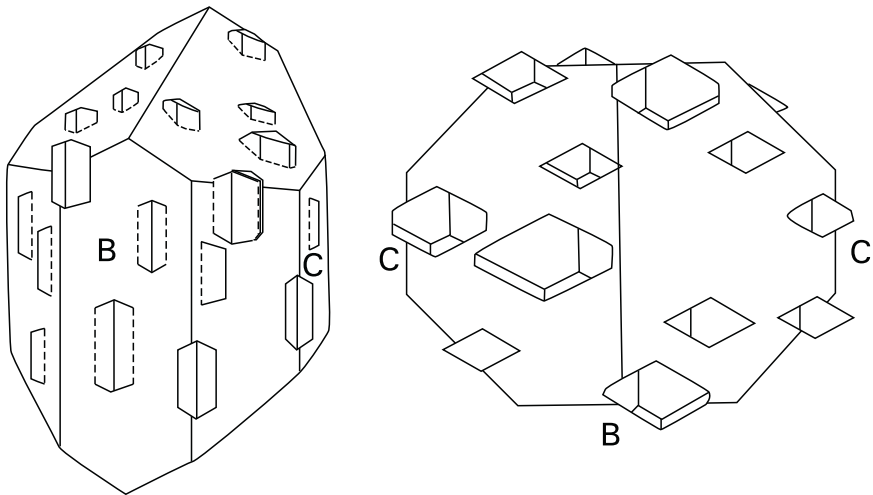
Reported data presented in Table 1.5 show that, according to available descriptions, majority of the positive products can be distributed among the proposed taxons, although, strictly speaking, metasomatic genesis seems to be doubtless only for polycrystalline pseudomorphs. Some examples of morphological analogs of synthetic products and natural formations are presented below. Zoned topaz crystals containing cores saturated with fluid inclusions (Fig. 1.21), poikilitic crystals of zircon (Figs. 1.22a–c) and tourmaline (Fig. 1.22d), and feldspar spheroid porphyroblasts of rapakivi (see Fig. 5.1) correspond to monocrystalline spongy pseudomorphs (Figs. 1.6a–c). Pseudomorph of actinolite on tremolite (Fig. 1.23) can be attributed to monocrystalline pseudomorphs



**Fig. 1.21** Zoned topaz crystals, each composed of a spongy core and a transparent outer zone (According to data obtained by Barabanov 1977)



**Fig. 1.22** Poikilitic (“skeletal” according to Rudenko) crystals of zircon (a–c) and tourmaline (d) (According to data obtained by Rudenko 1966)



**Fig. 1.23** Embossed monocrystalline pseudomorph of actinolite after tremolite having autoepitaxial excrecences (According to data obtained by Goldschmidt 1913)

with autoepitaxial excrescences (Fig. 1.3). Some examples of various polycrystalline pseudomorphs, both natural (Figs. 1.1*a, b* and 1.20) and synthetic (Figs. 1.1*c, d*, 1.7, 1.8*a*, 1.9), are described above. Orbicular crystal aggregates of feldspar (see Figs. 5.4 and 5.5) correspond to localized circular automorphs (Figs. 1.10 and 1.11).

Doubtless, most readily detected and reliable attributes of metasomatic process are polycrystalline pseudomorphs, although, they cannot be the only ones, since the products of solid-phase transformation may be presented by new formations having similar shape and structure, for instance, by graphite paramorphs on diamond (Slodkevich 1982).

However, localized automorphs may present enough information for arguments supporting metasomatic genesis of some geological bodies. In fact, it is really difficult to find out another interpretation for appearance of isolated accumulations of some minerals in a relatively uniform rock matrix. In Sect. 5.2 the above is presented as substantiation of metasomatic nature of some rapakivi granites (Glikin 1990, 1991, 2002). At present, though, it can be ascertained that reliable diagnostic methods for such natural formations are still absent.

Isomorphic replacement (and formation of crystals with variable composition in general) is considered by us as an unconventional fundamental phenomenon of crystallogenesis. The key morphological effects and the basic model for physicochemical analysis have been determined for this kind of replacement, although the attributes, essential to discover the monocrystalline replacement products and reconstruct their formation conditions, are not too numerous. Considering the data, presented in Chapters 3 and 4, it is clear that interpretation of distribution and composition of admixtures and fluid and solid inclusions in isomorphic-mixed crystals requires a new approach. Among the potential attributes of replacement, in addition to well-known monocrystalline rims (Betekhtin et al 1958; Polovinkina 1966; Atlas... 1976, and others), the following signs can be mentioned: autoepitaxial excrescences and a spongy constitution with absence of primary zoned and sectorial structures. Some minerals were found to contain individuals with specific spongy structure bearing a morphological similarity to synthetic spongy pseudomorphs (e.g., amphiboles – Galdin 1968; topaz – Barabanov 1977; astrophillite – MacKensie and Guilford 1980; hydrogarnets – Galuskina et al. 1998).

Crystals which underwent monocrystalline isomorphic replacement are expected to exhibit discrepancies in crystal-chemical and goniometric constants, e.g., different ratios of the elementary cell parameters and morphological factors, deviation of spherical coordinates of the crystal forms having arbitrary positions, or deviations of twin crystal angles from the standard values obtained for the given isomorphic composition. In this connection it is to be noted that common crystal-optical methods for determination of feldspars and amphiboles using the angle constants between the elements of indicatrix and faceting elements (Zavaritskii 1953; Dolivo-Dobrovolskii 1964; Saranchina and Kozhevnikov 1985) may provide with wrong information; this is a probable reason for obtaining some abnormal data (Dolivo-Dobrovolskii 1964). The data obtained are likely to further complicate the problem of estimating conditions of natural formation according to distribution of isomorphic impurities in minerals (Fonarev 1987, and others)

Analytical principles of replacement volume effects discussed above seem natural, supported by both the theory and the experimental laws of physical chemistry and thus doubtless. The most important factor for mineralogical reconstitutions is



difference in phenomenology and the mechanisms of the reactions proceeding with deficit and excess of volume.

The volume-deficit reactions resulting in increased rock porosity are considered to be quite possible (Lindgren 1933; Currier 1937; Grogan 1949; Nakovnik 1949; Ames 1961c, and others). Geological processes based upon the volume-excess reactions are surely to have specific mechanisms to compensate appearance of extra matter. Some of them have been discussed at least as general ideas, including, for example, local mechanical deformations and reduced porosity (Korzhinskii 1955, 1970), local tectonic phenomena (for instance, “salt tectonic,” accompanying anhydrite to gypsum transition – Betekhtin 1961), and dissolution of minerals under the action of crystallization pressure (Landa 1979). Probably, the most frequently occurring mechanism involves an infiltration or diffusion transport of the extra matter outside the reaction volume; at the micro level these processes can proceed as ingrowth of the replacing crystals into the matrix accompanied by diffusion removal of the reaction products through the film of solution surrounding the crystal without formation of any free volume (Figs. 1.8*b, d*; reaction 1*a/5*). The possibility of complete reaction termination with preservation of nonequilibrium associations cannot be excluded as well.

Material balance of reactions is defined by character of phase equilibria in the system. Calculations of the reaction coefficients on the basis of the postulated volume equality, as well as an assumption of particular nature of reactions proceeding in the earth crust, seem to be incorrect. Formula stoichiometry must be adhered to only when the product solubility is negligible in comparison with solubilities of the initial reactants.

It should be noted that all four supra-elementary classes, their definitions being given in Introduction, can be singled out in the generalized scheme of replacement of monocrystals.

The first class consists of monocrystalline pseudomorphs (phase borders between the sites of synchronized dissolution and growth are absent); the second class comprises all other pseudomorphs and localized automorphs (sites of synchronized dissolution and growth are separated by the phase borders, but spatially coordinated with each other in unambiguous way); the third class includes dissipated automorphs (dissolution and growth are substantially synchronized, but their spatial coordination is ambiguous); and the fourth class comprises translocated automorphs (dissolution and growth are non-synchronized and spatially uncoordinated). Actually, at present mineralogical concepts of replacement processes include only the first and partially the second class of replacement products and are to be extended to eliminate existing discrepancies, which, in our opinion, are mainly of imaginary nature.

## References

- Ames LL Jr (1960) Some cation substitutions during the formation of phosphorite from calcite. *Econ Geol* 55:2:354–362
- Ames LL Jr (1961a) Volume relationships during replacement reactions. *Econ Geol* 56:8:1438–1445

- Ames LL Jr (1961b) The metasomatic replacement of limestones by alkaline fluoride-bearing solutions. *Econ Geol* 56:4:730–739
- Ames LL Jr (1961c) Cation metasomatic replacement reaction. *Econ Geol* 56:6:1017–1024
- Amstutz GC (1981a) Kupfer nach aragonit. *Lapis* 6:11:19–21
- Amstutz GC (1981b) Malachit nach asurit. *Lapis* 6:11:22
- Amstutz GC (1981c) Pseudomorphosen – zum Thema. *Lapis* 6:115.
- Amstutz GC (1981d) Pseudomorphe fossilien. Durch Mineralien verdrängte organische Reste und Gegenstände. *Lapis* 6:11:27
- Anosov VYa, Ozerova MI, Fialkov YuA (1976) Fundamentals of physicochemical analysis. Nauka, Moscow (Russ.)
- Ansheles OM, Burakova TN (1948) Microchemical analysis on the base of crystal optics. Leningrad State University, Leningrad (Russ.)
- Atlas of textures and structures of nonferrous metal ores of Kazakhstan* (1976) Nauka, Alma-Ata (Russ.)
- Balitskii VS (1966) Transformation of granites under the action of silica-containing hydrothermal solutions under elevated pressures. *Doklady Acad Sci USSR* 171:5:1175–1178 (Russ.)
- Balitskii VS, Komova VV (1968) On interaction of sodium hydroxide solutions containing silica with various rocks and minerals at high temperatures and pressures. *Doklady Acad Sci USSR* 179:6:1444–1447 (Russ.)
- Barabanov VF (1977) Genetic mineralogy. Nedra, Moscow (Russ.)
- Barker AJ (1994) Introduction to metamorphic textures and microstructures. Blackie, Oxford
- Betekhtin AG (1961) Treatise on mineralogy. Gosgeoltekhizdat, Moscow (Russ.)
- Betekhtin AG, Genkin AD, Filimonova AA, et al. (1958) Textures and structures of ores. Gosgeoltekhizdat, Moscow. (Russ.)
- Beus AA (1961) On the mechanism of formation of idiomorphic crystals of rare metal minerals in replacement processes. *Proc Inst Miner Geochem Rare Elements USSR Acad Sci* 7:61–64 (Russ.)
- Blüm IR (1843) Die Pseudomorphosen des Mineralreichs. Stuttgart.
- Bogolepov VD (1965) Two periods of metasomatic mineral formation. *Zapiski Vsesoyuz Miner Obsh* 2:149–161 (Russ.)
- Brodin BV, Dymkova GA (1966) Contraction structures of hubnerite replacing scheelite. *Zapiski Vsesoyuz Miner Obsh* 5:570–572 (Russ.)
- Carl JD, Amstutz GC (1958) Three-dimensional Liesegang rings by diffusion in a colloidal matrix, and their significance for the interpretation of geological phenomena. *Geol Soc Amer Bull* 69:1467–1468.
- Chekin SS, Samotoin ND (1983) Peculiarities of weathering and kaolinization mechanisms in sheet silicates. In: Sapozhnikov DG (ed) *Weathering Crust* 18. Nauka, Moscow (Russ.)
- Chelishchev NF (1973) Ion-exchange properties of minerals. Nauka, Moscow (Russ.)
- Chernov AA (1984) Processes of crystallization. In: *Modern Crystallography III, Crystal Growth*. Springer, Berlin
- Chesnokov BV (1974) Relative age of mineral individuals and aggregates. Nedra, Moscow (Russ.)
- Chesnokov BV, Yakshin VI (1969) Shadow pseudomorphs after garnet in amphibolites of the Middle Urals. *Zapiski Vsesoyuz Miner Obsh* 1:85–89 (Russ.)
- Chukhrov FV (1955) Colloids in the earth crust. *Acad Sci USSR, Moscow* (Russ.)
- Collins LG (1988) Hydrothermal differentiation and myrmekite – a clue to many geological puzzles. Theophrastus Publications, Athens
- Currier LW (1937) Origin of the bedding replacement deposits of the fluorspar in the Illinois field. *Econ Geol* 32:364–386
- Dobrovol'skii EV (1975) Kinetic study of interaction between calcite and fluorine-containing solutions. In: *Problems of hydrogeology, engineering geology and soil science*. Naukova Dumka, Kiev (Russ.)
- Dolivo-Dobrovol'skii VV (1964) On a definition of optical orientation of plagioclase on a Fedorov's object stage. *Zapiski Vsesoyuz Miner Obsh* 4:390–398 (Russ.)
- Dolivo-Dobrovol'skii VV (1967) Physical geochemistry as a new scientific discipline and some characteristics of its development in our country. *Zapiski Vsesoyuz Miner Obsh* 5:526–531 (Russ.)

- Drüppel K, von Seckendorf V, Okrusch M (2001) Subsolidus reaction textures of anorthosites. *Eur J Miner* 13:2:289–309
- Egorov BL (1982) Diffusion-metasomatic method of crystal growth. *Izvestia VUZ (Proc High School)*. *Geol Explor* 10:161–164 (Russ.)
- Egorov BL (1983) The role of direct and reverse diffusion in metasomatic reactions. *Izvestia VUZ*. *Geol Explor* 12: Deposited papers (Russ.)
- Fersman AE (1952) Selected works 1. Acad Sci USSR, Moscow-Leningrad (Russ.)
- Fersman AE (1960) Selected works 6. Acad Sci USSR, Moscow-Leningrad (Russ.)
- Fisher GW (1973) Nonequilibrium thermodynamics as a model for diffusion controlled metamorphic processes. *Amer J Sci* 273:897–924
- Fonarev VI (1987) Mineral equilibria in Precambrian ferruginous formations. Nauka Moscow (Russ.)
- Fontbole L, Rastad E (1981) Pseudomorphosen als Schlüssel zur Erlagerstättendeutung. *Lapis* 6:11:12–13
- Frank-Kamenetskii VA, Kotov NV, Kotel'nikova EN (1981) Forms of inherited polytypism in the course of hydrothermal transformation of sheet silicates. In: Frank-Kamenetskii VA (ed) *Crystal chemistry of minerals*. Nauka, Leningrad (Russ.)
- Frank-Kamenetskii VA, Kotov NV, Goilo EA (1983) Transformations of sheet silicates at elevated P-T parameters. Nedra, Leningrad (Russ.)
- Franke VD, Glikin AE, Kryuchkova LYu, Tabuns EV (2007) Cocrystallization of isomorphic components in solutions and crystal zoning: an example of the Ba,Pb(NO<sub>3</sub>)<sub>2</sub> series. *Geol Ore Deposits* 49:7:641–647
- Galdin NE (1968) Investigation of elastic wave velocities measured under high pressures in the samples collected along a region line of Kola Peninsula. In: *Physicochemical properties of rocks in the upper part of the Earth crust*. Nauka, Moscow (Russ.)
- Galuskin E, Galuskina I, Winiarska A (1995) Epitaxy of achtarandite on grossular – the key of the problem of achtarandite. *Neues Jb Miner Mh* 7:306–320
- Galuskin EV, Golovanova TI (1987) Genetic peculiarities of polychromatic diopside crystals from skarns of the Polar Yakutia. *Zapiski Vsesoyuz Miner Obsh* 1:64–71 (Russ.)
- Galuskina I, Galuskin E, Sitarz M (1998) Atoll hydrogarnets and mechanism of the formation of achtarandite pseudomorphs. *Neues Jb Miner Mh* 2:49–62
- Galuskina I, Galuskin E, Sitarz M (2001) Evolution of morphology and composition of hibschite, Wiluy River, Yakutia. *Neues Jb Miner Mh* 2:49–66
- Geisler T, Ulonska M, Schlecher H, Pidgeon RT, von Bronswijk W (2001) Leaching and differential crystallization of metamict zircon under experimental hydrothermal conditions. *Contrib Miner Petrol* 141:53–65
- Geologic Dictionary* (1973) Nedra, Moscow (Russ.)
- Gerasimov YaI, Dreving VP, Eremin EN et al. (1970) Course of physical chemistry 2. Khimia, Moscow (Russ.)
- Glikin AE (1990) Crystallogenic model of isomorphic replacement and metasomatic formation of rapakivi type structures. In: Yushkin NP, Askhabov AM (eds) *Mineralogical crystallography, crystallogenesis, crystallosynthesis*. Ural Branch Acad Sci USSR, Syktyvkar (Russ.)
- Glikin AE (1991) Mechanisms of inheriting and losing the structural attributes of rocks in the course of metasomatism and recrystallization. In: Gelman ML (ed) *Metamorphic complexes of the North-East of USSR, their ore content and geological mapping*. SVKNII Far-East Branch Acad Sci USSR, Magadan (Russ.)
- Glikin AE (1995) On the theory of formation of isomorphic-mixed crystals. *Zapiski Vsesoyuz Miner Obsh* 5:125–134 (Russ.)
- Glikin AE (1996a) The physicochemical aspect of the unsteady state of metasomatic crystal production. *Geochem Intern* 33:8:117–128 (Russ.)
- Glikin AE (1996b) About equilibrium supercooled solutions related to formation of isomorphic-mixed crystals. *Zapiski Vsesoyuz Miner Obsh* 5:103–111 (Russ.)
- Glikin A (2002) Features of rapakivi origin in terms of polymineral-metasomatic crystallogenesis. *Miner Soc Poland. Spec Papers* 20:17–19.
- Glikin AE (2004) Polymmineral-metasomatic crystallogenesis. *Zhurnal "Neva"*, St. Petersburg (Russ.)

- Glikin AE (2007) On the genetic nature of isomorphism: mechanism of component selection during crystal growth. *Geol Ore Deposits* 49:8:806–810
- Glikin AE, Kasatkin AP (1976) A method for determining specific weight of solids and liquids. Authorship certificate 540195. *Bull Invent* 47 (Russ.)
- Glikin AE, Kaulina TV (1988) Kinetic model of epitaxial growth of crystals. *Zapiski Vsesoyuz Miner Obsh* 5:609–615 (Russ.)
- Glikin AE, Sinai MYu (1983) Experimental genetic study of monocrystal pseudomorphs. *Zapiski Vsesoyuz Miner Obsh* 6:742–748 (Russ.)
- Glikin AE, Sinai MYu (1988) Genetic role of crystal inclusions in metasomatism. In: Kalyuzhny VA (ed) *Geochemistry and thermobarometry of endogenous fluids*. Naukova Dumka, Kiev (Russ.)
- Glikin AE, Sinai MYu (1991) Morphological and genetic classification of crystal replacement products. *Zapiski Vsesoyuz Miner Obsh* 1:3–17 (Russ.)
- Glikin AE, Grunskii OS, Kaulina TV, et al. (1988) Crystallogenic aspect of experimental mineralogy. In: Zharikov VA (ed) *Experiment in mineralogy*. Nauka, Moscow (Russ.)
- Glikin AE, Leontyeva OA, Sinai MYu (1994a) Mechanisms of exchange of isomorphic components between crystal and solution and macrodefectiveness in secondary crystals. *J Struct Chem Russ* 35:5:642–646
- Glikin AE, Leont'eva OA, Sinai MYu, Zorina ML, Kirillov AS, Tabuns EV (1994b) Exchange with isomorphic components between a crystal and solution. *Vestnik St. Petersburg Univ* 4 Ser 2:11:111–112 (Russ.)
- Glikin AE, Kovalev SI, Rudneva EB, Kryuchkova LYu, Voloshin AE (2003) Phenomena and mechanisms of mixed crystal formation in solutions I. General concept on the example of the system  $\text{KHC}_8\text{H}_4\text{O}_4\text{-RbHC}_8\text{H}_4\text{O}_4\text{-H}_2\text{O}$ . *J Cryst Growth* 255:155–162
- Glikin AE, Kryuchkova LYu, Plotkina YuV (2007) Crystallogenic grounds of isomorphism: experimental data and theoretical approach. *Zapiski Russ Miner Soc, Crystallogenesis and Mineralogy, Spec Issue* 7–35. Nauka, St. Petersburg
- Glover ED, Sippel RE (1962) Experimental pseudomorphs: replacement of calcite by fluorite. *Geol Soc Amer Spec Papers* 68:1156–1165
- Goldschmidt V (1913) *Atlas der Kristallformen*. C. Winter. Universitätsbuchhandlung, Heidelberg
- Gordienko VV, Krivovichev VG, Syritso LF (1987) *Metasomatites of pegmatite fields*. Leningrad State Univ, Leningrad (Russ.)
- Grant JA (1986) The isocon diagram – a simple solution to Gresens' equation for metasomatic alteration. *Econ Geol* 81:1976–1982
- Grigor'ev DP (1948) Regularities of copper sulfide formations in deposits of the Middle Urals. *Zapiski Vsesoyuz Miner Obsh* 1:32–41 (Russ.)
- Grigor'ev DP (1961) *Ontogeny of Minerals*. Lvov University, Lvov (Russ.)
- Grigor'ev DP, Zhabin AG (1975) *Ontogeny of minerals: Individuals*. Nauka, Moscow (Russ.)
- Grogan RM (1949) Structures due to volume shrinkage in the bedding-replacement fluorspar deposits of Southern Illinois. *Econ Geol* 44:606–616.
- Haiüy RJ (1801) *Trate de mineralogie*. Chez Louis, Paris.
- Johannes W, Koepke J, Behrens H (1994) Partial melting reactions of plagioclases and plagioclase-bearing systems. In: Parsons I (ed) *Feldspars and their reactions*. NATO ASI series. Kluwer, Dordrecht, The Netherlands
- Karpov GA (1970) Experimental mineral formation in hydrothermal wells. In: *Mineralogy of hydrothermal systems of Kamchatka and the Kuril Islands*. Nauka, Moscow (Russ.)
- Kasatkin AP, Glikin AE (1974) A method for determining gas volume in a closed hole of changeable volume. Authorship certificate 429281. *Bull Invent* 19 (Russ.)
- Kazitsyn YuV (1979) *Metasomatism in the earth crust*. Nedra, Leningrad (Russ.)
- Kazitsyn YuV, Rudnik VA (1968) *A manual to the calculation of the matter and internal energy balance in metasomatic rocks*. Nedra, Moscow (Russ.)
- Kirgintsev AN (1976) *Sketches on thermodynamics of aqueous salt systems*. Nauka, Novosibirsk (Russ.)
- Kleber W, Pascal I (1960) Über das Achtaragdit-Problem. *Neues Jb Miner Abh* 94:2:1266–1276

- Korzhinskii DS (1952) Granitization as a magmatic replacement. *Izvestia Acad Sci USSR, Ser geol nauk* 2:56–69 (Russ.)
- Korzhinskii DS (1955) Sketches of metasomatic process. Main problems in the concept of magmatogene ore deposits. Acad Sci USSR, Moscow (Russ.)
- Korzhinskii DS (1970) Theory of metasomatic zoning. Clarendon Press, Oxford
- Korzhinskii DS (1993) Selected works. Principles of metasomatism and metamagmatism. Nauka, Moscow (Russ.)
- Kostov I (1956) Cordierite pseudomorphs. In: Ann publications Univ Sofia, Biol-Geol-Geogr Dept 2 – Geol XLIX 1954/55. Univ Sofia, Sofia (Bulgarian)
- Kostov I (1968) Mineralogy. Oliver and Boyd, London
- Krasnova NI, Petrov TG (1997) Genesis of mineral individuals and aggregates. *Nevskii Kur'er*, St. Petersburg (Russ.)
- Krotov BP (1925) Some pseudomorphs after rock-salt. *Zapiski Vsesoyuz Miner Obsh* 1:25–31 (Russ.)
- Kryuchkova LYu, Glikin AE, Voloshin AE et al. (2002) Kinetic and morphological phenomena of growth and isomorphic replacement of mixed crystals in solutions (in the series (Co,Ni)(NH<sub>4</sub>)<sub>2</sub>(SO<sub>4</sub>)<sub>2</sub>·6H<sub>2</sub>O). *Zapiski Vsesoyuz Miner Obsh* 3:62–77 (Russ.)
- Kukui AL (1969) Some transformations of minerals in NiSO<sub>4</sub>-H<sub>2</sub>O system. *Zapiski Vsesoyuz Miner Obsh* 1:94–96 (Russ.)
- Kulkov AM, Glikin AE (2007) Replacement of nickelhexahydrate with retgersite: polymorphic-metasomatic structures. *Geol Ore Deposits* 49:8:159–164.
- Landa EA (1979) Some facts about formation of metacrystals and blastocrystals. In: Works of All-Union Geol Inst 287:43–56 (Russ.)
- Laemlein GG (1929) Sekundäre Flüssigkeitseinschlüsse in Mineralen. *Zs Krist* 71:3:237–256
- Laemlein GG (1973) Morphology and genesis of crystals. Nauka, Moscow (Russ.)
- Lazarenko EK (1979) An attempt on genetic classification of minerals. *Naukova Dumka*, Kiev (Russ.)
- Levinson-Lessing FYu, Vorob'eva OK (1929) Some aspects of study of orbicular structures in igneous rocks. *Doklady Acad Sci USSR* (Russ.)
- Levinson-Lessing FYu, Struve EA (1963) Petrographical Dictionary. Gosgeoltekhizdat, Moscow (Russ.)
- Liesegang RE (1913) Geologische Diffusionen. Steinkopf, Dresden-Leipzig
- Lindgren W (1918) Volume changes in metamorphism. *J Geol* 26:542–554
- Lindgren W (1925) Metasomatism. *Bull Geol Soc Amer* 36:1:1–114 and 248–253
- Lindgren W (1933) Mineral deposits. McGraw-Hill, New York
- Lyakhovich VV (1954) New data on mineralogy of the Vilyui achtarandite deposit. In: Proc East-Siberian Branch Acad Sci USSR. Ser geol nauk 1. Acad Sci USSR, Moscow (Russ.)
- Lutz N (1989) Pseudomorphosen. *Fundgrube* 25:2:54–59
- MacKensie WS, Guilford C (1980) Atlas of rock-forming minerals in thin sections. Longman, New York
- Makhmudov SA, Babaev IA (1972) A new type of pseudomorph from the Dashkesan deposit of iron ore (Azerbaijan). *Zapiski Vsesoyuz Miner Obsh* 4:490–492 (Russ.)
- Nakovnik NI (1949) On metasomatic mineral formation and the equal volume rule. *Zapiski Vsesoyuz Miner Obsh* 4:270–272 (Russ.)
- Nakovnik NI (1958) Determining the quantitative transformations of matter in the course of hydrothermal metamorphism. *Zapiski Vsesoyuz Miner Obsh* 4:401–417 (Russ.)
- Nakovnik NI (1964) Determining the “removal-addition” of matter in the process of metasomatism and the Lindgren's rule. *Zapiski Vsesoyuz Miner Obsh* 1:110–113 (Russ.)
- Nazimova YuV (1984) Ultrabasites of Kamchatka and related copper-nickel ores. Diploma work. Geochem Dept St. Petersburg Univ, St. Petersburg
- Pelican A (1902) Pseudomorphose von Magnetit und Rutil nach Ilmenit. *Tschemm Miner Petrogr Mitt* 21:226
- Petrov TG, Treivus EB, Punin YuO et al. (1983) Growing crystals from solutions. Nedra, Leningrad (Russ.)
- Pidjan GO (1950) About chalcopyrite pseudomorphs after pyrite. *Zapiski Vsesoyuz Miner Obsh* 4:301–302 (Russ.)

- Plotnikov MA, Tatarskii VB (1946) A calcite pseudomorph after gaylussite from the tatar stage of the river Mezen'. *Zapiski Vsesoyuz Miner Obsh* 3:234–236 (Russ.)
- Polovinkina YuI (1966) Structures and textures of igneous and metamorphic rocks. Nedra, Moscow (Russ.)
- Popov VA (1984) Applied crystal morphology of minerals. Academy of Science USSR. Sverdlovsk (Russ.)
- Pospelov GL (1973) Paradoxes, physicochemical nature and mechanisms of metasomatism. Nauka, Novosibirsk (Russ.)
- Pospelov GL (1976) Replacements and intrusions of magmatism and ore formation. Nauka, Novosibirsk (Russ.)
- Pospelov GL, Kaushanskaya PI, Lapin SS (1961) On formation of the vein-shaped mineralization forms outside the fissures. *Geol Ore Deposits* 2:45–56 (Russ.)
- Prodan EA (1990) Topochemistry of crystals. Nauka i Tekhnika, Minsk (Russ.)
- Ramdohr P (1955) Die Erzminerale und ihre Verwachsungen. Akad. Verl, Berlin
- Rudashevskii NS (1984) Pseudomorphs after inclusions of olivine in the grains of platinoids and the nature of platinum mineralization in ultramafites. *Zapiski Vsesoyuz Miner Obsh* 2: 186–195 (Russ.)
- Rudenko SA (1951) Examination of perthite accretions of feldspars in connection with their internal structure. In: Shafranovskii II, Mikheev VI (eds) *Kristallografiya. Proc Fedorov Session. Ugletekhizdat, Moscow-Leningrad* (Russ.)
- Rudenko SA (1966) Skeletal growth of crystals in rocks and ores. *Zapiski Vsesoyuz Miner Obsh* 2:158–168 (Russ.)
- Rudnik VA (1962) Determination of quantitative matter changes in the course of a metasomatic process. *Zapiski Vsesoyuz Miner Obsh* 6:683–689 (Russ.)
- Rudnik VA (1978) The volume and reference atomic petrochemical converting systems. Nedra, Leningrad (Russ.)
- Saranchina GM, Kozhevnikov VN (1985) Fedorov's method. Nedra, Leningrad (Russ.)
- Saranchina GM, Shinkarev NF (1973) Petrology of magmatic and metamorphic rocks. Nedra, Leningrad
- Shergin IV (1970) Forms of origin, growth, and transformation of sillimanite. In: *Ontogenetic methods in the study of minerals*. Nauka, Moscow (Russ.)
- Shinkarev NF, Rundkvist ND (1986) Some aspects of rapakivi granite formation. *Zapiski Vsesoyuz Miner Obsh* 6:643–649 (Russ.)
- Sinai MYu (1991) Morphology and genesis of the products of metasomatic replacement of monocrystals in model systems. PhD thesis. Leningrad State Univ, Leningrad (Russ.)
- Sinai MYu, Glikin AE (1989) Formation of case-like and negative pseudomorphs. *Geol Explor* 4:31–35 (Russ.)
- Sinai MYu, Shakhmuradyan AR (1995) Comparison of natural and experimental products of crystal replacements. *Zapiski Russ Miner Obsh* 5:47–58 (Russ.)
- Slodkevich VV (1982) Paramorphs of graphite after diamond. *Zapiski Vsesoyuz Miner Obsh* 1:13–33 (Russ.)
- Stern KH (1954) The Liesegang phenomenon. *Chem Rev* 54:79–99
- Strunz H (1957) Mineralogische tabellen. Akademische Verlagsgesellschaft Geest & Portig K.-G., Leipzig
- Strunz H (1982) Pseudomorphosen – der derzeitige Kenntnisstand. Versuch einer Klassifizierung. *Der Aufschluss* 33:314–342
- Sudovikov NG (1967) Problems of rapakivi and later orogenic intrusions. Nauka, Moscow-Leningrad (Russ.)
- Tananaev NA (1954) Drop method. Goskhimizdat, Moscow-Leningrad (Russ.)
- Treivus EB (1979) Kinetics of crystal growth and dissolution. Leningrad University, Leningrad (Russ.)
- Treivus EB, Rozhnova GA (1962) Experimental reproduction of metasomatism in water-soluble salts. *Zapiski Vsesoyuz Miner Obsh* 2:219–222 (Russ.)
- Tsuchiyama A. Dissolution kinetics of plagioclase in the melt of the system diopside-albite-anorthite, and origin of dusty plagioclase in andesites. *Contrib Miner Petrol* 1985:89:1–16

- Velikoslavinskii DA (1953) Petrology of the Vyborg massif of rapakivi. Proc Lab Geol Pre-Cambrian Acad Sci USSR 3. Acad Sci USSR, Leningrad 5–142 (Russ.)
- Velikoslavinskii DA, Birkis AP, Bogatkov OA et al. (1978) Anorthosite-rapakivi-granite formation. East European platform. Nauka, Leningrad (Russ.)
- Voloshin AE, Glikin AE, Kovalev SI, et al. (2001) The mechanisms of mixed crystal formation in KAP–RbAP and KDP–ADP systems. The Thirteenth Intern Conf Cryst Growth. Abstracts. Kyoto, Japan
- Voloshin AE, Kovalev SI, Rudneva ED, Glikin AE (2004) Phenomena and mechanisms of mixed crystal formation in solutions II. Mechanism of interface processes // J. Cryst Growth 261:105–117
- Wark DA, Stimac JA (1992) The origin of feldspars with envelope (rapakivi structure): experimental evidence of dissolution. Contrib Miner Petrol 111:3:345–361
- Woensdregt CF, Glikin AE (2005) Ex situ scanning force microscopic observation of growth and dissolution phenomena on {010} surfaces of potassium hydrogen phthalate crystals (KAP) caused by isomorphic exchange reactions. J Cryst Growth 283:3–4:523–532
- Yakshin VI (1962) Rutilization of grothite in the alpine type veins. Zapiski Vsesoyuz Miner Obsh 2:222–225 (Russ.)
- Yardley BWD, MacKensie WS, Guilford C (1990) Atlas of metamorphic rocks and their textures. Longman, New York
- Yushkin NP (1990) Calcite pseudomorphs after gaylussite crystals. Zapiski Vsesoyuz Miner Obsh 2:75–81 (Russ.)
- Zaitsev AN, Sinai MYu (2001) Sphalerite of carbonatite series rocks of the Khibini massif: mineralogy, formation conditions and crystallogenic simulations. Zapiski Russ Miner Obsh 2:84–92 (Russ.)
- Zaitsev AN, Sinai MYu, Shakhmuradyan AR (1998) Peculiarities of chemical composition and interrelations of pyrrhotine and pyrite in carbonatite series rocks of the Khibini alkaline massif. Zapiski Russ Miner Obsh 4:110–119 (Russ.)
- Zaraiskii GP (1991) Zonality and conditions of formation of metasomatic rocks. Nauka, Moscow (Russ.)
- Zaraiskii GP (1993) Progress in the metasomatic zonality concept. Petrologia 1:1:4–28 (Russ.)
- Zaraiskii GP, Shapovalov YuB, Belyaevskaya ON (1981) Experimental investigations of acidic metasomatism. Nauka, Moscow (Russ.)
- Zavaritskii AN (1953) Development of the Fedorov's universal method and its use in study of feldspars. In: Fedorov's universal object stage. Acad Sci USSR, Moscow (Russ.)
- Zhabin AG (1960) Pseudomorph of actinolite after calcite. Zapiski Vsesoyuz Miner Obsh 1:106–107 (Russ.)
- Zhabin AG, Rusinov VL (1973) Classification and genesis of pseudomorphs. Zapiski Vsesoyuz Miner Obsh 3:241–253 (Russ.)
- Zhabin AG, Samsonova NS (1975) Indications of the former presence of pyrrhotine in pyrite deposits. Zapiski Vsesoyuz Miner Obsh 3:346–350 (Russ.)

## Chapter 2

# Joint Growth of Crystals of Different Phases

Our investigations of multicomponent systems showed that joint growth of crystals formed by different phases having stable compositions is affected by mutual influence of the crystals, i.e., phenomenon which does not occur in binary solutions. This phenomenon can be illustrated by processes taking place during joint growth of potassium and sodium chloride crystals in  $\text{KCl-NaCl-MgCl}_2\text{-H}_2\text{O}$  system, which is widely distributed in nature and is of industrial and scientific importance (Glikin et al. 2001).

Previously, this system was used as a convenient object for morphological and kinetic investigations of individuals growing in  $\text{KCl-H}_2\text{O}$  and  $\text{NaCl-H}_2\text{O}$  binary solutions (both pure and containing various admixtures) (Kleber 1964; Panov et al. 1969; Punin 1969; Punin and Petrov 1972; Treivus et al. 1985; König et al. 1987), as well as for kinetics study of mass precipitation (Khamskii 1979). The present chapter deals with behavior of individual KCl and NaCl seeds in three- and four-component solutions in the region of KCl and NaCl eutonic concentration and discusses previously ignored relationship between the process kinetics and essential features of phase equilibria.

## 2.1 Growth and Dissolving in Supercooled Solutions<sup>1</sup>

### 2.1.1 Technique

Crystallizations were conducted in solutions having eutonic compositions (binary equilibrium for KCl and NaCl) and containing the following concentrations of  $\text{MgCl}_2$ : 0.0, 1.06, 3.36, 7.10, 10, 12, and 20 wt% (0–30 g/100 g of  $\text{H}_2\text{O}$ ).

Potassium and sodium chlorides used to prepare the process solutions and seeds had been precipitated from solutions of natural sylvinit (Berezниковsky field, the Cisural region). Such technique ensured the absence of amines contaminating

---

<sup>1</sup> According to original experimental data provided by Dr. Yu.V. Plotkina (Plotkina 1998; Glikin et al. 2001).



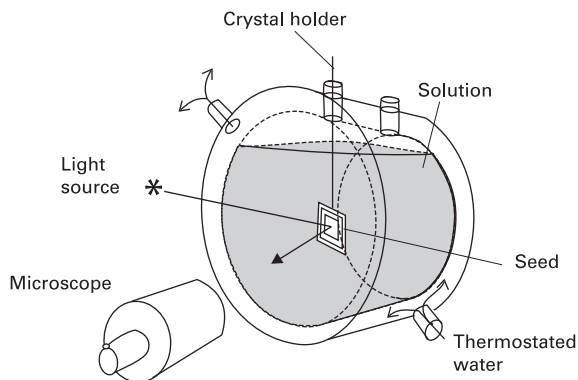
industrial reactants, which considerably affect both morphology and kinetics of growing KCl crystals (Punin 1969). Crystallization methods were used for primary separation of sylvinite from ferric oxides and for purification of experimental materials.

The process solutions containing eutonic concentrations of KCl and NaCl were prepared by means of combined mixing-in the reactants for 3–5 days at 35°C and  $40 \pm 0.1^\circ\text{C}$  in 0.5–0.6L of distilled water with or without addition of  $\text{MgCl}_2$  (Table 2.1) using ~10% excess of each reactant. All experiments were preceded by saturation temperature checkouts, which were conducted using a microcrystallization device with  $\pm 0.1^\circ\text{C}$  admissible measurement error. The device (Petrov et al. 1969) is schematically shown in Fig. 2.1. Each correspond-

**Table 2.1** Compositions (wt%) and saturation temperatures ( $^\circ\text{C}$ ) of KCl and NaCl eutonic solutions containing various concentrations of  $\text{MgCl}_2$

Experimental series	Components, wt%			Saturation temperature ( $^\circ\text{C}$ )
	$\text{MgCl}_2$	KCl	NaCl	
0	–	12.41	19.42	35.0
1	1.06	11.88	18.18	Idem
2	3.36	10.44	15.82	Idem
-	–	19.46	29.57	40.0
3	5.28	11.76	15.14	Idem
4	7.10	10.76	11.25	Idem
5	10.(35)	9.(75)	10.(73)	Idem
6	12.(92)	8.(37)	9.(06)	Idem
7	20.(01)	6.(02)	4.(03)	Idem

**Note:** At a low  $\text{MgCl}_2$  content the measurement error is about 0.01 wt%; this value increases when  $\text{MgCl}_2$  content exceeds 10 wt% (brackets enclose the doubtful values). Chemical assays were made in Russian Research Institute of Mineral-Salt Production. Compositions of triple-phase solutions at 40°C are cited according to Solubility (1961–1970).



**Fig. 2.1** Microcrystallization cell used to study morphology and kinetics of crystal formation and equilibria in solutions

ing saturation temperature was defined on the basis of the seed growing and dissolving signs, which appeared at higher and lower temperatures in comparison to that of equilibrium, respectively. Temperatures of saturation for KCl and NaCl, respectively, in four-component solutions containing known contents of other salts (Table 2.1) were determined in analogous manner in order to refine the phase diagram.

Each experimental series was carried out with the same solution, which was sealed and kept in a thermostat at the temperature exceeding that of saturation by 2–3°C. Each series took from 3 to 6 months to complete, and the differences in corresponding phase saturation temperatures for KCl and NaCl, which did not exceed 0.5°C in the beginning of a series, could reach 1.0°C by its end as a result of partial water evaporation.

Morphological and kinetic observations were conducted in the microcrystallization device. Supercooling values  $\Delta T$  for the solutions were 1.0°C and 2.0°C, with a solution volume in the cell being 25 mL. Seeds of KCl were transparent, while those of NaCl were impregnated with solution microinclusions; both salts formed slightly flattened, well-faceted cubes with 0.3–0.5 cm edges. Using seeds of such dimensions in the experiment allowed to minimize supersaturation lowering, which was 0.06 and 0.07% at  $\Delta T = 1.0$  and 2.0°C for KCl, and 0.03 and 0.04% at  $\Delta T = 1.0$  and 2.0°C for NaCl, respectively.

After defining the saturation conditions, a new, already slightly dissolved seed of KCl or NaCl was inserted into each tested solution. The seed regenerated in 10–15 min with the degree of supercooling being kept constant; after the indicated period, the growth rate and morphological characteristics of the crystals, including facet pattern, surface texture, and the properties of an excrescence phase (crystal shape and size, crystal distribution and orientation at the seed surface) were identified.

The seed growing rates for the first phase and the second phase inserted sequentially into the solution were measured as a result of the {100} crystal plane shift along the perpendicular axis in 10 min, which was observed with the aid of an ocular micrometer. Examination of each crystal took from 40 min to 1 h. Kinematical curves showing time variations of the growth rates were plotted on the basis of four to six measurements taken under stationary conditions. Usually by the end of each experiment the former seed was densely covered with grown crystals of the other phase. Morphology of these overgrowth formations and their orientation distribution were studied separately under an electron microscope. For both degrees of supercooling (1.0 and 2.0°C) investigations were conducted on 20 seeds of each KCl and NaCl.

The Schreinemakers concentration diagrams were used for genetic interpretations of crystallization characteristics (Anosov et al. 1976, pp. 176 and 280–281). As it was mentioned in Chapter 1, these diagrams provide visual representation of mutual influence of salts present in a solution upon the solubility of each other that makes them the most informative tool for crystal and genetic analysis of three-component and more complex systems (Glikin 1996a, b).

### 2.1.2 Crystal Morphology

In binary solutions crystals of both KCl and NaCl practically always take cubic shape. Octahedral crystals of KCl are only formed in the solutions with extremely low levels of supersaturation (Punin and Petrov 1972). Greater degrees of supercooling cause more pronounced roughening of the surface texture of the crystals of both phases that becomes apparent in thickening the growth layers and covering the surface of the crystal with oriented and disoriented bodies divided by deep channels (Bunn 1964; Punin and Petrov 1972).

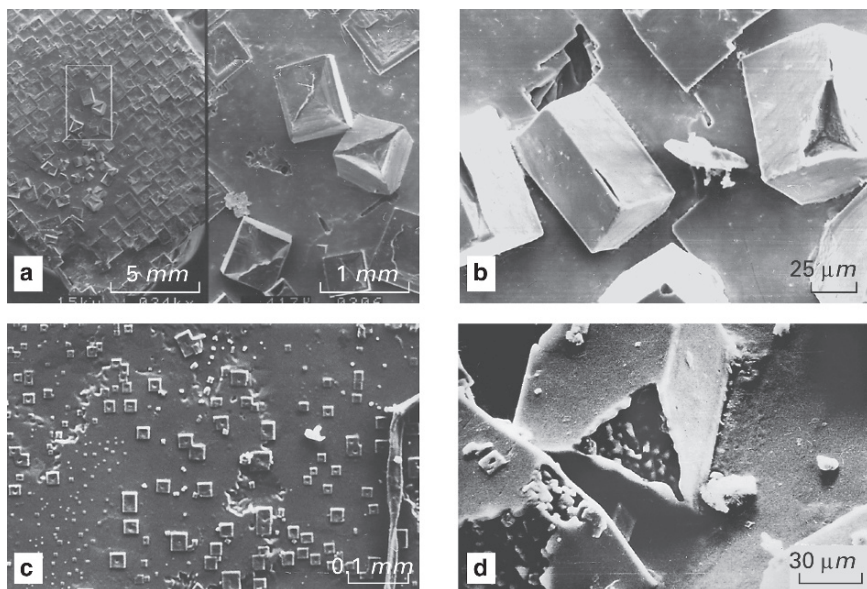
In ternary eutonic solutions of KCl and NaCl the crystal face patterns and surface topography of both phases (Fig. 2.2) vary with time that results in formation of octahedral faces on the cubic seeds or gaps in the places where these faces should be as a result of slowing-down along the [111] direction. In most cases, geometry of gaps replicates triangular form of the entire face and the gap surfaces bear caverns (Fig. 2.2d). After 5–10 min from the beginning of the experiment, the seed surfaces gradually become covered with spontaneously growing crystals of the partner phase. In about an hour or a little more after the addition of seeds, these overgrowing crystals block any further growth or dissolution completely.

In eutonic solutions, crystals of KCl and NaCl have different morphological characteristics. The surface texture of KCl crystals undergoes roughening with increasing degree of supercooling or when the crystal is kept in the solution with maintaining a constant level of supercooling. In this case, outgrowths of the partner-phase are distributed irregularly and arranged in the facet periphery; this distribution, however, becomes more regular as supercooling degree increases. On the contrary, the surface texture of NaCl crystals is smoothed out with enhancement of supercooling; the seed surface is characterized by relative uniformity of the partner-phase distribution, which can ultimately cover the entire surface of the seed.

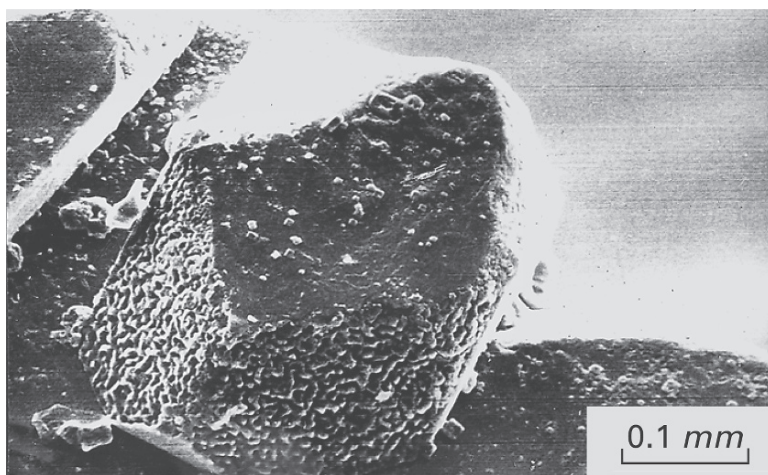
In the presence of  $\text{MgCl}_2$ , the faceting of KCl and NaCl crystals (both seeds and outgrowths) is represented by combinations of cubes and octahedrons. Formation of octahedrons on the seeds of the both phases occurs when  $\text{MgCl}_2$  concentration does not exceed 10 wt%. When  $\text{MgCl}_2$  content surpasses the above level, the octahedral formations disappear under the cover of newly growing crystals. If the content of  $\text{MgCl}_2$  is about 5.28 wt%, the facets of accretive KCl crystals (mostly octahedral) are curved and bear caverns (Fig. 2.3). Addition of  $\text{MgCl}_2$  (of any concentration in the above range) results in development of surface imperfection (cracking, caverns, macrolayering, and mosaicity) in both KCl and NaCl crystals.

Presence of  $\text{MgCl}_2$  in the solutions was observed to cause formation of partner-phase crystals on the seeds of the both substances. It is interesting to point out, that the greater is the  $\text{MgCl}_2$  content, the greater becomes the number of NaCl excrescences on KCl crystals, and the lesser is amount of KCl formations on NaCl phase.

Both combinations of the excrescence phase crystals (KCl on NaCl and NaCl on KCl) form two types of textures (Glikin and Plotkina 1999). The texturing is considered in detail in Chapter 6, so just a brief overview shall be given below. *Epitaxial texture*,  $\{100\}, [100]_{\text{KCl}} \parallel \{100\}, [100]_{\text{NaCl}}$  (Figs. 2.2a, c), is formed in



**Fig. 2.2** Morphology of crystals grown in KCl–NaCl–H<sub>2</sub>O solution **a, b** – Excrescences of NaCl on KCl substrate (**a** – general view showing elements of epitaxial and “vertical” textures; **b** – “vertical” texture). **c, d** – Excrescences of KCl on NaCl substrate (**c** – general view – epitaxial texture; **d** – gaps in the places of octahedron faces)



**Fig. 2.3** Surface of a KCl octahedral crystal grown on a NaCl crystal ( $\Delta T = 1.0^\circ\text{C}$ , 5.28 wt% of  $\text{MgCl}_2$ )

accordance with well-known Royer's principles of crystal chemistry (Royer 1928) and with participation of factors breaking parallelism of  $[100]_{\text{KCl}}$  and  $[100]_{\text{NaCl}}$  in coalescences of structurally similar  $\{100\}_{\text{KCl}}$  and  $\{100\}_{\text{NaCl}}$  faces (Glikin and Kaulina 1988; Glikin and Plotkina 1999). Simultaneously, growing cubic crystals can adhere to a substrate with their edges or vertexes, forming a "vertical texture" (Glikin and Kaulina 1988; Glikin and Plotkina 1999). In this case, the  $L_2$  or  $L_3$  axes of the cube are perpendicular to the substrate plane (Figs. 2.2*b*, *d*). The number of crystals forming the vertical structure does not exceed 10% of the total amount of the accretive crystals. Any influence of  $\text{MgCl}_2$  upon formation of these structures has not been revealed.

When  $\text{MgCl}_2$  content ranges from 12 to 20 wt%, formation of carnallite grains ( $\text{KMgCl}_3 \cdot 6\text{H}_2\text{O}$ ) was observed on the surface of KCl crystals. It is essential that this phenomenon takes place beyond the carnallite thermodynamic stability region: according to the phase diagram, carnallite crystallization at 35–40°C becomes possible only when  $\text{MgCl}_2$  content is about 25 wt% or more. Carnallite forms random aggregates of unfaceted individuals (Fig. 2.4*a*). After some time (up to 2 h), the amount of carnallite on the surface increases (Fig. 2.4*b*) and, ultimately, this mineral together with NaCl crystals block the entire seed surface. Unlike KCl substrates, crystals of NaCl can host only a few carnallite excrescences.

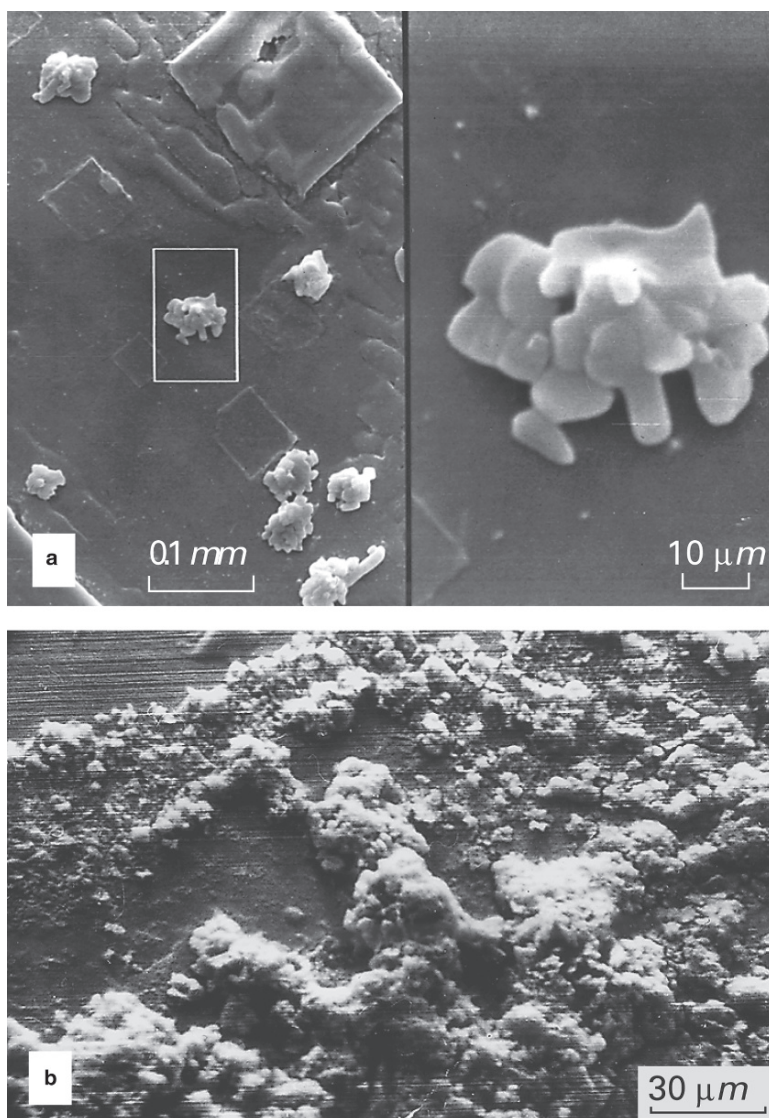
Unfortunately, lack of experimental data does not allow us to generalize the regularities of individual morphogenesis and explain its mechanisms. Nevertheless, influence of solution admixtures upon adsorption and diffusion processes can be stated unambiguously.

### 2.1.3 Kinetics

Crystallization of KCl and NaCl in ternary and quaternary solutions of the system in question differs from the processes proceeding in binary solutions of these salts. The most peculiar phenomenon occurring due to co-crystallization in the vicinity of the eutonic region is instability of the growth processes, which can be even reversed to dissolving at constant conditions of component concentration, temperature, and supercooling. It is interesting to point out that the growth rate can become nonmonotonous depending upon the contents of other components in solution.

*In supercooled binary aqueous solutions* of KCl and NaCl there were observed common kinetic phenomena, viz.: growth or its absence (described previously as "stability region" or "dead area" – Punin 1969; Treivus et al. 1985).

According to the data obtained by Punin (1969), the absolute growth rates of KCl isolated cubic crystals range from 0.1 to 18.0  $\mu\text{m}/\text{min}$ , when saturation temperature  $T_{\text{sat}}$  ranges from 5°C to 85°C, and supercooling  $\Delta T$  varies from 0.2°C to 2.0°C. In our experiments ( $T_{\text{sat}} = 40^\circ\text{C}$ ,  $\Delta T = 1.0$  and  $2.0^\circ\text{C}$ ) these parameters were 4.2 and 10.0  $\mu\text{m}/\text{min}$ , correspondingly. There is a direct, but not monotonic correlation between the growth rate and supercooling degree. The growth rates measured



**Fig. 2.4** Carnallite grains grown on the surface of an octahedral KCl crystal, which were formed beyond the bounds of the carnallite stability region (12.9 wt% of  $\text{MgCl}_2$ ) **a** – Simultaneous growth with NaCl crystals. **b** – Grain cluster formed in 2h after the beginning of the experiment

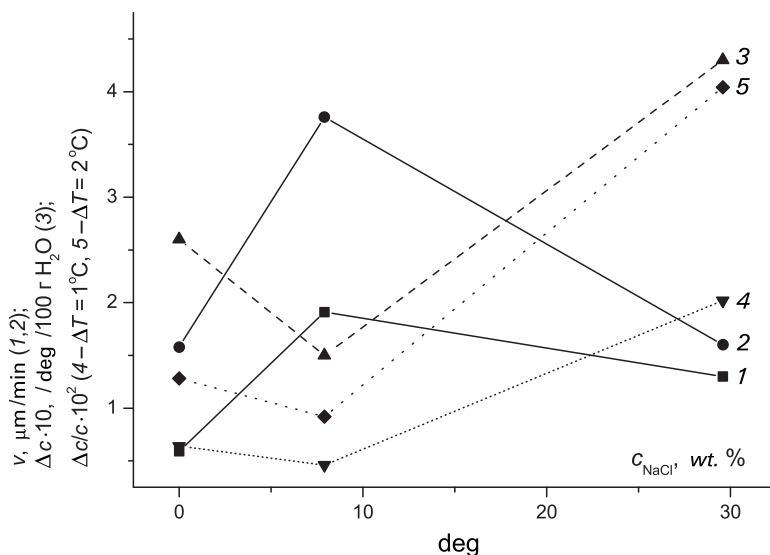
by us under the above conditions, being 0.59 and 1.58  $\mu\text{m}/\text{min}$ , appeared to be significantly lower (by an order of magnitude) in comparison with Punin's data. This difference is most likely due to the use of different reactants: in his experiments Punin used a reactant repeatedly purified by means of zone smelting, while

in our experiments we used the reactant obtained from natural ores. According to published data, growth of isolated crystalline seeds of KCl is diffusion-controlled (Kleber 1964; Panov et al. 1969; Punin and Petrov 1972; König et al. 1987).

According to the data obtained by Treivus et al. (1985), the absolute values of growth rates for NaCl isolated cubic crystals (chemically pure reactant) were within the range of 0.0–3.5  $\mu\text{m}/\text{min}$  (ranges: for saturation temperature  $T_{\text{sat}} = 33\text{--}48^\circ\text{C}$ , for supercooling  $\Delta T \approx 12\text{--}25^\circ\text{C}$ ), and at  $\Delta T = 1.0\text{--}2.0^\circ\text{C}$  the “dead area” was observed. We found a direct correlation between the growth rates of NaCl cubes in solution having saturation temperature of  $40^\circ\text{C}$  and supercoolings  $\Delta T = 1.0$  and  $2.0^\circ\text{C}$ ; the growth rates were 2.38 and 2.98  $\mu\text{m}/\text{min}$ , correspondingly. Growth rates of NaCl determined in mass crystallization process (Rumford and Bain 1960; Panov et al. 1969) and specific conditions of formation of fibrous crystals (“whiskers”) (Hayashi and Shichiri 1974) are not to be compared with the growth rates of isolated seeds.

The growth rates of cube facets of NaCl and KCl crystals in binary solutions can vary in wide ranges, being 0–45  $\mu\text{m}/\text{min}$  ( $\Delta T = 1.0^\circ\text{C}$ ) and 0.5–6  $\mu\text{m}/\text{min}$  ( $\Delta T = 2.0^\circ\text{C}$ ) for KCl, and 0–5  $\mu\text{m}/\text{min}$  ( $\Delta T = 1.0^\circ\text{C}$ ) and 0–7.5  $\mu\text{m}/\text{min}$  ( $\Delta T = 2.0^\circ\text{C}$ ) for NaCl. It is to be noted that within the temperature range of  $5\text{--}85^\circ\text{C}$  the crystals of KCl can show several anomalous bursts of the growth rates (up to 30%). These anomalies are accounted for by structural rearrangements occurring in the solutions (Punin and Petrov 1972). This phenomenon can be discovered only in high precision experiments. Random selection of the process variables that inevitably involve hitting the maxima or minima of the growth rate domain can create a wrong impression of the extended dispersion of the data. At the same time, measurements made in profoundly anomalous regions can result in real extension of data dispersion due to temperature variations within the margin of the temperature error.

*Crystallization of individual seeds of KCl and NaCl in ternary eutonic solutions* is not covered in literature except for some indications of the growth rate anomalies observed for KCl crystals in industrial solutions, which have compositions close to those of eutonic solutions (Punin 1969). We observed (Glikin et al. 2001) that the average growth rates of cubic faces of both investigated substances tend to increase with enhancing the supercooling. Thus, for KCl crystals at saturation temperature of  $40^\circ\text{C}$  and  $\Delta T = 1.0$  and  $2.0^\circ\text{C}$  the observed rates were  $1.3 \pm 0.01$  and  $1.6 \pm 0.01$   $\mu\text{m}/\text{min}$ , correspondingly; for NaCl crystals these values were  $0.8 \pm 0.01$  and  $0.9 \pm 0.02$   $\mu\text{m}/\text{min}$ . The values were averaged on the results of 20 experiments, which provided narrow confidence intervals. It can be seen that in ternary systems the growth of KCl crystals at  $\Delta T = 1.0^\circ\text{C}$  accelerates significantly, while growth rates of NaCl decrease substantially in comparison with growth rates obtained in their binary solutions; at  $\Delta T = 2.0^\circ\text{C}$  the growth rates for KCl are close to their values obtained for binary solutions, while growth of NaCl crystals becomes considerably slower. It should be noted that introduction of 7.9 wt% of NaCl into a KCl solution (approximately one third of NaCl content in eutonic solution at  $40^\circ\text{C}$ ) also increases growth rate of KCl, which can reach up to 1.91 and 3.76  $\mu\text{m}/\text{min}$  for  $\Delta T = 1.0$  and  $2.0^\circ\text{C}$ , respectively. The above figures exceed KCl growth rates in eutonic solution (1.3 and 1.6  $\mu\text{m}/\text{min}$  at  $\Delta T = 1.0$  and  $2.0^\circ\text{C}$ , respectively). In other words, function of KCl growth rate versus NaCl content in the solution has a maximum (see Fig. 2.5, curves 1 and 2).



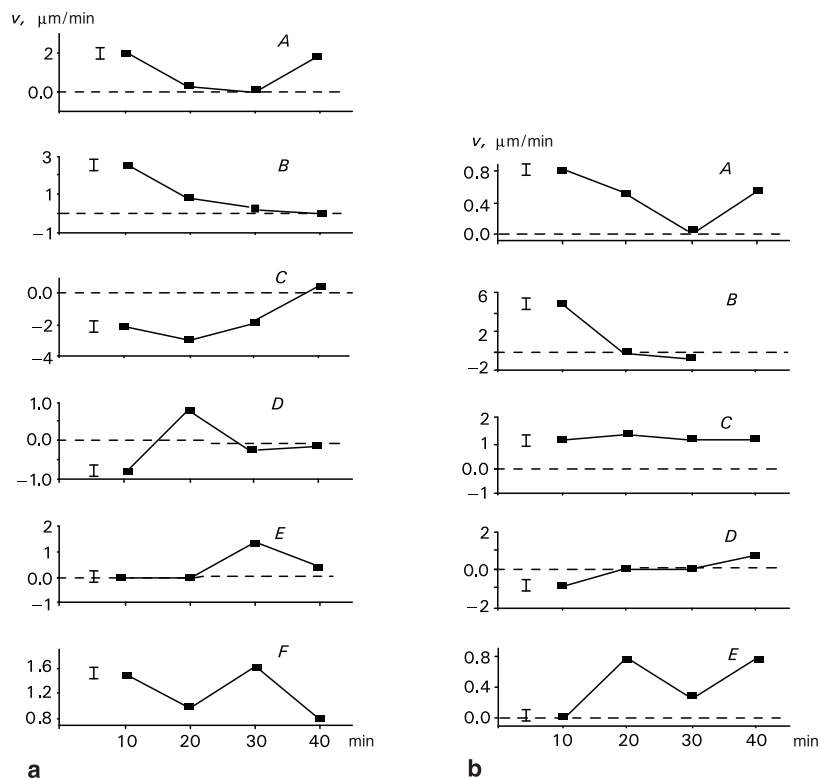
**Fig. 2.5** Nonmonotonous correlation between NaCl content in the solution and growth rate of KCl crystals ( $v$ , curves 1 and 2 for  $\Delta T = 1^\circ\text{C}$  and  $2^\circ\text{C}$ , respectively); saturation temperature =  $40^\circ\text{C}$ ; 3 – solubility temperature gradient ( $\Delta c/10$ ), 4 and 5 – supersaturation  $\Delta c/c$  at  $\Delta T = 1.0^\circ\text{C}$  and  $2.0^\circ\text{C}$ , respectively

It is essential to point out that the growth rates can vary (Fig. 2.6), despite the narrow confidence interval obtained for average values; the data dispersion at  $\Delta T = 1.0^\circ\text{C}$  ranges from 0.0 to 0.4 for KCl and from  $-3.2$  to 0.9 for NaCl, while at  $\Delta T = 2.0^\circ\text{C}$  it can vary from  $-0.25$  to 5.0 for KCl and from  $-1.0$  to 3.2 for NaCl. The most interesting phenomenon observed was negative growth rates of NaCl (Fig. 2.6): at various stages of the same experiment the seeds dissolved despite the fact that the solution remained under the same supercooling conditions as were maintained during the growth stage; the experiment was carried out uninterruptedly using the same seed and maintaining the constant temperature and level of supercooling.

Kinematical curves obtained for the time dependences of the growth rates of the both substances under constant conditions included sloping, elevating, and stability regions. In particular, various combinations of the growth and dissolution stages were observed for NaCl (Fig. 2.6). At  $\Delta T = 1.0^\circ\text{C}$  about 25% of the total of experiments with NaCl (5 out of 20) involved dissolution of the crystals, while at  $\Delta T = 2.0^\circ\text{C}$  this figure decreased to 10% (2 out of 20). Dissolving was not observed in experiments with KCl.

*In a quaternary system containing magnesium chloride, eutonic solutions of both KCl and NaCl ( $\Delta T = 1.0$  and  $2.0^\circ\text{C}$  with 5.28–20 wt% of magnesium chloride) display kinetic instability, which is also typical for crystallization of these salts in ternary solutions; in due time the growth rates become negligible and then the crystals start to dissolve. Kinematical variations of KCl growth rates (micrometer/minute) ranged*

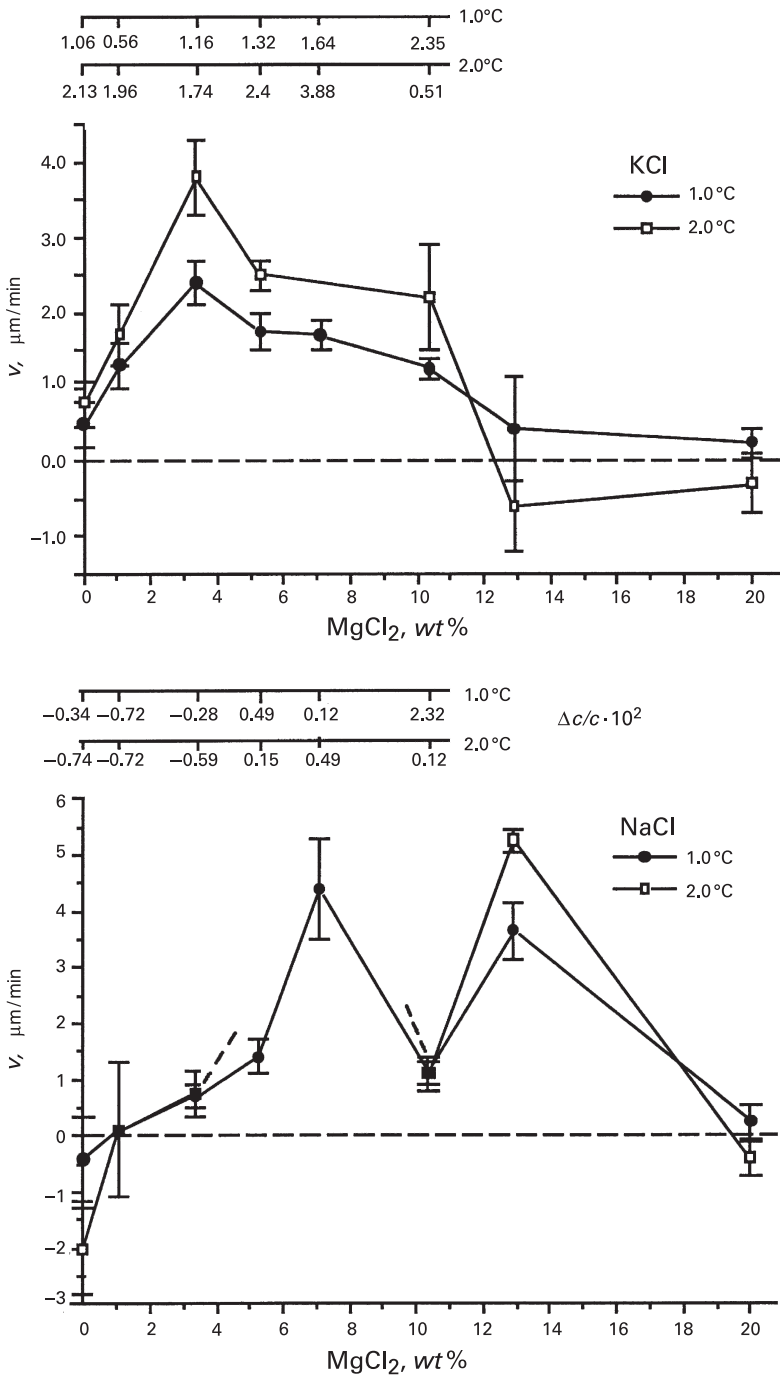




**Fig. 2.6** Time dependences of growth rate obtained for NaCl crystals **a** –  $\Delta T = 1.0^\circ\text{C}$ : A – including a growth rate minimum; B – monotonous slowing down to zero rate; C – increasing growth rate (from negative to positive values); D, E – including a rate maximum; F – including both the rate maximum and minimum. **b** –  $\Delta T = 2.0^\circ\text{C}$ : A – including a growth rate minimum; B – monotonous slowing down and transfer to dissolution; C – constant rate; D – increasing growth rate (from negative to positive values); E – including both the rate maximum and minimum

from 0.0 to 3.0 for  $\Delta T = 1.0^\circ\text{C}$  and from 0.3 to 7.0 for  $\Delta T = 2.0^\circ\text{C}$ , while for NaCl the rates varied from  $-3.0$  to  $2.0$  for  $\Delta T = 1.0^\circ\text{C}$  and from  $-1.0$  to  $5.0$  for  $\Delta T = 2.0^\circ\text{C}$ .

Presence of  $\text{MgCl}_2$  in solutions of the both phases complicated kinetic regularities (Fig. 2.7). According to data obtained in individual experiments, slow dissolution of NaCl crystals (rates varying from about  $-2$  to about  $-0.2 \mu\text{m}/\text{min}$ ) and slow growth of KCl crystals (rates varying from about  $0.5$  to about  $1.5 \mu\text{m}/\text{min}$ ) occurred in solutions containing low concentrations of  $\text{MgCl}_2$  (0–1 wt%). When concentration of  $\text{MgCl}_2$  ranged from about 3 to about 7 wt%, KCl growth rates reached  $3.8 \mu\text{m}/\text{min}$ , and those of NaCl were about  $4.5 \mu\text{m}/\text{min}$ . Further increase of  $\text{MgCl}_2$  concentration (up to 12–20 wt%) led to slowing down the growth of the both phases, and, ultimately, to dissolution (negative values of growth rates). At  $\Delta T = 2.0$  the crystals of KCl stopped growing and started dissolving when  $\text{MgCl}_2$  concentration exceeded about 13 wt%, while for NaCl seeds this transformation took place



**Fig. 2.7** Correlations between the growth rates of KCl (a) and NaCl (b) crystals and concentration of MgCl<sub>2</sub> at  $\Delta T = 1.0$  and  $2.0^\circ\text{C}$  and  $40^\circ\text{C}$  saturation temperature Scales in the upper part of the figure denote experimental supercooling degrees obtained from the phase diagram (Fig. 2.8)

when  $\text{MgCl}_2$  content was above 20 wt%. In contrast to supercooled binary and ternary systems, considerable concentrations of  $\text{MgCl}_2$  in supercooled quaternary solutions caused dissolving both KCl and NaCl seeds. Under the above conditions we observed the minimum of NaCl growth rate, which occurred at 10.35 wt% of  $\text{MgCl}_2$  and  $\Delta T = 1.0$  and  $2.0^\circ\text{C}$  and was proved by the coincidence of shapes of the curves obtained for both levels of supercooling.

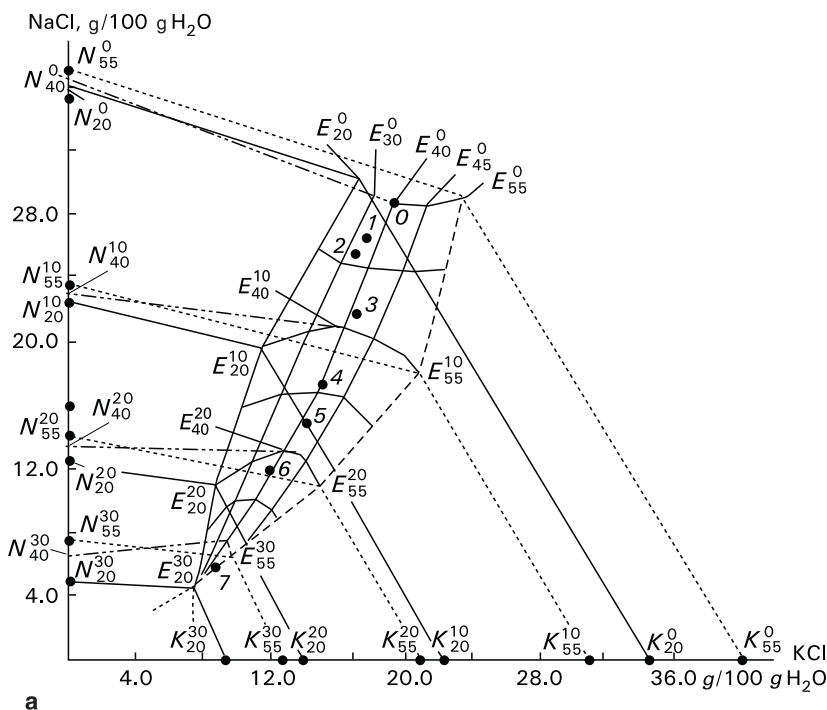
## 2.2 Physicochemical Model

### 2.2.1 Phase Equilibria in $\text{KCl-NaCl-MgCl}_2\text{-H}_2\text{O}$ System

Equilibria in  $\text{KCl-NaCl-MgCl}_2\text{-H}_2\text{O}$  system are usually represented as the Schreinemakers diagrams, which contain mutual solubility lines for the components and linear eutonic curves reflecting decreasing NaCl content with increasing KCl concentration and rising the temperature. The diagram was thoroughly investigated taking into consideration both the conventional solubility values (Buksha and Shestakov 1997) and results obtained in collaboration with a team of Research Institute of Mineral-Salt Production in 1989 (Glikin et al. 2001) to reveal more details including specific distortion of the main elements. Discovered peculiarities of phase equilibria allowed to interpret the above-mentioned phenomena of crystal growth/dissolution, and at the same time kinetic data obtained provided additional proofs for the proposed variant of the diagram (Fig. 2.8a).

In accordance with the Schreinemakers method, the absolute values of NaCl and KCl concentrations ( $N$  and  $K$ , correspondingly) in solution are plotted on the coordinate axes. Lines  $N_{20}^0-E_{20}^0-K_{20}^0$ ,  $N_{40}^0-E_{40}^0$ , and  $N_{55}^0-E_{55}^0-K_{55}^0$  represent solubility isotherms for NaCl and KCl ( $N$  and  $K$  branches, respectively) at  $20^\circ\text{C}$ ,  $40^\circ\text{C}$ , and  $55^\circ\text{C}$  in the ternary system in the absence  $\text{MgCl}_2$  (the intermediate isotherms are not shown); lines  $N_{20}^i-E_{20}^i-K_{20}^i$ ,  $N_{40}^i-E_{40}^i$ , and  $N_{55}^i-E_{55}^i-K_{55}^i$  are the solubility isotherms of these substances at  $20^\circ\text{C}$ ,  $40^\circ\text{C}$ , and  $55^\circ\text{C}$  in the quaternary system in the presence of  $i$ -content of  $\text{MgCl}_2$  ( $i = 10, 20, \text{ and } 30 \text{ g of } \text{MgCl}_2/100 \text{ g of } \text{H}_2\text{O}$ ). Eutonic dots  $E_{20}^0$ ,  $E_{30}^0$ ,  $E_{40}^0$ ,  $E_{45}^0$ , and  $E_{55}^0$  and the eutonic line connecting them designate binary equilibria of both solid NaCl and KCl in  $\text{MgCl}_2$ -free solution at the corresponding temperatures. Eutonic dots  $E_{20}^i$  and  $E_{55}^i$  with connecting lines of equal  $\text{MgCl}_2$  concentrations (hereinafter – “eutonic lines”) correspond to binary equilibria of solid NaCl and KCl at the constant  $i$ -content of  $\text{MgCl}_2$  and the temperatures ranging from  $20^\circ\text{C}$  to  $55^\circ\text{C}$ . Lines  $E_{20}^0-E_{20}^i$ ,  $E_{30}^0-E_{30}^i$ ,  $E_{40}^0-E_{40}^i$ ,  $E_{45}^0-E_{45}^i$ , and  $E_{55}^0-E_{55}^i$  represent isothermal univariant eutonic lines (hereinafter – “isothermal lines”) characterizing the shift of eutonic points of NaCl and KCl, obtained at 20, 30, 40, 45, and  $55^\circ\text{C}$ , as a function of  $\text{MgCl}_2$  content in solution.

The most significant feature of the diagram is distortion of the isoconcentration ( $E_{20}^0-E_{55}^0$  and  $E_{20}^i-E_{55}^i$ ) and isothermal ( $E_{20}^0-E_{20}^i$  and  $E_{55}^0-E_{55}^i$ ) eutonic lines.



**Fig. 2.8** Phase diagram of KCl–NaCl–MgCl<sub>2</sub>–H<sub>2</sub>O system **a** – According to reported and experimental data; our corrections are represented by dots 0–7. Dash-dotted lines – solubility isotherms for NaCl at 40°C. *E* – eutonic points, *K* – KCl, *N* – NaCl; superscripts – concentrations of MgCl<sub>2</sub> (wt%), subscripts – temperature (°C). For the other details, see text. **b** – Reported experimental data: 1 – 20°C, 2 – 30°C, 3 – 35°C, 4 – 38°C, 5 – 39°C, 6 – 40°C, 7 – 45°C, 8 – 50°C, 9 – 55°C (MgCl<sub>2</sub> content is in the range of 0–20 wt%). *References*: 1 and 9 – Kayser 1923 (*I* – Kayser’s calculation according to Pitzer’s method for 20°C); 2 – Shestakov and Pelsh 1977: private communication of NE Shestakov (1996) on the data obtained with Pelsh in 1977 (dash line) and unpublished data of 1989 (solid line); 6 – Kurnakov and Osokoreva 1935 and unpublished data of 1987–1989; 7 – Solov’eva et al. 1987 (dotted line) and unpublished data of 1989 (solid line); 8 – Korobkova 1987. Insert: enlarged portion of the diagram containing non-variant point defined by various authors (hollow circles); unpublished data kindly provided by Dr. S. N. Titkov were obtained from Research Institute of Mineral-Salt Production **c** – Isothermal eutonic (univariant) lines (1–9) calculated according to Pitzer’s method (Cheremnykh and Shestakov 1992). Temperatures (°C): 1 – 20; 2 – 30; 3 – 35; 4 – 38; 5 – 39; 6 – 40; 7 – 45; 8 – 50; 9 – 55. Concentrations of MgCl<sub>2</sub> (wt%): *a* – 1.06, *b* – 3.36, *c* – 5.28, *d* – 7.10, *e* – 10.35, *f* – 12.92, *g* – 20.01

It can be seen (Fig. 2.8 a) that the eutonic lines have their extremum points at  $\approx 40$ – $45^\circ\text{C}$ . The extremum is a minimum when solution does not contain any MgCl<sub>2</sub>, and a maximum when MgCl<sub>2</sub> concentration reaches or exceeds 5.28 wt%; the maxima become more pronounced when MgCl<sub>2</sub> content increases. Thus, the eutonic line corresponding to 0–5 wt% MgCl<sub>2</sub> concentrations approaches abscissa when the temperature rises to about 40–45°C and diverts from this axis when the temperature exceeds the above level (“inverted” and “direct” sections of eutonic

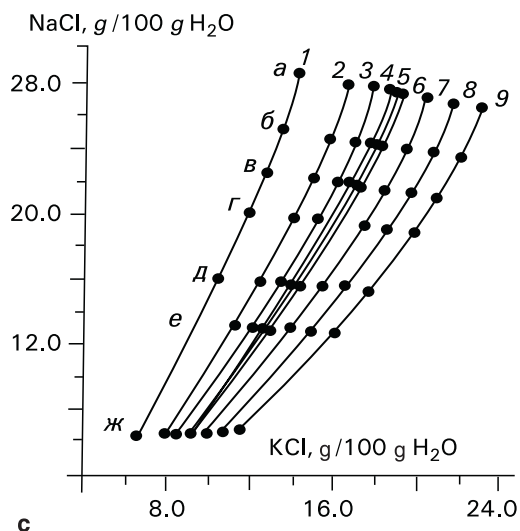
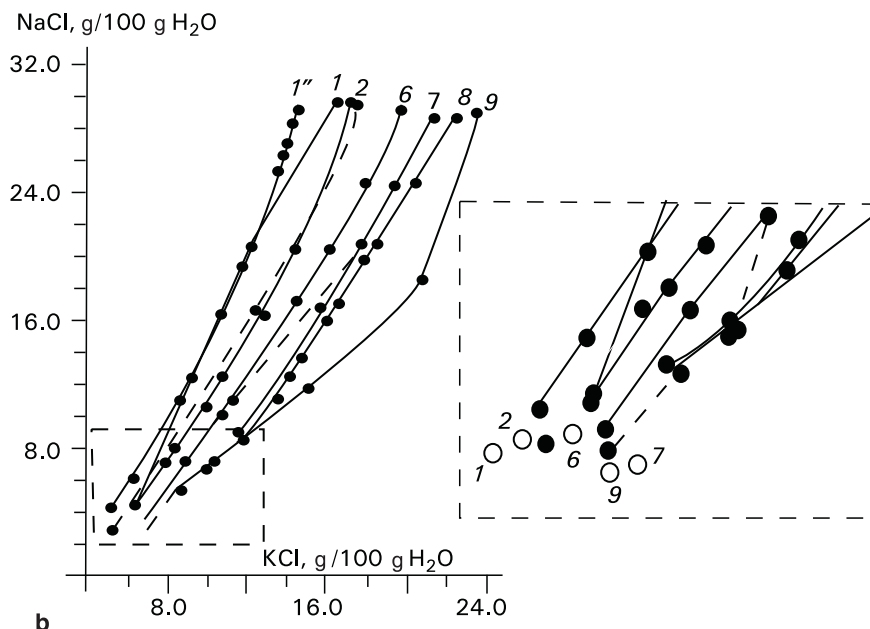


Fig. 2.8 (continued)

curve, correspondingly). When MgCl<sub>2</sub> content exceeds about 5 wt%, these sections switch places ("direct" and "inverted" sections correspond to the temperature ranges below and above approximately 40°C). "Inverted" eutonic line having no significant bending is observed when MgCl<sub>2</sub> content is about 5 wt% (≈10 g of

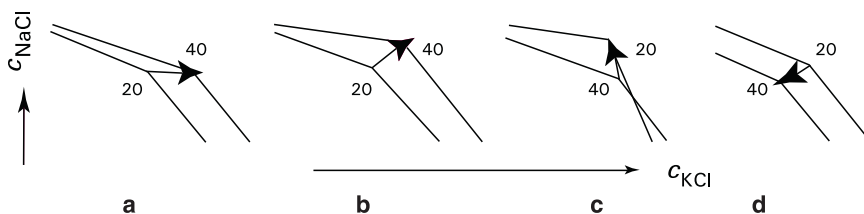
MgCl<sub>2</sub>/100 g of H<sub>2</sub>O). All reported diagrams of this system the author of the present monograph is aware of (Solubility 1954; Solubility 1979; Processing ... 1985; Buksha and Shestakov 1997) were plotted by simple connecting the eutonic points obtained at 20 and 50°C with straight lines that correspond to a monotonic shift from the “invert” eutonic line to the “direct” one with increase of Mg concentration in the solution.

Also, convexity of  $E_{20}^0-E_{20}^i$  isotherm is directed toward the ordinate, and that of the  $E_{55}^0-E_{55}^i$  line is directed toward the abscissa (Fig. 2.8a). Isotherms of 30, 40, and 45°C occupy intermediate positions. Extrapolating the converging  $E_{20}^0-E_{20}^i$  and  $E_{55}^0-E_{55}^i$  isotherms reveals their inversion in point A corresponding to about 22 wt% of MgCl<sub>2</sub> content ( $\approx 30$  g of MgCl<sub>2</sub>/100 g of H<sub>2</sub>O). The convergence of isothermal lines also appears in the diagram plotted according to Pitzer’s method, but in this case the convergence is insignificant in comparison with our data and the plotted lines cannot be inverted (Fig. 2.8c: the diagram was plotted by Dr. L.M. Cheremnykh, Research Institute of Mineral-Salt Production).

The convergence of isothermal lines and their inversion are accompanied by directional shift of eutonic lines in respect to the directions of the axes. This is schematically shown in Fig. 2.9. As MgCl<sub>2</sub> concentration increases, orientation of the eutonic line in temperature range of 20–40°C changes from “inverted,” converging with abscissa with increase of temperature (Fig. 2.9a,  $\sim 0$ –5 wt% of MgCl<sub>2</sub>), to “straight” (Fig. 2.9b,  $\sim 5$ –22 wt% of MgCl<sub>2</sub>), and then again to “inverted,” converging, as the temperature rises, with the ordinate axis (Fig. 2.9c;  $>22$  wt% of MgCl<sub>2</sub>). Subsequent extrapolation assumes a possible transition to the “reversed” eutonics (Fig. 2.9d). At the same time, in the 40–55°C interval, orientation of the eutonic line changes in accordance with another scheme: “direct” – “inverted toward the abscissa” – “reversed.” The new terms mentioned above need explanation. “*Eutonics inverted toward the abscissa axis*” corresponds to a positive temperature gradient of KCl solubility and a negative temperature gradient of NaCl solubility, i.e., as the temperature rises, the equilibrium concentration of KCl increases, while that of NaCl diminishes. “*Direct eutonics*” corresponds to positive solubility temperature gradients for the both substances. “*Eutonics inverted toward the ordinate axis*” corresponds to a negative temperature gradient of KCl solubility and a positive temperature gradient of NaCl solubility. Finally, the “*reversed eutonics*” corresponds to negative temperature solubility gradients for the both substances, i.e., as the temperature rises, the equilibrium concentrations of both components decrease.

Noteworthy is the fact that at high concentrations of MgCl<sub>2</sub> (above  $\approx 20$  wt% of MgCl<sub>2</sub>, or  $\approx 30$  g of MgCl<sub>2</sub>/100 g of H<sub>2</sub>O), both isothermal and isoconcentration eutonic lines almost merge in the neighborhood of point A (Fig. 2.8a). In particular, it is typical for the left-wing region of  $E_{20}^{30}$  isotherm. It means that in this region the equilibrium and kinetic properties of the system become irresponsive toward the minor changes of MgCl<sub>2</sub> content and the solution temperature.

The curved isothermal and isoconcentration eutonic lines plotted above disagree with the reported data (Figs. 2.8b, c). However, taking into consideration their compliance with kinetic data (see below) and with our control measurements of



**Fig. 2.9** Shift of the eutonic line between the KCl and NaCl regions with increase of  $\text{MgCl}_2$  concentration (a–d) at the temperatures ranging from 20°C to 40°C resulting in transition from positive temperature gradients to negative ones (schematic representation)

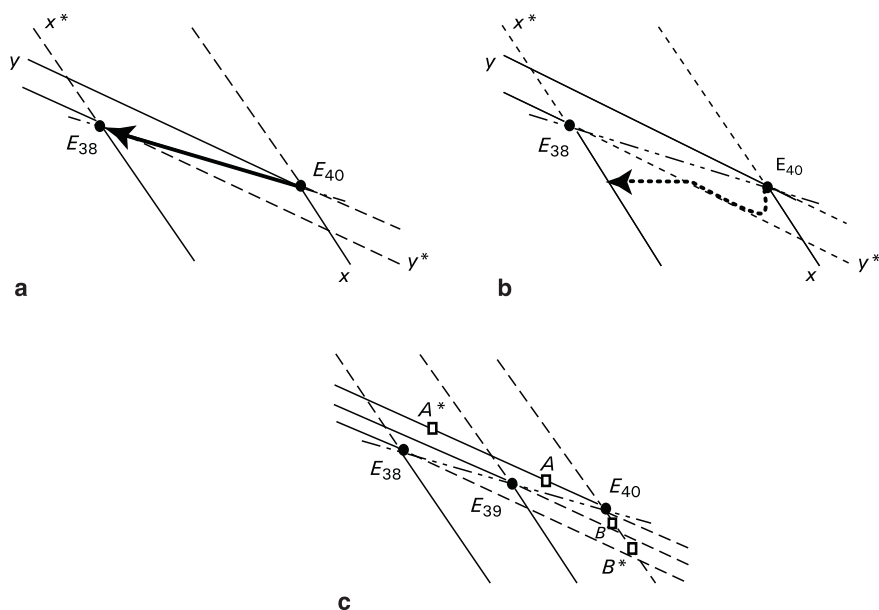
solubility conducted by means of precision method based upon an isolated seed observation, we consider our detailing to be rightful. However, we have to point out a strong disagreement existing among the numerous reported experimental and calculated solubility data (Kayser 1923; Kurnakov and Osokoreva 1935; Solubility 1954, 1979; Processing... 1985; Korobkova 1987; Solov'eva et al. 1987; Zdanovskii 1990; Cheremnykh and Shestakov 1992) especially obtained in the presence of high concentrations of magnesium chloride in the solutions (see insert in Fig. 2.8b).

## 2.2.2 Kinetic Effects and Peculiarities of Phase Equilibria

The plotted phase diagram allows to explain some unusual stages of NaCl dissolution in supercooled ternary solutions occurring under conditions of abrupt kinetic instability (Fig. 2.6). It can also help to understand the existence of nonmonotonous changes in crystal growth rates induced by variation of the solution composition, and by influence of  $\text{MgCl}_2$  content (Fig. 2.7) upon both the phases and effect of dissolved NaCl on the growth of KCl crystals (Fig. 2.5).

Morphological peculiarities of KCl and NaCl crystals and nucleation and subsequent growth of the partner-phase crystals directly on the seed surface indicates a significant diffusion limitation of crystallization processes. This conclusion can be further proved by formation of carnallite crystals on the seed surfaces, which occurs far outside the carnallite thermodynamic stability domain. The above statement also means that diffusion layer around the crystal can be considered as an area relatively isolated from the rest of the solution, and concentration variations in the solution caused by crystal growth/dissolving can be attributed mainly to the influence of the diffusion layer. Due to a relatively great volume of crystallization cell, the net composition of the solution changes insignificantly during the experiment; so, the above conclusion is very important in crystallogenic analysis of the mutual phase influence.

At first it is necessary to consider an equilibrium process that escaped our investigation before (Fig. 2.10a). When using an excess of both solid phases in heterogeneous KCl–NaCl– $\text{H}_2\text{O}$  system, change in temperature in proximity of 40°C, i.e.,



**Fig. 2.10** Illustration for physicochemical interpretation of crystal behavior in eutonic KCl–NaCl–H<sub>2</sub>O solutions at a lowering temperature  $E$  – Eutonic points for 38°C, 39°C, and 40°C, *dash-dotted lines* – eutonic lines, *solid lines* – stable equilibrium isotherms, *dash lines* – continuation of the isotherms toward the metastable region, *solid and dotted arrows* – trajectories of the solution compositions during crystallization. **a** – Excesses of both crystalline phases **b** – An isolated seed in a homogenous solution **c** – Supercooled solution state in the region of the concentration deviation from the eutonic point

within the “inverted” eutonic area, is usually characterized by conjugated growth and dissolution of KCl and NaCl crystals (Glikin 1996a). For example, lowering the temperature of the solution saturated at  $E_{40}$  results in shifting the trajectory of equilibrium composition toward  $E_{38}$  that corresponds to dissolution of NaCl and growth of KCl. Raising the temperature of the solution saturated at  $E_{38}$  reverses direction of the trajectory and thus a correlation between the growth and dissolution processes. The obvious conclusion about NaCl *dissolution* at lowering temperature seems at least peculiar given the fact that the figurative point of the solution concerned lies within the area of the both phase *supersaturation domain* circumscribed by  $xE_{40}y$  lines. Similarly uncommon is the conclusion about NaCl *growth* at the rising temperature, when the solution is *undersaturated* with both phases (the region circumscribed by  $x^*E_{38}y^*$  lines).

The isolated seed behaviour in homogenous solution has a number of peculiarities (Figs. 2.10b, c).

*Dissolution of NaCl crystals* in supercooled eutonic solutions and *kinetic instability* of both phase seeds observed in the absence and at a low MgCl<sub>2</sub> concentration



are probably of common origin. In our opinion, the above phenomena occur due to inhomogeneous accumulation of  $\text{MgCl}_2$  and the partner-substance in the diffusion layer formed around the seed and owing to uncontrollable crystallization of both partner-substance and carnallite on the seed surface. Alterations in composition of the diffusion layer, which has a very small volume, occur spontaneously and rapidly that results in fluctuations of the growth rate registered in kinematical curves (Fig. 2.6).

Figure 2.10*b* shows a hypothetic change of the solution composition in the diffusion layer around a point-like seed of NaCl occurring in the course of transition from  $E_{40}$  to  $E_{38}$  dot ( $\Delta T = 2^\circ\text{C}$ ). In the beginning the seed starts to grow; this leads to depletion of the solution in sodium chloride that is shown by the trajectory segment, which is parallel to the ordinate axis. When the trajectory approaches  $E_{38,y}^*$  boundary (metastable equilibrium for NaCl), the growth of the seed is slowing down and KCl accumulated in the diffusion layer reaches its labile state and starts precipitating on the seed. As a result, the trajectory bends (slowing down NaCl growth) and then, due to impossibility of crossing the metastable equilibrium line, takes a direction proceeding along this line toward  $E_{38}$  point. This process corresponds to the stage of NaCl dissolution and KCl growth. As NaCl concentration in the solution is limited, the trajectory reaches the level of initial NaCl concentration and then goes toward the  $38^\circ\text{C}$  isotherm, being parallel to the abscissa axis. Stages of NaCl seed growth characterized by lowering the growth rate and starting the dissolution can be matched with corresponding segments of kinematical curve *B* shown in Fig. 2.6*b*. It is possible to trace the potential trajectories of figurative points in kinematical curves of various types and correlate them with the processes occurring in the diffusion layers.

At least at the first steps of the experiment a probability for dissolution to occur decreases with increasing the supercooling degree. If supercooling is quite pronounced, nucleation of KCl crystals occurs in the region, which is sufficiently remote from the line of NaCl metastable equilibrium, so the tendency for the trajectory to reverse its direction (NaCl dissolution) appears to be slowed down. This phenomenon can be considered as one of the reasons for scarcity of the reported experiments in which it was possible to register dissolution phases when changing from the series with  $\Delta T = 1^\circ\text{C}$  to the series with  $\Delta T = 2^\circ\text{C}$ .

Such deviation of solution composition from the eutonic concentrations resulting from the metastable growth of one of the phases makes undersaturation exist only for NaCl phase, while for KCl phase it proves to be impossible due to the diagram asymmetry. Growth of KCl seeds is represented by the trajectory that is parallel to the abscissa. Precipitation of NaCl crystals followed by their dissolution when the trajectory crosses the metastable segment of  $E_{38,y}^*$  isotherm causes the trajectory to bend toward the abscissa (as in the case of NaCl seeds), but would not result in dissolution of KCl seeds.

The above considerations explain the presence of dissolution stages in NaCl growth process and their absence in transformations of KCl seeds. Since binary equilibrium  $E_{38}$  is inaccessible for any of the seeds, the solution remains undersaturated with NaCl.

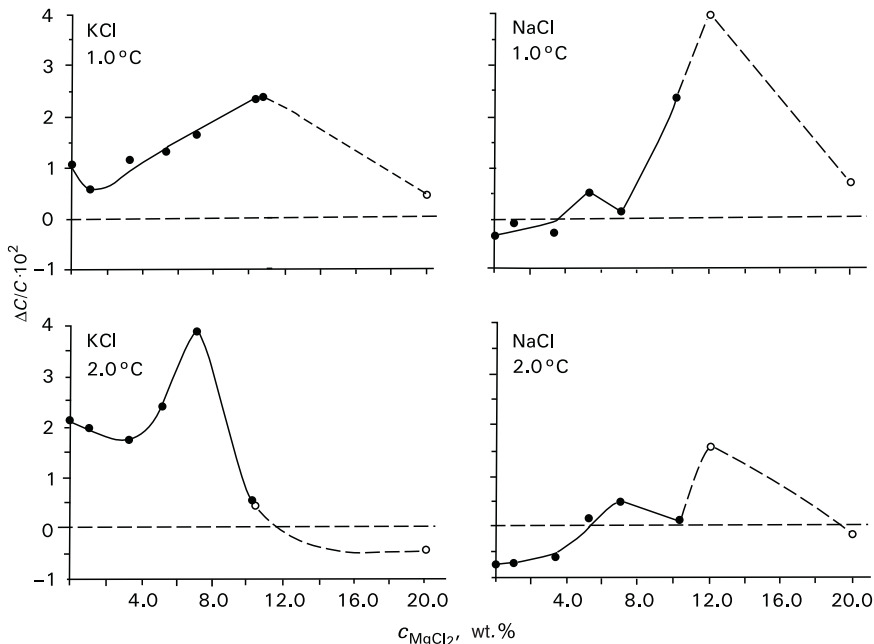
Thus, dissolution of crystals in supercooled ternary and, obviously, more complex solutions, depends upon differences between the solution composition and the eutonic concentrations of its components.

Of course, the crystals can dissolve due to a simple mistake made in the course of solution preparation (like in binary systems). In such a case a greater supercooling compensates the deviation, and the greater is the deviation, the deeper must be the supercooling applied to initiate the crystal growth. It can be seen (Fig. 2.10c) that figurative points *A* and *B* located at some distance from eutonic point  $E_{40}$  fall into the supersaturated solution domain at  $\Delta T = 1^\circ\text{C}$ , whereas the points  $A^*$  and  $B^*$  positioned at a greater distance from the eutonics appear in the supersaturated domain at  $\Delta T = 2^\circ\text{C}$ . However, dissolution initiated by a preparative mistake must become apparent in the very beginning of the experiment and persist all the way though it, showing in both NaCl and KCl transformations. In our experiments, dissolution processes were observed at different stages of the experiments and they were quite unstable (Fig. 2.6). Besides, KCl seeds did not tend to dissolve at all. Thus, the observed stages of NaCl dissolution are most likely related to the kinetic processes discussed above.

Nonmonotonous dependence of KCl and NaCl growth rates  $v$  on  $\text{MgCl}_2$  concentration in the solution (Fig. 2.7) is determined by configurations of isoconcentration and isothermal eutonic lines. Values of supersaturation  $\Delta c/c$  calculated at constant supercooling degree for KCl and NaCl in accordance with configuration of the eutonic lines reveal similar nonmonotonous dependence of supersaturation upon  $\text{MgCl}_2$  content in the solution (Fig. 2.11).

Nonmonotonous character of the growth rates (Fig. 2.7) is characterized by small absolute values of  $\Delta c/c$  and  $v$  at various concentrations of  $\text{MgCl}_2$ , either low or high, and by high absolute values of these parameters at medium  $\text{MgCl}_2$  concentrations. Dissolving KCl and NaCl in solutions containing considerable amounts of  $\text{MgCl}_2$  at  $2.0^\circ\text{C}$  of supercooling confirms inversion of the eutonic lines predicted by extrapolation of  $E_{20}^0-E_{20}^i$  and  $E_{55}^0-E_{55}^i$  curves and the presence of a region containing the “reversed” eutonic line. The position of the inversion point ( $\approx 22$  wt% of  $\text{MgCl}_2$ ) is proved by kinetic data. The fact that the both phases dissolve slowly at  $\Delta T = 2.0^\circ\text{C}$ , but grow slowly at  $\Delta T = 1.0^\circ\text{C}$  can possibly indicate a transition from the “direct” eutonic area to the “reversed” one and emphasize a narrowness of the intermediate area that is “directed toward the ordinate.” Explanation of the mutual locations of  $\Delta c/c$  and  $v$  maxima along  $\text{MgCl}_2$ -concentration axis and their relative widths (Figs. 2.7 and 2.11) cannot be made at present state of knowledge and requires further physicochemical adjustment of the phase diagram and acquiring additional kinetic data.

For the solutions containing high concentrations of  $\text{MgCl}_2$  ( $>12$  wt%), the isothermal eutonic lines almost merge that makes experimental determination of  $c$  and  $\Delta c$  exact values difficult; at any rate, under these conditions supersaturation/undersaturation in the solutions supercooled by  $1.0$  and  $2.0^\circ\text{C}$  cannot reach the point where growth/dissolution becomes observable that corresponds to zero growth rates (Fig. 2.7).



**Fig. 2.11** Correlation between the KCl and NaCl supersaturations and  $MgCl_2$  concentrations in the solutions at equal supercooling degrees 1 and 2°C (40°C saturation temperature) Solid circles – data obtained from the phase diagram (Fig. 2.8a), hollow circles – data obtained from kinetic investigations

Nonmonotonous character of KCl crystal growth rate with increasing NaCl content in the solution (Fig. 2.5, curves 1 and 2) can be considered from the point of view of the alterations in the system state. Effect of NaCl upon KCl solubility is actually more complicated than that presented schematically by the straight isotherms in the right part of the diagram (Fig. 2.8). The correlation varies with the temperature (Fig. 2.12) that, in turn, provides different temperature gradients of KCl solubility in solutions containing various NaCl concentrations. We obtained the following gradient values (Fig. 2.5) for several kinetic points (g/grad 100 g of  $H_2O$ ) at 40°C: in the absence of NaCl – 0.26, at 7.9 wt% of NaCl – 0.15 (the closest isotherms in Fig. 2.12), and in the eutonic area at 29.6 wt% of NaCl – 0.43. The above values correspond to the supersaturations  $\Delta c/c$  equal to 0.0064, 0.0046, and 0.0202 at  $\Delta T = 1^\circ C$ , or 0.0128, 0.0092, and 0.0404 at  $\Delta T = 2^\circ C$ .

As it can be seen in Fig. 2.5 (curves 3–5), the growth rate maximum corresponds to the minimum supersaturation, so the process kinetics cannot be explained away by the peculiarities of phase equilibria. The kinetic phenomena are most likely to be caused by structural rearrangements in the solutions, which are expected to occur at temperatures varying around 40°C, where some investigators observed

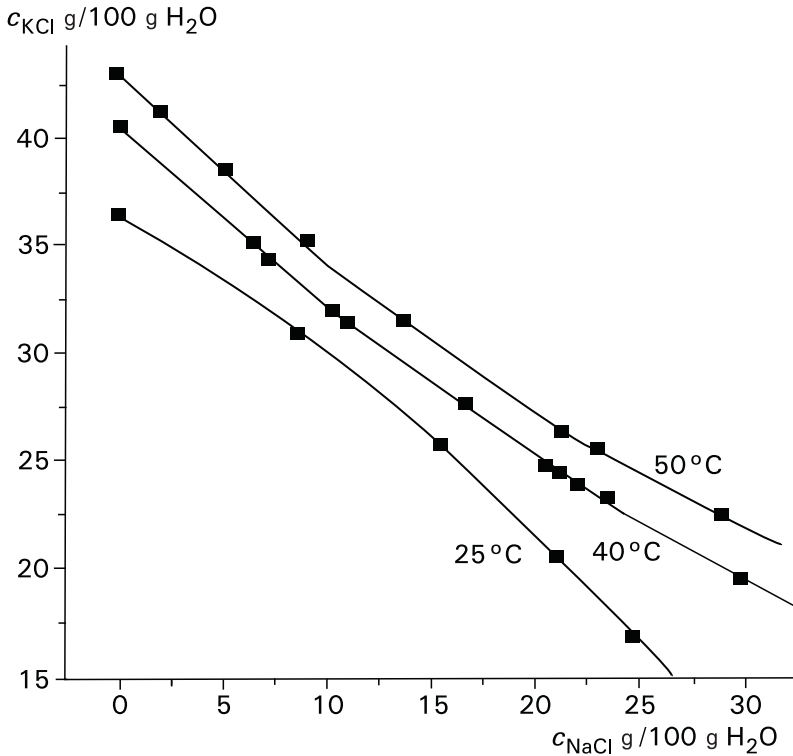


Fig. 2.12 Influence of NaCl upon KCl solubility at various temperatures (see Solubility, 1961–1970)

various temperature nonmonotonies showing in a series of peculiar phenomena registered in the solutions (see Franke and Punin 1972).

In fact, at any concentration of MgCl<sub>2</sub>, the eutonic lines contain extremum points in the neighborhood of 40°C, which are minima when MgCl<sub>2</sub> content is less than 10 g/100 g, and maxima when MgCl<sub>2</sub> content is about 10–30 g/100 g (Fig. 2.8a). Presence of KCl results in appearance of extremum points in NaCl solubility curves (minima and maxima at respective MgCl<sub>2</sub> contents). They can be deduced from the mutual arrangement of NaCl solubility isotherms at 20°, 40° (dash-dotted line), and 55°C (Fig. 2.8a), this conclusion being drawn irrespective to bending of the isotherms.

Thus, kinetic and morphologic characteristics of crystallogenesis in complex systems differ from those observed in binary solutions. Nevertheless, the data obtained in the binary systems are generally taken as a basis for interpretation of natural mineral formation and laboratory observations. The said significant differences manifest themselves in general instability of the process proceeding and nonmonotonous effect of the basic parameters upon the process kinetics.

Instability of the process proceeding (including dissolving the crystals at a supersaturated state of the solution bulk) is a result of phase interactions between the crystals of different phases mediated by changes in solution composition within the diffusion layer. It is important to note that this interaction results from a cause–effect relationship between the growth and dissolution of the partner phases, i.e., metasomatic component prevails in the process of joint crystal growth, which becomes apparent from the process kinetics.

Nonmonotonous influence of multicomponent system parameters upon the kinetics of crystal formation can result from nonmonotony of equilibrium properties of the system in question that require a detailed investigation to be revealed and cannot be predicted a priori on the basis of the particular case of a binary subsystem. Also, possible influence of some factors unknown at present cannot be discarded. In other words, using simplified crystal-genetic conceptions comprising, first of all, a direct correlation between the growth rate and a level of supercooling, solution composition, and temperature can hardly be fruitful for interpreting the processes taking place in complex systems, natural mineral formation including.

## References

- Anosov VYA, Ozerova MI, Fialkov YuA (1976) *Fundamentals of Physicochemical Analysis*. Nauka, Moscow (Russ.)
- Buksha YuV, Shestakov NE (eds) (1997) *Physicochemical Properties of Halurgy Solutions and Salts*. Reference Book. Khimia, St. Petersburg (Russ.)
- Bunn C (1964) *Crystals: Their Role in Nature and Science*. Academic, New York/London
- Cheremnykh LM, Shestakov NE (1992) Phase equilibria in NaCl–KCl–MgCl<sub>2</sub>–H<sub>2</sub>O system at 273–373K. *Zhurn Prikl Khimii* 65:3:507–512 (Russ.)
- Franke VD, Punin YuO (1972) Investigation of viscosity of potassium chloride solutions in the region of the phase transition in solution In: Frank-Kamenetskii VA (ed) *Crystallography and Crystallochemistry*. Leningrad State University, Leningrad (Russ.)
- Glikin AE (1996a) The physicochemical aspect of the unsteady state of metasomatic crystal production. *Geochem Intern* 33:8:117–128 (Russ.)
- Glikin AE (1996b) About equilibrium supercooled solutions related to formation of isomorphic-mixed crystals. *Zapiski Vsesoyuz Miner Obsh* 5:103–111 (Russ.)
- Glikin AE, Kaulina TV (1988) Kinetic model of epitaxial growth of crystals. *Zapiski Vsesoyuz Miner Obsh* 5:609–615 (Russ.)
- Glikin A, Plotkina J (1999) Disorientation effects of epitaxy at aqueous media. *materials structure*. *Bull. Czech Slovak Cryst Assoc* 6:2:155–158
- Glikin AE, Titkov SN, Plotkina YuV et al. (2001) Peculiarities of polymineral crystallogenesis (KCl–NaCl–MgCl<sub>2</sub>–H<sub>2</sub>O exemplary system). *Zapiski Vsesoyuz Miner Obsh* 6:100–114 (Russ.)
- Hayashi M, Shichiri T (1974) Theoretical and experimental study of the growth of perfect crystals. *J Cryst Growth* 21:254–260
- Kayser E (1923) Substitution factors for dissimilarly saturated solutions of potassium chloride and sodium chloride. *Kali* 17:1–9:37–42
- Khamskii EV (1979) *Crystallization in Chemical Industry*. Khimia, Moscow (Russ.)
- Kleber W (1955/1956) Über Hypomorphie. *Wiss Zs Humboldt-University Berlin, Math-Natur R* 5:1–13

- Kleber W (1964) Über die linearen Verschiebungsgeschwindigkeiten beim Wachstum komplexer Mischkristalle. *Z Phys Chem* 227:5/6: 289–295
- Korobkova EV (1987) Solubility in quaternary sub-systems of a quinary marine system containing Na, K, Mg//Cl,  $\text{SO}_4\text{-H}_2\text{O}$  at 50°C. In: *Solubility of Aqueous Salt Systems*. Collected science papers. All-Union Research Institute Halurgy, Leningrad (Russ.)
- König Ax, Emons H-H, Nývlt J (1987) The influence of sodium chloride on the driving force of the crystallization of potassium chloride from aqueous solutions at 25°C. *Cryst Res Technol* 22:1:13–19
- Kurnakov NS, Osokoreva NA (1935) *The Solikamsk Carnallites*. ONTI, Moscow-Leningrad (Russ.)
- Panov VI, Novikov AN, Prisyazhnik VA (1969) Rates of growth and dissolution of crystals in the presence of a surfactant. In: *Industrial Crystallization XX*. Khimia, Leningrad (Russ.)
- Petrov TG, Treivus EB, Kasatkin AP (1969) *Crystal Growing from Solutions*. Academic, New York.
- Plotkina YuV (1998) Morphologic, kinetic and epitaxial effects of crystallogenesis in the system KCl-NaCl-MgCl<sub>2</sub>-H<sub>2</sub>O. PhD thesis. St. Petersburg State University, St. Petersburg (Russ.)
- Punin YuO (1969) Kinetics of crystal growth of potassium chloride. PhD thesis. Leningrad State University, Leningrad (Russ.)
- Punin YuO, Petrov TG (1972) Anomalies of growth rates of potassium chloride crystals growing from aqueous solutions. In: Sheftal NN, Givargizov EI (ed) *Growth of Crystals IX*. Nauka, Moscow (Russ.)
- Solubility* (1954) *Solubility of Salt Systems*. Reference Book 2. Goskhimizdat, Leningrad (Russ.)
- Solubility* (1961–1970) Reference Book 1–3. Nauka, Moscow (Russ.)
- Solubility* (1979) Reference Book. Nauka, Moscow (Russ.)
- Processing of Natural Salts and Brines* (1985) Reference Book. Khimia, Leningrad (Russ.)
- Royer L (1928) Recherches experimentales sur l'epitaxie on orientation mutuelle des cristaux des espices differentes. *Bull Soc Franc Miner* 51:77–159
- Rumford F, Bain J (1960) The controlled crystallisation of sodium chloride. *J. Trans Inst Chem Eng* 38:10–20
- Solov'eva EF, Yakovleva NF, Abutkova LM (1987) Solubility in four-component systems: Na, K//Cl,  $\text{SO}_4\text{-H}_2\text{O}$ ; K, Mg//Cl,  $\text{SO}_4\text{-H}_2\text{O}$ ; Na, K, Mg//Cl-H<sub>2</sub>O at 45°C. In: *Solubility of Aqueous Salt Systems*. Vsesouz Institute of Halurgy, Leningrad (Russ.)
- Treivus EB, Kamentsev IE, Gaidamako IM (1985) Crystallization of halite from an aqueous solution in the presence of urea. In: Frank-Kamenetskii VA (ed). *Crystallography and Crystallochemistry 5*. Leningrad State University, Leningrad (Russ.)
- Zdanovskii AB (1990) Calculation of isohydral lines and solubilities of NaCl and KCl in NaCl-KCl-MgCl<sub>2</sub>-H<sub>2</sub>O system at various temperatures. *Zhurn. Prikl. Khimii* 5:966–972 (Russ.)

## Chapter 3

# Formation of Mixed Crystals in Solutions

### 3.1 Particular Characteristics of the Process and Historical Survey

A concept of isomorphism, principles of which were enunciated by E. Mitscherlich, D. I. Mendeleev, V. Goldschmidt, V. I. Vernadskii, and A. E. Fersman, is considered to be one of the foundation stones of crystal chemistry. It has been developed for many decades in numerous scientific works concerning both fundamental concepts and individual inorganic and organic compounds (Belov 1960, 1976; Frank-Kamenetskii 1964; Lebedev 1964; Kirkinskii and Yaroshevskii 1967; Bokii 1971; Kitaigorodskii 1971; Makarov 1973; Urusov 1977; Vainshtein 1982; Filatov and Bubnova 1986; Urusov 1987; Bohm 1995; Urusov et al. 1997; Kotel'nikova and Filatov 2002, and others). Data on structural arrangement, crystal imperfection, and thermodynamic stability of natural and synthesized crystals of variable compositions, obtained in complex experimental and theoretical researches, formed a solid basis for a fundamental theory, though interpretations of some phenomena still remain ambiguous. Unfortunately, available data do not cover principles of selecting and incorporating the components in the processes of crystal growth and isomorphic exchange between crystals and media, which determine compositions and imperfections of mixed crystals formed by different compounds.

Crystallogenic interpretations of isomorphism, which have been fully developed by the beginning of 1980s and are dominating at present, are summarized in A. A. Chernov's review (Chernov 1984, pp. 134–157). They are based on analysis of individual incorporations of admixture particles. Incorporation is usually divided into two types: homogeneous (incorporation of atom-molecule particles) and heterogeneous (incorporation of colloid particles). The former process can proceed under thermodynamically equilibrium or nonequilibrium conditions depending upon the process kinetics: with increase of growth rate the distribution coefficient of isomorphic components tends to 1 (Zhmurova et al. 1963; Zhmurova and Khaimov-Mal'kov 1970a, b; Petrov et al. 1983). Incorporation of the second type always takes place under thermodynamically nonequilibrium conditions. Nonuniform incorporation results in formation of heterogeneous crystals

(Laemlein 1948, 1973). Heterogeneity of the crystals produced can be classified as follows: sectorial heterogeneity formed owing to differences in adsorption properties of various crystal faces; zonal heterogeneity caused by alterations in growth rate; and structural heterogeneity caused by concentration changes in imperfect regions of a crystal. Selection of admixtures proceeds at the atomic level and depends upon the admixture solubility (the Ruff rule: Chernov 1984) and solubility of surface compounds formed by the admixture (the Panet rule: Laemlein 1948, 1973). The process has statistical nature regulated by difference in characters of the bonds formed by the crystal's own constituents and the admixture particles that results in development of local deformations and changing in elastic energy of the crystal lattice. The concepts developed to elucidate the growth mechanisms of mixed crystals, as well as use of elements of external and internal crystal morphology (faceting, details of the surface relief, inclusions, and other defects) for genetic examinations of mixed crystals, do not principally differ from a similar studies of crystals having constant compositions.

As stated in Chapter 1 (Sects. 1.1, 1.2, 1.4, and 1.5), in 1983 we discovered (optical microscope resolution) nontrivial phenomena of isomorphic exchange between a crystal and solution and developed a first model of monocrystal isomorphic substitution comprising synchronized processes of crystal dissolution and growth (Glikin and Sinai 1983). Next, the place for this process among the variety of exchange reactions was determined (Glikin and Sinai 1991). Later, the proposed mechanism was proved by quantitative physicochemical results (Glikin et al. 1994), and, then, we formulated a conceptual physicochemical basis combining regularities of isothermal substitution, growth, and heterogeneous metastable equilibria in supercooled solutions (Glikin 1995, 1996a). During the last decade this model was elaborated to incorporate the results of detailed optical-microscopic and kinetic researches (Kryuchkova et al. 2002; Glikin et al. 2003) and data obtained by means of several high-resolution methods including X-ray topography (Glikin et al. 2003), electron microscopy (Putnis et al. 2001; Putnis 2002), and atomic-force microscopy (Voloshin et al. 2004; Woensdregt and Glikin 2005).

These findings comprising incorporation of impurities into a crystal; formation of autoepitaxial excrescences; influence of the component solubilities and volume effect of substitution upon these phenomena; correlations between replacement, growth, and dissolution; heterogeneous metastable equilibria; and other parameters partially discussed in Chapter 1 appeared to be far beyond the boundaries of traditional interpretations developed for growth of crystals having constant compositions and co-crystallization of isomorphic substances (Melikhov and Merkulova 1975; Chernov 1984). Analysis of capturing individual atoms appears to be insufficient for interpretations, as it is capable of clarifying neither mechanism of information transaction between different sites of the crystal defining the contents of individual components, nor the feedbacks regulating these contents in accordance with the growth conditions. Physicochemical analysis of formation of a mixed crystal considered as an integral entity of interrelated isomorphic components may



present a feasible alternative to the above method. This approach is being developed in the present monograph; in our opinion it should be considered as a fundamental problem of crystallogensis.

The common principles involved in physicochemical analysis of equilibrium co-crystallization of isomorphous substances are fully developed only for the binary systems (various “fish”-modifications: Gerasimov et al. 1970; Anosov et al. 1976; Saranchina 1994; Treivus 2000, and others). They involve models of component interchange between the liquid and solid phases, both of which are continuously changing their compositions, i.e., the process, which at lowering temperature is accompanied by synchronous crystallization. Thus, according to the models, substitution is considered to be a constituent part of precipitation of mixed crystals; however, no valid basis for exchange mechanism, or kinetic-morphological consequences, or the substitution itself was suggested.

Unusual phenomena were observed in the processes of mixed crystal formation earlier, but they were never concerned in connection with physicochemical aspects of the process.

The most systematic research was carried out by Yu. B. Bolkhovityanov's research group. They studied a liquid phase heteroepitaxy in solid solutions of semiconductors having formula  $A^{III}B^V$  (Bolkhovityanov 1981, 1983, 1990; Bolkhovityanov et al. 1986 and others). The systems consisted of a multicomponent flux and a crystal having nonequilibrium (foreign<sup>1</sup>) composition. Substrate dissolution and its metastable equilibrium with the flux, as well as growth of a new solid phase accompanied by substrate simultaneous dissolution were observed under supercooling conditions. Such phenomena are similar to those observed by us in aqueous solutions, although the former are less expressed. They are in a good agreement with Bolkhovityanov's concept suggesting formation of a strained diffusion “skin-layer” on the substrate surface as a result of lattice discordance. However, this approach does not explain specific characteristics of morphology or a role of volume effect induced by crystal-liquid interaction, while analytical model developed by A. E. Voloshin (Voloshin et al. 2003, 2004) determines contribution of the physicochemical factors defined by us as more important.

Unfortunately, evidences of such uncommon phenomena are too rare, and, perhaps, in some cases they have not been published as mistaken for artifacts. In a few works concerning growth of mixed crystals references were made to morphological formations similar to autoepitaxial excrescences described above, for example,  $(Ba,Sr)SO_4$  (Melikhov et al. 1977) and  $K_2(S,Cr)O_4$  (Kasatkin 1993). Melikhov et al. (1977) mentioned heterogeneous metastable equilibria as unusual phenomena observed in the course of  $(Ba,Sr)SO_4$  crystallization. Both formations of excrescences and abnormal equilibria were explained away by structural disagreements between the seed constitution and that of overgrowing layers. Metastable heteroge-

---

<sup>1</sup>“Own composition” is referred to as an isomorphous composition corresponding to thermodynamic equilibrium between the solid and fluid phases under fixed conditions.

neous equilibrium of aqueous  $K_2(S,Cr)O_4$  solution overcooled by about  $20^\circ\text{C}$  was explained by accidental poisoning of the initially precipitated crystals. Formation of pure (or almost pure) isomorphous-capacious compounds in natural environment inevitably containing some or other isomorphous component is a well-known fact accepted without any explanations. Examples of such formations include copper, silver, grossular, andradite, fayalite, tephroite, clinoenstatite, enstatite, pyrochlore, muscovite, phlogopite and many others (Betekhtin 1950; Minerals 1960, 1967, 1972, 1981, 1992, and others); in particular, gold of high purity precipitating from neotectonic volcanic gases saturated with isomorphous copper should be mentioned (Vergasova et al. 1982).

Our findings indicate that formation of mixed crystals is determined by extremely closely related and complex interactions between the elemental acts of growth and dissolution that in common cases of overheated or supercooled solutions involve superimposed development of metasomatic component and ordinary growth or dissolution components. The main peculiarity of such interactions is lack of phase boundaries separating sites of dissolution and growth in a monocrystal that causes predominance of totally new macroscopic effects. In this connection, the above and some other processes can be included into the specific first over-elemental class. Sub-elemental phenomena of such unordinary replacement take place in microscopic sites of the surface, while suppression of metasomatic component can induce spreading of direct growth and dissolution phenomena over the whole crystal surface.

### 3.2 Material Balance and Mechanisms of Replacement

In the previous sections it has been shown that there are two variants of metasomatic transformation of monocrystal isomorphous composition that result in formation of products having different structures: solid (continuous) (Table 1.1, reactions *Ib/24, 26, 28, 30, 32, 33, 34*) or spongy (reactions *Ib/25, 27, 29, 31–33, 35*). It has been proved that these products are monocrystals inheriting initial orientation of the protocrystal, and their particular structures are determined by volume-deficit or volume-excess replacements, correspondingly (Glikin and Sinai 1983). Mechanisms of these reactions should be given a particular concern.

The key step in understanding of both replacement mechanisms is a quantitative evaluation of the component interchange, which was obtained by us for  $KAl(SO_4)_2 \cdot 12H_2O - KCr(SO_4)_2 \cdot 12H_2O - H_2O$  system (Glikin et al. 1994) in the course of monocrystal replacement with volume excess, and for a reversed case, with volume deficit (Table 1.1, reactions *Ib/28* and *Ib/29*, respectively).

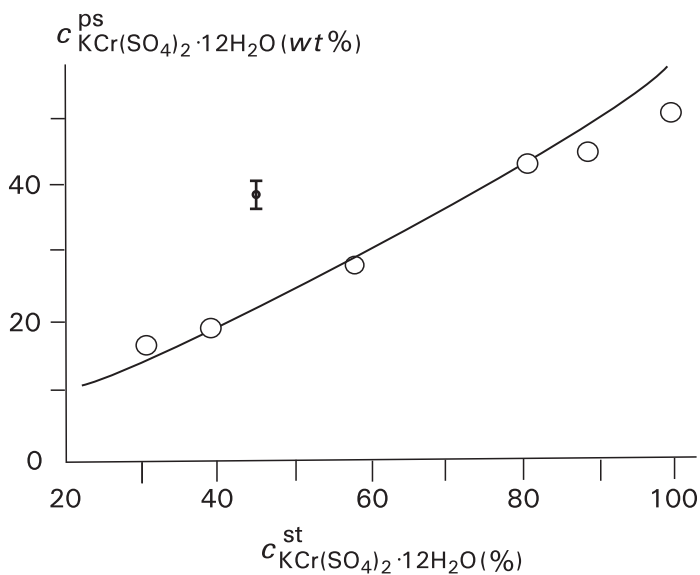
Initial alum crystals representing the extreme (Al and Cr) and intermediate (30–90 wt% of Cr component) members of the isomorphous series were grown under

ambient conditions to the sizes of 5–10 mm by means of either evaporation or lowering the solution temperature. Then the crystals were merged into a replacing solution: Al-K crystals were placed into Cr-K solution (slow replacement with volume excess), and crystals containing chromium into Al-K solution (fast replacement with volume deficit). Reactions were conducted at ambient temperature without water evaporation. Duration of experiments varied from several days to several months for volume-deficit and volume-excess processes, correspondingly. Morphological attributes were examined visually and under optical microscopes. The matter interchange was investigated separately for three kinds of the components by means of special methods as follows.

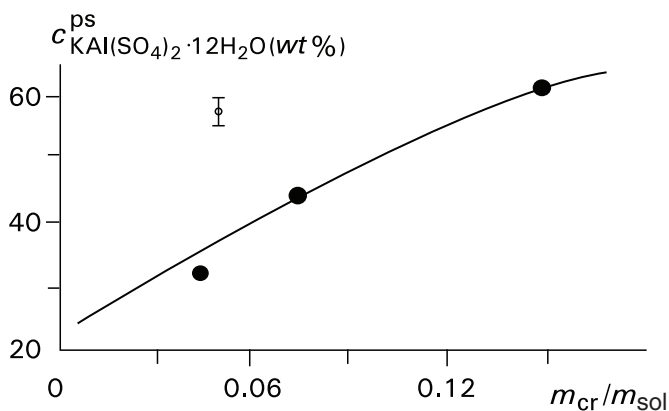
*Chromium ↔ aluminium interchange*, which was accompanied by a visible change in colors of solution and substituted crystals from violet to colorless, was detected by defining  $\text{Cr}^{+3}$  content in the solid phase using X-ray fluorescent analyzer SPARK-1 (Mr. E. B. Tabuns, Laboratory of Rare Element Geochemistry of the Earth Crust Research Institute, St. Petersburg State University). Pseudomorphs with volume deficit were formed when the protocrystals with different Cr/Al ratios were used. Dependence of chromium content in a pseudomorph versus the chromium content in the initial crystal was in a good agreement with theoretical data (Fig. 3.1). Pseudomorphs with volume excess were formed only when pure aluminum-containing protocrystals were used. The process pathway depended upon the mass ratio between the crystal and solution and was also in a good agreement with theoretical data (Fig. 3.2). Theoretical values were calculated ( $\pm 5\%$ ) for equilibrium processes with an aid of a phase diagram (Fig. 3.3) adjusted by Ms. O. A. Leont'eva (1990).

*Potassium interchange* was studied using labeled  $^{41}\text{K}$  atoms. To introduce a label, weighed amounts of KCl with the ratio of  $^{39}\text{K}/^{41}\text{K} = 0.5$  were added into the starting solutions. The ratio of  $^{39}\text{K}/^{41}\text{K}$  was evaluated first in the starting crystals and solutions, and then in the substituted crystals and residual solutions using a mass-spectrometer KI-1305 (Dr. A. S. Kirillov, Laboratory of Physical and Chemical Methods of the Earth Crust Research Institute, St. Petersburg State University). Crystals undergoing both volume-excess and volume-deficit replacements became enriched with  $^{41}\text{K}$  isotope contained in the solution, while the residual solutions became depleted in respect to this isotope. When the difference between isotope compositions of the phases was lessening, the crystal enrichment with the heavy isotope was inversely proportional to the crystal size (Table 3.1).

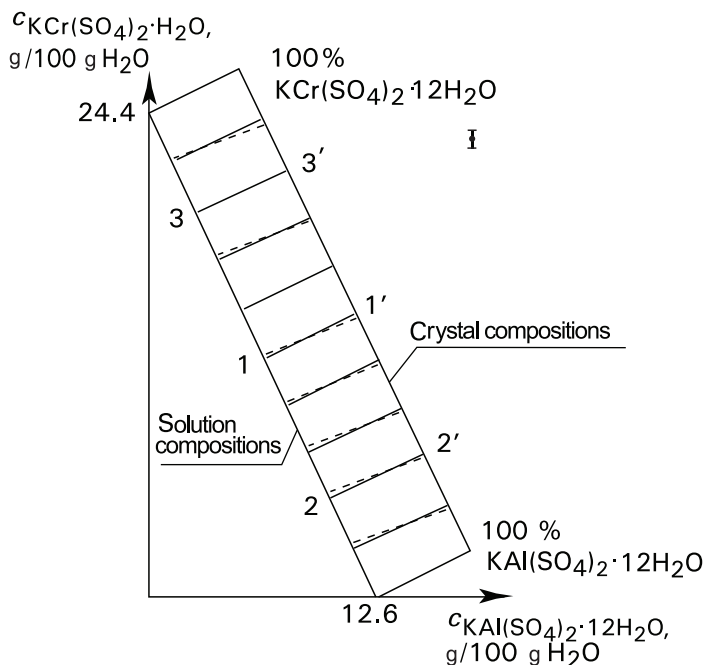
*Water interchange* was studied using deuterium labeling. Primary deuterated crystals of K-Al and K-Cr alums ( $\text{H}_2\text{O} < 3\%$ ) were grown from heavy-water solutions. After replacements had been completed in usual aqueous solutions,  $\text{D}_2\text{O}$  contents were determined in the residual solutions using spectrometer UR-20 (Dr. M. L. Zorina, Department of Geochemistry of St. Petersburg State University). Contents of heavy water transferred from crystal into solution were evaluated in all residual solutions studied and found to be



**Fig. 3.1** Function of Cr-K-component content in pseudomorphs  $c^{\text{ps}}$  versus its content in starting crystals  $c^{\text{st}}$ . Volume-deficit replacement of Cr-K-alum with Al-K-alum (simultaneous replacement of several crystals at mass ratio of crystal to solution  $m_{\text{cr}}/m_{\text{sol}} = 0.25$ ). The solid line represents calculated function



**Fig. 3.2** Function of Al-K-component content in pseudomorphs  $c^{\text{ps}}$  versus mass ratio of crystal to solution  $m_{\text{cr}}/m_{\text{sol}}$ . Volume-excess replacement of Al-K-alum with Cr-K-alum. The solid line represents calculated function



**Fig. 3.3** Equilibria in  $\text{KAl}(\text{SO}_4)_2\text{-KCr}(\text{SO}_4)_2\text{-H}_2\text{O}$  (Measured by Ms. O. A. Leont'eva, St. Petersburg University) Dash lines – experimental conodes. Solid parallel conodes indicate hypothetical constant distribution coefficient

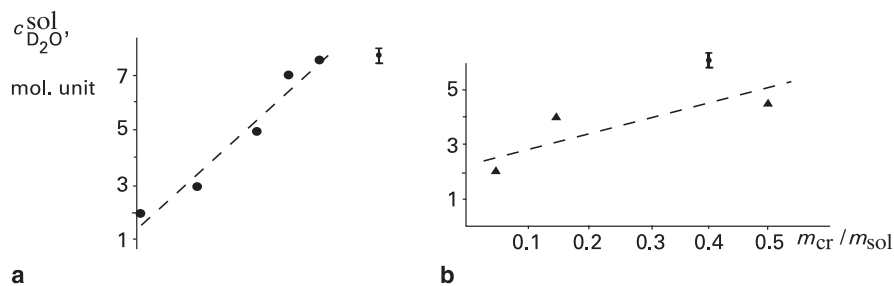
directly proportional to the mass of the crystal for all samples representing both types of replacement (Fig. 3.4).

Agreement between the experimental and theoretical characteristics of  $\text{Al} \leftrightarrow \text{Cr}$ -interchange and strict correlation of final contents of  $^{41}\text{K}$  and  $\text{D}_2\text{O}$  with relative phase volumes proves the tendency of the system to reach a physicochemical equilibrium in reactions with both deficit and excess of secondary volume, regardless to mechanism differences. The results obtained allow to conclude that metasomatic transformations of isomorphous mixed crystals are accompanied by equal participation of all the components in the matter interchange between the crystal and the medium, where the components can be both different ( $\text{Al} \leftrightarrow \text{Cr}$ ) and the same ( $\text{K}_{\text{cryst}} \leftrightarrow \text{K}_{\text{sol}}$  and  $\text{H}_2\text{O}_{\text{cryst}} \leftrightarrow \text{H}_2\text{O}_{\text{sol}}$ ). Interchange of sulfate ions was not studied, but there are no reasons for considering them inert and not participating in the process. These conclusions agree with the basic principles of chemical reaction of salting-out (Anosov et al. 1976), so we just need to determine the feedback mechanism controlling the ratios of all solid and liquid phase components in the course of the reaction.

**Table 3.1** Alteration of potassium isotope content (% to the total potassium content) in crystals and solutions during replacement

Sample	$^{39}\text{K}/^{41}\text{K}$	Content of $^{41}\text{K}$ , %
<b>Replacement of Cr-K-alum with Al-K-alum (volume deficit)</b>		
Initial solution	$11.51 \pm 0.07$	7.90
Crystal		
Initial	$13.76 \pm 0.07$	6.77
Replaced		
Sample 1	$12.44 \pm 0.04$	7.44
Sample 2	$12.81 \pm 0.05$	7.19
<b>Replacement of Al-K-alum with Cr-K alum (volume excess)</b>		
Solution		
Initial	$12.70 \pm 0.10$	7.29
Residual		
Sample 3	$13.35 \pm 0.09$	6.97
Sample 4	$13.51 \pm 0.06$	6.89
Crystal		
Initial	$14.28 \pm 0.04$	6.54
Replaced		
Sample 3 ( $m_{\text{cr}}/m_{\text{sol}} = 0.25$ )	$13.56 \pm 0.08$	6.87
Sample 4 ( $m_{\text{cr}}/m_{\text{sol}} = 0.15$ )	$13.40 \pm 0.01$	6.94
Sample 5 ( $m_{\text{cr}}/m_{\text{sol}} = 0.05$ )	$13.27 \pm 0.2$	7.0

**Note:**  $m_{\text{cr}}$  and  $m_{\text{sol}}$  are weights of the crystal and solution respectively.



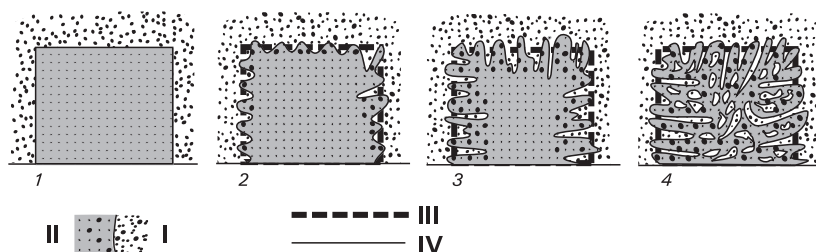
**Fig. 3.4** Function of  $\text{D}_2\text{O}$  content in residual solutions versus mass ratio of crystal to solution  $m_{\text{cr}}/m_{\text{sol}}$ . **a** – volume-deficit replacement of Cr-K-alum with Al-K-alum; **b** – volume-excess replacement of Al-K-alum with Cr-K-alum

The mechanism of the above-mentioned feedbacks consists in precipitating the “own” crystal matter and dissolving the crystalline material having isomorphic composition, which is “foreign” to the process solution. As it was mentioned

before, the processes of crystal dissolution and growth occur simultaneously at microsites randomly distributed over the “mosaic” crystal surface and differing in composition. Nonequilibrium conditions for the adjoining sites of the mosaics are different, so some of them start dissolving, while others are growing. The distribution of mosaics changes every moment (up to the point of changing from dissolution to growing and vice versa) according to composition variations in solution and crystal caused by local fluctuations in composition of the near-surface solution layer.

The above processes can be observed at the microscopic level and were registered in situ under volume-deficit conditions (Fig. 1.5). This type of replacement is accompanied by formation of numerous narrow channels filled with solution, which penetrate the bulk of a crystal, where some of them can become separated forming closed inclusions filled with solution. The same “mosaic” dissolution and growth processes take place on the surface of the channels and inclusions adjacent to the solution and having very complicated shapes, thus, providing fast tangential movement of inclusions and transformation of the whole crystal. It is to be noted that extent of replacement and structure of pseudomorphs having identical history of formation and transformation of their initial crystal may be different, i.e., pseudomorphs of different stages of conversion contain intact regions of various sizes (“blocks”) and implanted inclusions dividing them. This difference is discussed below for  $(\text{Co,Ni})(\text{NH}_4)_2(\text{SO}_4)_2 \cdot 6\text{H}_2\text{O}$  series.

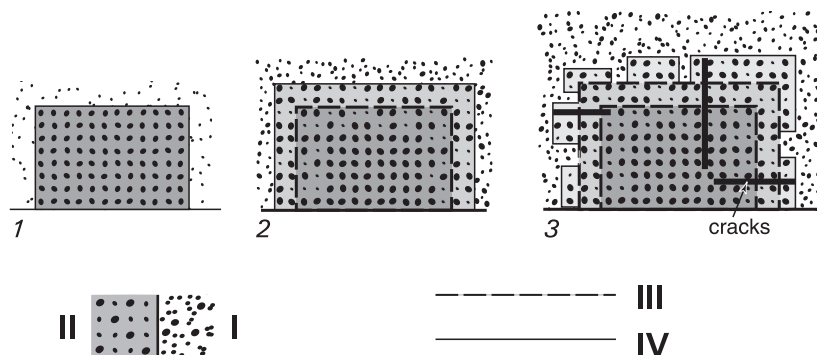
A volume-deficit process is schematically represented in Fig. 3.5 and is as follows. At first, the surface layer of the crystal starts to dissolve causing supersaturation of the solution. Salting-out does not provide appropriate amount of precipitating material, so the growing layer of the new formation has gaps facilitating the salting-out process. As a result, the solution composition changes and the substance, having



**Fig. 3.5** Schematic representation of volume-deficit replacement (crystal section) I – solution components; II – crystal components; III – the initial surface of the crystal; IV – real surface of the crystal. 1 – initial moment of the contact between the crystal and solution; 2 – transformation of the faces into a constantly changing scalloped surfaces with alternating protuberances and pockets; 3 – transformation of the deepest pockets into numerous channels penetrating the crystal at perpendicular direction to its surface; 4 – bending and tangent movement of the channels resulting in formation of a spongy crystal containing numerous inclusions

precipitated earlier and also containing breaks in the newly formed layers, enters the reaction. The process continues until reaching the equilibrium state. This mechanism explains formation of inclusions compensating the volume deficit with simultaneous preservation of the total volume the crystal had before the process beginning. At the same time, it is important to note that precipitation is autoepitaxial, and salting-out does not require nucleation of new individuals, thus ensuring a monocrystalline structure of the new formation.

Volume-excess replacement involves changing the composition of the external zone accompanied by formation of the surface excrescences and sometimes cracks. The edge of the replacement front is sharp and irregular, and the thickness of the replaced region may differ for faces of various crystal forms. The details of this slow process are impossible to be discerned visually, and its mechanism cannot be visualized either. The basic question is how the proportion of interchanging components corresponding to physicochemical parameters of the process is ensured. Since this replacement also involves salting-out, its course can be represented as follows (Fig. 3.6). As the reaction begins, a thin reacting film is produced on the surface of a crystal as a result of salting-out caused by dissolution of the first layer of the solid matter. The film has monocrystalline structure and autoepitaxial orientation, but does not contain any gaps as replacement is volume-excessive. It is important that the film appears to be in equilibrium with solution and envelops the crystal surface thus terminating the reaction. At the same time, nonequilibrium state existing between the film and the crystal matter induces a solid-phase diffusive



**Fig. 3.6** Schematic representation of volume-excess replacement I–IV – see: Fig. 5. 1 – initial moment of the contact between the crystal and solution; 2 – dissolving a thin surface layer and subsequent growth of a continuous autoepitaxial isomorphous film having a greater thickness; diffusion component interchange between the protocystal and the film, dissolving a thin surface layer and subsequent growth of a continuous autoepitaxial isomorphous film having a greater thickness; 3 – formation of defect parts containing clusters of dislocation and cracks, formation of autoepitaxial excrescences and pertite structures



interchange of ions between them. This results in changing the film composition, which, in turn, leads to resuming the salting-out, formation of a new equilibrium film, and repeating the whole sequence. As a result of this process, the volume of the crystal increases.

Prima facie, this process should be extremely slow, as diffusion rate in crystal, especially at low temperatures, is believed to be negligible. However, noticeable diffusion and replacement rates may be stimulated by crystal defects (strains, dislocations, and point deformations; microcracks; or solution microinclusions), and localization of autoepitaxial excrescences in vicinity of defects confirms this conclusion. It is clearly seen in Fig. 1.3c that excrescences produced are distributed along the edges and the scratch, i.e., regions of strained lattice and dislocations. Figure 1.4 shows that replacement proceeds along the cracks. For example, in reaction *Ib/24*, the cracks are developed directly during the replacement, probably, due to heterometry effect (Sternberg 1962): nonuniform distribution of isomorphic components results in development of stresses and cracks along the cleavage. Both cracks and dislocations developed according to various schemes of heterometry strain removal (Punin 1994), as well as lattice deformations in strained regions, accelerate diffusion in the bulk of crystal to the following effect: the greater the number of defects, the faster is the diffusion, and the faster the diffusion, the more rapid is the replacement and formation of new strained areas and defects owing to heterometry.

The results of the experiments described in the previous paragraph unambiguously demonstrate importance of the crystal imperfection for volume-excess replacements. Development of strains and corresponding imperfections during the process can be shown by formation of secondary cracking in pseudomorphs of  $(\text{Mg,Ni})\text{SO}_4 \cdot 7\text{H}_2\text{O}$  after  $\text{NiSO}_4 \cdot 7\text{H}_2\text{O}$  (reaction *Ib/24*). Moreover, published data obtained by Voloshin and collaborators present in situ X-ray topographic observation of developing the inhomogeneous strain on the sites of heterogeneous replacement of  $\text{KHC}_8\text{H}_4\text{O}_4$  crystals with  $(\text{K,Rb})\text{HC}_8\text{H}_4\text{O}_4$  (Glikin et al. 2003).

The author has not succeeded in finding any direct data on acceleration of diffusion in imperfect and strained crystals. However, mechanisms suggested for transport phenomena in crystals (Friedel 1964; Geguzin 1970; Shuvalov et al. 1988) make this process likely to occur.

Hence, both volume-deficit and volume-excess monocrystalline replacements involve a common physicochemical scheme of salting-out, i.e., via local acts of dissolution and subsequent growth. However, they have different mechanisms of the limiting stages. The former replacement is undoubtedly limited by diffusion of components in the solution. The latter process is assumed with a high degree of certainty to be limited by solid-phase diffusion of components.

Proposed model of isomorphic replacement interrelates some of the fundamental conceptions of chemistry and mineralogy. First of all, a quantitative aspect of the process has been brought to conformity with the principle of thermodynamic equilibrium. A priory and ambiguous principle “particle for particle” is replaced by exact quantitative characteristics of the salting-out reaction and mechanisms of conjugated dissolution and growth, which control the proportion of components in crystal and solution. At the same time, the volume effect of the process can be exactly expressed

depending upon components' solubility ratio. Second, the above process of volume-excess continuous replacement determines the application terms for a well-known model of diffusion component interchange between crystal and solution (Lindgren 1925; Grigor'ev 1961; Grigor'ev and Zhabin 1975; Frank-Kamenetskii et al. 1983). It is to be noted that the above process is a single and by now unique phenomenon of crystal formation in solutions where sub-elemental solid-state diffusion plays the key role; in other cases this type of diffusion may be ignored. Third, the model of spongy replacement, which has no analogs, removes the problem of lack of transportation and precipitation space under conditions of ultimate consolidation of matter undergoing replacement. In other cases this problem is not so important due to the presence of pores, cracks, intercrystalline boundaries, etc. At the same time, the model covers only the principal aspects of isomorphic replacement. Influence of phase equilibria in particular ternary and multicomponent systems and non-isothermal character of the process are described in the following paragraphs.

### 3.3 Physicochemical Model

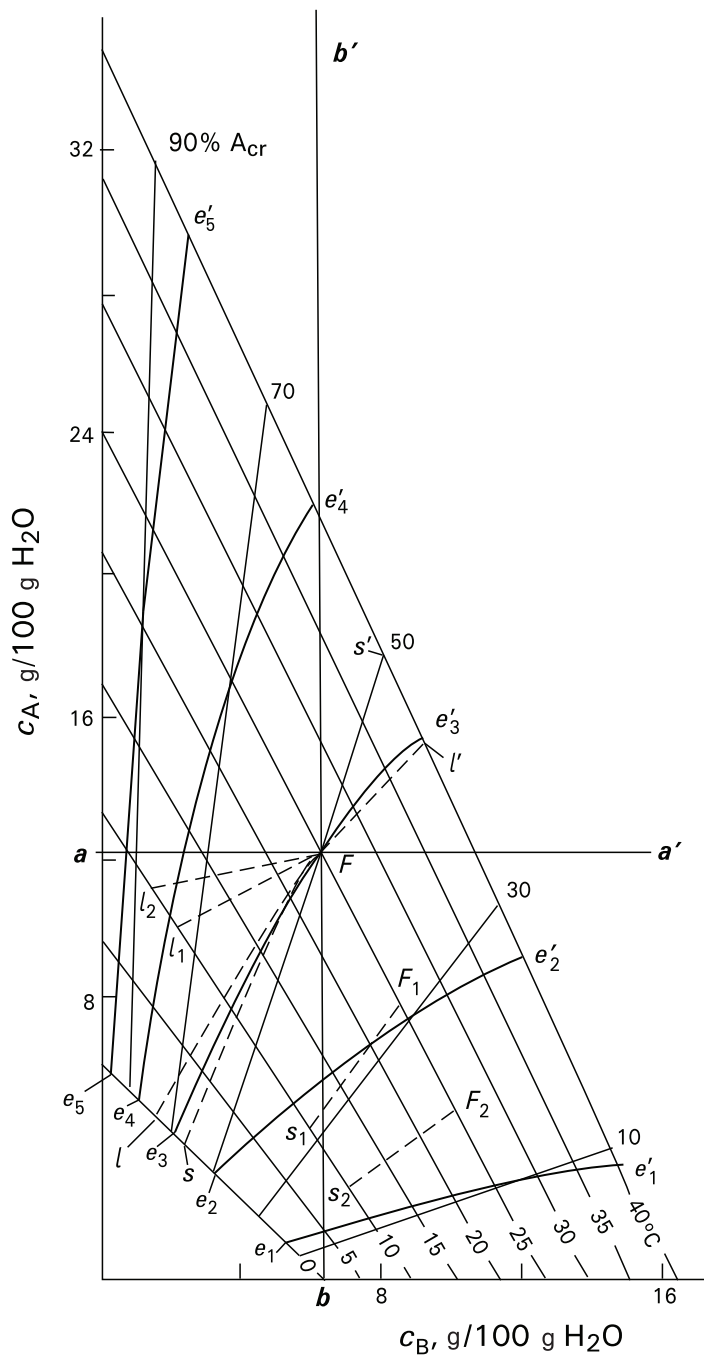
#### 3.3.1 *Modified Concentration Diagrams*

Concurrent analyses of composition changes in solid and liquid phases require combination of two coordinate systems, where the crystal composition is characterized by the component proportions, whereas solution composition also must include the amount of a solvent.

The Schreinemakers concentration phase diagrams (Anosov et al. 1976) are used to define the solution composition. They are convenient and provide with valuable information for analysis of metasomatic crystallogenic processes (Treivus and Rozhnova 1962; Korzhinskii 1970; Treivus 1977; Glikin and Sinai 1983, 1991; Glikin 1995, 1996a, b, c).

The axes of the diagram (Fig. 3.7) are expressed in absolute contents of components A and B in a fixed quantity of a solvent (e.g., in grams per 100 g of H<sub>2</sub>O) with marked values of the component solubilities at certain temperatures (in Fig. 3.7 the temperature ranges from 0 to 40°C with the step of 5°C). The lines connecting the values of components solubility at equal temperatures are the isotherms of the solution equilibrium compositions (liquidus isotherms); they are plotted on the basis of data on mutual solubility of the components.

Isotherm lines representing composition scales are used to determine the crystal composition. The points of 0%, 10%, 30%, 50%, 70%, 90%, and 100% content of substance A in the solid phase are superposed with such compositions of the isotherm that are in equilibrium with the crystals (of course, the selected crystal compositions can be optional, but the scale is the same for a particular isotherm). Homologous isotherm points are to be connected with radial "solidus isocomposites" (hereinafter, "isocomposites").



**Fig. 3.7** Main domains and evolution of crystal formation in a ternary system with continuous isomorphous miscibility of the components A and B. Explanations are given in the text

Ensemble of such isotherms and isocomposites completely describes conditions of thermodynamic equilibria in a system, as each point of the diagram corresponds to the only temperature, composition of the solution, and composition of the crystal determined by the diagram grid.

It is to be emphasized that compositions of solution and crystal in the modified diagram are presented in different coordinate systems. At the same time, the coordinate system of the solid phase is “adapted” to the Schreinemakers diagram, as the values of selected crystal compositions are marked in the points experimentally obtained under equilibrium conditions.

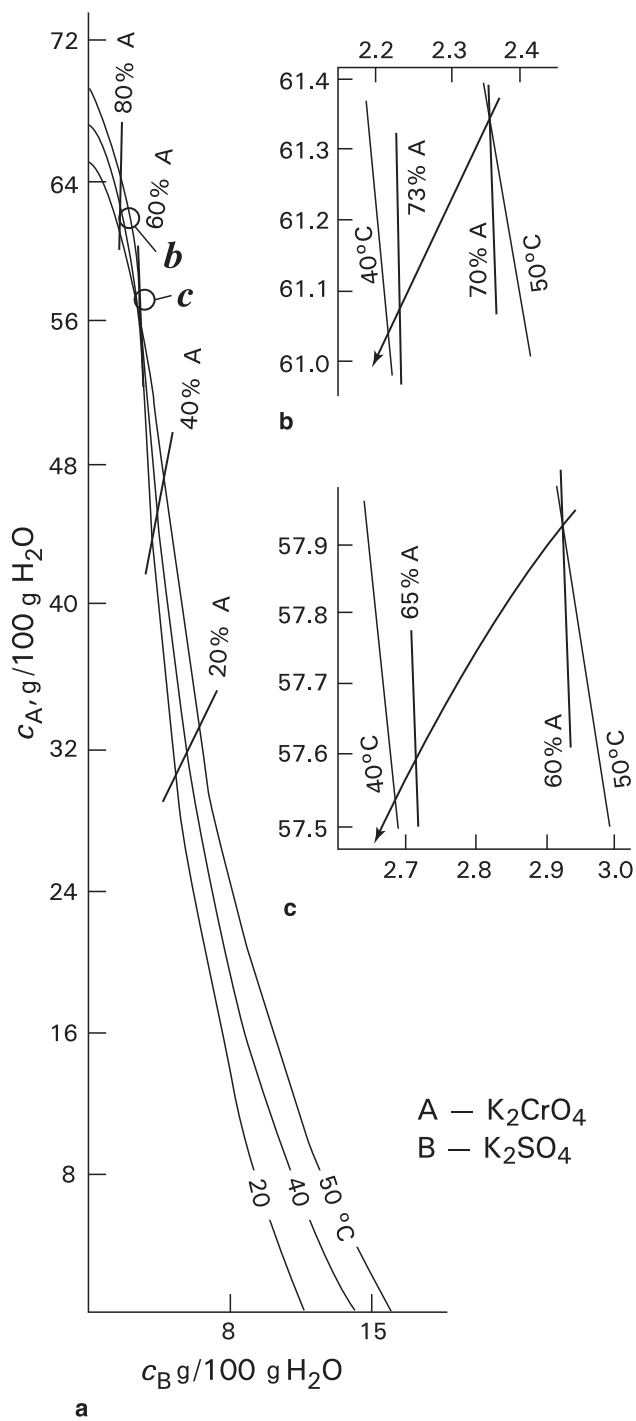
Figure 3.7 represents the case of linear partition of the isotherms with the lines defining equilibrium compositions of the solid phases. Such partition corresponds to a constant coefficient of distribution of the main components between the phases at given temperature. The represented diagram reflects slightly idealized phase states of  $\text{KCr}(\text{SO}_4)_2 \cdot 12\text{H}_2\text{O} - \text{KAl}(\text{SO}_4)_2 \cdot 12\text{H}_2\text{O} - \text{H}_2\text{O}$  system (Fig. 3.3) in 0–40°C range.

In general, the isotherms are not linear, and isocomposite distribution is irregular, i.e., the distribution coefficient at given temperature is not a constant. There exists a great variety of variants, and some of them are discussed below.

Systems  $\text{K}_2\text{CrO}_4 - \text{K}_2\text{SO}_4 - \text{H}_2\text{O}$  (Fig. 3.8) and  $\text{Pb}(\text{NO}_3)_2 - \text{Ba}(\text{NO}_3)_2 - \text{H}_2\text{O}$  (Franke et al. 2007) are characterized by sharp differences in solubility of individual components and changing the isotherm curvatures from concave to convex in the regions of a less- and more-soluble component, respectively. A considerable part of equilibrium crystal compositions of the former system is concentrated in the solution region enriched with more-soluble  $\text{K}_2\text{CrO}_4$ , i.e., in this region the crystal composition is extremely sensitive to the changes of solution composition. On the contrary, in the region enriched with  $\text{K}_2\text{SO}_4$ , the crystal composition is only slightly affected by the changes in solution composition. Also, in the  $\text{K}_2\text{CrO}_4$ -enriched region the isotherms almost merge and isocomposites are almost parallel to the ordinate, i.e., compositions of crystals enriched with  $\text{K}_2\text{CrO}_4$  are practically unaffected by temperature. A considerable difference in the component solubilities corresponds to a strong influence of volume effect resulting, in particular, in fragmentation of a pseudomorph formed under volume-deficit conditions (Fig. 1.6d).

System of acidic phthalates,  $\text{RbHC}_8\text{H}_4\text{O}_4 - \text{KHC}_8\text{H}_4\text{O}_4 - \text{H}_2\text{O}$ , contains individual components having similar values of solubility (slightly higher for  $\text{RbHC}_8\text{H}_4\text{O}_4$ ), and is characterized by convexity of the isotherms (Glikin et al. 2003). This convexity means that replacement of pure  $\text{RbHC}_8\text{H}_4\text{O}_4$  and  $\text{KHC}_8\text{H}_4\text{O}_4$  crystals in initially pure solutions of  $\text{KHC}_8\text{H}_4\text{O}_4$  or  $\text{RbHC}_8\text{H}_4\text{O}_4$ , respectively, proceeds with changing the volume-deficit mechanism to volume-excess scenario (see Sect. 3.4.2).

System  $\text{KCl} - \text{KBr} - \text{H}_2\text{O}$  has convex isotherms (data from Durham et al. 1953; Solubility 1961–1970), similar to their configuration in  $\text{KHC}_8\text{H}_4\text{O}_4 - \text{RbHC}_8\text{H}_4\text{O}_4 - \text{H}_2\text{O}$  system. Replacement of pure  $\text{KCl}$  and  $\text{KBr}$  crystals in initially pure solutions saturated by  $\text{KBr}$  and  $\text{KCl}$ , respectively, proceeds with changing the volume-deficit mechanism to volume-excess scenario. According to our data some intermediate compound  $\text{KCl}_x\text{Br}_{1-x}$  of a fixed alyotropic composition with molar ratio  $\text{Cl}/\text{Br} \approx 1/2$  is present in this series. Crystals grown in the region corresponding to vicinity



**Fig. 3.8** Phase equilibria (a) and evolution of co-crystallization (b and c — trajectories are designated with arrows) in  $K_2CrO_4$ - $K_2SO_4$ - $H_2O$  system containing isomorphous components (isotherms: 20, 40, and 50°C; solidus isolines: 20, 40, 60, and 80% of A) (Data for 40 and 50°C: Kasatkin and Leont'eva 1992, Kasatkin 1993; data for 20°C: Solubility 1961–1970)

of this composition are of a higher perfectness in comparison with that of pure and other intermediate compounds (Taratin et al. 2007).

System  $\text{NaBrO}_3\text{--NaClO}_3\text{--H}_2\text{O}$  is characterized by significant difference in solubilities of individual components, and has concave isotherms (data from Reference book... 1970). This means that replacement of pure  $\text{NaBrO}_3$  and  $\text{NaClO}_3$  crystals in initially pure solutions saturated with  $\text{NaClO}_3$  and  $\text{NaBrO}_3$ , respectively, proceeds with changing volume-excess mechanism to volume-deficit scenario. This series is also likely to contain an intermediate compound  $\text{NaCl}_x\text{Br}_{1-x}\text{O}_3$  having a fixed alyotropic composition with molar ratio  $\text{Cl/Br} \approx 30:1$ .

System  $\text{Co}(\text{NH}_4)_2(\text{SO}_4)_2 \cdot 7\text{H}_2\text{O}\text{--Ni}(\text{NH}_4)_2(\text{SO}_4)_2 \cdot 7\text{H}_2\text{O}\text{--H}_2\text{O}$  is characterized by insignificant isotherm concavity and a relatively uniform fan of isocomposite lines (Kryuchkova et al. 2002). The system characteristics are close to linear, and processes proceeding in different regions do not significantly differ. This was the reason for this system to be chosen as an exemplary one for detailed examinations (see Sect. 3.4.1).

System  $\text{NH}_4\text{H}_2\text{PO}_4\text{--KH}_2\text{PO}_4\text{--H}_2\text{O}$  is characterized by considerable isotherm convexity (Srinivasan et al. 1995) and, it also seems, by presence of an intermediate compound having fixed alyotropic composition –  $(\text{NH}_4)_{0.67}\text{K}_{0.33}\text{H}_2\text{PO}_4$ . This system showed some signs of volume-deficit replacement and transfer to a volume-excess mechanism. Influence of the intermediate compound upon the process was not studied.

### 3.3.2 *Formation of Crystals Under Equilibrium, Quasi-equilibrium, and Non-equilibrium Conditions*

Principles of mixed crystal precipitation will be discussed below with the aid of an exemplary system, i.e.,  $\text{KCr}(\text{SO}_4)_2 \cdot 12\text{H}_2\text{O}\text{--KAl}(\text{SO}_4)_2 \cdot 12\text{H}_2\text{O}\text{--H}_2\text{O}$  (Fig. 3.7). Idealized physicochemical analysis of the system is presented below, assuming the processes proceed in kinetic regime, i.e., with uniform distribution of isomorphous components in a bulk of the solution (including diffusion layer). This analysis was taken into account when planning experiments with  $\text{Co}(\text{NH}_4)_2(\text{SO}_4)_2 \cdot 7\text{H}_2\text{O}\text{--Ni}(\text{NH}_4)_2(\text{SO}_4)_2 \cdot 7\text{H}_2\text{O}\text{--H}_2\text{O}$ ,  $\text{RbHC}_8\text{H}_4\text{O}_4\text{--KHC}_8\text{H}_4\text{O}_4\text{--H}_2\text{O}$ , and  $\text{K}_2\text{CrO}_4\text{--K}_2\text{SO}_4\text{--H}_2\text{O}$  systems, also discussed below, which illustrate a general case of combining a metasomatic reaction with growth or dissolution in supercooled or overheated solutions. The results obtained proved that, as a whole, a theoretical prognosis agreed with experimental findings qualitatively, while rather considerable quantitative discrepancies arose due to limitative influence of diffusion stage upon the process kinetics.

A priori any figurative point of the diagram can correspond to several regions differing in the pathways of the system reactions induced by temperature changes. For example, point *F* in Fig. 3.7 corresponds to 25°C isotherm and solidus composition of 50% A; the contents of A and B in the solution are marked as values *a* and *b* on the ordinate and abscissa respectively. Straight lines *bb'* and *aa'* passing through the point *F* are parallel to the coordinate axes, and delimit the following regions:

1. The isotherm line is a region, where the pure metasomatic processes take place, which, as was shown in Sect. 3.2, can proceed with the volume deficit or excess, if crystal compositions are above or below the point  $F$ , respectively. Trajectories of changing the solution and crystal compositions coincide with the isotherm and are directed toward each other. The point where the trajectories meet corresponds to an equilibrium state of the system, with its position in the isotherm depending upon the initial quantitative proportion of the phases. If a large crystal undergoes replacement in a little volume of solution, the point is located in the neighborhood of the crystal composition; if the ratio is inversed, the point lies within the neighborhood of the initial composition of solution  $F$ . Thus, there should be expected a direct dependence of replacement rate upon increasing the difference between compositions of solution and crystal.
2. Sector  $aFb$  delimits compositions of solutions obtained if spontaneous co-crystallization of both substances takes place in the initially homogeneous solution  $F$  due to lowering the temperature. (Apparently, a region situated beyond the boundaries of  $aFb$  sector can be reached if the system contains an excess of the solid component A or B, which undergoes dissolution.) Here solutions are supersaturated with each substance; supersaturation for the each of the components can be derived from the distance between the coordinates of the initial and the final figurative points on the abscissa and the ordinate.

Proportions of components in solid and liquid phases vary with time. Nevertheless, the process direction and position of the final figurative point can be determined with the aid of the described diagram with any prescribed accuracy only in the case of quasi-equilibrium or equilibrium process.

- (a) If a system keeps a state of quasi-equilibrium, any moment a new layer having a composition, which is in equilibrium with the solution composition, grows on a crystal. Diffusion rate within the crystal under these conditions is negligible.

To determine a pathway of the process starting from the initial point ( $F$ , Fig. 3.7) it is necessary to set up an absolute mass of the crystallizing phase (the less the value, the more precise are the calculations). Then, proportion of isomorphous components in the crystallizing phase can be determined from the initial scale on the isotherm, and their absolute quantities are calculated. Then, these amounts are subtracted from the quantities of dissolved components, thus, allowing to evaluate a new composition of the solution. After that, the isotherm corresponding to the new composition of solution is plotted via interpolation, and a composition of the solid phase, which is in equilibrium with this solution, is estimated with an aid of the solidus isoline grid. Then the new absolute value of composition of precipitating solid phase is set again, and the process is repeated till desirable isotherm is obtained. Appropriate values of the solution composition and total composition of the solid phase are marked on each isotherm.

Figure 3.7 represents trajectory  $F-l$  of the altering solution composition, which coincides with the trajectory of changing composition of the crystal surface layer, while the trajectory of the solid-phase total composition coincides with the line  $F-s$ ,

which is located below the previous one, as the solution is enriched with more-soluble component A and the crystal – with less-soluble component B. It is evident, that the crystal acquires a zonal structure, and, as a whole, the system remains unbalanced.

- (b) If the system is in equilibrium state, it differs from the previous case in having a sufficiently slow rate of precipitation, which is compatible with diffusion rate in the crystal. This ensures the crystal uniformity. Under these conditions the system is in equilibrium, and the trajectories  $F-l$  and  $F-s$  described above coincide with the intermediate line  $F-e_3$ .

Plotting the line  $F-e_3$  involves estimating the compositions of the products formed via isothermal interaction between the quasi-equilibrium solution and crystal. It is to be noted that this interaction is a monocrystalline volume-excess replacement. In this case it is conveniently to use the isotherms plotted during the calculation of quasi-equilibrium trajectories.

Total proportion of component contents in the solid phase and composition of the initial solution correspond to the points of intersection of the isotherm and the lines  $F-s$  and  $F-l$ , respectively. Then  $n = 3-5$  of control dots are selected randomly within the interval delimited by the intersection points. Then the changes in concentrations of the components contained in the solution are calculated for each control point with the aid of the diagram of mutual solubility:  $a_n$  transfers from the crystal into the solution, while  $b_n$  precipitates from the solution. Conjectural amounts of components  $A'_n = A - a_n$  and  $B'_n = B + b_n$  and their ratios  $A'_n/B'_n$  in the solid phases are calculated for all control points from the absolute amounts of components A and B in the precipitated substance, which have been previously derived in the course of plotting the quasi-equilibrium trajectories. Concurrently, proportions  $A''_n/B''_n$  of the components are estimated with the aid of the scale of the solid-phase compositions positioned along the isotherm. The point of the solid-phase composition scale having the same values of  $A'_n/B'_n$  and  $A''_n/B''_n$  is the required point of the equilibrium line  $F-e_3$ . Also, it can be determined as an intersection of the auxiliary graphs  $A'_n/B'_n = f'(n)$  and  $A''_n/B''_n = f''(n)$ .

Thus, the assembly of trajectories  $e'_n-e_n$  depicted in Fig. 3.7 together with the isotherms makes up a nomogram, which allows to determine a pathway of equilibrium crystallization and thermodynamic supersaturation in any figurative point under particular supercooling conditions. It is to be noted that the above estimation technique is valid only for examining a spontaneous crystallization; seed crystallization (including the seeds, which are in the equilibrium with the initial solution) changes proportion of components in the system.

- (c) Nonequilibrium system differs from the previous two cases in having a specific final supercooling, arbitrary precipitation rate, and absence of equilibrium between the crystal surface layer and the solution. Ranges of divergence of the trajectories  $F-l$  and  $F-s$  inside the  $aFb$  region have not been determined for real processes. Such divergences may be considerable at sufficiently strong supercoolings and growth rates. The data obtained by us showed a 30% and greater divergence of crystal compositions from the equilibrium values in



(Co,Ni)(NH<sub>4</sub>)<sub>2</sub>(SO<sub>4</sub>)<sub>2</sub>·7H<sub>2</sub>O–H<sub>2</sub>O and (Pb,Ba)(NO<sub>3</sub>)<sub>2</sub>–H<sub>2</sub>O systems with supercooling ranging from 2 to 20°C and at about 2°C, respectively.

This divergence induces the component interchange between the crystal and solution, i.e., it determines a metasomatic component of the crystal-formation process. The crystal becomes enriched with a less-soluble component, so the reaction proceeds with the volume excess. The reaction must be accompanied by formation of replacement blocking layers including specific autoepitaxial excrescences, and thus result in lowering the growth rate and convergence of  $F-l$  and  $F-s$  trajectories. These effects become obvious if growth rates of the faces, rates of metasomatic interchange, and solid-state diffusion interchange along the dislocation channels or cracks with attached excrescences are commensurable. Combination of autoepitaxial excrescences and growth layers on K<sub>2</sub>(S,Cr)O<sub>4</sub> crystals (Kasatkin 1993) can be accounted for by an intensive metasomatic reaction proceeding at the stage of growing the faces.

Divergence of trajectories at relatively high crystallization rate reflects lowering the rate of capturing a more-soluble component. At the same time, the solution composition trajectory flattens having position of the initial point fixed (e.g.,  $F-l_1$  and  $F-l_2$  in Fig. 3.7), and the limiting position of the trajectory is the line parallel to the abscissa ( $F-a$ ), which corresponds to a zero supersaturation with the component A and crystallization of the pure component B; this conclusion is applicable for initial solutions of any composition. The trajectory of crystal composition leaves the initial point and flattens as well, moving toward the abscissa ( $F_1-s_1$  and  $F_2-s_2$  corresponding to the trajectories  $F-l_1$  and  $F-l_2$ ) and coinciding with it if crystallization of the pure component B takes place.

Whether this limit is attainable still remains unclear; however, the above explanation may help in interpreting formation of pure minerals having high isomorphous capacity under unsterile natural conditions.

It is to be noted that the common consequence of the three phenomena described above is unavailability of solution compositions below the equilibrium line during spontaneous crystallization (e.g., for the initial solution  $F$ , compositions below  $F-e_3$  line are unattainable).

3. Sector  $a'Fb''$  delimits the region of the substance dissolution. The solutions are undersaturated with both substances; degree of undersaturation can be estimated from distances between coordinates of the initial and final figurative points in the abscissa and ordinate for each component separately. Proceeding the dissolution is somewhat analogous to precipitation in the sector  $aFb$ . However, these processes differ, as dissolution includes no analog to a spontaneous growth, and the system is heterogeneous in the initial point.

(a) Equilibrium dissolution of the substance crystallized spontaneously in accordance with the equilibrium trajectory  $e'_3-F$  ( $F-e_3$  is its continuation) occurs in the reversed sequence along the  $F-e'_3$  trajectory. So, determination of undersaturation degree and analysis of the process development can be advantageously made with the aid of a growth nomogram described above.

The equilibrium state is maintained due to sufficiently slow dissolution of substance. As long as the solution composition changes with the process development, the crystal continues entering into metasomatic reaction with the solution, and so the surface layer will be also changing until the equilibrium with the solution is reached. Thus, to attain a total equilibrium the dissolution rate must be lower than the rate of evening-out the concentration differences within the crystal.

In contrast to growth process ( $aFb$  sector), metasomatic component in this case is characterized by volume deficit, and so must have a considerably higher rate.

(b) Quasi-equilibrium dissolution takes place when matter interchange within the crystal bulk is negligibly small, and dissolution is slow enough to maintain equilibrium between the solution and the crystal surface.

In contrast to the growth processes, the particular case given above is meaningless. On one hand, the composition of the initial solid phase may be considered as homogeneous. When the volume of an equilibrium layer tends to a minimum (similarly to the case described in point 2(a) of this section), its bulk composition remains almost the same, and quantitative estimations of the process would not differ from the nonequilibrium case (see below). On the other hand, if a crystal has zoned structure formed in the course of quasi-equilibrium growth, sequential dissolution of the crystal growth layers is impossible due to the principal differences in morphology between the growth and dissolution surfaces.

(c) Nonequilibrium system is distinguished by a high dissolution rate and negligible metasomatic interaction between the crystal and solution. The crystal composition remains the same and the corresponding trajectory coincides with the solidus isocomposite that crosses the initial point; in this example it is  $F-s'$  trajectory. At any moment solution is enriched with both components in constant proportion corresponding to their ratio in the crystal, and the trajectory of changing the solution composition is a half-line starting from the initial point, which in the example discussed is  $F-l'$  trajectory making the angle of  $45^\circ$  with the coordinate axes.

In accordance with initial conditions, the solid phase dissolves completely at  $40^\circ\text{C}$ . In this case, the points  $l'$  and  $e'_3$  should coincide. At lower temperatures solution compositions depend upon efficiency of the metasomatic component and should be located between the trajectories  $F-e'_3$  and  $F-l'$ , whereas the crystal compositions are to be positioned between the lines  $F-e'_3$  and  $F-s'$ .

4. Sectors  $aFb'$  and  $a'Fb$  comprise different regions of metasomatic replacement proceeding at varied temperature. Figure 3.9 represents four types of replacement occurring in the initial solution  $F$  and corresponding to the following final points:  $M_1, M_2, M_3$ , and  $M_4$ , where  $M_1$  and  $M_3$  correspond to cooling, and  $M_2$  and  $M_4$  – for heating;  $M_1$  and  $M_2$  show replacement in the crystal enriched with the component A;  $M_3$  and  $M_4$  indicate replacement in the crystal enriched with the component B.

(a) Replacement at rising temperature (regions  $a_iFb'_i$  and  $a'Fb_i$ ) is analogous to isothermal substitution, which corresponds to line  $ab_i$  (see point 1 of this section), but with some complications caused by indefinite degree of concurrence with ordinary dissolution.



One of the complications is an arbitrary configuration of the composition trajectory of solution interacting with the crystal that undergoes replacement, which may affect a zoned structure and shape of the produced pseudomorphs.

For example, transition of the system to state  $M_2$  occurring during replacement of initially pure K-Cr alum may proceed, generally with volume deficit, along any pathways within the limits of quadrangle  $Fi_2'b_2M_2$ . If the trajectories coincide with the extreme lines  $F-b_2-M_2$  and  $F-i_2'-M_2$ , their sectors  $b_2-M_2$  and  $F-i_2'$  correspond to the periods of isothermic replacement with volume deficit. When the process proceeds along the trajectory  $F-b_2-M_2$ , the produced pseudomorph will bear some signs of the initial crystal dissolution, while if it assumes  $F-i_2'-M_2$  trajectory, the signs of the pseudomorph dissolution will appear. Location of the process trajectory within the limits of quadrangle  $Fi_2'b_2M_2$  indicates absence of dissolution independent stage. It can be considered that replacement is accompanied by extra dissolution, similar to metasomatic component accompanying the dissolution within the sector  $a'Fb'$ .

On one hand, configurations of the trajectories are determined by size and composition of the protocystal, and on the other hand, by the ratio between the rates of heating and metasomatic reaction. If the protocystal contains (A,B)-component, the right line of the delimiting quadrangle shifts into the region of dissolution  $a'Fb'$  (e.g., along the line  $Fb_2'b$ ).

Another complication occurs in the region  $a'Fb_i$ . The main analysis of the process is similar in to the previous one, the exception being that  $a'Fb_i$  region is divided into two parts. In  $b_iFv_b$  part and the adjoining sector of the isotherm  $Fb_i$  the process proceeds with volume excess, while in  $a'Fv_b$  part the process proceeds with volume deficit.

(b) Replacement at lowering temperature (regions  $aFa_i$  and  $bFb_i$ ) is also complicated in comparison with isothermal process or replacement at rising temperature. It is caused by the indefinite character of combination with the normal growth.

One of the complications (as in the case of replacement when the system is heated) consists in arbitrary appearance of the trajectory of liquidus composition corresponding to a specific shape and zonal structure of pseudomorphs. For example, the system transition from the state  $F$  to the state  $M_3$  during replacement of crystal B can take any pathway within the limits of the quadrangle  $Fb_1'i_3'M_3$ . When the trajectory occupies the extreme position  $F-b_1-M_3$ , the replacement is preceded by autoepitaxial growth of the pure phase A over the initial crystal B, and the replacement proceeds according to volume-excess isothermal mechanism. Naturally, shielding layer A causes additional complexities, but they are not considered at present. Another extreme trajectory  $F-i_3'-M_3$  corresponds to the initial stage of volume-excess isothermal replacement followed by growth of the pure phase B over a pseudomorph. Composition of the protocystal, its mass, and cooling and replacement rates determine configuration of the trajectory.

One more complication, which is also similar to the above replacement with heating, consists in dividing the region  $aFa_i$  into two parts. Within the part  $a_iFv_a$  and in the adjoining sector of isotherm  $Fa_i$  the process is volume-deficient, while in the part  $aFv_a$  it is volume-excessive.

### 3.3.3 *Heterogeneous Metastable Equilibrium Between Crystals and Solutions*

Heterogeneous metastable equilibria between crystals and supercooled solutions are peculiar states of systems containing isomorphous components (Glikin 1996a). Lowering temperature to a considerable degree can prevent metasomatic replacement and bring the whole system into an unusual metastable state, when the phenomena inducing the salting-out are compensated by supercooling.

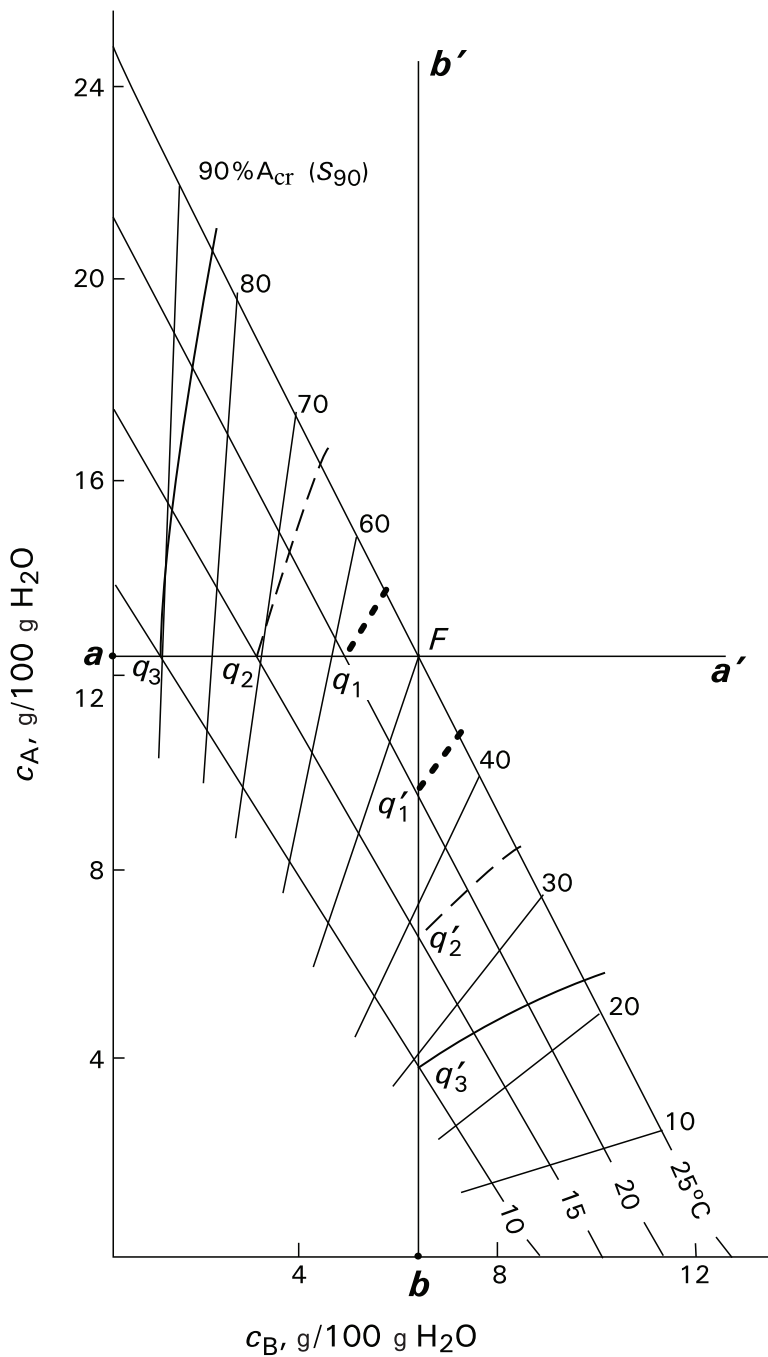
Indeed, replacement (salting-out) originated from dissolution of the initial crystal, which can be terminated by supercooling the system. The required degree of supercooling depends upon solution composition and nature of the crystal undergoing replacement. The value of supercooling can be defined (Fig. 3.10) as a difference between the equilibrium temperature of the initial solution (e.g., 25°C for the point  $F$ ) and the temperature of the isotherm passing through the intersections between a composition isoline of the crystal undergoing replacement and the lines  $Fa$  and  $Fb$ . For example, for solution  $F$ , it is the point  $a$  when the crystal A is being replaced or the point  $b$  when the crystal B is being replaced.

Hereinafter, solutions and crystals coexisting in the state of heterogeneous equilibrium supercooling, and the diagram elements corresponding to the above solutions and crystals (including the lines  $Fa$  and  $Fb$ ) will be referred to as meta-equilibrium elements.

Examination of the diagram represented in Fig. 3.10 can furnish the following conclusion: at a given supercooling degree two solid phases with different isomorphous compositions can exist simultaneously in meta-equilibrium state with the solution. In contrast to the composition of a crystal being in thermodynamic equilibrium with solution (without any supersaturation), compositions of both two phases are enriched with one of the extreme member of the series. In the solution  $F$  supercooled by 5°C, the corresponding crystals are  $q_1$  and  $q'_1$ , while at supercooling of 10°C they are  $q_2$  and  $q'_2$ , and at 15°C supercooling they correspond to  $q_3$  and  $q'_3$ , respectively (Fig. 3.10). In the phase diagram these crystals correspond to two “ternary” crosspoints of the following lines: isotherm of the specified supercooling, two meta-equilibrium lines ( $aF$  and  $bF$ ), and two isocomposites ( $S_i$ ).

At the same time, the supercooled solution is metastably supersaturated in comparison with crystals having any intermediate composition within the sector  $aFb$ , but it is undersaturated in comparison with any crystals corresponding to the other regions  $aFa_i$  and  $bFb_i$  of extreme compositions (Fig. 3.9). Such interpretation gives lines  $Fa$  and  $Fb$  a physical meaning, i.e., they mark conditions of heterogeneous metastable equilibrium and separate regions of crystal compositions, which can be supersaturated or undersaturated compared to the solution  $F$ .

It is essentially to distinguish supercooled solutions under conditions of heterogeneous metastable equilibrium from solutions being in the state of metastable supersaturation. The latter are similar to the metastable supersaturated solutions in binary systems and are homogeneous, i.e., they contain no seeds for which solution is supersaturated. Meta-equilibrium crystals contained in the solution can be



**Fig. 3.10** Equilibria existing between supercooled solution  $F$  and the crystals having different compositions (%A):  $q_1 = 59, q'_1 = 45, q_2 = 72, q'_2 = 39, q_3 = 90, q'_3 = 28$

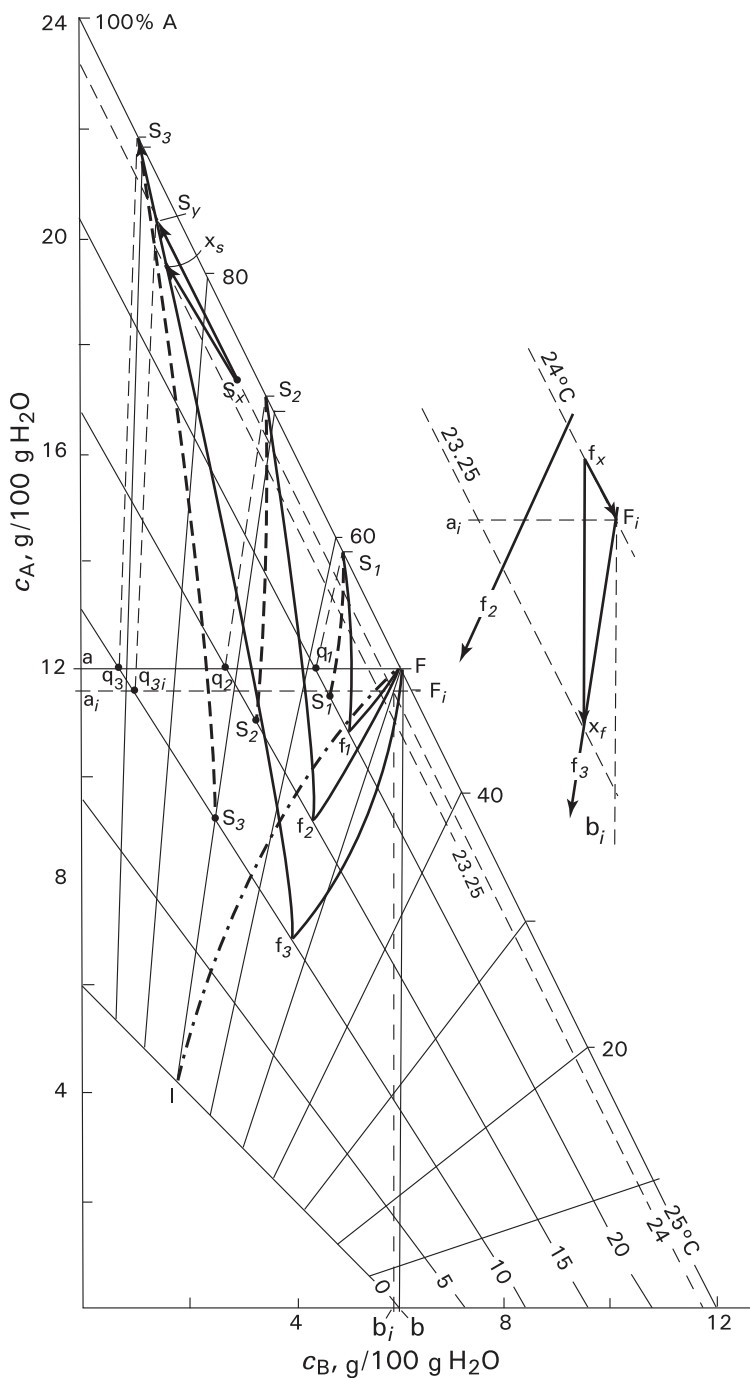
considered as inert bodies, similar to the vessel walls. Heterogeneous meta-equilibria are unattainable in binary systems.

It is interesting to consider a mechanism of meta-equilibrium crystallization of a supercooled solution in a way, analogous to that used for examination of the above model of quasi-equilibrium crystallization discussed in Sect. 3.3.2. Diffusion resistance effect should be ignored. By definition, composition of the solid phase precipitating in this way at any moment of the process corresponds to a state of meta-equilibrium with saturated solution. Compositions of both metastable phases are determined from the graph at the specified supercooling, and trajectories of changes in phase compositions are defined in the same way: quantities of both isomorphous components leaving the initial solution are equal to their amounts contained in the given mass of the precipitating solid phase, which is minimized in accordance with required calculation accuracy. The operation is performed repeatedly for all the compositions obtained in every particular step; it is obvious that degree of supercooling decreases with each subsequent step, and the compositions of precipitating crystals change accordingly. Graphically, in the diagrams, the process termination corresponding to thermodynamic equilibrium of the crystal surface and the solution coincides with intersection of trajectories of solid and liquid phases of the final isotherm.

The above estimations (Glikin 1996a) are similar to those described in Sect. 3.3.2 for quasi-equilibrium systems (Glikin 1995), the difference being the method of determining the solid-phase composition. The examples are shown in Fig. 3.11. Composition of the initial solution  $F$  corresponds to that of the equilibrium crystal containing equal contents of both components – 50% of A and 50% of B (same as for the examples described in Sect. 3.3.2). There are three cases possible (Fig. 3.11): (a) the crystals are enriched with A-component (ternary points of the isoconcentrate  $aF$ , e.g.,  $q_i$ ; Fig. 3.11a), (b) crystals are enriched with B-component (ternary points of  $bF$ , e.g.,  $q'_i$ ; Fig. 3.11b), and (c) both crystals precipitate simultaneously (ternary points of  $aF$  and  $bF$ , e.g.,  $q_i$  and  $q'_i$  respectively; Fig. 3.11c; rates of precipitation of both phases correlate so that both the crystal compositions are in meta-equilibrium at any moment). Trajectories of phase compositions for the initial supercoolings equal to 5, 10, and 15°C are represented in the figures.

Iteration procedure applied, for example, to a diagram plotted for supercooling of 15°C (Fig. 3.11a, b) shows that at the first step the solid phases have the following compositions (%A):  $a - S_3 = 91$  (ternary point  $q_3$ ),  $b - S'_3 = 28.5$  ( $q'_3$ ). Precipitation 0.5 g of crystals would cause the compositions of the solutions to reach points  $F_i$  and  $F'_i$ , i.e., crosspoints of the new isoconcentrates  $F_i a_i$  and  $F'_i b_i$ ,  $F'_i a'_i$  and  $F_i b'_i$ , and the new isotherms, as in each case, supercooling decreases by the value of a difference between the temperatures of the previous and subsequent isotherms. The second step consists in precipitating the crystals having the following compositions:  $a - S_{3-\Delta} = 87.5$  ( $q_{3i}$ ),  $b - S'_{3-\Delta} = 33$  ( $q'_{3i}$ ) and plotting the new points for solution compositions and drawing the new isoconcentrate lines. Continued iterations allow to find the final points  $f_3$  and  $f'_3$ .

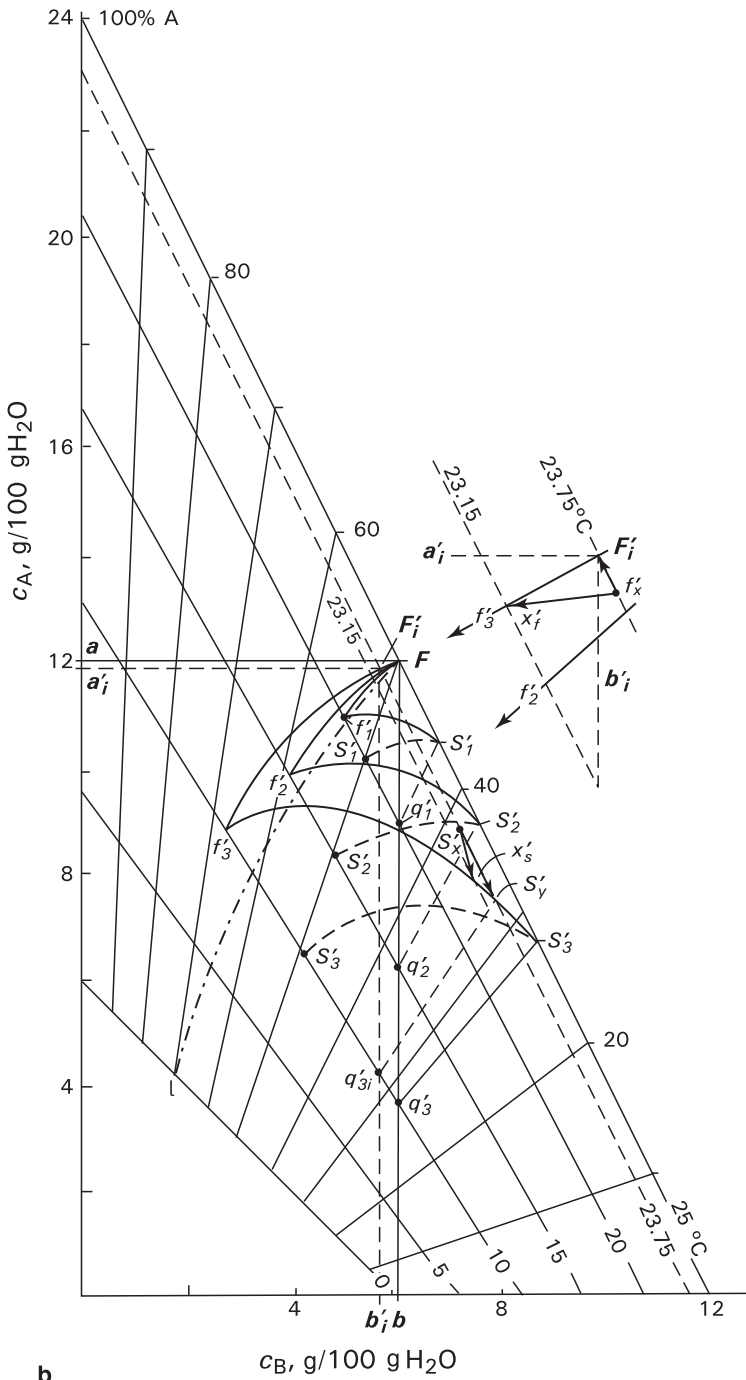
Iterations used in the last example (Fig. 3.11c) involve similar steps of finding compositions of crystals enriched with different components. It is to be noted that



**a**

**Fig. 3.11** Proceeding the quasi-equilibrium crystallization in a supercooled solution of two isomorphous components A and B **a, b** – precipitating the crystals enriched with components A (**a**) and B (**b**); **c** concurrent depositing the crystals of the two types.  $F$  – experimental solution;  $Ff_i$  – trajectories of changing the solution compositions (hereinafter  $i = 1, 2, 3$  correspond to the initial supercoolings 5, 10, and 15°C);  $Sf_i$  – trajectories of changing the compositions of the crystal surface zones,





**b**

**Fig. 3.11** (continued) –  $S_i, s_i$  trajectories of changing the total compositions of the crystals;  $Ff$  – trajectory of changing the compositions of the solution and crystal during equilibrium crystallization. Lines 0–25°C – solubility isotherms; radial lines – isolines of crystal compositions (isocomposites);  $Fa$  and  $Fb$  – isoconcentration lines for A and B components, respectively; thin dash lines corresponding to the isoconcentration line families are shown for estimation assistance. Other explanations are given in the text

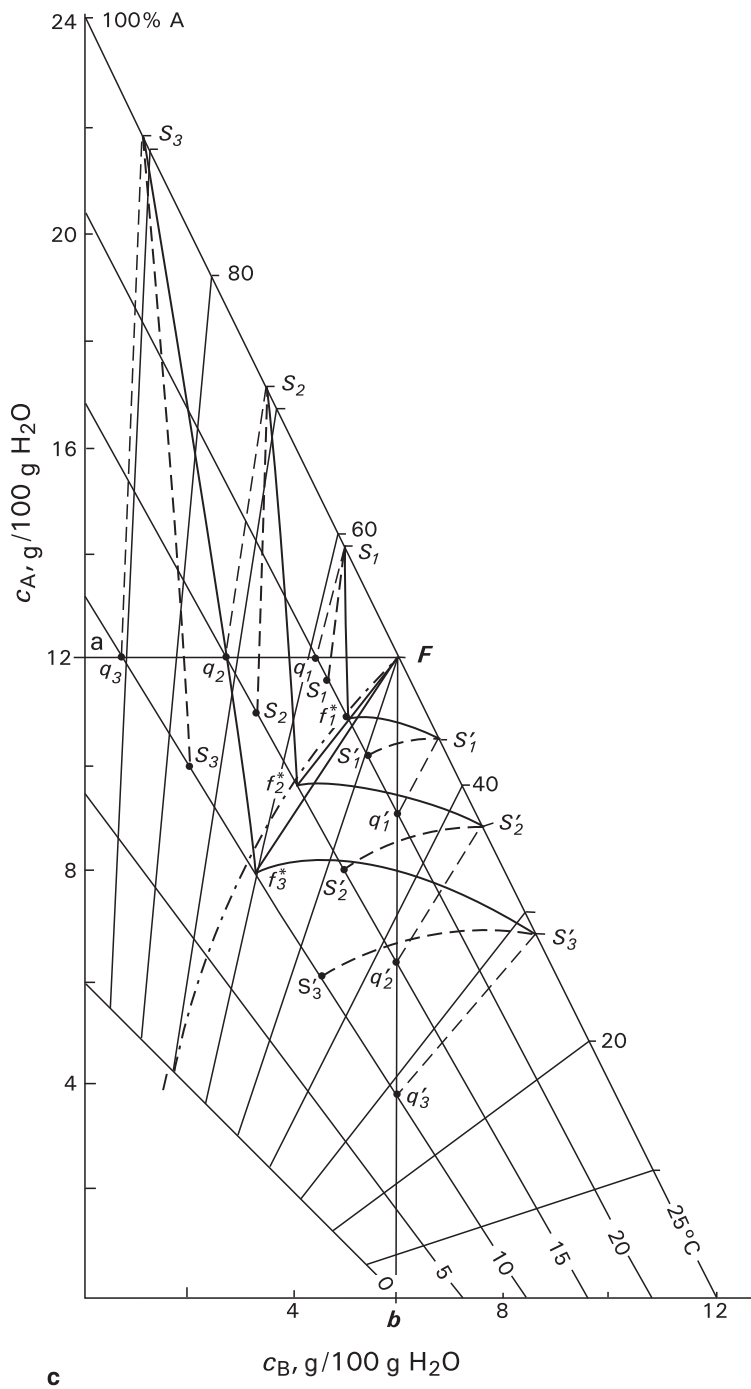


Fig. 3.11 (continued)

simultaneous precipitation of the crystals of two different types results in the reversed variation of the crystal compositions from the periphery toward the centre of the diagram.

Similar methods can be used for determination of changes in phase compositions at a constant supercooling or under specified conditions of supercooling variation during meta-equilibrium crystallization; they are also applicable for the process of solution evaporation, which additionally requires an adjustment of the coordinate scales.

Thus, any solution containing fixed concentrations of two isomorphic components at sufficient supercoolings is metastable for isomorphic-mixed crystals having two different compositions, with the difference diminishing to zero as the supercooling decreases. Thermodynamic equilibrium can be reached only in a solution existing in equilibrium with crystals of only one particular composition.

Meta-equilibrium crystallization in question is a real process that was first proved by insignificant partial precipitation of the solid phase from deeply supercooled solutions of  $K_2(Cr,S)O_4$  (Glikin 1996a). Such meta-equilibrium may be reasonably stable, and so may require a special mechanism providing shifting the phase compositions toward the point  $f_i$ . This mechanism can be assumed to involve some temperature fluctuations resulting in temporal multidirectional disturbances of the equilibrium (Glikin 1996a). Thus, shifting the figurative points inside or outside the region  $Ff_iS_i$  induces growth of crystals or metasomatic alterations in near-surface regions of the crystals, while the cyclic proceeding of the process leads to a gradual disappearance of the composition differences between the phases.

Two pathways of metasomatic reactions, which alternate at lowering or elevation of temperature, are considered below. They produce multidirectional disturbances in meta-equilibrium supercooled solutions. It is to be noted that if the total composition of the system is constant (i.e., the system does not contain any seeds or is not undergoing dilution or evaporation), positions of figurative points of the solution are conjugated with those of crystals at the moments of spontaneous disturbances of meta-equilibrium, and solutions compositions do not diverge significantly from equilibrium lines  $Ff_i$ . This is represented graphically in Fig. 3.11, which shows proportions between the trajectories drawn at different levels of supersaturation.

1. Figurative points of solution and crystal are situated in the region  $Ff_iS_i$  (e.g.,  $f_x$  and  $s_x$  are in the region  $Ff_3S_3$ , or  $f'_x$  and  $s'_x$  are in the region  $Ff'_3S'_3$ ; see Figs. 3.11a, b respectively). As reaction proceeds, points move toward the corresponding meta-equilibrium lines: in the examples concerned, the solution points move to  $Ff_3$  and  $Ff'_3$ , and the crystal points shift toward  $S_3f_3$  and  $S'_3f'_3$ . The respective displacement vectors for the solution are  $f_xF_i$  and  $f'_xF'_i$ , and for the crystal they are  $s_xS_y$  and  $s'_xS'_y$ ; they are shown in the 10-fold magnified inserts of Figs. 3.11a, b. It is to be noted that, in comparison with isothermal reaction, the displacement appears inversed when the trajectory vectors are directed toward each other and join in the equilibrium point.

At the same time, as the solution is supersaturated with the crystal matter, the crystal transformation should be accompanied by an additional growth component that

causes vectors of both trajectories deviate toward the region of lowering temperatures ( $f'_x x_f$  and  $s'_x x_s$ ,  $f'_x x'_f$  and  $s'_x x'_s$ ).

2. Figurative points of crystal and solution are outside the region  $Ff_i S_i$ . As the reaction proceeds, the points also move toward the corresponding meta-equilibrium lines, and the solution points shift toward  $Ff_3$  and  $Ff'_3$ , while the crystal points transfer toward  $S_3 f_3$  and  $S'_3 f'_3$ ; here, vectors of displacement are directed toward each other, but their final meta-equilibrium points are separated. As the solution is undersaturated with the crystal matter, transformation of these crystals should be accompanied by an additional dissolution component. The resultant vectors should be directed toward the region of increased temperature. If the divergence is less than in the previous case, meta-equilibrium crystallization actually occurs.

The first case also takes place during spontaneous crystallization, thus presenting serious uncertainty. In Sect. 3.3.2, we assumed that compositions of spontaneously formed crystals tend to one of the extreme members of the series. The model considered corrects this assumption by delimiting compositions of solutions and crystals with the lines of quasi-equilibrium crystallization and allowing precipitation of crystal of two types, which tend to compositions of different components. In the presented examples (Figs. 3.11a–c), for the deepest supercooling of 15°C, these lines are  $Ff_3^* - S_3 f_3^*$  (a),  $Ff'_3 - S'_3 f'_3$  (b), and  $Ff_3^* - S_3 f_3^* - S'_3 f'_3$  (c).

The analysis given above clearly indicates a possibility for spontaneously formed crystals to have bimodal composition distribution and shows movement of composition of crystals belonging to different modes in opposite directions from the centre to periphery.

The pathway of spontaneous crystallization proceeding is determined by deviation of compositions of initially precipitated crystals from their meta-equilibrium values and also by the ratio between the growth and metasomatic components (i.e., orientation of the resultant vectors). The resultant vectors  $f'_x x_f$  ( $s'_x x_s$ ) and  $f'_x x'_f$  ( $s'_x x'_s$ ), represented in Figs. 3.11a, b, bring the system back to its meta-equilibrium state. This phenomenon was observed in  $K_2(S, Cr)O_4 - H_2O$  system as termination of crystallization mentioned above. Naturally, the metasomatic constituent should impede growth of isomorph-mixed crystals in comparison with the rate of growth of single-component solid phase; such proportion of the growth rates was determined for crystals of  $K_2(S, Cr)O_4$  and  $K_2SO_4$  (Kasatkin 1993; Kasatkin et al. 1995). The growth rates of isomorph-mixed crystals are expected to be unstable as a result of alternating modes with a greater or less metasomatic constituent caused by fluctuations of supercooling that even can lead to a complete termination of the growth due to reaching a meta-equilibrium state.

Use of sufficiently large seed crystals complicates the process analysis as the solution composition shifts due to unavoidable interchange processes.

The model comprising various aspects of mixed crystal formation is proposed as a working hypothesis for explanation of the process peculiarities and for planning the new experiments. It can predict some aspects of the real systems, which can provide several possibilities for its thorough experimental verification (some of the aspects have already been proved and are described in the following sections).

Some experimental results for several model systems are given below. It is to be noted that the quantitative data may differ essentially from the predictive estimations as a result of impossibility of the in situ control of such fundamental system properties as compositions of diffusion layer and that of the crystal surface. Besides, an accuracy of quantitative measurements is limited by impossibility of obtaining the seeds of specified mixed composition, and also by the fact that from the moment of contact between a seed and a foreign solution the surface composition starts changing, thus affecting the process kinetics during the measurements. However, this problem is avoided when working with crystals having fixed compositions. Difference between the real and idealized processes is represented by the example of  $(\text{Co,Ni})(\text{NH}_4)_2(\text{SO}_4)_2 \cdot 6\text{H}_2\text{O}$  series described in Sect. 3.4.1.

### 3.4 Morphological and Kinetic Behavior of Monocrystals

#### 3.4.1 *Tutton Salt Series* $(\text{Co,Ni})(\text{NH}_4)_2(\text{SO}_4)_2 \cdot 6\text{H}_2\text{O}$ <sup>[2]</sup>

##### 3.4.1.1 Methods

Researches were carried out with crystals of  $\text{Co}(\text{NH}_4)_2(\text{SO}_4)_2 \cdot 6\text{H}_2\text{O}$  or  $\text{Ni}(\text{NH}_4)_2(\text{SO}_4)_2 \cdot 6\text{H}_2\text{O}$  in solutions containing various contents of these salts under ambient conditions in flat preparations (Fig. 1.2a) and in a thermostatically controlled microcrystallization cell (Fig. 2.1).

A flat preparation containing a plate of  $\text{Co}(\text{NH}_4)_2(\text{SO}_4)_2 \cdot 6\text{H}_2\text{O}$  or  $\text{Ni}(\text{NH}_4)_2(\text{SO}_4)_2 \cdot 6\text{H}_2\text{O}$  with average dimensions of about  $5 \times 4 \times 0.25 \text{ mm}^2$  was placed between an object carrier and a cover glass. The plate was cut out in a random direction from an isometric crystal (size up to 10 mm), which did not contain any visible inclusions. The plates of  $\text{Co}(\text{NH}_4)_2(\text{SO}_4)_2 \cdot 6\text{H}_2\text{O}$  were glued between the object and cover glasses with water-resistant synthetic glue leaving all the ends opened, while plates of  $\text{Ni}(\text{NH}_4)_2(\text{SO}_4)_2 \cdot 6\text{H}_2\text{O}$  were not glued at all. Acetone lacquer was used as glue, because it does not cause noticeable deformations of the crystal during drying. The gaps between the glasses were sealed hermetically with vacuum lubricant. Saturated solutions containing definite concentration ratios of Ni- and Co-components were introduced into the corresponding preparations into the space between the glasses via a syringe. Each preparation was used to study kinetic–morphological phenomena of interaction with seeds of both pure compositions; behavior of crystals in “own” solution of the same composition was not examined. Previously, only morphological phenomena were studied for reactions of crystals and solutions represented by extreme members of isomorphic series

---

<sup>[2]</sup>Using materials of original published works (Kryuchkova et al. 2002; Glikin et al. 2007).

[e.g., reactions of  $\text{Co}(\text{NH}_4)_2(\text{SO}_4)_2 \cdot 6\text{H}_2\text{O}$  crystals with  $\text{Ni}(\text{NH}_4)_2(\text{SO}_4)_2 \cdot 6\text{H}_2\text{O}$  solution and vice versa; (Glikin and Sinai 1983; Glikin and Sinai 1991)]. Volume of solution added to each plate sample amounting to approximately 0.2 ml was determined by the sample thickness (0.25–0.30 mm) and by the size of the cover glass (15 × 15 mm). Only ends of the “glued” plates reacted with the solution allowing to observe morphological changes including macroscopic changes of the end-face relief and to detect the progress of the reaction front from the crystal periphery toward its center. Interaction of “nonglued” samples with solution occurred on the whole sample surface, also allowing to detect changes of relief. Observations were carried out with binocular and optical microscope.

A microcrystallization device was used for experiments in thermostatically controlled conditions (Petrov et al. 1969). It allowed simultaneous determination of solution saturation state, controlling the equilibrium temperature of the solid and liquid phases, cooling the solution to a necessary temperature, and visual observation of seeds. The quartz cell (Fig. 2.1) was connected to the thermostat and fixed on the vertical objective table of an optical microscope equipped with an ocular micrometer and photo- (or video-) recorder. The test solution and the seeds were introduced into the inner vessel of the cell. A seed was fixed on the crystal-holder capable of axial rotation. Composition of the solution was maintained constant during the test by using great volumes of the solutions (50 ml), small seeds (up to 2 × 2 × 2 mm), and absence of other crystals. Signs of growth/dissolution on the crystal surface (sharpening/rounding of edges, direction of the layers movement, etc.) were examined in situ in solutions of fixed compositions under microscope in transmitted or reflected light at temperatures set in neighborhood of saturation.

The saturation point was accepted as a medium value of the minimum temperature interval (0.1°C generally), at the upper and lower limits of which there were respectively observed growth and dissolution of an equilibrium seed.

It is impossible to prepare a seed of specified intermediate composition because the actual final supercooling causes deviation of the crystal composition from the equilibrium one by an uncertain, but probably significant value (Glikin 1996a; Franke et al. 2007), and controlling the crystal composition requires destruction of the sample. So, to attain the equilibrium composition the seeds of pure  $\text{Co}(\text{NH}_4)_2(\text{SO}_4)_2 \cdot 6\text{H}_2\text{O}$  or  $\text{Ni}(\text{NH}_4)_2(\text{SO}_4)_2 \cdot 6\text{H}_2\text{O}$  were subjected to step-by-step direct overgrowing in a portion of the test solution. First, a temperature was set at such a value that a seed started to grow. The seed appeared to be covered with a sufficient quantity of material in 20–30 min. Then the temperature was gradually risen till the first signs of dissolution appeared, and then again the temperature was lowered till the growth recommenced, and was continued for another 20–30 min. This procedure was repeated until the 0.1°C interval between the growth and dissolution processes ceased its shifting (i.e., surface of the seed acquired its equilibrium composition); the middle value of this interval was taken as the saturation temperature. States of growth or dissolution of a seed were additionally controlled by monitoring the directions of convective streams. So, the measurement error for saturation temperatures was ±0.05°C within the interval of 26.5–30.5°C.

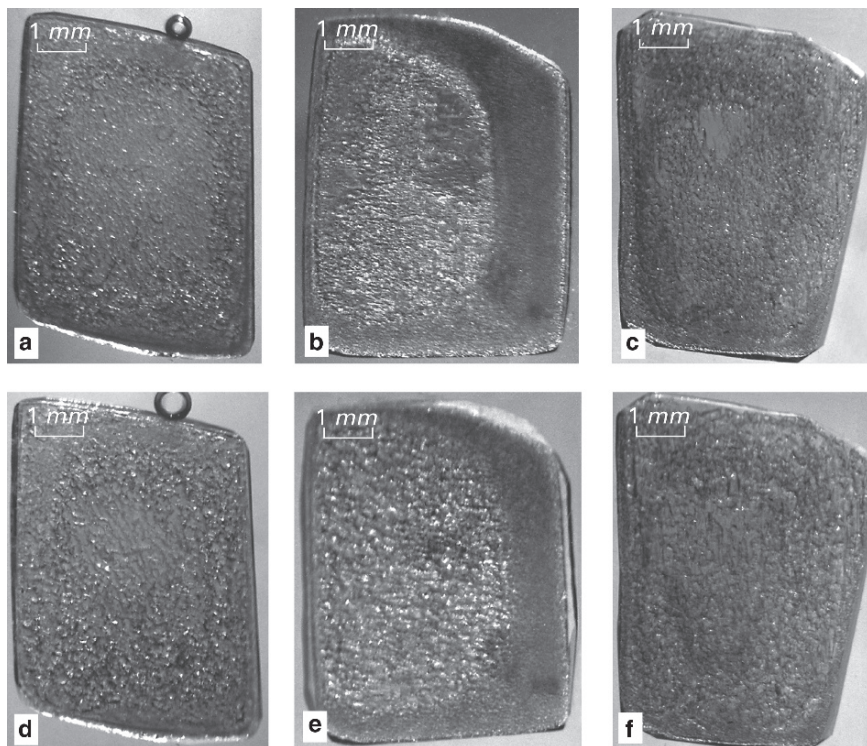
All observations and kinetic measurements were taken at different values of supercooling with the step of 0.2–0.3°C (the minimal supercooling was 0.2–0.3°C, and the maximal one varied in the range 0.7–1.5°C, the measurement error was  $\pm 0.05^\circ\text{C}$ ). A seed was inserted into a previously supercooled solution. To prevent solution contamination by spontaneous nuclei, a seed was washed with water before introducing into a corresponding solution, so that seed surfaces became covered with numerous etching pits. Only spontaneously precipitated crystals of the extreme members of the series, i.e.,  $\text{Co}(\text{NH}_4)_2(\text{SO}_4)_2 \cdot 6\text{H}_2\text{O}$  and  $\text{Ni}(\text{NH}_4)_2(\text{SO}_4)_2 \cdot 6\text{H}_2\text{O}$ , were used as the seeds. Each measurement (observation) was performed with a new seed having an unchanged surface composition.

The experiments were conducted with the same proportions of the components in the solutions as were used in the flat preparation studies. Interaction of each solution with the seeds of both types was studied. Changes in the surface relief caused by metasomatic reaction and direct processes of growth and dissolution were monitored.

#### 3.4.1.2 Isothermal Reactions of Flat Preparations

The “foreign” saturated solutions were observed to profoundly affect the crystals. In all cases interchange of isomorphic components took place, easily detected from the change in coloration from red to brown and then to green or vice versa, as experiments involved use of chromophores  $\text{Co}^{+2}$  and  $\text{Ni}^{+2}$ . According to known data (Glikin and Sinai 1983), enrichment of Co-crystal with Ni-component is accompanied by rapid invasion of spongy macrostructure from the crystal periphery toward its centre (Fig. 3.12). The inversed reaction of Ni-crystal with Co-containing solution resulted in slow formation of replacement rims enriched with Co and having a distinct border with the Ni-relic (Fig. 3.13). As it was expected, ortho- and conoscopic patterns in crossed nicols demonstrated preservation of monocrystalline structure in all the flat samples accompanied by some other differences in morphological replacement attributes that had not been detected earlier in solutions having different composition.

Top (*a–c*) and bottom (*d–f*) rows of Fig. 3.12 show the early and late (2 and 8 days) stages of replacement of Co-crystals in solutions containing successively decreasing initial contents of Ni (from left to right). “Grained” and nontransparent regions of the crystals are formed by monocrystalline sponges of  $(\text{Co,Ni})(\text{NH}_4)_2(\text{SO}_4)_2 \cdot 6\text{H}_2\text{O}$  composed of large ( $\approx 0.04\text{ mm}$ ) and small ( $\approx 0.002\text{ mm}$ ) cell-inclusions and “blocks” located between them. In solutions of intermediate composition (Ni/Co = 50/50 wt%; Figs. 3.12*b*, *e*) the spongy structure replaces the crystal almost completely within 2 days. In solutions containing other concentrations of Ni-component (low or, especially, high; Figs. 3.12*a*, *d* and 3.12*c*, *f*), a relic can be still found in the centre of the crystal after 2 days; after 8 days a less changed core still can be discerned. Also, in all cases the spongy structure expands with time and acquires an even distribution within the crystal. The photos show (Figs. 3.12*a–c*) that fine- and coarse-grained spongy zones appear in the edge region and in the central area, respectively, at the



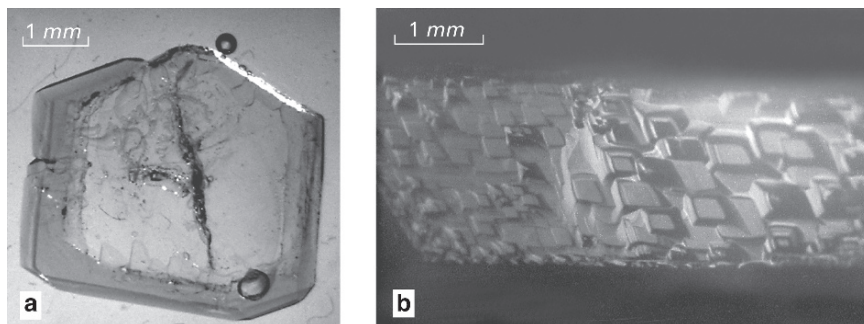
**Fig. 3.12** Volume-deficit replacement. A crystal of  $\text{Co}(\text{NH}_4)_2(\text{SO}_4)_2 \cdot 6\text{H}_2\text{O}$  in solution containing various proportions of Ni/Co-components Ratio Ni/Co (wt%): **a, d** – 100:0; **b, e** – 50:50; **c, f** – 30:70. Reaction duration: **a, b, c** – 2 days; **d, e, f** – 8 days

reaction beginning stage. In solutions of intermediate compositions (Figs. 3.12*b, e*) the fine-grained regions are the most distinct and stable during the both stages of the experiment, while in the other solutions the regions disappear by the end of the first stage (Figs. 3.12*a, d* and 3.12*c, f*). It can be seen that the fine-grained region shrinks due to enlargement of the coarse-grained core (Figs. 3.12*b, e*).

Generally, it takes from several days up to a month, depending on the solution composition, for complete replacement of a 5 mm crystal of  $\text{Co}(\text{NH}_4)_2(\text{SO}_4)_2 \cdot 6\text{H}_2\text{O}$ . Progress of the spongy region toward the crystal center is as fast as about 0.2–0.3 mm a day; the coarse-grained region penetrates into the fine-grained one at a rate of about 0.02–0.04 mm in 5–6 days. In a number of cases a strong anisotropy of the replacement rate was detected (Figs. 3.12*b, e*).

Figure 3.13*a* demonstrates a zoned structure formed during replacement of Ni-crystals in solution of  $\text{Co}(\text{NH}_4)_2(\text{SO}_4)_2 \cdot 6\text{H}_2\text{O}$ . These reactions proceed with volume excess and result in formation of solid pseudomorphs. Formation of autoepitaxial excrescences on the crystal surfaces was detected before (Glikin and Sinai 1983).





**Fig. 3.13** Zoned structure and relief of crystals formed via volume-excess replacement. Crystals of  $\text{Ni}(\text{NH}_4)_2(\text{SO}_4)_2 \cdot 6\text{H}_2\text{O}$  in solution  $\text{Co}(\text{NH}_4)_2(\text{SO}_4)_2 \cdot 6\text{H}_2\text{O}$

Yet, observation of the crystals end-faces showed that faces of such pseudomorphs may be plane, without any signs of isolated excrescences. Formation of a replacement zone (monocrystalline rim) does not occur simultaneously on every side of a crystal, and the rate of its ingress into the crystal is not uniform. In experiments with equal reaction time, the lesser difference is observed between compositions of the crystal and solution, i.e., the lesser is a content of Co-component in the solution, the narrower is the replaced region. Rate of replacement decreases with time. So, a 5 mm crystal of  $\text{Ni}(\text{NH}_4)_2(\text{SO}_4)_2 \cdot 6\text{H}_2\text{O}$  may be replaced within the period of a few months. The observed maximal rate of replacement region ingress into a crystal is about 0.01–0.02 mm a day, i.e., by an order of magnitude less than that for replacement with volume deficit.

### 3.4.1.3 Reactions in the Thermostatically Controlled Cell

Monitoring the crystal surface relief while the crystal was reacting with “foreign” *supercooled solutions* allowed to estimate a ratio between metasomatic and growth constituents. After introducing the seed into a supercooled solution, its surface developed a “replacement relief” gradually changing to a “growth relief.” Duration of “pre-growth stage of replacement” depended upon solution and seed compositions and supercooling degree and was estimated as a period passing until the appearance of the first signs of the “growth relief.” The shorter the stage was, the less was the proportion of metasomatic component in this process. Kinetic estimation involved determination of time interval (“pre-growth period”) between the seed introduction and appearing the first signs of growth on the initial rough surface, typical for replacement. Zero value of this interval was considered to mean a “minimal growth supercooling,” i.e., growth was proceeding without preliminary replacement. The methods used did not allow to determine this point directly, so it was estimated by means of experimental data extrapolation.

Under volume-deficit conditions of pre-growth replacement, the surface relief obtains random rough (scalloped in the section) pattern of the entire surface or some of its parts (e.g., if replacement is slow, the scalloped pattern is formed on steps only). Character of this relief is determined by alternative development of the dissolution and growth elements, location of which is constantly varying (Glikin and Sinai 1983). The first elements of the growth relief appear in the bottom part of a vertical face as multiple small light-reflecting growing elements of the surface. Subsequently, growth layers become discernible in these elements, and the elements' arrangement acquires a regular flaky pattern (Fig. 3.13*b*). Initially details of the pattern are fine and indistinct, but with time they enlarge, and eventually the entire surface develops a coarse flaky pattern with smooth rounded edges of the "flakes." The surface of a seed become smooth with time: e.g., at  $\Delta T = 0.2^\circ\text{C}$  it happens in 1 h or more, and at  $\Delta T = 1.0^\circ\text{C}$  the change takes place in 10–20 minutes.

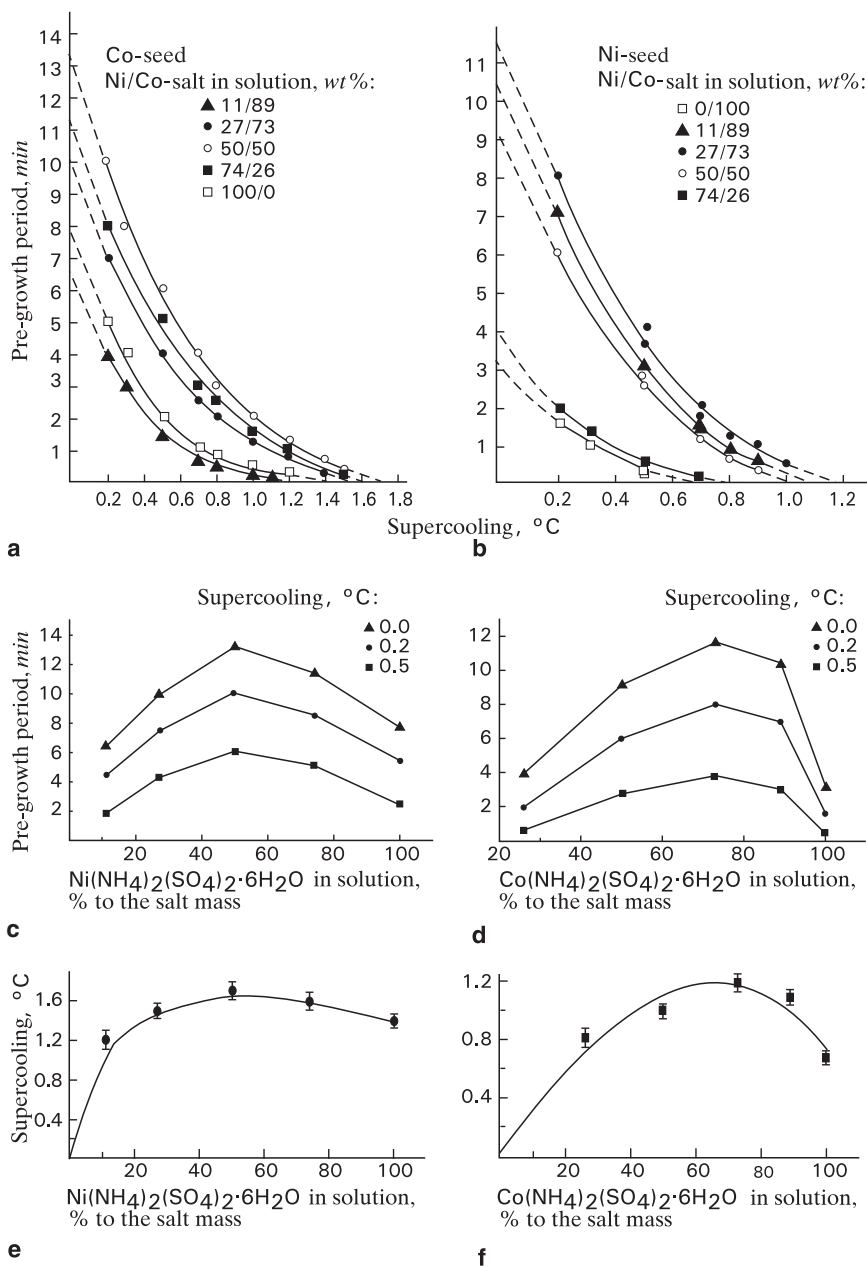
In the course of volume-excess pre-growth replacement the surface relief comprises slowly changing, twisting, and sluggishly moving steps, having appeared in the very beginning of the process. The moment of the first discernible ordering of the crystal surface elements in the bottom part of the vertical face is considered as the starting moment of growth. This moment was registered with accuracy of about 0.5 min (including subjective perception of the moment). Later on, the surface obtains a flaky appearance, but the "flakes" are of polygonal or irregular shape. Filling up the etching pits formed during preparation of the seeds for introducing into the solution leads to a gradual change of the surface relief into polygonal flake-shaped clusters of layers, inheriting the pattern of the etching pit distribution. As the time passes, the surface of a seed gets smoothed too, but faster than in the previous case: e.g., smoothing takes 2–3 min in 100% solution of  $\text{Co}(\text{NH}_4)_2(\text{SO}_4)_2 \cdot 6\text{H}_2\text{O}$  at  $\Delta T = 1.2^\circ\text{C}$ .

Start of growth is easier to detect for  $\text{Co}(\text{NH}_4)_2(\text{SO}_4)_2 \cdot 6\text{H}_2\text{O}$  seeds than for  $\text{Ni}(\text{NH}_4)_2(\text{SO}_4)_2 \cdot 6\text{H}_2\text{O}$  seeds (volume-deficit and volume-excess pre-growth replacement respectively). That is the reason of difference in accuracy of estimating the pre-growth period for seeds of different composition. The accuracy for Co-crystals is estimated to be about 0.2–0.3 min and for Ni-crystals it is about 0.5–1 min. The pre-growth period shortens steadily as supercooling deepens for both Co and Ni seeds in reactions with solutions of any composition (Figs. 3.14*a, b*). Extrapolation of the diagrams on the abscissa and the ordinate allows to estimate influence of the solution composition upon duration of pre-growth period in saturated and oversaturated "foreign" solutions (Figs. 3.14*c, d*) and upon the value of "minimal supercooling" defining the absence of the pre-growth period (Figs. 3.14*e, f*).<sup>3</sup> The dependencies contain maxima approximately corresponding to the intermediate compositions of solutions.

Also, it is to be noted that in a number of cases when supercooling ranged from about  $0.2^\circ\text{C}$  to about  $0.5^\circ\text{C}$  it was possible to detect sufficiently long (up to 5–6 min) stages of changeless state of the crystal surface subsequently transforming into a

---

<sup>3</sup>Pre-growth period was first observed by A.E. Voloshin and S.I. Kovalev in the course of replacement in (K,Rb)HC<sub>8</sub>H<sub>4</sub>O<sub>4</sub> series.



**Fig. 3.14** Kinetic characteristics of the process of combined growth and metasomatic replacement  
**a, c, e** – volume-deficit replacement; **b, d, f** – volume-excess replacement **a, b** – dependence of pre-growth period versus supercooling; **c, d** – dependence of pre-growth period versus solution composition; **e, f** – dependence of minimal supercooling when the pre-growth period is absent versus solution composition

state of growth. At those stages no signs of replacement, growth, or dissolution were observed, i.e., the conditions corresponded to a metastable equilibrium of the system.<sup>4</sup>

A combination of signs of dissolution and replacement was observed in *overheated solutions*. In contrast to dissolution of crystals in “own” solutions (the same component in crystal and solution), the relief pattern altering in the course of the process also is different for various parts of the surface. Investigations were conducted in solutions saturated with Co- and Ni-components contained in equal weight ratios at 26.5 and 28.8°C (dots 3 and 7, respectively, in Fig. 3.15a).

Dissolution of  $\text{Co}(\text{NH}_4)_2(\text{SO}_4)_2 \cdot 6\text{H}_2\text{O}$  crystals is accompanied by volume-deficit replacement. If overheating does not exceed 18°C, a seed obtains a spongy surface relief immediately after its introduction into solution (the greater the overheating, the smaller are the spongy elements), and after that the surface gradually starts to dissolve. If overheating exceeds 18°C, the signs of replacement and dissolution appear at the initial stage of reaction between the seed and solution. If overheating is about 30°C, the seed starts to dissolve from the moment of its introduction showing no signs of replacement.

Dissolution of  $\text{Ni}(\text{NH}_4)_2(\text{SO}_4)_2 \cdot 6\text{H}_2\text{O}$  crystals accompanied by volume-excess replacement consists in a combination of formation of autoepitaxial excrescences and surfaces of dissolution. If overheating is below 6°C, the process starts with generation of autoepitaxial excrescences. Then etching pits start to appear between the excrescences, while the excrescences can be also located on the bottoms of these pits. If overheating exceeds 6°C, development of excrescences and pits starts from the very beginning of the process; increasing the overheating results in reduction of growth components and expansion of dissolution region.

Rapid dissolution without any signs of growth and replacement was detected when overheating exceeded 20°C.

So, reaction between a seed and overheated foreign solution either starts with replacement and changes to dissolution, or starts with a combination of replacement and dissolution (without pre-dissolution period), or directly begins with dissolution. Corresponding values of overheating significantly exceed similar values of supercooling for combinations of replacement and growth.

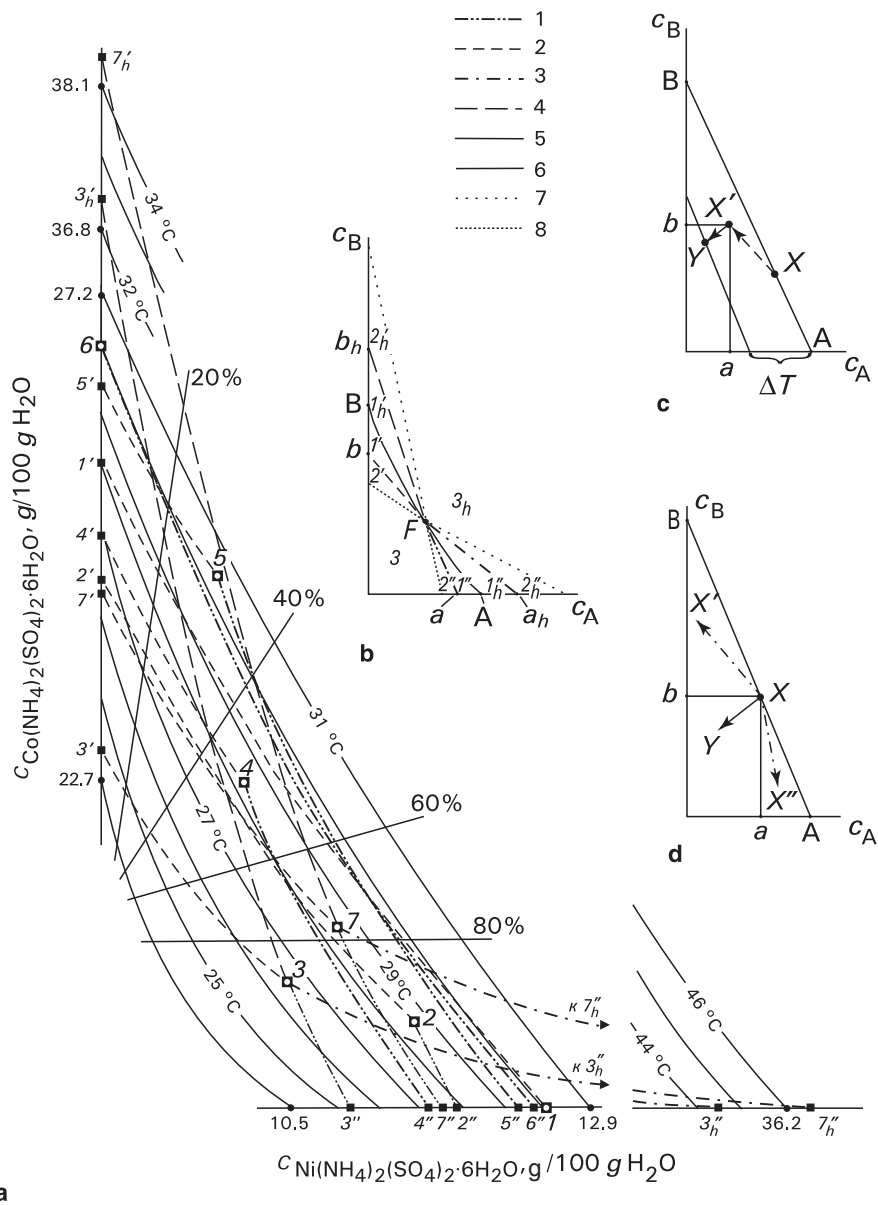
#### 3.4.1.4 Physicochemical Interpretation

Physicochemical interpretation (Fig. 3.15) is based on the phase equilibria data obtained in the system under investigation.

Figure 3.15a shows that isotherms are almost linear (a slight concavity in the region of compositions enriched with Ni-component is negligible). According to the data obtained for such systems (see Sect. 3.3.2), reaction of Co-crystals with solution of Ni-component or solution of any other intermediate composition would result in formation of spongy pseudomorphs (volume-deficit replacement), while reaction of Ni-crystals with Co-containing solution or with any solution of

---

<sup>4</sup>This period exceeds 20 min for  $(\text{Ba,Pb})(\text{NO}_3)_2$  series (microcrystallization observations).



**Fig. 3.15** Schreinemakers diagram for  $(\text{Ni,Co})(\text{NH}_4)_2(\text{SO}_4)_2 \cdot 6\text{H}_2\text{O} - \text{H}_2\text{O}$  system. The scale is distorted. Dots 1–7 – starting solutions with the following Ni/Co-salt ratios (%wt): 1 – 100:0; 2 – 74:26; 3 and 7 – 50:50; 4 – 27:73; 5 – 11:89; 6 – 0:100. Lines 1 and 2 – boundaries of regions with and without pre-growth replacement period, respectively; lines 3 and 4 – boundaries of dissolution regions with and without signs of replacement, respectively (lines joining dots 1–7 with abscissa and ordinate – volume-excess and volume-deficit replacements, respectively); lines 5 – isotherms 24–31°C; lines 6 – isocomposites of the crystal phase (20–80%). Lines 7 and 8 in the insert **b** – boundaries of dissolution  $3_h$  and growth  $3$  regions. Explanations are given in the text. In inserts – schemes: **b** – location of the regions having different ratios between metasomatic replacement and growth or dissolution; **c** – change of the solution composition in the diffusion layer; **d** – types of the kinetic mode processes in supercooled solutions ( $X-Y$  – growth,  $X-X'$  – combination of growth and volume-deficit replacement,  $X-X''$  – combination of growth and volume-excess replacement)

intermediate composition would produce solid pseudomorphs (volume-excess replacement). This can be observed in flat preparations.

Coarsening the elements of spongy replacement structures mentioned above (inclusions and blocks), occurring as time passes, can be attributed to coalescence of inclusions, which should accompany inclusion migration within the bulk of a crystal, and also to alternating growth/reduction of inclusion caused by temperature fluctuations (similar to transformation of an ensemble of crystals; see Punin 1964, 1965). Probability of formation of new barriers within an inclusion, the process, which is opposite to coalescence, is obviously close to zero. Yet the reasons for the coarse-grained region consuming the fine-grained zone are not clear. Formation of finely dispersed structure can be explained by a high initial rate of the process caused by a great initial difference in the compositions of solution and crystal at the beginning of the reaction when the diffusion layer that could obliterate this difference has not been formed. When the diffusion layer comes to a stable state and the difference in compositions is smoothed over, the entire process turns to a stiller mode resulting in enlargement of the relief elements. These effects require further investigations.

Kinetic results obtained are summarized in the diagram represented in Fig. 3.15a, which was plotted on the basis of a modified concentration diagram (see Sect. 3.3.1). The diagram comprises the following main elements: coordinate axes with concentration values of  $\text{Co}(\text{NH}_4)_2(\text{SO}_4)_2 \cdot 6\text{H}_2\text{O}$  and  $\text{Ni}(\text{NH}_4)_2(\text{SO}_4)_2 \cdot 6\text{H}_2\text{O}$  salts in water, solubility isotherms of the mixed salts of  $(\text{Co},\text{Ni})(\text{NH}_4)_2(\text{SO}_4)_2 \cdot 6\text{H}_2\text{O}$ , and a group of "isocomposites" (including the coordinate axes) for 0, 20, 40, 60, 80, and 100 wt% content of Ni-component in the solid phase.

The diagram contains figurative points 1–7 of the investigated solutions. "Kinetic points" 1'–5', 7', and 2''–7'' are marked on the isocomposites of pure Co- and Ni-crystals, which at the same time are the coordinate axes. There are no kinetic points 6' and 1'', because the figurative points 6 and 1 are situated directly on the axes. Each kinetic point is located at a distance from the figurative point, which is equal to an estimated "minimal supercooling" (Fig. 3.15a). The figurative and kinetic points are connected with the lines having the same curvature as the adjacent isotherms.

The test experiments conducted in solutions containing equal proportions of components did not reveal any significant temperature dependence of kinetics in the investigated interval of saturation temperatures (points 3 and 7 in Fig. 3.15a). For that reason all kinetic data were combined and normalized to 29°C, i.e., intermediate value of saturation temperature.

According to morphologic attributes, kinetic phase diagram<sup>5</sup> of a ternary system with continuous isomorphic miscibility may be divided in any intermediate point of

---

<sup>5</sup>The concept of kinetic phase diagram may be considered to characterize the system state under different conditions of nonequilibrium with participation of metasomatic constituent in the process of crystal formation. This approach elaborates the previously introduced concept (Borisov 1962; Treivus 1982, 2000) by including the metasomatic constituent. The term "kinetic phase diagram" is not generally accepted and, thus, can be widened to assume a more general interpretation.

the diagram into a number of domains, showing correlations between replacement, growth, and dissolution processes (Fig. 3.15*b*). Two regions of pure replacement (with volume deficit or excess) are located along the isotherm on the opposite sides of the figurative point. Within the four regions adjacent to the isotherm ( $I'$  and  $I''$ , corresponding to low supercooling,  $I'_h$  and  $I''_h$  corresponding to weak overheating), the process starts with replacement. Upon completion of the pre-growth or pre-dissolution periods the replacement is gradually inhibited by growth or dissolution, respectively. Within the next four regions ( $2'$  and  $2''$  corresponding to intermediate supercooling;  $2'_h$  and  $2''_h$  corresponding to intermediate overheating), the process starts with a combination of replacement and either growth or dissolution; the replacement is also gradually slowing down in the course of the process. Boundaries between the regions corresponding to the weak and intermediate supercoolings (dash and dash-dot lines in Fig. 3.15*b*) represent regions of metastable heterogeneous equilibrium between the supercooled solutions and crystals. Growth and dissolution in regions  $3$  and  $3_h$  are not accompanied by any evident signs of replacement.

Experimental points 3 and 7 (Fig. 3.15*a*) have been completely described in respect to the growth and dissolution regions.<sup>6</sup> They correspond to the point  $F$  in the scheme (Fig. 3.15*b*); points  $a$  and  $b$  (meta-equilibria in supercooled solutions) correspond to supercooling of 1.7°C for Ni-seeds and 1.2°C for Co-seeds, dots  $a_h$  and  $b_h$  (meta-equilibria in overheated solutions) correspond to overheating of 18°C for Ni-seeds and 6°C for Co-seeds. The boundary points of the inner regions  $3$  and  $3_h$  (growth or dissolution without evident signs of replacement in solutions with considerable supercooling and overheating, respectively) are as follows: supercoolings for Ni- and Co-seeds are 6.0 and 3.2°C, degrees of overheating are 30 and 20°C, respectively.

Thus, morphological attributes make it possible to introduce four additional regions which have not been included into the idealized diagrams (see Sect. 3.3.2). The additional domains can be included owing to differentiation of replacement regions into subregions with or without pre-growth (pre-dissolution) periods. The new diagram differs from the idealized form in containing profoundly non-orthogonal meta-equilibrium lines. These features of the real processes can be explained by influence of diffusion resistance.

Highly important is experimental detection of kinetic points  $1'-5'$ , and  $2''-7''$  (Figs. 3.15*a, b*), as it proves both their predictive existence and the general concept of mixed crystals suggested above (see Sects. 3.3.2 and 3.3.3). Physical meaning of these points includes the following: A crystal introduced into a solution saturated with its isomorphic component must dissolve inducing a salting-out reaction and autoepitaxial precipitation of some quantity of a mixed compound having an intermediate composition on the crystal surface. If the solution is supercooled, dissolution and all subsequent stages of the process slow down. If supercooling degree is sufficient, these stages terminate completely; this degree of supercooling

<sup>6</sup>As the main diagram contains too many details (Fig. 3.15*a*), only meta-equilibrium lines corresponding to certain supercoolings are plotted. Boundaries of the pure dissolution regions ( $3_h$  in Fig. 3.15*b*) are marked for the points 3 and 7.

corresponds to the points  $1'-5'$ ,  $7'$  and  $2''-7''$  obtained by means of extrapolation (Figs. 3.14*a*, *b*). These points describe metastable heterogeneous equilibrium between the supercooled solution and the solid phase, which can be observed as above-mentioned periods of invariable state of the crystal surface.

Each point of the lines arising from the points 1–7 and terminating at the points  $1'-7'$  of the abscissa and  $1''-7''$  of the ordinate are kinetic points corresponding to equilibria between the solutions 1–7 and crystals of intermediate compositions; some of the compositions are plotted as isocomposites 20%, 40%, 60%, and 80% in the diagram. In other words, these lines represent temperatures of metastable heterogeneous equilibria (meta-equilibria) for crystals of different composition in a given solution. They are plotted assuming that supercooling, which is necessary for attaining meta-equilibrium between a solution and a “foreign” crystal, should be increasing as the content of the “foreign” isomorphous component increases in a crystal. The exact location of the meta-equilibrium lines might be determined by testing a series of seeds having known intermediate composition, which is highly problematical.

Another experimental verification of the predicted effects can be derived from the shapes and positions of meta-equilibrium lines, which are close to isotherms, while their branches representing Co- and Ni-enriched crystals form an obtuse angle in the solution initial figurative point. The prognostic analysis (see Sects. 3.3.2 and 3.3.3) was carried out assuming the angle  $a \times b$  between these branches to be  $90^\circ$  (Fig. 3.15*c*), since directions of the trajectories of changing solution compositions in the initial figurative point determine the processes of direct growth and metasomatic dissolution. In fact, any trajectory within a right angle (e.g., X–Y, Fig. 3.15*d*) corresponds to precipitation of both isomorphous components, i.e., to direct growth, which can be accompanied by replacement. The trajectories outside the angle (e.g., X–X' or X–X'') characterize precipitation of one of the components accompanied by dissolution of the other, i.e., metasomatic replacement, which can be accompanied by direct growth. We observed direct growth in the replacement region that disagrees with ideas about interaction between these processes and requires an explanation.

The contradiction mentioned above is most likely to be illusory and is determined by generating a diffusion layer of solution around the crystal. The process observed is to take place within the diffusion layer, when its isomorphous composition rapidly approaches that of the crystal. At the same time, conditions of the direct growth are provided on the local microscopic level despite the fact that the total characteristics of the system should correspond to replacement conditions. Thus the scheme shown in Fig. 3.15*c* represents a probable local trajectory of altering a diffusion layer composition from the total figurative point X toward the local figurative point X'', which is the vertex of the right angle under discussion, in the course of metasomatic interaction between the crystal and solution. The point X' is positioned at a little distance from the initial isotherm, being shifted toward the lowered temperatures owing to supercooling and presence of the corresponding component of direct growth. This induces a change in surface composition of a crystal of initial composition B to form mixed compounds. Further the trajectory is directed toward



*Y*, because the surface having a new composition undergoes a direct growth caused by supercooling. The total state of the solution does not vary during this process, while monitoring the crystal composition *in situ* is impossible.

It is important that the value of meta-equilibrium supercooling depends only upon a proportion of isomorphous components in solution and the crystal composition. No temperature dependence of meta-equilibrium supercooling upon absolute concentrations of the components in the solution was observed. So, it can be seen that data obtained for  $(\text{Co,Ni})(\text{NH}_4)_2(\text{SO}_4)_2 \cdot 6\text{H}_2\text{O}-\text{H}_2\text{O}$  system at different saturation temperatures ranging from 26°C to 30.5°C form homotypic dependences (Fig. 3.15*a*). It is to be noted that the test measurements of meta-equilibrium supercoolings for Co- and Ni-seeds in solutions with 50:50 (%wt) ratio of isomorphous components at saturation temperatures of 26 and 28.4°C (points 3 and 7) agreed within 0.1°C ( $\Delta T = 1.7^\circ\text{C}$ ).

In a similar way it can be supposed that the system is in a metastable overheated state comprising a short interruption of growth phase induced by a salting-out effect of the protocystal. Actually, this state has not been detected, but if it existed, it could not be considered as a symmetrical process to one discussed above. Overheating can inhibit only the second stage of salting-out, i.e., growth, termination of which would not affect dissolution, but not the initial stage, i.e., dissolution that limits the entire process, including the growth stage. No crystals of any composition can resist dissolution in an overheated system, since undersaturation conditions have no analogy to the metastable supersaturated state.

Scheme of the process proceeding under kinetic conditions in the systems, similar to  $(\text{Co,Ni})(\text{NH}_4)_2(\text{SO}_4)_2 \cdot 6\text{H}_2\text{O}-\text{H}_2\text{O}$ , was discussed in Sects. 3.3.2 and 3.3.3. It allows concluding that increased difference between the crystal and solution compositions results in acceleration of isothermal replacement and raising the degree of meta-equilibrium supercooling and prolongation of the pre-growth period. So, kinetic-morphological nonmonotony of changes in the solution composition observed in the course of volume-deficient replacement as acceleration of the replacement rate of in solutions of intermediate composition (Figs. 3.12*b*, *e*) and as peaks of curves in Figs. 3.14*c-f* was totally unexpected.

Nature of the revealed nonmonotony is unclear, but most probably it results from the difference in diffusion processes occurring in the crystal neighborhoods during interaction with solution of different compositions. Indeed, the rate of salting-out is directly proportional to the rate of delivering the solution particles to the crystal. Dissolution accelerates with increasing the difference between the crystal and solution compositions, but if the difference is relatively small, dissolution is not too intense and it limits the entire reaction. As the compositional differences and dissolution rate increase, diffusion from the solution becomes the limiting stage, since the diffusion layer becomes saturated with the crystal components and the salting-out flows reach the state of equilibrium. Then, as saturation increases, inflow of the solution particles becomes blocked and thus the entire reaction is inhibited.

It is interesting to point out that effect of the solution composition upon characteristics of the process with both volume-deficit and volume-excess is quite similar in nature and in absolute values (Fig. 3.14). According to the proposed explanation

of nonmonotonies, it means that contribution of the diffusion stage is equal in both processes. However, this appears dubious, at least at zero supercooling.

Important data for proving or denial of this or any other interpretation may be obtained in examining the influence of stirring upon dependencies under discussion, yet such data are still scarce. Investigations of interaction between  $\text{NiSO}_4 \cdot 7\text{H}_2\text{O}$  crystals and solutions of  $\text{MgSO}_4 \cdot 7\text{H}_2\text{O}$  showed that at  $0.2^\circ\text{C}$  supercooling stirring ( $\approx 100$  rps) decreases the pre-growth period from 6 to 3 min, while at  $0.4^\circ\text{C}$  supercooling the period diminishes from 3 to 1 min. However, effect of stirring is opposite for the series of  $(\text{K,Rb})\text{HC}_8\text{H}_4\text{O}_4$  (see below).

### 3.4.2 Series of Potassium–Rubidium Acidic Phthalates $(\text{K,Rb})\text{HC}_8\text{H}_4\text{O}_4$ <sup>[7]</sup>

#### 3.4.2.1 Methods

Study of formation of potassium–rubidium acidic phthalate crystals (KAP and RbAP) are similar to that used for investigation of the Tutton salts described in Sect. 3.4.1.1.

*In flat preparations* (Fig. 1.2a). A crystal plate of KAP or RbAP having a size of about  $7 \times 5 \times 0.25$  mm was chipped from a carved crystalline column along the cleavage surfaces (010).<sup>8</sup> The surfaces of samples (KAP mainly) were covered with chemically resistant lacquer exposing the end-faces. The surfaces of the other samples (RbAP mainly) were left entirely exposed. Solutions containing definite concentration ratios of KAP/RbAP (about 15 compositions, the ratios ranged from 0:100 to 100:0) were introduced into the corresponding samples into the space between the glasses by means of a syringe. Volume of solution added to each flat sample was determined by the sample thickness (0.25–30 mm) and the size of a cover glass ( $15 \times 15$  mm). Observations were carried out with optical microscope.

Investigations of supercooled solutions were performed in the *thermostatically controlled cell* (Fig. 2.1).

Initial stages of replacement processes were examined using *atomic-force microscopy*.

#### 3.4.2.2 Isothermal Reactions in Flat Preparations

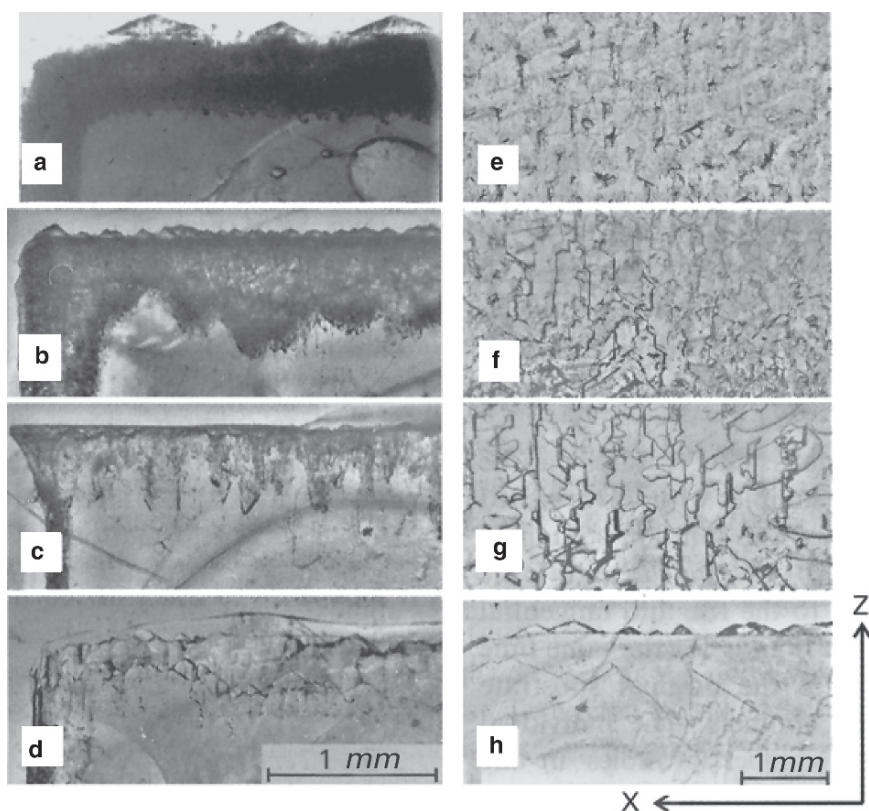
Isomorphic replacement of the crystal periphery zones or that of the entire crystal was observed. Interference ortho- and conoscopic patterns in crossed nicols showed preservation of monocrystalline structure in all the samples.

<sup>7</sup>Using data of original publications (Kryuchkova et al. 2002; Glikin et al. 2003; Woensdregt and Glikin 2005).

<sup>8</sup>A conventional rhombic setting was used. Actually, the crystals had monoclinic structure, and their cleavage was oriented along (100) (Glikin et al. 1979).

Imperfection zones penetrating the crystal were observed in “lacquered” samples of RbAP (Figs. 3.16*a–d*). Application of practically pure solutions of KAP (8% of RbAP – Fig. 3.16*a*) caused formation of imperfection region comprised by a net of fine channels, significantly penetrating into the crystal bulk and containing inclusions of solution. The inner boundary of the imperfection zone is relatively sharp and straight, but its section made in parallel to the (001) surface, contains a sequence of small juts and cavities. The end-face of the (001) crystal bears faceted autoepitaxial excrecences.

The channels width increases with increase of RbAP content (35 %wt – Fig. 3.16*b*) in the solution. The inner edge of the imperfection region is relatively sharp and even on the section parallel to the (100) surface, but distinctively wavy on the part parallel to the (001) surface. Faceted autoepitaxial excrecences can be seen on the end-face (001) of the crystal, while on the (100) surface they join in to form a continuous layer. Then, when the content of RbAP is about 67% (Fig. 3.16*c*), the number of the channels decreases, but they become wider, so that formation of the

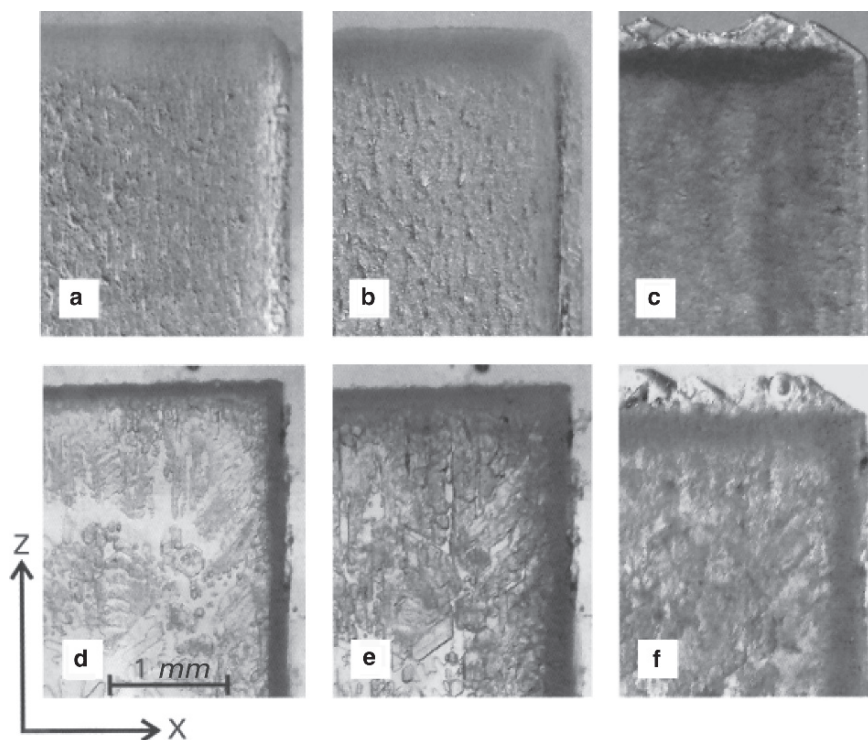


**Fig. 3.16** Crystals of RbAP (**a–d**) and KAP (**e–h**) replaced in solution with various KAP/RbAP ratios (%wt): **a** – 92:8, **b** – 65:35, **c** – 33:67, **d** – 17:83; **e** – 0:100, **f** – 9:91, **g** – 33:67, **h** – 17:83. Sections are parallel to the (010) cleavage

inner-faceted regions is observed. Faceted autoepitaxial excrescences buried under a solid layer of the new formation can be discernible on the end-face surface (001) of the crystal. A spongy structure saturated with solution inclusions is formed at a small distance from the crystal surface, its edge being parallel to the surface. As the difference between the compositions of the crystal and solution grows smaller (83% of RbAP – Fig. 3.16*d*), the inner-faceted regions form a uniform zone, and a region of loose chains of isolated inclusions is formed under it. The excrescences of the end-face surface (001) are buried under a uniform layer of the new formation.

Thus, at a high relative concentration of KAP in the solution, the process starts with development of a spongy structure composed of channels penetrating the external zone of the initial crystal of RbAP. After that, in 1–2 h, the channel development slows down abruptly and a visible formation of autoepitaxial structures begins. Their growing up to the state shown in Fig. 3.16 takes several days.

Features of an epitaxial texture can be seen in the KAP preparations with exposed surface (Figs. 3.17*e–h*). If a solution contains a small concentration of KAP, viz.: 0–9% (Figs. 3.16*e, f*), the autoepitaxial layer develops in the course of nucleation



**Fig. 3.17** Stages of crystal replacement: KAP in solution of RbAP (**a, b, c**) and RbAP in solution of KAP (**d, e, f**) **a, d** – 15 min; **b, e** – 100 min; **c, f** – 170 h

and tangential growth of multiple excrescences. Uncovered parts of the initial substrate remain at the boundaries between the excrescences. The individual excrescences grow bigger, while the number of uncovered spaces in the epitaxial layer decreases, as the difference between the solution and substrate compositions diminishes (Fig. 3.16g). If a solution contains about 65% of KAP (Fig. 3.16h), the crystal surface gets covered with a uniform transparent layer of the new formation containing traces of excrescences resembling the layer shown in Fig. 3.16d. An advanced autoepitaxial excrescence texture can be seen on the end-face of a crystal.

Monitoring dynamics of isomorphic replacement of KAP and RbAP initial crystals revealed a similarity in the replacement development. Figure 3.17 shows photos of cleavage chips of KAP and RbAP crystals at different moments of their interaction with solutions of RbAP and KAP, respectively. In all cases the process starts with the crystal dissolution. After 5 min, distinctly visible imperfection zones are formed in the peripheral zones of both the crystals as the processes progresses at the end-faces. Even at the initial stage, in both cases the process substantially consists in formation of a spongy texture. Also noteworthy is formation of excrescences on the end-faces (001) of both type crystals; but while the KAP face is almost completely covered, there is still a significant part of RbAP surface that remains exposed.

Difference in the processes occurring in crystals of KAP and RbAP becomes less pronounced with time. After 1.5 h, the KAP surface becomes entirely covered with solid rough layer of the new formation, and degree of covering the RbAP surface with the new phase excrescences also rises significantly, though uncovered spaces of substrate still remain. At the same time, formation of the spongy structure continues on the RbAP end-faces, but it almost terminates on the faces of KAP crystal. Yet, 170 h later both crystals are indistinguishable from each other, with all faces covered with similar excrescences, whose shapes depend upon the type of the sample face.

It is to be noted that in KAP–RbAP–H<sub>2</sub>O system under discussion formation of the replacement texture proceeds differently from that of the above Tutton (Co,Ni)-salts. It is to be remembered that the Tutton salts generate the spongy texture only if the crystal matter is more soluble than the dissolved partner-component. In such systems the spongy structure evenly and quickly occupies the entire volume of the crystal undergoing replacement, thus terminating the process. On the contrary, autoepitaxial texture is formed on the Tutton salt crystals when the crystal matter is less soluble than the dissolved matter of the partner-component; it is limited by a thin near-surface zone of the crystal and isolated excrescences do not tend to merge together, and replacement progress inside the crystal is extremely slow.

### 3.4.2.3 Reactions in the Thermostatically Controlled Cell

Kinetic characteristics of reaction between KAP crystals and solution of RbAP (Table 3.2) are widely different from those of the Tutton salts (Fig. 3.14). Levels of supercooling at which the system has a pre-growth period and can acquire a

**Table 3.2** Pre-growth period of  $\text{KC}_8\text{H}_5\text{O}_4$  in  $\text{RbC}_8\text{H}_5\text{O}_4$  solution at different supercoolings (Data obtained by Mr. S. I. Kovalev in Crystallography Institute of Russian Academy of Sciences)

$T_{\text{sat}}$ (°C)	$\text{RbC}_8\text{H}_5\text{O}_4$ in solution (g/100 g $\text{H}_2\text{O}$ )	Supercooling (°C)	Pre-growth period (min)
26.5	16.8	0.0 (Extrapolation)	9.5
	1.0	6–7	
	2.0	5–6	
	5.0	1.5–2	
	7.0 (Extrapolation)	0 (Meta-equilibrium)	
39.5	21.4	0.0 (Extrapolation)	6.5
	1.0	4.5–5	
	2.0	2–3	
	5.0	0.5–1	
		7.0 (Extrapolation)	0 (Meta-equilibrium)

meta-equilibrium state are considerably greater (in the case of Tutton salts they do not exceed 1.2–1.7°C). Pre-growth period without supercooling is also longer (for the Tutton salts it is about 3–8 min), and its duration, also shortening as degree of supercooling increases, is less affected by it. Finally, in KAP–RbAP– $\text{H}_2\text{O}$  system the pre-growth period is affected by temperature influences, decreasing with the rate of 0.23 min per degree; for the Tutton salt systems this difference, being only 2°C, ranged within the measurement error due to a modest difference between the temperatures of conditions 3 and 7, which were compared (see Fig. 3.15a).

Stirring the solution also considerably affects the process. Pre-growth period, being 2–3 min in the absence of stirring, reaches 15–17 and 50–53 min at 2 and 8 rps of the agitator rate, respectively. Yet, as it was mentioned before, stirring ( $\approx 100$  rps) causes shortening of the pre-growth period of interaction between  $\text{NiSO}_4 \cdot 7\text{H}_2\text{O}$  crystals and  $\text{MgSO}_4$  solutions, which decreases from 6 to 3 min (at supercooling of 0.2°C) and from 3 to 1 min (at supercooling of 0.4°C).

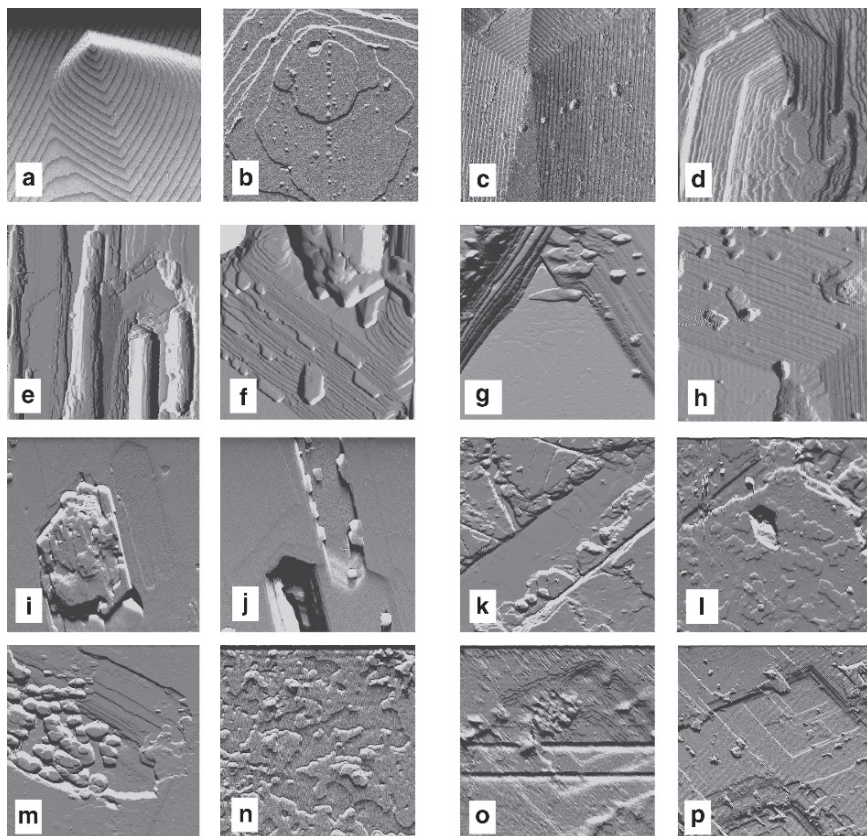
#### 3.4.2.4 Atomic Force Microscopy

Atomic force microscopy was carried out on Park CP Scanning Microscope equipment provided with a high-resolution optical microscope.<sup>9</sup> The initial stages of replacement process were observed in cleaved chips of KAP and RbAP crystals (supplied by Dr. A. E. Voloshin, Crystallography Institute of Russian Academy of Sciences) and in natural {010} surfaces of (K,Rb)AP grown up by solution evaporation at ambient temperature (the same technique was used to prepare crystals of KAP and RbAP used for comparison of the surface relief). The initial crystals were

<sup>9</sup>The study was performed in collaboration with Prof. C. Woensdregt at Earth Science Department of Utrecht University with financial support of A.E. Glikin by the Netherlands Organization of Scientific Research (NWO).

contacted with saturated foreign solution for 1–10 s. The reaction was terminated by blowing the solution away with an air gun.

Figure 3.18 represents details of the natural growth relief of crystals and relief obtained in replacement process. Growth hillocks consisting of periodic spirals and



**Fig. 3.18** Surfaces of KAP, RbAP, and (K,Rb)AP crystals obtained in growth processes (*a–d*) and in short-term interactions with solutions of various compositions (*e–p*) **a, b** – KAP, vicinal hillock: monolayer steps, frame 11.3  $\mu\text{m}$  (**a**), and a complex core structure, 2.1  $\mu\text{m}$  (**b**) **c, d** – RbAP, vicinal hillock: monolayer steps, frame 60  $\mu\text{m}$  (**c**), and a complex core structure, 3.75  $\mu\text{m}$  (**d**) **e, f** – KAP in solution of RbAP, 10 s: etch pits with excrescences, 38.2  $\mu\text{m}$  (**e**) and growth spots on the etch pit slopes, 2.1  $\mu\text{m}$  (**f**) **g, h** – RbAP in solution of KAP: etch pits with excrescences (growth spots on the etch pit slopes): 1 s, 7.6  $\mu\text{m}$  (**g**); 3 s,  $\mu\text{m}$  (**h**) **i, j** – KAP in 1:1 solution of (K,Rb)AP, 1 s: excrescence overlapping the etch pit, 20.5  $\mu\text{m}$  (**i**), and excrescences in an etch pit, 12.  $\mu\text{m}$  (**j**) **k, l** – in 1:1 solution of (K,Rb)AP, 1 s: excrescences in an etch pit, 24  $\mu\text{m}$  (**k**), and growing layers, 12  $\mu\text{m}$  (**l**) **m, n** – (K,Rb)AP in solution of RbAP, 1 s: excrescences in an etch pit, 14.6  $\mu\text{m}$  (**m**), and growing layers, 2.6  $\mu\text{m}$  (**n**) **o, p** – (K,Rb)AP in solution of KAP, 1 s: excrescences in etch pits, 3.4  $\mu\text{m}$  (**o**), 14.1  $\mu\text{m}$  (**p**)

complex cores were detected in crystals of KAP and RbAP grown up in pure solutions (*a–d*). The hillocks of KAP and RbAP differ respectively by absence and presence of faceting, isometry, and oblongness, and also in having monolayer and multilayer growth steps. Reactions between crystals and foreign solutions (*e–r*) are represented by different combinations of simultaneously generated elements of growth and dissolution. They include autoepitaxial excrescences on the bottoms of the etch pits (*e, j, m, o*), step sites growing on the inner sides of the etch pits (*f, g, h, p*), overlapping the pits with excrescences (*i*), and formation of layers covering the dissolution surface (*k, l, n*). These interactions undoubtedly represent mutual correlation between dissolution and growth processes at the starting stages of replacement: judging by the distinct development of elements at both stages, it can be concluded that after 1 s interaction (*g, i–p*), initiating of salting-out requires less than several tenths or even hundredths of a second. The process rate is so high that monitoring requires to be done with a step, which would not exceed 0.1–1 s, and thus was unavailable.

Difference in the excrescence morphology seems to qualitatively reflect their composition in accordance with morphology of hillocks observed in pure media: the elongated hillocks are enriched with rubidium component (*e, o*), while isometric hillocks are enriched with potassium component (*i, k, m*). Shapes of the etching pits also vary from elongated (*e, j, k*) to isometric (*i, o, p*) regardless to associated excrescence habits. The etching pits are usually, but not necessarily, joint with the growth formations: the pits may be free from apparent growth elements (*i*, a shallow long pit on the right) and the growth layers may be developed separately from the etching formations (*l, n*). These peculiarities are likely to represent compositional heterogeneity of the diffusion layer in longitudinal direction. Absence of apparent correlation in localization of the dissolution and growth elements does not allow to determine, whether the initial process mechanism was volume-deficient (*m–p*) or volume-excessive (*i–l*).

### 3.4.2.5 Physicochemical Interpretation

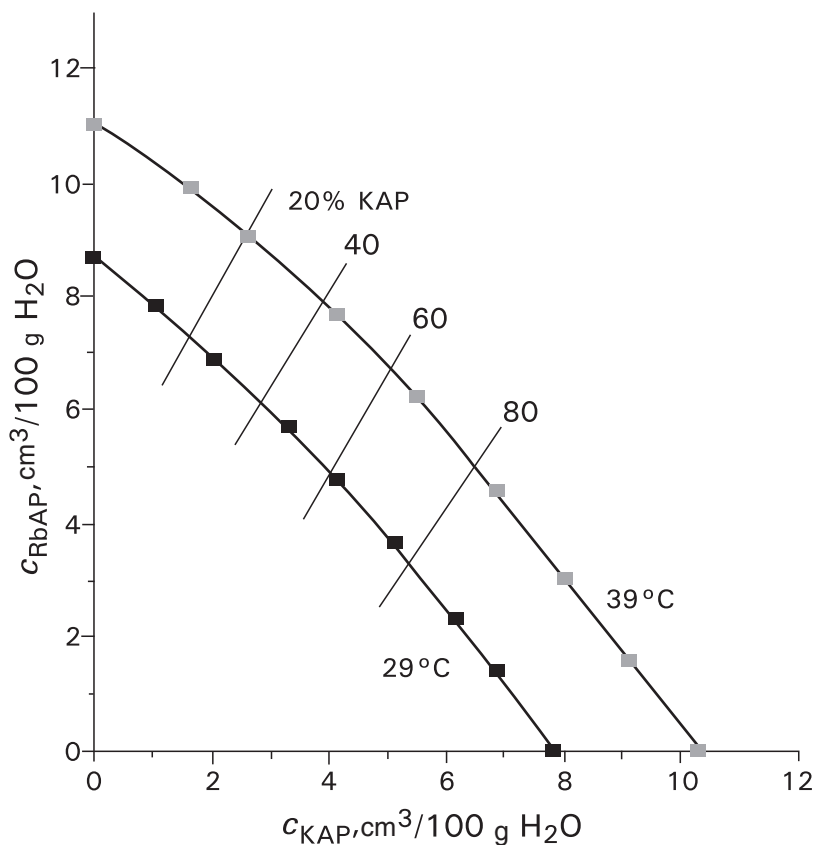
Replacement processes in (K,Rb)AP series are more complicated in comparison with those occurring in (Co,Ni)(NH<sub>4</sub>)<sub>2</sub>(SO<sub>4</sub>)<sub>2</sub>·6H<sub>2</sub>O series. The former systems develop the spongy structure only within the edge region, while in the latter series it consumes the whole crystal. In the former systems the autoepitaxial excrescences are coupled with development of the spongy region, while in the latter series these formations are produced independently. This dissimilarity arises from different solubility ratios in the systems concerned, which is reflected in convex shapes of isotherms plotted for the former system and absence of convexity in the isotherms of the latter system.

Total solubility in (Co,Ni)(NH<sub>4</sub>)<sub>2</sub>(SO<sub>4</sub>)<sub>2</sub>·6H<sub>2</sub>O–H<sub>2</sub>O system in any figurative point is lower than the solubility of any crystal, relatively enriched with the Co-component in comparison with the equilibrium crystal, thus total solubility derivative of a pure Ni-component content in solution is always less than unity. When a Co-enriched



crystal interacts with a Ni-enriched solution, these terms provide favorable conditions for the process of the spongy structure formation to continue from the very beginning till the very end of the reaction, until a complete equilibrium is reached. On the contrary, reaction between a Ni-enriched crystal and Co-enriched solution occurs under conditions corresponding to a lesser solubility of the crystal, and from the very beginning the process is hampered by volume-excess growth of the new formation blocking the crystal surface, and this mode remains unchanged throughout the whole process.

Volume solubilities of KAP and RbAP are nearly the same, and due to the isotherm convexity (Fig. 3.19), the (K,Rb)AP solubility derivative with respect to any pure component content in solution changes from the values exceeding unity toward the values less than unity. The change takes place in the region of flattening the convex solubility isotherms. Thus, only when the solution composition is nearly similar to that of the pure crystal of KAP or RbAP the volume-excess replacement is not accompanied by formation of the spongy structure. When the crystals of

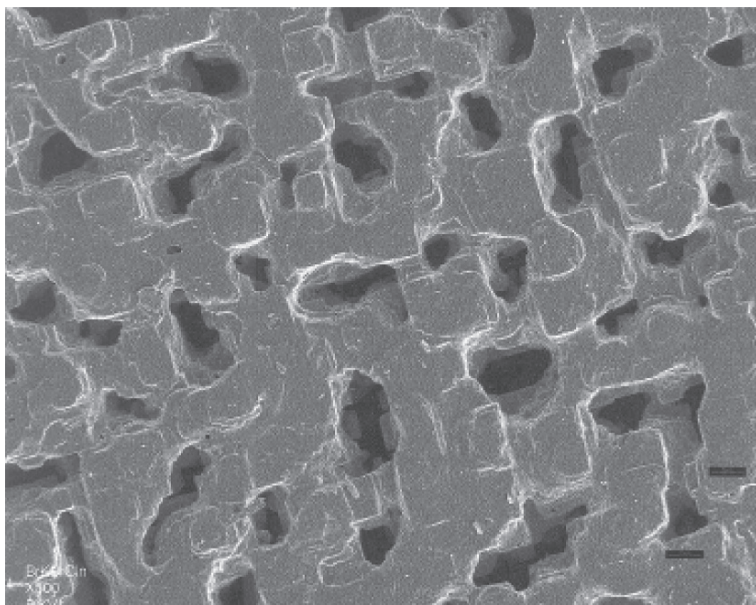


**Fig. 3.19** KAP-RbAP-H<sub>2</sub>O system. Solubility isotherms at 29 and 39°C and isocomposites at 20, 40, 60 and 80% of KAP in solid phase

either KAP or RbAP interact with solutions of profoundly different compositions, the mechanism of the sponge formation changes from volume-deficit to volume-excess. The latter process leads to blocking the complex spongy surface inside the crystal, thus preventing deeper ingress of the sponge into the crystal, and results in formation of autoepitaxial excrescences on the external crystal surface.

This interpretation was proved by two-step replacement in  $(\text{Co,Ni})(\text{NH}_4)_2(\text{SO}_4)_2 \cdot 6\text{H}_2\text{O}-\text{H}_2\text{O}$  system carried out with forced change of the mechanism. At the first stage a crystal of  $\text{Co}(\text{NH}_4)_2(\text{SO}_4)_2 \cdot 6\text{H}_2\text{O}$  reacted with solution of  $\text{Ni}(\text{NH}_4)_2(\text{SO}_4)_2$  according to volume-deficit mechanism, so that a  $(\text{Co,Ni})$  spongy pseudomorph was obtained. At the second stage the pseudomorph was introduced into a  $\text{Co}(\text{NH}_4)_2(\text{SO}_4)_2$  solution, so that the subsequent reaction proceeded according to volume-excess mechanism. This precluded the ingress of the spongy structure into the centre of the crystal and resulted in formation of a stable and relatively sharp edge between the crystal center and its periphery accompanied by a gradual formation of faceting and ordering the contours of the previously generated inclusions. Thus, the mechanism and the result of the process are similar to those obtained in KAP-RbAP- $\text{H}_2\text{O}$  system.

Faceting and subsequent ordering the inclusions of the same reason can also be readily discernible in the images of replacement occurring in  $\text{K}(\text{Cl,Br})$  isomorphic series (Fig. 3.20). When replacement was involving the extreme members of  $(\text{K,NH}_4)\text{H}_2\text{PO}_4$  series, at some stage we observed an abrupt inhibition of it followed



**Fig. 3.20** Faceting and ordering the inclusions in the course of change the volume-deficit mechanism of replacement into the volume-excess one. Reaction of KBr crystal in KCl solution. Scale marks are of  $5\mu\text{m}$  (SEM-image by C. Putnis, University of Muenster, Germany)

by formation of autoepitaxial excrescences over the spongy structure. On the contrary,  $\text{Na}(\text{Cl},\text{Br})\text{O}_3\text{-H}_2\text{O}$  system is characterized by shift from volume-excess to volume-deficit replacement and by concave solubility isotherms.<sup>10</sup>

Kinetic effects in supercooled solutions, including pre-growth period of replacement, which decreases as supercooling deepens, heterogeneous meta-equilibria, and nonmonotonous correlation between the system characteristics and the ratio of isomorphic components, represent combination of metasomatic and growth components, which was thoroughly studied for  $(\text{Co},\text{Ni})(\text{NH}_4)_2(\text{SO}_4)_2\cdot 6\text{H}_2\text{O}$  and  $(\text{K},\text{Rb})\text{HC}_8\text{H}_4\text{O}_4$  series. The process mechanisms in these systems have a great deal in common, yet the data comparison displays significant quantitative differences resulting, first of all, from different proceedings of diffusion processes in solutions. Considerable influence of the other factors should also be taken into account. Thus, Dr. A.E. Voloshin, Dr. E.B. Rudneva, and Mr. S.I. Kovalev (Crystallography Institute of Russian Academy of Sciences) showed by means of X-ray topography in situ at ambient temperature that replacement of KAP crystal in RbAP solution is the fastest in the stressed regions and that the stresses are gradually alleviated in the course of reaction to be regenerated and redistributed in other regions, but without any generation of new dislocations (Glikin et al. 2003).

### 3.4.3 *Arcanite-Tarapacaite $\text{K}_2(\text{S},\text{Cr})\text{O}_4$ Series*<sup>11</sup>

Formation of crystals in  $\text{K}_2\text{SO}_4\text{-K}_2\text{CrO}_4\text{-H}_2\text{O}$  system was studied in flat preparations (Fig. 1.2a) using the thermostatically controlled microcrystallization cell (Fig. 2.1) described above.

In spite of the isotherm nonlinearity and uneven distribution of the solidus isocomposites of  $\text{K}_2(\text{S},\text{Cr})\text{O}_4$  system (Fig. 3.8), the features of the replacement products and some kinetic characteristics, such as trajectories of figurative points in the course of growth and polythermal replacement and heterogeneous meta-equilibria, are qualitatively similar to the corresponding characteristics of  $(\text{Co},\text{Ni})(\text{NH}_4)_2(\text{SO}_4)_2\cdot 6\text{H}_2\text{O}$  and  $(\text{K},\text{Rb})\text{AP}$  series discussed above.

Isothermal interaction between a  $\text{K}_2\text{CrO}_4$  crystal and  $\text{K}_2\text{SO}_4$  solution or between a  $\text{K}_2\text{SO}_4$  crystal and  $\text{K}_2\text{CrO}_4$  solution occurs according to monocrystalline replacement mechanism, but is accompanied by an extremely powerful volume effect. A great deficit of volume accompanying replacement of a  $\text{K}_2\text{CrO}_4$  crystal results in disintegration of pseudomorph and in disorientation of its isolated fragments (Fig. 1.6d). Under the volume-excess conditions the  $\text{K}_2\text{SO}_4$  crystals undergo intensive

---

<sup>10</sup>Monitoring the substitution and estimation of solubility in  $(\text{K},\text{NH}_4)\text{H}_2\text{PO}_4$  and  $\text{Na}(\text{Cl},\text{Br})\text{O}_3$  series were carried out in collaboration with Prof. H. Klapper at Bonn University with financial support of German Fund for Academic Interchange (DAAD).

<sup>11</sup>Using data of original publications (Kasatkin et al. 1995, Glikin 1996a).

cracking to form wide replacement zones along the cracks dissevering the entire crystal. Relatively rapid volume-excess replacement is likely to be caused by development of microcracks on the edges of blocks.

Zoned structure of a  $K_2(Cr,S)O_4$  pseudomorph after a  $K_2CrO_4$  crystal is of special interest (Fig. 1.6*d*). The peripheral zone has essentially continuous uniform structure; the next region, on the contrary, contains fragmented crystalline material, while the central zone is continuous. These zones may be associated with three sectors of the system solubility curve (Fig. 3.8*a*). The sector, adjoining the abscissa and corresponding to the initial stage of replacement in solution enriched with sulfate component, is slightly flattened; so, the volume deficit at this stage is not the greatest in the system. Besides, isocomposites of this sector are positioned far apart from each other, so, the composition of the solid phase changes insignificantly, and composition nonuniformities of surfaces of the crystal and diffusion layer are negligible,<sup>12</sup> while in the other systems they result in formation of inclusions. As a result, dissolution prevails in this sector accompanied by more or less uniform precipitation of the material undergoing salting-out on the surface of crystals. Then, after the solubility curve passes the point of about 24 g of  $K_2CrO_4$  per 100 g  $H_2O$ , the slope of the isotherm sharpens abruptly, isocomposites converge, and the reaction assumes the mechanism of volume-deficit replacement, but as the deficit of volume is too great in this region, that results in fragmentation of the crystal instead of inclusion formation, as it happened in the previous case. At the same time, the fastest reaction preferably occurs in the unchanged regions of the crystal, because in these parts difference between the crystal and solution composition is maximal. Reaction of the changed external zone with solution is slower preserving a more or less continuous ring around the region of fragmentation. The third sector of the isotherm is straighter and the difference in compositions of crystal and solution becomes lesser, so, the reaction slows down in the region of Cr-enriched compositions and the central relic remains intact. These replacement zones must differ in compositions, so the structure represented in Fig. 1.6*d* is to change gradually in the course of the process.

Figure 3.8*b* shows that lowering temperature results in the combining the processes of growth and replacement according to the mechanism described for the idealized case of  $K(Cr,Al)(SO_4)_2 \cdot 12H_2O$  series (Sect. 3.3.2) and observed experimentally in  $(Co,Ni)(NH_4)_2(SO_4)_2 \cdot 6H_2O$  series (Sect. 3.4.1). Irregular distribution of isocomposites is supposed to cause variations in proportions of metasomatic and growth components in different parts of the system. The role of metasomatic component should be insignificant in the region of sulfates, where the crystal composition does not depend upon the solution composition. On the contrary, it must have a great influence in the region of chromates. Indirect evidence for this supposition is development of autoepitaxial excrescences during the process of layer growth

---

<sup>12</sup>To date this is the only and indirect evidence of influence of crystal composition variations upon the texture of volume-deficit replacement.

(Fig. 3.21) and inhibition of growth in mixed-composition solutions in comparison with the growth in binary solutions (Kasatkin 1993; Kasatkin et al. 1995).

Data on metastable heterogeneous equilibria in the system under consideration evoke a considerable interest. Saturation temperatures of the mixed solutions, which were measured using seeds of  $K_2(\text{Cr,S})O_4$  spontaneously grown up in separate portions of corresponding experimental (“own”) solutions and seeds of pure  $K_2\text{CrO}_4$  and  $K_2\text{SO}_4$ , were compared. The experiments were carried out according to the methods used for observations in  $(\text{Co,Ni})(\text{NH}_4)_2(\text{SO}_4)_2 \cdot 6\text{H}_2\text{O}$  series (Sect. 3.4.1); each test was performed using a new seed.

In most cases saturation temperature of any one of single-component crystals is significantly lower than that of any mixed crystal (Table 3.3). This indicates that supercooling necessary to achieve a meta-equilibrium state deepens as the difference between the crystal composition and composition corresponding to thermodynamic equilibrium for the given solution increases. This fact also agrees with the proposed model. It is interesting to note that in the system under consideration the meta-equilibrium state is extremely stable: a solution containing crystals supercooled



**Fig. 3.21** Autoepitaxial excrescences on the growing surface of  $K_2(\text{Cr,S})O_4$  (Photo by I.A. Kasatkin, St. Petersburg University)

**Table 3.3** Equilibria in supercooled solutions containing crystals of different composition

No	Concentration (g/100 g H <sub>2</sub> O)		Saturation temperatures for different seeds (°C)				
	K <sub>2</sub> CrO <sub>4</sub>	K <sub>2</sub> SO <sub>4</sub>	K <sub>2</sub> (CrO <sub>4</sub> ,SO <sub>4</sub> )	K <sub>2</sub> CrO <sub>4</sub>	K <sub>2</sub> SO <sub>4</sub>		
<b>Solutions enriched by K<sub>2</sub>CrO<sub>4</sub></b>							
1	65.1	1.0	38.4 ± 0.2	33.85 ± 0.2	(4.55)	30.7 ± 0.2	(7.7)
2	64.0	1.5	36.7 ± 0.1	30.6 ± 0.1	(6.1)	27.75 ± 0.15	(8.95)
3	63.0	1.8	33.2 ± 0.2	18.9 <sup>a</sup>	(14.3)	23.85 ± 0.15	(9.35)
4	62.1	2.25	43.4 ± 0.1	33.8 ± 0.2	(9.6)	37.2 ± 0.2	(6.2)
5	62.0	2.0	36.4 ± 0.1	21.9 ± 0.2	(14.5)	23.8 ± 0.1	(12.6)
6	61.66	2.1	36.7 ± 0.1	32.1 ± 0.1	(4.6)	27.9 ± 0.15	(8.8)
7	61.4	2.2	38.2 ± 0.2	33.0 ± 0.1	(5.2)	35.45 ± 0.15	(2.75)
8	61.35	2.36	39.05 ± 0.15	38.1 ± 0.1	(0.95)	35.25 ± 0.2	(3.8)
9	61.2	1.9	32.0 ± 0.1	19.85 ± 0.15 <sup>a</sup>	(12.15)	27.75 ± 0.15	(4.25)
<b>Solutions enriched by K<sub>2</sub>SO<sub>4</sub></b>							
10	0.8	16.0	49.45 ± 0.15	Less ambient <sup>a</sup>	(>30)	49.25 ± 0.15	(0.25)
11	1.5	16.0	50.1 ± 0.1	Less ambient <sup>a</sup>	(>30)	26.0 <sup>a</sup>	(24.1)
12	2.0	15.9	50.1 ± 0.1	Less ambient	(>30)	21.0 <sup>a</sup>	(29.1)
13	3.5	15.8	51.85 ± 0.15	Less ambient	(>32)	25.0 <sup>a</sup>	(26.85)
14	4.0	15.0	54.35 ± 0.15	<40.0 <sup>a</sup>	(>14)	37.0 <sup>a</sup>	(17.35)
15	4.0	15.0	54.35 ± 0.15			54.2 ± 0.2	(0.15)
16	4.0	15.0	51.7 ± 0.1	Less ambient	(>32)	<28.0 <sup>a</sup>	(>23)
17	5.0	14.8	52.25 ± 0.15	Less ambient	(>32)	<23.0 <sup>a</sup>	(>29)
18	6.0	14.5	50.7 ± 0.1	Less ambient	(>30)	<28.0 <sup>a</sup>	(>22)
19	9.0	14.5	47.5 ± 0.2	Less ambient	(>27)	<26.0 <sup>a</sup>	(>21)
20	10.0	13.5	51.4 ± 0.1	Less ambient	(>31)	<24–30 <sup>a</sup>	(>27)
21	12.0	13.0	47.85 ± 0.15	Less ambient	(>27)	<21.0 <sup>a</sup>	(>26)
22	13.0	12.0	54.6 ± 0.1	<38 <sup>a</sup>	(>16)	<39 <sup>a</sup>	(>15)
23	16.0	11.0	54.8 ± 0.2	<30 <sup>a</sup>	(>25)	<33 <sup>a</sup>	(>22)

**Note:** Values given in brackets are deviations from saturation temperatures for seeds of K<sub>2</sub>(CrO<sub>4</sub>,SO<sub>4</sub>) grown in the same K<sub>2</sub>(CrO<sub>4</sub>,SO<sub>4</sub>) solutions as used for experiments.

<sup>a</sup>Tests conducted in contaminated solutions (Measurements were performed by Mrs. O.I. Artamonova Laboratory of Crystallogenesis, St. Petersburg State University).

by about 20°C or more is stable at least for several days. This fact can be explained by small distances between the isotherms (Fig. 3.8), which define small supersaturations for crystals having composition points located between the meta-equilibrium states (see Sect. 3.3.3).

Experimental results and predictive estimations obtained graphically on the basis of equilibria data for this system (Fig. 3.8) are close enough (Table 3.4). Only a few instances, excluding evident artifacts, show considerable divergence between the experimental and predictive estimations, sometimes reaching about half an order. Yet, it should be pointed out that sometimes quantitative estimations are not available due to the absence of data for equilibria at temperatures exceeding 50°C and those below 20°C, and also because of insufficient degrees of experimental supercooling.

**Table 3.4** Differences in saturation temperatures ( $^{\circ}\text{C}$ ) measured in the same solution using mixed crystals and single-component seeds of  $\text{K}_2\text{CrO}_4$  and  $\text{K}_2\text{SO}_4$ 

Group of tests (see Table 3.3)	$\text{K}_2\text{CrO}_4$		$\text{K}_2\text{SO}_4$	
	Predicted value	Experimental value	Predicted value	Experimental value
1–9	20	4.55–14.5 <sup>a</sup>	$\approx 20$	3.8–12.6
10–18	30	$>14 - >32^a$	5–10	17.35 – $>29$
19–23	30	$>16 - >31$	30–40	$>15 - >27$

**Note:** <sup>a</sup>Tests conducted in contaminated solutions. Values at 0.95, 0.25, and 0.15 $^{\circ}\text{C}$  (Table 3.3: tests 8, 10, and 15) are artifacts.

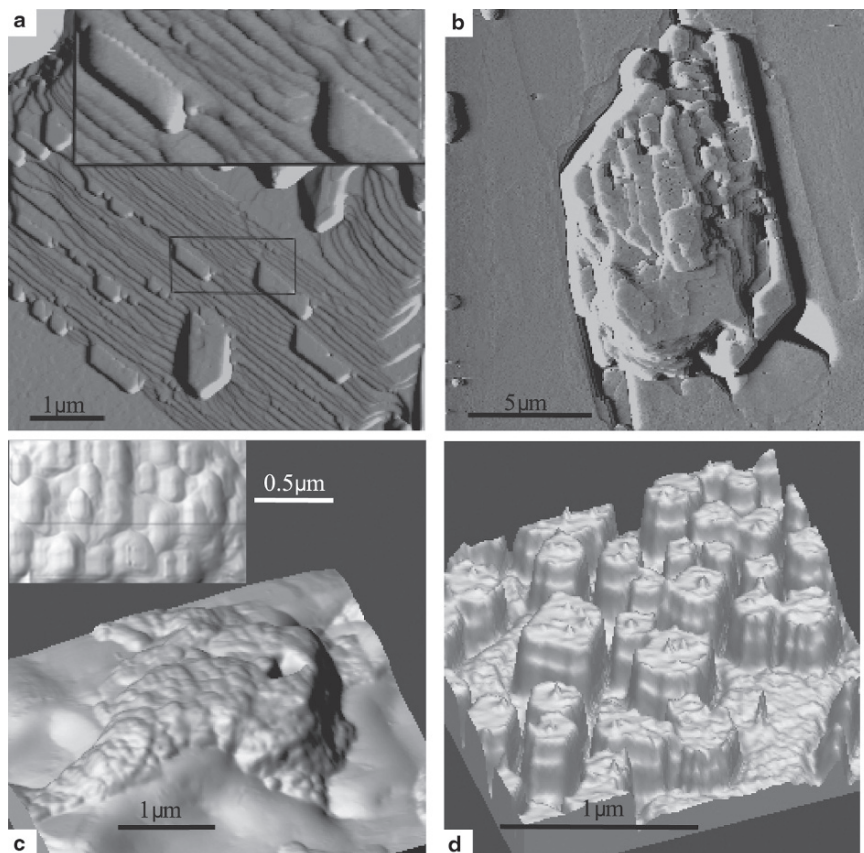
Reasons for divergence between the experimental and theoretical data are probably the same as were proposed in description of  $(\text{Co},\text{Ni})(\text{NH}_4)_2(\text{SO}_4)_2 \cdot 6\text{H}_2\text{O}$  series (Sect. 3.4.1). First of all, they include impossibility for theoretical model to take into account diffusion resistance and impossibility of experimental controlling the surfaces compositions of crystal and diffusion layer. Analysis of  $\text{K}_2(\text{Cr},\text{S})\text{O}_4\text{--H}_2\text{O}$  system is complicated by an additional circumstance, i.e., impossibility of controlling compositions of the mixed crystal seeds that was not encountered in  $(\text{Co},\text{Ni})(\text{NH}_4)_2(\text{SO}_4)_2 \cdot 6\text{H}_2\text{O}\text{--H}_2\text{O}$  system, where the seeds having extreme compositions of the series were used. This reason probably accounts for widespread values in tests 4–6, 6–9, and 14–16, which were carried out under similar or the same conditions.

### 3.5 Inhomogeneity of Crystals

The above consideration reveals an unordinary compositional inhomogeneity of mixed crystal surface in the course of growth and replacement processes.

AFM pictures of mixed crystal surfaces (Fig. 3.22) display a combination of simultaneous dissolution and growth just at the beginning of crystal-solution interaction. A clear appearance of such textures was recorded by experiments of the shortest duration for the  $(\text{K},\text{Rb})\text{HC}_8\text{H}_4\text{O}_4$ -series described in Sect. 3.4.2 and  $\text{K}(\text{Cl},\text{Br})$ -series (Woensdregt and Glikin 2005; Glikin et al. 2007). The short duration of the process (about 10 s) permits to suppose the observed picture to be close to a momentary state of the system.

Figure 3.22a displays a texture of  $(\text{K},\text{Rb})\text{HC}_8\text{H}_4\text{O}_4$  protuberances developed autoepitaxially in etching pit in  $\text{KHC}_8\text{H}_4\text{O}_4$ . Each protuberance appears to include a spontaneous ensemble of isomorphic particles formed due to combined stages of isomorphic replacement and growth caused by droplet evaporation. The forms of dissolving steps indicate the adjoining protuberances to be growing out directly from the steps without two-dimensional nucleation or additional dislocation sources. Meanwhile imperfection rows between the protuberances and the steps indicate their compositional difference (see insertion in Fig. 3.22a).



**Fig. 3.22** Surface inhomogeneities resulted from isomorphic exchange between the crystals and solutions:  $(\text{K,Rb})\text{HC}_8\text{H}_4\text{O}_4$  (**a**, **b**) and  $\text{K}(\text{Br,Cl})$  (**c**, **d**) series **a**, **c** – volume-deficit replacements (enlarged fragments are in the insertions); **b**, **d** – volume-excess replacements

Substantially, protuberances are characterized by a strong dispersion in habits, faceting degree, and at least by a 1.5-order difference in sizes. As it has been mentioned in Sect. 3.4.2, different habits correspond to different compositions: protuberances countering the surface steps and those growing out across the steps are enriched with K and Rb, respectively. This is proved by the corresponding habits of the hillocks growing on the faces of pure  $\text{KHC}_8\text{H}_4\text{O}_4$  and  $\text{RbHC}_8\text{H}_4\text{O}_4$ : the former are isometric, but the latter are elongated (Figs. 3.18a–d).

Different faceting degrees of protuberances indicate their different stability: the faceted ones grow or maintain the equilibrium state, but the rounded ones dissolve. Different sizes of protuberances show their different growth rate: the big ones are formed under favorable conditions, while the small ones are formed under adverse conditions. The following tendencies can be outlined. (1) Stable (faceted) protuberances

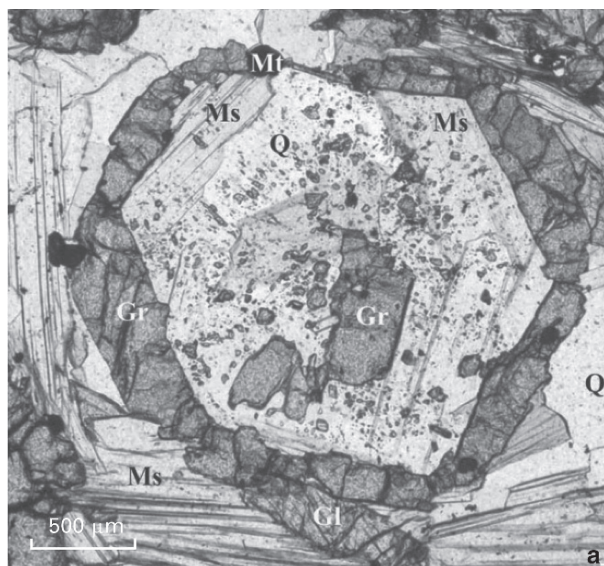


are large and enriched with either potassium or rubidium; protuberances of intermediate habits and compositions are nearly absent among the faceted ones. (2) Unstable (rounded) protuberances are small; their isometry shows an intermediate composition. Such a bimodal compositional distribution of protuberances is a consequence of heterogeneous metastable equilibrium existing between the crystal and supercooled solution that was discussed in Sect. 3.3.3.

Surface inhomogeneities induce inhomogeneous distribution of isomorphic components within the crystal bulk. It is to be noted that traditional bulk inhomogeneity includes the forms of crystal zoning and those of growth pyramids; the first discussions of the inhomogeneity origin appeared as early as in the middle of the twentieth century (Laemmlein 1948, 1973). At the present state of experimental techniques, the compositional inhomogeneity can be observed at a considerably higher level of resolution. Obviously, a surface homogeneity is unavailable under conditions of the surface rapid spontaneous change. Sites varying in composition are buried under new overgrowing formations making up clusters of nano-micrometer sizes. A negligible intercrystal diffusion provides a stable cluster texture of a mixed crystal undergoing growth or replacement.

Obviously, the forms of surface relief vary profoundly depending upon physico-chemical properties of the system in question and the process conditions (Figs. 3.18 and 3.22), and, therefore, the cluster textures should vary accordingly.

For example, some metasomatically transformed garnet crystals of pyrope–almandine–grossular series display a cluster texture. These box-like monocrystals (Fig. 3.23*a*) were formed via a two-stage replacement of initial garnets having solid



**Fig. 3.23** Bulk inhomogeneities resulted from isomorphic exchange between the crystals and solutions: the series of natural pyrope–almandine–grossular garnets from Maksyutovo metamorphic complex, the South Urals (**a** – general view, **b** – case fragment) and synthetic  $(\text{Pb,Ba})(\text{NO}_3)_2$  (**c**)

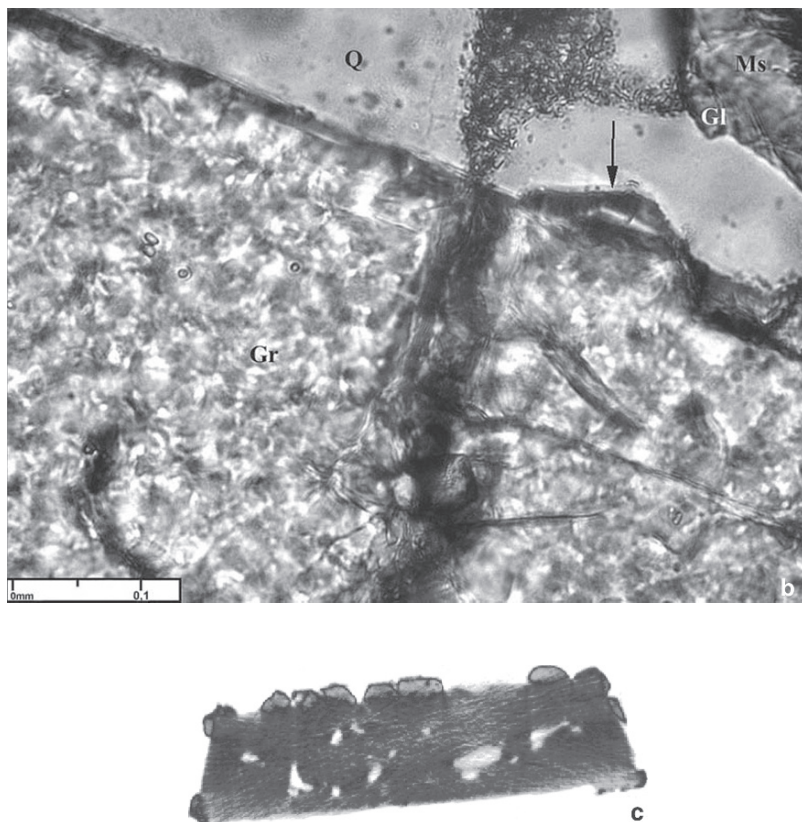


Fig. 3.23 (continued)

textures (Zhdanov and Glikin 2006). The first stage resulted in a volume-excess isomorphic replacement of the crystal periphery. Such kind of the replacement is particularly proved by the distinctive excrescences and crossing cracks with dispersed material clouds formed at the crystal-solution interaction (Fig. 3.23*b*). Then, during the second stage, the internal relics were substituted by mica and some other minerals. Figure 3.23*b* displays the cluster texture of the box-like blocks.

In addition to the clusters, it was possible to discern a compositional specificity of a thin rim (0.03–0.05 mm) formed at the boundary of the box-like block and bordering cracks due to enrichment with Mg-component; this rim includes an excrescence originated at the volume-excess replacement (see the arrow in Fig. 3.23*b*). A similar rim was observed on  $(\text{Pb,Ba})(\text{NO}_3)_2$  volume-excess monocrystal pseudomorphs after  $\text{Ba}(\text{NO}_3)_2$  (Fig. 3.23*c*). The rim probably indicates a spontaneous precipitation of some material having statistical isomorphic composition, components of which undergo redistribution to form a mosaic surface, which subsequently transforms into the bulk clusters in accordance with local conditions.

The phenomena of compositional inhomogeneity have an utmost importance for mineralogical interpretations and preparation of new materials. However, their investigations have been so far insufficient and still require special experimental and theoretical approaches.

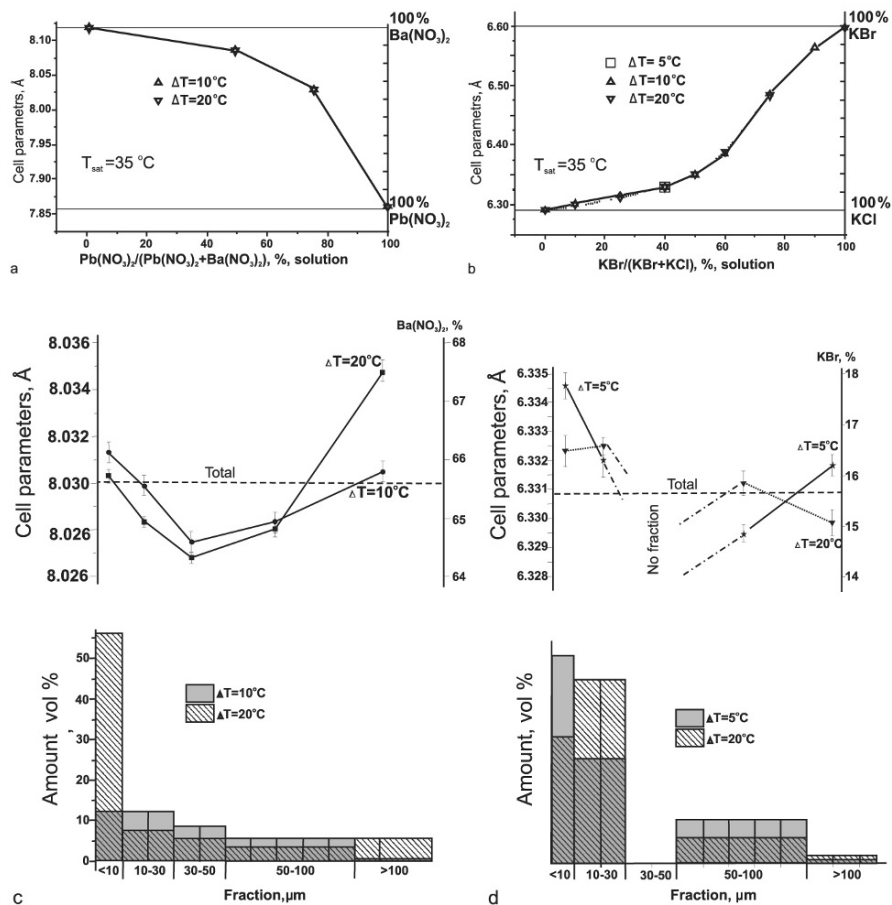
### 3.6 Mass Precipitation of Mixed Crystals: Distribution by Compositions and Sizes

Different authors used spontaneous mass precipitation of mixed crystals in experiments for plotting phase diagrams which coordinate compositions of solidus and liquidus. However, the process peculiarities including distribution of crystals by composition have not been investigated. Experiments show an unexpected behavior of such systems.

The precipitation was carried out in  $(\text{Pb,Ba})(\text{NO}_3)_2$  and  $\text{K}(\text{Br,Cl})$  series induced by intensive stirring of preliminary supercooled solutions (100 ml). Solutions were stirred for 15 s, supernatant liquid decanted, and the precipitated samples were dried with filter paper. In such a process the change in solution composition should be negligible, and precipitation can be considered as momentary. The  $(\text{Pb,Ba})(\text{NO}_3)_2$ -ensembles were obtained when the component ratios in solutions were 40:60 and 60:40 (wt%), and the supercoolings were 10 and 20°C. The  $\text{K}(\text{Br,Cl})$ -ensembles were obtained when the component ratios in solutions were 10:90, 25:75, 40:60, 50:50, 60:40, 75:25, and 90:10 (wt%), and the supercoolings were 10 and 20°C for all the compositions, except for the solution with 40:60 ratio, which was also supercooled by 5°C. The samples obtained in the solutions of  $\text{Pb}(\text{NO}_3)_2/\text{Ba}(\text{NO}_3)_2 = 40:60$  and  $\text{KBr}/\text{KCl} = 60:40$  were separated into the size fractions of <10, 10–30, 30–50, 50–100, and >100 μm by means of plastic sieves. The total and fraction compositions were determined on the basis of the cubic cell parameters defined by means of X-ray diffractometry (STOE-diffractometer, Mo-radiation, transmission conditions in the range of  $2\theta = 5\text{--}46^\circ$ ), taking into account reported data on the linear Vegard functions for these series. An accuracy of the parameter measurements was within 0.0003–0.0004 Å, which meant a corresponding composition accuracy within the following diapasons: 0.12–0.16 mol.% of  $\text{Ba}(\text{NO}_3)_2$  in a  $(\text{Pb,Ba})(\text{NO}_3)_2$ -sample, and 0.17–0.23 mol.% of  $\text{KBr}$  in a  $\text{K}(\text{Br,Cl})$ -sample.

For both series the total composition of a precipitate depended only upon the solution composition (Figs. 3.24a, b). Supercooling did not influence the total composition, while the curves obtained for each series at different supercoolings (10 and 20°C for  $(\text{Pb,Ba})(\text{NO}_3)_2$ ; 5, 10, and 20°C for  $\text{K}(\text{Br,Cl})$ ) coincided in the diagrams within the accuracy limits. Effect of saturation temperature (concentration of the salt mass) was not recorded.

At the same time, the above fractions were different in sizes and compositions, which corresponded to a bimodal distribution of individuals forming the ensembles (Figs. 3.24c, d). Small and large crystals of  $(\text{Pb,Ba})(\text{NO}_3)_2$  were enriched with the less-soluble Ba-component in comparison with the intermediate



**Fig. 3.24** Crystal compositions in the course of mass precipitation **a**, **b** – effect of solution composition on isomorphous composition of the crystals in the absence of solution supercooling (**a** –  $(\text{Pb,Ba})(\text{NO}_3)_2$ ; **b** –  $\text{K}(\text{Br,Cl})$ ); **c**, **d** – dependence of crystal compositions on size and distribution of crystals by size into fractions (**c** –  $(\text{Pb,Ba})(\text{NO}_3)_2$ ; **d** –  $\text{K}(\text{Br,Cl})$ )

crystal compositions. On the contrary, small and large crystals of  $\text{K}(\text{Br,Cl})$  were enriched with the more-soluble  $\text{KBr}$ . The fractions displayed a bimodal distribution by volume, which changed with alterations in supercooling. In the case of  $\text{K}(\text{Br,Cl})$ , the 30–50  $\mu\text{m}$  fraction was absent.

The results given above do not agree with usual concepts. First, a perceptible sensitivity of crystal composition to supersaturation, which was proved experimentally for monocrystal growth of soluble salts, was not observed (Zhmurova et al. 1963; Zhmurova and Khaimov-Mal'kov 1970a, b). Second, the crystal composition, growth rate, and sizes do not conform to more or less simple statistical regularities that can be also expected from a general point of view. This contradiction is obviously fallacious, as it results from an unjustified direct comparison between the

mass precipitation and monocrystal growth in spite of obviously different growth conditions. A mass precipitation should result in formation of crystals having a wide range of compositions caused by influence of heterogeneous metastable equilibrium states (see Sects. 3.3.2 and 3.3.3).

Unusual uniformity of total compositions obtained at different degrees of supercooling can be a consequence of similarity between the crystallization trajectories plotted at various supercooling degrees, which can be concluded from consideration of the phase relations visualized by means of the concentration diagrams (Fig. 3.11c).

The bimodal distribution of spontaneously precipitated crystals both by compositions and sizes displays the direct effect of metastable equilibrium states. Nucleation is supposed to proceed spontaneously in a wide range of crystal compositions, but only those nuclei whose compositions correspond to the meta-equilibrium states can remain in the solution giving rise to the bimodal distribution. Thus, the process discussed has the same origin as formation of surface protuberances, and these cases should be distinguished as three- and two-dimensional processes, respectively.

In Figs. 3.24c, *d* it can be seen that crystal compositions of individual fractions depend upon a supercooling degree. However, this dependence is not uniform for different fractions that can be attributed to quite rough distribution estimation resulting from the wide ranges of fraction sizes.

We would also note that the smallest and largest fractions of both ensembles are always enriched with the same component (Figs. 3.24c, *d*), i.e., crystals formed at low and high growth rates have a similar rate of capturing the impurities. This is in accordance with conclusion made by Dr. Z. I. Zhmurova, who stated the process of capturing the impurities to be independent from the growth rate, but dependent upon degree of supersaturation. However, physical nature of the dependence is not clear.

### **3.7 On the Mechanism of Isomorphic Component Selection during the Crystal Formation**

The main genetic problem of isomorphism, i.e., mechanism of controlling the component ratio, which would satisfy the formation conditions, appears to be unsolved within the framework of conventional interpretations of mixed crystal formation. Processes involved in formation of crystals having either variable or constant composition are considered as acts of building-in some certain particles into fractures formed in the crystal steps. The process mechanism suggested for systems containing isomorphic components involves statistical selection of individual particles followed by diffusion equalization of resulting composition throughout the crystal. Nevertheless, high supersaturations are believed to trigger a mechanism of “nonselective” crystallization (Chernov 1984). Also, the lattice deformations induced around a captured particle are supposed to serve as regulating factor (Iiyama 1974, quoted by Urusov et al. 1997). Such assumptions do not allow a reliable correlation between the isomorphic composition of crystals and their formation parameters to be deduced.

The above concepts elucidating a specific genetic nature of isomorphic-mixed crystals allow to solve this problem. The main peculiarity of the mixed crystal formation can be essentially stated as a chemical exchange with components between the crystal and solution involved. The reaction unambiguously corresponds to a metasomatic replacement of a crystal in a saturated solution under isothermal–isobaric conditions and is accompanying the growth and dissolution in supersaturated and undersaturated solutions, respectively. The replacement proceeds via a plurality of interrelated local elementary acts of substrate dissolution and autoepitaxial growth of a new formation occurring simultaneously at numerous sites of the crystal surface, alternating and interchanging throughout the whole surface of the crystal. Physicochemical aspect of the replacement consists in movement of compositional figurative points of the solid and liquid phases from their starting positions toward each other until a thermodynamic equilibrium is reached. The process is accompanied by dissolution of the crystal caused by “foreign” composition of the solution that, in turn, initiates the solution supersaturation in respect of the “own” crystal phase and deposition of this phase (salting-out takes place). In supercooled and overheated solutions the salting-out process is accompanied by direct growth and dissolution.

This concept is a key to regulation of a crystal isomorphic composition. Suggested “ensemble” mechanism for a crystal to select such a ratio of isomorphic components that is defined by existing conditions (solution composition, supercooling/overheating, temperature, etc.) involves the following principles.

1. Various crystal ensembles of particles having some statistical composition distribute precipitate according to autoepitaxial mechanism onto a crystal surface or are nucleated in the bulk of the solution.
2. The only ensembles that can exist under the above conditions must have “own” composition.
3. The other particle ensembles having “foreign” compositions undergo dissolution thus initiating the salting-out of the “own” ensembles.

Several examples of ensemble textures are given in the previous sections. The examples include development of two-dimensional textures formed on the crystal surface (Sect. 3.5, Fig. 3.22) and three-dimensional structures in the solution bulk (Sect. 3.6, Fig. 3.24). It is to be mentioned that in both cases compositions of the “survivor” ensembles correspond to the compositions of crystals existing in heterogeneous metastable equilibrium with supercooled solutions (Sect. 3.3.3). The physical meaning of this correlation consists in stability of such ensembles in the surrounding solution. The process can be schematically represented as follows. The bulk of the solution is not compositionally homogeneous as its various regions become depleted in some isomorphic components due to spontaneous nucleation of the crystal ensembles. During this process, each crystal ensemble is quite dependent upon its surrounding portion of the solution, and its existence within this portion is of some duration determined by the time of interchange between the solution portions. All these micro-portions, except those, which accidentally acquired their metastable equilibrium states, become the regions of proceeding such processes as

growth, dissolution, and replacement that result in variations in the phase compositions and lack of ensemble stability. The life spans of the micro-regions, which have acquired the metastable equilibrium states, are the longest; that ensures “survival” of their ensembles. Also, ensembles, having accidentally moved into the regions having characteristics, favoring the corresponding equilibrium states of the ensembles, reach their stable states.

So, the mechanism suggested for selection of the components during formation of the mixed crystals involves participation of sufficiently big particle aggregations, which can “survive” (“own composition”), or dissolve (“foreign composition”) in the surrounding solution. Conventional statistical mechanism involving distribution of individual ions proves to be valid for a preselection stage of the process. Statistical selection of ions is likely to occur in systems containing a sufficiently small amount of one of the isomorphic components, i.e., when the composition of the solution approaches its ideal state. Also, nonselective crystallization is possible to occur when supersaturation in the system is high enough. However, experimental data obtained for supercooled by 20°C crystals of  $K(\text{Br},\text{Cl})$  and  $(\text{Pb},\text{Ba})(\text{NO}_3)_2$  (Sect. 3.6) make such a contingency highly improbable.

Thus, the model proposed integrates various circumstances of formation of mixed crystals, therefore providing a unified systematical concept. Experimental researches comprising the studies of theoretically predicted phenomena prove appropriateness of the model including the main role of the metasomatic stage, which regulates the process course. It is to be noted that the morphological features observed are combinations of well-known forms of dissolution and growth of crystals in solutions, although their specific combinations and corresponding cause–effect relations lie outside the sphere of classical concepts of crystallogeny. At the same time, experiments have been revealing kinetic effects that are typical for multicomponent systems comprising isomorphic components. This is true, above all, for processes related to metastable heterogeneous equilibria. The main factors defining morphological and kinetic aspects of formation of mixed crystals, which are worth to mention, are as follows: initial compositions of crystal and solution, degree of supercooling or overheating, quantitative ratio between the solution and crystal amounts, peculiarities of the system equilibria, and diffusion characteristics of both solution and crystal. Physicochemical and crystallogenic approaches, which take into consideration the above factors, must be given a priority in suggested genetic interpretations. Simplification without a special basis seems to be unacceptable.

## References

- Anosov VYa, Ozerova MI, Fialkov YuA (1976) *Fundamentals of Physicochemical Analysis*. Nauka, Moscow (Russ.)
- Belov NV (1960) Crystallochemical concepts of isomorphic intrusion of boron into silicates. *Geokhimiya* 6:551–557 (Russ.)
- Belov NV (1976) *Sketches on Structural Mineralogy*. Nedra, Moscow (Russ.)

- Betekhtin AG (1950) Mineralogy. Gosgeolizdat, Moscow (Russ.)
- Bohm J (1995) Realstruktur von Kristallen. E. Schweizerbart'sche Verlagsbuchhandlung (Nägele u. Obermiller), Stuttgart
- Bokii GB (1971) Crystallochemistry. Nauka, Moscow (Russ.)
- Bolkhovityanov YuB (1981) The peculiarities of isothermal contact of liquid and solid phases during the LPE of  $A^{III}B^V$  compounds. *J Cryst Growth* 55:591–597
- Bolkhovityanov YuB (1983) Contact phenomena in acquisition stage of an equilibrium between liquid and solid phases for liquid phase heteroepitaxy of compounds  $A^{III}B^V$ . In: Materials for Electronics 1: Physicochemical Basis of the Preparative Methods. Nauka, Novosibirsk (Russ.)
- Bolkhovityanov YuB (1990) Integrated mechanism of relaxation of a non-equilibrium solid-liquid interface before the liquid phase heteroepitaxy of the III–V group compounds. In: Givargizov EI, Ginberg SA (eds) *Crystal Growth* 18. Nauka, Moscow (Russ.)
- Bolkhovityanov YuV, Bolkhovityanova RI, Vaulin YuD, GavriloVA TA, Olshanetsky BZ, Stenin SI (1986) The formation of  $Al_xGa_{1-x}$  As layers by regrowth on the surface of GaAs during its with the undersaturated liquid containing Al. *J Cryst Growth* 78:335–341
- Borisov VT (1962) Kinetic diagrams of melt crystallization. *Doklady Acad Sci USSR* 142:1:69–71 (Russ.)
- Chernov AA (1984) Processes of crystallization. In: Vainshtein BK, Chernov AA, and Shuvalov LA (eds) *Modern Crystallography III, Crystal Growth*. Springer, Berlin.
- Durham GS, Rock EJ, Frayn SF (1953) Solid solution of the alkali halides. I. The systems KBr-KCl- $H_2O$ , RbBr-RbCl- $H_2O$ , RbBr-KBr- $H_2O$  at 25°C. *J Amer Chem Soc* 75:5793–5794.
- Filatov SK, Bubnova RS (1986) Influence of the crystal media upon extent of isomorphic replacements. *Zapiski Vsesoyuz Miner Obsh* 4:423–437 (Russ.)
- Frank-Kamenetskii VA (1964) Nature of Structural Admixtures and Inclusions in minerals. Leningrad State University, Leningrad (Russ.)
- Frank-Kamenetskii VA, Kotov NV, Goilo EA (1983) Transformations of Sheet Silicates at Elevated P-T Parameters. Nedra, Leningrad (Russ.)
- Franke VD, Glikin AE, Kryuchkova LY., Tabuns EV (2007). Cocrystallization of isomorphic components in solutions and crystal zoning: An example of the  $(Ba,Pb)(NO_3)_2$  series. *Geol Ore Deposits* 49:7:641–647.
- Friedel G (1964) *Lecons de cristallographie*. Paris
- Geguzin YaE (1970) Sketches on the Diffusion in Crystals. Nauka, Moscow
- Gerasimov YaI, Dreving VP, Eremin EN et al. (1970) Course of Physical Chemistry 2. Khimia, Moscow (Russ.)
- Glikin AE (1995) On the theory of formation of isomorphic-mixed crystals. *Zapiski Vsesoyuz Miner Obsh* 5:125–134 (Russ.)
- Glikin AE (1996a) About equilibrium supercooled solutions related to formation of isomorphic-mixed crystals. *Zapiski Vsesoyuz Miner Obsh* 5:103–111 (Russ.)
- Glikin AE (1996b) The physicochemical aspect of the unsteady state of metasomatic crystal production. *Geochem Intern* 33:8:117–128 (Russ.)
- Glikin AE (1996c) Modeling of metasomatic crystallogenesis in aqueous-salt systems. Dr Sci thesis. St. Petersburg State University, St. Petersburg (Russ.)
- Glikin AE, Sinai MYu (1983) Experimental genetic study of monocystal pseudomorphs. *Zapiski Vsesoyuz Miner Obsh* 6:742–748 (Russ.)
- Glikin AE, Sinai MYu (1991) Morphological and genetic classification of crystal replacement products. *Zapiski Vsesoyuz Miner Obsh* 1:3–17 (Russ.)
- Glikin AE, Nikolaeva VP, Petrov TG (1979) Crystallization of potassium biphthalate from neutral and alkaline aqueous solutions. In: Smirnov YuM (ed) *Physics of Crystallization*. Kalinin State University, Kalinin (Russ.)
- Glikin AE, Leontyeva OA, Sinai MYu (1994) Mechanisms of exchange of isomorphic components between crystal and solution and macrodefectiveness in secondary crystals. *J Struct Chem (Russia)* 35:5:642–646.
- Glikin AE, Kovalev SI, Rudneva EB et al. (2003) Phenomena and mechanisms of mixed crystal formation in solutions I. General concept on the example of the system  $KHC_8H_4O_4$ - $RbHC_8H_4O_4$ - $H_2O$ . *J. Cryst. Growth* 255:150–162



- Glikin AE, Kryuchkova LYu, Plotkina YuV et al. (2007) Crystallogenic grounds of isomorphism: Experimental data and theoretical approach. In: Krivovichev SV (ed) *Crystallogenes and Mineralogy* (Zapiski RMO: special issue). Nauka, St. Petersburg
- Grigor'ev DP (1961) *Ontogeny of minerals*. Lvov University, Lvov (Russ.)
- Grigor'ev DP, Zhabin AG (1975) *Ontogeny of Minerals: Individuals*. Nauka, Moscow (Russ.)
- Kasatkin IA (1993) Interrelations of morphology and kinetics of mixed crystal growth and peculiarities of phase equilibria in the system  $K_2SO_4$ - $K_2CrO_4$ - $H_2O$ . PhD thesis. St. Petersburg State University, St. Petersburg (Russ.)
- Kasatkin IA, Leont'eva OA (1992) Phase equilibria in aqueous-salt systems with isomorphic components. *Inorganic Materials* 28:6:1169–1172
- Kasatkin IA, Glikin AE, Bradaczek H, et al. (1995) Kinetics of mixed crystal  $K_2(SO_4, CrO_4)$  growth from aqueous solutions. *Cryst Res Technol* 30:5:659–666
- Kirkinskii VA, Yaroshevskii AA (1967) Physicochemical aspect of isomorphism. *Zapiski Vsesoyuz Miner Obsh* 5:532–546 (Russ.)
- Kitaigorodskii AI (1971) *Molecular Crystals*. Nauka, Moscow (Russ.)
- Korzhinskii DS (1970) *Theory of metasomatic zoning*. Clarendon Press, Oxford
- Kotel'nikova EN, Filatov SK (2002) Crystal chemistry of paraffins. *Zhurnal "Neva"*, St. Petersburg (Russ.)
- Kryuchkova LYu, Glikin AE, Voloshin AE, et al. (2002) Kinetic and morphological phenomena of growth and isomorphic replacement of mixed crystals in solutions (in the series (Co,Ni)(NH<sub>4</sub>)<sub>2</sub>(SO<sub>4</sub>)<sub>2</sub>·6H<sub>2</sub>O). *Zapiski Vsesoyuz Miner Obsh* 3:62–77 (Russ.)
- Laemmlin GG (1948) *Sectorial Structure of Crystals*. Academy of Science, USSR. Moscow [see also in: Laemmlin GG (1973)] (Russ.)
- Laemmlin GG (1973) *Morphology and Genesis of Crystals*. Nauka, Moscow (Russ.)
- Lebedev VI (1964) Some general aspects of isomorphism. *Zapiski Vsesoyuz Miner Obsh* 2:126–138 (Russ.)
- Lindgren W (1925) *Metasomatism*. *Bull Geol Soc Amer* 36:1:1–114 and 36:1:248–253
- Makarov ES (1973) *Isomorphism of Atoms in Crystals*. Atomizdat, Moscow (Russ.)
- Melikhov IV, Merkulova MS (1975) *Co-crystallization*. Khimia, Moscow (Russ.)
- Melikhov IV, Komarov VF, Podoinitsyn VA, et al. (1977) Investigating the action of a seed in the process of a mass crystallization. In: *Mass Crystallization*. IREA, Moscow (Russ.)
- Minerals 1* (1960) Reference Book. Acad Sci USSR. Moscow (Russ.)
- Minerals 2:3* (1967) Reference Book. Nauka. Moscow (Russ.)
- Minerals 3:1* (1972) Reference Book. Nauka. Moscow (Russ.)
- Minerals 3:2* (1981) Reference Book. Nauka. Moscow (Russ.)
- Minerals 4:1* (1992) Reference Book. Nauka. Moscow (Russ.)
- Petrov TG, Treivus EB, Kasatkin AP (1969) *Crystal growing from solutions*. Academic, New York
- Petrov TG, Treivus EB, Punin you, et al. (1983) *Growing Crystals from Solutions*. Nedra, Leningrad (Russ.)
- Punin YuO (1964) Recrystallization in aqueous solutions accompanied by grain coarsening. *Zapiski Vsesoyuz Miner Obsh* 3:364–367 (Russ.)
- Punin YuO (1965) On mechanism of recrystallization. *Zapiski Vsesoyuz Miner Obsh* 4:459–462 (Russ.)
- Punin YuO (1994) *Autodeformation defects in crystals*. Dr Sci thesis. St. Petersburg State University, St. Petersburg (Russ.)
- Putnis C, Pina CM, Pollok K, Glikin A (2001) Mineral replacement reactions in solid solution-aqueous solution systems. In: *The 11th Annual Goldschmidt Conference*. May 2001. Abstracts. Hot Springs. Virginia, USA
- Putnis A (2002) Mineral replacement reactions: From macroscopic observations to microscopic mechanisms. *Miner Mag* 66:5:689–708
- Solubility* (1961–1970) Reference Book 1–3. Nauka, Moscow (Russ.)
- Saranchina GM (1994) *Physical chemistry for geologists*. St. Petersburg State University, St. Petersburg (Russ.)
- Shuvalov LA, Urusovskaya AA, Zheludev IS et al. (1988) *Physical Properties of Crystals*. In: Vainshtein BK, Chernov AA, Shuvalov LA (eds) *Modern Crystallography IV*; Springer, Berlin

- Srinivasan K, Anbukumar S, Ramasamy P (1995) Mutual solubility and metastable zone width of  $\text{NH}_4\text{H}_2\text{PO}_4$ – $\text{KH}_2\text{PO}_4$  mixed solutions and growth of mixed crystals. *JCG* 151:226–229.
- Sternberg AA (1962) On the relation of crystal cracking and morphology with impurities. *Kristallografiya* 7:1:114–120 (Russ.)
- Taratin NV, Kryuchkova LYu, Glikin AE (2007) Features of substance distribution in mixed crystal volume (on the example of the system  $\text{KCl}$ – $\text{KBr}$ – $\text{H}_2\text{O}$ ). In: *Crystallogeneses and Mineralogy. II International Conference*. October 1–5, 2007. Abstracts. St. Petersburg State University, St. Petersburg (Russ.)
- Treivus EB (1977) Elaboration of the state diagrams of multi-component systems. In: *Mass Crystallization*. IREA. Moscow (Russ.)
- Treivus EB (1982) A method of depicting the compositions of isomorphous crystals and three-component solutions equilibrium to them. In: Frank-Kamenetskii VA (ed) *Crystallography and Crystallochemistry*. Leningrad State University, Leningrad (Russ.)
- Treivus EB (2000) About isothermal diagrams of ternary systems containing binary solid solution. *Vestnik St. Petersburg State Univ Ser 7:2:15:14–22* (Russ.)
- Treivus EB, Rozhnova GA (1962) Experimental reproduction of metasomatism in water-soluble salts. *Zapiski Vsesoyuz Miner Obsh* 2:219–222 (Russ.)
- Urusov VS (1977) *A Theory of Isomorphous Miscibility*. Nauka, Moscow (Russ.)
- Urusov VS (1987) *Theoretical Crystal Chemistry*. Moscow State University, Moscow (Russ.)
- Urusov VS, Tauson VL, Akimov VV (1997) *Geochemistry of Solids*. GEOS, Moscow (Russ.)
- Vainshtein BK (1982) Principles of formation of atomic structure of crystals. In: Vainshtein BK, Fridkin VM, Indenbom VL (eds) *Modern Crystallography 2*. Springer, Berlin
- Vergasova LP, Naboko SI, Serafimova EK, Filatov SK (1982) Exhalation native gold. *Doklady Acad Sci USSR* 264:1:201–204 (Russ.)
- Voloshin AE, Glikin AE, Kovalev SI, et al. (2003) Morphological effects of liquid phase epitaxy (in a model system of  $\text{C}_8\text{H}_5\text{O}_4\text{K}$ – $\text{C}_8\text{H}_5\text{O}_4\text{Rb}$ – $\text{H}_2\text{O}$ ). *Kristallografiya* 48:6:1112–1123 (Russ.)
- Voloshin AE, Kovalev SI, Rudneva ED, et al. (2004) Phenomena and mechanisms of mixed crystal formation in solutions II. Mechanism of interface processes. *J Cryst Growth* 261:105–117
- Woensdregt CF, Glikin AE (2005) Ex situ scanning force microscopic observation of growth and dissolution phenomena on {010} surfaces of potassium hydrogen phthalate crystals (KAP) caused by isomorphous exchange reactions. *J Cryst Growth* 283:3–4:523–532
- Zhdanov VV, Glikin AE (2006) Sheatlike metasomatic garnet crystals from the Maksyutovo metamorphic complex, the Southern Urals. *Doklady Earth Sci.* 409:5:814–817.
- Zhmurova ZI, Khaimov-Mal'kov VYa (1970a) Dependence of distribution of impurities during crystallization of isomorphous systems from aqueous solutions. *Kristallografiya* 15:1:136–141 (Russ.)
- Zhmurova ZI, Khaimov-Mal'kov VYa (1970b) Distribution of isomorphous impurities during crystallization from aqueous solutions. *Kristallografiya* 15:1:142–148 (Russ.)
- Zhmurova ZI, Khaimov-Mal'kov VYa, Akulenok EM et al. (1963) Distribution of isomorphous impurity in crystals of  $\text{Zn}(\text{NH}_4)_2(\text{SO}_4)_2 \cdot 6\text{H}_2\text{O}$ – $\text{K}_2\text{SO}_4$  during crystallization. *Kristallografiya* 8:6:936–937 (Russ.)

# Chapter 4

## Physicochemical Analysis of Metasomatic Crystallogenesis

### 4.1 Brief Overview

Thorough examination of phenomena observed during formation of isomorphic-mixed crystals revealed that classification attributes of structures and shapes of monocrystal replacement products are complicated by some complementary effects. Some of them may remain unnoticed unless certain indications are found in preliminary theoretical analysis (e.g., faceting and ordering of the incorporated inclusions in KCl–KBr series). This is a reason for further elaboration of genetic approach presented in Chapter 1.

As it was mentioned before, the most efficient analysis of crystal-genetic processes comprising a metasomatic component can be performed with aid of the Schreinemakers concentration diagrams. Their coordinates are expressed in absolute values of the component solubilities that enable to follow the progress of a process and influence of the volume effect by direct observing the plot shape. Before the publication of our works (Glikin 1995a, 1996a, b, c), these diagrams had been used extensively for presenting phase equilibria in aqueous-salt systems, but only for relatively simple eutonic systems (Anosov et al. 1976). The diagrams have been virtually unknown in mineralogical–petrological methodology, and several sporadic instances of their application have been limited by interpretation of phase associations in metasomatic columns (Treivus and Rozhnova 1962; Korzhinskii 1970).

Solid phases of systems containing isomorphic components have variable compositions, which should be taken into account, and, thus, the diagrams had to be modified accordingly (Glikin 1995a, 1996b, c; Kryuchkova et al. 2002; Glikin et al. 2007; see Chapter 3 of the present monograph). As shown in Chapter 3, the modified diagrams graphically and in detail represent equilibrium states of systems, composition trajectories of both phases obtained for the processes of formation of mixed crystals, and regions having various proportions of metasomatic replacement, direct growth, and direct dissolution. Yet, some or other part of valuable information gets inevitably lost in the process of plotting any diagram, and the Schreinemakers diagrams are not the exception: they cannot clearly show the sin-

gular points that should characterize isodimorphism, regions of discontinuous miscibility, additional compounds, and metastable states.

The peculiarities mentioned above are apparent from examination of diagrams, which were studied in details (Treivus 1982, 2000) with reference to a series of aqueous-salt and dry high-temperature systems [(Co,Mg)(NO<sub>3</sub>)<sub>2</sub>·6H<sub>2</sub>O–H<sub>2</sub>O, (Mg,Ni)SeO<sub>4</sub>·7H<sub>2</sub>O–H<sub>2</sub>O, K(Br,Cl)–H<sub>2</sub>O, (Mg,Cu)SO<sub>4</sub>·5H<sub>2</sub>O–H<sub>2</sub>O, (K,NH<sub>4</sub>)Cl–H<sub>2</sub>O, (Mg,Fe)SiO<sub>4</sub>–SiO<sub>2</sub>, (Na,K)AlSiO<sub>3</sub>–SiO<sub>2</sub>]. The diagrams show a correlation between the total salt content in a saturated solution (the ordinate) and relative fractions of the individual salt components (the abscissa).<sup>1</sup> They contain various “fish-shapes,” similar to the well-known Roseboom diagrams plotted for binary systems having isomorphic miscibility; composition of the equilibrium solid phase is characterized in analogous manner as it is done in the Roseboom diagrams. High sensitivity of these diagrams to the slightest changes in the equilibrium states caused by influence of isodimorphism was shown, for example, for K(Cr,S)O<sub>4</sub>–H<sub>2</sub>O system. The diagrams of such systems are characterized by smooth, but well-distinguishable breaks in the regions of medium solidus compositions and corresponding compositions of the solution (Kasatkin and Leont’eva 1992; Kasatkin et al. 1995), while no singularities have been observed in the Schreinemakers diagrams, except of some points of inflection (Fig. 3.8). However, such diagrams do not provide any direct data on volume effect of isothermal reactions of replacement, while examination of a polythermal process on their basis is highly complicated due to multiple overlapping of various liquidus and solidus isotherms.

The Treivus diagrams can be converted into the Schreinemakers charts via a simple calculation. Thus, physicochemical analysis of crystallogeneses in systems with isomorphism is to be performed with the aid of the diagrams of both types. For instance, simultaneous examination of these diagrams can furnish precise values of solubility. Experimental points correspond to different saturation temperatures and various isomorphic compositions of both phases. All the necessary interpolations for plotting the solubility isotherms can be advantageously plotted in the Schreinemakers diagrams, although experimental and extrapolation errors and singular points can be readily discovered with the aid of the Treivus diagrams. So, the most accurate graphs can be obtained by means of successive adjustments of interpolated dots in the diagrams of both types, when intercorrelated functions plotted in both diagrams acquire a reasonable curvature (Franke et al. 2007).

---

<sup>1</sup> Elements of the diagrams (Treivus 2000) are calculated on the basis of an equilibrium content of the total salt mass and a constant amount of water. They are more representative than the Jeneke diagrams, which are calculated on the basis of a ratio between amount of water and a constant total mass of salts (Anosov et al. 1976). The Lippman diagrams calculated for a fixed amount of water have the same properties, but total solubility of the salt mass in the diagrams is expressed as ion activities (see, e.g., Putnis 2002).

The most possible pathways of metasomatic reactions are discussed below with reference to the Schreinemakers diagrams plotted for three-component systems (Fig. 4.1).

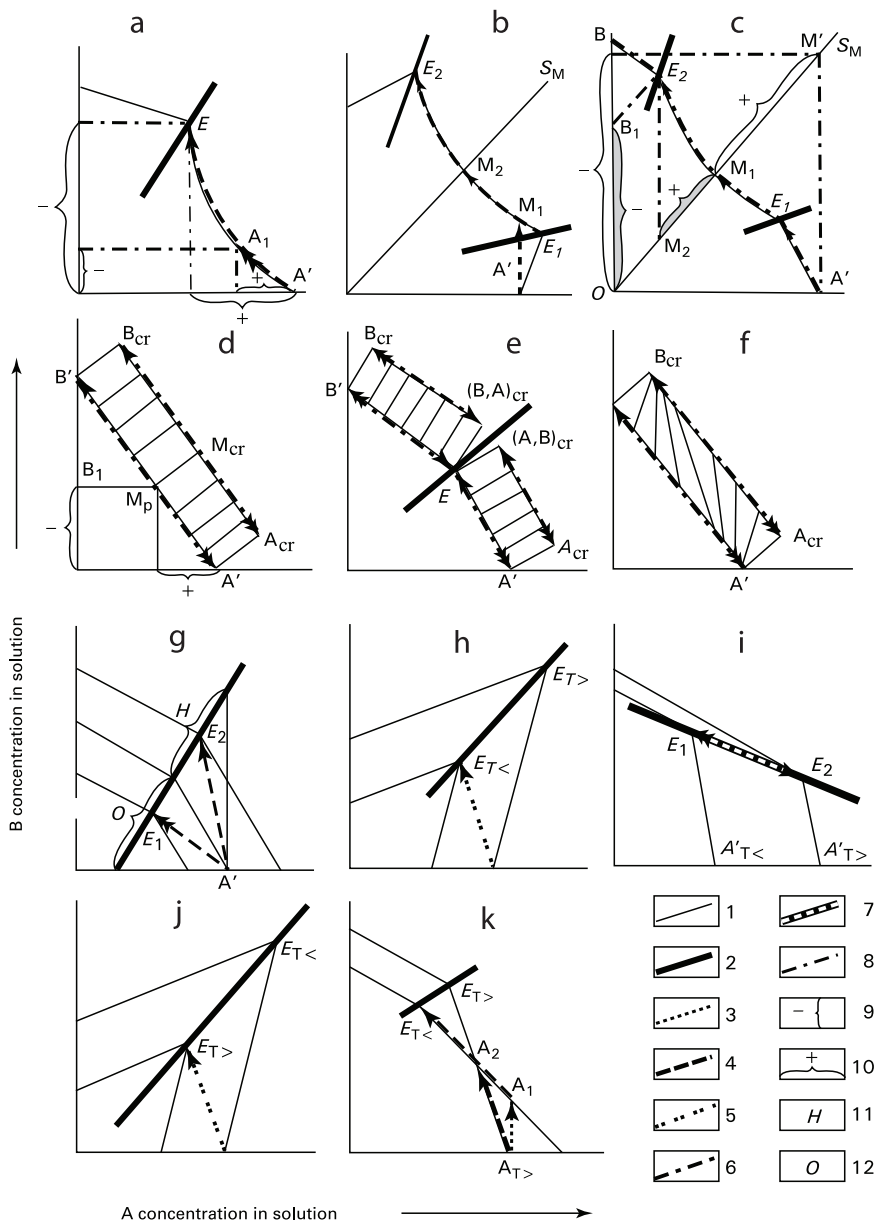
It is useful to remind that the units of both orthogonal coordinate axes represent solubilities  $c_A$ ,  $c_B$  of the main components of the system at the corresponding temperatures. The main elements of the diagrams are solubility isotherms of the system components, and most of the diagrams also contain eutonic lines  $E$  that divide regions of crystallization of the components. The half-lines  $S$  starting from zero point of the coordinates show compositions of solutions containing a stoichiometric content of one of the components. In systems with eutonic equilibria (similar to eutectic equilibria in binary systems) the half-lines are located in the region of stability of the corresponding component, and in particular cases coincide with the coordinate axes. If a compound is a part of a peritonic system (similar to a peritectic alloy), its corresponding half-lines are located outside the region of its stability. The basic definitions for systems comprising isomorphous components (Figs. 4.1*d-f*) are given in Chapter 3, and when references are made to the respective definitions it is important to separate scales of crystal compositions from the solubility isotherms.

Physicochemical nature of a metasomatic reaction consists in its mechanism, according to which the mineral substance to be replaced initiates precipitation of the substituting phase due to salting-out of the latter or owing to proceeding of some incongruent reactions. It is worth to remind that in systems (or their parts) with “salting-out” the isotherm converges with a coordinate axis of the dissolving component ( $\partial c_A / \partial c_B < 0$  – Fig. 4.1*a*), while in systems with “salting-in” the isotherm and the axis diverge ( $\partial c_A / \partial c_B > 0$  – Fig. 4.1*h*). Introducing a component into one of the above systems can either lower or increase solubility of the other component, respectively (Anosov et al. 1976; Kirgintsev 1976). It is important to mention incongruent systems, where introducing a new component results in its reaction with the components of the solution and in precipitating compounds  $M$  (Figs. 4.1*b, c*), which are referred to as “additional compounds.”

The systems also differ in arrangement of isotherms and in location of the stoichiometric composition lines within the characteristic regions or outside of them.

Accordingly, it is possible to distinguish a number of pathways for replacement process to proceed and to present each one of them as a combination of salting-out, salting-in, and incongruent reactions by correlating them with correspondent sectors of isotherms in the standard diagrams. If there is a sufficient amount of the initial crystalline phase, its transformation corresponds to transition from one sector of the diagram to the other in accordance with various process mechanisms, which can be accompanied by a variety of effects.

Some possible variants of replacement processes are discussed below with reference to Fig. 4.1. It is assumed that in all systems, except for some special modifications, initial concentration of the solution is the equilibrium concentration, with its figurative point located on the abscissa, while the protocystal composition (its amount is not limited) corresponds to the component, solubilities of which are plotted on the ordinate axis.



**Fig. 4.1** Pathways of metasomatic replacement in various (a–k) physicochemical systems: (1) coordinate axes (showing stoichiometric compositions of solutions A, B, and M); (2) eutonic compositions of solutions; (3–7) trajectories of figurative points: 3 – dissolving, 4 – salting-out, 5 – replacement with salting-in, 6 – incongruent reactions, 7 – alternating change of the trajectory direction; (8) auxiliary lines; (9) amount of dissolving protocystal; (10) amount of a new formation; (11, 12) regions of possible replacement with elevation (11) and lowering (12) the temperature. Single arrows – volume-deficit replacement, double arrows – volume-excess replacement;  $T >$  and  $T <$  – dots corresponding to elevated and decreased temperatures

## 4.2 Isothermal Replacement in Ternary Systems

Systems containing two non-isomorphous compounds with mutual salting-out effect (the lines of stoichiometric compositions coincide with the coordinate axes) are the simplest examples shown in Fig. 4.1*a*. Isothermal replacement can only take place according to the salting-out mechanism without being accompanied by additional growth or dissolution processes. The reaction comprises successive stages of the protocystal dissolution, supersaturation of the solution with a newly generated substance, and precipitation of such quantity of the products, which corresponds (but is not equal!) to the amount of the dissolved substance. The substances being non-isomorphous, precipitation involves growth of spontaneously nucleated crystals of the new formation that results in generation of polycrystalline products (reactions *Ia11*, 2, 8, 9, 11, 14, 18 in Table 1.1). The interaction is graphically represented by the trajectory drawn over the isotherm stretching between the figurative points  $A'$  and  $E$ , which designate the extreme points of the initial and residual solution compositions. Curvature of the isotherm reflects change in volume effect in the course of the reaction concerned from the volume-excess to the volume-deficit (see Sect. 4.6). Crystals composed of substances A and B are characterized by morphological features of dissolution and growth, respectively.

Different polymorphs possess individual dependencies of solubility versus temperature in spite of them having the same chemical compositions. They behave as non-isomorphous components specified by typical salting-out curves crossed in eutonic point  $E$  like in Fig. 4.1*a*. Therefore transformations between polymorphs run in solutions by means of metasomatic reactions similarly to that for the retgersite-nickelhexahydrite couple described in Sect. 1.3 (see Kulkov and Glikin 2007). Substantially these compounds reveal only a weak difference in solubility dependencies. This makes available a low supersaturation of the secondary phase during the replacement process causing specific textures of pseudomorphs. The polymorph couple  $\alpha\text{-LiIO}_3\text{-}\beta\text{-LiIO}_3$  is of similar physicochemical features and their mutual transformations should run similarly causing similar textures. Another example of polymorph transformation through metasomatic reaction is well-known synthesis of diamond after graphite in Ni-Fe-fluxes.

If a system contains double salts or any other additional compounds of fixed discrete composition (Figs. 4.1*b*, *c*), the replacement process also results in formation of polycrystalline products (Table 1.1, reactions *Ia5*, 6, 10, 19, 22, 23). However, the replacement appears complicated due to accompanying precipitation of the extra phases. The Schreinemakers diagrams allow to divide replacement with formation of an additional compound into several stages, where the first stage is defined by stability region of the dissolved substance A, and the others are determined by stability region of the additional compound M.

Proceeding of the first stage, which should be considered in the AB coordinates, depends upon the slope of  $A'E_1$  sector of the isotherm, which determines whether

the process involves salting-out or salting-in.<sup>2</sup> If it involves salting-in (Fig. 4.1*b* schematically representing replacement of  $\text{CuSO}_4 \cdot 5\text{H}_2\text{O}$  crystals in  $\text{K}_2\text{SO}_4$  solution: reaction 1*a*/22), the protocystal dissolves without generation of any new phases, while composition of the solution changes along the linear trajectory  $A'M_1$  that partially crosses the M region. If the process involves salting-out (Fig. 4.1*c*), dissolution of the protocystal is accompanied by metasomatic precipitation of the solid-phase A and by change in the solution composition in accordance with trajectory  $A'E_1$ .

The second stage involves metasomatic precipitation of the additional phase M and changing the solution composition to agree with the corresponding stoichiometry; in the systems under discussion, these are sectors positioned along  $M_1M_2$  or  $E_1M_1$  parts of the isotherm (Figs. 4.1*b* and 4.1*c*, respectively). There, incongruent chemical reaction takes place between the protocystal substance B and the dissolved substance A, which is present in the solution in an excessive amount in respect to the stoichiometry of compound M. Reaction in Fig. 4.1*b* is additionally complicated by simultaneous action of the second precipitation mechanism induced by secondary replacement of the initial products, i.e., by replacement of crystals A with crystals M. This mechanism slows down the movement of the figurative point from the dot  $E_1$  toward the dot  $E_2$  (corresponding to the basic, incongruent reaction) setting its movement in the opposite direction; as long as crystals A are present in the system, the process takes place at the point  $E_1$ , provided the secondary reaction is relatively fast. This stage should be considered in skew coordinates  $AS_M$ , where it is easier to realize that the secondary replacement (A with M) can be described by the scheme represented in Fig. 4.1*a*.

The third stage should be contemplated in skew coordinates  $S_MB$ . If substance B exerts a salting-out effect upon the substance M, precipitation of the M phase, after passing the line  $S_M$ , continues up to the point  $E_2$ , but according to the other, congruent mechanism; the process also agrees with the scheme, presented in Fig. 4.1*a*. If the substance B exerts a salting-in effect upon the substance M, precipitation of the latter after crossing the line  $S_M$  transforms into its dissolution, so, reaching the point  $E_2$  (and, consequently, association of B and M) is a question of whether the quantity of the M phase generated in the previous reactions is enough for it.

If the line of stoichiometric composition of the additional compound falls into the stability region of the initially dissolved substance, the stage of incongruent replacement is absent, and until the system reaches the point  $E_2$ , the system undergoes only salting-out. If this stoichiometric line falls into the region of the protocystal matter, the protocystal undergoes replacement according to incongruent mechanism until the system reaches the point  $E_2$ . In such systems, the initial new formation A deposited due to its salting-out from the protocystal substance is replaced in the vicinity of  $E_1$  point thus inhibiting alteration of the solution composition proceeding in the direction of  $E_2$  (similar to the process shown in Fig. 4.1*b*).

---

<sup>2</sup>Of course, the isotherm shape reflects phase equilibria in the systems and does not determine the process. However, we purposely introduced this stylistic inaccuracy to simplify the text.



A variety of additional compounds may exist (e.g.,  $\text{KOH}-\text{K}_2\text{CrO}_4-\text{K}_2\text{Cr}_2\text{O}_7-\text{K}_2\text{Cr}_3\text{O}_{10}-\text{K}_2\text{Cr}_4\text{O}_{13}-\text{H}_2\text{CrO}_4-\text{H}_2\text{O}$  system). If the system can produce any additional compounds, the reaction proceeds as a series of alternating and partially overlapping stages.

It is to be noted that presence of additional compounds prompts the change in mineral associations in the course of a single metasomatic process. So, crystals of the new formations, which are growing at the early stages, would dissolve at the later stages of the process. If the rate of the process is sufficiently low, the system state in each moment would be close to that of equilibrium, so that only crystals stable under these conditions would remain. Yet if the process is sufficiently rapid, the mineral associations may retain some dissolving relics of the substances generated at the early stages and unstable under the new conditions.

Precipitation of an insoluble compound (reactions of type *III* in Table 1.1), in spite of its peculiarity, is also classed as a replacement pattern *c*, and this is apparent after plotting the diagram in logarithmic scale. In linear scale, isotherms and regions of the “extremities” in the diagram almost merge with the coordinate axes, while the entire field between them is occupied by the region of an insoluble additional compound. Thus, replacement in this system is an interaction between the initial compounds, the only difference from a well-known reaction of chemical quantitative analysis being solid state of one of the compounds.

Systems saturated with isomorphous substances (Table 1.1, reactions *Ib*) show the most complicated pattern of replacement. Physicochemical analysis of such systems is discussed in Chapter 3, so only some of their aspects are pointed out in the present section. It is to be reminded that reactions occurring in the above systems change not only the composition of the solution, but also the composition of the crystal. So, to represent this coupled change the diagrams must be either modified (as it was proposed in Chapter 3), or provided with linear scales of solidus composition (Figs. 4.1*e, f*). If the latter are used, the correspondent compositions marked on the solidus lines and liquidus isotherms are to be connected via conodes, mutual positions of which can be arbitrary: they may be parallel (Fig. 4.1*d* – systems *Ib/24, 25, 28, 29*), concurrent, or divergent (Fig. 4.1*f* – *Ib/34, 35*). The only limitation is that the crystal composition must be enriched with a substance, which is the least soluble in the existing solution.

Isotherms or some of their parts, which characterize equilibria with crystals formed by members of a continuous series of solid solutions, take the shape of smooth lines; they can be straight lines [e.g., system  $\text{K}(\text{Al,Cr})(\text{SO}_4)_2 \cdot 12\text{H}_2\text{O}-\text{H}_2\text{O}$ , Fig. 3.3] or curves [ $(\text{Co,Ni})(\text{NH}_4)_2(\text{SO}_4)_2 \cdot 7\text{H}_2\text{O}-\text{H}_2\text{O}$ ; Fig. 3.15*a*]. If a diagram is represented by a single continuous region, such systems contain components having infinite additive miscibility (Fig. 4.1*d*).

The area of additive miscibility corresponds to a continuous interchange of components between the solution and the crystal, bringing such variation in their compositions that the figurative points of the liquidus and solidus appear to be permanently advancing toward each other from their initial locations until

they reach some of their common conodes. The conode position depends upon proportion of the phases and is limited by two extreme points: if the initial ratio between the solid and liquid phases is sufficiently great, the composition of the newly generated crystals is virtually identical to that of the protocrystal. On the contrary, if this proportion is sufficiently small, the composition approaches that of the other extreme member of the series. Accordingly, the former process results in almost complete transformation of the salt component present in the liquid into the isomorphic one, while in the latter case it remains virtually invariable.

Such nearly ideal systems cannot be too abundant. Systems with different singular points of the solubility isotherms, various isotherm curvature, variable coefficient of distribution, etc., are to be more numerous. Data reported for such systems are fragmentary, so just some assumptions about the processes peculiarities can be given at present, hopefully, creating a foundation for the forthcoming research. It is to be reminded that for reliable determination of singularities it is essential to use the Treivus diagrams.

In singular points corresponding to discontinuity regions of solid-phase miscibility (the most powerful failure of additivity), crystals change their polymorphic modifications; for example, in  $(\text{Ni},\text{Co})\text{SO}_4 \cdot 7\text{H}_2\text{O}$  series the crystal symmetry changes from orthorhombic to monoclinic. This results in breaking the isotherms in their crosspoints with eutonic lines and dividing the diagram into stability regions corresponding to different solid phases, which have variable compositions (Fig. 4.1e). If in the vicinity of a break the compositions of protocrystal and solution occupy opposite regions divided by the eutonic (Fig. 4.1e), the entire process starts with replacement of phase B with a non-isomorphic phase (A,B), and until the system reaches the point E, the protocrystal continues to dissolve accompanied by simultaneous continuous alterations in composition of newly generated crystals according to the scheme represented in Fig. 4.1d. In this example nucleation of the new phase proceeds in the same manner as in the systems with discrete compositions of components (see Figs. 4.1a–c). If the system state corresponds to the point E, replacing of the protocrystal relic B continues, but it is now being replaced by the isomorphic phase (B,A). This process is accompanied by replacement of the crystals (A,B) precipitated earlier with the same (B,A) phase, which inhibits the system moving away from the point E along the trajectory EB', as it was observed in the presence of an additional compound in the system having fixed compositions of the solid phases (Fig. 4.1b).

Mechanism of the process proceeding in the vicinity of the isodimorphism singular point can probably be considered in the same vein, but crystal-chemical difference and additivity failure should be significantly less pronounced under these conditions. Thus, structures of  $\text{K}_2\text{SO}_4$  and  $\text{K}_2\text{CrO}_4$  crystals are considered as similar (Wyckoff 1965, 1966). According to the phase equilibria data these substances form isodimorphous series, but the corresponding breaks of the Treivus diagrams are not too sharp (Kasatkin and Leont'eva 1992; Kasatkin et al.

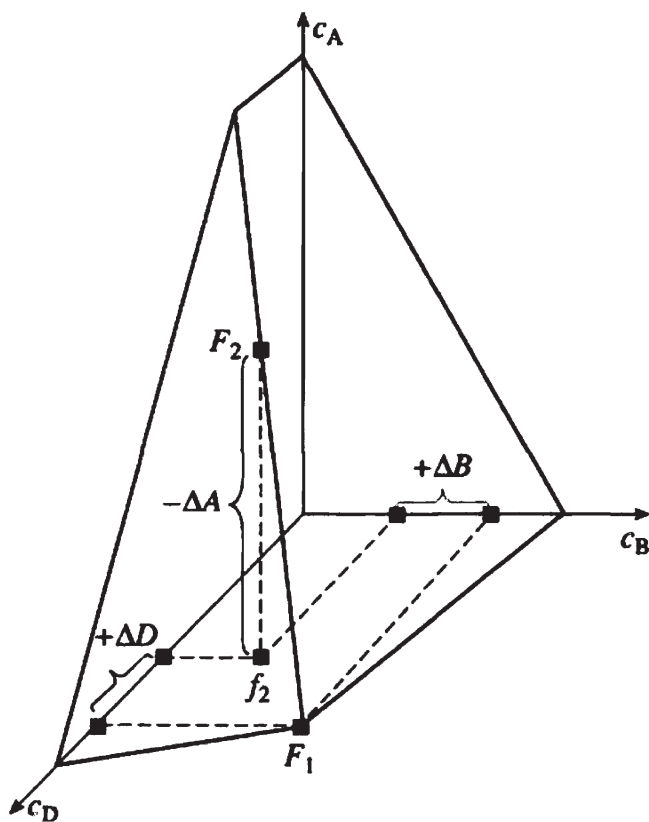
1995). In the Schreinemakers diagrams the breaks are completely absent (Fig. 3.8). Interpretation of the process occurring in this system quite agrees with conception of continuous miscibility (see Sect. 3.4.3). It is quite unlikely that those insignificant structural differences hamper autoepitaxial precipitation, and the mechanism of monocrystalline replacement remains the same even after passing the point of isodimorphism. At the same time one cannot exclude the possibility that the observed heterogeneity of replacement (Fig. 1.6*d*) is caused by isodimorphism of the compounds.

Some systems with absence of additivity failures contain an intermediate additional compound (so-called alyotropic compound) corresponding to a singular point detected as a maximum or a minimum of the total solubility in the Treivus diagram without breaks in the Schreinemakers isotherms. These points have been revealed in  $\text{K}(\text{Cl},\text{Br})\text{-H}_2\text{O}$  and  $(\text{Na},\text{K})\text{AlSiO}_3\text{-SiO}_2$  systems (Treivus, 2000). Most likely, at least three systems we tested exhibit similar singular points:  $(\text{K},\text{Rb})\text{HC}_8\text{H}_4\text{O}_4\text{-H}_2\text{O}$ , characterized by close solubility values of the extreme members and a convex Schreinemakers isotherm (Fig. 3.19);  $(\text{K},\text{NH}_4)\text{H}_2\text{PO}_4\text{-H}_2\text{O}$ , also characterized by a convex isotherm; and  $\text{Na}(\text{Cl},\text{Br})\text{O}_3\text{-H}_2\text{O}$ , having a profoundly concave isotherm. Monocrystalline isomorphic replacements, characterized by change of mechanism from volume-deficit to volume-excess [ $\text{K}(\text{Cl},\text{Br})$ ,  $(\text{K},\text{Rb})\text{HC}_8\text{H}_4\text{O}_4$  and  $(\text{K},\text{NH}_4)\text{H}_2\text{PO}_4$  series] or vice-versa [ $\text{Na}(\text{Cl},\text{Br})\text{O}_3$  series], take place in four of the above systems. We consider this phenomenon to result from variation of the isotherm steepness in different sectors of the replacement trajectory (see Sect. 3.4.2). However, this might be a property of the systems forming additional compounds. From the above it can be concluded that when examining systems, which form additional compounds, it is necessary to take into account both the isotherm shapes and the process regularities.

In general, conodes connecting corresponding compositions of liquidus and solidus in the Schreinemakers diagrams are not parallel, indicating variation of the distribution coefficient according to changes occurring in the solution composition [Fig. 4.1*f*; see also  $\text{K}(\text{Cr},\text{S})\text{O}_4\text{-H}_2\text{O}$  system in Fig.3.8]. If the conodes converge at the solidus line, the composition of the newly generated crystals corresponding to this section of the isotherm changes insignificantly, but if the conodes converge at the liquidus line, the composition changes abruptly and quickly. This phenomenon is referred to as a “wide fish” in the Treivus diagram. As it was pointed out in Sect. 3.4.3, volume-deficit replacement in the region of slowly changing solid-phase composition produces insignificant variations of composition at the crystal surface and in the diffusion layer and, thus, does not result in formation of inclusions. Evidently, the signs of volume-excess replacement in such a case should also be expressed weakly. As a result, the most expectable is prevalence of dissolution accompanied by more or less uniform deposition of material undergoing salting-out on the surface. On the contrary, in the region of a rapid change of the solid-phase composition the volume effect of replacement should be apparent.

### 4.3 Isothermal Replacement in Complex Systems and Formation of Poikilitic Crystals

The next level of complication consists in increasing the number of system components, thus approaching the naturally occurring systems. It can be stated that physicochemical factors of salting-out processes and crystallogenic mechanisms of replacement in quaternary or more complex systems are principally analogous to those of ternary systems. Nevertheless, for description of processes taking place in quaternary systems it is essential to use three-dimensional diagrams, where isothermal equilibria are depicted as planes, plane intersection lines, and crosspoints of the lines. The Schreinemakers diagrams are still important for analysis of metasomatic processes in these systems, though methods of their application in a three-dimensional space (Fig. 4.2) have not been considered yet.



**Fig. 4.2** Schematic representation of interrelationships between physicochemical processes proceeding during a metasomatic formation of poikilitic crystals in A–B–D three-salt system occurring in the course of metasomatic replacement of crystal A with mixed component (A,B) and with the matter of compound D having a fixed composition:  $c_A$ ,  $c_B$  and  $c_D$  represent concentrations of the components A, B, and D, respectively;  $F_1$  and  $F_2$  are the initial and final figurative point of the solution;  $f_2$  represents a projection of  $F_2$  on  $c_B c_D$  plane.  $-\Delta A$  is a quantity of the protocystal matter undergoing dissolution;  $+\Delta B$  and  $+\Delta D$  are the quantities of the salt components of the initial solution undergoing precipitation

The most important feature of all multicomponent systems is that dissolution of a protocystal leads to salting-out of two or more substances that formerly were to enrich the solution, so that the result is generation of products of combined replacement. Different phases of such products precipitate in a relatively independent way in the form of different pseudomorphs or automorphs, so that they may either grow through each other or can be deposited in various sectors of the reaction volume. If a system contains compounds having fixed compositions, the products are polymineralline pseudomorphs (replacement of alum crystal with combined  $K_2CrO_4$  and  $K_2Cr_2O_7$  aggregates – reaction *1a/5*, Fig. 1.8). Their analogs in systems saturated with compounds of isomorphic series and substances, which do not belong to this series, are monocrystalline pseudomorphs with implanted solid inclusions, which can be classed as poikilitic (Glikin and Sinai 1991, 2004; Glikin 1996a, 2002), or myrmekitic formations.

The most pronounced poikilitic crystals obtained in the first experiments are shown in Figs. 1.6e–g (Glikin and Sinai 2004). The matrix (the dark, extinguished part) is a spongy volume-deficit monocrystalline pseudomorph of  $(Fe,Co)SO_4 \cdot 7H_2O$  after  $CoSO_4 \cdot 7H_2O$ . The light regions are composed of randomly oriented secondary crystals implanted into the matrix, which have probably the composition corresponding to the following formula:  $(Fe,Co)(NH_4)_2(SO_4)_2 \cdot 6H_2O$ . The implanted crystals precipitate in the bulk of the matrix undergoing replacement, either in its center (Fig. 1.6e) or in the periphery (Fig. 1.6f), directly in the course of replacement.

Metasomatic formation of poikilitic crystals in quaternary and more complicated systems was predicted (Glikin 1996a) on the basis of experimental and theoretical data obtained for replacement of monocystals in ternary systems (Glikin and Sinai 1991), and physicochemical nature of this formation involves the following. Dissolving a protocystal of  $CoSO_4 \cdot 7H_2O$  results in simultaneous salting-out of isomorphic  $(Fe,Co)SO_4 \cdot 7H_2O$  compound and non-isomorphic  $(Fe,Co)(NH_4)_2(SO_4)_2 \cdot 6H_2O$  component. Isomorphic salting-out proceeds according to volume-deficit mechanism and, owing to decreasing solubility of compounds in  $(Fe,Co)SO_4 \cdot 7H_2O$  series as the content of Fe in the series increases, results in formation of a monocrystalline spongy pseudomorph. Non-isomorphic salting-out results in precipitation of crystals in pores of the spongy pseudomorph due to a higher diffusion rate of the precipitating substance in comparison with that of the substance undergoing salting-out (see Sect. 1.5). A variation in inclusion distribution depends upon the process kinetics.

As a rule, the process involves the following stages: formation of the external spongy zone, nucleation of the double-salt crystals on the pseudomorph surface and in inclusions within the matrix in the vicinity of the replacement front, expansion of the spongy zone toward the centre of the pseudomorph accompanied by ingrowth of the double-salt crystals (in a way similar to that of metacrystals into the polycrystal pseudomorph – see Figs. 1.8b–d). Progress of the spongy zone front toward the centre of the protocystal is accompanied by formation of zones (from one to three) containing crystals of the double salt. Their number depends upon a proportion between the volume of protocystal and that of the solution. The spongy pseudomorph preserves both its monocrystalline nature and the initial orientation

of the protocrystal until the process is complete; on the contrary, orientation of the double-salt crystals is random. The process can be accompanied by dissolution of the inclusions previously formed in the peripheral zones with subsequent precipitation of the new inclusions in the central zones of the matrix.

It is to be noted that the result of the process described quite agrees with character of replacements in the ternary (two-salt) parts of the quaternary system under discussion. Replacement of  $\text{CoSO}_4 \cdot 7\text{H}_2\text{O}$  crystal in solution of  $\text{FeSO}_4 \cdot 7\text{H}_2\text{O}$  results in formation of a spongy pseudomorph of  $(\text{Fe,Co})\text{SO}_4 \cdot 7\text{H}_2\text{O}$ , while its replacement in  $(\text{NH}_4)_2\text{SO}_4$ -containing solution produces a polycrystalline pseudomorph of  $(\text{NH}_4)_2\text{Co}(\text{SO}_4)_2 \cdot 6\text{H}_2\text{O}$  made of well-faceted crystals. However, this correspondence cannot be a rule, as particular places of deposition of replacement products in complex systems and some parts of the complex systems containing a lesser number of components might be different due to alterations in diffusion characteristics of the system caused by change in its composition.

#### 4.4 Polythermal Processes

Variation of temperature complicates any process as it presents an additional independent factor influencing solubility of the components. General analysis of such apparently diversified processes requires special researches; nevertheless, a number of important subclasses may be singled out a priori allowing a chemical scheme of supra-elementary processes to be completed.

1. As a rule, a monotonous variation of temperature within the limits defined by the system phase equilibria does not change the general mechanism of metasomatic process, while affecting its particulars.

During polycrystalline replacement of *Ia* type in systems with salting-out (Fig. 4.1g), the initial and final figurative points are located on different isotherms. Effects and mechanisms of replacement stated above also take place in systems of this type, being more profound or less expressed depending upon lowering or raising the temperature. In fact, the only limit of temperature variation consists in a higher solubility of the substance B undergoing replacement and a lesser solubility of the replacing substance A in the final figurative point in comparison with the corresponding solubilities in the initial figurative point, i.e., the final point must be located within a right-angled triangle having its apex in the point  $A'$  and hypotenuse at the eutonic line. It is obvious that variation of temperature can affect the volume effect and even change its sign to the opposite.

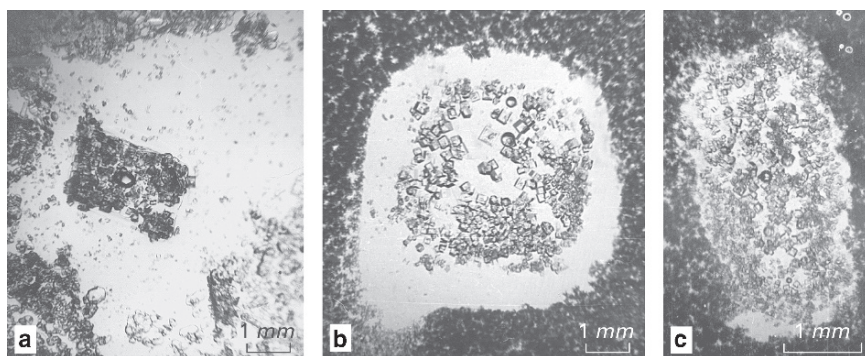
Varying temperature in systems forming additional compounds (Figs. 4.1b, c) affects not only the volume effect and kinetic properties of the system, but it also changes the mechanism of the initial stage of the process, corresponding to its proceeding within the stability region of the component A and in vicinity of the eutonic line  $E_1$ . For example, if the system *b* is cooled sufficiently, the initial dissolution along  $A'M_1$  line is averted. Deeper cooling causes this dissolution to transform into

replacement, as it is the case in the system *c*. On the contrary, in the system *c*, the initial replacement transforms into dissolution as the temperature rises. In the course of formation of an insoluble additional compound (a modification of the system *c*), changes in temperature affect only kinetic properties of the process.

If a process occurs under non-isothermal conditions, replacement can take place even in salting-in systems (type *II*, see Sects. 1.2 and 1.4). The scheme of the process is shown in Fig. 4.1*h*; it results in formation of negative products (Sinai and Glikin 1989, 1991). It is obvious that this process can occur under a wide range of conditions and when the slope of the trajectory ranges from  $0^\circ$  to  $90^\circ$ . Examples of the process products are shown in Fig. 4.3.

Non-isothermal processes of crystal formation in the systems containing isomorphic components were discussed in detail in a series of articles (Glikin 1995a, b; Kryuchkova et al. 2002; Glikin et al. 2003, 2007) and are summarized in Sect. 3.3 with reference to some illustrative examples. Two of the most important regularities are as follows. First, it is a regular suppression of a metasomatic component combined with growth or dissolution under conditions of increased supercooling or overheating. Second, it is a metastable heterogeneous equilibrium existing between the crystal matter and a supercooled solution containing isomorphic substances dissolved in any “foreign” ratio.

If a system contains components with negative thermal gradient of solubility, this significantly increases diversity of the process modifications, but does not change it in essentials. If the isotherms are “inversed” (systems with inversed solubility gradients of all the components), all the processes, described above as taking place at lowering temperature, should occur at increasing temperature. For example, a system in which negative products can be formed only with elevation of temperature is depicted in Fig. 4.1*j*; principally it is similar to the process occurring



**Fig. 4.3** Combined pseudomorphs after  $\text{NaNO}_3$ : positive pseudomorphs formed by  $\text{NaCl}$  (central parts of the picture) located inside the negative ones, which are surrounded with  $\text{K}_2\text{Cr}_2\text{O}_7$  aggregates: (a–c) products of replacement obtained at various degrees of supercooling  $\Delta T$ ,  $^\circ\text{C}$ : a –  $\Delta T = 8$ ; b –  $\Delta T = 15$ ; c –  $\Delta T = 25$

with temperature decrease shown in chart *h*. If isotherms intercross (combination of components with direct and inversed solubility gradients – Fig. 4.1*k*) the vicissitude of the process can probably change. Thus, in this case, abrupt decrease of temperature causes the protocystal to dissolve at the initial stage of the process without accompanying precipitation of any new formations (trajectory  $A'_{T>} A_1$ ); then replacement starts according to an ordinary scheme presented in Fig. 4.1*a*. If the temperature decrease is sufficiently slow, an ordinary replacement corresponding to the trajectory  $A'_{T>} A_2 E_{T<}$  may occur.

2. Oscillating temperature regime involves a series of recrystallizations of monomineral aggregates in solutions caused by cyclic alternations of the crystal growth and dissolution stages, which were shown (Shubnikov 1918; Punin 1964, 1965) to be accompanied by gravitational separation of solution into layers. In general, if the aggregate has polymineral composition, redistribution comprises a significant proportion of metasomatic components (Glikin 1991, 1995b; Glikin and Petrov 1998) that makes it rather different from the particular process involving monomineral formations. Recrystallization experiments are given some attention in Chapter 5, so at present only their main physicochemical aspects are pointed out.

Variations of temperature define the states of the system varying within the range limited by eutonic points  $E_{T>}$  and  $E_{T<}$  of two isotherms corresponding to the upper and lower values of temperature (e.g., Figs. 4.1*h*, *i*). Generally, the trajectories of the solution compositions are more or less arbitrary distributed between these points, while in a particular quasi-equilibrium case they coincide with the eutonic lines. It is possible to distinguish systems with ordinary (Fig. 4.1*h* and similar) and inversed (Fig. 4.1*i*) eutonic lines.

Local metasomatic reactions of different types occur in the systems. Mutual influence of crystals formed by different phases consists in salting-out or salting-in reactions, which can accelerate or inhibit both growth and dissolution of individuals induced by temperature variations. These reactions are induced by alterations in concentration of the second salt component in the vicinity of one individual, while its neighboring individual consisting of the second component also undergoes dissolution or growth under the action of temperature variations.

If the trajectory diverges from the quasi-equilibrium state, it falls within the stability region of one of the phases. When the eutonic line has an ordinary shape (Fig. 4.1*h*), this is the region of a slowly growing phase, while the rapidly growing phase appears to be unstable or metastable under discussed conditions. On the contrary, if the eutonic line is inversed (Fig. 4.1*i*), this is the region of a rapidly growing phase, while the slowly growing one appears to be unstable or metastable. The first exemplary system is likely to be more unbalanced.

Recrystallization (see Sect. 5.3) in the systems with the inversed eutonic line may be interpreted as an alternating proceeding of direct and inverse reactions of replacement (Fig. 4.1*i*). Elevation of temperature makes the system to transfer from  $E_{T<}$  to  $E_{T>}$  state and brings about a replacement of A with B, while lowering the temperature causes the reverse change and B is to be replaced with A.



It is worth mentioning that influence of temperature variation upon the kinetic properties of the process and thereby the morphology of metasomatic reaction products is in agreement with the concepts set forth in Sect. 1.5.3.

#### **4.5 Common and Different Features of the Processes Proceeding in Systems Containing either Isomorphic or Non-isomorphic Components**

In spite of the fact that replacement products produced in eutonic systems and in the systems containing isomorphic components are radically different in composition, being polycrystalline and monocrystalline, respectively, still they have much in common both in their properties and in their physicochemical and crystallogenic nature.

Physicochemical nature of salting-out of isomorphic substances is quite similar to that of non-isomorphic compounds, as in both the cases the substance of the protocrystal dissolves making the solution supersaturated with dissolved matter, which, consequently, crystallizes out. One of the differences is formation of monocrystalline and polycrystalline products. Monocrystalline pseudomorphs allow visualization of some features of the volume-deficit and volume-excess processes as implanted inclusions and autoepitaxial accretions. Attributes of volume effect cannot be discerned in polycrystalline products, because they are hidden in their friable constitution.

Loosening the substance structure and its impregnation with solution in the course of metasomatic replacement is demonstrated by volume-deficit monocrystalline replacement. This is an example of an extreme case, because the above-mentioned transformations occur in the most consolidated, i.e., monocrystalline, solid object, which, at the same time, preserves its monocrystal state. Structure loosening and its impregnation with the solution in the course of polycrystalline replacement proceed in a similar way, but probably more efficiently. This mechanism can be the reason of rock permeability for metasomatic solutions (an appropriate term may be “autopermeability”), which does not really depend upon the natural porosity, fissuring, and intercrystal boundaries of the rock.

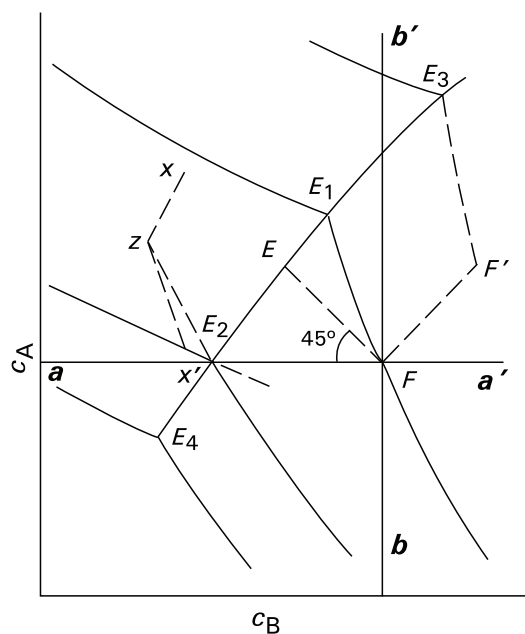
On the contrary, monocrystalline volume-excess replacement prevents this reaction and forms a barrier for the permeability. In the course of polycrystalline replacement an excessive substance precipitates in the rock cavities, thus blocking ways for solutions.

Polymineral products in the form of monocrystalline and polycrystalline pseudomorphs also have a common physicochemical nature. In both cases the crystal dissolution results in salting-out of two or more substances. The difference is as follows: the monocrystalline products contain hard inclusions implanted within a mass of solid crystal (this may seem to be paradoxical, because formation of such inclusions as well as introduction of fluid inclusions is not considered in traditional theories), while the polycrystalline products result from ordinary growth of polymineral aggregate.

Pathways of monocrystalline and polycrystalline replacements also have some common, and some different stages.

An equilibrium diagram of a eutonic system contains a number of regions (Fig. 4.4) differing in the mode of processes proceeding and separated from each other with four lines intercrossing in the figurative point  $F$ . These lines are isoconcentration lines  $aa'$  and  $bb'$  (isolines of the solution compositions containing equal contents of the components A and B, respectively), the isotherm  $FE_1$ , and the slant line  $FE$  forming a  $45^\circ$  angle with  $aa'$ . Domains of direct crystallization and dissolution coincide for both types of the systems, while regions of metasomatic replacement overlap only partially. At the same time, in a eutonic system the regions of direct crystallization and dissolution are characterized by the presence of a metasomatic component, and termination of metasomatic process is also possible due to supercooling (like in systems with isomorphous components – see Sect. 3.3).

1. The region circumscribed with  $aF$  and  $Fb$  half-lines is a domain of simultaneous growth of phases A and B. Supersaturation can be calculated for each phase as a difference between a corresponding coordinate, i.e., abscissa or ordinate, respectively, of the initial figurative point  $F$  and the eutonic point  $E_r$  determined at a specified temperature  $T$ . The sequence of substance precipitation in this region is rather complicated and involves metasomatic stages comprising a combination of growth of one of the substances and dissolution of the other. Such a combined case is depicted by  $z-x'$  trajectory, provided the compounds have been



**Fig. 4.4** The main domains and processes of crystal formation in a ternary system containing immiscible components A and B. Explanations are given in the text

previously deposited as indicated by  $x-z$  line (Treivus 1977). However, physical nature of metasomatic component in this process is not related to the isomorphous exchange of matter between the crystal and solution.

2.  $d'Fb'$  region is a domain of simultaneous dissolution of the phases A and B, where a metasomatic component may also occur, although the nature of the component differs from that of the system containing isomorphous components. This may happen, for instance, if the trajectory of varying solution composition (line  $F-F'$ ) reaches a certain isotherm and further proceeds along this isotherm  $F'-E_3$ , where dissolution of the crystals in phase B continues accompanied by a simultaneous growth of the phase A according to the mechanism of volume-deficit polycrystalline replacement.
3. Eutonic lines are functionally similar to the equilibrium trajectories  $Fe_i$  in the systems containing isomorphous substances (Fig. 3.7).
4.  $E_1Fb'$  region, which represents metasomatic replacement at elevating temperature, is similar to  $a_iFb'$  region in Fig. 3.9, the only difference being that such a replacement produces polycrystalline products. The replacement is volume-deficit, somewhat similar to the isothermal replacement corresponding to the isotherm  $FE_1$ , but the deficit is greater.
5.  $E_1FE_2$  region of metasomatic replacement at decreasing temperature is analogous to the region  $aFa_i$  depicted in Fig. 3.9, but differing in formation of polycrystalline replacement products. As it is in the systems with isomorphous components, the line of  $45^\circ$  divides this region into two parts (if the coordinates are expressed in volume units). Replacement reactions are volume-deficit within the region  $E_1FE$  (the deficit is lesser than it is for isothermal replacement corresponding to the adjacent isotherm  $FE_1$ ), and volume-excess within  $EFE_2$  region.
6. A particular case, similar to that discussed for systems containing isomorphous components, results in termination of metasomatic process, when the temperature lowers, if ordinates of the dots  $F$  and  $E_2$  coincide; supercooling, which is necessary for such termination, must ensure equal solubilities  $c_A$  of the substance undergoing replacement in the initial figurative point and in the eutonic point corresponding to the new value of temperature (Fig. 4.4). The system remains in metastable equilibrium, if supersaturation with B component corresponding to  $FE_2$  interval is less than the width of the metastable region.
7. For the systems under discussion,  $d'Fb$  region and the region above the eutonic line  $E_3E_4$  are forbidden, because the compositions falling within their boundaries are unattainable for any combination of salting-out processes and temperature variations at the initial figurative point  $F$ . There is no such prohibition for systems containing isomorphous components. The reason for such a difference is as follows: In a eutonic system, the only permissible movement of the composition figurative points is that along the isotherm and toward the eutonic line, which limits the admissible domain, while in the systems with continuous miscibility the movement is permissible in both directions without limits within the range of the isotherm.

The nature of isomorphous replacement processes may be interpreted as a particular case of replacement in systems containing phases of fixed compositions that may

form an infinite number of additional compounds. The diagram of a system with infinite miscibility of solid components may be represented as a set of infinitely narrow regions divided by extremely close eutonic lines. The process may be represented as a continuous series of successive elemental stages, similar to the discrete replacements with formation of a number of additional compounds mentioned before (see Sect. 3.2). Essentially, only a continuous change of the solid-phase composition (that is the reason for the reaction to be unconditionally considered as incongruent) makes this process different from the discrete one, shown in Fig. 4.1*b*. This approach may be fruitful in estimation of permissible divergence of composition trajectories of the solid and liquid phases in the course of direct crystallization, in discussion of polymodal distribution of spontaneously formed crystals in accordance with their isomorphic compositions, and for analysis of other crystallogenic features of systems containing isomorphic components. However, this approach requires a solid theoretical basis taking into account the phase rule.

#### 4.6 Some Methods of Estimation of Reaction Volume Effect

Physicochemical analysis is used to estimate phase relations in various systems, and in general it cannot provide reliable information about structure and shapes of the products formed in the course of certain processes. Nevertheless, discovering a correlation between the process mechanism and volume effect can help in revealing some structural-morphological properties of the products. An illustrative example is formation of monocrystalline pseudomorphs having a spongy structure or possessing autoepitaxial accretions that can be quite confidently predicted on the basis of solubility data.

Volume effects in reactions of non-isomorphic salts can be directly derived from their diagrams.

In the simplest diagram containing only two regions (Fig. 4.1*a*), the distances between the initial and final figurative points in the ordinate and abscissa axes are confined between the dash lines and correspond to the quantities of dissolved protocrystal substance and the newly generated phase. Obviously, such replacement results in excessive volume of the new formation if the angle between the isotherm (or a tangent to the curved isotherm in the point of interest) and the coordinate axis of the new formation does not exceed  $45^\circ$  ( $A'A_1$  trajectory), and in deficit of its volume, if the angle exceeds  $45^\circ$  ( $A_1E$ ).

This means that if the amount of substance undergoing replacement is great enough to induce a sufficient change in the solution composition, a considerable curvature of the isotherm may be the reason for an essential change of volume effect at different stages of the replacement process. Thus, if the isotherm is concave, as shown in Fig. 4.1*a*, the process results in formation of box-like pseudomorphs, which were observed in the course of KCl and KBr replacements in solution of  $K_2Cr_2O_7$ , as well as during replacement of  $CuSO_4 \cdot 5H_2O$  crystals in  $K_2SO_4$  solution (reactions 1*a*/11, 14, 22; see Table 1.1, Fig. 1.9). Formation of a

localized automorph with a hard central core and a loose periphery is most likely to occur if an isotherm has a convex trajectory (Fig. 4.1k). It is to be noted that the above phenomena can only occur in a relatively small quantity of solution, assuming, of course, that after accessing the eutonic point in a congruent system the replacement stops and excessive matter of the protocystal remains preserved in relics. If the amount of a solution is relatively great, the process is characterized by a short sector of the isotherm and the system state is close to a stationary one, with formation of an almost homogeneous structure of the replacement products.

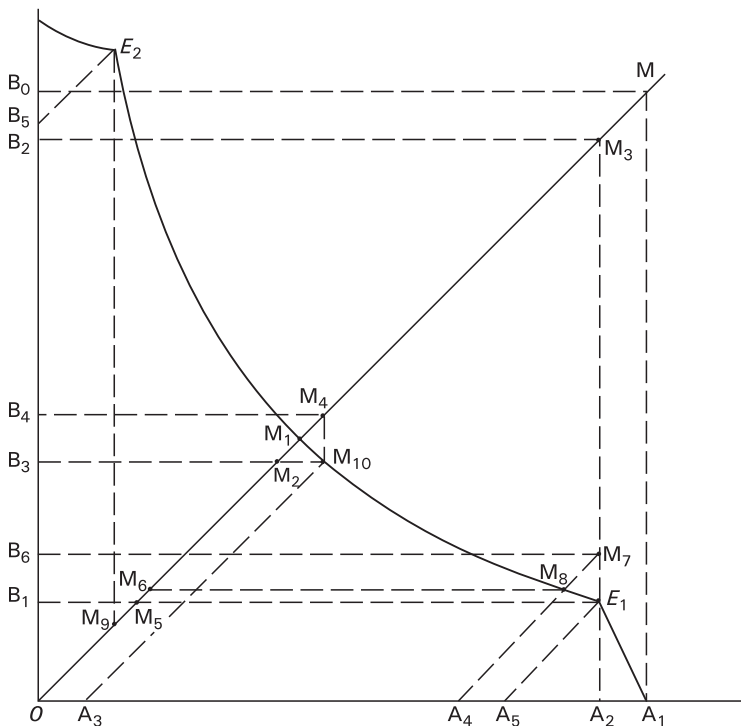
The process becomes more complicated in presence of additional compounds (Fig. 4.1c). The quantity  $A'$  of a dissolved substance makes it possible to generate a quantity  $M'$  of an additional phase, which requires a quantity  $B'$  of the dissolving substance. This mechanism is represented by auxiliary dash-dot lines in  $A'OB$  coordinates. At the same time,  $M'M_1$  part of the extra phase would crystallize, while the other part  $OM_1$  would remain in the solution. Further dissolution of  $B$  results in crystallization of the additional substance  $M$ , which proceeds until the dot  $E_2$  is attained; quantities of substances undergoing dissolving and salting-out ( $B_1$  and  $M_1M_2$ ) can be readily estimated using  $BOM$  coordinates (see corresponding auxiliary dash-dot lines). The total balance of the process is as follows: amount  $B' + B_1$  of the protocystal dissolves, and  $M'M_2$  quantity of a new formation crystallizes out. This formal conclusion is only a partial representation of the real process, which becomes quite complicated due to salting-out followed by dissolution of substance  $A$  according to the sector  $A'E_1$ , as it was mentioned before.

This process, including a number of uncertainties caused by kinetic effects, is shown in details in Fig. 4.5.

At the first stage (trajectory  $A_1E_1$ ), the quantity of dissolving protocystal  $B$  is characterized by the sector  $OB_1$ , while the amount of the new formation  $A$  is described by the sector  $A_1A_2$ .

At the second stage the process proceeds along  $E_1M_1$  trajectory and its estimation should be performed in  $A_1OM$  coordinates. At this stage the substance  $A$  dissolves completely accompanied by continuous dissolution of the substance  $B$  and initiating the salting-out of the substance  $M$ . The quantity of the substance  $M$  undergoing salting-out ranges from  $M_5M_6$  to  $M_1M_2$  and depends upon the ratio between the rate of replacement of the substance  $B$  and that of the substance  $A$ . These sections are plotted on the abscissa as sectors  $OA_3$  and  $A_4A_5$ , which are equal to section  $A_1A_2$ ; after that it is possible to draw the lines  $A_3M_{10}$  and  $A_4M_8$ , as well as the lines  $M_{10}M_2$  and  $M_8M_6$  ( $E_1A_5$ ,  $A_3M_{10}$ , and  $A_4M_8$  are parallel to  $OM$ , while  $M_{10}M_2$  and  $M_8M_6$  are parallel to the abscissa). To reach the position  $M_1$  it is necessary to dissolve the main quantity  $B_1B_2$  of the substance  $B$  (thus precipitating  $M_1M_3$  amount of  $M$ ) and an additional quantity, which is described by the interval  $B_1B_6 - B_3B_4$  (thus precipitating  $M_7M_8 - M_1M_4$  quantity of  $M$ ). Dissolution of the additional part of  $B$  compensates the movement of the system toward the dot  $E_1$  that is caused by the replacement of the substance  $A$ .

The additional part of the substance  $B$  and a quantity of the substance  $M$  corresponding to that part, and the additional ratios of  $B$ ,  $M$ , and  $A$  cannot be estimated precisely, as their reactions are prolonged, and so their volume effect changes in the



**Fig. 4.5** Scheme for graphic determination of the volume effect at a multistage replacement of crystals B in solution of the initial composition  $A_1$  in a system containing additional compound M (for a more schematic representation see Fig. 4.1c)

course of the process in accordance with the isotherm curvature. Reaching the extreme values of  $B_1B_6-M_7M_8$  is possible if an extremely fast secondary replacement takes place completely in the point  $E_1$ , and the values of  $B_3B_4-M_1M_4$  are feasible, and if an extremely slow replacement of A proceeds almost completely at the third stage.

The third stage of the process corresponds to the trajectory  $M_1E_2$  and all calculation should be performed in BOM coordinates. Here, amount of dissolving substance B can be calculated from the sector  $OB_5$ , while the quantity of precipitating substance M is described by  $M_1M_9$  section.

If an insoluble additional compound is present in the system (reactions of type III; e.g., system  $KAl(SO_4)_2 \cdot 12H_2O - BaSO_4 - BaCl_2 \cdot 2H_2O - H_2O$ ), the points  $M_1$ ,  $M_2$ ,  $E_1$ , and  $E_2$  coincide with zero point of the coordinates. The amount of the new formation precisely corresponds to the section  $OM$  and may be calculated from ordinary chemical equations describing exchange reactions.

It is desirable that solubilities plotted on the axes should be expressed as volume units indicating ratio of a substance volume to a fixed amount of a solvent (e.g., 1 cm<sup>3</sup> of a substance per 100 g of H<sub>2</sub>O or any other solvent having a fixed composition).

In a double-salts system (Fig. 4.1*a*) the axes scales are mutually independent and can be arbitrary chosen in accordance with the formula composition of the substances involved, which, if present, should also include water of crystallization. If the system contains any additional compounds (Figs. 4.1*b, c*), using this direct method is impossible. Quantitative indices of all the three axes may be consistent only when the measurement units of the main axes are expressed in equal molar or weight units of components, a sum of which makes the formula of the additional compound. For example, in analyzing replacement of  $\text{KAl}(\text{SO}_4)_2 \cdot 12\text{H}_2\text{O}$  alum with  $\text{BaSO}_4$  in solution of  $\text{BaCl}_2 \cdot 2\text{H}_2\text{O}$ , the main axes should indicate contents of  $\text{Ba}^{2+}$  and  $\text{SO}_4^{2-}$  ions determined in equilibrium solutions, while the intermediate axis should indicate content of  $\text{BaSO}_4$ . To use the diagram it is convenient to convert the chosen solubility units of each axis into volume contents of substances in their formula representations. The scales thus obtained would be different, but compatible with each other.

Naturally, graphic representation of multi-type systems must be different, and exemplary examination of some incongruent systems – systems with several additional compounds – or quaternary and more complex systems proves this in full measure. Isomorphic replacement cannot be exactly examined in volume unit coordinates, as the densities of the solid phases vary. Quantitative graphical analysis of such replacement processes requires plotting special nomograms.

This section was not written to present any analytical algorithms. The examples cited are to demonstrate a practicality of an important physicochemical approach to replacement processes. It is to be noted that volume effect of replacement (under the non-isothermal conditions too) entirely depends upon the equilibrium parameters of a system. The proposed approach of physicochemical analysis combined with crystallogenic interpretation of structural-morphological and kinetic phenomena is supposed to reveal the essence of metasomatic reactions and at present has no valid alternatives. Of course, known variety of natural physicochemical systems does not comprise all the possible cases, so only indirect features are available for analysis of the process mechanisms, its driving forces and characteristic features. However, the proposed approach provides a solid basis for mineral-genetic examinations. At the same time, it is necessary to emphasize a difference between volume effect of crystal replacement, which depends upon equilibrium characteristics of a system, and a metasomatic change of the entire bulk of a mountain rock, which is substantially defined by its mechanical characteristics and the process kinetics.

## References

- Anosov VYa, Ozerova MI, Fialkov YuA (1976) Fundamentals of physicochemical analysis. Nauka, Moscow (Russ.)
- Franke VD, Glikin AE, Kryuchkova LYu et al. (2007) Cocrystallization of isomorphic components in solutions and crystal zoning: an example of the  $(\text{Ba,Pb})(\text{NO}_3)_2$  series. Geol Ore Deposits: 49:7:641–647

- Glikin AE (1991) Mechanisms of inheriting and losing the structural attributes of rocks in the course of metasomatism and recrystallization. In: Gelman ML (ed) *Metamorphic complexes of the North-East of USSR, their ore content and geological mapping*. Russian Academy of Science, Magadan (Russ.)
- Glikin AE (1995a) On the theory of formation of isomorphic-mixed crystals. *Zapiski Vsesoyuz Miner Obsh* 5:125–134 (Russ.)
- Glikin AE (1995b) Crystallogenesis and geological-mineralogical sciences – coordination problems (by example of metasomatism phenomena). *Zapiski Vsesoyuz Miner Obsh* 4:116–125 (Russ.)
- Glikin AE (1996a) The physicochemical aspect of the unsteady state of metasomatic crystal production. *Geochem Intern* 33:8:117–128 (Russ.)
- Glikin AE (1996b) About equilibrium supercooled solutions related to formation of isomorphic-mixed crystals. *Zapiski Vsesoyuz Miner Obsh* 5:103–111 (Russ.)
- Glikin AE (1996c) Modeling of metasomatic crystallogenesis in aqueous-salt systems. Dr Sci thesis. St. Petersburg State University, St. Petersburg (Russ.)
- Glikin AE (2002) Features of rapakivi origin in terms of polymineral-metasomatic crystallogenesis. *Miner Soc Poland. Special Papers* 20:17–19
- Glikin AE, Petrov SV (1998) Recrystallization of bimineral aggregates. *Zapiski Vseross Miner Obsh* 4:79–88 (Russ.)
- Glikin AE, Sinai MYu (1991) Morphological and genetic classification of crystal replacement products. *Zapiski Vsesoyuz Miner Obsh* 1:3–17 (Russ.)
- Glikin AE, Sinai MYu (2004) Metasomatic formation of poikilitic crystals: experimental modeling. *Doklady Earth Sci* 396: 4: 563–566
- Glikin AE, Kovalev SI, Rudneva EB, et al. (2003) Phenomena and mechanisms of mixed crystal formation in solutions I. General concept on the example of the system  $\text{KHC}_8\text{H}_4\text{O}_4\text{-RbHC}_8\text{H}_4\text{O}_4\text{-H}_2\text{O}$ . *J. Cryst Growth* 255:150–162
- Glikin AE, Kryuchkova LYu, Plotkina YuV (2007) Crystallogenic grounds of isomorphism: experimental data and theoretical approach. *Zapiski Russ Miner Soc, Crystallogenesis and Mineralogy, Special Issue* 7–35. Nauka, St. Petersburg
- Kasatkin IA, Leont'eva OA (1992) Phase equilibria in aqueous salt systems containing isomorphic components. *Inorganic materials* 28:6:1169–1172 (Russ.)
- Kasatkin IA, Glikin AE, Bradaczek H, et al. (1995) Kinetics of mixed crystal  $\text{K}_2(\text{SO}_4\text{,CrO}_4)$  growth from aqueous solutions. *Cryst Res Techn* 30:5:659–666
- Kirgintsev AN (1976) Sketches on thermodynamics of aqueous salt systems. Nauka, Novosibirsk (Russ.)
- Korzhinskii DS (1970) *Theory of metasomatic zoning*. Clarendon Press, Oxford
- Kryuchkova LYu, Glikin AE, Voloshin AE, et al. (2002) Kinetic and morphological phenomena of growth and isomorphic replacement of mixed crystals in solutions (in the series  $(\text{Co,Ni})(\text{NH}_4)_2(\text{SO}_4)_2\cdot 6\text{H}_2\text{O}$ ). *Zapiski Vsesoyuz Miner Obsh* 3:62–77 (Russ.)
- Kulkov and Glikin (2007) Replacement of nickelhexahydrate with retgersite: polymorphic–metasomatic structures. *Geol Ore Deposits* 49:8:159–164
- Punin YuO (1964) Recrystallization in aqueous solutions accompanied by grain coarsening. *Zapiski Vsesoyuz Miner Obsh* 3:364–367 (Russ.)
- Punin YuO (1965) On mechanism of recrystallization. *Zapiski Vsesoyuz Miner Obsh* 4:459–462 (Russ.)
- Putnis A (2002) Mineral replacement reactions: from macroscopic observations to microscopic mechanisms. *Miner Mag* 66:5:689–708
- Shubnikov AV (1918) Influence of temperature fluctuations upon crystals. *J Russ Physicochem Soc. Phys Branch* 50:39–44 (Russ.) (see also in: *Zs Krist* 1941 54:3–4:417–433)
- Sinai MYu, Glikin AE (1989) Formation of case-like and negative pseudomorphs. *Geol Explor* 4:31–35 (Russ.)
- Treivus EB (1977) Elaboration of the state diagrams of multi-component systems. In: *Mass crystallization*. IREA, Moscow (Russ.)



- Treivus EB (1982) A method of depicting the compositions of isomorphic crystals and three-component solutions equilibrial to them. In: Frank-Kamenetskii VA (ed) Crystallography and Crystallochemistry. Leningrad State University, Leningrad (Russ.)
- Treivus EB (2000) About isothermal diagrams of ternary systems containing binary solid solution. Vestnik St. Petersburg State University 7 Ser 2:15:14–22 (Russ.)
- Treivus EB, Rozhnova GA (1962) Experimental reproduction of metasomatism in water-soluble salts. Zapiski Vsesoyuz Miner Obsh 2:219–222 (Russ.)
- Wyckoff R (1965) Crystal structures 1. Wiley, New York/London/Sidney
- Wyckoff R (1966) Crystal structures 3. Wiley, New York/London/Sidney

## Chapter 5

# Metasomatic Transformation of Aggregates

### 5.1 On Replacement and Growth of Monocrystals in the Course of Transformation of Aggregates

The processes of metasomatic transformation of aggregates can be conveniently represented as a series of isolated replacements of single individuals. It is obvious that replacement of individuals in aggregates conforms to the rules discussed above for single protocrytals (see Chapter 1). Experiments conducted by Dr. M. Yu. Sinai showed that a compact crystal aggregate behaves in a course of replacement as an entity transforming either into a single pseudomorph, or a single automorph. It can be accounted for by formation of a common diffusion field around the aggregate undergoing dissolution, which induces precipitation of a new formation in the periphery of the aggregate (pseudomorphic replacement) or at some distance from the initial aggregation (automorphic replacement). Moreover, if the distance between the individuals undergoing replacement is sufficient, the morphological patterns are expected to be complicated as a result of overlapping the areas occupied by the new formations produced around various individuals. Variation of temperature causes direct processes of growth and dissolution to occur, which would take place mainly on the border of a compact aggregate, subsequently penetrating its inner part as the structure of the aggregate undergoes loosening. At the same time, loosening the aggregates should induce an abrupt acceleration of restructuring the solution.

Thus, metasomatic transformation of aggregates covers all four overelementary classes of metasomatic crystallogensis (see Introduction). During pseudomorphic replacement of aggregates or individuals composing the aggregates, the basic features of the initial structure (the first and second classes) should generally remain, while during automorphic replacement of individuals the overlapping areas of the products would to some extent conceal the protostructure (mainly, the third and fourth classes). At the same time, structural-morphological diversity of the product characteristics can be practically unlimited, being determined by the number and quantitative ratio of solid reactants, their granulometric composition, spatial distribution, as well as their physicochemical properties and kinetic characteristics of growth and dissolution. Therefore, in contrast to replacement of monocrystals,

these processes should mostly belong to the reactions of the third and fourth classes, as their products do not maintain any spatial and spatiotemporal relations to the initial individuals.

Investigations of aggregate metasomatic replacement have been mainly focused on the general phenomena and mechanisms of replacement of rock massifs (Irving 1911; Lindgren 1925; Pospelov 1976; Zavaritskii 1950; Korzhinskii 1955, 1970; Demin et al. 1979; Zaraiskii 1979, 1991; Zaraiskii et al. 1981, 1986; Petrov 1983; Yardley 1989; Barton et al. 1991; Aleksandrov 1995; and others). These investigations made the grounds for a diffusion–infiltration theory of metasomatic process and allowed to formulate valid approaches to such well-known problems as analysis of changes in total chemical composition of the rocks, construction of metasomatic columns, and discovering succession of stages in metasomatic processes.

In this connection, a great attention is focused on the volume effect of metasomatic process. In contrast to unambiguous volume relations between the educt and product observed during replacement of monocrystals (see Sects. 1.5.2 and 4.6), effect of the replacement process upon the total volume of a rock formation cannot be determined since it is mediated by the forms of mineral replacement, initial rock porosity, and the rock expansive or compressive properties. Volume-deficit in a rock massif can be compensated by increase in the rock friability and contraction, which also can be accompanied by the removal of a new formation from the reaction area. Also, the extreme case of volume compensation, which is formation of spongy mixed crystals, would affect neither intercrystal space nor the total amount of rock or any of its blocks. On the contrary, variations of the volume characteristics of rocks are probably difficult to be evaluated when friability of the rocks increases in various ways accompanied by contraction and removal of the secondary material. The volume excess can be expressed as an increased volume of the mixed crystals, filling up the pores and cracks with secondary crystals, removing the new formation outside the reaction space, and as expanded dimensions of the massif undergoing replacement.<sup>1</sup> Moreover, these processes are very likely to occur in combination and their results appear to be rather uncertain; for example, removal of a new formation outside the reaction volume can lead to the total volume-deficit, despite the fact that the reaction balance is volume-excessive.

So, it is important to distinguish analysis of the volume transformations of individual crystals from examination of rocks undergoing metasomatic transformations. It is to be noted that all the above-mentioned factors determining the volume effect are well-known, and any concept implying the volume constancy cannot be accepted as justifiable.

---

<sup>1</sup>The most demonstrative example of the massif extension is a volume-excess replacement of anhydrite with gypsum accompanied by development of local tectonic phenomena (Betekhtin 1961). It is to be noted that reactions of anhydrite transformation into gypsum and those of dehydration of anhydrite (Prodan 1990) are typical reactions of metasomatic replacement and they always involve salting-out.

Another trend includes studying the metasomatic formation of individuals and local peculiarities of structures of rocks and vein-shaped bodies (e.g., Ramdohr, 1955; Betekhtin et al. 1958; Atlas... 1976; MacKensie and Guilford 1980; Adams et al. 1984; Yardley et al. 1990; Barker 1994; Craig and Vangham 1994). This concept comprises two popular replacement models, namely a solid-phase model (Lindgren 1925; Grigor'ev 1961) and a three-zone model (Beus 1961; Pospelov 1973). Numerous investigations encompass uncountable metacrystals, pseudomorphs, rims, and other specific aggregates, which in some cases allow to reveal (including reported descriptions, regardless of the questions considered by authors) some attributes of inheriting the primary aggregate structure by pseudomorphs (Lyakhovich 1954), by formations, which here are referred to as localized automorphs (Tatarskii 1939; Velikoslavinskii 1953; Sudovikov 1967; Adams et al. 1984), by shadowed pseudomorphs (Chesnokov 1974), and some other formations.

Compositions and spatial distributions of minerals in numerous experimental samples belonging to various metasomatic columns have been thoroughly investigated; the results obtained have been generalized in the well-known concept of column zonality (Zharikov and Zارايسkii 1973; Zارايسkii 1991; and others). The descriptions contain data on some features of aggregate structure and in some cases on metacrystal morphology (Schouten 1934; Garrels and Dreyer 1952; Ol'shanskii and Brusilovskii 1958; Pospelov et al. 1961; Treivus and Rozhnova 1962; Zارايسkii 1979; Zارايسkii et al. 1981; Krasnova et al. 1983; Zارايسkii et al. 1986; Zارايسkii 1991; Krasnova and Petrov 1997; and others). Only a few reported works include crystallogenic analysis of behavior of individuals (Krasnova et al. 1983; Krasnova and Petrov 1997).

The forms of metasomatic crystal growth were studied in precipitation experiments using the method of reactant counter diffusion (Henisch 1970; Wilke 1973; Petrov et al. 1983; Askhabov 1984; Givargizov et al. 1984; and others), which is one of the experimental analogs of a contact-reaction process. The minerals prepared belong to all mineral classes, the examples including gold (Kratochvil et al. 1968), cinnabar (Murphy et al. 1968), nantokite, miersite, and fluorite (Armington and O'Connor 1968; Murphy et al. 1968; Kiryanova et al. 1984; Kiryanova and Glikin 1999), magnetite and structural analogs of garnet ( $Y_3Fe_2[FeO_4]_3$  – Y-Fe-garnet) and perovskite ( $YFeO_3$  – Y-Fe-perovskite or orthoferrite) (Mikhailov et al. 1973), celestine (Ulyanova and Petrov 1971), calcite (Kiryanova et al. 1998; Kiryanova and Glikin 1999, and some others).

Y-Fe-garnet, Y-Fe-perovskite, fluorite, and calcite were synthesized for researches of crystal morphogenesis (Mikhailov et al. 1973; Kiryanova et al. 1984). These substances are interesting examples of metasomatic replacements in aggregates having different primary structures. The experiments differed in having various manners of arranging the reactant powders in solutions. The first experimental series involved divided weights of pure initial reactants (in fluorite preparations the distance between the reactant portions was about 20 cm, in calcite preparations it was about 5 cm, and in Y-Fe-garnet and Y-Fe-perovskite preparations it was about 1–2 cm). Another variant comprised contacting portions of pure reactants (Y-Fe-garnet

and Y-Fe-perovskite syntheses). The third series included mixtures of reactants (Y-Fe-garnet and Y-Fe-perovskite synthesis), and the fourth variant consisted in reactions of calcite crystals with fluorine-containing solutions. Crystallizations of fluorite and calcite were conducted via diffusion in water of a number of soluble salts containing calcium and fluorine (fluorite) or calcium and carbonate ion (calcite) at room temperature and under low-temperature hydrothermal conditions in solution having various pH values. Joint synthesis of Y-Fe-garnet and Y-Fe-perovskite was carried out via a reaction of iron and yttrium oxides in hydrothermal solutions of KOH. In this experimental series, diffusive influx of hydrogen into the solution caused reduction of initial hematite that resulted in crystallization of magnetite in association with the above minerals. It is to be reminded that hydrogen metasomatism is classified as an independent type of metasomatic process (Rus'ko 1976; Lazarenko 1979).

It was possible to observe various distributions of new formations of Y-Fe-garnet and Y-Fe-perovskite in container corresponding to the theory of precipitating the new formations due to counter diffusion of components (Petrov et al. 1983). When the reactants were divided, Y-Fe-garnet and Y-Fe-perovskite crystals were formed at the border between a free volume of the solution and iron oxide, which had a significantly lower solubility than yttrium oxide. Fluorite was also formed on the surface of the less-soluble reactant or in relative proximity to it in a free solution volume. When the reactants were in contact, precipitation of the new formation (Y-Fe-garnet and Y-Fe-perovskite) was asymmetric in respect to the contact interface, proceeding in the way analogous to that observed in model bimetasomatic columns (Zaraiskii et al. 1986). In the case considered, it is possible to conclude that precipitation of the new formations occurs within the mass of the less-soluble iron oxide at different distances from the surface of contact. In the mixtures of the initial reactant the new formations precipitated chaotically within the whole bulk. Degree of hematite replacement with magnetite (proceeding under the action of hydrogen in accordance with usual scheme of regenerative process) decreased along the column in downward direction, as the distance from the top of container where hydrogen penetrated the system via holes in the cover. Thus, the area of precipitation of the new formation was characterized by "common" replacement front, which resulted from superposition of diffusive fields induced by different individuals composing the aggregate. In this case, the aggregate behaved as a whole entity and spatial coordination between the products and the individuals undergoing replacement became lost completely, i.e., the system was found to display all the attributes of the third overelementary class of metasomatic crystallogenesis (see Introduction).

Synthesized crystals of Y-Fe-garnet, Y-Fe-perovskite, and magnetite looked like a uniform fragile aggregate or could be distributed in a polycrystalline mass of unreacted but partially recrystallized initial substances, mainly, in the mass of iron oxides. Metacrystals could reach 1 mm in size. This result is an illustration for a model of metasomatic formation of crystals in a solid medium proceeding in accordance with the three-zone mechanism (Beus 1961; Pospelov 1973).

As a rule, crystals of metasomatic new formations have full-faceted, sometimes skeletal, form with usual relief elements (growth layers, vicinal hillocks), typical

for the process of free growth from the solution; the same features have been also detected in natural crystals (Novgorodova 1968). It should be emphasized that morphological peculiarities of metasomatically formed fluorite and fluorite obtained in direct growth experiments appear to be the same. It is a direct evidence of common morphogenesis mechanisms of both types of crystallizations.

Faceting of crystals prepared by means of counter-diffusion method (analog of bimetasomatic process) can include a small set of crystal forms (e.g., only {111} for magnetite). Nevertheless, occurrence of some forms, atypical for synthesized crystals, is also observed rather frequently, for instance: fluorite can develop the {111}, {100}, {110}, and {112} faces instead of usual {111} and {100} combination; calcite occurs in the {0001}, {10 $\bar{1}$ 1}, {01 $\bar{1}$ 2}, and {08 $\bar{8}$ 1} faces instead of the {0001} and {101 $\bar{1}$ } ones, Y-Fe-garnet forms {112}, {110}, {123}, {130}, and {100} faces instead of {110} and {112}. The number of crystal forms for the orthorhombic orthoferrite reaches 16. The faceting variety can be explained by nonstationarity of preparative conditions (Glikin and Glazov 1979; Grunskii 1988; Kasatkin et al. 1995) reflecting a specificity of metasomatic crystallogeneses, which has been stated to be determined by nonstationary nature of metasomatic reactions (Dolivo-Dobrovolskii 1967; Glikin 1996a; and others). Of course, this assumption requires thorough investigation since the variations of the forms can be induced by usual influence of medium composition, supersaturation, and temperature.

Metasomatic phenomena can accompany direct growth of polymineral aggregates; it has been discussed in Chapter 2. One of the extreme cases of such a process is probably formation of a metastable phase followed by its dissolution caused by change in the solution composition induced by growth of the other phase (these processes can be classified as belonging to any one of the two to four overelementary classes). The metastable phase can be partially dissolved (see Sect. 4.5 and comments to Fig. 4.4) or disappear completely, as it happens, for example, during evaporation of an aqueous KNO<sub>3</sub> solution, where a hexagonal modification of KNO<sub>3</sub>, having precipitated originally, dissolves, being automorphically replaced with an orthorhombic modification (these phenomena can be classified as belonging to the third overelementary class). A phase can be dissolved partially or completely, and then get crystallized again. For example, according to our data,<sup>2</sup> at the first stage of the experiments involving Na<sub>2</sub>S<sub>2</sub>O<sub>3</sub>-NaNO<sub>3</sub>-H<sub>2</sub>O system, evaporation followed by cooling resulted in formation of an aggregate composed of three to four alternating polycrystalline zones consisting of Na<sub>2</sub>S<sub>2</sub>O<sub>3</sub> and NaNO<sub>3</sub>. During the second stage of the experiment, zones of one of the substances dissolved completely accompanied by continuous growth of the second phase. During the third stage, both substances precipitated again in a whole bulk of the residual solution (the fourth-class phenomena).

Growing of crystals via dissolution of polycrystalline substance having another composition accompanied by a convective transport of the matter to the growth

---

<sup>2</sup>Ms M. V. Togatova performed the experimental investigations.

zone gives rise to the products, all of which are represented by translated monocrystalline and polycrystalline automorphs (see Sect. 1.2) randomly divided from the starting material. The examples include the hydrothermal processes of growing the crystals of Y-Fe-garnet and Y-Fe-perovskite (Mill and Klevtsov 1966; Mikhailov et al. 1973), anhydrous iron fluoride (Glikin et al. 1974), wolframite (Panov 1979), polycrystalline aggregates of ornamental malachite and rosasite (Petrov et al. 1977a, b), lithium iodate and other water-soluble compounds (Kidyarov and Mitnitskii 1977; Petrov et al. 1983) and so forth. It is highly probable that some part of metasomatic veins is of the same nature.

The most complicated metasomatic transformation appears to be a polymineral recrystallization (see Sect. 5.3), which is a series of matter redistribution processes occurring under the action of oscillations and/or gradients of temperature, pressure, and other intensive parameters. This type of recrystallization can manifest itself in macroscopic and local phenomena of stratification–homogenization of aggregates and extension–reduction of grains appearing as a result of the aggregate heterogeneity and accompanied by a strong influence of salting-in and salting-out processes. The elementary processes of growth and dissolution during the recrystallization are characterized by lack of spatiotemporal correlations; this allows to classify the recrystallizations of this type as phenomena belonging to the fourth overelementary class of metasomatic crystallogenesis (see Introduction).

So, both external effects and mechanisms of metasomatic processes occurring in aggregates can be extensively variable. The metasomatic processes can belong to different classes of metasomatic crystallogenesis depending upon their various spatiotemporal correlations of elementary processes of growth and dissolution. However, fragmentary experimental data present a poor basis for a unified systematic concept. We shall not go beyond a hypothesis of formation of rapakivi-type structures in the course of metasomatic transformation of isomorphic–mixed crystal aggregates and models of recrystallization of polymineral aggregates.

## 5.2 A Model of Formation of Rapakivi-Type Structures

Formation of rapakivi-type structures can be a result of replacement of a massif of mixed crystals in a multicomponent solution. The model is suggested (Glikin 1990, 1991, 1995a, 2002) on the basis of comparison made between the main structural features of various rapakivi granites (observed mainly in the facing materials and partially in the so-called Gubanovskaya intrusion of the Vyborg massif and described in the published literature) and morphological characteristics of synthetic products of monocrystal replacement described in Chapters 1 and 3.

Rapakivi structures have been continuously studied for at least a century-and-a-half, and still their origin remains a traditional subject for discussions (Delesse 1848; Chrustschoff 1894; Sederholm 1928; Levinson-Lessing and Vorob'eva 1929; Escola 1938; Velikoslavinskii 1953; Sudovikov 1967; Sviridenko 1968; Levkovskii 1975; Velikoslavinskii et al. 1978; Shinkarev and Rundkvist 1986; Koval and

Valasis 1989; Meyer 1989; Dempster et al. 1991; Collins 1994; Price et al. 1996; and many others). The greatest attention is focused on rapakivi granites; however, similar structures also occur among the other rocks, e.g., tonalites, diorites, gabbros, norites, and peridotites (Delesse 1848; Nockolds 1931; Carstens 1957; Viluksela 1965; Leveson 1966; Van Diver and Maggetti 1975; Dahl and Palmer 1983; and others). Investigations have generally dealt with morphological and chemical peculiarities of phenocrysts and well-marked textural features. The most popular is magmatic genesis of rapakivi granites and similar rocks (see, e.g., review by Rämö and Haapala 1995). However, the data obtained, which also include experimental researches conducted under higher parameters (Seck 1971; Fenn 1977; Donaldson 1979; Lofgren 1980; Tingle 1981; Lofgren 1983; Grove et al. 1984; Wark and Stimac 1992; and others), show that not all the rapakivi characteristic features can be accounted for by magmatic origin, and at least a part of them can be attributed to action of metasomatic processes (Velikoslavinskii 1953; Sudovikov 1967; Levkovskii 1975; Glikin 1990, 1991, 1995a, 2002).

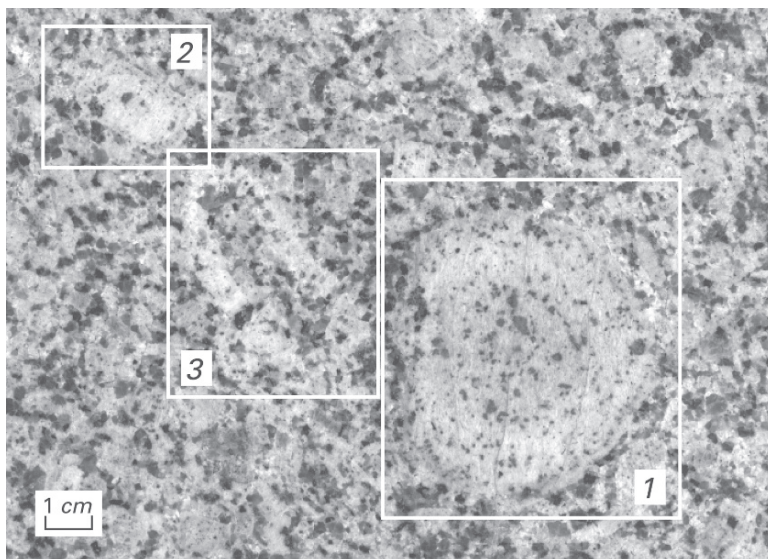
The tasks set forth in the present monograph do not include opening a discussion of rapakivi granite genesis from the points of view of conventional comparison of magmatic and metasomatic interpretations; here the problem is considered from positions involving metasomatism.

Experimental data (Glikin and Sinai 1983, 1988, 1991, 2004; Kryuchkova et al. 2002; Glikin et al. 2003) show phenomena of metasomatic replacements of monocrystals, which are similar to the basic morphologic features of rapakivi. Hence, we consider rapakivi granites as products of metasomatic transformation of magmatogene feldspar rocks. The primary rocks are supposed to have had a heterogeneous giant-grained structure, which comprised crystals reaching 10–20 cm in sizes. Taking into account a petrogenic type of rapakivi granites (Velikoslavinskii et al. 1978; Koval and Valasis 1989; and others), the primary rocks are likely to be anorthosites. The entire or almost entire rapakivi mass can be considered as a totality of innumerable interpenetrated and separated polymineral (mainly quartz-feldspar) pseudomorphs and automorphs after feldspar crystals. Distinctions in the forms of replacement products result from a significant dispersion of isomorphic component ratios in the initial crystals and the influence of compounds belonging to the same isomorphic line and non-isomorphic compounds present in the forming solution. Similar structures can also appear as a result of metasomatic transformations of amphibolites, pyroxenites, and other monomineral rocks characterized by variable contents of isomorphic components in individuals.

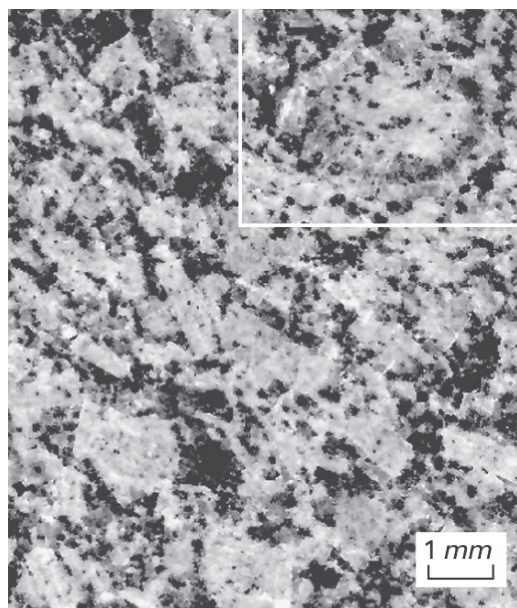
Further, attention will be paid to some structural peculiarities of the granites, which can have a great importance for our conclusions.

The most important and enigmatic rapakivi elements are considered to be feldspar phenocrysts, which are most explicitly described in published literature. It is to be reminded that phenocrysts can have spheroid, faceted, and partially faceted form (Figs. 5.1–5.3). As a rule, they are separated from each other by the medium-grained and coarse-grained quartz-feldspar mass, where spheroid and faceted phenocrysts can be co-located, or, in some rare cases, interlock with each other.

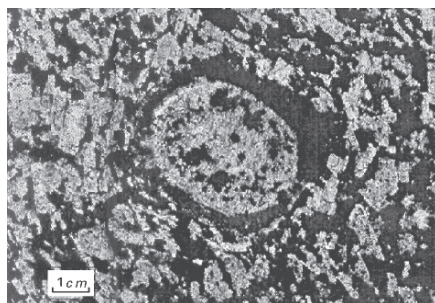




**Fig. 5.1** A typical fragment of a rapakivi structure. A sample from collection of Petrography Department of St. Petersburg State University: (1) spherical phenocryst containing concentric solid inclusions and an intermittent external zone; (2) combined phenocryst including a spherical superficial zone containing solid inclusions; (3) a polymineral faceted-blurred case-shaped pseudomorph



**Fig. 5.2** A mass of rapakivi granite. Adjoining faceted and spherical feldspar phenocrysts: *Framed* is a spherical phenocryst surrounded by a circular polycrystalline rim



**Fig. 5.3** A fragment of a rapakivi structure containing a spherical phenocryst surrounded by a faceted polycrystalline rim (Photo by Prof. V. A. Popov)

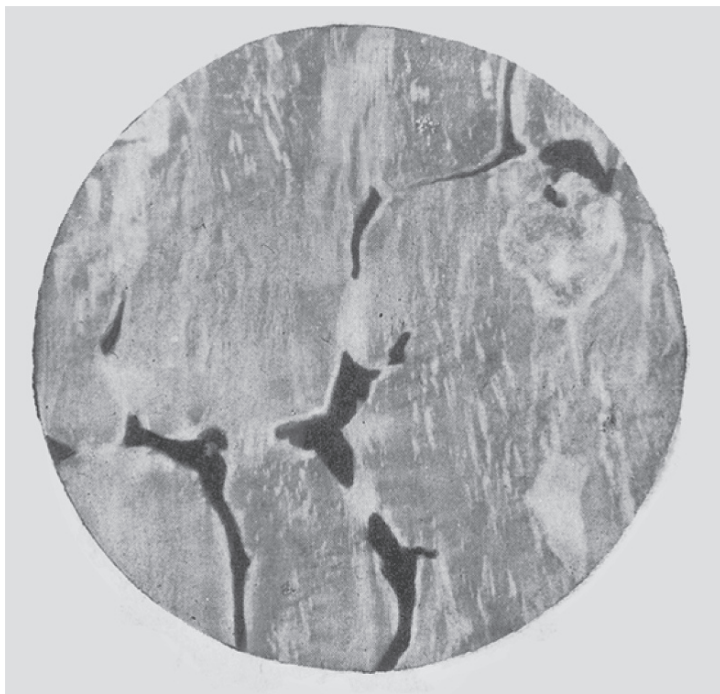
Spheroid phenocrysts have rough surfaces and are usually zoned (Fig. 5.1) as a result of heterogeneous distribution of mineral inclusions and isomorphic components in individuals. In general, spheroid phenocrysts are characterized by concentric location of the zones, a uniform zone thickness, localization of inclusions in the core parts of the crystals, and absence of internal growth pyramids (sectors). If a phenocryst is sufficiently saturated with inclusions, its central part acquires a polycrystalline structure. The external zones can be intermittent. Quartz inclusions often have bizarre vermiform shapes (Fig. 5.4).

Faceted phenocrysts show a typical zonal–sectorial texture determined, as a rule, by compositional changes. At the same time, the central zone frequently does not coincide with the crystal geometrical center, and thicknesses of various zones can vary along their contours.

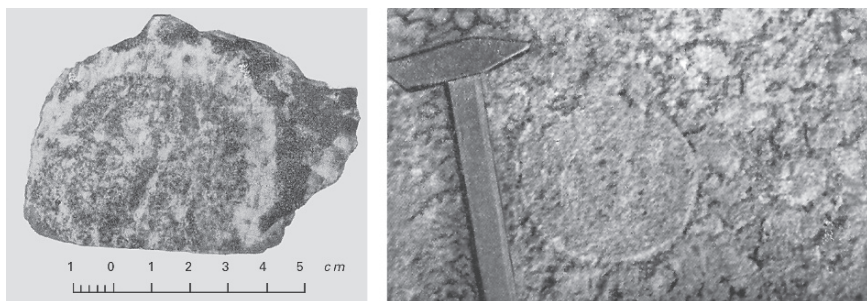
According to our classification, combined phenocrysts include partially faceted phenocrysts, faceted phenocrysts containing spheroid zones in their central parts, and spheroid phenocrysts comprising polygonal zones.

Structural heterogeneities of the main granite mass comprise “granite ovoids” (Velikoslavinskii 1953) or “orbiculars” (Sudovikov 1967), which are spheroid ensembles of feldspar crystals having diameters up to 10–15 cm; sometimes they have cyclic-concentric forms (Figs. 5.5 and 5.6). As a rule, feldspar crystals forming the orbiculars are isolated composing “chain-like orbiculars” (Fig. 5.6). Additionally, solid feldspar shells with thickness up to 1–2 cm and containing the granite mass inside and also surrounded with it can also occur (“shell orbiculars,” Fig. 5.5). Such shells (solid and chain-like) can encompass spheroid phenocrysts (Figs. 5.2 and 5.3). The shells surrounding the phenocrysts can be polygonal (Fig. 5.3). There are also observed locked polygonal crystal chains, which can be reliably defined as faceted-blurred case-like pseudomorphs (Figs. 5.1 and 5.3).

Structural-morphological characteristics of spheroid phenocrysts apparently form a continuous series. In general, the mentioned heterogeneities of the rapakivi structure



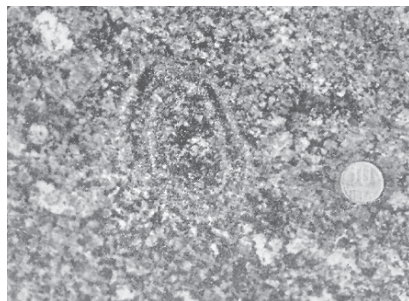
**Fig. 5.4** A feldspar crystal comprising monocrystalline quartz inclusions having bizarre shapes (According to data provided by Velikoslavinskii, 1953)



**Fig. 5.5** "Shell orbiculars" (According to data provided by Velikoslavinskii, 1953)


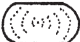






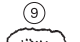


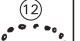
and found correlations can be presented in the form of a diagram (Table 5.1) constructed on the basis of the replacement product classification (see Table 1.2).

Metasomatic development after anorthosite of rapakivi is in a good agreement with some indications of metasomatic contacts between these rocks (Koval and



**Fig. 5.6** “Chain orbiculars” (According to data provided by Sudovikov, 1967)

**Table 5.1** Systematization of the main heterogeneities of the rapakivi structure with references to the classification of replacement products of monocrystals (Table 1.3–1)

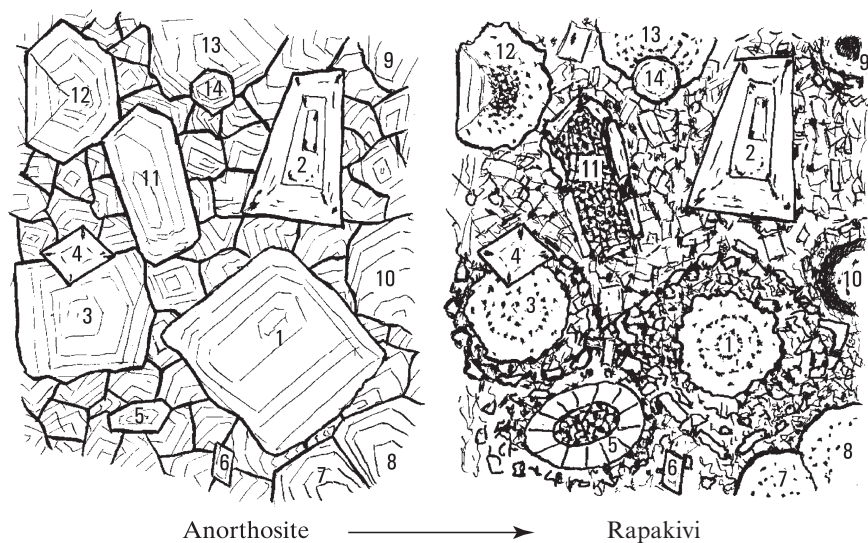
Shape		Structure		
products of replacement (Table 1.2)	inhomogeneities of rapakivi	monocrystalline		polycrystalline
		without inclusions	with inclusions	
Pseudomorphs		①		
faceted	faceted			
blurred	combined		  	 
Automorphs localized	spheroidal		   	 

**Note:** Figures in the circles are index figures. Division of monocrystalline formations into those containing inclusions and those, which do not contain any inclusions, is an example of introduction of additional taxons discussed in Sect. 1.5.

Valasis 1989); however, the authors consider that anorthosites are developed after rapakivi and not the other way around.

Close location of faceted (growing) and spheroid (dissolving) crystals is an evidence of metasomatic replacement, as this process consists in growth of crystals due to dissolution of the other (see Chapters 1 and 4). Dissimilarities in behavior of adjoining feldspar crystals can be accounted for by differences in their isomorphous compositions. Additional evidence is separation of phenocrysts: this phenomenon supports the above assumption about their being relics in a bulk of metasomatite mass. In some rare cases of formation of intergrown (or, probably, twinned) phenocrysts, resorption attributes on the intergrowth borders are observed.

A scheme of formation of a rapakivi structure, which unites the elements described above, is represented in Fig. 5.7.



**Fig. 5.7** A suggested scheme of formation of a rapakivi structure after anorthosite substrate (the relative locations in the initial and secondary structures are numbered equally)

As mentioned above, structural heterogeneities of rapakivi fall into classification of products of monocrystal replacement occupying several positions of this classification (compare Tables 1.2 and 5.1). In Table 5.1 all the phenocrysts are classified as monocrystalline replacement products, while the shell-like and orbicular forms, including polygonal ones, are considered to be polycrystalline products. With all this, according to the definitions given in Sect. 1.2, the faceted phenocrysts are considered as faceted pseudomorphs, the spheroid phenocrysts are defined as localized automorphs, and combined phenocrysts together with polygonal orbiculars are determined as blurred pseudomorphs.

Among these formations, only the shell-like and chain-like orbiculars (indices 11 and 12 in Table 5.1) can be reliably interpreted as the products of metasomatic replacement. Their well-known analogs are the Lisegang rings, which positively have a metasomatic origin; a double concentric orbicular shown in Fig. 5.6 supports the analogy. Among the replacement products obtained by us, the circular (in cross section) and bag-shaped localized automorphs (reactions *Ia/6*, *III/3*, *45*, *47*, *48* in Table 1.1; Figs. 1.10 and 1.11) can serve as analogs. The mechanism of their formation has been already discussed (Glikin and Sinai 1991; Glikin 1996a, b; and Sect. 1.4.3 of the present monograph), and reported data contain no other alternative models.

The chain-like polygonal orbiculars provide with almost the same information (indices 5 and 6 in Table 5.1). Reliability of describing these orbiculars as the blurred automorphs and also reliability of their identification are not high as they normally are not too distinctly developed. Also, any chain-like orbiculars can be visually identified only in a few particular cases due to their overlapping with the

automorphs. Sometimes, in private discussions, the origin of the orbiculars has been explained by specific conditions of nucleation of new individuals created by a diffusion field induced at the growth front of a crystal growing in magma (index 5 in Table 5.1) or they appear as a result of skeletal growth (index 6 in Table 5.1). These alternative views seem lame; a polygonal shape of diffusion fields surrounding the crystal has not been proved yet; at present what is known is a polygonality of thermal fields for specific conditions of crystallization from a melt (see, e.g., Klapper 1994), and the type of skeletal growth discussed also has not been proved either experimentally or theoretically.

So, we consider the orbicular crystal ensembles as the key evidence of metasomatic genesis of rapakivi.

In the present monograph spheroid phenocrysts are considered to be the products of isomorphic monocystal replacement, which had proceeded with a partial volume-deficit of feldspar, similar to that observed in the model reactions *Ib/27, 29, 31, 35* (Tables 1.1 and 1.2). Roundish forms are also typical for the model pseudomorphs of this type (Figs. 1.5*b* and 1.6*d*). There are two reasons for their formation. One of them is a significant volume-deficit, which induces decomposition of the peripheral part undergoing replacement into several isolated fragments; a simulation analog of this process is reaction *Ib/35* (Fig. 1.6*d*). Another reason is a usual dissolution. It can precede the replacement, if the solution is undersaturated in the beginning of the process, or accompany it, if the temperature raises simultaneously with the replacement or the process is accompanied by an additional salting-in reaction.

We consider solid concentric inclusions in rounded phenocrysts to be secondary formations implanted in the course of replacement process. Implanting the fluid inclusions, typical for volume-deficit replacements, is discussed in detail in Sect. 3.2; the inclusions have been observed not only in water-soluble model systems (Figs. 1.6*a–d*), but also in feldspar, which was subjected to an autoclave treatment (Tsuchiyama 1985; Wark and Stimac 1992; Johannes et al. 1994). It was demonstrated (see Sect. 4.3) that fluid inclusions in systems containing isomorphic compounds and an additional non-isomorphic compound can be partially or entirely filled with the non-isomorphic compound in crystal form (Figs. 1.6*e–j*), which gives rise to poikilitic crystals (Glikin and Sinai 2004). The vermiform quartz inclusions in the phenocrysts (Velikoslavinskii 1953) are morphologically similar to the fluid inclusions observed in the model crystals; a similar structure has been demonstrated in myrmekite formations, the genesis of which is considered by some authors as metasomatic (Tikhonenkov 1961; Collins 1988; Garcia et al. 1996). Another evidence of secondary, hydrothermal origin of quartz in these inclusions can be derived from the fact that temperature of quartz crystallization did not exceed 570°C (Koval and Valasis, 1989), which was proved by the absence of wavy extinction (Fig. 5.4), typical for magmatic quartz, having undergone the  $\alpha$ – $\beta$ -transition.

Concentricity of zones formed by inclusions in spheroid phenocrysts corresponds to a volume-deficit replacement. It reflects a diffusion nature of the replacement, as diffusion of components in the solutions captured within the implanting inclusions is a limiting stage of the process. Alternative concepts assuming the capture of solid inclusions to occur during the growth process cannot explain

**Table 5.2** Differentiation of polymineral mixtures into layers in the course of their recrystallization

Description of the experiment	Amount of the separated component (wt%)				
	In the initial mixture (P, %)	Separated (L, % of P)	Remaining in the aggregate (R)	Content in the aggregate (M)	
<b>NaNO<sub>3</sub>-K<sub>2</sub>Cr<sub>2</sub>O<sub>7</sub></b> Separated is NaNO <sub>3</sub> , 125 tests, 42°C, fraction 0.25–0.5 mm	20	0.0	100.0	20.0	
	30	0.0	100.0	30.0	
	35	0.0	100.0	35.0	
	40	1.3	96.8	39.2	
	45	8.8	80.4	41.9	
	50	20.0	60.0	37.5	
	55	25.0	54.5	40.0	
	60	40.0	33.3	33.3	
	70	51.3	26.7	38.4	
	80	68.8	14.0	34.8	
<b>Ba(NO<sub>3</sub>)<sub>2</sub>-BaCl<sub>2</sub>·2H<sub>2</sub>O</b> Separated is Ba(NO <sub>3</sub> ) <sub>2</sub> , 43 tests, 42°C, fraction 0.25–0.5 mm	10	0.0	100.0	10.0	
	20	1.4	93.0	18.9	
	30	8.8	70.7	23.2	
	40	22.3	44.2	22.8	
	50	36.0	28.0	21.9	
	60	48.8	18.7	21.9	
	70	61.0	12.9	23.1	
	42°C, fraction 0.5–1.0 mm	10	0.0	100.0	10.0
		20	0.8	96.0	19.4
		30	9.8	67.3	22.3
40		24.1	39.8	20.9	
50		36.6	26.8	21.1	
60		49.1	18.2	21.4	
70		63.5	9.3	17.9	
80		74.8	6.5	20.6	
90		88.1	2.1	16.0	
21°C, fraction 0.25–0.5 mm	10	0.0	100.0	10.0	
	20	0.0	100.0	20.0	
	30	5.2	82.7	26.2	
	40	14.7	63.0	29.6	
	50	20.3	59.4	37.3	
	60	45.5	24.2	26.6	
	70	62.2	11.1	20.6	
	80	76.1	4.9	16.3	
	90	87.7	2.6	18.7	
21°C, fraction 0.5–1.0 mm	10	0.0	100.0	10.0	
	20	0.0	100.0	20.0	
	30	6.4	78.7	25.2	
	40	13.2	67.0	30.9	
	50	27.6	44.8	30.9	

(continued)

**Table 5.2** (continued)

Description of the experiment	Amount of the separated component (wt%)			
	In the initial mixture ( <i>P</i> , %)	Separated ( <i>L</i> , % of <i>P</i> )	Remaining in the aggregate ( <i>R</i> )	Content in the aggregate ( <i>M</i> )
	60	43.2	28.0	29.6
	70	60.5	13.6	24.1
	80	72.3	9.6	27.8
	90	84.2	6.4	36.7
<b>KAl(SO<sub>4</sub>)<sub>2</sub>·12H<sub>2</sub>O–NiSO<sub>4</sub>·7H<sub>2</sub>O</b>	15	2.0	86.7	13.3
Separated is KAl(SO <sub>4</sub> ) <sub>2</sub> ·12H <sub>2</sub> O, 25 tests, 42°C, fraction 0.02 mm	40	20.0	50.0	25.0
	60	48.5	19.2	22.7
42°C, fraction 0.1 mm	15	6.3	58.0	9.3
	40	25.0	37.5	20.0
	60	54.5	9.3	12.3
	85	80.0	5.9	24.2
<b>NaCl–K<sub>2</sub>Cr<sub>2</sub>O<sub>7</sub></b> , Separated is NaCl 40 tests, 42°C, fraction 0.25–0.5 mm	10	0.0	100.0	10.0
	20	0.0	100.0	20.0
	30	3.2	89.3	27.5
	40	6.3	84.2	36.0
	50	7.9	84.2	45.5
	60	9.1	84.8	56.0
	70	10.8	84.6	67.0
	80	20.7	74.1	75.0
	90	28.0	68.9	86.0
42°C, fraction 0.5–1.0 mm	10	0.0	100.0	10.0
	20	1.9	90.5	18.5
	30	4.9	83.7	26.1
	40	11.7	70.8	32.0
	50	17.5	65.0	39.5
	60	31.2	48.0	42.0
	70	44.0	37.1	46.5
	80	69.8	12.8	34.0
	90	82.3	8.6	43.5
21°C, fraction 0.25–0.5 mm	10	0.0	100.0	10.0
	20	0.0	100.0	20.0
	30	1.4	95.3	29.0
	40	1.7	95.8	38.0
	50	2.5	95.0	49.0
	60	2.8	95.3	59.0
	70	3.3	95.4	69.0
	80	3.1	96.1	79.5
21°C, fraction 0.5–1.0 mm	10	0.0	100.0	10.0
	20	0.0	100.0	20.0
	30	0.0	100.0	30.0
	40	2.7	93.0	38.5
	50	2.1	95.8	49.0
	60	11.3	81.2	55.0

(continued)



**Table 5.2** (continued)

Description of the experiment	Amount of the separated component (wt%)			
	In the initial mixture ( <i>P</i> , %)	Separated ( <i>L</i> , % of <i>P</i> )	Remaining in the aggregate ( <i>R</i> )	Content in the aggregate ( <i>M</i> )
	70	12.2	82.6	66.0
	80	15.2	81.0	76.5
	90	19.8	77.8	87.5
<b>NH<sub>4</sub>Cl–K<sub>2</sub>Cr<sub>2</sub>O<sub>7</sub></b> Separated is NH <sub>4</sub> Cl 20 tests 42°C, fraction 0.25–0.5 mm	10	0.0	100.0	10.0
	20	0.0	100.0	20.0
	30	0.0	100.0	30.0
	40	13.7	66.8	30.8
	50	34.3	31.4	23.9
	60	48.3	19.5	22.6
	70	60.1	14.1	24.8
	80	74.2	7.2	22.5
	90	87.1	3.2	22.5
21°C, fraction 0.25–0.5 mm	10	0.0	100.0	10.0
	20	0.0	100.0	20.0
	30	7.6	80.7	24.0
	40	8.3	86.8	34.5
	50	16.3	67.4	40.5
	60	22.2	64.7	49.5

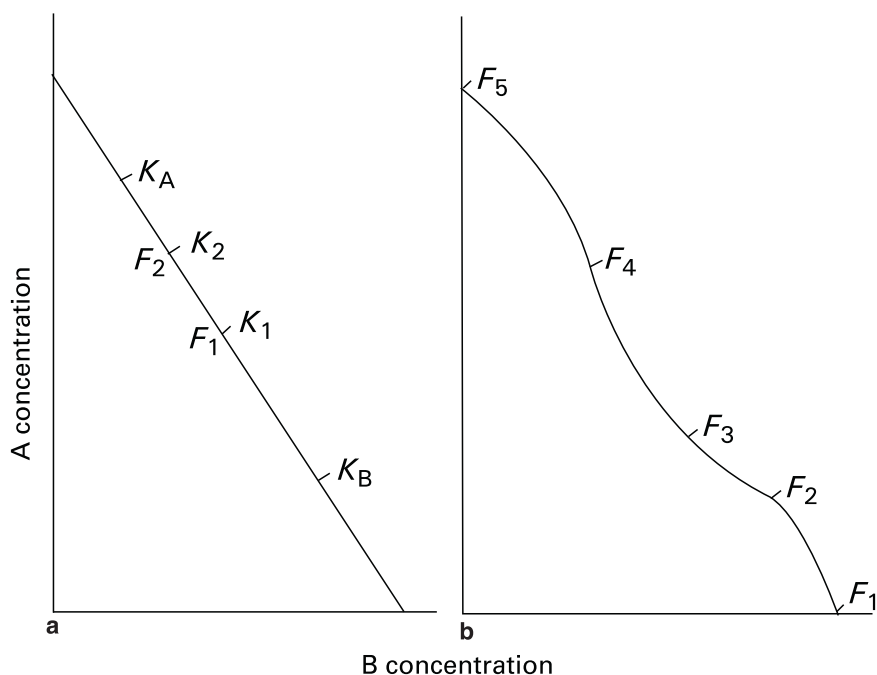
the concentricity observed at least as a mass phenomenon: convection inevitably taking place during the crystal growth in a mobile solution or magmatic melt results in formation of an asymmetrical growth zone (Lemlein 1948; Grigor'ev 1961; Shafranovskii 1968; Petrov et al. 1983).

It should be noted that the absence of sectoriality attributes is typical for both spheroid phenocrysts and their model analogs (spongy monocrystal pseudomorphs), as the composition of the solid part gradually becomes uniform due to random migration of inclusions. The breaks in external zones of the phenocrysts are results of formation of replacement products in places of individual fine crystals, which previously formed accretions on the basic protocryystal.

Metasomatic origination of the faceted phenocrysts agrees with the model of the volume-excess monocrystal isomorphic replacement (Glikin and Sinai 1983, 1991; Glikin et al. 1994, 2003; Kryuchkova et al. 2002; see also Sect. 3.2). These pseudomorphs differ from the crystals grown in a usual manner only in having a few subtle signs, which include autoepitaxial surface excrescences, perthite-type replacements along the cracks, and complex microdistribution of isomorphic components in zones of diffusion interchange like in the metasomatic garnets (Zhdanov and Glikin 2006; this attribute is likely to be useful, but it has not been investigated in the model crystals). The corresponding research of phenocrysts has not been carried out. Of course, the model suggested also includes growth of faceted phenocrysts as metacrystals.

Association of different types of phenocrysts can be accounted for by simultaneous proceeding of the volume-deficit isomorphous replacement processes (spheroid phenocrysts containing solid-phase inclusions), and those with volume-excess (faceted phenocrysts having a zoned-sectorial growth structure). Such simultaneous processes in aggregates (rocks) result from a significant dispersion of isomorphous compositions of individuals and an intermediate composition of the solution. Figure 5.8a schematically shows qualitative distribution of crystals in a system comprising isomorphous components A and B, which originally contained a solution having composition  $F_1$  and an aggregate of crystals having compositional dispersion ranging from  $\kappa_A$  to  $\kappa_B$  ( $\kappa_1$  is a solidus composition existing in equilibrium with solution  $F_1$ ). Crystals of  $K_1$ – $K_A$  compositions undergo a volume-deficit replacement, while the crystals of  $K_1$ – $K_B$  compositions, on the contrary, undergo a volume-excess replacement that corresponds to occurrence of two basic types of phenocrysts in rapakivi structure.

Peculiarities of zoned structure of spheroid phenocrysts can also be explained from this point of view. However, lack of data concerning effects of overlapping different metasomatic reaction allows only a schematic representation of some ways to form a zoned structure, which can arise due to nonuniform distribution of inclusions and heterogeneity of the chemical composition of the crystals.



**Fig. 5.8** Changes in the volume effect of replacement caused by different rates of shifting the compositions of crystals and solution (a) and by the isotherm curvature (b). Explanations are given in the text

1. As the rate of a volume-deficit reaction is considerably faster, solution becomes enriched with component A (Fig. 5.8a). When the solution reaches the figurative point  $F_2$ , the reaction direction for crystal relics  $K_1-K_2$ , which originally was a volume-deficit replacement, transforms into replacement with volume-excess. Besides, crystals having  $K_2-K_A$  and  $K_1-K_B$  compositions are still undergoing replacement in accordance with the former reaction direction. This interpretation is proved by structural and imperfection peculiarities usually occurring in the external zone of spheroid relics. Disappearance of the inclusions can be a result of their healing caused by increasing volume of the surrounding crystal matrix. Also, implanted solid inclusions can undergo dissolution, if the mechanism of their reactions transforms from salting-out into salting-in.
2. If nonlinearities of liquidus and/or solidus isotherms are high enough, the change in solution structure described above can also be accompanied by alterations of said replacement mechanisms. For example, during the interaction of crystals A with solution  $F_1$  (Fig. 5.8b), a volume-deficit reaction taking place within the sector  $F_1F_2$  would transform into a volume-excess reaction within the sector  $F_2F_3$ . Numerous variations of the process are possible depending upon the character of nonlinearity, position of initial figurative point of liquidus, and compositional distribution of initial crystals. If the process is accompanied by isodimorphism or jump in miscibility (e.g., in point  $F_2$ ), its continuation would result in full or partial replacement of the crystals with a polycrystalline aggregate (see Sect. 4.2) followed by monocrystal replacement of the new formation corresponding to the sector  $F_4F_5$ .
3. Proceeding of the metasomatic process at a lowering temperature (see Sect. 4.4), or under the action of other driving forces inducing crystallization results in crystal growth accompanied by rather slow replacement. Most frequently this process has been observed in volume-excess replacement of individuals and in volume-deficit reactions, which correspond to insignificant deviation of the crystal composition from the equilibrium contents. This can explain formation of some zoned crystals (see Table 5.1, index 3).
4. Primary zonality of crystals is also one of the factors determining a zoned structure of pseudomorphs. Replacement of zones, compositionally similar to the equilibrium solid solution, would obviously proceed less vigorously than that of zones with profoundly nonequilibrium compositions.

The details of these and some other ways of zonality formation, as well as development of a system under conditions of their superposition, are still rather poorly investigated. However, it seems possible that occurrence of solid-phase inclusions in the core parts of spheroid phenocrysts is related either to peculiarities of primary zonality (Table 5.1, index 4), or to change of the reaction direction (Table 5.1, indices 1 and 2), or to kinetic effects (Figs. 1.6e–g).

The concept mentioned above explains characteristic features of rapakivi structure from independent crystallogenic point of view. It is clear that the model described above should be applied to investigations of feldspar crystal structures and analysis of possible peculiarities of phase equilibria in a system consisting predominately of feldspar components and quartz.

## 5.3 Recrystallization of Polymineral Aggregates<sup>3</sup>

### 5.3.1 *Natural and Experimental Products of Recrystallization*

In published literature the term “recrystallization” is applied to any macrostructural morphological transformations of mineral individuals and aggregates, including processes with preservation and change of chemical and mineral composition, with or without participation of solutions, as well as to a typical reprecipitation of minerals (Grigor’ev 1956, 1961; Grigor’ev and Zhabin 1975; Popov 1984). The scope of this term has been expanded owing to absence of an unequivocal approach to classification of certain phenomena. Thus, “recrystallizations of individuals” are divided into recrystallization in the solid state and recrystallization of needle-like and plate-like individuals accompanied by their decomposition (morphological approach), the Rikke recrystallization and the Curie recrystallization (morphology plus operating factor), and recrystallization with partial addition or removal of the matter (chemical balance). Phenomena of “recrystallization of aggregates” are divided into recrystallization accompanied by the grain coarsening (morphology of individuals) and cumulative recrystallization (spatial distribution of the matter).

Moreover, this classification cannot be considered complete, as it does not include recrystallization of aggregates in solutions accompanied by grain refinement, reacting minerals, stratification of matter under the action of gravitation, stressing and thermal influences, and other important characteristics. Recrystallization forms can depend upon extent of isomorphic miscibility between the phases of an aggregate, ratio of phase solubilities, temperature solubility gradients of the phases, granulometric compositions of aggregates, their porosity, and so forth.

It is obvious, that all these phenomena and processes are inseparable and their rational classification must take into account mutual relations of the process constituents and their mechanisms. However, a unified recrystallization concept cannot be developed as state of the art due to scarcity of experimental data. The available information concerns only some special cases mainly including monomineral systems, and, besides, their interpretations are not always convincing.

Recrystallization is one of the important geological processes. It is believed to be a necessary stage in the course of formation of pegmatites (Zavaritskii 1947, 1950; Nikitin 1949, 1952; Gordienko 1959; Tibilov and Glikin 1981, and others), monomineral siderite aggregates (Grigor’ev 1961), marbles (Kaleda 1956; Skropyshev 1961), jaspers (Kaleda 1956), carbonatites (Zhabin 1979), and so forth. The process of coarsening the aggregate grains can be explained by differences in solubility rates of large and small crystals (Grigor’ev 1961 and others) and also by pulsation of hydrothermal solutions (Zavaritskii 1950) and their temperature fluctuations (Tibilov and Glikin 1981). There were some indications that recrystallization is promoted by impurities facilitating solubility of solid phase (Kaleda 1956).

---

<sup>3</sup>The major part of investigations was conducted in collaboration with Dr S. V. Petrov (Petrov et al. 1988; Glikin and Petrov 1998).

Cumulative recrystallization can be accounted for by mineral redistributions within the volume during the processes of dissolution and growth (Zavaritskii 1947; Nikitin 1949, 1952, 1955, 1958; Rudenko 1951; Grigor'ev 1961; Lazarenko 1961). Both the nature of collecting centers and the degree of participation in the process of various aggregate components have been discussed; however, the process factors and mechanisms have not been suggested yet. In general, some recrystallization models have been created on the basis of already developed, mainly intuitional concepts explaining formation of isolated crystals or some simple aggregates (Korzhinskii 1955, 1993; Grigor'ev 1961; Zhabin 1979; Popov 1984; and others). However, extreme complexity of the process requires some alternative approaches.

Experimental and theoretical studies of recrystallization processes occurring in aggregates have been conducted for a long time (see Askhabov 1984).

Thermodynamic approach is most popular in geology. It is assumed that the difference in grain sizes determines the difference in amount of surface energy per mass unit and, in accordance with the principle of energy minimization in a developing system, causes dissolution of fine grains and growth of large ones to occur (Korzhinskii 1955, 1993; Grigor'ev 1961; Bazhal and Kurilenko 1975; and others). This mechanism of recrystallization, so-called Ostwald's ripening, actually occurs in systems having micron-sized grains; however, it cannot be applied to coarse-grained aggregates with the sizes of more than  $10\mu\text{m}$ , since the amount of surface energy in them becomes negligibly small (Punin 1965; Khamskii 1979; Askhabov 1984).

The process of recrystallization of coarse-grained *monomineral aggregates* in solution has kinetic nature. It is determined by solution temperature fluctuations in vicinity of saturation point and by differences in kinetic properties of crystals having various degrees of imperfection. Imperfection does not affect the rate of dissolution, but the growth rate is considerably influenced by it. Therefore, alternating periods of lowering and elevation of temperature affect various crystals differently: dissolution is similar for all crystals of an ensemble, whereas the growth rate depends on degree of imperfection of particular individuals and is faster for individuals with higher number of defects. Less-imperfect individuals eventually dissolve completely, and the substance grains become bigger throughout the total volume (Punin 1964, 1965). Unfortunately, this concept is practically unknown to geologists. The effect of temperature oscillations was later discovered by other authors (Gordeeva and Shubnikov 1967; Melikhov 1968; Vacek et al. 1975a, b), who related it to influence of grain sizes upon the differences in the surface energy or upon growth rate of the crystals forming an ensemble. These phenomena can be accompanied by gravitational differentiation of solution resulting in a greater coarsening of the grains located in the bottom parts of experimental columns (Askhabov 1984). It is also noted that the process can be divided into three stages having different transformation rates (Gordeeva and Shubnikov 1967; Bazhal and Kurilenko 1975; Askhabov 1984).

The first experimental results obtained for *polyminerall aggregates* (Krasnova et al. 1985) were dedicated to cumulative recrystallization using one of water-soluble systems. The authors explained the process by combination of mechanical redistri-

bution of matter, gravitational stratification of concentration flows, and substance transfer from the crystal surfaces having a greater curvature to those having a relatively lesser curvature.

Our experiments were carried out using 12 polymineral aqueous salt systems and they revealed a series of morphological and kinetic patterns of structural transformation of polymineral aggregates and their correlations with physicochemical properties of the systems. The results allowed to determine the position of the process in metasomatic crystallogenesis concept (Glikin et al., 1988; Petrov et al., 1988; Glikin 1991, 1995b, 1996a, b; Glikin and Petrov, 1998). There are no other data available in published literature.

Askhabov (1984) believed that mechanisms of recrystallization in solution have principal differences in comparison to other crystallogenesis processes, and E.A. Landa (1979) emphasized close spatiotemporal and genetic interrelations between metasomatism and recrystallization processes. On the basis of our experimental results we can conclude that recrystallization of a polymineral aggregate in solution is a complex crystallogenic process comprising effects of metasomatic replacement, direct growth and direct dissolution, diffusion and infiltration mass transfer, and gravitational and thermal stratification of solution.

Metasomatic processes are the most important constituents of recrystallization. From physicochemical point of view, recrystallization can be represented (Glikin 1991) as a series of local salting-out and salting-in processes described in Chapters 1, 3, and 4. Accordingly, changes in configurations of intergrain borders can be considered as replacement of one phase by another in the process of joint expansion/contraction of adjacent grain borders. Intermediate formation of pseudomorphs (Zhabin 1979) was observed in some particular recrystallizations in the nature. We also could observe net structures of recrystallization, which could be interpreted as a set of negative automorphs, in some model preparations (Glikin et al. 1988; Glikin 1996b; Glikin and Petrov 1998). Cumulative recrystallization (Krasnova et al. 1985; Glikin et al. 1988; Glikin 1996b; Glikin and Petrov 1998) can be accounted for by translocated automorphic replacement of initial crystals. Recrystallization accompanied by refinement of grains in systems with inverted eutonics (such as KCl–NaCl–H<sub>2</sub>O) can be represented as a series of alternating processes of polycrystalline replacement (KCl by NaCl and NaCl by KCl) (Glikin 1996a, b).

Random spatiotemporal correlations between the processes of dissolution and growth make it possible to classify recrystallization as belonging to a supreme overelementary class of metasomatic crystallogenesis (see Introduction).

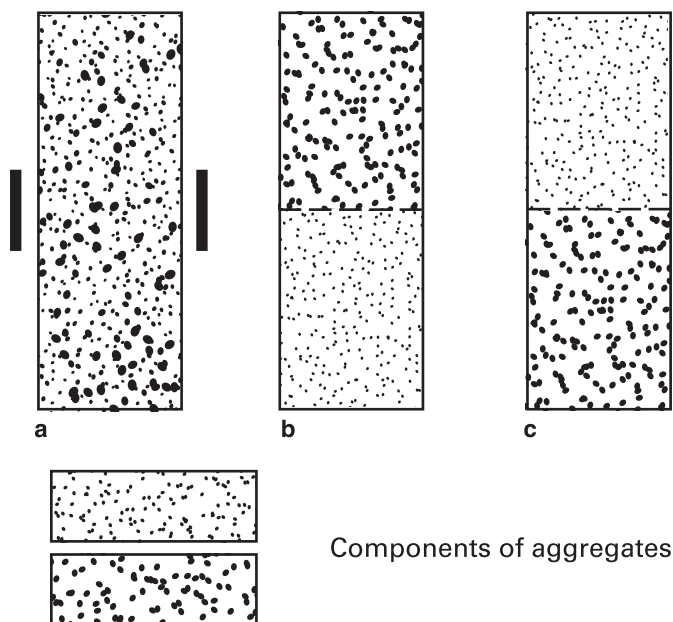
### ***5.3.2 Technique and Experimental Results***

In general, experiments were carried out using pairs of water-soluble salts. Pairs of powdered substances were loaded into an oblong vertical container and were impregnated with a solution having eutonic composition. There were used two temperature regimes: oscillatory (in an air chamber) and gradient mode (ambient

conditions with continuous local heating of a small central zone). Glass test tubes ( $20 \times 2$  cm or  $15 \times 1.5$  cm) were used to conduct reactions in oscillatory mode, and glass cylinders ( $35 \times 4$  cm) having a 4-cm-wide heating zone in their middle parts were used as containers for experiments in gradient mode. In some cases the process details were observed in thin sections (see Fig. 1.2a) having a 0.5 mm gap between the glasses.

The starting columns for standard tests (Fig. 5.9) were prepared as homogeneous mechanical mixtures of two powdered substances, or as two monomineral powder parts having equal volumes and located one atop of another in both possible combinations. Grain size of the powder fractions were 0.25–0.5 mm and 0.5–1.0 mm, and also approximately 0.02 mm and 0.1 mm. Experiments conducted in the cylinders lasted up to 24 months, and those in flat samples lasted up to 26 days. The temperature parameters are represented in Fig. 5.10.

The processes in  $K_2Cr_2O_7$ – $NaNO_3$ – $H_2O$  system were the most thoroughly investigated. The study included monitoring the evolution of macro- and micromorphology of aggregates, their granulometric and mineral compositions, and changes in kinetics. Also, the estimations included influence of initial component ratio, presence of big individuals in powder fractions, and temperature conditions. Only some



**Fig. 5.9** Location of the initial columns intended for recrystallization in the containers: (a) reactant mixture; (b and c) two combinations of monomineral parts. *Vertical lines* outside the container (a) – external heaters at the gradient mode; *dash lines* (b, c) – filter paper

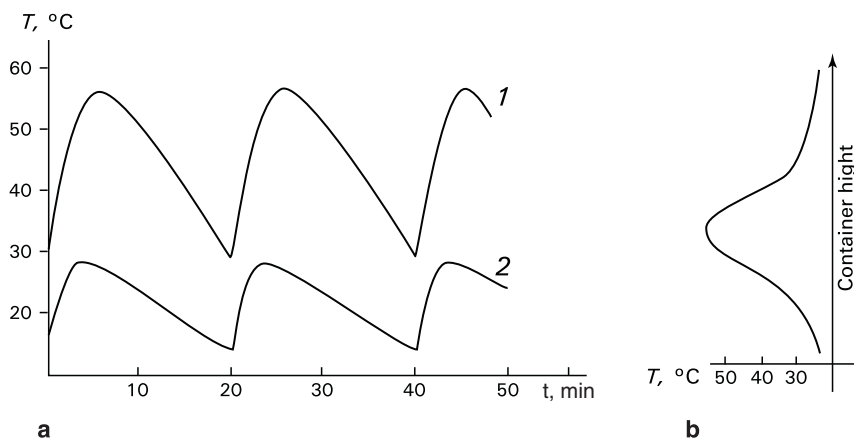


Fig. 5.10 Oscillatory (a) and gradient (b) temperature modes at experiments on recrystallization

aspects were studied in the other systems, which were used to compare with some physicochemical characteristics of the exemplary system. Morphological researches were visually carried out and under microscope, colorimetric analysis in solutions was used to determine mineral compositions of the mixtures, phase diagrams of the systems were plotted approximately based on data obtained from Solubility (1961–1970) and data obtained by us in experiments of mixing the weighed amounts of substances in water. The main regularities are considered below.

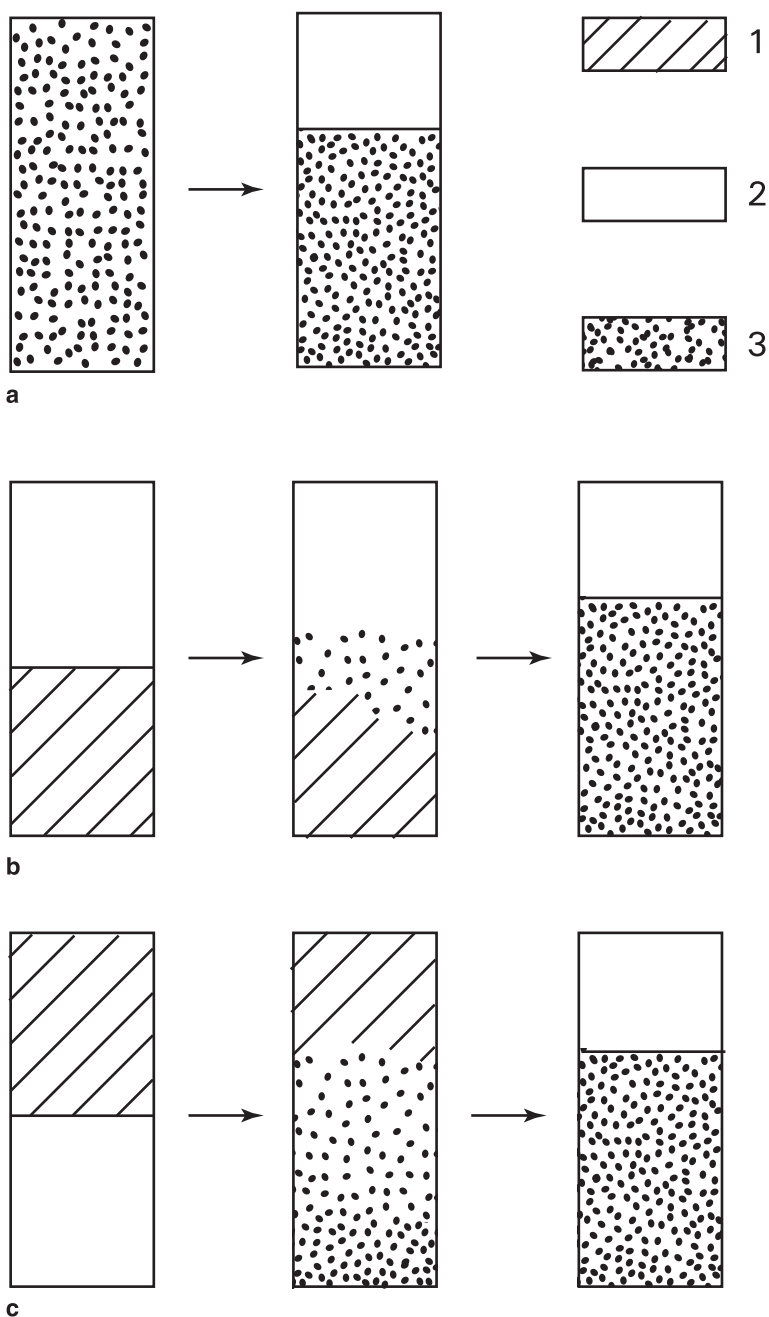
*Thermooscillatory recrystallization* was most thoroughly investigated for the pair  $\text{NaNO}_3\text{--K}_2\text{Cr}_2\text{O}_7$  (mode 1 in Fig. 5.10a, 125 experiments).

Schematic representation of alterations in macrostructure of powder mixtures (0.25–0.5 mm fraction) is shown in Fig. 5.11. Homogeneous mixture (a) became layered and partial mixing occurred in combinations of two monomineral powders (b, c). As a result, identical columns with monomineral upper  $\text{NaNO}_3$  layer and bimineral lower layer consisting of  $\text{K}_2\text{Cr}_2\text{O}_7$  and  $\text{NaNO}_3$  were obtained. Intermediate stages were different for particular columns.

The *mixture columns* became separated into two layers in 4 months after beginning the experiment, and the upper layer consisted of a monomineral  $\text{NaNO}_3$  aggregate. The border between the two layers was gradually falling and stopped approximately after 10 months.

In *separated columns* where  $\text{NaNO}_3$  was placed over  $\text{K}_2\text{Cr}_2\text{O}_7$ , the contact between them started eroding after 6 months due to the formation of “foreign” crystals in each area. In the process of formation of the lower bimineral layer, approximately by the 13th month of the experiment, the contact with  $\text{NaNO}_3$  layer became distinct, and by the 16th month, the substance redistribution stopped. At the reverse position of monomineral powders,  $\text{K}_2\text{Cr}_2\text{O}_7$  crystals started to appear in  $\text{NaNO}_3$  area within 1 month; their nucleation and growth started first at the bottom part of the column and then spread upward forming a bimineral aggregate having a





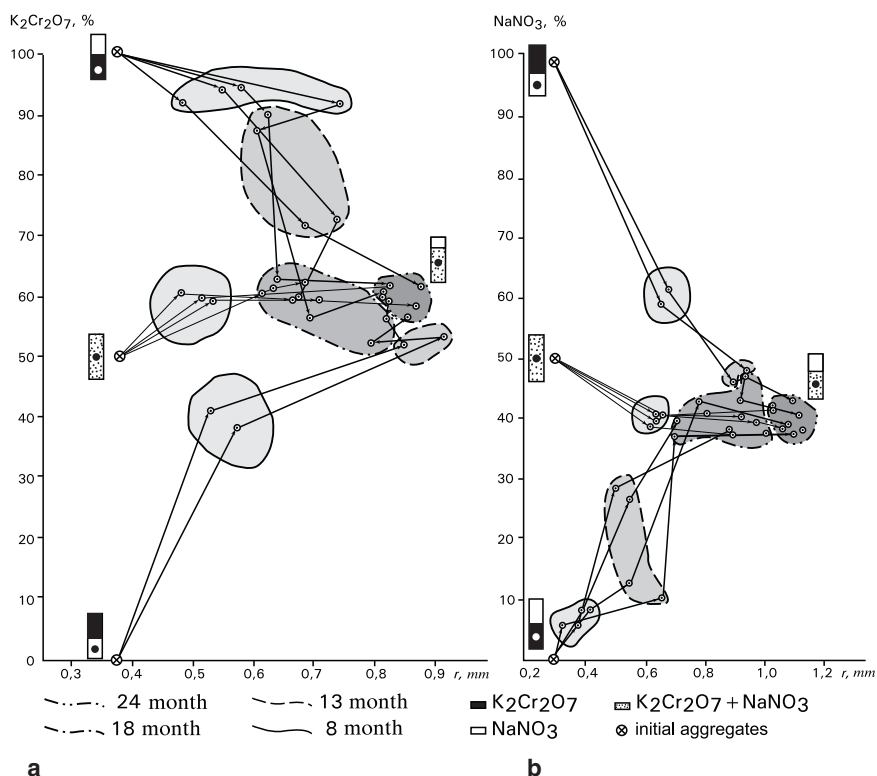
**Fig. 5.11** Schematic representations of  $K_2Cr_2O_7$ - $NaNO_3$  aggregate transformations in the columns having various initial configurations (a-c) (see Fig. 5.9) in thermo-oscillatory mode: (1)  $K_2Cr_2O_7$ , (2)  $NaNO_3$ , (3) mixture of  $K_2Cr_2O_7$  and  $NaNO_3$

sharp contact with the monomineral block of  $\text{NaNO}_3$ , which was mechanically pushed upward.

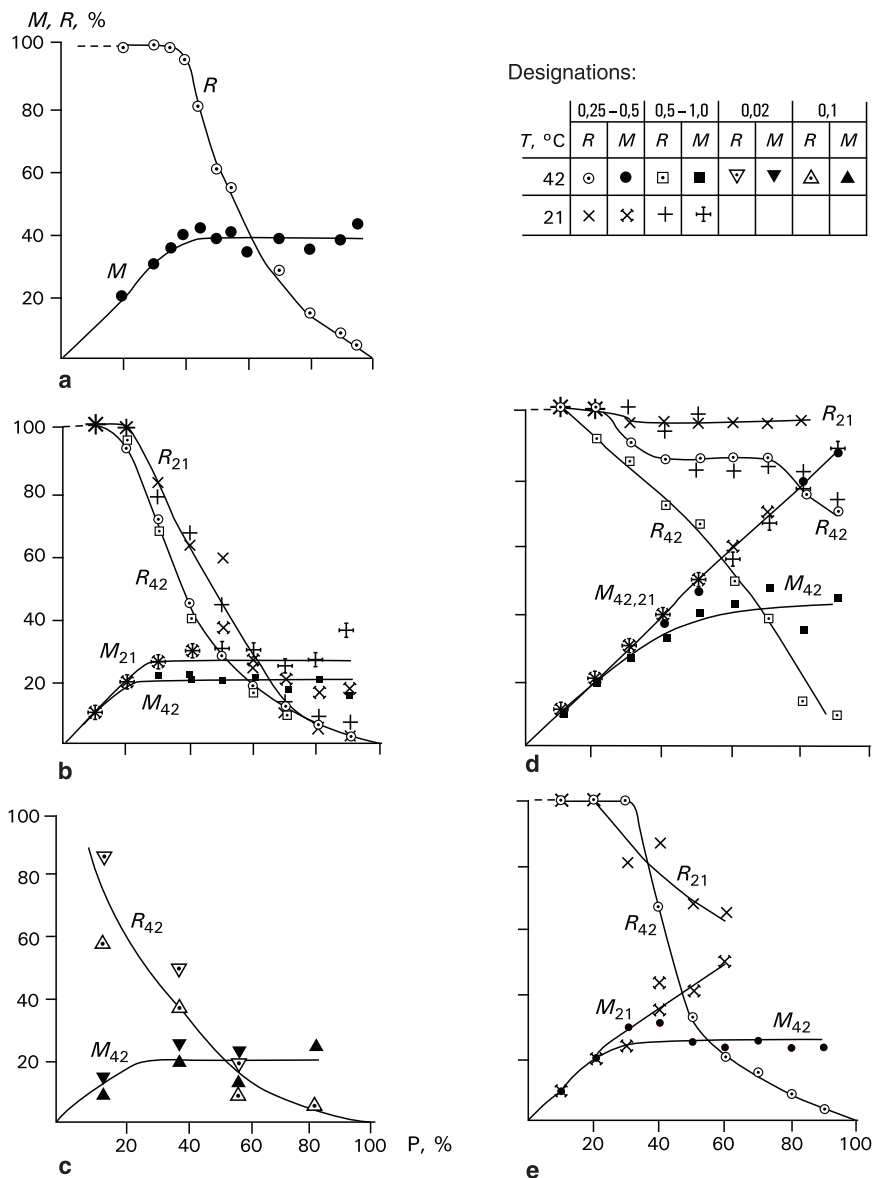
Distinct tendency to form bimineral aggregates with similar granulometric and phase compositions was detected in all three above types of columns (Fig. 5.12).

The average size of crystals in each point was measured by averaging the sizes of 100 selected crystals and confidence range for similarity of final size distributions of crystal was at least 0.95 ( $\lambda$ -criterion of Kolmogorov–Smirnov test).

The major factor of the compositional layering of the aggregates is the initial ratio of the phases. The process in mixture columns can be characterized by behavior of the component transferred into the upper monomineral layer, i.e., its content in the initial mixture ( $P$ , wt%); amount of the substance in the separated layer ( $L$ , wt% of  $P$ ); the residual amount of this substance in the lower bimineral layer [ $R = 100(P-L)/P$ ]; and its content in the bimineral layer ( $M$ , wt%). These characteristics are presented in Fig. 5.13a plotted in accordance with data presented in Table 5.2 (pages 190–192).



**Fig. 5.12** Behavior of crystals of  $\text{K}_2\text{Cr}_2\text{O}_7$  (a) and  $\text{NaNO}_3$  (b) in the course of recrystallization of bimineral aggregates having various configurations: temporal evolution of substance contents (wt%) and average crystal sizes ( $r$ ): Rectangles designate configurations of the initial aggregates (circles – the places where the samples were taken). Outlined and darkened are fields of the points of different experimental series corresponding to different expositions



**Fig. 5.13** Dependencies of compositional characteristics of recrystallized mixture aggregates on their initial total composition (Data from Table 5.2 (pages 190–192), explanations are given in the text): **(a–e)** – mixtures (separated component is printed in bold): **(a)**  $\text{NaNO}_3\text{--K}_2\text{Cr}_2\text{O}_7$ , **(b)**  $\text{Ba}(\text{NO}_3)_2\text{--BaCl}_2\cdot 2\text{H}_2\text{O}$ , **(c)**  $\text{KAl}(\text{SO}_4)_2\cdot 12\text{H}_2\text{O--NiSO}_4\cdot 7\text{H}_2\text{O}$ , **(d)**  $\text{NaCl--K}_2\text{Cr}_2\text{O}_7$ , **(e)**  $\text{NH}_4\text{Cl--K}_2\text{Cr}_2\text{O}_7$ . Indices 42 and 21 – temperature modes 1 and 2 from Fig. 5.10a; numeric values in the designation table are fractions of the powders (in millimeters)

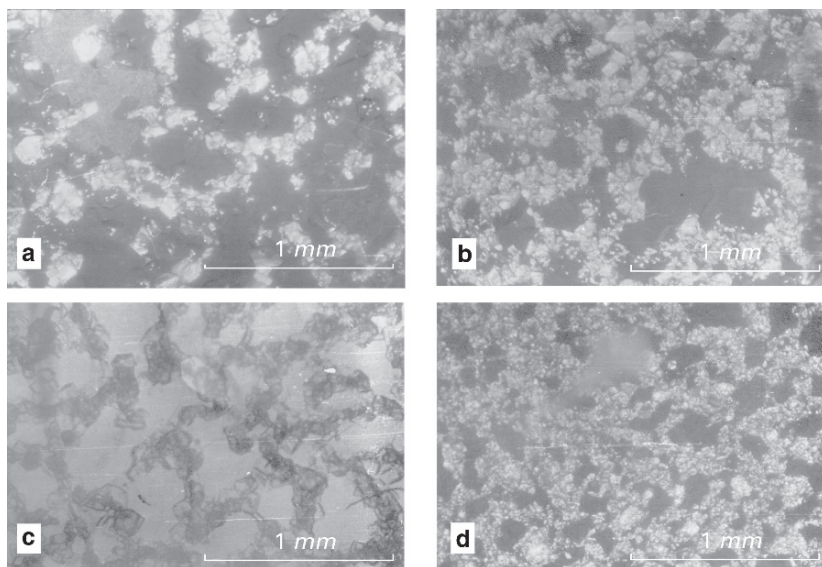
It can be seen that if initial content of  $\text{NaNO}_3$  was less than 35 wt%, this component was contained solely in the aggregate, i.e., the layering did not occur. With higher initial amounts of  $\text{NaNO}_3$  layering resulted in obtaining identical composition of bimineral aggregate, which consisted of about 61.6 wt% of  $\text{K}_2\text{Cr}_2\text{O}_7$  and 38.4 wt% of  $\text{NaNO}_3$  (Fig. 5.12). Compositions of aggregates obtained via recrystallization of divided monomineral powders were also close to the above values: 34.0 wt% of  $\text{NaNO}_3$  and 66.0 wt% of  $\text{K}_2\text{Cr}_2\text{O}_7$ , correspondingly, if  $\text{K}_2\text{Cr}_2\text{O}_7$  was initially placed in the upper part of the container; and 37.5 wt% of  $\text{NaNO}_3$  and 62.5 wt% of  $\text{K}_2\text{Cr}_2\text{O}_7$ , if  $\text{NaNO}_3$  was initially in the upper part of the container.

If initial contents of  $\text{NaNO}_3$  are high, recrystallization in this system is accompanied by formation of intermediate unstable macrostructures resulting from cumulative recrystallization in the lower part of the container. They exist for about 1.5–2 months and then transform into the bimineral aggregate described above. Big sectors (10–12 mm) highly enriched with  $\text{K}_2\text{Cr}_2\text{O}_7$  are formed, when the initial  $\text{NaNO}_3$  content is about 70–80%, and when this content is about 80–90%, it results in formation of 3–4 mm thick layers stretching in perpendicular directions and enriched with  $\text{K}_2\text{Cr}_2\text{O}_7$ , located at the distance of 5–6 mm from each other; the layers are gradually merged to form a bimineral aggregate. Contents of  $\text{NaNO}_3$  ranging from 90% to 95% cause formation of large joint crystals of  $\text{K}_2\text{Cr}_2\text{O}_7$  (the aggregate sizes are about 4–6 mm, while the sizes of individual crystal in the aggregates are about 2.5 mm; content of  $\text{K}_2\text{Cr}_2\text{O}_7$  in this zone is about 2–3%) with their longer [001] axes located in perpendicular directions to the column vertical axis and also a thin bottom bimineral layer. When the content of  $\text{NaNO}_3$  in flat samples exceeds 80%, accumulations of diffused  $\text{K}_2\text{Cr}_2\text{O}_7$  can be visible in randomly located sites of the column. If the component contents are close to equal, formation of intermediate net structures gradually transforming in uniformly grained bimineral aggregates is observed (Fig. 5.14a).

Kinetic curves of layering the mixture containing 40–95% of  $\text{NaNO}_3$  are represented in Fig. 5.15. Each curve can be divided into three definite parts and corresponding to three following stages: incubation interval *I* (merges with abscissa), active stage *A*, and stationary stage *S*. Increasing the initial contents of  $\text{NaNO}_3$  results in shortening incubation interval and active stage as well as accelerating the active stage.

It is important to note that recrystallization kinetics depend essentially upon the structure of an initial aggregate. The differences in the process of transformation of mixtures and various monomineral combinations (Figs. 5.11 and 5.12) are discussed above. Also, influence of primary granulometric heterogeneity of the aggregates should be taken into consideration. It can be seen in Fig. 5.16 that the active stage of bimineral aggregate formation in a mixture containing equal amounts of  $\text{NaNO}_3$  and  $\text{K}_2\text{Cr}_2\text{O}_7$  abruptly slows down if the mixture is seeded with individual large crystals (5–8 mm, 4–7 wt%).

At the later stages of process, morphology of individuals is characterized by a high degree of idiomorphism. Crystals of  $\text{K}_2\text{Cr}_2\text{O}_7$  are faceted as monohedrons {100}, {010}, {001}, {110}, {1 $\bar{1}$ 0}, and {11 $\bar{1}$ } and, as a rule, flattened in parallel to {010} (crystal class 1, indexing according to Groth, 1906) that corresponds to

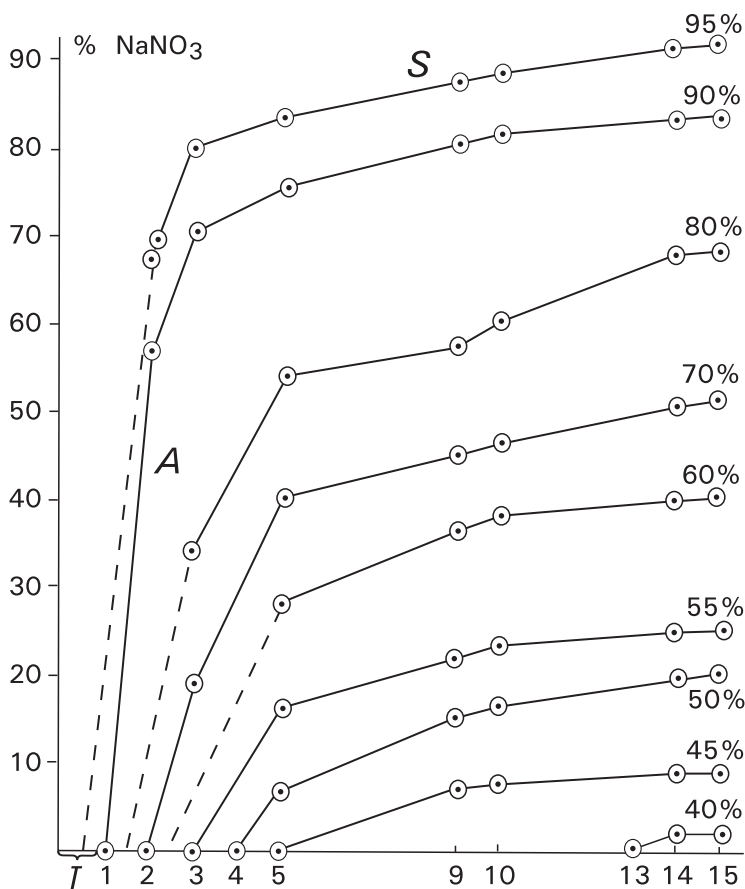


**Fig. 5.14** Intermediate net structures formed in thin sections via recrystallization of finely fractionated mixtures  $\text{NaNO}_3\text{-K}_2\text{Cr}_2\text{O}_7$  (a),  $\text{Ba}(\text{NO}_3)_2\text{-BaCl}_2\cdot 2\text{H}_2\text{O}$  (b),  $\text{KAl}(\text{SO}_4)_2\cdot 12\text{H}_2\text{O}\text{-NiSO}_4\cdot 7\text{H}_2\text{O}$  (c) and  $\text{KAl}(\text{SO}_4)_2\cdot 12\text{H}_2\text{O}\text{-CuSO}_4\cdot 5\text{H}_2\text{O}$  (d)

their most abundant form. Crystals of  $\text{NaNO}_3$  (crystal class  $\bar{3}m2$ ) are faceted with  $\{10\bar{1}1\}$ , and surprisingly have faces  $\{0001\}$  (up to 60% of crystals) and  $\{11\bar{2}1\}$ . The crystal idiomorphism distinctly increases in transition from monomineral sectors to bimineral ones, idiomorphism of  $\text{K}_2\text{Cr}_2\text{O}_7$  being always higher than that of  $\text{NaNO}_3$ . At the same time,  $\text{K}_2\text{Cr}_2\text{O}_7$  crystals initially appearing in  $\text{NaNO}_3$  mass have needle-like shape elongated along  $[001]$ .

Observations conducted in thin sections (see Fig. 1.2a) used to minimize gravitation influence upon the mass exchange showed that large crystals of both  $\text{NaNO}_3$  and  $\text{K}_2\text{Cr}_2\text{O}_7$  dissolved when placed in monomineral fine-grained mass of the other substance, which formed druses in cavities appearing due to dissolution. Dissolution of  $\text{NaNO}_3$  crystals was approximately twice as fast in comparison with that of  $\text{K}_2\text{Cr}_2\text{O}_7$ . At the same time, big crystals located in fine-grained mass of the same substance did not change significantly at least for 1 month. Development of “comb structures” was observed in vertical section-type samples. The structures appeared on large (5–8 mm) flat crystals of  $\text{K}_2\text{Cr}_2\text{O}_7$  surrounded by  $\text{NaNO}_3$  mass; the “comb cogs” (usually about 10) had almost the same length as the crystal and were its continuation; they were surrounded with fine-grained  $\text{NaNO}_3$  mass (Fig. 5.17).

Recrystallization results in enlargement of  $\text{NaNO}_3$  and  $\text{K}_2\text{Cr}_2\text{O}_7$  grains, which can reach their maximal sizes observed under stationary condition, i.e., 2–2.5 mm and 1.5–2 mm, respectively. The size distribution of the crystal grains is multimodal.

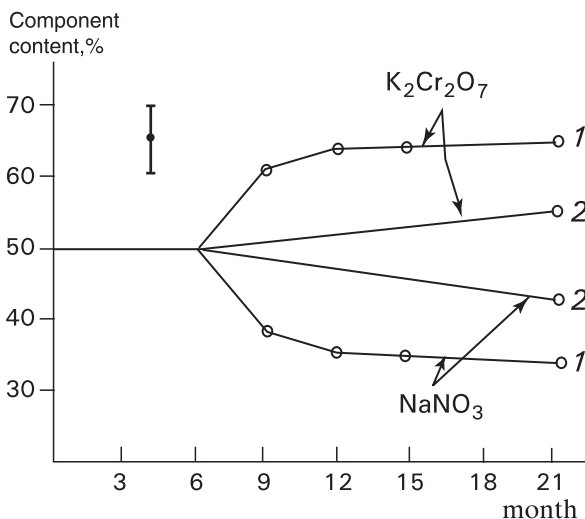


**Fig. 5.15** Time variation of separated amount of monomineral  $\text{NaNO}_3$  in the course of recrystallization of mixtures containing  $\text{NaNO}_3$  (40–95%) and  $\text{K}_2\text{Cr}_2\text{O}_7$

dal. Reaching the stationary stage leads to disappearance of all differences in the multimodal distributions of the grain sizes obtained in different series of experiments (Petrov et al. 1988). Coarsening the fine-grained (0.005–0.008 mm) mixtures of  $\text{NaNO}_3$  and  $\text{K}_2\text{Cr}_2\text{O}_7$  (as well as other mixture discussed below) in the course of recrystallization in thin sections proceeds with a high rate and includes an incubation interval, and the active and stationary stages (Fig. 5.18).

Other systems are characterized by various tendencies though scarcity of the data prevents development of an unequivocal picture.

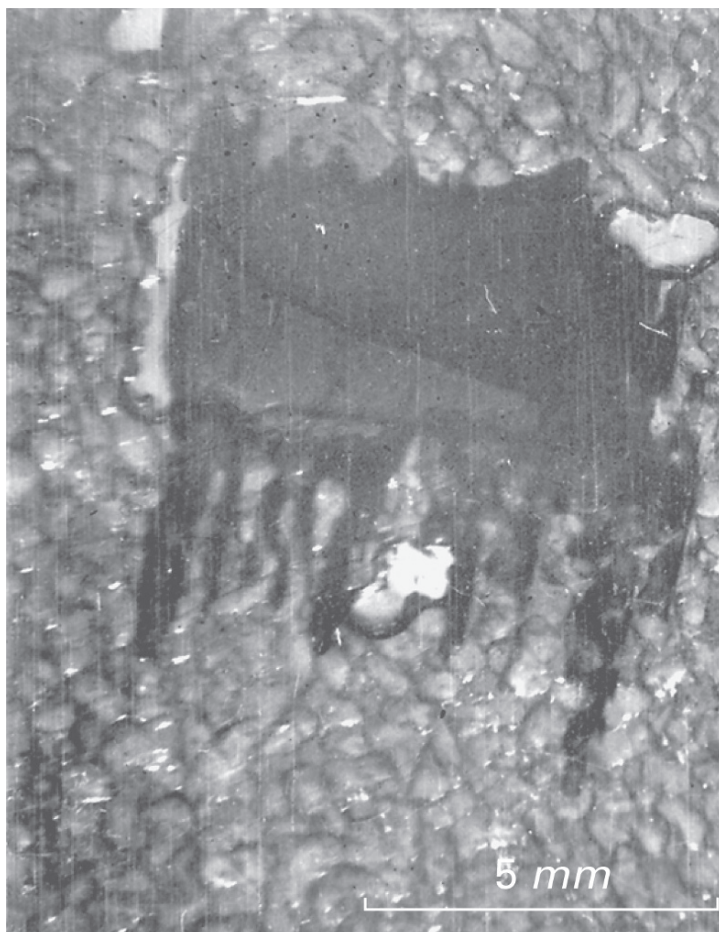
During recrystallization, mixtures of  $\text{Ba}(\text{NO}_3)_2\text{-BaCl}_2\cdot 2\text{H}_2\text{O}$  and  $\text{KAl}(\text{SO}_4)_2\cdot 12\text{H}_2\text{O-NiSO}_4\cdot 7\text{H}_2\text{O}$  undergo separation into layers in accordance with the above scheme (Figs. 5.13*b, c*; Table 5.2), but a fraction of substance transferred to the



**Fig. 5.16** Formation of bimineral aggregate in a 50%:50% mixture of  $\text{NaNO}_3$ - $\text{K}_2\text{Cr}_2\text{O}_7$  of homogeneous structure (1) and that containing big crystals of both substances (2)

monomineral part is higher in comparison with that of  $\text{NaNO}_3$ - $\text{K}_2\text{Cr}_2\text{O}_7$  mixture. The amount of separated substance insignificantly depends upon the temperature conditions of recrystallization; it is indicated by a slight divergence of plots showing separation of  $\text{Ba}(\text{NO}_3)_2$ - $\text{BaCl}_2 \cdot 2\text{H}_2\text{O}$  mixture into layers in different temperature modes. The fraction size does not affect or only slightly affects the separation; the plots drawn for different fractions of this mixture coincide almost completely. Also, there is not any significant difference in the curves drawn for  $\text{KAl}(\text{SO}_4)_2 \cdot 12\text{H}_2\text{O}$ - $\text{NiSO}_4 \cdot 7\text{H}_2\text{O}$  mixture, and their absolute values do not much differ from the characteristics of the two previous compounds, despite the fact that the difference in the grain sizes is about an order of magnitude. A mixture of  $\text{KAl}(\text{SO}_4)_2 \cdot 12\text{H}_2\text{O}$  and  $\text{CuSO}_4 \cdot 5\text{H}_2\text{O}$  also undergoes layering with formation of a monomineral alum aggregate in the upper part of the container and a bimineral aggregate in its lower part.

Unstable intermediate structures, analogous to those of  $\text{NaNO}_3$ - $\text{K}_2\text{Cr}_2\text{O}_7$ , were observed during recrystallization of  $\text{Ba}(\text{NO}_3)_2$ - $\text{BaCl}_2 \cdot 2\text{H}_2\text{O}$ ,  $\text{KAl}(\text{SO}_4)_2 \cdot 12\text{H}_2\text{O}$ - $\text{NiSO}_4 \cdot 7\text{H}_2\text{O}$ , and  $\text{KAl}(\text{SO}_4)_2 \cdot 12\text{H}_2\text{O}$ - $\text{CuSO}_4 \cdot 5\text{H}_2\text{O}$  mixtures. The net structures formed by fine-grained aggregates of one substance grain surrounding the individuals of the other were observed in flat samples in the fine-grained (0.01 mm) aggregates of all three pairs of compounds (Figs. 5.14b-d); the individuals were represented by a separated component, and the nets were formed by the other one. In the cylindrical columns the mixture of  $\text{KAl}(\text{SO}_4)_2 \cdot 12\text{H}_2\text{O}$  and  $\text{NiSO}_4 \cdot 7\text{H}_2\text{O}$  formed isometric spotty segregations enriched with  $\text{NiSO}_4 \cdot 7\text{H}_2\text{O}$ , which subsequently transformed into a layered structure (in perpendicular direction to the gravitation vector) containing 3–5 mm thick alternating layers. Contacting of monomineral  $\text{KAl}(\text{SO}_4)_2 \cdot 12\text{H}_2\text{O}$  and  $\text{CuSO}_4 \cdot 5\text{H}_2\text{O}$  columns resulted in formation of the “upper” substance aggregates

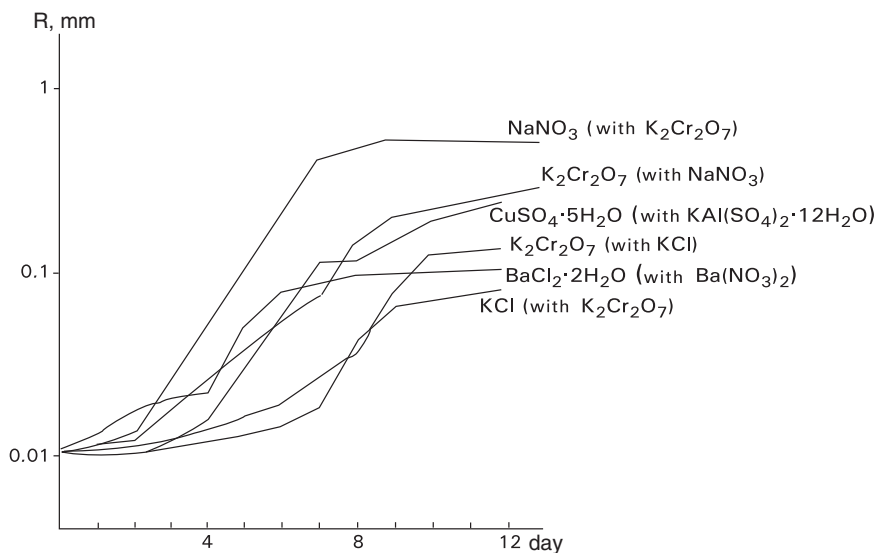


**Fig. 5.17** A “comb-like” structure on a big crystal of  $K_2Cr_2O_7$ , surrounded by  $NaNO_3$

(K-Al-alum) in the mass of the “lower” substance. When  $KAl(SO_4)_2 \cdot 12H_2O$  was arranged in the lower zone, large (up to 2–4 mm) joints of  $CuSO_4 \cdot 5H_2O$  crystals were formed in its bulk; and if the arrangement was inverted, the lower  $CuSO_4 \cdot 5H_2O$  mass became broken into blocks divided by veins composed of  $KAl(SO_4)_2 \cdot 12H_2O$ .

Behavior of  $NaCl-K_2Cr_2O_7$  and  $NH_4Cl-K_2Cr_2O_7$  mixtures (Figs. 5.13*d, e*; Table 5.2, pages 190–192) and mixtures of  $KCl$  and  $K_2Cr_2O_7$  reveals other regularities. During recrystallization of a fine-grained fraction under low-temperature conditions, mixtures of  $NaCl$  and  $K_2Cr_2O_7$  do not practically undergo any separation into layers, while elevation of temperature (and increase in the amplitude of temperature fluctuations; see Fig. 5.10*a*) or increasing the amount of the fraction increases the tendency of the separation. At elevated temperature and increasing the amount of the fraction, the plot shapes become similar to those of the layered systems. Under





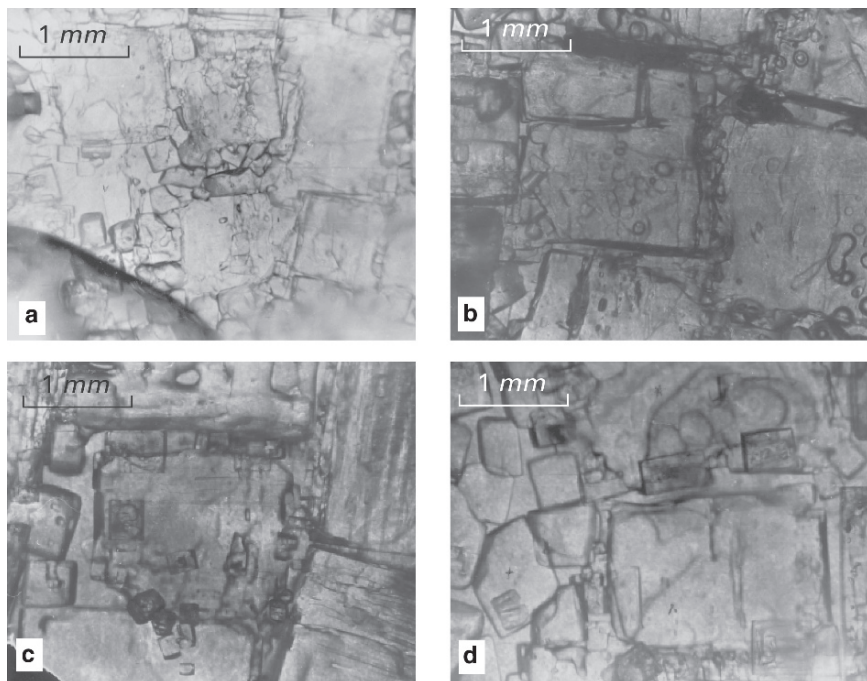
**Fig. 5.18** Temporal evolution of grain size in the course of recrystallization of mixtures containing equal amounts of finely fractionated components

low-temperature conditions the mixture  $\text{NH}_4\text{Cl}-\text{K}_2\text{Cr}_2\text{O}_7$  undergoes insignificant layering; elevated temperatures produce alterations similar to those occurring in the layering systems. Mixture of equal contents of  $\text{KCl}$  and  $\text{K}_2\text{Cr}_2\text{O}_7$  (78 experiments) does not undergo layering, but predominance of  $\text{KCl}$  (80–90%) results in accumulation of potassium dichromate in the form of big crystal joints chaotically distributed within the container and undergoing no changes for a long time in contrast to the morphologically similar but unstable joint crystals of  $\text{NaNO}_3(95\%)-\text{K}_2\text{Cr}_2\text{O}_7$  mixture. When a monomineral mass of  $\text{K}_2\text{Cr}_2\text{O}_7$  is placed over a mass of  $\text{KCl}$ , big stable joint crystals of  $\text{K}_2\text{Cr}_2\text{O}_7$  are also formed in the mass of  $\text{KCl}$ ; the crystals grow bigger in the narrow bordering zones of the both substances. It is to be noted that recrystallization of the above mixture was accompanied by mutual epitaxial growth of components, including formation of  $\text{KCl}$  incrustations all over big  $\text{K}_2\text{Cr}_2\text{O}_7$  crystals.

Coarsening the grains, which was determined in the series of mixtures in the fine-grained preparations (Fig. 5.17), includes three stages (similar to the coarsening in a  $\text{NaNO}_3-\text{K}_2\text{Cr}_2\text{O}_7$  mixture). As a result, the aggregate acquires a stationary state. Coarsening of crystals in  $\text{KCl}-\text{K}_2\text{Cr}_2\text{O}_7$  mixture proceeds with the least extent and the rate in comparison with coarsening processes taking place in  $\text{NaNO}_3-\text{K}_2\text{Cr}_2\text{O}_7$ ,  $\text{Ba}(\text{NO}_3)_2-\text{BaCl}_2\cdot 2\text{H}_2\text{O}$ , and  $\text{KAl}(\text{SO}_4)_2\cdot 12\text{H}_2\text{O}-\text{CuSO}_4\cdot 5\text{H}_2\text{O}$  mixtures.

Recrystallization of coarse-grained (1–2 mm) ordered NaCl–KCl (1:1) aggregates was studied in nine experiments in flat samples.<sup>4</sup> Amplitudes of the temperature fluctuations ranged from ambient conditions to 50–55°C and the period varied from 20 to 60 min. The main peculiarity of the process appeared to be formation of fine-grained fraction consisting mainly of KCl surrounding individual initial crystals and the whole aggregate (Fig. 5.19). Newly formed crystals precipitated at the beginning of the process; subsequently they become coarser and sometimes intergrown. The process terminates when an aggregate consisting of coarse and fine grains acquires a stationary state (or extremely sluggishly altering state).

*Thermogradient recrystallization* of aggregates was observed in four binary powder mixtures:  $\text{KAl}(\text{SO}_4)_2 \cdot 12\text{H}_2\text{O} - \text{NiSO}_4 \cdot 7\text{H}_2\text{O}$ ,  $\text{KAl}(\text{SO}_4)_2 \cdot 12\text{H}_2\text{O} - \text{CuSO}_4 \cdot 5\text{H}_2\text{O}$ ,  $\text{KCl} - \text{K}_2\text{Cr}_2\text{O}_7$ ,  $(\text{NH}_4)_2\text{Ni}(\text{SO}_4)_2 \cdot 6\text{H}_2\text{O} - \text{CuSO}_4 \cdot 5\text{H}_2\text{O}$  (three of them were tested under thermo-oscillatory conditions) and one ternary mixture  $\text{NaNO}_3 - \text{K}_2\text{Cr}_2\text{O}_7 - (\text{NH}_4)_2\text{Ni}(\text{SO}_4)_2 \cdot 6\text{H}_2\text{O}$ . The columns contained equal amounts of components, and the experiments were carried out using the temperature mode shown in Fig. 5.10b.

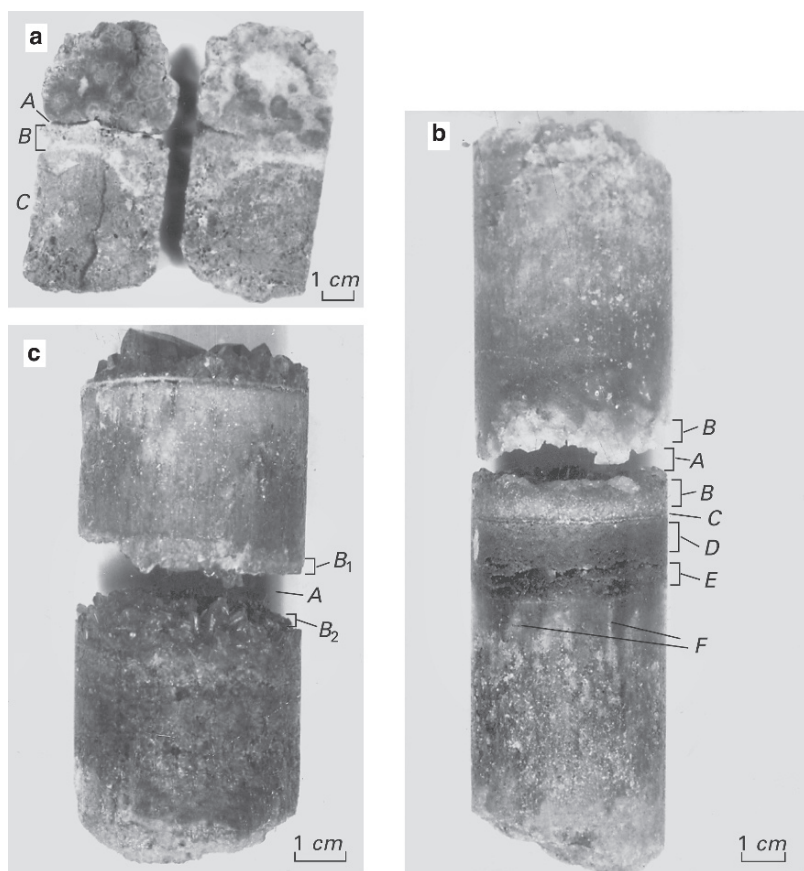


**Fig. 5.19** Exemplary recrystallized aggregate of KCl–NaCl surrounded by fine-grained precipitated crystals, which also fill up the intercrystalline cavities: (a–d) various parts of the sample (45 periods of temperature oscillations)

<sup>4</sup>Mr. A. V. Talyzin performed the experimental investigations.

The main result was common for all the mixtures and consisted in separating the mixtures into a series of zones located in perpendicular direction to direction of coinciding vectors of the temperature and gravity gradients. Zonal structures of all investigated systems included a central cavity having a thickness of about 5–10 mm, sharp contacts between the selvage zones, and asymmetric configurations of the upper and lower selvages in respect to the cavity (Fig. 5.20). The process of separation into layers takes about 2–3 months, and after that the column is not perceptively changing for at least the same period.

In  $\text{KAl}(\text{SO}_4)_2 \cdot 12\text{H}_2\text{O} - \text{NiSO}_4 \cdot 7\text{H}_2\text{O}$  mixture (Fig. 5.20a) the cavity A is delimited by the crystal druses (3–6 mm) of both substances. Zone B having the thickness up to 50 mm and containing large (up to 10–12 mm) zonal idiomorphic crystals of



**Fig. 5.20** Columns obtained after recrystallization of mixtures in a thermogradient mode. Explanations are given in the text

$\text{NiSO}_4 \cdot 7\text{H}_2\text{O}$  bound with  $\text{KAl}(\text{SO}_4)_2 \cdot 12\text{H}_2\text{O}$  crystals having the sizes up to 4 mm is located lower. A fine-grained zone *C* is located below the zone *B*; it is enriched with  $\text{NiSO}_4 \cdot 7\text{H}_2\text{O}$  and is gradually transformed into a bound primary aggregate.

The cavity *A* in  $\text{KAl}(\text{SO}_4)_2 \cdot 12\text{H}_2\text{O}$ – $\text{CuSO}_4 \cdot 5\text{H}_2\text{O}$  mixture (Fig. 5.20*b*) is delimited by crystal druses (8–10 mm) of both substances growing upward from the zone *B* and also containing crystals of  $\text{Cu}_3\text{SO}_4(\text{OH})_4$ . Below that cavity are the following zones: *C*, which is a monomineral aggregate of  $\text{CuSO}_4 \cdot 5\text{H}_2\text{O}$  having the thickness up to 3–4 mm; *D*, which is a monomineral aggregate of  $\text{Cu}_3\text{SO}_4(\text{OH})_4$  having the thickness of about 2–12 mm; *E*, which is practically a monomineral aggregate containing phenocrysts of  $\text{CuSO}_4 \cdot 5\text{H}_2\text{O}$ ; *F*, which is a series of vertical tapered out monomineral veins having the length up to 20–35 mm. These veins look like a continuation of the zone *E* and are surrounded by a fine-grained bound aggregate of  $\text{KAl}(\text{SO}_4)_2 \cdot 12\text{H}_2\text{O}$  and  $\text{CuSO}_4 \cdot 5\text{H}_2\text{O}$  (the initial ratio 1:1). The upper zones represent gradual transition from a zone similar to *B* to the bound primary aggregate.

The cavity in  $\text{KCl}$ – $\text{K}_2\text{Cr}_2\text{O}_7$  mixture is delimited by large (4–6 mm) crystals of  $\text{K}_2\text{Cr}_2\text{O}_7$  and by relatively symmetric upper and lower zones enriched with the same substance and having sharp contact zones with a primary aggregate.

The cavity *A* in  $\text{CuSO}_4 \cdot 5\text{H}_2\text{O}$ – $(\text{NH}_4)_2\text{Ni}(\text{SO}_4)_2 \cdot 6\text{H}_2\text{O}$  mixture (Fig. 5.20*c*) is delimited by crystal druses (up to 8–10 mm) made up of the substances composing the system and  $(\text{NH}_4)_2\text{Cu}(\text{SO}_4)_2 \cdot 6\text{H}_2\text{O}$ . The borders between the selvages and the main volume are sharp and their compositions are distinctly asymmetric. The upper selvege is enriched with  $(\text{NH}_4)_2\text{Ni}(\text{SO}_4)_2 \cdot 6\text{H}_2\text{O}$  (*B*<sub>1</sub>), whereas the lower one with  $(\text{NH}_4)_2\text{Cu}(\text{SO}_4)_2 \cdot 6\text{H}_2\text{O}$  and  $\text{CuSO}_4 \cdot 5\text{H}_2\text{O}$  (*B*<sub>2</sub>). The upper and lower parts of the main mass are represented by a bound primary aggregate enriched with corresponding substances. The upper part contains a druse grown above the mass in a free part of the solution and consisting of crystals of  $(\text{NH}_4)_2\text{Ni}(\text{SO}_4)_2 \cdot 6\text{H}_2\text{O}$ ,  $\text{CuSO}_4 \cdot 5\text{H}_2\text{O}$ , and  $(\text{NH}_4)_2\text{H}(\text{SO}_4)_2$ .

In ternary  $\text{NaNO}_3$ – $\text{K}_2\text{Cr}_2\text{O}_7$ – $(\text{NH}_4)_2\text{Ni}(\text{SO}_4)_2 \cdot 6\text{H}_2\text{O}$  mixture, the cavity is delineated from above and below by crystal druses composed of  $(\text{NH}_4)_2\text{Ni}(\text{SO}_4)_2 \cdot 6\text{H}_2\text{O}$  (up to 8–10 mm) with insignificant amounts of  $\text{NaNO}_3$  and  $\text{K}_2\text{Cr}_2\text{O}_7$  crystals. On either side of the druse boundaries there are located a strong porous macrocrystalline aggregate made up of  $(\text{NH}_4)_2\text{Ni}(\text{SO}_4)_2 \cdot 6\text{H}_2\text{O}$ . After the aggregate there are zones of dense macrocrystalline aggregates of  $\text{K}_2\text{Cr}_2\text{O}_7$  containing up to 20% of  $\text{NaNO}_3$ , which form sharp contact zones with the main bound mass. These borders exist even at the upper zone, but at the lower zone they have wedges intruding into the main bound mass and gradually disappearing in it.

The results discussed in this section show a variety of transformations of individuals and phenomena of matter redistribution occurring during recrystallizations in solutions. However, they have a number of regularities that can be traced despite the incoherence of the experimental data.

### 5.3.3 General Regularities and Possible Mechanisms

The results obtained are too incoherent to allow development of a unified theory of recrystallizations in solutions. However, some fundamental tendencies can be briefly summarized as follows.

*Activity and passivity* are the main peculiarities of mixture aggregates, which are recrystallized under thermo-oscillation conditions. Active aggregates undergo significant fast changes and passive ones preserve basic elements of initial structure for a long period of time.

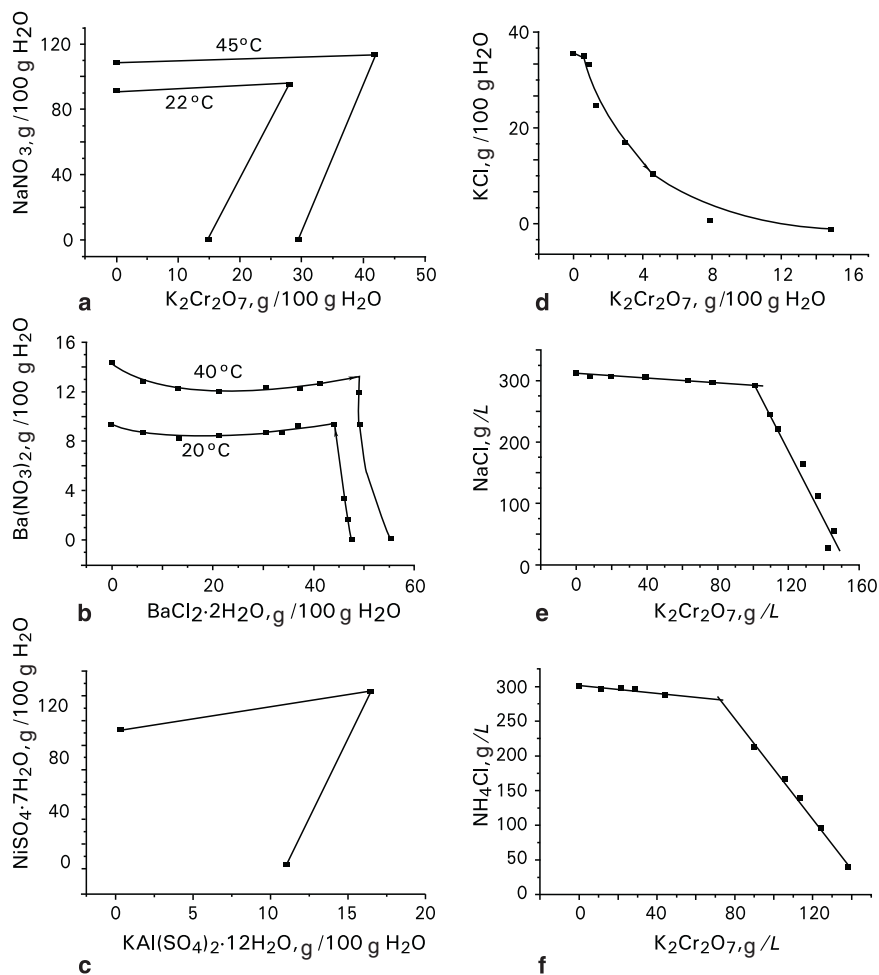
A mixture of  $\text{NaNO}_3$  and  $\text{K}_2\text{Cr}_2\text{O}_7$  can be an example of an active aggregate, because the time required for a complete transformation of its macrostructure varies depending on composition from several weeks to several months (Figs. 5.15 and 5.16). A mixture of  $\text{KCl}$  and  $\text{K}_2\text{Cr}_2\text{O}_7$  is an example of a passive aggregate, because its macrostructure does not significantly alter for at least 2 years.

The following mixtures  $\text{NaNO}_3\text{--K}_2\text{Cr}_2\text{O}_7$ ,  $\text{Ba}(\text{NO}_3)_2\text{--BaCl}_2\cdot 2\text{H}_2\text{O}$ , and  $\text{KAl}(\text{SO}_4)_2\cdot 12\text{H}_2\text{O}\text{--NiSO}_4\cdot 7\text{H}_2\text{O}$  were active in all studied experimental series (Fig. 5.13a–c). For each mixture there is an extreme content of a component, and if a content of the component exceeds the extreme value, the mixture separates into a monomineral part and bimineral part. The compositions of bimineral parts do not depend upon the initial aggregate compositions. As a whole, quantitative characteristics of transformed aggregates are almost unaffected by the temperature conditions and sizes of the initial fractions.

On the contrary, there are not any extreme contents for mixtures of  $\text{NaCl}$  and  $\text{K}_2\text{Cr}_2\text{O}_7$  (in majority of series) and  $\text{NH}_4\text{Cl}\text{--K}_2\text{Cr}_2\text{O}_7$  (at  $21^\circ\text{C}$ ), or they are indistinct, while bimineral parts form almost the same compositions at various component ratios of the initial mixtures (Figs. 5.13d, e). These mixtures, and also  $\text{KCl}\text{--K}_2\text{Cr}_2\text{O}_7$  mixture, can be classified as passive ones, though under certain conditions they can behave as active systems.

Despite a wide spread of the experimental points and incompleteness of the data obtained for different mixtures, some other tendencies can be derived from Fig. 5.13. In each case, high-temperature conditions ( $42^\circ\text{C}$ ) cause more intensive separation into layers in comparison with that observed in the low-temperature mode ( $21^\circ\text{C}$ ). This tendency is more expressed in the passive mixtures (5.13d, e) than in the active ones (5.13b). Increase of the fraction content also leads to more intensive separation, which appears to be significant in the passive mixture (5.13d), and visible in the active mixtures (5.13b, c).

Activity and passivity of mixtures is regarded as the system belonging to the particular type with “salting-in” and “salting-out” respectively (Glikin et al. 1988; Petrov et al. 1988; Glikin 1991; Glikin and Petrov 1998; see Sects. 1.5.1 and 4.1). Comparison of data obtained for capabilities of certain mixtures to undergo recrystallization with the data available on phase equilibria (Figs. 5.13 and 5.21) shows that the active systems studied belong to the type “with salting-in” (Figs. 5.21a–c) either in the whole compositional range of saturated solutions ( $\text{NaNO}_3\text{--}$



**Fig. 5.21** Phase concentration diagrams of active (a–c) and inert (d–f) systems: Data for NaNO<sub>3</sub>–K<sub>2</sub>Cr<sub>2</sub>O<sub>7</sub>–H<sub>2</sub>O and KAl(SO<sub>4</sub>)<sub>2</sub>·12H<sub>2</sub>O–NiSO<sub>4</sub>·7H<sub>2</sub>O–H<sub>2</sub>O systems were provided by Dr S. V. Petrov, data for Ba(NO<sub>3</sub>)<sub>2</sub>–BaCl<sub>2</sub>·2H<sub>2</sub>O–H<sub>2</sub>O, KCl–K<sub>2</sub>Cr<sub>2</sub>O<sub>7</sub>–H<sub>2</sub>O, NaCl–K<sub>2</sub>Cr<sub>2</sub>O<sub>7</sub>–H<sub>2</sub>O, and NH<sub>4</sub>Cl–K<sub>2</sub>Cr<sub>2</sub>O<sub>7</sub>–H<sub>2</sub>O systems were taken from Solubility (1961–1970). Isotherms for systems (c–f) 20°C

K<sub>2</sub>Cr<sub>2</sub>O<sub>7</sub>–H<sub>2</sub>O and KAl(SO<sub>4</sub>)<sub>2</sub>·12H<sub>2</sub>O–NiSO<sub>4</sub>·7H<sub>2</sub>O–H<sub>2</sub>O), or at least for compositions, which are close to their eutonic points (Ba(NO<sub>3</sub>)<sub>2</sub>–BaCl<sub>2</sub>·2H<sub>2</sub>O–H<sub>2</sub>O). On the contrary, passive systems KCl–K<sub>2</sub>Cr<sub>2</sub>O<sub>7</sub>–H<sub>2</sub>O, NaCl–K<sub>2</sub>Cr<sub>2</sub>O<sub>7</sub>–H<sub>2</sub>O, and NH<sub>4</sub>Cl–K<sub>2</sub>Cr<sub>2</sub>O<sub>7</sub>–H<sub>2</sub>O belong to the type “with salting-out” (Figs. 5.21d–f).

Positive feedbacks act in the active mixtures ensuring maximal rates and efficiency of recrystallization due to salting-in effect. Elevation of temperature

increases dissolution rate of each component due to salting-in effect of the dissolving partner component which goes into solution. Similarly, lowering the temperature accelerates precipitation of each component due to diminishing the concentration of the partner component.

Passive mixtures form negative feedbacks, which slow down recrystallization process due to salting-out effect. Elevation of temperature slows down dissolution of each component due to salting-out influence of the partner component, which dissolves. Analogously, lowering the temperature causes slowing down of the precipitation of each component as a result of the decrease in the partner component concentration.

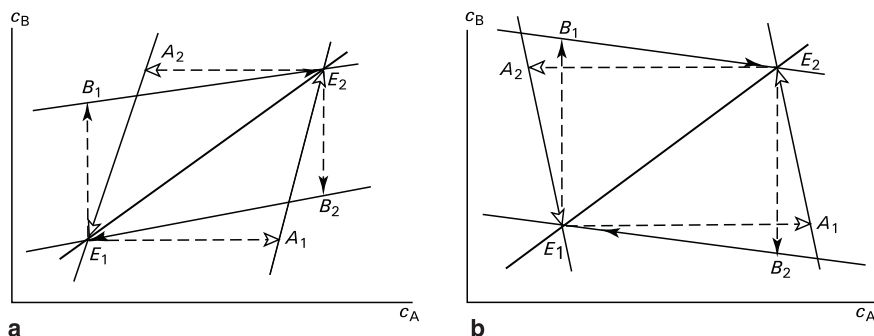
The feedback efficiency obviously weakens with increase of distances between the crystals of different phases, since the time necessary for saturation of a great volume of solution and transportation of substance to partner-crystal increases. It can be seen as reduced passivity of  $\text{NaCl-K}_2\text{Cr}_2\text{O}_7$  mixtures containing fractions of greater sizes and, correspondingly, greater intercrystalline intervals (Fig. 5.13*d*). However, changes observed in active  $\text{Ba}(\text{NO}_3)_2\text{-BaCl}_2\cdot 2\text{H}_2\text{O}$  and  $\text{KAl}(\text{SO}_4)_2\cdot 12\text{H}_2\text{O-NiSO}_4\cdot 7\text{H}_2\text{O}$  mixtures (Figs. 5.13*b, c*) are opposite to the expected.

Diminishing passivity of  $\text{NaCl-K}_2\text{Cr}_2\text{O}_7$  mixture and increasing activity of  $\text{Ba}(\text{NO}_3)_2\text{-BaCl}_2\cdot 2\text{H}_2\text{O}$  mixture with elevation of temperature and transition from the low-temperature to high-temperature mode can be induced not only by change of the absolute temperature, but also by alteration of the amplitude of oscillating temperature perturbation.

System of  $\text{NH}_4\text{Cl-K}_2\text{Cr}_2\text{O}_7\text{-H}_2\text{O}$  is a system with salting-out, but separation of the corresponding mixture into layers is rather fast. In a low-temperature mode (21°C, 0.25–0.5 mm fraction) it behaves similar to a passive  $\text{NaCl-K}_2\text{Cr}_2\text{O}_7$  mixture capable of layering (high-temperature mode 42°C, 0.5–1 mm fraction). Probably, different conditions compensate the differences in properties of the systems, and the processes eventually lead to similar results. In a high-temperature mode,  $\text{NH}_4\text{Cl-K}_2\text{Cr}_2\text{O}_7\text{-H}_2\text{O}$  behaves as a typical active mixture, but this can be a result of an equilibrium transformation occurring above 40°C and the system conversion into a  $\text{KCl-Na}_2\text{Cr}_2\text{O}_7\text{-H}_2\text{O}$  mixture.<sup>5</sup> Probably, in contrast to low-temperature conditions, the resulting system is a system with salting-in; moreover, transition from one state to another should be accompanied by a metasomatic transformation of the mixture phase composition, which would profoundly affect the process of recrystallization (especially if the transition point lies within the interval of the temperature oscillations).

---

<sup>5</sup>Such conversion remains unfortunately uninvestigated despite the fact that it frequently occurs in complex systems. Representative examples of the systems comprise a phthalate mixture  $\text{KHC}_8\text{H}_4\text{O}_4\text{-K}_2\text{C}_8\text{H}_4\text{O}_4\cdot 4\text{C}_8\text{H}_6\text{O}_4\cdot 4\text{H}_2\text{O-H}_2\text{O}$  (Fig. 7.13). For this system the eutonic line intersects the line of the solution composition stoichiometric in respect to  $\text{KHC}_8\text{H}_4\text{O}_4$  in the area located between the regions of  $\text{KHC}_8\text{H}_4\text{O}_4$  and  $\text{K}_2\text{C}_8\text{H}_4\text{O}_4\cdot 4\text{C}_8\text{H}_6\text{O}_4\cdot 4\text{H}_2\text{O}$ . That results in alterations in the composition of the phase undergoing crystallization occurring in accordance with the change in temperature. To prevent this alteration it is necessary to add KOH into solution (Glikin et al. 1979).



**Fig. 5.22** Changes in total compositions of solutions during recrystallization of active biminerals with salting-in (a) and passive biminerals with salting-out (b):  $E_1E_2-E_2E_1$  – equilibrium trajectories at lowering or elevating temperatures,  $E_1A_2E_2-E_2B_2E_1$  or  $E_1B_1E_2-E_2B_2E_1$  – extreme nonequilibrium trajectories

Variety of curve types plotted for passive mixtures and similarity of dependencies drawn for active systems indicates a greater sensitivity of the negative and less susceptibility of the positive feedbacks to various factors of the process. The conclusion seems quite logical as variations of multidirectional factors can lead to the qualitative changes in the process taking place in passive mixtures, while variations of unidirectional factors in active mixtures change only their quantitative characteristics.

A physicochemical aspect of recrystallization in systems of main types having fixed phase compositions<sup>6</sup> and positive temperature gradients of solubilities is schematically shown in Fig. 5.22. The temperature varies within the range  $T_1-T_2$  corresponding to the solubility isotherms containing eutonic points  $E_1$  and  $E_2$ . The mixture contains excesses of both crystal phases, which exceed fluctuations of their contents in solution induced by changes of temperature.

At elevating temperature the total solution compositions in any systems move from the neighborhood of the eutonic points  $E_1$  to the neighborhood of  $E_2$  along an arbitrary trajectory lying within the limits of quadrangles  $E_1A_1E_2B_1$ . The trajectory is determined by the dissolution rates of different phases and elevation of temperature. If the temperature rises sufficiently slowly, the equilibrium dissolution takes place and the trajectory coincides with the eutonic line. The trajectory of a nonequilibrium process depends upon a ratio between the rates  $\nu$  of solution saturation with components A and B; the difference in values  $\nu$  can be determined by differences in dissolution kinetics and the sizes of crystals formed by different phases. The extreme trajectories are lines  $E_1A_1E_2$  or  $E_1B_1E_2$  (if  $\nu_B < \nu_A$  or  $\nu_B > \nu_A$ , respectively). If  $\nu_B$  and  $\nu_A$

<sup>6</sup>Recrystallization of mixtures containing isomorphic components cannot be discussed at present. Preliminary investigations gave ambiguous results ranging from a complete passivity to an active separation of system into layers. This can be accounted for by a great complexity of crystallogenic processes proceeding in the systems, which at the present state-of-the-art makes any predictions impossible.



are of the same order of magnitude, the intermediate trajectories lie within  $E_1A_1E_2$  or  $E_1B_1E_2$  regions, and their extreme points may or may not coincide with  $E_1$  and  $E_2$ .

At lowering temperature the total solution compositions change in the opposite direction (from the neighborhood of  $E_1$  to the neighborhood of  $E_2$ ) and within the limits of other quadrangles:  $E_2B_2E_1A_2$ . If the temperature lowering is sufficiently slow, the composition trajectory of the solution undergoing equilibrium crystallization of both phases accompanied by the solution depletion coincides with the eutonic line in the way similar to the dissolution stage. The extreme trajectories of nonequilibrium processes are  $E_2A_2E_1$  (if  $v_B < v_A$ ) or  $E_2B_2E_1$  (if  $v_B > v_A$ ), whereas the intermediate trajectories lie within the areas  $E_2A_2E_1$  or  $E_2B_2E_1$ . Nonequilibrium trajectories for the stages corresponding to elevation of temperature and its lowering lie on the opposite sides of the eutonic lines.

The shapes of trajectories of the processes occurring in the systems with salting-in and salting-out (Figs. 5.22a and 5.22b respectively) differ. The trajectories of the former process (Fig. 5.22a) always have positive values of  $\partial c_A / \partial c_B$  regardless to elevation or lowering the temperature. For the latter system (Fig. 5.22b) the sign of the derivative can change, for example, on the extreme trajectories in the points  $A_1$  and  $B_1$  at increasing temperature and in the points  $A_2$  and  $B_2$  at lowering temperature; the course of process after a change of the sign corresponds to a metasomatic salting-out reaction, which impedes the process.

It should be noted that physicochemical scheme described covers variations of the total solution composition and is intended for providing an explanation for activity and passivity of polymineral mixtures undergoing recrystallization.

*Three-stage* division of thermo-oscillatory recrystallization of active mixtures is the next important feature of the process which terminates by the aggregate, reaching a stationary state with respect to the macrostructure, granulometric, and mineral composition (Figs. 5.12, 5.15, and 5.16). The three-stage sequence of monomineral aggregate recrystallization was in general described as resulting from a superposition of several competing mechanisms (Askhabov 1984). The results presented allow to conclude that all the recrystallization processes involve a participation of a three-stage mechanism, which can be further adjusted to describe the processes occurring in polymineral aggregates.

The mechanism suggested below for polymineral recrystallization is considered (Glikin 1991; Glikin and Petrov 1998) as generalization of a model proposed for monomineral recrystallization, which is based on cyclic alternations of processes of dissolution and growth of grains and takes into consideration essential differences in rate disorders of the growth and dissolution processes (Punin 1965). The process in question is characterized by a high structural stability of the final aggregate, abrupt transitions between the stages, and fast termination of layering caused by changes in ratios between the solid phases. Heterogeneous distribution of crystals by imperfection, which determines monomineral recrystallization (Punin 1965), cannot explain these phenomena.

The major factor of polymineral recrystallization is considered to be heterogeneous and nonoptimal spatial distribution of crystals belonging to different phases and having various sizes. In general, it is distribution of crystals having different proper-

ties, and then monomineral recrystallization appears to be a particular case of the process. In accordance with the mechanism suggested by Krasnova and co-workers (1985), temperature fluctuations result in solution enrichment or depletion with different components in various points (during dissolution or growth of the aggregate crystals, correspondingly), thus acquiring concentration heterogeneity. Light and heavy portions of the solution migrate along the intergrain interstices upwards and downwards. Crystallization of separated solutions at lowering temperature leads to the layering of an aggregate.

The term “grain coordination” hereinafter means a number of grains of one mineral surrounding a central grain composed of the other mineral (by analogy with crystallochemical terminology) in a conventional “coordination cell.” The greater the coordination number of a cell and, respectively, the smaller the sizes of coordinating grains, the greater are their relative surfaces and the faster the concentration of the grain substance varies under the action of the changing temperature in the solution surrounding the central grain. Therefore, a greater coordination number is the reason for a faster reaction of the central grain to the temperature change, as it results from a faster saturation of the solution with the component of the substance inducing salting-in. Heterogeneous structure of an aggregate defines various coordination numbers for the grains of the same substance thus resulting in variations of solution density from cell to cell.

This mechanism is also considered to be responsible for formation of the block and layered heterogeneities in intermediate macrostructures of cumulative recrystallization. According to it, polymineral ensembles initially enriched with some compound are represented as the centers of “macrocells.” Each ensemble behaves as an entity towards the medium (similarly to the dense aggregates of crystals during metasomatic replacement), and “coordination cells” described above are formed inside the ensembles. The cells promote dissociation of macroheterogeneities. If a system contains large crystals, the kinetics of recrystallization changes (Fig. 5.16) and that can also be explained as follows: these crystals act as “continuous macrocells,” and their dissociation can be induced only by resorption of external contours. It explains formation of the above comb crystals (Fig. 5.17). Separation into layers stops when the aggregate reaches a homogeneous composition.

Criteria of uniformity of the aggregate composition are absent. From the point of view of the model discussed, the composition can be determined as homogeneous if the solution composition and density vary equally in all the coordination cells under the action of temperature perturbations. This could be true if ensembles of crystals forming the cells had definite combinations of geometrical characteristics of individuals (shapes, sizes, and coordinations) ensuring identical responses of the cells to perturbation. In some sense, such structure is so highly ordered that it disagrees with supposition of equilibrium systems losing perfection of mineral distribution (Aleksandrov 1995).<sup>7</sup>

---

<sup>7</sup>Universal approach to definitions of homogeneity and ordering in structures of polymineral aggregates seems to be impossible, as impossible is creation of a universal classification.

Another effective factor is apparently a degree of system deviation from the equilibrium during dissolution or growth. At increasing temperature rates, increasing the concentrations of both substances can be arbitrary (Fig. 5.22a and comments to it). Thus, if the dissolution rate of the component A is essentially greater, there are no obstacles for solution composition to move along the trajectory  $E_1A_1E_2$ . On the contrary, the inverse symmetric change of solution composition along the trajectory  $E_2A_2E_1$  in accordance with a formal hysteresis principle is apparently hampered, since growth of the crystals A should occur in a stability domain of the phase B. Most likely, optimal aggregate composition is a composition, which counterbalances rates of dissolution and growth of both phases so that change of solution composition during the temperature fluctuations occurs along the eutonic line.

It is to be reminded that an important structural feature of a recrystallized aggregate is its multimodal granulometric composition (Petrov et al. 1988). Taking into consideration this experimental fact, it is possible to demonstrate geometrically that one of the conditions of permanent-equilibrium state of an aggregate under conditions of temperature oscillations should be optimal multimodal granulometric composition of the aggregate. An example of such a system is an elementary case of monomineral ensemble consisting of  $i$  number of grains having mass  $M$  and  $j$  number of grains having mass  $m$  (the total aggregate mass is  $iM + jm$ ). During dissolution the masses of corresponding grains decrease by  $\Delta M^-$  and  $\Delta m^-$ , while during growth, they increase by  $\Delta M^+$  and  $\Delta m^+$  respectively. Maintaining the equilibrium should correspond to the following condition:  $i\Delta M^- + j\Delta m^- = i\Delta M^+ + j\Delta m^+$ , or  $i(\Delta M^- - \Delta M^+) = j(\Delta m^- - \Delta m^+)$ ; or:  $i/j = (\Delta m^- - \Delta m^+)/(\Delta M^- - \Delta M^+)$ . This example proves a possibility of reaching the equilibrium state during a monomineral recrystallization. It can also at least partially explain the experimental results showing granulometric multimodality of these aggregates (Punin 1964) and slowing down the process at the final stage (Askhabov 1984). Despite the obvious complexity of strict calculation, the physical meaning of above formula must be applicable for polymineral aggregates containing crystals of random shapes, including variants of variable growth and dissolution rates.

Hence, stationary states of recrystallized aggregates having close granulometric and mineral compositions, achieved irrespective to their initial compositions, can be explained by formation of homogeneous structures providing conditions for preservation of uniform structures ensuring local (for individual cells) and common equilibrium between the aggregates and solution under the action of temperature perturbations. However, a reason for a system to choose a direction of structural transformation is still unclear. It is possible to assume that the basic role belongs to asymmetry of trajectories defining movement from  $E_1$  to  $E_2$  and back (Fig. 5.22), which disappears when they merge with the eutonic line: as mentioned earlier, dissolution trajectory can be arbitrary, while configuration of the growth trajectory should be delimited, since, in general, the components crystallize within a "foreign" domain. Solution of this problem requires experimental or at least physico-chemical computer examination of the sites located around separate grains and

analysis of the system evolution caused by interactions of different sites of this liquid mosaic.

Among the other mechanisms leading to a stationary condition, it is necessary to mention plugging of intergrain interstices as a result of the aggregate condensation, and slowing down the alternating processes of saturation–depletion of the solution caused by reduction in dispersivity of the aggregate. They should induce a gradual change of the process rate, and, probably, these mechanisms prevail in the course of separation of passive  $\text{NaCl-K}_2\text{Cr}_2\text{O}_7$  mixtures into layers (at  $42^\circ\text{C}$ , see Figs. 5.13*d, e*).

All the information stated above allows the following assumptions concerning the nature of recrystallization stage to be made. Incubation interval *I* (Fig. 5.15) is determined by isolation of those coordination cells or their ensembles in which deviations of concentration from the average induced by temperature changes are most significant. The active stage *A* comprises convective infiltration of light and heavy portions of solution through the aggregate mass, decomposition of cells whose kinetic parameters significantly deviate from the average values, and formation of new cells with approximately average characteristics. The stationary stage *S* includes self-regulation of structure to acquire an optimum-homogeneous distribution of the crystal phase.

Quantitative estimation of the individual process components determining the composition of recrystallized aggregates was performed by S. V. Petrov and G. N. Polishchuk (Petrov et al. 1988). Five major components covering about 80% of the total dispersion of attributes (the remaining 20% cover the components of small importance) were determined using *R*-modification of factor analysis, which included:

1. Crystal coarsening accompanied by phase redistributions (45%)
2. Transformation of monomodal grain-size distribution into a multimodal distribution (13%)
3. Profound heterogeneity of initial granulometric composition (10%)
4. Formation of metacrystals (6%)
5. Increase of the average grain size in the column in downward direction (6%)

*Change of grain size* accompanies recrystallization of aggregates in the form of either coarsening or reduction.

Grain coarsening is considered as one of the basic characteristics of the process (Grigor'ev 1961; Punin 1964; Grigor'ev and Zhabin 1975; Askhabov 1984; and others). Our experiments show that granulometric effects of recrystallization of the active polymineral mixtures are similar to those observed in monomineral aggregates and include statistical grain coarsening, multimodal size distribution, and a three-stage process. However, these effects are different in their nature. In monomineral process the leading factors are heterogeneous distribution of crystals according to their imperfection (Punin 1965) and the crystal sizes (Gordeeva and Shubnikov 1967; Vacek et al. 1975a, b). In polymineral process, the leading role is believed to belong to heterogeneity of spatial distribution of solid components and to physicochemical parameters of the solution, which were discussed above in the present section.

Grain reduction seems to be unusual process; we observed it during polymineral recrystallization and consider it to be induced by its metasomatic component.<sup>8</sup>

Two types of processes take place in active mixtures (see Sect. 5.3.1): fragmentation of the large crystals surrounded by the fine-grained aggregate of the other substance (formation of druse cavities, and also, probably, the comb crystals; see Fig. 5.17), and development of net fine-grained ensembles of one substance along the intergrain borders of the other (Fig. 5.14). We consider both processes to be examples of formation of Type *II* negative replacement products due to salting-in at lowering temperature (see Sects. 1.2, 1.4, and 1.5.1).

Grain fragmentation seems to be usual enough for passive mixtures. It can be logically deduced from a significant role the metasomatic stage plays in the mechanism ensuring mixture passivity (Fig. 5.22*b* and comments to it), as, according to conclusions presented in Sect. 1.5.1, replacement of Type *Ia* results in polycrystalline replacement.

We observed a special case of recrystallization proceeding according to a metasomatic mechanism involving the grain fragmentation in passive NaCl–KCl mixture, which does not undergo layering. In this system, fragmentation of aggregates occurs along the intergrain borders; it is shown in Fig. 5.19. It is defined by “inverted” eutonic line determined by significant difference in the temperature solubility gradients (Glikin 1996a) (Figs. 2.8*a* and 4.1*i* and explanations given in Sects. 2.2 and 4.4). At fluctuating temperatures the process proceeds in cyclic mode from the neighborhood of  $E_1$  to the neighborhood of  $E_2$  and vice versa. Each stage includes dissolution of one phase and growth of the other, and their change leads to inversion of the phase functions, i.e., the replacing phase becomes a phase undergoing replacement and vice versa.

This type of replacement results in formation of polycrystalline products, and the process includes a stage of nucleation, which requires at least a minimal supersaturation. After precipitation of a sufficient amount of a fine-grained fraction, which has high specific surface, supersaturation abruptly slows down as temperature drops, and subsequent nucleation does not occur. Fragmentation stops, and the process turns into its slow stage. The trajectory of figurative point during this process apparently coincides with the eutonics. Short duration of the experiments does not allow to define whether this stage is stationary or if it is a preliminary stage for a subsequent gradual evening-out of grain-size distribution. It is interesting to note that such stationary state is quite possible; in this case, the resulting structure consisting of a large and fine crystal mixture should be considered homogeneous in accordance with our definition mentioned in this section.

Classification of mixtures in accordance with their thermo-oscillatory recrystallization ability, as well as division of crystals in accordance with their susceptibility to isothermal metasomatic replacement is determined by physicochemical types of

---

<sup>8</sup>We do not speak of a trivial variant, which is diminishing the grain sizes in some fraction of an aggregate due to coarsening of the others.

corresponding systems. It should be noted that recrystallization proceeds in systems with salting-in, and metasomatic replacement, on the contrary, takes place in systems with salting-out.

Passivity of a mixture is rather a conditional concept describing relative stability of its macrostructure in the course of thermo-oscillatory recrystallization; in systems of this type, intensive processes proceed at the level of individuals or even at a macrostructural level if temperature gradients exist in the system.

*Thermogradient recrystallization* phenomena complete the schematic picture of the fourth class of overelementary metasomatic processes (see Introduction). The main tendencies are described briefly as follows.

Different mixtures are transformed into columns having similar macrostructures and containing a central druse cavity and a series of layers differing partially or entirely in their mineral composition and divided, as a rule, by sharp borders, which are perpendicular to the temperature gradient (Fig. 5.20). The most important fact is that the resulting structure does not depend upon the system belonging to one of the above types, i.e., with salting-in or salting-out. Therefore, it can be concluded that mechanisms of thermogradient and thermo-oscillatory recrystallizations are different.

Thermogradient columns have at least three characteristic features. The first one is a central druse cavity appearing as a result of contraction due to condensation of near-selvage zones; they are likely to bear a genetic similarity to the axial cavities in the alpine veins. The second feature is asymmetry of the upper and lower zoned structures determined by gravitation factor. The asymmetry shows in vertical crystal bunches, breaking the sharpness of contacts that confirms existence of concentration flows, similar to the flows causing layering of aggregates during thermo-oscillation processes (see this Section). The third peculiarity consists in the presence of large metacrystals both in the druse cavity and the fine-grained matrix of the partner component. These formations are results of convective mass transfer (so-called autoclave effect) and can assist in distinguishing recrystallization from thermo-oscillation recrystallization, provided they do not occur simultaneously.

Judging from the signs mentioned above and microstructural attributes, the resulting columns (Fig. 5.20) can be considered to be identical to experimental metasomatic or bimetasomatic columns (Zaraiskii 1979, 1991; Zaraiskii et al. 1986). Photos and drawings presented in the cited publications allow to draw rightful analogies. The common feature is also a gradual extinction of the processes with time. These similarities indicate identity of the both recrystallization mechanisms, and thus, evolution of thermogradient recrystallization columns is determined by differential mobility of the components participating in the process and by local equilibrium in various column zones, which is in a good agreement with theory of metasomatic zonality (Korzhinskii 1970, 1993). Classical processes and the processes described above differ in driving forces – concentration and temperature gradients, respectively – and this difference can be easily included in theoretical basis of the cited works.

Preservation of mineral composition is not an essential condition of recrystallization. It can be changed under the action of a metasomatic component of the processes; in fact, this was observed in systems undergoing transformations in thermo-oscillatory mode ( $\text{NH}_4\text{Cl}-\text{K}_2\text{Cr}_2\text{O}_7$ ), and thermogradient mode [ $\text{CuSO}_4 \cdot 5\text{H}_2\text{O}-\text{KAl}(\text{SO}_4)_2 \cdot 12\text{H}_2\text{O}$  and  $(\text{NH}_4)_2\text{Ni}(\text{SO}_4)_2 \cdot 6\text{H}_2\text{O}-\text{CuSO}_4 \cdot 5\text{H}_2\text{O}$ ]. Systems containing isomorphic components will certainly have their mineral composition varied within the limit of the series owing to dispersion of crystal compositions in the initial massif and kinetic effects (see Chapter 3).

Disclosed data are believed to provide with enough material for a preliminary search of recrystallization criteria. Also, it is important to point out that reliable criteria should be based on a complex of macroscopic and microscopic features including chemical properties of minerals having variable compositions, which are not discussed in the present monograph.

Specific zonality of crystals can indicate alternating stages of growth and dissolution occurring under thermo-oscillatory recrystallization conditions; this feature supports a corresponding conclusion about the nature of numerous pegmatite-like formations determining composition and relief of granite massifs in Central Chukotka (Tibilov and Glikin 1981).

Zonality of aggregates can indicate gradients of parameters, namely temperature and pressure, influencing solubility of minerals. Possible origination of cavities in the alpine veins during a thermogradient recrystallization in a zone of locally risen temperature was mentioned above. It is possible to assume that local cooling would lead to inverse zonality. Antisymmetric zonality was observed by us in structures of pegmatite–aplite veins of Tremearne Cove in Cornwall. A brief description is given below (Bromley et al. 1996). Clearly defined precise aplite and macrocrystalline zones having identical compositions (basically feldspar with various accessory minerals) can be distinguished in numerous veins having the thickness of about 10–15 cm. Furthermore, in a pair of neighbor veins located at about 15–20 cm from each other, one of the veins has aplite selvages, while the other contains an axial part composed of aplite. Close localization prompts a supposition of identity of temperature for both veins. Meanwhile the veins have different spatial position and located at an angle of more than  $60^\circ$  to each other. Besides, one of them lies in parallel with schistosity of the host rocks, while the other dissects them. It allows to suppose that the total stress pressure in veins could be decomposed into components so that one of the veins was subjected to compression, and the other, on the contrary, to expanding. Therefore, barogradient recrystallization could lead to antisymmetric mineral redistribution.

Macro- and microstructural heterogeneity of a rock massif can indicate the process termination at active intermediate recrystallization stage, while uniform distribution of minerals and homogeneous granulometric characteristics display the process completeness. In some cases, heterogeneities can also indicate passivity of the rock.

We would like to emphasize the fact that the examples mentioned do not pretend to reconstruct the rock genesis; they are given for demonstration of possible ways to search some signs of recrystallization in natural formations. Thus, the problem of recrystallization concludes the present review of overelementary processes of metasomatic crystallogenesis.

## References

- Adams AE, MacKensie WS, Guilford C (1984) Atlas of sedimentary rocks under the microscope. Longman, New York
- Aleksandrov SM (1995) Self-organization phenomena in progressive metasomatism of carbonate rocks. *Geokhimiya* 9:1323–1338 (Russ.)
- Armington AF, O'Connor JJ (1968) Gel growth cuprous halide crystals. *J Cryst Growth* 3:4:367–371
- Askhabov AM (1984) Processes and mechanisms of crystallogenesis. Nauka, Leningrad (Russ.)
- Atlas of textures and structures of nonferrous metal ores of Kazakhstan* (1976) Nauka, Alma-Ata (Russ.)
- Betekhtin AG (1961) Treatise on mineralogy. Gosgeoltekhizdat, Moscow (Russ.)
- Barker AJ (1994) Metamorphic textures and microstructures. Blackie, Oxford
- Barton MD, Ilchik RP, Marikos MA (1991) Metasomatism. In: Kerrick DM (ed) *Reviews in mineralogy* 26. Mineralogical Society of America, Washington
- Bazhal IG, Kurilenko OD (1975) Re-condensation in disperse systems. *Naukova Dumka*, Kiev (Russ.)
- Betekhtin AG (1961) Treatise on mineralogy. Gosgeoltekhizdat, Moscow (Russ.)
- Betekhtin AG, Genkin AD, Filimonova AA, et al. (1958) Textures and structures of ores. Gosgeoltekhizdat, Moscow (Russ.)
- Beus AA (1961) On the mechanism of formation of idiomorphic crystals of rare metal minerals in replacement processes. *Proceedings of the Institute of Mineralogy and Geochemistry of Rare Elements Academy of Science USSR* 7:61–64 (Russ.)
- Bromley A, Camm S, Glikin AE et al. (1996) Zoned aplite-pegmatite veins at Tremearne Cove and experimental recrystallization columns. In: Kurilenko VV (ed) *Regularities of the earth crust evolution. The Jubilee International Conference of the Research Institute of Earth Crust. Abstracts*. St. Petersburg State University, St. Petersburg
- Carstens H (1957) On the orbicular structure in the norite of Romsaas, Norway. *Nor Geol Tidsskr* 37:279–280
- Chesnokov BV (1974) Relative age of mineral individuals and aggregates. Nedra, Moscow (Russ.)
- Chrustschoff K (1894) Über holokrystalline mikrovariolitische Gesteine. *Mem Imper Acad Sci SPb* 7 Ser 42:3:1–243
- Collins LG (1988) Hydrothermal differentiation and myrmekite – a clue to many geological puzzles. Theophrastus, Athens
- Collins LG (1994) The origin of granite and continental masses in an expanding Earth. In: Barone M, Selleri F (eds) *Frontiers of fundamental physics*. Plenum, New York
- Craig JR, Vangham DJ (1994) *Ore microscopy and ore petrography*. Wiley, New York
- Dahl PS, Palmer DF (1983) The petrology and origin of orbicular tonalite from western Taylor Valley, southern Victoria Land, Antarctica. In: *Antarctic Earth sciences program. 4th International Symposium*. Cambridge University Press, Cambridge
- Delesse A (1848) Sur la diorite orbiculaire de Corse. *Ann Chim Phys* 3 Ser 24:435–442
- Demin YuI, Dmitriev VI, Zharikov VA (1979) Mathematic model of diffusion metasomatism with interaction of zones. In: Korzhinskii DS, Zharikov VA (eds) *Problems of physicochemical petrology* 2. Nauka, Moscow (Russ.)
- Dempster TJ, Hutton DHW, Harrison TN, et al. (1991) Textural evolution of the rapakivi granites, South Greenland Sr, O and H isotopic investigations. *Contrib Miner Petr* 107:459–471
- Dolivo-Dobrovol'skii VV (1967) Physical geochemistry as a new scientific discipline and some characteristics of its development in our country. *Zapiski Vsesoyuz Miner Obsh* 5:526–531 (Russ.)
- Donaldson CH (1979) An experimental investigation of the delay in nucleation of olivine in mafic magmas. *Contrib Miner Petrol* 69:21–32
- Escola P (1938) On the esboitic crystallisation of orbicular rocks. *J Geol* 46:448–485
- Fenn PM (1977) The nucleation and growth of alkali feldspars from hydrous melts. *Canad Miner* 15:135–161



- Garcia D, Pascal M-L, Roux J (1996) Hydrothermal replacement of feldspars in igneous enclaves of the Velay granite and the genesis of myrmekites. *Eur J Miner* 8:4:703–717
- Garrels RM, Dreyer RM (1952) Mechanism of limestone replacement at low temperature and pressure. *Geol Soc Amer Bull* 63:325–380
- Givargizov EI, Bagdasarov KhS, Kuznetsov VA, et al. (1984) Growing of crystals. In: Vainshtein BK, Chernov AA, and Shuvalou LA (eds) *Modern Crystallography III, Crystal Growth*. Springer, Berlin
- Glikin AE (1990) Crystallogenic model of isomorphic replacement and metasomatic formation of rapakivi type structures. In: Yushkin NP, Askhabov AM (eds) *Mineralogical crystallography, crystallogenesis, crystallosynthesis*. Ural Branch Academy of Science USSR, Syktyvkar (Russ.)
- Glikin AE (1991) Mechanisms of inheriting and losing the structural attributes of rocks in the course of metasomatism and recrystallization. In: Gelman ML (ed) *Metamorphic complexes of the north-east of USSR, their ore content and geological mapping*. SVKNII Far East Branch Academy of Science USSR, Magadan (Russ.)
- Glikin AE (1995a) New metasomatic concept on granite-rapakivi origin in connection with experimental crystallogeny data. In: *Precambrian of Europe: Stratigraphy, Structure, Evolution and Mineralization*. 9th Meet of the Association of the European Geological Society. Abstracts. Nauka, St. Petersburg
- Glikin AE (1995b) Crystallogenesis and geological-mineralogical sciences – coordination problems (by example of metasomatism phenomena). *Zapiski Vsesoyuz Miner Obsh* 4:116–125 (Russ.)
- Glikin AE (1996a) The physicochemical aspect of the unsteady state of metasomatic crystal production. *Geochem Intern* 33:8:117–128 (Russ.)
- Glikin AE (1996b) Modeling of metasomatic crystallogenesis in aqueous-salt systems. Dr Sci thesis. St. Petersburg State University, St. Petersburg (Russ.)
- Glikin A (2002) Features of rapakivi origin in terms of polymineral-metasomatic crystallogenesis. *Miner Soc Poland. Special Papers* 20:17–19
- Glikin AE, Glazov AI (1979) Problem of genetic interpretation of the crystal habit. *Zapiski Vsesoyuz Miner Obsh* 5:536–551 (Russ.)
- Glikin AE, Petrov SV (1998) Recrystallization of bimineral aggregates. *Zapiski Vseross Miner Obsh* 4:79–88 (Russ.)
- Glikin AE, Sinai MYu (1983) Experimental genetic study of monocystal pseudomorphs. *Zapiski Vsesoyuz Miner Obsh* 6:742–748 (Russ.)
- Glikin AE, Sinai MYu (1988) Genetic role of crystal inclusions in metasomatism. In: Kalyuzhny VA (ed) *Geochemistry and thermobarometry of endogenous fluids*. Naukova Dumka, Kiev (Russ.)
- Glikin AE, Sinai MYu (1991) Morphological and genetic classification of crystal replacement products. *Zapiski Vsesoyuz Miner Obsh* 1:3–17 (Russ.)
- Glikin AE, Sinai MYu (2004) Metasomatic formation of poikilitic crystals: experimental modeling. *Doklady Earth Sci* 396:4:563–566.
- Glikin AE, Krivosheev BV, Petrov TG, et al. (1974) A method for preparation of monocystals. Authorship certificate 429610 (Russ.)
- Glikin AE, Nikolaeva VP, Petrov TG (1979) Crystallization of potassium biphthalate from neutral and alkaline aqueous solutions. In: Smirnov YuM (ed) *Physics of crystallization*. Kalinin State University, Kalinin (Russ.)
- Glikin AE, Grunskii OS, Kaulina TV et al. (1988) Crystallogenic aspect of experimental mineralogy. In: Zharikov VA (ed) *Experiment in mineralogy*. Nauka, Moscow (Russ.)
- Glikin AE, Leontyeva OA, Sinai MYu (1994) Mechanisms of exchange of isomorphic components between crystal and solution and macrodefectiveness in secondary crystals. *J. Struct. Chem.* (Russ.). 35:5:642–646 (Translated into English from *Zhurnal Strukturnoi Khimii*. 35:5:79–83)
- Glikin AE, Kovalev SI, Rudneva EB et al. (2003) Phenomena and mechanisms of mixed crystal formation in solutions I. General concept on the example of the system  $\text{KHC}_8\text{H}_4\text{O}_4\text{-RbHC}_8\text{H}_4\text{O}_4\text{-H}_2\text{O}$ . *J Cryst Growth* 255:150–162

- Gordeeva NV, Shubnikov AV (1967) Coarsening of Seignette salt grains in the same salt solution under the action of temperature fluctuations. *Kristallografiya* 12:2:186–190 (Russ.)
- Gordienko VV (1959) A special type of pegmatite recrystallization. In: *Materials on the Kola Peninsula mineralogy 1*. Acad Sci USSR, Kirovsk (Russ.)
- Grigor'ev DP (1956) Recrystallization of minerals. *Zapiski Vsesoyuz Miner Obsh* 2:147–170 (Russ.)
- Grigor'ev DP (1961) Ontogeny of minerals. Lvov University, Lvov (Russ.)
- Grigor'ev DP, Zhabin AG (1975) Ontogeny of minerals. *Individuals*. Nauka, Moscow (Russ.)
- Groth P (1906) *Chemische Kristallographie*. Leipzig
- Grove TL, Baker MB, Kinzler J (1984) Coupled CaAl–NaSi diffusion in plagioclase feldspar: experiments and applications to cooling rate speedometry. *Geochim Cosmochim Acta* 48:2113–2121
- Grunskii OS (1988) Morphology and kinetics of crystal growth in non-stationary regimen. PhD thesis. Leningrad State University, Leningrad (Russ.)
- Henisch HK (1970) *Crystal growth in gels*. Pennsylvania State University Press, University Park, PA/London
- Irving JD (1911) Replacement ore deposits and criteria for their recognition. *Econ Geol* 6:527–561 and 6:619–699
- Johannes W, Koepke J, Behrens H (1994) Partial melting reactions of plagioclases and plagioclase-bearing systems. In: Parsons I (ed) *Feldspars and their reactions*. NATO ASI series. Kluwer, Dordrecht
- Kaleda GA (1956) On recrystallization of carbonate rocks. In: *Aspects of mineralogy of the sedimentary rocks 2*. Lvov University, Lvov (Russ.)
- Kasatkin IA, Glikin AE, Grunskii OS (1995) Multi-headed (multi-edged) and parallel-block structures of crystals resulting from their growth in non-stationary conditions. In: Tikhonov AN (ed) *Geology 2*. Moscow State University, Moscow (Russ.)
- Khamskii EV (1979) Crystallization in chemical industry. *Khimiya*, Moscow (Russ.)
- Kidyarov BI, Mitnitskii TL (1977) Method for growing the crystals of lithium iodate from solutions under static conditions. *Kristallografiya* 22:5:1113–1114 (Russ.)
- Kiryanova EV, Glikin AE (1999) The laws of fluorite and calcite habit formation in terms of the morphogenetic structural-chemical concept. *J Cryst Growth* 198/199:697–703
- Kiryanova EV, Glikin AE, Kazitsyna OYu (1984) Acid-alkaline influence of a medium upon the fluorite crystal habit (in the course of low-temperature mineral formation). *Zapiski Vsesoyuz Miner Obsh* 5:628–632 (Russ.)
- Kiryanova EV, Glikin AE, Krivovichev VG (1998) Calcite shape origin at natural and experimental crystal formation. *Zapiski Vsesoyuz Miner Obsh* 6:96–104 (Russ.)
- Klapper H (1994) *Kristalle, die geerntet werden*. *Die Waage* 33:1:28–34
- Korzhinskii DS (1955) Sketches of metasomatic process. Main problems in the concept of magmatogenic ore deposits. *Academy of Science USSR, Moscow* (Russ.)
- Korzhinskii DS (1970) *Theory of metasomatic zoning*. Clarendon Press, Oxford
- Korzhinskii DS (1993) *Selected works: principles of metasomatism and metamagmatism*. Nauka, Moscow (Russ.)
- Koval' VB, Valasis AG (1989) Problem of anorthosite-rapakivi-granite formation. *Geol Zhurn* 2:48–54 (Russ.)
- Krasnova NI, Petrov TG (1997) Genesis of mineral individuals and aggregates. *Nevskill kur'er*, St. Petersburg (Russ.)
- Krasnova NI, Petrov TG, Rundkivist TV (1983) Determining crystal growth direction at metasomatism. *Zapiski Vsesoyuz Miner obsh* 6:738–742 (Russ.)
- Krasnova NI, Petrov TG, Zolotrareva NYU (1985) Experimental study of the cumulative recrystallisation process. *Miner J* 7:4:66–72
- Kratochvil P, Sprusil B, Heyrovsky M (1968) Growth of gold single crystals in gels. *J Cryst Growth* 3–4:360–36
- Kryuchkova LYu, Glikin AE, Voloshin AE, et al. (2002) Kinetic and morphological phenomena of growth and isomorphic replacement of mixed crystals in solutions (in the series (Co,Ni)(NH<sub>4</sub>)<sub>2</sub>(SO<sub>4</sub>)<sub>2</sub>·6H<sub>2</sub>O). *Zapiski Vsesoyuz Miner Obsh* 3:62–77 (Russ.)

- Landa EA (1979) To the problem of formation conditions of metacrystals and blastocrystals. *Proc Vsesyuzn Geol Inst* 287:43–56
- Lazarenko EK (1961) Treatise on mineralogy. Vysshaya Shkola, Moscow. (Russ.)
- Lazarenko EK (1979) An attempt on genetic classification of minerals. *Naukova Dumka*, Kiev (Russ.)
- Lemmlein GG (1948) Sectorial structure of crystals. Academy of Science USSR. Moscow [see also in: Laemmlein GG (1973)] (Russ.)
- Leveson DJ (1966) Orbicular rocks: a review. *Geol Soc Amer Bull* 77:409–426
- Levinson-Lessing FYu, Vorob'eva OK (1929) Some aspects of study of orbicular structures in igneous rocks. *Doklady Acad Sci USSR* 351–356 (Russ.)
- Levkovskii RZ (1975) Rapakivi. Nedra, Leningrad (Russ.)
- Lindgren W (1925) Metasomatism. *Bull Geol Soc Amer* 36:1:1–114 and 36:1:248–253
- Lofgren GE (1980) Experimental studies on the dynamic crystallization of silicate melts. In: Hargraves RB (ed) *Physics of magmatic processes*. Princeton University Press, Princeton
- Lofgren GE (1983) Effect of heterogeneous nucleation on basaltic textures: a dynamic crystallization study. *J Petrol* 24:229–255
- Lyakhovich VV (1954) New data on mineralogy of the Vilyui ahtarandite deposit. In: *Works of the East-Siberian Branch of the Academy of Science USSR* 1. Ser. geol. nauk. Academy of Science USSR, Moscow (Russ.)
- MacKensie WS, Guilford C (1980) *Atlas of rock-forming minerals in thin sections*. Longman, New York
- Melikhov IV (1968) Investigation of re-deposition of admixtures. PhD thesis. Moscow State University, Moscow (Russ.)
- Meyer H-P (1989) Zur Petrologie von Orbiculiten. Dissertation. University (TH) Fridericiana Karlsruhe, Karlsruhe
- Mikhailov MA, Sipovskii DP, Glikin AE, et al. (1973) Crystallization of yttrium-iron garnet and orthoferrite under hydrothermal conditions. In: Frank-Kamenetskii VA (ed) *Crystallography and Crystallochemistry* 2. Leningrad State University, Leningrad (Russ.)
- Mill BV, Klevtsov PV (1966) Studying the conditions of hydrothermal synthesis of yttrium-iron garnet. *Doklady Academy of Science USSR. Inorganic mater* 2:10:1865–1867 (Russ.)
- Murphy JC, Kues H, Bohandy J (1968) Growth of crystals in silica gel using a co-solute. *Nature* 218:5134:165–166
- Nikitin VD (1949) Main peculiarities of genesis of the South Karelia ceramic pegmatites. *Zapiski Vsesoyuz Miner Obsh* 3:207–226 (Russ.)
- Nikitin VD (1952) Processes of recrystallization and metasomatism in the mica-containing and muscovite pegmatites. *Zapiski Leningrad Mining Inst* 27:2:107–157 (Russ.)
- Nikitin VD (1955) Features of mineral formation processes at metasomatic phenomena. In: *Crystallography*. Leningrad State University, Leningrad (Russ.)
- Nikitin VD (1958) Structure and origin of graphic granites in pegmatite veins. *Zapiski Leningrad Mining Institute* 33:2:47–68
- Nockolds SR (1931) On an orbicular diorite from the Island of Alderney *Geol Mag* 68:499–506
- Novogordova MI (1968) On Morphology of chalcopyrite crystals obtained from deposits belonging to various genitic types. *Zapski Vsesoyuz Miner Obsh* 5:582–582 (Russ.)
- Ol' shanskii LI, Brusilovskii SA (1958) Simple laboratory experiments displaying phenomena of the infiltration metasomatic zoning
- Panov EN (1979) Some peculiarities of morphology and composition of wolframite re-precipitated on the rock-forming minerals of granitoids. *Zapiski Vsesoyuz Miner Obsh* 1:86–91 (Russ.)
- Petrov SV (1986) Modeling of the processes of aggregate recrystallization in solutions. Diploma work. Crystallography Department Leningrad State University, Leningrad (Russ.)
- Petrov SV, Polishchuk GN, Glikin AE (1988) Estimations of recrystallization modeling results. In: II All-Union Conference “Computer physicochemical simulations in geochemistry and petrology”. Abstracts II. Academy of Science USSR, Irkutsk (Russ.)
- Petrov TG (1983) Method of equal ratios for discovering passive components and determining behaviour of active components in geochemical processes. *Zapiski Vsesoyuz Miner Obsh* 6:641–651 (Russ.)
- Petrov TG, Glikin AE, Moshkin SV (1977a) Authorship certificate 102486 (Russ.)

- Petrov TG, Glikin AE, Moshkin SV (1977b) Authorship certificate 110407 (Russ.)
- Petrov TG, Treivus EB, Punin YuO, et al. (1983) Growing crystals from solutions. Nedra, Leningrad (Russ.)
- Popov VA (1984) Applied crystal morphology of minerals. Academy of Science USSR. Sverdlovsk (Russ.)
- Pospelov GL (1973) Paradoxes, physicochemical nature and mechanisms of metasomatism. Nauka, Novosibirsk (Russ.)
- Pospelov GL (1976) Replacements and intrusions of magmatism and ore formation. Nauka, Novosibirsk (Russ.)
- Pospelov GL, Kaushanskaya PI, Lapin SS (1961) On formation of the vein hyshaped mineralization forms outside the fissures. Geol Ore Deposits 2:45–56 (Russ.)
- Price JD, Hogan JP, Gilbert MC (1996) Rapakivi texture in the Mount Scott Granite, Wichita Mountains, Oklahoma. Eur J Miner 8:435–451
- Punin YuO (1964) Recrystallization in aqueous solutions accompanied by grain coarsening. Zapiski Vsesoyuz Miner Obsh 3:364–367 (Russ.)
- Punin YuO (1965) On mechanism of recrystallization. Zapiski Vsesoyuz Miner Obsh 4:459–462 (Russ.)
- Ramdohr P (1955) Die Erzminerale und ihre Verwachsungen. Akad Verl, Berlin.
- Rämö OT, Haapala I (1995) One hundred years of rapakivi granite. J Miner Petrol 52:3–4:129–185
- Rudenko SA, (1951) An experience in studying peritic intergrowth of feldspars to their internal structure In: Crystallography 2. Ugletkhitzdat, Moscow–Leningrad (Russ.)
- Rus'ko YuA (1976) Kaolization and kaolins of the Ukrainian Shield. Naukova Dumka, Kiev (Russ.)
- Schouten C (1934) Structures and textures of synthetic replacements in “open space”. Econ Geol 29:611–658
- Seck HA (1971) Koexistierende Alkalifeldspäte und Plagioklase im System  $\text{NaAlSi}_3\text{O}_8$ – $\text{KAlSi}_3\text{O}_8$ – $\text{CaAlSi}_2\text{O}_8$ – $\text{H}_2\text{O}$  bei Temperaturen von 650°C bis 900°C. Neues Jb Miner Abh 115:315–345
- Sederholm JJ (1928) On orbicular granites, spotted and nodular granites etc. and on the rapakivi texture. Bull Comm Geol Finl 83:1–105
- Shafranovskii II (1968) Lectures on crystal morphology of minerals. Vysshaya Shkola, Moscow (Russ.)
- Shinkarev NF, Rundkvist ND (1986) Some aspects of rapakivi granite formation. Zapiski Vsesoyuz Miner Obsh 6:643–649 (Russ.)
- Skropyshev AV (1961) On recrystallization and distribution of mechanic admixtures in crystals. Zapiski Vsesoyuz Miner Obsh 5:521–534 (Russ.)
- Sudovikov NG (1967) Problems of rapakivi and later orogenic intrusions. Nauka, Moscow–Leningrad (Russ.)
- Sviridenko LP (1968) Petrology of Salmin massif of granites rapakivi (in Karelia). Karel, Petrozavodsk (Russ.)
- Tatarskii VB (1939) Lithology of oil carbonate rocks of the Central Asia and the origin of oil-bearing dolomites. GONTI, Leningrad–Moscow (Russ.)
- Tibilov IV, Glikin AE (1981) On recrystallization of granitoids of the Central Chukotka. In: Petrology of lithosphere and ore-capacity. Proc 6 Petrographical Congress. Nauka, Leningrad (Russ.)
- Tikhonenkov IP (1961) Some graphic replacement structures in alkaline rocks. Zapiski Vsesoyuz Miner Obsh 2:252–255 (Russ.)
- Tingle TN (1981) An experimental study of liquid immiscibility in the Davie Country orbicular rock, Central North Carolina, Piedmont. BOS 62:45:1063–1064
- Treivus EB, Rozhnova GA (1962) Experimental reproduction of metasomatism in water-soluble salts. Zapiski Vsesoyuz Miner Obsh 2:219–222 (Russ.)
- Tsuchiyama A (1985) Dissolution kinetics of plagioclase in the melt of the system diopside–albite–anorthite, and origin of dusty plagioclase in andesites. Contrib Miner Petrol 89:1–16

- Vacek V, Žáček S, Horsák J (1975a) Recrystallization rates at periodic temperature changes. *Kristall und Technik* 11:1141–1145
- Vacek V, Žáček S, Skřivánek J (1975b) Periodical temperature changes and the behaviour of individual crystals. *Kristall und Technik* 11:1147–1155
- Van Diver BB, Maggetti M (1975) Orbicular gabbro from Reichenbach in the Bergstraesser Odenwald, Germany. *Neues Jb Miner Abh* 125:1–26
- Velikoslavinskii DA (1953) Petrology of the Vyborg massif of rapakivi. In: *Proc Lab Geol Pre-Cambrian Acad Sci USSR* 3. Academy of Science USSR. Leningrad (Russ.)
- Velikoslavinskii DA, Birkis AP, Bogatikov OA et al. (1978) Anorthosite-rapakivi-granite formation. East European platform. Nauka, Leningrad (Russ.)
- Viluksela E (1965) Om Klotperidotit. *Geol Soc Finl* 9–10:144
- Wark DA, Stimac JA (1992) The origin of feldspars with envelope (rapakivi structure): experimental evidence of dissolution. *Contrib Miner Petrol* 111:3: 345–361
- Wilke K-Th (1973) *Kristallzüchtung*. VEB Deutscher Verlag der Wissenschaften, Berlin
- Yardley BWD (1989) *An introduction to metamorphic petrology*. Longman, New York
- Yardley BWD, MacKensie WS, Guilford C (1990) *Atlas of metamorphic rocks and their textures*. Longman, New York
- Zhabin AG (1979) Ontogeny of minerals. *Aggregates*. Nauka, Moscow (Russ.)
- Zaraiskii GP (1979) On differential mobility of the components in experiments on diffusion metasomatism. In: *Problems of physicochemical petrology 2*. Nauka, Moscow (Russ.)
- Zaraiskii GP (1991) Zonality and conditions of formation of metasomatic rocks. Nauka, Moscow (Russ.)
- Zaraiskii GP, Shapovalov YuB, Belyaevskaya ON (1981) Experimental investigations of acidic metasomatism. Nauka, Moscow (Russ.)
- Zaraiskii GP, Zharikov VA, Stoyanovskaya FM, Balashov VN (1986) Experimental investigation of bimetasomatic formation of minerals. Nauka, Moscow (Russ.)
- Zavaritskii AN (1947) Consideration of pegmatites as intermediate formations in respect to igneous rocks and ore veins. *Zapiski Vsesoyuz Miner Obsh* 1:37–50 (Russ.)
- Zavaritskii AN (1950) Metamorphism and metasomatism in pyrite deposits of the Urals. In: *Pyrites deposits of the Urals*. Academy of Science USSR, Moscow (Russ.)
- Zharikov VA, Zaraiskii GP (1973) Experimental studies of metasomatism: state and prospects. *Geol Ore Deposits* 15:4:3–18 (Russ.)
- Zhdanov VV, Glikin AE (2006) Sheathlike metasomatic garnet crystals from the Maksyutovo metamorphic complex, the southern Urals. *Doklady Earth Sci* 409:5:814–817

# Chapter 6

## Epitaxy and Quasiepitaxy in Solutions

### 6.1 Principle Phenomena

Formation of aggregate textures is affected by various factors and the leading role in the process belongs to mutual orientation influence of individuals (Zhabin 1979). The most renowned phenomenon is epitaxy, which means a regular growth of crystals of a new formation all over a substrate. Epitaxy considered from the classical point of view is referred to as a structural similarity of the accreting surfaces of the partner crystals. The similarity is defined in accordance with crystallochemical criteria, i.e., closeness between the interatomic distances of the accreting planes and similarity in the nature of atoms or atomic groups and chemical bonds in the crystals. The principles of crystallochemical approach were formulated by L. Royer about a century ago (Royer 1928) and have survived almost unaltered until now. However, some modification of the principle concerning nucleation, strength of bonds formed between the precipitate and the substrate, deformations in the overgrowing layers, and stability ratio between the oriented and disoriented nuclei have been developed (Deicha 1947; Yanulov 1948, 1958; Neuhaus 1952; Pashley 1952, 1965; Frank-Kamenetskii 1964; Palatnik and Papirov 1964; Simanovskii 1965; Distler 1968; Palatnik and Papirov 1971; Distler 1975; Schneider and Ruth 1976; Chernov 1984; Hurlle 1994; Pina et al. 1995; Haag and Dabringhaus 1997a, b, c; and others).

Published data contain a vast variety of exemplary epitaxial pairs occurring in nature and obtained artificially; some part of them was covered in four extensive reviews (Mügge 1903; Vultee 1952; Ramdohr 1955; Gebhardt and Neuhaus 1972). Some examples include grown-together pairs of samarskite and columbite (Grigor'ev 1945); olivine, garnet, and chromspinel with diamond (Futergendler and Frank-Kamenetskii 1961); feldspar and quartz (Rudenko et al. 1975); pyrite and chalcopyrite (Novgorodova 1977); sodium nitrate with calcite and potassium; or ammonium iodide with mica (Wulff 1908; Kamentsev 1956; Chernov 1984; Gaidamako et al 1983). Crystallochemical interpretations of orientation regularities are prevailing, but they do not contemplate any correlation between the observed phenomena and the growth conditions or the process mechanisms. Thus, the nature of epitaxy remains unclear, and despite their easy detection, the observed phenomena do not provide valuable information useful for genetic reconstructions.

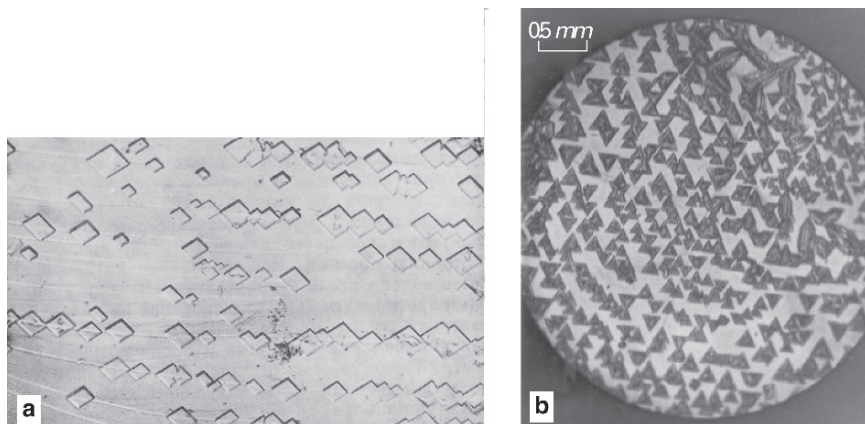
At the same time it is well-known that joint growth of the same pairs of epitaxial crystals results in formation of both oriented and disoriented accretions. For example, quartz and feldspar form oriented accretions (Grigor'ev and Shafranovskii 1946; Rudenko et al. 1975), but produce randomly oriented formations in granitoids. Experiments showed degree of mutual orientation to be affected by temperature, supersaturation, and substrate imperfection (Bauer 1956; Behrndt 1963; Chernov 1984; Givargizov et al. 1984). These effects are accounted for by variations in energy of bonds formed between crystal and substrate, and theoretical evaluations prove validity of conclusions made for both gaseous systems and solutions (Chernov 1984). Perfection of precipitate orientation depends upon substrate purity and its degree of imperfection (Kleber 1958; Kleber and Mietz 1963; Distler 1968, 1975). Some data were reported showing changes of epitaxy perfection in accretions formed by various alkali metal halides on a fluorite substrate (Krastanov and Stranski 1938; Kleber et al. 1967). Moreover, influence of a crystallochemical factor is not unconditional, since closeness of structural parameters in various "metal-alkali halide substrate" pairs can either increase or decrease degree of epitaxy depending upon the strength of the chemical bonding between precipitate and substrate (Chernov 1984).

All proposed mechanisms of epitaxial excrescence formation can be generalized as follows: (1) oriented heterogeneous nucleation of crystals and growth of the precipitating crystals on a substrate; (2) heterogeneous nucleation of randomly oriented crystals followed by their turning to acquire an epitaxial orientation; (3) heterogeneous nucleation of randomly oriented crystals with following destruction of all nuclei having nonepitaxial orientation; (4) adhesion of homogeneously nucleated crystals accompanied by their turning to acquire an epitaxial orientation; and (5) capturing molecular particles of precipitating crystals by the surface vacancies and micropores of substrate. The concept of epitaxial growth has also been applied to oriented excrescences grown on substrates, which do not have any structural similarity with precipitating crystals, and on amorphous substrates or substrates having artificially obtained regular microrelief (Stulov 1939, 1954; Simanovskii 1965; Sheftal et al. 1977; and others).

Our experimental data allowed to propose a crystallogenic model combining phenomena and criteria of a texture formation induced by interaction between substrate and precipitate (Glikin et al. 1988; Glikin and Kaulina 1988; Glikin and Plotkina 1999).

We consider *epitaxial textures* to include ensembles of crystals accreted to a substrate with their structurally similar surfaces. Regular orientation is defined by a crystallochemical factor inducing heterogeneous epitaxial nucleation. Nevertheless, kinetic processes accompanying growth or dissolution can cause a turn of the precipitating crystals. The classical textures made up of crystals with parallel orientation in respect to each other (Fig. 6.1) represent a particular case.

We assume *quasiepitaxial textures* to comprise ensembles of crystals with regular orientation, which, however, are not the result of structural similarity between the crystals and substrate. Orienting action of the crystallochemical factor is obviously absent; so, strictly speaking, these phenomena do not conform to a classical



**Fig. 6.1** Epitaxial excrescences: (a) sodium nitrate on calcite (Chernov 1984); (b) – potassium iodide on mica (Photo by Dr. I. E. Kamentsev)

definition of epitaxy. The precipitating crystals are homogeneously nucleated in a bulk of solution and subsequently become adhered to a substrate due to electrostatic interaction between the crystals and the substrate. If precipitated crystals become adhered to the substrate with their faces (and, especially, if there is a structural similarity between the substrate and precipitate), the resulting texture may be absolutely undistinguishable from an epitaxial formation. If the crystal edges or vertexes adhere to the substrate, some of characteristic morphologic elements of the crystals are aligned approximately in perpendicular direction to the substrate plane (e.g., flattening the crystals of  $K_2Cr_2O_7$ , body diagonals or planes of calcite and cubic crystals of KBr, KCl, and NaCl).<sup>1</sup>

The nature of any texture, which, in a general case, can be a combination of epitaxial and quasiepitaxial textures, depends upon the ratios between crystallochemical, kinetic, and electrostatic (adhesion) factors.

Experimental data forming the main principles of the concept are considered below.

## 6.2 Technique

The experiments comprised two types of assays: the assays of the first type included growing epitaxial textures on an unstable substrate, which was either dissolving or growing; those of the second type involved a quasiepitaxial adhesion of suspension particles onto a substrate.<sup>2</sup>

<sup>1</sup>This was a reason to introduce the term “vertical textures” (Glikin and Kaulina 1988, Glikin and Plotkina 1999).

<sup>2</sup>Growth on a dissolving substrate is a metasomatic process.

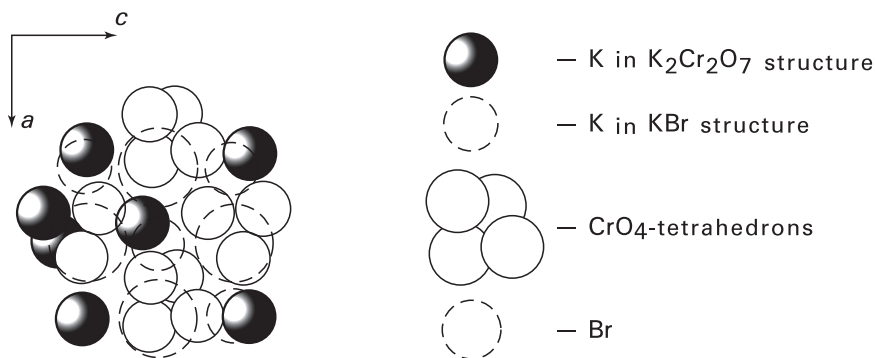


Synthetic lopecite,  $K_2Cr_2O_7$ , and KBr were selected as the principle pair tried in experiments of growing on an unstable substrate (Glikin and Kaulina 1988). This pair (as well as its isostructural pair,  $K_2Cr_2O_7$ -KCl) was found to form epitaxial textures according to the following rule:  $(010)[100]_{K_2Cr_2O_7} || (100)[001]_{KBr}$ . The result was repeatedly observed in numerous experiments involving spontaneous precipitation; the crystallochemical nature of orientation was proved by an agreement between potassium-anionic nets (Fig. 6.2) in structures of the test compounds (Wyckoff 1965). Epitaxy in KCl-NaCl pair, i.e., the substances having matching structures (space group:  $Fm\bar{3}m$ ,  $a_{KCl} = 6.29 \text{ \AA}$ ,  $a_{NaCl} = 5.64 \text{ \AA}$ ), was also thoroughly investigated (Glikin and Plotkina 1999).

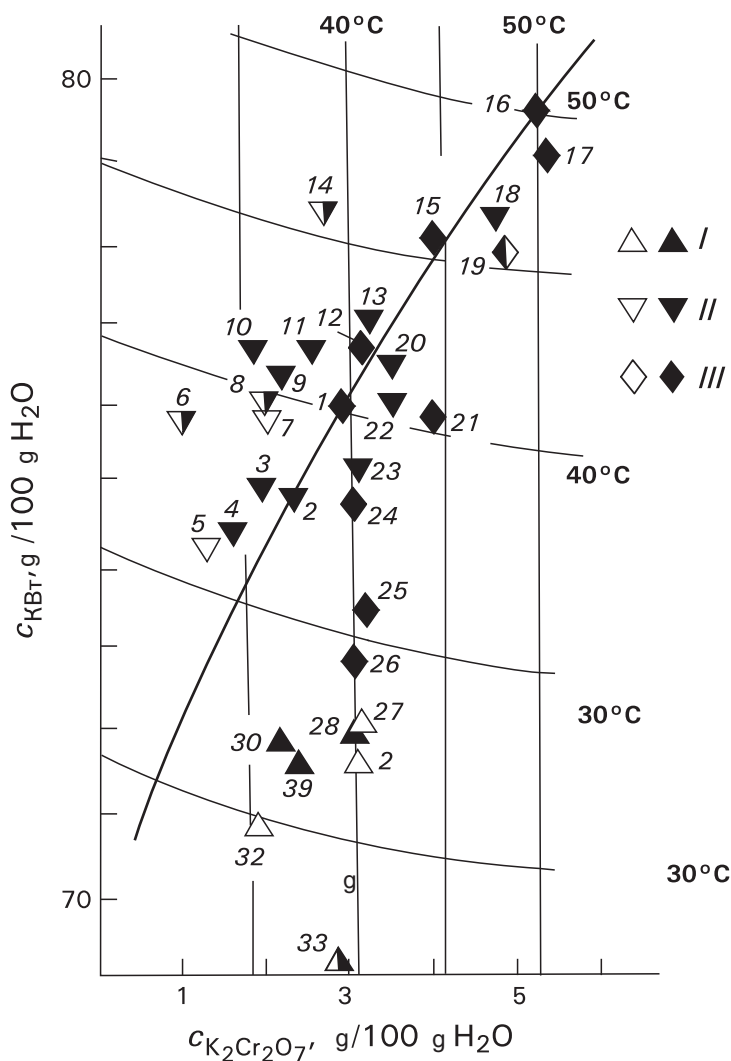
The state diagrams for  $K_2Cr_2O_7$ -KBr- $H_2O$  (grid in Fig. 6.2) and KCl-NaCl- $MgCl_2$ - $H_2O$  (see Fig. 2.8) were adjusted before commencing the experiments.

The experiments were conducted in the following manner. Saturation temperatures were measured with an accuracy of  $\pm 0.1^\circ\text{C}$  in solutions containing weighed amount of the components. Characteristics of  $K_2Cr_2O_7$ -KBr- $H_2O$  solutions were measured in 77 points in 33 solutions having various compositions; they are represented in Fig. 6.3. Conditions maintained in KCl-NaCl- $(MgCl_2)$ - $H_2O$  system corresponded to eutonic compositions in the neighborhood of  $40^\circ\text{C}$  and to supercooling degrees of 1.0 and  $2.0^\circ\text{C}$ ; contents of  $MgCl_2$  were varied in the range of 0–20 wt%. Various experimental solutions were either undersaturated (metasomatic replacement of substrate with precipitate) or supersaturated (joint growth of substrate and precipitate), or saturated (growth of precipitate on a stable substrate) in respect to the substrate composition. In respect to the phase undergoing precipitation, all solutions were always supersaturated.

A monocrystal substrate (separately grown crystals having the sizes up to 3–5 mm) was placed vertically in a thermostatically controlled cell (see Fig. 2.1).



**Fig. 6.2** Crystallochemical matching the nets  $\{010\}$  of  $K_2Cr_2O_7$  and  $\{100\}$  of KBr:  $K_2Cr_2O_7$ ; space group  $P1$ ,  $a = 7.52 \text{ \AA}$ ,  $b = 13.43 \text{ \AA}$ ,  $c = 7.39 \text{ \AA}$ ,  $\alpha = 98^\circ 00'$ ,  $\beta = 90^\circ 51'$ ,  $\gamma = 96^\circ 13'$ ; KBr: space group  $Fm\bar{3}m$ ,  $a = 7.10 \text{ \AA}$



**Fig. 6.3** Phase diagram of  $K_2Cr_2O_7$ -KBr- $H_2O$  system and compositions of test solutions: *thin lines* – solubility isotherms and their temperatures ( $^{\circ}C$ ), *bold line* – eutonic equilibrium curve. Substrates: *I* – KBr, *II* –  $K_2Cr_2O_7$ , *III* – KBr and  $K_2Cr_2O_7$  (*solid symbols* – growing substrate, *hollow symbols* – dissolving substrate; *half-hollow symbols* – both dissolving and growing substrate). *Crystallization temperatures of the solutions 1–33* ( $^{\circ}C$ ): 1–31.5, 33.5, 36.0, 36.5; 2–37.0; 3–35.1; 4–32.0, 34.0; 5–34.3; 6–32.0, 35.5, 37.0, 38.0; 7–37.6; 8–34.0, 34.4, 35.6, 37.3, 38.0, 38.3; 9–35.9; 10–34.6; 11–35.6, 38.0; 12–37.0, 37.5; 13–41.0; 14–38.1, 44.0; 15–41.2, 42.9, 44.5; 16–48.0; 17–46.3; 18–44.0; 19–41.0, 41.5, 42.5, 45.0, 46.2, 47.2; 20–35.8, 37.0, 38.0, 40.1; 21–37.7, 38.5; 22–37.5, 37.8, 40.1; 23–33.0, 35.0; 24–34.0, 36.0, 37.0; 25–34.5, 35.0; 26–30.6; 33.0; 27–34.5, 35.1, 36.3; 28–32.0; 29–34.0; 30–28.9, 30.0; 31–30.3, 31.0; 32–30.1; 33–24.1, 31.4

This position allowed preventing the crystals homogeneously nucleated in a bulk of the solution from dropping down onto the substrate. Both substances composing the pairs served as substrates and precipitates.

Temperature of  $K_2Cr_2O_7$ -KBr- $H_2O$  solutions was gradually lowered until precipitated matter became visible (eightfold magnification) on the substrates and then it was maintained constant for 15–20 min (the size of the precipitated crystals was about 0.1–1 mm). Solutions of KCl-NaCl-( $MgCl_2$ )- $H_2O$  were supercooled by 1.0 or 2.0°C; the residence times were 40–60 min. Then the samples were isolated, dried, and distribution of angles of deviation from the epitaxial direction was studied under an optical or electron microscope. Growth and dissolution rates were also measured in situ by means of an optical microscope under the above conditions according to movement of the {010} face for  $K_2Cr_2O_7$ , and the {100} faces for KBr, KCl, and NaCl. Growth rates of  $K_2Cr_2O_7$  and KBr were determined independently in different portions of the same solutions. In experiments with KCl and NaCl first the growth rates of the substrates had been measured, and after that, the partner-phase crystals were caused to precipitate on the substrates. Growth rates of the precipitating crystals were determined independently.

Histograms of orientation distribution were plotted for each experiment. The histogram step in each case was 2°. Deviation angles were measured in diapason 0–45°. Measurements in diapason 45–90° were not conducted, as it would result in mirrored distribution pattern. Distributions have maxima in the epitaxial direction; when the angle of deviation from the epitaxial direction increases, the number of oriented crystals diminishes until reaching the background line. Orientation degree was determined as the value of  $E = s(h - a)/nh$ , where  $s$  was a number of crystals occupying the peak domain down to the baseline,  $h$  – a number of epitaxially oriented crystals,  $a$  – the average background value,  $n$  – the total number of the grown crystals. The value  $E$  takes into account both a fraction  $(h - a)/n$  of the precisely oriented crystals, and the fraction  $s/n$  of crystals having various degrees of orientation. Complete disorientation ( $E = 0$ ) is shown as an absence of the maxima in the histograms and  $s = a = h$ ; precise orientation looks like a sharp maximum and absence of the background with  $a = 0$ ,  $s = h = n$ .

The most valuable data on orientation of adhered crystals were obtained in the experiments involving precipitation of the cleaved microfragments from a suspension of  $CaCO_3$  onto horizontal rhombohedral cleaved chips of calcite or onto growing faces of sodium nitrate rhombohedrons, which had almost similar structures (space group  $R\bar{3}c$ ; for  $CaCO_3$   $a_{th} = 6.42$ ,  $\alpha = 101^\circ 55'$ ; for  $NaNO_3$   $a_{th} = 6.49$ ,  $\alpha = 102^\circ 40'$ ). Calcite is insoluble, and, thus, its heterogeneous nucleation is impossible. Therefore, calcite is useful in the studies of crystal orientation in precipitates which exclusively adhere to the substrate. Precipitation onto a calcite substrate was conducted in suspensions prepared in different solvents (water, acetone, dioxane, etc.) at ambient temperature. Precipitation onto a sodium nitrate substrate was performed in aqueous suspensions of  $NaNO_3$  obtained by 3°C supercooling the corresponding aqueous solutions prepared at 35°C. The experiments were conducted in vigorously stirred media. The optimum consistence of the suspensions ( $\approx 0.02$  g/ml) ensuring smooth precipitation of sufficient amounts of separated and unsticking fragments was deter-

mined empirically. The fragment sizes ranged from 15 to 500  $\mu\text{m}$ ; the lesser fragments were observed to stick to each other. Duration of each test was about 40 min.

Orientation of the crystals with their rhombohedral faces stuck to the substrates was determined in the way, similar to that used for epitaxial determinations. Deviation angles were measured in diapason 0–50°. In determining the orientations of flat-cleaved chips of calcite it had to be taken into account that the chips situated in twin position in respect to each other appeared indistinguishable. In a particular case, the chips situated in epitaxial twinned position in respect to the substrate also cannot be distinguished. As the degree of preference of epitaxial position over the twinned one is unknown that makes any corrections impossible. The fraction of the crystals with their vertexes or edges stuck to the substrates was also determined.

Orientation of the crystals stuck to the substrates with their vertexes or edges was also studied in the experiments involving  $\text{K}_2\text{Cr}_2\text{O}_7$ –KBr and KCl–NaCl pairs, as it was supposed that this orientation was a result of the crystal adhesion to the substrate.

### 6.3 Epitaxial Regularities on a Growing or Dissolving Substrate

Growing on an unstable substrate is a common and likely to be the most frequently occurring natural manifestation of epitaxy.

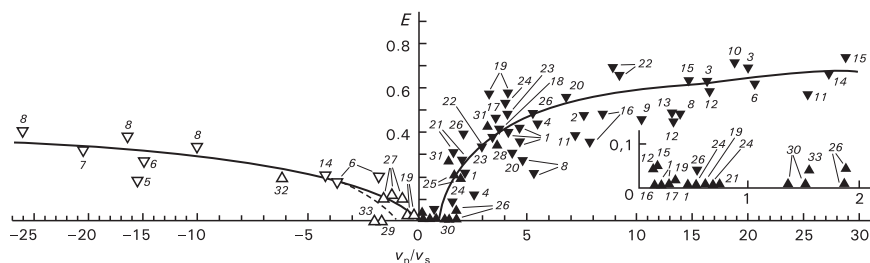
First of all, it should be emphasized that morphology of crystals precipitating from the solutions of  $\text{K}_2\text{Cr}_2\text{O}_7$ –KBr– $\text{H}_2\text{O}$  is, as a whole, similar to that of crystals growing from the mono-salt aqueous solutions.  $\text{K}_2\text{Cr}_2\text{O}_7$  forms rectangular (almost square) or octagonal flat plates flattened along the (010) monohedron and delimited by monohedrons of the [001] and [100], [101] and  $[\bar{1}01]$  zones or by their combination. Crystals of KBr always have the cubic faceting.<sup>3</sup>

When these crystals accrete with the structurally similar faces, i.e., (010) or (0 $\bar{1}0$ ) of  $\text{K}_2\text{Cr}_2\text{O}_7$  and (100) of KBr, they form *E* texture characterized by various degrees of orientation of the precipitated crystals in the plane of accretion.

In spite of a great spread of the experimental data, dependence of the turn value upon the growth rates of the precipitating crystals ( $v_p$ ) and the rates of growth or dissolution of the substrate crystals ( $v_s$ ) was rather distinct. If the substrate is growing (Fig. 6.4, the right wing), increasing  $v_p/v_s$  causes increase of *E* within the range 0–1, while *E* = 0 for  $0 < v_p/v_s < 1-2$ . If the substrate is dissolving (Fig. 6.4, the left wing), the dependence is similar, but has the less-sharp slope, and, according to the primal data (Glikin and Kaulina 1988), it intersects zero point of the coordinates.<sup>4</sup>

<sup>3</sup>In a ternary system the KBr crystals grow in the form of twins according to the fluorite law; twinned individuals are, as a rule, flattened up to tenths of a millimeter, while their size along the flattened face can exceed 10 mm.

<sup>4</sup>According to unpublished data obtained by Dr. Yu. V. Plotkina, the left wing of the curve also crosses the abscissa in the neighborhood of the point  $v_p/v_s = -1$  (dot line in Fig. 6.4). It does not principally affect the proposed model.



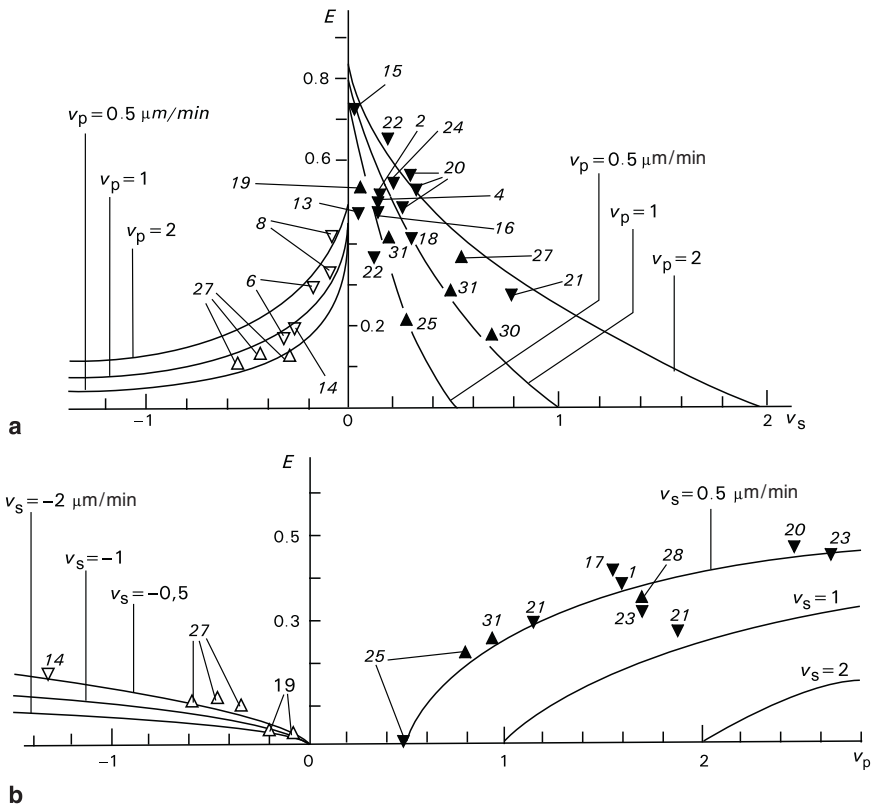
**Fig. 6.4** Dependence of the epitaxy degree (relative units) upon the ratio between the growth rate of the precipitate and the rate of growth and dissolution of the substrate  $v_p/v_s$  (the right and the left wings of the curve, respectively). The insert shows an enlarged portion near the coordinate origin

Effects of the substrate and the precipitating crystals in the above process can be expressed as dependences of  $E$  upon the absolute values of the growth and dissolution rates (Fig. 6.5). They are calculated from the averaged curves (Fig. 6.4) for values  $v_p$  and  $v_s$  equal to 0.5, 1.0, and 2.0  $\mu\text{m}/\text{min}$ , respectively. The experimental points  $v_p$  and  $v_s$  having the values, equal to 0.5, 1.0, and 2.0  $\mu\text{m}/\text{min} \pm 30\%$ , respectively, are marked on the curves. Majority of the points (54 out of 77) coincide with the theoretical curves within the accuracy limits that indicated independence of  $E$  on  $v_p$  and  $v_s$  when  $v_p/v_s = \text{constant}$ . Therefore, the main curves in Fig 6.5 unite the whole set of data regardless of the absolute values of the rates or the natures of the substrate and the precipitating substances.

Formation of a vertical texture  $V$  was observed (Fig. 6.6) in eight assays, and these results should be considered separately. The texture consists of the  $\text{K}_2\text{Cr}_2\text{O}_7$  plates aligned in perpendicular direction to the plane of the growing KBr substrate and disoriented in the plane of accretion. These assays belong to the experimental series with  $E = 0$  (see the dot congregation at the coordinate origin in the insert of Fig. 6.4). The texture  $V$  coexists in various proportions (from 0% to 100% of the total number of the accreted crystals) with the totally disoriented epitaxial texture ( $E = 0$ ). The value  $V$  abruptly increases with decrease of the  $v_p/v_s$  ratio and increase of absolute value of  $v_s$ ; at the same time, any distinct dependence upon the value of  $v_p$  was not detected (Fig. 6.7).

Comparison of the experimental results, having close values of  $v_p/v_s$ , but differing in presence or absence of the vertical texture is shown in Table 6.1. The left and right parts of the table designated as  $V > 0$  and  $V = 0\%$  correspond to the presence and absence of the texture. It can be seen that development of the texture depends upon the growth rate of the substrate. In all the cases the texture is developed at higher absolute values of the substrate growth rates (e.g.,  $V = 100\%$  at 3.260  $\mu\text{m}/\text{min}$ , while  $V = 0\%$  at 1.593 and 1.647  $\mu\text{m}/\text{min}$ ). Moreover, values  $V > 0\%$  are directly proportional to  $v_s$  and  $\Delta v_s$ .

In some experiments it was possible to observe formation of a vertical texture composed of cubic crystals of KBr aligned along the axis  $L_3$ , which was perpen-

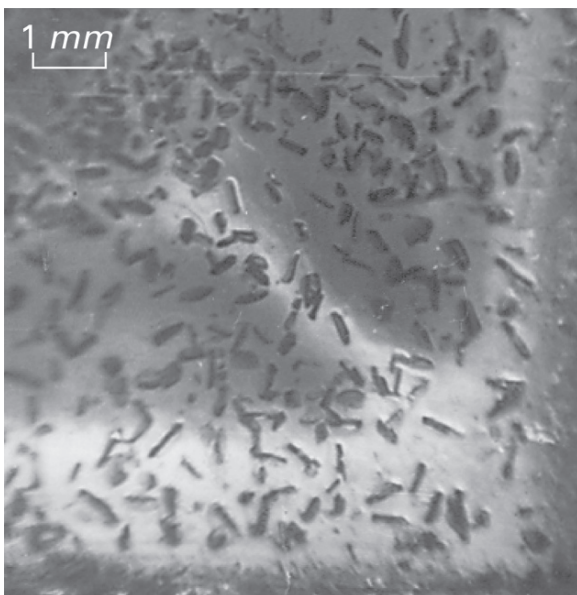


**Fig. 6.5** Dependence of the epitaxy degree upon the absolute values of the growth rates of substrate (a) and precipitate (b). The curves represent calculated dependences

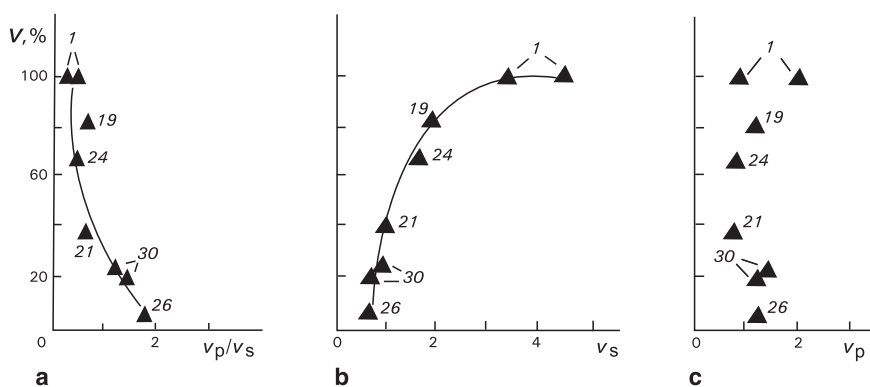
dicular to the growing substrate  $(010)_{\text{K}_2\text{Cr}_2\text{O}_7}$ . The relative amount of thus oriented crystals ranged from 0% to 100%. Unfortunately, a thorough examination of the texture has been precluded by scarcity of experimental data.

Regularities of accretion formation in the pair  $\text{KCl}-\text{NaCl}$  are qualitatively similar but differ in quantitative aspect. Under discussed conditions both the substances show cubic faceting.

Correlation between the crystal orientation and the process kinetics is shown in Fig. 6.8. In this case, like in the case of  $\text{K}_2\text{Cr}_2\text{O}_7-\text{KBr}$  (Fig. 6.4), all the data are plotted in one diagram regardless of the nature of substrate and precipitate, supercooling degree, and presence of  $\text{MgCl}_2$  in solution. It can be seen that crystals forming the epitaxial texture  $(100)_{\text{KCl}} \parallel (100)_{\text{NaCl}}$  are oriented in the plane of accretion in the vicinity of the  $[100]_{\text{KCl}} \parallel [100]_{\text{NaCl}}$ . Majority of the experimental epitaxy degrees fall within the following diapason:  $0.8 < E < 1$ , while the ratios between the growth rates of the precipitate and substrate crystals are as follows  $-3.5 < v_p/v_s < 5.5$ . In 12



**Fig. 6.6** Vertical texture of the flattened crystals of  $K_2Cr_2O_7$  on the KBr substrate



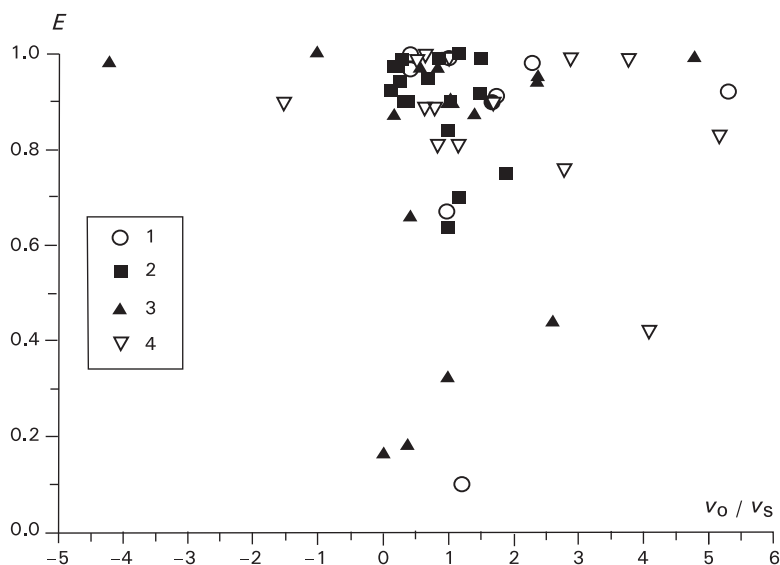
**Fig. 6.7** Dependence of relative amount  $V$  of crystals forming vertical textures upon the relative (a) and absolute (b, c) growth rates of substrate ( $v_s$ ) and precipitate ( $v_p$ )

assays out of 56 (21.5%) the orientation lowers to  $0.1 < E < 0.8$ , while the growth rate ratio for almost all the tests of this diapason falls within  $0 < v_p/v_s < 3$ .

The dependence depicted in Fig. 6.8 can be regarded as a rough estimation since the growth rates of the crystals were rather unstable (see Section 2.1.3) and data were obtained only for two values of supercooling. Nevertheless, the dots obtained allow to draw two wings of the curve originating from the vicinity of  $0 < v_p/v_s < 1$ , abruptly raising along the abscissa and sharply diverging at  $0.9 < E < 1.0$ . It can be

**Table 6.1** Absolute growth rates of  $K_2Cr_2O_7$  and  $KBr$  crystals ( $\mu\text{m}/\text{min}$ ) related to the existence of the vertical texture [ $v_s$  and  $v_s^0$  in the samples showing a vertical texture ( $V > 0\%$ ) and those without it ( $V = 0\%$ ) at close values of  $v_p/v_s$ ]

Solution	Temperature of the experiment ( $^{\circ}\text{C}$ )	Vertical texture presence			Solution	Temperature of the experiment ( $^{\circ}\text{C}$ )	Vertical texture absence			$\Delta v_p = v_p - v_p^0$
		$V$ (%)	$v_p/v_s$	$v_s$			$V$ (%)	$v_p/v_s$	$v_s^0$	
1	33.5	100	0.24	3.260	1	36.5	0	0.21	1.647	1.613
1	33.5	100	0.24	3.260	17	46.3	—	0.26	1.593	1.667
24	34.0	69	0.52	1.654	33	24.1	—	0.51	1.308	0.346
21	38.5	40	0.69	1.066	24	36.0	—	0.69	0.748	0.318
30	30.0	21	1.67	0.752	31	30.3	—	1.66	0.531	0.221



**Fig. 6.8** Dependence of epitaxy perfection  $E$  in the pair  $KCl$ – $NaCl$  upon the ratio  $v_p/v_s$  between the growth rates of precipitate and substrate: 1, 2 – the  $KCl$  substrate; 3, 4 – the  $NaCl$  substrate; 1, 3 –  $\Delta T = 1^{\circ}\text{C}$ ; 2, 4 –  $\Delta T = 2^{\circ}\text{C}$

seen that a vertical section of the curve is shifted toward the positive  $v_p/v_s$  values by about a unity (probably the left wing, responsible for the substrate dissolution, practically merges with the abscissa, and the right wing is located at some distance from it). If this assumption is taken as a working hypothesis, dependencies of  $E$  upon  $v_p/v_s$  will be analogous for both the investigated pairs, including asymmetry of the plots in respect to the abscissa. The only differences are the sharpness of the slopes in the proximity of the curve origin and the maxima of  $E$ .

A vertical texture of  $KCl$ – $NaCl$  pair was observed in majority of the experiments; it consisted of cubic crystals oriented with their axis  $L_3$  in nearly perpendicular direction to the substrate. The proportion of thus oriented crystals did not exceed 10%.



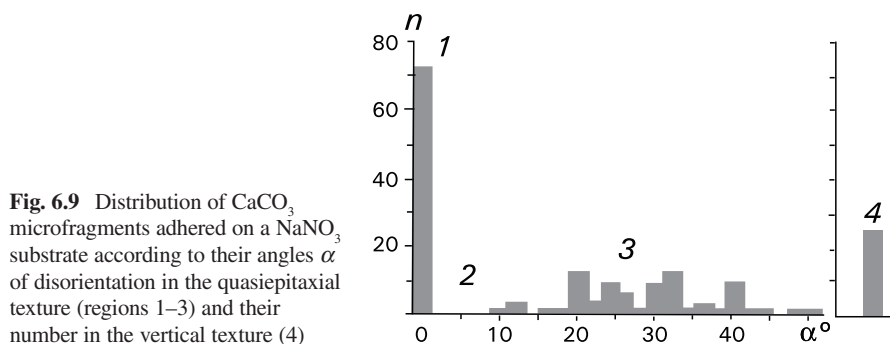
## 6.4 Regularities of Orientation of $\text{CaCO}_3$ Microcrystals Adhered to a Substrate

Microfragments of  $\text{CaCO}_3$  precipitating onto a growing  $\text{NaNO}_3$  rhombohedron adhere to it with their rhombohedron faces (quasiepitaxial texture composed of flattened crystals with the size ratios falling within the following range: 1.3:1.3:1–3:3:1) or with their edges or vertexes (vertical texture) stuck to the substrate as a result of adhesion. In contrast to the epitaxial texture formed by  $\text{NaNO}_3$  on  $\text{CaCO}_3$ , which is characterized by  $E = 1$  (Fig. 6.1a), orientation of studied  $\text{CaCO}_3$  crystals falls within the following diapason:  $0.1 < E < 0.7$ .

Distribution of crystals by the angles of disorientation in the quasiepitaxial texture calculated for one of the substrates is rather bizarre (Fig. 6.9). Three angle regions can be discerned in the diagram. The region 1 comprises 72 crystals (40%) having a thickness of about  $15\mu\text{m}$  (some of them have the thickness up to  $40\text{--}50\mu\text{m}$ ) and a quasiepitaxial orientation with  $\alpha = 0\text{--}2^\circ$ . The region 2 occupying the range  $2^\circ < \alpha < 10^\circ$  does not correspond to any crystals. The region 3 including 86 crystals (46%) having a thickness of about  $30\text{--}90\mu\text{m}$  (with predomination of those having the thickness up to  $60\text{--}70\mu\text{m}$ ) is characterized by a uniform or normal distribution with  $10^\circ < \alpha < 50^\circ$ .

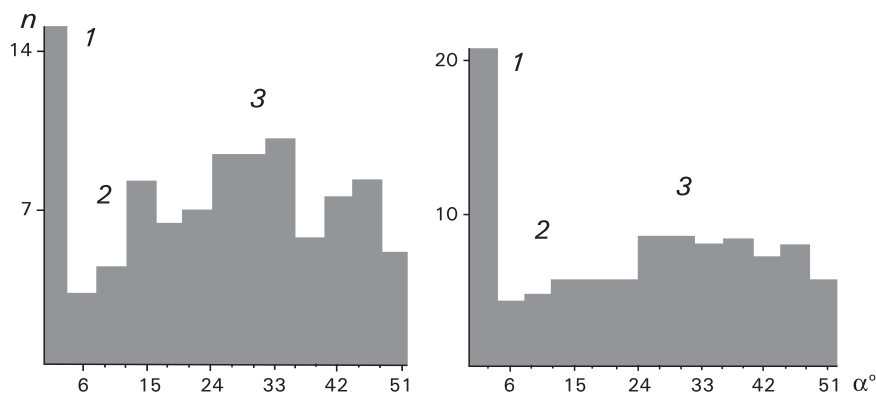
The remaining 26 crystals (14% with the sizes of about  $120\mu\text{m}$  or more) belong to the vertical texture corresponding to the region 4. Here, rhombohedron cleavage microfragments having isometric habits ( $\approx 1:1:1$ ) are fixed on the substrate with their vertexes, their  $L_3$  axes being perpendicular to the substrate. The fraction of thus oriented crystals in the vertical texture is about 86%. Microfragments having a prismatic habit ( $\approx 1:1:1.3\text{--}1:1:2$ ) are fixed on the substrate at their elongated edges. Their proportion is about 14%.

Calcite microfragments adhered to the cleavage surface of the calcite substrate with their rhombohedron surfaces are oriented in a similar manner (Fig. 6.10).<sup>5</sup> There, three angle regions can be distinguished. The region 1 corresponds to an epitaxial



**Fig. 6.9** Distribution of  $\text{CaCO}_3$  microfragments adhered on a  $\text{NaNO}_3$  substrate according to their angles  $\alpha$  of disorientation in the quasiepitaxial texture (regions 1–3) and their number in the vertical texture (4)

<sup>5</sup>A detailed report is being prepared for publication.



**Fig. 6.10** Distribution of calcite microfragments adhered onto a calcite substrate during precipitation from an acetone (a) and aqueous (b) suspension according to their disorientation angles  $\alpha$

orientation with  $\alpha = 0-2^\circ$ . The region 2 is characterized by the minimal content of the crystals,  $4^\circ < \alpha < 12^\circ$ . The region 3 is characterized by a uniform or normal distribution with  $12^\circ < \alpha < 50^\circ$ . The above peculiarities are more clearly seen in the texture precipitated from a less-viscous suspension in acetone (Fig. 6.10a).

## 6.5 Model of Formation of Epitaxial and Quasiepitaxial Textures

Experiments showed that epitaxial phenomena are more diversified than those concerning oriented accretions of crystals induced by crystallochemical factors. The most important epitaxial phenomena include disorientation of crystals under the action of kinetic processes and their orientation caused by adhesion interaction assisted by electrostatic forces.

Disorientating kinetic effects are observed, first of all, in the epitaxial textures. They can be described as a single two-stage process.

The first stage includes a heterogeneous epitaxial nucleation of the precipitating individuals on the substrate in accordance with the crystallochemical model. Preference of crystallographic orientation of a nucleus over a random orientation is ensured by a less work of the oriented nucleation (Chernov 1984). Structures of the accreting surfaces of the experimental pairs described above agree with generally accepted criteria. Compounds of the pair  $K_2Cr_2O_7$ -KBr have the same cation, but essentially different anions. Nevertheless, in the plane of accretion these anions have close sizes, and accreting planes  $(010)_{K_2Cr_2O_7}$  and  $(100)_{KBr}$  have similar structural configurations, i.e., distorted and regular square nets, respectively, composed

of the same alternating patterns of cations and anions, the difference in translations being about 14% (Fig. 6.2). Compounds of KCl–NaCl pair also have ionic nature and have the same anion and similar cations. Their crystallochemical similarity is proved by isomorphism observed at high temperatures. The accreting planes {100} have structurally similar nets made up by the same alternating patterns of cations and anions, the difference in translations being about 11%. These data prove a great structural similarity of compounds in pair KCl–NaCl.

The second stage involves a mechanical turning of the nuclei (or microcrystals) into random positions due to the movement of the growing substrate layers and those of the nuclei. This process caused by action of crystallization pressure developed in front of a growth step. The turn can be accomplished either due to nonuniform incursion of the substrate growth layers upon a nucleus or owing to self-repulsion of the nucleus growth layers from the substrate rough parts.

Epitaxy in a series of compounds with gradually increasing structural dissimilarity in respect to a particular substrate is also gradually worsening when these compounds are grown on that substrate. For example, this regularity can be observed in the series of alkali halides precipitating onto fluorite (Krastanov and Stranski 1938; Kleber et al. 1967). The regularity cannot be explained by the conventional crystallochemical model, as in the example cited the substances possess similar chemical bonds and all of them form strong bonding with the substrates. The possible explanation is an increasing efficiency of the nuclei self-repulsion and lessening of the adhesion between the crystals and the substrates in the series.

If the substrate is dissolving, its growth layers cannot move the nuclei, but self-repulsion of the lateral and underlying layers growing on the accreting surface still continues to act during the nucleus growth, as the surface of the substrate under a growing nucleus recedes. The nuclei can also drop onto the dissolving substrate and repeat the process of bonding formation in a manner similar to that observed for homogeneous nucleation (see below).

The ideas discussed above can assist in interpretation of quantitative correlations shown in Figs. 6.4 and 6.5. It is obvious that an adhesion between a nucleus and substrate resisting the turn of the former during growth or dissolution of the substrate is directly proportional to the area of accretion, i.e., the size of the nucleus. When the rates of the precipitate growth  $v_p$  are sufficiently high and the rates of the substrate growth  $v_s$  are sufficiently low, the nuclei, which have been nucleated in the oriented positions, have enough time to reach considerable sizes and form a strong attachment to the substrate before the beginning of incursion of the growing substrate layers. This results in a low mobility of the precipitating crystals and a high perfection of epitaxy. The reversed correlations result in a great mobility of the precipitating crystals and the absence of epitaxy. Different slopes of the dependencies of  $E$  versus  $v_s$  and  $v_p$  (Figs. 6.5a, b) indicate a higher sensitivity of the precipitate orientation to the substrate growth in comparison to self-repulsion effect; this can be explained by a smaller tangential constituent of self-repulsion created by growth layers of the nucleus as they are thinner than the growth layers of the substrate.

If substrate dissolves, disorienting action of the both phases increases (Figs. 6.5a, b). The precipitate plays a greater role in this case that can be seen in Fig. 6.4,

as  $E$  values in its left part are smaller than those in the right. On the one hand, this can be accounted for by increasing self-repulsion of the nuclei due to involving the layers located on their accretion surface, which becomes free as the substrate dissolves. Tangential growth component exerted by these layers is great and their growth rates also increase due to salting-out influence of the dissolving substrate. On the other hand, falls of the nuclei caused by dissolution of the substrate also make their contribution into the nuclei mobility.

Degree of epitaxy in  $K_2Cr_2O_7$ -KBr pair reaches  $E \approx 0.7$ . Curves depicted in Figs. 6.4 and 6.5a, b show that the extreme case  $E = 1$  corresponds to either a known phenomenon of the stable substrate ( $v_s = 0$ ), or to the theoretical assumption  $v_p \gg v_s$ . The latter is unlikely to be attained in the system in question even at the rate  $v_s = 0.1 \mu\text{m}/\text{min}$  due to inevitable mass crystallization, as the required growth rates of the precipitating crystals correspond to supersaturations, which are situated in the domain of an unstable solution.

On the contrary,  $E \approx 1$  is attained in KCl-NaCl pair when  $v_p/v_s$  ratio is close to 0 (Fig. 6.8). The dependence, as it has been mentioned before, is likely to be represented by two wings, similar to those plotted for  $K_2Cr_2O_7$ -KBr, but having a much sharper slope. In such a case the dependence should be interpreted in accordance with the two-stage crystallogenic process involving oriented heterogeneous nucleation followed by disorientation of the growing nuclei. The difference between the  $K_2Cr_2O_7$ -KBr and KCl-NaCl epitaxy is surely a result of the stronger crystal-chemical similarity between the members of the latter pair.

Bonding a nucleus to a substrate is obviously stronger if the structural similarity between the nucleus and the substrate is greater. Thus, considering autoepitaxy (maximum structural similarity), it can be said that the orientation is almost perfect even when the system undergoes intensive mutual growth-dissolution; it was observed as formation of monocrystalline pseudomorphs (Glikin and Sinai 1983; Kryuchkova et al. 2002). In the series of alkali halides with gradually lessening structural similarity, epitaxy on a stable fluorite substrate is also worsening (Krastanov and Stranski 1938; Kleber et al. 1967). Worse epitaxy in  $K_2Cr_2O_7$ -KBr pair in comparison with that of KCl-NaCl also proves the supposition of the structural similarity defining the epitaxy degree. Nevertheless, it should be reminded that this regularity is observed only if the bonding between the substrate and the precipitate is sufficiently strong and nucleation proceeds according to the Frank-Van der Merwe mechanism, while if the bonding is weak, the mechanism is that of Volmer-Weber, and correlation can appear to be reversed (Chernov 1984).

The concept of crystal disorientation in the course of their growth described above for epitaxial structures can be also realized in quasiepitaxial processes (see below). However, if in the former process there is a natural reference mark of epitaxial orientation allowing to evaluate the contributions of various disorienting factors, in the latter processes the crystals have initial disorientation and this reference mark is absent. Thus, adhesion of  $CaCO_3$  on the growing  $NaNO_3$  substrate with the growth rate ranging from 3.8 to 4.7  $\mu\text{m}/\text{min}$  is possibly accompanied by additional disorienting influence of the substrate growth layers upon the crystals.

The other phenomena of oriented growth observed by us are not directly related to crystallochemical similarity between the precipitate and substrate and can be referred to as quasiepitaxial. The main idea consists in adhesion of crystalline particles suspended in a liquid (homogeneously nucleated particles of suspension microcrystals). In the course of their attachment to the substrate, they are turned to acquire an optimal position due to interacting anisotropic electrostatic fields caused by the substrate and the precipitating crystals (i.e., due to so-called long-range forces).

The best illustration of the long-range force influence is orientation of calcite microfragments. In this case, as it was mentioned above, heterogeneous nucleation is impossible and a stable space orientation of crystals in the solution under a vigorous stirring is also hardly possible.

Predominating epitaxial orientation (angle region 1,  $\alpha \approx 0$ ) of flattened microfragments adhering with their rhombohedral faces to the isostructural surfaces of calcite and sodium nitrate can be distinctly seen in Figs. 6.9 and 6.10. The only probable explanation of this orientation is turning the adhering particle under the action of long-range forces. The most important additional evidence proving such interpretation is the region 2 in Figs. 6.9 and 6.10 characterized by the absence or a decreased amount of microfragments. Depletion of these regions is accounted for by turning the microfragments having a slight deviation from the epitaxial direction during their attachment to the substrate to acquire the epitaxial position. Obviously, efficiency of the turning should increase in less viscous acetone medium in comparison to that in aqueous medium, and such a tendency, however weak, was observed experimentally (Fig. 6.10).

It is to be noted that data shown in Figs. 6.9 and 6.10 are direct and unambiguous experimental proof of influence of the long-range forces.

It is obvious that such a process does not require a structural similarity between the interacting crystals, having been defined by anisotropy of the long-range forces. This concept at least partially allows to solve the long-discussed problem of a regular orientation of structurally dissimilar crystals (Pashley 1965; Chernov 1984; and others). The concept also offers an explanation for graphoepitaxy, i.e., orientation of crystals on a substrate, which has an artificially created regular relief (Sheftal et al. 1977; and others).

Another illustration of the long-range force influence is formation of vertical textures involving a selective orientation of elongated calcite crystals that cause their adhesion along the edges, and that of the isometric crystals, which get attached with their vertexes. The other vertical textures observed seem to have the same morphological origin and also have adhesion nature. These structures include, among the others, the textures described above for NaCl–KCl and  $K_2Cr_2O_7$ –KBr.<sup>6</sup>

---

<sup>6</sup>Earlier it was supposed (Glikin and Kaulina 1988) that formation of the vertical texture of  $K_2Cr_2O_7$ –KBr (Fig. 6.6) proceeded as follows: a flat nucleus under compression action of rapidly and forcefully approaching layers, which surround it, becomes detached from the substrate and oriented along the direction, perpendicular to that of the layer movement, similar to an object compressed by pincers. This modification of a quasiepitaxial process can be realized in some cases, but total vertical arrangement seems to be highly improbable under such conditions.

For the first time such textures were discovered and identified as a result of electrostatic interaction as early as a half a century ago, when investigating deposition of NaCl crystals from aqueous salt solutions onto various metal and amorphous (glass, plastics) substrates, as well as in natural fluorite aggregates (Stulov 1939, 1954). These textures were investigated among the other epitaxial and quasiepitaxial phenomena in our experiments that allowed a considerable elaboration of the concept of vertical structure formation.

It is to be noted that the problem of vertical texture formation has not been solved completely as the reason for crystal stability in a vertical position is still not clear. At present it is assumed that attraction forces exerted by different surfaces of a crystal are balanced. For example, isometric calcite fragments attached with their vertexes must have attraction forces developed by the three rhombohedral faces balanced, and prismatic fragments attached with their edges must have attraction forces exerted by two rhombohedral faces balanced, while flat fragments are attached with their biggest surfaces. However, such interpretation can hardly be considered as satisfactory. Thus, flat calcite microfragments are oriented in parallel to a substrate, while flat microfragments of  $K_2Cr_2O_7$  are oriented in perpendicular to that. It can be supposed that there exists a complex equilibrium between the attraction and repulsion forces, which can be induced by nonuniformities of a double electric layer surrounding both the substrate and the precipitating crystal.

The experimental data and their interpretations described above allow a new approach to the phenomena, which is usually considered as epitaxial exclusively from the crystallochemical point of view. The perspectives of its use can be correctly evaluated only in the course of thorough simulative investigations of correlative factors guiding orientation and disorientation of the accretive crystals, as well as effects of temperature and other parameters of the media. Nevertheless, with the state of the art it is possible to study a mutual orientation influence of epitaxial pairs, which can provide with valuable information about processes of nucleation and spatiotemporal changes in relative growth-dissolution rates. Discovering such structures can be done in accordance with a proposed method (Panov 1983, 1987), while the quantifications can be performed using the method described above.

Mechanisms of growth and dissolution of crystals, adhesion, and electrostatic interaction are not affected by thermodynamic conditions. The exemplary substances were arbitrary chosen and, so, there are no grounds to consider them special. Therefore, discovered regularities should be unaffected, at least qualitatively, by the nature of crystals and media (magma, hydrothermal solution, gaseous emanations, etc.) or the driving forces. In the other words, the regularities must be observed in the courses of both direct crystallization of accreting epitaxial minerals and their precipitation induced by metasomatic replacement.

## References

- Bauer E (1956) Über Orientierungserscheinungen beim Kristallwachstum fern vom Phasengleichgewicht. *Zs Krist* 107:4:290–317

- Behrndt KH (1963) Influence of the deposition conditions on growth and structure of evaporated films. *Vacuum* 13:9:337–347
- Chernov AA (1984) Processes of crystallization. In: Vainshtein BK, Chernov AA, Shuvalov LA (eds) *Modern crystallography III*. Crystal Growth. Springer, Berlin
- Deicha G (1947) Epitaxie du chlorure de potassium sur les micas (orientation suivant les faces du cube). *Bull Soc Franc Miner Crist* 70:1–6:318–324
- Distler GI (1968) Actual structure, activity and long-range interaction of crystal surfaces. In: Sheftal NN (ed) *Growth of crystals 8*. Nauka, Moscow (Russ.)
- Distler GI (1975) Crystallization as a matrix replicative process. In: Chernov AA, Bagdasarov KhS, Givargizov EI (eds) *Growth of crystals XI*. Erevan University, Erevan (Russ.)
- Frank-Kamenetskii VA (1964) Nature of structural admixtures and inclusions in minerals. Leningrad State University, Leningrad (Russ.)
- Futergendler SI, Frank-Kamenetskii VA (1961) Oriented accretions of olivine, garnet and chrome-spinelide in diamonds. *Zapiski Vsesoyuz Miner Obsh* 2:230–236 (Russ.)
- Gaidamako IA, Treivus EB, Kamentsev IE (1983) Effect of epitaxial substrate on the crystal growth rate of ammonium iodide. *Kristallografia* 1:200–202
- Gebhardt M, Neuhaus A (1972) *Epitaxie-daten anorganische und organische Kristalle*. Springer. Heidelberg/New York (Landolt-Börnstein. Neue Ser III: 8)
- Givargizov EI, Bagdasarov KhS, Kuznetsov VA, et al. (1984) Growing of crystals. In: Vainshtein BK, Chernov AA, Shuvalov LA (eds) *Modern Crystallography III*. Crystal Growth. Springer, Berlin
- Glikin AE, Kaulina TV (1988) Kinetic model of epitaxial growth of crystals *Zapiski Vsesoyuz Miner Obsh* 5:609–615 (Russ.)
- Glikin A, Plotkina J (1999) Disorientation effects of epitaxy at aqueous media. *Materials Structure*. *Bull. Czech Slovak Cryst Assoc* 6:2:155–158
- Glikin AE, Sinai MYu (1983) Experimental genetic study of monocystal pseudomorphs. *Zapiski Vsesoyuz Miner Obsh* 6:742–748 (Russ.)
- Glikin AE, Grunskii OS, Kaulina TV et al. (1988) Crystallogenic aspect of experimental mineralogy. In: Zharikov VA (ed) *Experiment in mineralogy*. Nauka, Moscow (Russ.)
- Grigor'ev DP (1945) Regular accretions of samarskite and columbite of the Ilmen' Mountains. *Zapiski Vsesoyuz Miner Obsh* 1:57–61 (Russ.)
- Grigor'ev DP, Shafranovskii II (1946) Epitaxial growth of quartz on feldspar. *Zapiski Vsesoyuz Miner Obsh* 4:265–272 (Russ.)
- Haag M, Dabringhaus H (1997a) Epitaxial growth of alkaline earth fluorides on the (001) surface of lithium fluoride I. The system  $MgF_2/LiF_{(001)}$ . *J Cryst Growth* 178:287–297
- Haag M, Dabringhaus H (1997b) Epitaxial growth of alkaline earth fluorides on the (001) surface of lithium fluoride II. The system  $CaF_2/LiF_{(001)}$ . *J Cryst Growth* 178:298–309
- Haag M, Dabringhaus H (1997c) Epitaxial growth of alkaline earth fluorides on the (001) surface of lithium fluoride III. The system  $BaF_2/LiF_{(001)}$  – epitaxial growth of  $LiBaF_3$ . *J Cryst Growth* 179:477–487
- Hurle DTJ (ed) (1994) *Handbook of crystal growth 3*. North-Holland/Elsevier, Amsterdam
- Kamentsev IE (1956) Aspects of oriented crystallization of potassium iodide and bromide on muscovite. *Kristallografiya* 1:2:240–243 (Russ.)
- Kleber W (1958) Über Adsorption und Epitaxie. *Fortschr Miner* 36:1:38–51
- Kleber W, Mietz I (1963) Über den Einfluss der Oberflächen Realstruktur auf die Keimbildung bei der Epitaxie. *Akad. Verlag, Berlin*
- Kleber W, Ickert L, Ahrens E (1967) Ein Beitrag zur Epitaxie von Alkalihalogeniden auf Calcium und Bariumfluorid. *Krist. und Techn* 2:1:47–54
- Krastanov L, Stranski I (1938) Über die Kristallisation von Alkalihalogenidkristallen auf Fluorit. *Zs. Krist Bd* 99:5:444–451
- Kryuchkova LYu, Glikin AE, Voloshin AE et al. (2002) Kinetic and morphological phenomena of growth and isomorphic replacement of mixed crystals in solutions (in the series  $(Co,Ni)(NH_4)_2(SO_4)_2 \cdot 6H_2O$ ). *Zapiski Vsesoyuz Miner Obsh* 3:62–77 (Russ.)
- Mügge O (1903) Die segelmassigen Verwachsungen von Mineral verschiedener Art. *Neues Jb Miner* 16:1–335

- Neuhaus A (1952) Orientierte Substanzabscheidung (Epitaxie). *Fortschr Miner* 29–30:2:136–296
- Novgorodova MI (1977) Epitaxial accretions of pyrite crystals on chalcopyrite crystals. *Zapiski Vsesoyuz Miner Obsh* 1:99–102 (Russ.)
- Palatnik LS, Papirova IP (1964) Oriented crystallization. *Metallurgia*, Moscow (Russ.)
- Palatnik LS, Papirova IP (1971) Epitaxial films. *Nauka*, Moscow (Russ.)
- Panov EN (1983) On accretions of magnetite and acidic plagioclase in granitoids. *Zapiski Vsesoyuz Miner Obsh* 5:573–577 (Russ.)
- Panov EN (1987) On accretions of magnetite and hornblende in granitoids. *Zapiski Vsesoyuz Miner Obsh* 6:702–705 (Russ.)
- Pashley DW (1952) Oriented deposits on crystalline substrates. *Proc Phys Soc* A65:33
- Pashley DW (1965) The nucleation, growth, structure and epitaxy of thin surface films. *Adv Phys* 14:55:327–416
- Pina CM, Fernandez-Diaz L, Lopes-Garsia, J et al. (1995) Growth of  $\beta$ -LiNaSO<sub>4</sub> and Li<sub>2</sub>SO<sub>4</sub>·H<sub>2</sub>O: epitaxy and intergrowth phenomena. *J Cryst Growth* 148:283–288
- Ramdohr P (1955) *Die Erzminerale und ihre Verwachsungen*. Akad. Verlag, Berlin.
- Royer L (1928) Recherches experimentales sur l'epitaxie on orientation mutuelle des cristaux des especes differentes. *Bull Soc Franc Miner* 51:77–159
- Rudenko SA, Rudenko SS, Ivanov MA (1975) Attempt of genetic-geometrical classification of mineral aggregates. *Zapiski Vsesoyuz Miner Obsh* 2:129–144 (Russ.)
- Schneider HG, Ruth V (1976) Advances in epitaxy and endotaxy. *Acad. Kiado*, Budapest
- Sheftal NN, Klykov VI, Sheftal RN (1977) Oriented crystallization on amorphous and polycrystalline substrates (artificial epitaxy). In: NV Belov (ed) *Processes of real crystal formation*. Nauka, Moscow (Russ.)
- Simanovskii AA (1965) Mechanism of an epitaxial growth on the orienting and non-orienting substrates. In: Sheftal NN (ed) *Growth of crystals VI*. Nauka, Moscow (Russ.)
- Stulov NN (1939) Oriented crystallization of NaCl. *Zhurn Experim Techn Phys* 9:5:630–633 (Russ.)
- Stulov NN (1954) About orienting influence of electric charges upon crystallization. *Zapiski Vsesoyuz Miner Obsh* 3:241–242 (Russ.)
- Vultee I (1952) Die orientierten Verwachsungen der Mineralen. *Fortschr Miner* 29–30:2:297–378
- Wulff G (1908) Über die Kristallisation des Kaliumjodids auf dem Glimmer. *Zs Krist* 45:4:335–345
- Wyckoff R (1965) *Crystal structures* 1. Wiley, New York/London/Sydney
- Yanulov KP (1948) On the law of limits for epitaxial accretions. *Doklady Acad Sci USSR* 62:6:813–814 (Russ.)
- Yanulov KP (1958) Isomorphism and epitaxial accretions. *Doklady Acad Sci Tadjik SSR. Natural Sci Branch* 2:41–51 (Russ.)
- Zhabin AG (1979) *Ontogeny of minerals: aggregates*. Nauka, Moscow (Russ.)



## Chapter 7

# Crystal Faceting

The concept of polymineral-metasomatic crystallogenesis discussed above allows to state that sub-elemental phenomena limited by growth or dissolving domains are universal for all variety of crystallization conditions in solutions. They manifest themselves in crystal nucleation, formation of stepped surface relief, faceting the growing individuals, and rounding the crystals in the course of dissolution. These phenomena do not depend on the technique for presetting the driving force, whether it is a change in temperature, pressure or concentration of the solution, or chemical reactions including metasomatic salting-out and salting-in reactions, etc. Crystal faceting is widely used for genetic reconstructions, though usually without contemplating any supporting theoretical or experimental basis. Reported data do not cover the matter completely and systematically; and some research and development works of the latest decades eluded the attention of both mineralogists and crystallographers. A sketch of the problem is presented below.<sup>1</sup>

### 7.1 Stationary Forms of Faceting

Faceting is one of the most prominent properties of minerals. It has been traditionally investigated since the seventeenth century to reveal mineral typomorphic properties, discover mechanisms of crystal formation, and optimize crystal-growth conditions. Investigation of faceting can be divided into several successively emerging branches, which have been evolving in parallel until now. Evolution of the most common views to consider these phenomena is marked by search of universal crystal-structural attributes of morphogenesis. Such models can vary in simplification degree, but limitations imposed on each model are usually too strict and, as a

---

<sup>1</sup> See also a previous review (Glikin et al 2002). It is to be noted that this chapter mainly contains works determining the stages of development in this field as well as presenting some important discussions and comments; it does not pretend to be a complete review.

rule, genetically uninformative, which has not been taken into consideration (Glikin 1978; Glikin and Glazov 1979). An alternative approach consists in analyzing the multivalued morphogenetic diversity arising from atomic–molecular interaction between a crystal and a medium, which is specific for particular substances and conditions. Prolonged discussion on the subject (Glikin and Glazov 1979, 1983; Shafranovskii 1981; Glazov and Glikin 1981, 1983; Evzikova 1983, 1984; Frank-Kamenetskii et al. 1987) indicates preference of simplified structural models over the complex crystal-genetic ones. The reasons for that are outlined in Conclusion of the present monograph (see also Glikin 1995).

The earliest primary concepts of crystal morphology theory were proposed by I. Kepler (in 1611), M. V. Lomonosov (in 1750), and R.-J. Haüy (in 1801). The concepts were generalized in “diminution theory” (Haüy 1801; Shafranovskii 1968) explaining appearance of different faces in crystals having the same atomic structure. In fact, it was a first attempt to find a correlation between the faces and the flat nets, which had not been invented by that time.

Next (in time and according to a degree of generalization) a “structural-geometric” approach was developed (Bravais 1866; Friedel 1904; Donnay and Harker 1937; Evzikova 1965). It was based upon quantitative assessment of significance of crystal forms expressed as a direct function of their reticular density. An initial indication that such a tendency, however complicated by numerous complementary factors, may exist (Bravais 1866) was subsequently absolutized as a unique dependence known as “Bravais Law” (Friedel 1904; and others). Later on, due to serious discrepancies existing between the law and reality, the attempts to find a universal form and physical sense of that hypothetical interrelation have been made. The best-known propositions are as follows. The first one consists in modifying the theoretical succession of face densities by means of transition from Bravais lattice to regular point systems (Donnay and Harker 1937). The other proposition is postulating the role of one of the medium parameters as a universal regulator of face significance, i.e., “activity” of the crystal components in the medium (Wells 1946a; Shafranovskii 1957) or supersaturation (Evsikova 1965, 1984). This concept was used for genetic interpretations of faceting in such minerals as fluorite, sphalerite, garnet, and cassiterite (Wells 1946a; Shafranovskii 1957; Yaroshevskii 1959; Gendeleev 1963; Evzikova 1984; and others). However, those attempts have not produced and could not produce (Tatarskii 1967; Glikin and Glazov 1979; Treivus 1986) a beneficial effect.

This conclusion is a special case of a more general principle of impossibility to use a single parameter of a multivariable process for unification of the participating system behavior. Similarly, several of other widespread concepts were disputed, including order of mineral crystallization (Dolivo-Dobrovolskii 1968, 1973; Petrov 1977), “corresponding” habits of different minerals (Treivus 1986), and optimal orientation of grain boundaries in rocks (Treivus 1989).

Later, J. Gibbs (in 1892), G. Wulff (in 1898), I. Stranskii (in 1932), P. Hartman (in 1955), N. Cabrera (in 1956), etc., developed a thermodynamic concept of correlation between increasing significance of a face and the face-surface

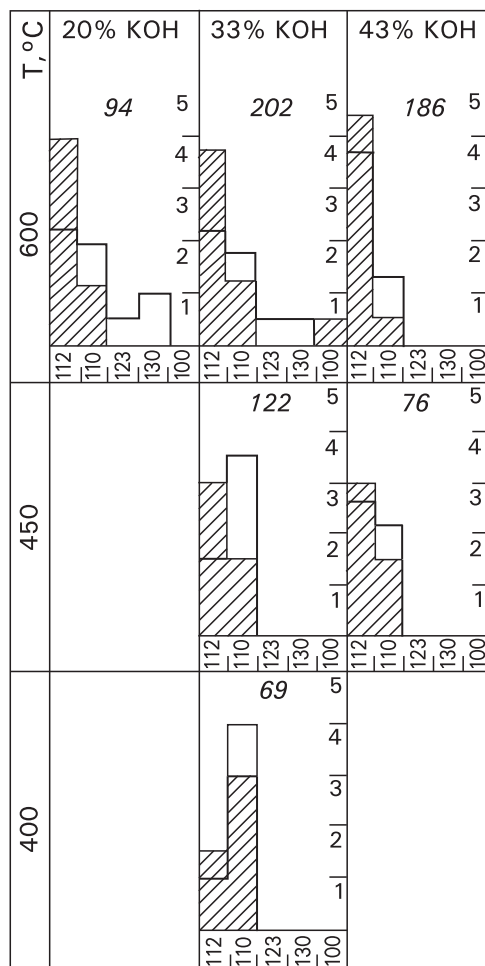
energy, thus, taking into account influence of medium and conditions upon crystal faceting. Polar diagrams of surface energy with selected singular orientations are well-known. Also known is structural division of crystal faces into flat faces  $F$ , which form stationary crystal habits, and unstable rough faces  $S$  and  $K$  (Hartman and Perdok 1955a, b, 1956; Honigman 1958; Hartman 1963; Chernov 1984). However, none of the methods for determination of stable faces – singular, or  $F$ -faces – in complex systems has been developed yet. The role of medium in the above concepts is limited by abstract notes on existing medium effect, and morphogenetic regularities are expounded in terms of crystal-structural attributes. Theoretical data are in a good agreement only with experimental data obtained for single-phase gaseous medium, and allow to construct an ideal model, deviation from which testifies a profound influence of medium components upon the crystal growth.

Extension in knowledge of mechanisms of crystal growth in solutions allowed to propose a concept of adsorptive influence of the medium components upon the crystal faceting (Bunn 1933; Laemmlein 1948; Kern 1968; Laemmlein 1973). Based on the concept, a model of adsorption-solvent film (Petrov 1964), and later on, a structure-chemical model of faceting were developed (Glikin 1978, 1981; Glikin and Glazov 1979, 1983; Kiryanova and Glikin 1986). The latter model is discussed in Sect. 7.4.

Instability of faceting is also typical for minerals (Shafranovskii 1957; Yaroshevskii 1959; Minerals 1960–2003; Novgorodova 1968; Pupin and Turco 1972; Evzikova 1984; Popov 1984; Popov and Popova 1996; Kostov and Kostov 1999; Sunagawa 2005; and others) and synthetic analogs of minerals, e.g., alum (Zemyatchenskii 1909, 1911), fluorite (Glikin and Petrov 1966; Kiryanova and Glikin 1986), tourmaline (Voskresenskaya and Barsukova 1968), Y-Fe-garnet (Gendelev 1963; Mikhailov et al. 1973), Y-Fe-perovskite (Mikhailov et al. 1973), calcite (Ikornikova 1975), ammonium dichromate (Glikin et al. 1994), etc. Therefore, faceting is commonly referred to as a typomorphic property of crystals. Along with that experimental investigations and theoretical analysis indicate that faceting is determined by numerous cofactors. The same effect may be achieved via a change in different parameters, and a change in a definite parameter may lead to different effects. As a result, this feature appeared to be highly convergent, and development of reliable genetic criteria on its base is impossible. Below a number of examples are discussed.

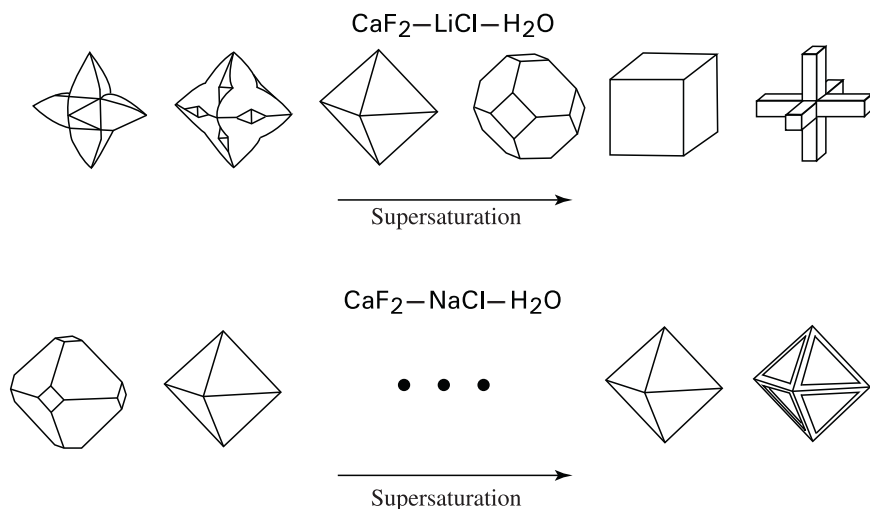
Y-Fe-garnet crystals formed under hydrothermal conditions (Mikhailov et al. 1973) in a type *III* metasomatic reaction of  $Y_2O_3$  and  $Fe_2O_3$  (Sect. 1.2) are faceted mainly as  $\{112\}$  and  $\{110\}$ , the fraction of  $\{123\}$ ,  $\{130\}$ , and  $\{100\}$  faceting being insignificant. Relative development of rhombic dodecahedron decreases with lowering the temperature, or with diminishing the content of mineralizing KOH or hydrogen concentration in the solution (Fig. 7.1).

Faceting of synthetic fluorite (Glikin and Petrov 1966) is determined by solution composition. For this compound, a correlation between appearing like a particular habit and supersaturation degree can vary and even can reverse depending upon the solution composition (Fig. 7.2). In such a case, it is obvious that crystals can have



**Fig. 7.1** Correlation between the shapes of Y-Fe-garnet crystals and crystallization conditions (Mikhailov et al. 1973) Shaded and hollow histograms (with thin and bold contours, correspondingly) correspond to low and high hydrogen concentrations in the solution. Figures at histograms show a number of crystals measured

a skeleton shape at both high (a well-acknowledged phenomenon) and sufficiently low supersaturation level. The nature of skeleton crystals varies (Glikin 1982): at high supersaturation it is, as a rule, determined by diffusion limit of crystal feeding, while at low supersaturation it is affected by adsorption poisoning, which is analogous to that leading to wedging-out of crystals typically occurring in  $\text{KH}_2\text{PO}_4$  or  $\text{NH}_4\text{H}_2\text{PO}_4$ . Skeleton shapes represent one of a few sources of information about



**Fig. 7.2** Correlation between the fluorite crystal shape and supersaturation in hydrothermal  $\text{CaF}_2\text{-LiCl-H}_2\text{O}$  systems (formation of skeleton crystals at low and high supersaturations) and  $\text{CaF}_2\text{-NaCl-H}_2\text{O}$  systems (Glikin and Petrov 1966)

supersaturation of ore-forming solutions; however, the rare instance mentioned above indicates a certain convergence of that property (Glikin 1982).

Faceting of Y-Fe-perovskite (orthoferrite) formed in association with Y-Fe-garnet mentioned above is notable for its complexity (Mikhailov et al. 1973). The crystals of this compound belong to orthorhombic symmetry and have been found to occur in 16 crystal forms, viz.:  $\{100\}$ ,  $\{010\}$ ,  $\{001\}$ ,  $\{111\}$ ,  $\{011\}$ ,  $\{110\}$ ,  $\{103\}$ ,  $\{210\}$ ,  $\{021\}$ , and several non-indexed forms including  $\{0kl\}$ , two  $\{h0l\}$ , and four  $\{hkl\}$ . The degree of development of the above forms may be different depending upon variations of conditions; it can be seen in different well-marked crystal habits formed. However, histograms of the face size similar to those depicted in Fig. 7.1 are inexpressive and do not allow a quantitative estimation of the differences. This example illustrates a fundamental but practically unused methodological rule stating that an objective quantitative measure of the face size is its growth rate, which can be approximately estimated by measuring the center distances, or, in the case of considerable time variation of the crystal habit, the growth rate can be estimated by measuring the boundary trajectory between the internal sectors. Unfortunately, only general concepts of those methods have been discussed (Laemmlein 1948, 1973; Glikin and Glazov 1979). Face size can be used directly only for simple isolated cases, with two to four habits predominating (their number depends on the crystal symmetry).

It is to be specially noted that in experiments on metasomatic precipitation of Y-Fe-garnet and orthoferrite the habit of formed crystal was not observed to be affected in any direct way by the method of introducing the reactants into a con-

tainer, whether it was their mixture or divided monomineral masses. Furthermore, regularities of fluorite faceting observed in numerous crystallizing systems do not depend upon a precipitation technique, be it metasomatic or direct precipitation.

Typical for the crystal habits of water-soluble ammonium dichromate  $(\text{NH}_4)_2\text{Cr}_2\text{O}_7$  (Glikin et al. 1994) is their pronounced susceptibility to influence of a solution supersaturation and concentrations of components in it. This case can serve as a negative illustration of quantitative interpretation of Bravais Law and its modifications.

Structural constants of  $(\text{NH}_4)_2\text{Cr}_2\text{O}_7$  are as follows:  $C2/c$  or  $Cc$ ,  $a = 13.26 \text{ \AA}$ ,  $b = 7.54 \text{ \AA}$ ,  $c = 7.74 \text{ \AA}$ ,  $\beta = 93^\circ 12'$  (Bystrom and Wilhelmi 1951; Wyckoff 1966; Dalgaard et al. 1974; *ICPDF*, 1999); they correspond to the following crystal optics data:  $+2V = 104^\circ$ ,  $Nm = b$ ,  $cNg = 35^\circ$ ,  $Ng = 1.905$ ,  $Nm = 1.80$ ,  $Np = 1.725$  (Winchell and Winchell 1964), and, partially, to following morphology parameters:  $2/m$ ,  $a:b:c = 1.0277:1:1.766$ ,  $\beta = 93^\circ 42'$ ; flattening along  $\{001\}$ ,  $\{101\}$ , or  $\{100\}$ , elongation along  $[010]$ , faceting by 12 pinacoids and prisms; cleavage along  $\{101\}$  (Groth 1906; Winchell and Winchell 1964; Dalgaard et al. 1974). However, symmetry 2 occurs systematically in its faceting (Kozlova et al. 1979; Glikin et al. 1994) and this is a subject of a special consideration.

To conduct a detailed investigation of crystal symmetry and to discover a correlation between the crystal habit and growth conditions, crystals of  $(\text{NH}_4)_2\text{Cr}_2\text{O}_7$  were grown according to a temperature-reduction technique using seeds under controlled stationary conditions (Petrov et al. 1983) or spontaneous nucleation in bulk with approximate estimation of supercooling degree, and including the method of sphere regeneration. Goniometric investigations (scale interval was equal to  $4'$ ) were carried out according to a standard technique using a two-circle instrument (Bulakh 1981) and photogoniometer with a parabolic mirror (Glazov 1981). Orientation and perfection of cleavage were studied according to the known (Tatarskii 1965) quantitative method.

The results obtained are shown in Tables 7.1 and 7.2 and in Figs. 7.3 and 7.4. Investigations revealed a wide range of face and habit types reducing symmetry class to 2, which was earlier defined as  $2/m$  (Winchell and Winchell 1964), but preserving the basic geometric constants, viz.:  $a:b:c = 1.77:1:1.03$ ,  $\beta = 94^\circ 12'$ . This allowed the crystal forms to be indexed as monohedrons, pinacoids, and dihedrons. On the contrary, data obtained for cleavage number and orientations proved to be widely different from the reported values. The most perfect cleavage with 63–64% occurrence was found to be parallel to  $\{010\}$ , while occurrences of the other two  $\{h0l\}$  cleavages were found to amount to 6–10% (the cleavage in the vicinity of the circular section of indicatrix) and 13–23%. Orientation of optical indicatrix turned out to be absolutely different:  $Np = b$ .

The data obtained reflect clearly a decisive influence of medium upon the development of various crystal forms the structure of the crystallizing compound can allow. Development of the habit types described (Fig. 7.5) is determined by supercooling conditions in the solution. It is to be noted that supercooling ranges defining formation of a particular habit are different for freshly prepared and aged solutions (Table 7.2). Consequently, a crystal habit is affected by the ratio  $\text{NH}_4/\text{Cr}_2\text{O}_7$ , which varies with time due to evaporation of ammonia.

**Table 7.1** Spherical coordinates  $\varphi$  and  $\rho$  and face symbols ( $hkl$ ) of ammonium dichromate crystals

Face number	Experimental device		Standard device		$(hkl)$
	$\varphi$	$\rho$	$\varphi^\circ$	$\rho^\circ$	
<b>Monohedrons</b>					
1	0°04′	90°01′	0	90	(0 1 0)
2	180°24′	90°03′	180	90	(0 $\bar{1}$ 0)
<b>Pinacoids</b>					
3	–	0°00′	90	90	(1 0 0)
4	–	180°00′	270	90	( $\bar{1}$ 0 0)
5*	Not measured		90	4	(0 0 1)
6	270°18′	57°12′	90	33	(1 0 $\bar{1}$ )
7	90°00′	122°39′	270	147	( $\bar{1}$ 0 $\bar{1}$ )
8	90°08′	62°00′	90	152	(1 0 $\bar{1}$ )
9	269°58′	117°42′	270	28	( $\bar{1}$ 0 1)
10*	Not measured		90	50	(2 0 1)
11*	Not measured		270	50	( $\bar{1}$ 0 1)
<b>Dihedrons</b>					
12	316°00′	65°53′	32	50.5	(1 1 1)
13	44°16′	114°03′	328	130.5	( $\bar{1}$ 1 $\bar{1}$ )
14	223°49′	65°42′	148	50.5	(1 $\bar{1}$ $\bar{1}$ )
15	135°50′	114°25′	212	130.5	( $\bar{1}$ $\bar{1}$ $\bar{1}$ )
16	43°59′	69°47′	26.5	130	(1 1 $\bar{1}$ )
17	315°54′	110°04′	333.5	50	( $\bar{1}$ $\bar{1}$ 1)
18	136°14′	69°37′	153.5	130	(1 $\bar{1}$ $\bar{1}$ )
19	224°08′	110°05′	206.5	50	( $\bar{1}$ $\bar{1}$ 1)
20	359°59′	60°28′	30	90	(1 1 0)
21	359°39′	119°37′	330	90	( $\bar{1}$ 1 0)
22	180°03′	60°20′	150	90	(1 $\bar{1}$ 0)
23	180°10′	119°38′	210	90	( $\bar{1}$ $\bar{1}$ 0)
24*	Not measured		2.5	46	(0 1 1)
25*	Not measured		12	72	(1 3 1)
26*	Not measured		44	29	(1 5 2)
27*	Not measured		34	39	(5 5 6)
28*	Not measured		61	64	(3 1 1)
29*	Not measured		144	30	(1 $\bar{1}$ 2)
30*	Not measured		145	34	(4 3 6)
31*	Not measured		162	17	(2 $\bar{3}$ $\bar{6}$ )
32*	Not measured		234	32	( $\bar{3}$ $\bar{1}$ 3)
33*	Not measured		312	27	(213)
34*	Not measured		312	90	( $\bar{2}$ 10)

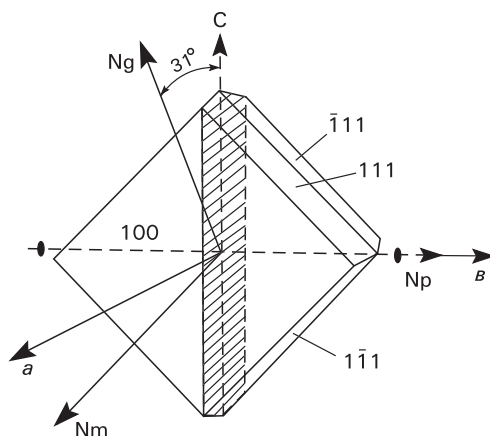
**Notes:** (1) Asterisks are used to denote the facets observed at the initial stages of regenerating the spheres and measured with the aid of photogoniometric technique only ( $\pm 0.5^\circ$ ). (2) For experimental setting: the crystals were measured using a two-circle goniometer and averaged on 20 measurements (five crystals of each habit type indicated in Table 7.2; instrumental error  $\pm 4^\circ$ ). For the standard setting: approximated ( $\pm 0.5^\circ$ ) values obtained taking into account a pseudorhombic symmetry of the crystals. (3) Different crystal forms are marked by dislocated positions of their face numbers.

Like in potassium chromate system (Solubility 1961–1970), solutions in question may be expected to contain impurities, such as  $(\text{NH}_4)_2\text{CrO}_4$ ,  $(\text{NH}_4)_2\text{Cr}_2\text{O}_7$ ,  $(\text{NH}_4)_2\text{Cr}_3\text{O}_{10}$ , and  $(\text{NH}_4)_2\text{Cr}_4\text{O}_{13}$ . The amounts of components containing high

**Table 7.2** Habit types of ammonium dichromate crystals and their formation conditions

Habit type	Supercooling interval (°C)		Predominant crystal forms
	Aged	Freshly prepared	
Pseudotetrahedral	1.5–2	0.5–5	$\{1\bar{1}\bar{1}\}^*$ , $\{11\bar{1}\}^*$ , $\{100\}$ , $\{110\}$
Tabular	2–5	5–10	$\{100\}^*$ , $\{11\bar{1}\}$ , $\{110\}$ , $\{111\}$ , $\{101\}$
Plank-like	5–8	Not found	$\{100\}^*$ , $\{101\}$ , $\{11\bar{1}\}$ , $\{110\}$
Needle-like	8–15	10–17	$\{100\}^*$ , $\{101\}^*$ , $\{1\bar{1}\bar{1}\}$ , $\{110\}$

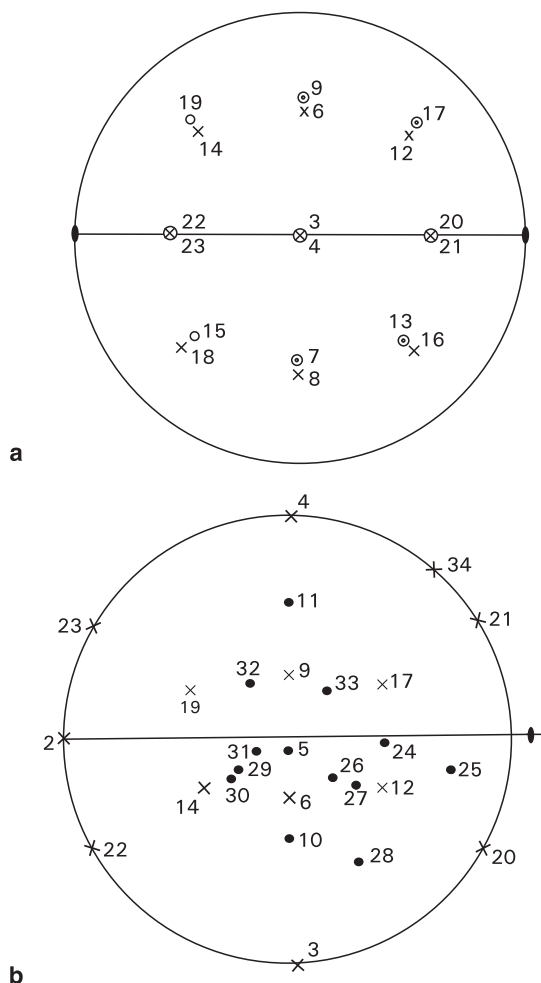
**Notes:** (a) Asterisks are used to denote the crystal forms most developed in the corresponding habit. (b) A sequence of the faces according to relative structural densities (Donnay-Harker computation; forms most developed under particular conditions are marked out) is given below for comparative purposes:  $\{001\} - 2.00$ ,  $\{100\}^* - 1.71$ ,  $\{1\bar{1}0\}$  and  $\{110\}^* - 1.70$ ,  $\{1\bar{1}\bar{1}\}$  and  $\{11\bar{1}\}^* - 1.31$ ,  $\{1\bar{1}\bar{1}\}^*$  and  $\{111\} - 1.28$ ,  $\{010\} - 0.98$ ,  $\{021\} - 0.88$ ,  $\{1\bar{1}2\} - 0.87$ ,  $\{10\bar{1}\}$  and  $\{112\} - 0.85$ ,  $\{101\}^* - 0.84$ ,  $\{221\} - 0.79$ ,  $\{221\} - 0.77$ ,  $\{011\} - 0.70$ ,  $\{201\} - 0.67$ ,  $\{210\} - 0.64$ ,  $\{201\} - 0.63$ ,  $\{211\} - 0.55$ ,  $\{211\} - 0.53$ ,  $\{120\} - 0.47$ ,  $\{012\} - 0.44$ ,  $\{121\} - 0.43$ ,  $\{121\} - 0.42$ ,  $\{212\} - 0.40$ ,  $\{212\} - 0.39$ ,  $\{122\}$  and  $\{1\bar{2}2\} - 0.34$ ,  $\{102\}$  and  $\{102\} - 0.24$ ; Bravais computation changes the situation insignificantly, bringing one of the most developed and frequent  $\{100\}$  form from the second to the first place and moving an exceptionally rare  $\{010\}$  form from the ninth to the third place.



**Fig. 7.3** Scheme of orientation of crystallographic axes, optical indicatrix elements and dominant cleavage along  $\{010\}$  (shaded) in ammonium dichromate (Glikin et al. 1994). One of widespread habits having the following crystal forms: 3, 12, 16, 17 – Figs. 7.4 and 7.5b, Table 7.1

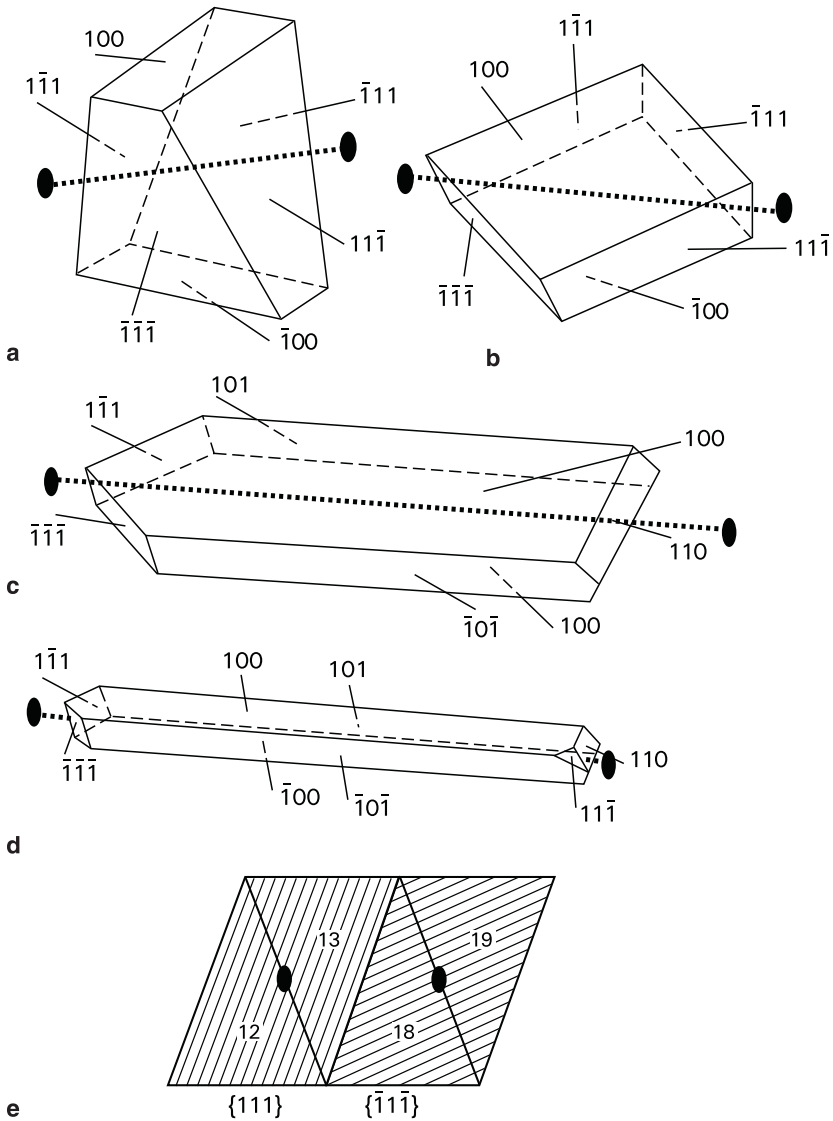
chromium contents are increasing with time that leads to a change in the composition and the structure of adsorption layers, which determine faceting. The details of the process mechanism cannot be elucidated at present. However, a similar cause–effect relationship (ratio of the crystal components in the solution  $\rightarrow$  absorption mode  $\rightarrow$  crystal habit) was found to hold for potassium acidic phthalate,  $\text{KHC}_8\text{H}_4\text{O}_4$  (Glikin et al., 1979).





**Fig. 7.4** Reciprocal projections of ammonium dichromate crystals (Glikin et al. 1994): (a) Basic habit facets in the experimental setting, (b) cumulative projection in the standard setting (shows facets with  $\rho \leq 90$ ); solid circles – facets formed at initial stage of the sphere regenerations.

Data presented in Tables 7.1 and 7.2 indicate that faces (including majority of regenerated faces) are characterized by Miller index values that do not exceed 3, and by comparatively high structural densities. However, no quantitative correlations between the shape and the structure have been found. The faces demonstrating the slowest growth and, consequently, maximal size, do not necessarily have the highest structural density, and their numerical values do not reflect their morphological importance in any possible way. Thus, obviously high-density  $\{001\}$  faces are extremely uncommon, and sizes of the  $\{111\}$  and  $\{1\bar{1}1\}$ ,  $\{11\bar{1}\}$  and  $\{\bar{1}\bar{1}1\}$  faces having the same densities of the flat nets are inevitably different. On the con-



**Fig. 7.5** Crystal habits of ammonium dichromate (Glikin et al. 1994) **(a–d)** – types of habits corresponding to different supercooling conditions (Table 7.2): **(a)** Pseudotetrahedral, **(b)** tabular, **(c)** plank-like, **(d)** needle-like; **(e)** schematic sweep of pseudotetrahedron formed by two dihedrons. Shading and  $L_2$  directions are shown for the  $\{111\}$  dihedrons (faces 12 and 13) and the  $\{\bar{1}\bar{1}\bar{1}\}$  dihedrons (faces 18 and 19).

trary, the  $\{101\}$  and  $\{100\}$  faces having rather different densities reach the same sizes in needle-like crystals, and the list of examples can be extended. Furthermore, the main cleavage position  $\{010\}$  does not correspond to the most developed crystal

forms, as {010} direction does not occur among them. It is to be noted that A. Bravais himself emphasized a conditional character of the analogy between the structural concept of crystal-faceting mechanism and his thoroughly developed cleavage theory (Bravais 1866).

Thus, data obtained in experiments on ammonium dichromate faceting further illustrate lack of quantitative estimation in Bravais' Law. Crystal structure can define the crystal faceting as far as it can define a set of crystal forms that can be developed depending upon the particular growth conditions (Glikin and Glazov 1979). This statement can be illustrated by structural features and habits of ammonium dichromate crystals. According to X-ray diffraction analysis, the symmetry of ammonium dichromate crystals is  $2/m$  or  $m$ ; however, the "hidden" structural asymmetry forbids formation of high-symmetry habits corresponding to these groups ("hypomorphy"), while pseudo-symmetrical structural patterns can result in formation of morphological pseudo-symmetry ("hypermorphy").

The term "hypomorphy" was introduced (Kleber 1955/1956) to denote reduction in external symmetry of crystals in comparison to structural symmetry determined by independent techniques. Hypomorphy manifests itself in systematical absence of mirror planes and symmetry center in faceting patterns, which should be expected to be revealed by structural measurements (Kozlova et al. 1979). Absence of any symmetry elements except of the only  $L_2$  symmetry is proved by a polar distribution of regeneration faces (Fig. 7.4b), pseudotetrahedron habit formed by two dihedrons (Fig. 7.5a-d), prominently different combinative striations (Fig. 7.5e), and asymmetrically blurred reflexes in photogoniometer pictures.

The term "hypermorphy" was introduced (Kleber 1960) to denote an increase in external crystal symmetry in comparison with structural symmetry determined by independent techniques. In this case, high-symmetry faceting patterns are quite diverse. Tetragonal pseudosymmetry  $4/mmm$  is clearly discernible in Fig. 7.5a due to pseudodipyramidal arrangement of faces 12–19 (pseudodipyramid {111}' with  $\varphi_{\text{theor}} = 45^\circ 0'$  and average  $\bar{\rho} = 67^\circ 45'$ ) and 6–9, 20, 23 ({101}' with  $\varphi_{\text{theor}} = 90^\circ 0'$  and  $\bar{\rho} = 60^\circ 0'$ ). Experimental average and maximum (in brackets) deviations from the specified values of  $\varphi_{\text{theor}}$  and  $\bar{\rho}$  found for the {111}' and {101}' pseudodipyramids are as follows:  $\bar{\Delta}\varphi_{\{111\}'} = 0^\circ 58' (1^\circ 14')$ ,  $\bar{\Delta}\varphi_{\{101\}'} = 1^\circ 56' (2^\circ 11')$ ,  $\bar{\Delta}\varphi_{\{101\}'} = 0^\circ 9' (0^\circ 21')$ ,  $\bar{\Delta}\rho_{\{101\}'} = 1^\circ 24' (2^\circ 48')$ .

Figure 7.5b shows pseudosymmetry  $6/mmm$ , provided unplotted faces with  $\rho > 90^\circ$  are taken into account. In this case, projections of faces 3, 4, and 20–23 form a hexagonal pseudoprism, where  $\bar{\varphi} = \bar{\Delta}\varphi = 0^\circ$ , and projections of faces 10–12, 14, 17, and 19 form a top of a pseudopyramid with  $\bar{\rho} = 50^\circ$ , where  $\bar{\Delta}\varphi = 2^\circ 10'$  (descriptions corresponding to pseudosymmetries  $222$ ,  $mmm$ ,  $2/m$  are possible too). The alternate versions listed above reflect arrangement patterns for the centers of  $\text{Cr}_2\text{O}_7$  diorthogroups (Wyckoff 1966) in the nets arranged in planes, which are parallel to the {100} and {001} directions; the patterns appear to be close to a tetragonal structure (more precisely, to doubled rhombic:  $\beta \cong 90^\circ$  if  $b \cong c$  with about 2.6% error) and hexagonal structure (deviations do not exceed  $25^\circ$ ).

It is to be noted that shape is not the only crystallographic property which can correspond to a symmetry type differing from that of the structure. At the same

time, exaggerated symmetry of any given property of a particular substance may be revealed only if measurement accuracy would be sufficiently high; this was observed for the crystal habits of ammonium dichromate and potassium acidic phthalate (Glikin et al. 1979). In other cases, overrated symmetry is typical for a particular crystal property as a whole, regardless of the measurement accuracy; the examples include nonpolarity of cleavage and optical indicatrix in relatively low-symmetrical crystals, occurrence of hexagonal crystal forms in trigonal substances, and existence of orthorhombic forms in monoclinic substances. Neumann principle (Shuvalov et al. 1988) designates the lowest symmetry as the true one: structural symmetry is to be favored in case of hypermorphism (that is beyond question, as diffraction methods are commonly considered as the most reliable), while morphological symmetry is to be selected in case of hypomorphism (the reasons given in Conclusion make this statement somewhat ambiguous).

To conclude this section it should be noticed that  $(\text{NH}_4)_2\text{Cr}_2\text{O}_7$  proved to be quite a promising substance for crystal-genetic modeling owing to its high morphological sensitivity to the growth conditions.

## 7.2 Crystal Habit under Nonstationary Growth Conditions

Time variation of the process conditions is typical for mineral formation in nature, and metasomatic process (see Chapter 4) is not an exception. In this connection development of crystal morphology under such conditions is of a great interest. The data available allow to distinguish variability of growth conditions as a specific morphogenetic factor.

Abrupt changes in growth conditions determine development of various textures and imperfections of shape, which were studied in regeneration experiments using dissolved and mechanically treated surfaces (Artem'ev 1914; Sipovskii 1964; Askhabov 1979), various degrees of supersaturation (Stroitelev 1961; Punin and Nekhorosheva 1987), or hydrodynamic regime (Nikolaeva and Petrov 1973; Petrovskii 1983).

Development of crystal morphology under conditions of smoothly changing supersaturation is considered below. Earlier, we suggested (Glikin and Glazov 1979) that it was smooth variation in the growth regime conditions that caused formation of nonsingular faces with high indices, typical for natural minerals and uncommon for synthetic crystals. We suggested those faces to be regarded as vicinal. It can be suggested that natural processes occurring normally in aggregates proceed with gradual variation of conditions that facilitates formation of high specific surface area of reacting phases.

We have investigated morphological evolution of crystals of  $(\text{NH}_4)_2\text{Cr}_2\text{O}_7$  and  $\text{KAl}(\text{SO}_4)_2 \cdot 12\text{H}_2\text{O}$  proceeding under gradually changing supersaturation conditions (Kasatkin et al. 1995).

The crystals were grown on seeds under both static and dynamic conditions. The temperature was varied according to parabolic modes, and the deviations did not exceed  $\pm 0.01^\circ\text{C}$ . Supersaturation was either monotonously decreasing, or monotonously increasing, or it was being changed nonmonotonically (Fig. 7.6). Control of

supersaturation was held within the range of  $\pm 0.05^\circ\text{C}$  by taking solution samples during the process and measuring their saturation temperatures by microcrystallization method (Petrov et al. 1969). More than 50 crystals (41 of ammonium dichromate and 10 of potassium alum) were grown.

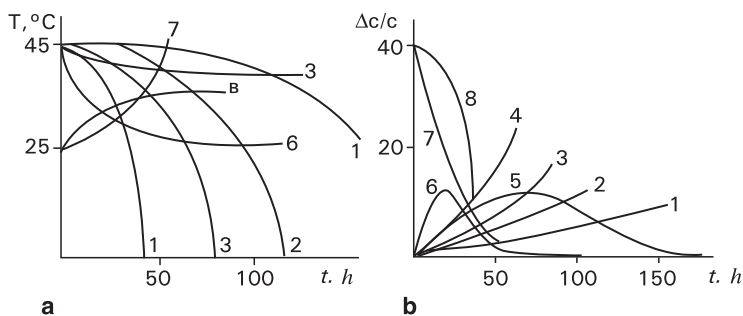
Majority of ammonium dichromate crystals had pseudotetrahedral habit and were faceted as the  $\{\bar{1}11\}$  and  $\{1\bar{1}1\}$  dihedrons, and the  $\{100\}$  pinacoids; poorly developed  $\{110\}$  and  $\{101\}$  faces also occurred. The examples of crystal grown at the conditions indicated above (Fig. 7.6) are shown in Fig. 7.7. All the crystals of potassium alum had usual faceting (Shubnikov 1975), namely, octahedron, cube, and rhombic dodecahedron.

Ammonium dichromate crystals grown under the above varying conditions (3–5 cm sized) had the following shape peculiarities.

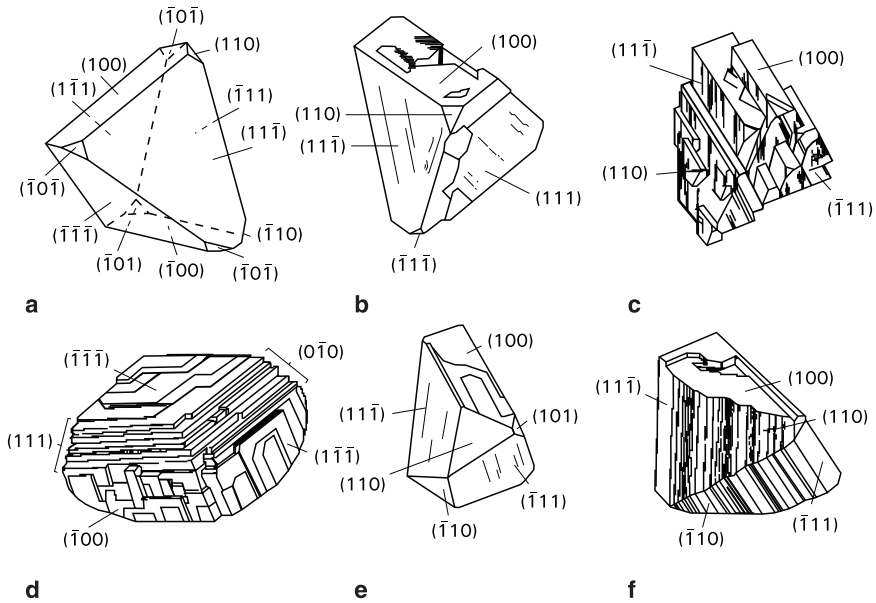
*Combined striations.* They have different patterns depending upon a crystallization mode, and are located on various faces. Under near-stationary conditions, all the dihedral  $\{\bar{1}11\}$  faces bore the stepped striation (striation types were determined by Gendelev 1961). Depending upon the regime, the width of flat  $\{\bar{1}11\}$  “terraces” varies from about 0.1 mm to about 3 mm and their step height ranges from about 0.05 mm to about 1 mm. Dihedral  $\{1\bar{1}1\}$  faces, forming together with the  $\{\bar{1}11\}$  dihedral a pseudo-tetrahedron habit, usually bear vicinal bulges arranged in direction, nonparallel to any of the edges.

According to their intensities, the striations are conventionally divided into “weak,” “medium,” and “pronounced” ones. The “pronounced” striations can be seen by naked eye as smooth ends of macrosteps growing in layers. The step height is about 0.5 mm or more and can be detected under a microscope by measuring a distance between dust particles situated on the adjacent terraces. The “medium” striations (the step height is about 0.1–0.5 mm) were distinguished with 36-fold or greater magnification. The “weak” striations (height up to 0.1 mm) were distinguished with magnification exceeding that of 36-fold.

*Multiheaded structure.* These structures can also be divided into “weak” (3–5 subindividuals on one crystal), “medium” (up to several tens of subindividuals



**Fig. 7.6** Temperature variations (a) and corresponding changes in supercooling degree (b) in ammonium dichromate solutions during growing the crystals (Kasatkin et al. 1995)



**Fig. 7.7** Ammonium dichromate crystals (a–f) obtained under varying temperature and supercooling conditions 1–6 shown in Fig. 7.6 (Kasatkin et al. 1995)

on a “main” crystal looking like a central large block; see Fig. 7.7c), and “pronounced” (a main crystal cannot be distinguished among the numerous parallel subindividuals clustered to form an aggregate).

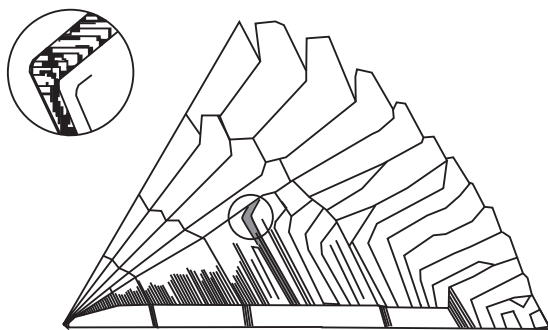
*Multi-edged structure.* This structure is an analog of the previous phenomenon. It is referred to as a cluster of parallel faceted ridges having lateral dimensions differing from those of the crystal by approximately an order of magnitude (Fig. 7.7d).

*Pseudoface.* This appears as a cluster of closely arranged multi-edged subindividuals having almost coplanar edges that look like an enlarged striation on a face corresponding to that face, e.g., (111) and (010) in Fig. 7.7d.

*Curved faces.* Curved faces are staggered quasi-cylindrical (Fig. 7.7f) and quasi-spherical surfaces. Macrosteps with unidirectional ends can be distinguished on the quasi-cylindrical faces. The quasi-spherical surfaces are always opaque.

*Sectoriality.* In crystal structure, multiheaded and multi-edged subindividual ensembles are regarded as optically parallel blocks represented by laminar and pencil-shaped sectors of growth (Fig. 7.8).

The characteristic properties mentioned above can transform into each other under the following conditions: (a) when relatively smooth supersaturation regime changes to more abrupt one, and (b) when a single crystal undergoes a long-term growth process in any mode indicated in Fig. 7.6. For example, if supersaturation is continually rising (Fig. 7.6b, curves 1–4), weak combined striations appear on the crystals immediately after regeneration mode had changed to programmable lowering of the temperature. As the process progresses, the striations become



**Fig. 7.8** Schematic cross-section of multiheaded (multi-edged) crystal of ammonium dichromate grown under static conditions of increasing supersaturation (Kasatkin et al. 1995)

coarser and transform into medium, and then into pronounced striations. And finally, formation of multiheaded and multi-edged crystals is observed (first weak, then medium, and, finally, pronounced) culminating in generation of pseudofaces.

On the whole, for both substances in question, gradually and gently rising supersaturation (Fig. 7.6*b*, curves 1 and 2) resulted in development of weak, and then pronounced striation, culminating in formation of multiheaded crystals within the period of the first hundreds of hours (up to 200h). “Abrupt” regimes (Fig. 7.6*b*, curves 3 and 4) caused all the evolution stages from weak striation to pseudofaces to take place within the first tens of hours. A similar evolution scheme was observed for decreasing supersaturations (Fig. 7.6*b*, curves 7 and 8). Somewhat different scheme was detected at nonmonotonic change of supersaturation (Fig. 7.6*b*, curves 5 and 6) from rise to lowering.

The experiments showed morphology of ammonium dichromate crystals (Fig. 7.7*a–d*) to depend upon the rate of increasing the supersaturation. Crystals of *a*-type were obtained at relatively slowly lowering temperature at practically constant supersaturation. They developed smooth  $\{\bar{1}11\}$  and  $\{1\bar{1}1\}$  dihedron and  $\{100\}$  pinacoid faces. Crystals of *b*-type were grown under conditions of very smooth increase of the supersaturation (about 0.03%/h), their faceting mainly including the  $\{\bar{1}11\}$ ,  $\{1\bar{1}1\}$ , and  $\{100\}$  faces, and poorly developed  $\{110\}$  and  $\{101\}$  faces. As a whole, the surfaces did not have a vicinal texture. The  $\{\bar{1}11\}$  faces bore weak combined striations, direction of which was parallel to the pseudotetrahedron edges (Fig. 7.7*b–e*), with the latter having the height not exceeding 0.02 mm; these usually formed several parallel blocks. Crystals of *c*-type were grown at a rather fast constant increase of supersaturation (about 0.1%/h); their faceting was similar to that of the above-mentioned crystals. Usually the crystals of this type bore up to several tens of parallel blocks. The  $\{\bar{1}11\}$  faces had combined striations of medium type with step heights amounting to 0.2 mm, while the  $\{1\bar{1}1\}$  faces showed a pronounced vicinal relief. Crystals of *d*-type were formed at the highest rate of increasing the supersaturation (about 0.5%/h). They did not develop combined striations, but bore multi-edged formations with

ridges forming the (111) and (0 $\bar{1}$ 0) pseudofaces. Further increasing the rate of raising the supersaturation caused abundant formation of multiheaded crystals.

In case of nonmonotonously changing supersaturation (Fig. 7.6*b*, curves 5 and 6), morphology evolution of ammonium dichromate crystals follows a different scheme. It consists of the following stages.

In the opening stage (supersaturation rises), observations showed development of combined striations and multi-edged (multiheaded) structure. In the second stage (practically stationary supersaturation in the neighborhood of its maximum), striations grew thinner and disappeared when supersaturation degree reached its maximum. This process resulted in formation of a multi-edged or multiheaded crystal without any striations on its faces. In the third stage (supersaturation decrease), multi-edged surfaces transformed into roundish-stepped ones as new cycles of striation development and its coarsening on the subindividual faces started to proceed.

It is to be noted that sharpening the maximum on the supersaturation curve corresponds to enlargement of relative dimensions of the {110} and {101} faces and appearance of roundish-stepped growth surfaces. For example, *e*-type crystals (Fig. 7.7) grown under conditions of smooth wide supersaturation maximum (Fig. 7.6*b*, curve 5) are faceted as the  $\{\bar{1}11\}$  and  $\{1\bar{1}1\}$  dihedrons and the {100} pinacoid; at the same time, this type of crystals also develops {110} and {101} faces, which assume the habit significance, but have neither obvious vicinal relief, nor the above characteristic features. Crystals of *f*-type (Fig. 7.7) grown under conditions of sharp supersaturation transition from rise to fall (Fig. 7.6*b*, curve 6) develop roundish-stepped quasi-cylindrical and quasi-spherical surfaces on the crystal forms  $\{\bar{1}11\}$  and {101} respectively. The process is accompanied by considerable coarsening of the vicinal formations grown on the  $\{1\bar{1}1\}$  faces; at the same time, the crystals develop {110} faces, which bear striations that are not observed under other conditions.

Crystals of potassium alum grown under nonstationary conditions develop combined stepped and comb striations on the {111} and {100} faces, respectively. Monotonous decrease in supersaturation makes these striations coarser and causes their transformation into multi-edged forms, which are also typical for ammonium dichromate crystals (Fig. 7.6*b*, curves 7 and 8).

In the course of crystal growth under unstable conditions, forced stirring of the solution results in noticeable simplification of the crystal shapes. Thus, even at the highest rate of increasing supersaturation, ammonium dichromate crystals grown under dynamic conditions bear only weak or medium combined striations on their  $\{\bar{1}11\}$  faces. Apart from it, the {110} and {101} faces have diminished sizes. Potassium alum crystals grown with stirring have their face relief almost completely smoothed, with the disappearing  $\{100\}$  and {110} forms.

If similar supersaturation regimes are used to grow crystals of ammonium dichromate and potassium alum, the former have more complicated shapes than the latter. This is due to higher sensitivity of ammonium dichromate habit to supersaturation.

Investigation of internal morphology of ammonium dichromate crystals was conducted in thick (up to 2–3 mm) sections cut in perpendicular direction to elonga-



tion of subindividuals of multi-edging. Studying the shapes of growth sectors allowed to single out two types of subindividuals (Fig. 7.8).

Sectors of Type I subindividuals are laminar. They start to grow from a seed and directed at an angle to the base plane of a subindividual.

Sectors of Type II subindividuals are laminar as well, but they start growing from the crystal and substrate junction line. Being parallel to the lateral faces in the beginning, later they follow the direction of the Type I sectors.

The Type I subindividuals are formed in the course of coarsening the macrosteps of the combined striations appearing on the seed. The Type II subindividuals are formed due to change in the preferred growth direction of the layers, which are parallel to the faces, and owing to formation of subindividuals on the ends of these layers.

Multi-edged and multiheaded subindividuals generally grow on the faces forming a positive angle with the substrate plane. In this case, the  $\{\bar{1}\bar{1}1\}$  faces of ammonium dichromate and the  $\{111\}$  faces of potassium aluminum sulfate, which under stationary conditions do not develop any combined striations, bear Type II subindividuals. Type I subindividuals are always formed on the  $\{\bar{1}\bar{1}1\}$  faces of ammonium dichromate under dynamic conditions, and on the  $\{100\}$  faces of potassium alum under static conditions. Static conditions facilitate formation of both Types I and II subindividuals on the  $\{\bar{1}\bar{1}1\}$  face of ammonium dichromate; the Type II formations usually grow on the lower parts of the faces oriented at a positive angle (Fig. 7.8). It should be noted that the number of Type I subindividuals stops growing at a certain stage of crystal evolution. Number of Type II subindividuals is directly proportional to alteration of supersaturation rate.

The mechanism of changing the preferred growth direction of multi-edged subindividual growth sectors (Fig. 7.8) may be presented as follows (Kasatkin et al. 1995). Growth layers nucleating on the plane of crystal and substrate junction spread upward in the direction, parallel to the face. When their end-faces reach the middle part of the face, tangential growth rate slows down considerably because of diffusion depletion, which can be observed via formation of the solution inclusions in these parts of growth pyramids of the faces. Under such conditions, growth direction of a layer section located at the edge end changes due to the presence of the edge between the terrace and end-face of the layer, where the solution circulation is more intensive (the layer thickness amounts to 1–3 mm). As a result, this sector grows in the direction that makes a certain angle with the surface, sometimes the angle coming up to 90°. Preferred growth of the edge sections is probably determined by shielding the rest of the terrace by the newly growing layers.

Combined striations on positively inclined faces occur mainly on their upper parts; the macrostep end-faces also have upward direction. This is likely to be caused by diffusion depletion: as a growth layer reaches the middle section of the face, where solution circulation reduces, the growth rate decreases. Thus, the end-face of the layer starts to grow layer-by-layer. This results in formation of combined striations. The suggestion mentioned above can also explain a normally observed uneven development of positively inclined faces (coarsening their relief in upward direction). As supersaturation increases, striations at the top of the faces coarsen, multi-edged and multiheaded subindividuals are formed, the diffusion depletion

regions approach the edges, and the process of forming and coarsening the striations repeats again and again.

The examples given above of specific morphological crystal features appearing even in “morphologically inert” substances (potassium alum) under conditions of smoothly changing supersaturation indicate that nonstationary mode of growth, along with presence of admixtures, absolute supersaturations, etc., is one of the most important factors determining the final shape of a real crystal. Intension of development of the shape peculiarities, determined by nonstationary mode of supersaturation, is directly proportional to the change in supersaturation rate and sensitivity of the crystal habit to this factor. Development of the face relief in the process of growth under conditions of monotonously changing supersaturation is characterized by its gradual coarsening, and the final crystal can be formed by subindividuals of two types. Forced stirring of the solution results in smoothing the relief, which is most pronounced in the crystals having lesser sensitivity to supersaturation. Apparently, those effects depend not only upon nonstationary behavior of the temperature, but also upon varying chemical composition of the medium, or another factor affecting solubility of the crystal phases.

The shapes described above can be expected to be formed when crystal faceting occurs under metasomatic conditions involving variations in chemical composition and supersaturation. Since the processes normally occur in aggregates, abrupt changes in conditions are rapidly smoothed over owing to a relatively great specific surface of the crystals involved. Thus, combined striations appear to be the most likely element to complicate faceting. However, a high sensitivity of a mineral habit to supersaturation or chemical composition of the medium can be expected to cause more complex relief formations of large crystals growing in cavities.

### 7.3 Regularities of Fluorite Faceting

Fluorite is one of the most extensively studied substances. Faceting its crystals, both natural and synthetic, is commonly used to reconstruct mineral formation and analyze crystal-genetic mechanisms. Generalization of experimental and naturally obtained data is of interest for both applications, including development of structure-chemical morphogenesis model discussed below (Glikin 1978, 1981; Glikin and Glazov 1979; Kiryanova and Glikin 1986, 1999; Glikin et al. 2002).

Faceting of natural fluorite was stated to comprise more than a hundred of crystal forms, including cube, octahedron, and rhombic dodecahedron, which are the most abundant (79.3, 49.2, and 25.2% of occurrence, correspondingly) and have the greatest sizes among the others (reviewed in Holzgang 1930; Minerals 1963). Other forms are much less common. Principal schemes of habit evolution are summarized in Table 7.3. Most investigators consider the most recent fluorite in hydrothermal deposits to have cubic faceting, while the crystals formed at earlier stages are normally octahedral. Rhombic dodecahedron is a relatively frequent intermediate shape and in certain circumstances it becomes the main one; nevertheless, there

**Table 7.3** Faceting of natural fluorite crystals

Conditions assumed	Evolution of faceting	Reference
<b>Hydrothermal deposits</b>		
Decrease in temperature	{111} → {110} → {100}	3, 6, 16, 17, 20, 21, 22, 24, 25, 33, 36, 37
Decrease in both temperature and supersaturation	{111} → {110} → {100}	15, 22, 23,
Decrease in temperature and pH increase	{111} → {100} → {110}	7, 9
	{111} → {100}	12, 13, 14, 19, 34
Increase in Ca/F ratio and decrease in supersaturation	{111} → {110} → {100}	31
	{111} → {110} → {100}	8, 27, 30, 32
Increase of CaO content in the host rock	{111} → {100}	28, 29,
Host rock influence:		
Granitoids, Eastern Pamir	{100} → {111}, {110}	26
Granitoids, Central Tajikistan	{100} → {111}, {110}	32
Limestones, Eastern Pamir	{111}, {110} → {100}	26
Limestones, Central Tajikistan	{100}	32
Andesite porphyrites	{100} → {111} → {110}	32
<b>Pegmatites</b>		
–	{111}, {100}	1, 17, 28
–	{111} → {100} → {110}	34
<b>Epigenetic deposits: sedimentary rocks</b>		
–	{100}	2, 4, 10, 11, 18, 35
–	{111}	5

**Note:** Authors and years of publications: 1 – Kalb 1923, 2 – Bushinskii 1936, 3 – Ermakov 1948, 4 – Kazakov and Sokolova 1950, 5 – Volkova 1953, 6 – Dymkov 1957, 7 – Evzikova 1958, 8 – Barabanov 1959, 9 – Evzikova 1959, 10 – Abramovich 1960, 11 – Minerals 1963, 12 – Pavlishin et al. 1963, 13 – Arkhipchuk 1971, 14 – Arkhipchuk and Lokerman 1966, 15 – Vovk and Mel'nikov 1966, 16 – Moskaluk and Zakharchenko 1966, 17 – Pleskova and Balitskii 1966, 18 – Avdonin 1968, 19 – Zatsikha 1968, 20 – Bogoyavlenskaya 1968, 21 – Aliev 1971, 22 – Arkhipchuk 1971, 23 – Arkhipchuk and Vovk 1971, 24 – Vasil'kova et al. 1972, 25 – Korytov 1972, 26 – Faiziev 1973, 27 – Barabanov 1977, 28 – Vasil'kova and Kukushkina 1976, 29 – Vasil'kova et al. 1976, 30 – Kukushkina et al. 1976, 31 – Zidarova et al. 1978, 32 – Faiziev 1978, 33 – Vasil'kova et al. 1980, 34 – Zatsikha et al. 1971, 35 – Preuss 1981, 36 – Yushkin et al. 1982, 37 – Balitskii et al. 1983.

was proposed a different scheme, viz.: {111} → {100} → {110}. This scheme is also observed in pegmatites, where {111} and {100} are prevailing; in these minerals solution inclusions of octahedral crystals are more acidic than the inclusions of the cubic ones (Zatsikha et al. 1971). Sedimentary fluorite is mostly faceted as a cube.

Interpretations of these data vary. Faceting variations are mostly explained as results of lowering the growth temperature, which was substantiated by measurements of homogenization temperature in fluid inclusions or by indirect means. Without solid reasoning it was stated that either decrease in supersaturation or simultaneous decrease in both supersaturation and temperature influences the shape. Some authors postulated a correlation between fluorite shape and Ca/F ratio or pH of the

solution, which they attempted to estimate on the basis of such data as compositions of fluid inclusions, impurities in crystals and mineral associations. Combined influence of these parameters and supersaturation was under consideration as well.

Data on fluorite morphology was generalized as follows. Octahedral, cubic, and rhombic dodecahedral faces are the densest, their predominance following the qualitative interpretation of Bravais Law. Octahedron was referred to as the most important *F*-shape (Honigman 1958; Hartman 1974). Development of the other shapes was accounted for by influence of supersaturation and impurities; however, the mechanism of the process was not defined in details (Hartman 1974).

Morphology evolution sequence  $\{111\} \rightarrow \{100\} \rightarrow \{110\}$  corresponding to Donnay–Harker’s order of decreasing the face density was assumed as a ubiquitous transformation taking place at decreasing supersaturation (Evzikova 1958). Furthermore, changing Ca/F ratio and pH of the solution controlling the relative activity of these ions were also suggested as universal morphogenetic factors. The point was reasoned by assuming different net stoichiometry in various faces (Wells 1946a) or different activity of Ca- and F-sublattices in fluorite structure in various media (Shafranovskii 1957). Wrongness of such reasoning is obvious and it was repeatedly spoken of (Tatarskii 1967; Glikin and Glazov 1979; and others).

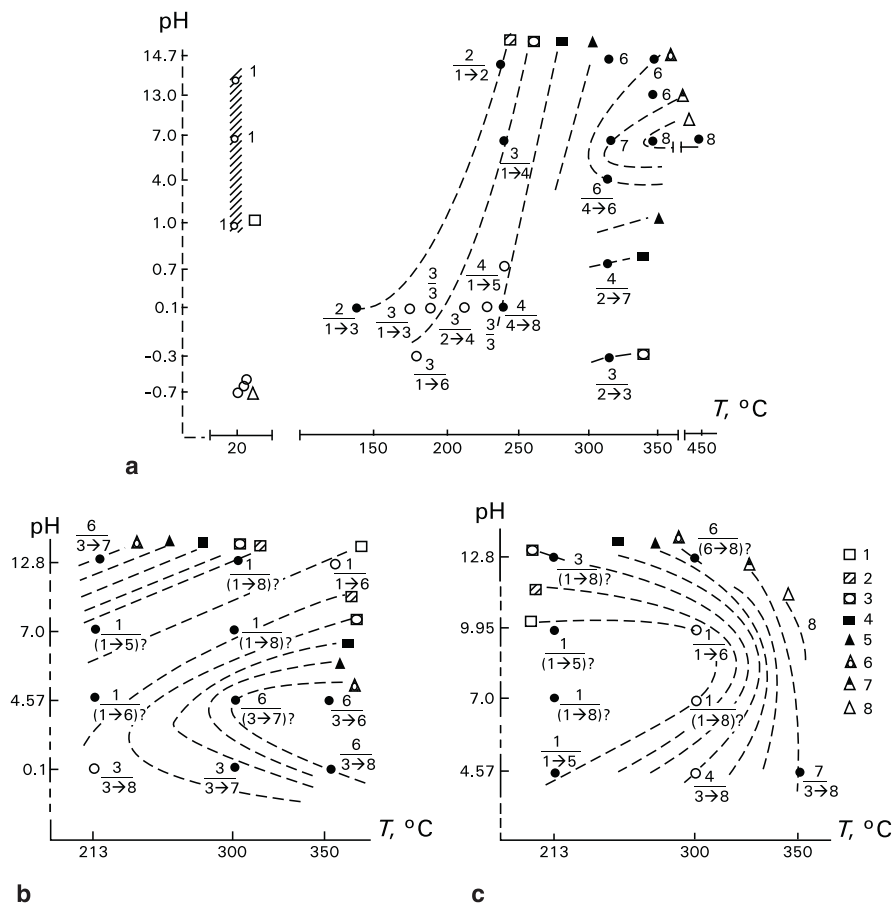
Finally, as it has been mentioned above, many authors explain the  $\{111\} \rightarrow \{110\} \rightarrow \{100\}$  sequence by lowering the temperature. Probably, a tendency to form a cubic crystal habit, which increases with decrease of temperature, is the only real genetic regularity resulted from generalization of phenomena observed in nature. This conclusion has both experimental and theoretical background (see below). At the same time, there are some experimental and theoretical data that allow to explain certain observations, e.g., the correlation between an octahedral habit and excessive acidity of the fluid inclusions (Zatsikha et al. 1971).

Experimental investigations of fluorite faceting are numerous. We synthesized our crystals in a wide range of media compositions, pH, temperatures, and supersaturation regimens, in hydrothermal and low-temperature aqueous solutions and in dry flux systems. The results obtained were combined with random reported data and provided a basis for our structure-chemical model.

Synthetic fluorite is practically always faceted only as the  $\{100\}$  form or the  $\{111\}$  form, or both. The habits may vary under different conditions with pronounced tendency to form cube in close to neutral aqueous solutions at a low temperature, and with gradual switching from the cube to octahedron as the temperature rises and pH changes from neutral.

Consideration of the most thoroughly investigated hydrothermal systems, namely,  $\text{CaF}_2\text{-NaCl-H}_2\text{O}$ ,  $\text{CaF}_2\text{-CaCl}_2\text{-H}_2\text{O}$ ,  $\text{CaF}_2\text{-KF-H}_2\text{O}$ , and  $\text{CaF}_2\text{-LiCl-H}_2\text{O}$  (Glikin and Petrov 1966; Kiryanova and Glikin 1986), shows that distribution of fluorite habit according to the conditions depicted in Fig. 7.9 can be represented as a complex dependence of relative evolution of cube and octahedron upon temperature, pH, and supersaturation. These and next images are similar to “morphodromes” introduced by Prof. R. Kern (Bienfait et al. 1964).

Formation of octahedral crystals in  $\text{CaF}_2\text{-NaCl}_{(30\%)}\text{-H}_2\text{O}$  system (Fig. 7.9a) takes place in approximately neutral solutions and at temperatures of above 350°C.



**Fig. 7.9** Fluorite morphodromes in hydrothermal systems (Kiryanova and Glikin 1986): (a)  $\text{CaF}_2\text{-NaCl-H}_2\text{O}$ , (b)  $\text{CaF}_2\text{-CaCl}_2\text{-H}_2\text{O}$ , (c)  $\text{CaF}_2\text{-KF-H}_2\text{O}$ ; figures at isolines: the upper value is an averaged habit characteristics (the greater the value, the more pronounced is octahedron), the lower value is a tendency to change the habit with decrease of supersaturation

At lower temperatures the predominating formation of cube is observed over a wide range of pH; it transforms into octahedron under highly acidic conditions. The same transformation occurs as supersaturation decreases. It is to be noted that at low-temperature the cubic fluorite is formed in association with  $\text{Ca(OH)}_2$  (portlandite) flattened along  $\{0001\}$ .

For  $\text{CaF}_2\text{-CaCl}_{2(10\%)}\text{-H}_2\text{O}$  system (Fig. 7.9b) there are two ranges of parameters for fluorite to have the octahedral faceting with insignificant development of cube, i.e., (1) in acidic solutions ( $\text{pH} < 4.5$ ) at temperatures above  $350^\circ\text{C}$  and (2) in alkali solutions ( $\text{pH} > 13$ ) at temperatures below  $200^\circ\text{C}$ . Under the other conditions investigated, predominating habit was the cubic one. Decrease in supersaturation results

in formation of cube. At pH = 13 formation of fluorite faceted as the cube is also associated with portlandite crystals flattened along {0001}.

In  $\text{CaF}_2\text{-KF}_{(20.5\%)}\text{-H}_2\text{O}$  system, fluorite has octahedron faceting at temperatures above 350°C (Fig. 7.9c). Transition to cube is observed with lowering temperature: the transition is more abrupt at pH = 7–9 and smoother in acidic and highly alkaline media. Decrease in supersaturation also leads to formation of cube. The cubic-faceted fluorite (220°C, pH = 10) is developed in association with portlandite flattened along {0001}; fluorite faceted by a combination of cube and octahedron (220°C, pH = 13) associates with some undiagnosed hexagonal-pyramidal crystals.

As supersaturation in  $\text{CaF}_2\text{-LiCl}_{(44\%)}\text{-H}_2\text{O}$  system (467°C in the absence of either acid or alkali) diminishes, the crystal faceting changes from cube to octahedron, while specific adsorption skeletons accompanied by insignificant rhombic dodecahedron faces are formed at a quite low supersaturation (Fig. 7.2).

In approximately neutral aqueous solutions, fluorite of  $\text{CaF}_2\text{-H}_2\text{O}$  system (200–300°C) has cubic faceting; it changed into a cubic-octahedron combination with addition of HCl to bring pH values to 0. The transition is more pronounced at elevated temperatures (Kunz 1974; Kiryanova and Glikin 1999).

Experimental data on fluorite faceting obtained under hydrothermal conditions are presented in Table 7.4. Unfortunately, systematic results are reported only in our works cited above. Nevertheless, even desultory reports agree with the principal regularities, i.e., preferred cubic and octahedral faceting of fluorite, absence of direct and unambiguous correlation between the faceting and leading genetic factors, and a tendency to form cubic crystals in less acidic solutions and lower temperatures.<sup>2</sup>

A method of counter-diffusion at room temperature comprising interaction of 16 pairs of reactants was used to prepare fluorite. Taking into account additions of acid–base agents, crystallization has been studied in 34 systems (Table 7.5).

It is noteworthy that in all low-temperature systems in the absence of either acids or alkalis the fluorite forms exceptionally the crystals of cubic habit. This tendency was mentioned earlier (Chizhov et al. 1973) when summarizing the data obtained for a few systems. However, the new information derived from a considerable number of systems, including acidic and alkaline media, and hydrothermal systems (Kiryanova et al. 1984; Kiryanova and Glikin 1986, 1999), allows this tendency to be spoken of as regularity. Addition of either acid or alkali does not change the faceting pattern in some low-temperature systems, while in the others the same operation causes the cubic habits to transform into octahedrons. In some systems, e.g.,  $\text{NH}_4\text{F} + \text{Ca}(\text{CH}_3\text{COO})_2$ ,  $\text{KF} + \text{Ca}(\text{NO}_3)_2$ , and  $\text{KF} + \text{CaCl}_2$ , this transformation takes place in both acidic and alkaline media, while in the others, e.g.,  $\text{NaF} + \text{CaCl}_2$  and  $\text{HF} + \text{Ca}(\text{OH})_2$ , it takes place only under the action of an acid. In some systems, the faceting pattern could not be changed in all the studied ranges of pH.

In a number of reactions we succeeded in finding pH values to cause transition from cube to octahedron and also in defining the acid–alkaline domains of the

<sup>2</sup>Predomination of cube in fluorite synthesized in aqueous solutions at lower temperatures was recognized for the first time by Shushkanov (1969).

**Table 7.4** Faceting of fluorite synthesized under hydrothermal conditions

Solution components	Parameters	Faceting	Reference
LiF (TR)	250–300°C	{100}	6
LiF, NaOH (TR)	250–300°C	{100} + {111}	6
LiF (TR)	400–500°C	{100}	6
LiF, CaCO <sub>3</sub> , CaMg(CO <sub>3</sub> ) <sub>2</sub> (TR)	250–300°C	{100}	6
NH <sub>4</sub> F (20.14%)	400–450°C	{111}	3
NH <sub>4</sub> F (2–8%)	450 → 300°C	{111} → {111} + {100}	7
NH <sub>4</sub> F (3, 5, 7%)	600 → 200°C	{111} → {100}	9,11
NH <sub>4</sub> F (5, 7.2, 10.1%)	500 → 350°C, Δc↓	{100} → {111}	12
LiCl (22, 44%)	250–300°C	{100}	10
LiCl (22, 44%), NaOH, F	250–300°C	{100} + {111}	10
LiCl (22, 44%), CaCO <sub>3</sub> (TR)	250–300°C	{111}	10
LiCl (22, 44%), MnF <sub>2</sub> (TR)	250–300°C	{100}	10
LiCl (23, 44%)	550 → 150°C	{111} → {100}, &:{110},{120},{112}	5
LiCl (44%, pH 6.15)	460 → 250°C	{111} → {100}	11
LiCl (44%)	470°C, Δc↓	{100} → {111}, &:{110}	4
LiCl (10–44%)	360°C, Δc↓	{100} → {100}+{111}	11
LiCl (22.6, 44.6%)	500 → 350°C, Δc↓	{100} → {111}, &:{110}	12
NaCl (30%)	470°C, Δc↓	{111}→{111}+{100}	4
NaCl (30%, pH –0.3–+14.7)	140–450°C, ⇔Δc	Y:{111},{111}+{100}, {100}	14
NaHCO <sub>3</sub> , HCl	250°C	{100} + {111}	2
HCl (4%)	500°C, ↑Δc	{100}	8
KF (22.57%, pH 4.57–12.8)	213–350°C, ⇔Δc	Y:{111},{111} + {100}, {100}	14
CaCl <sub>2</sub> (10.14%, pH 0.1–12.8)	213–350°C, ⇔Δc	Y:{111},{111} + {100}, {100}	14
KCl (18.3%, pH 5–12)	250–420°C, ⇔Δc	{111},{111} + {100}	15
K <sub>2</sub> SO <sub>4</sub> (10.0%, pH 7–12)	420 → 250°C, ⇔Δc	{100} + {111} → {100}, &:{110}	15
HCl (4%, pH 0.05)	300 → 200°C	{111} → {100} + {111}	11
HCl (pH 0.01)	284 → 100°C	{111} + {100} → {100}	15
HCl (pH 0.01–7)	350°C, pH↓	{100} → {111} + {100}	15
YF <sub>3</sub>	300–500°C	{111} + {100}	13
CaSiF <sub>6</sub> , CaCl <sub>2</sub> (chemical reaction)	250°C	{100} + {111}	1

**Notes:** (a) Pressure is not shown. (b) Symbols: Δc↓ and pH↓ denote decrease of supersaturation and pH, ⇔Δc denotes wide supersaturation range, ↑Δc denotes high supersaturation, & – additional faces, Y – morphodromes; solid arrows – directions of changing the temperature and faceting. (c) Authors and years of publications: 1 – Scheerer and Drechsel 1873, 2 – Groth 1906, 3 – Lieberts 1965, 4 – Glikin and Petrov 1966, 5 – Shushkanov 1969, 6 – Vasil'kova et al. 1972, 7 – Rykl and Bauer 1972, 8 – Chizhov et al. 1973, 9 – Kunz 1974, 10 – Vasil'kova and Kukushkina 1976, 11 – Kunz 1976, 12 – Zidarova et al. 1978, 13 – Kunz 1982, 14 – Kiryanova and Glikin 1986, 15 – Kiryanova and Glikin 1999.

**Table 7.5** Faceting of fluorite synthesized by counter-diffusion method at 20°C

Crystal form	Reactions in aqueous solutions		
	Acid medium	No additives	Alkaline medium
{100}	NaF + Ca(NO <sub>3</sub> ) <sub>2</sub> [5] NaF + Ca(CH <sub>3</sub> COO) <sub>2</sub> [5] NH <sub>4</sub> F + Ca(NO <sub>3</sub> ) <sub>2</sub> [5]	NaF + Ca(NO <sub>3</sub> ) <sub>2</sub> [5] NH <sub>4</sub> F + Ca(CH <sub>3</sub> COO) <sub>2</sub> [5] NH <sub>4</sub> F + Ca(NO <sub>3</sub> ) <sub>2</sub> [5] NaF + CaCl <sub>2</sub> [3, 5] KF + Ca(NO <sub>3</sub> ) <sub>2</sub> [5] KF + CaCl <sub>2</sub> [3,5] NH <sub>4</sub> F + CaCl <sub>2</sub> [2,4,5] LiF + CaCl <sub>2</sub> [3] BaF <sub>2</sub> + CaSO <sub>4</sub> <sup>***</sup> [1]	NaF + Ca(NO <sub>3</sub> ) <sub>2</sub> <sup>*</sup> [5] NaF + Ca(CH <sub>3</sub> COO) <sub>2</sub> <sup>*</sup> [5] NH <sub>4</sub> F + Ca(NO <sub>3</sub> ) <sub>2</sub> <sup>*</sup> [5] NaF + CaCl <sub>2</sub> <sup>*</sup> [5] AlF <sub>3</sub> + Ca(CH <sub>3</sub> COO) <sub>2</sub> <sup>*</sup> [5] AlF <sub>3</sub> + Ca(NO <sub>3</sub> ) <sub>2</sub> <sup>*</sup> [5] HF + Ca(OH) <sub>2</sub> <sup>*</sup> [6] KF + CaCl <sub>2</sub> <sup>*</sup> [6]
{111}	AlF <sub>3</sub> + Ca(H <sub>2</sub> PO <sub>4</sub> ) <sub>2</sub> [5] or NH <sub>4</sub> F + CaCl <sub>2</sub> [5]		AlF <sub>3</sub> + Ca(CH <sub>3</sub> COO) <sub>2</sub> [5] NH <sub>4</sub> F + CaCl <sub>2</sub> [5]
{111} + {100}	NH <sub>4</sub> F + Ca(CH <sub>3</sub> COO) <sub>2</sub> [5] KF + Ca(NO <sub>3</sub> ) <sub>2</sub> <sup>***</sup> [5] KF + CaCl <sub>2</sub> <sup>**</sup> [5] KF + Ca(CH <sub>3</sub> COO) <sub>2</sub> <sup>**</sup> [5] NaF + CaCl <sub>2</sub> [5] HF + Ca(OH) <sub>2</sub> [6]		NH <sub>4</sub> F + Ca(CH <sub>3</sub> COO) <sub>2</sub> [5] KF + Ca(NO <sub>3</sub> ) <sub>2</sub> [5] NH <sub>4</sub> F + Ca(H <sub>2</sub> PO <sub>4</sub> ) <sub>2</sub> [5] AlF <sub>3</sub> + Ca(NO <sub>3</sub> ) <sub>2</sub> [5]

**Notes:** (a) *One asterisk:* fluorite in association with portlandite flattened by {0001}; *two asterisks:* fluorite in association with undiagnosed hexagonal-pyramidal crystals; *three asterisks:* unreliable {110} faces. (b) Fluorite crystallization regions in HF + Ca(OH)<sub>2</sub> system, adjacent to HF and Ca(OH)<sub>2</sub> domains, are considered separately as acidic and alkaline media, respectively. (c) Authors and years of publications: 1 – Scheerer and Drechsel 1873, 2 – Becquerel 1874, 3 – Chizhov et al. 1973, 4 – Glikin 1982, 5 – Kiryanova et al. 1984, 6 – Kiryanova and Glikin 1999.

systems, where fluorite crystallizes in association with portlandite or some undiagnosed hexagonal-pyramidal phase. The values obtained vary for different systems; for example, the transition for NH<sub>4</sub>F + CaCl<sub>2</sub> takes place at pH = -0.1, and formation of portlandite at pH > 10; for NaF + CaCl<sub>2</sub> system the transition occurs within -0.8 < pH < 1 interval, formation of portlandite at pH > 12; for NH<sub>4</sub>F + Ca(CH<sub>3</sub>COO)<sub>2</sub> system the transition proceeds within -0.8 < pH < 1 interval; for KF + Ca(NO<sub>3</sub>)<sub>2</sub> system the transition occurs at pH = -0.8, and formation of undiagnosed phase at pH < -0.8. The results obtained for materials prepared through NaF + CaCl<sub>2</sub> reaction and the data obtained for chemically identical hydrothermal CaF<sub>2</sub>-NaCl-H<sub>2</sub>O systems are in a good agreement (Fig. 7.9): transition at pH = -0.8, formation of the undiagnosed phase at pH < -0.8. Probably, in some systems the transition was not observed due to a low concentration of the acidic or alkaline reactant added.

Fluorite faceting has been studied by us (see, e.g., Glikin 1981; Kiryanova et al. 1984; Kiryanova and Glikin 1986; and others) and some other investigators in a great number of dry flux binary and ternary, and sometimes quaternary, systems (Table 7.6, Fig. 7.10).

Any obvious regularities that can be general for all systems have not been revealed mostly due to a complex relationship existing between crystal habit and system com-



**Table 7.6** Fluorite faceting in dry flux systems

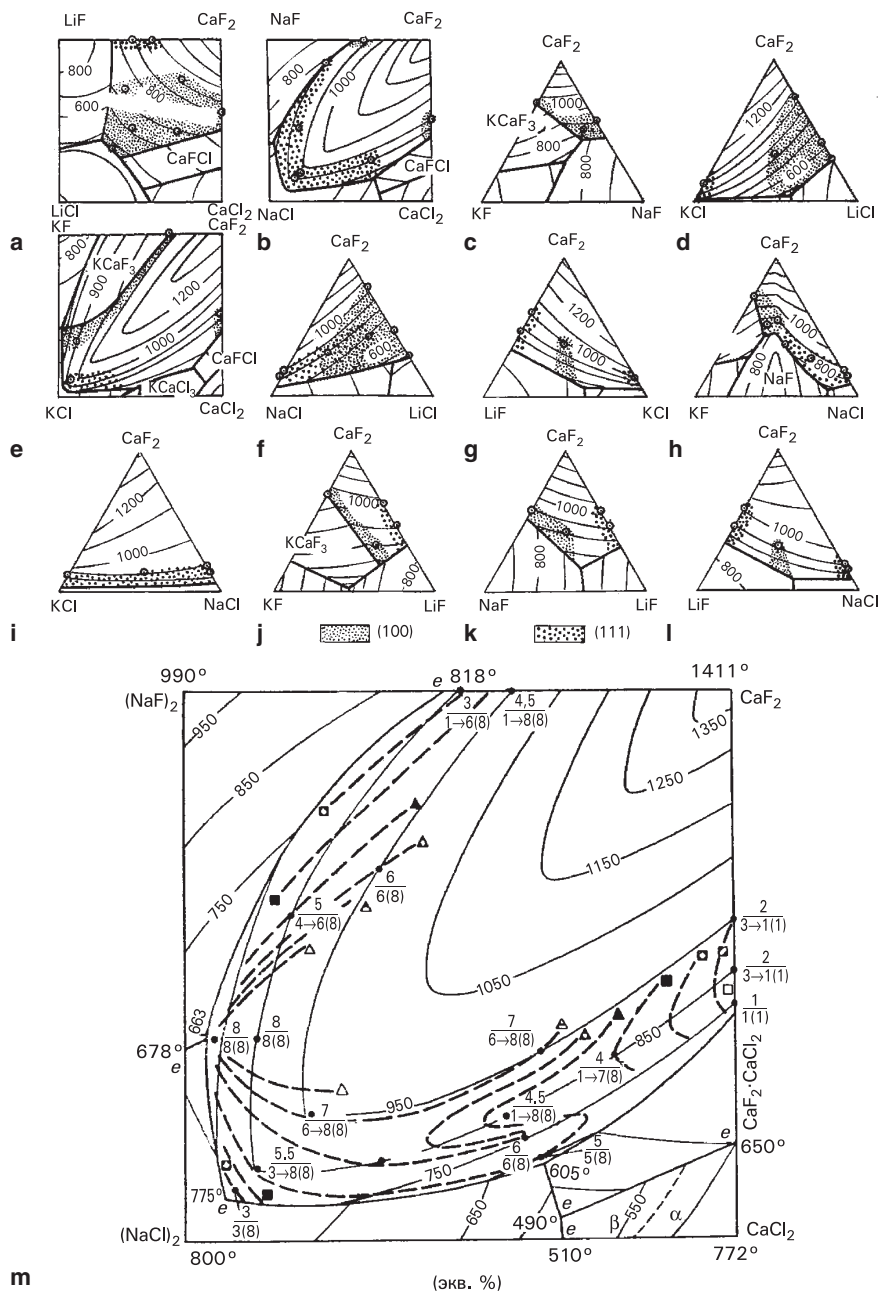
{111}	{100}	{111} + {100}
<b>Solvents in binary systems [1–7]</b>		
LiF, LiBr, Li <sub>2</sub> CO <sub>3</sub> ;	LiCl, Li <sub>2</sub> SO <sub>4</sub> ;	LiF**
NaCl, NaBr, NaJ, Na <sub>2</sub> CO <sub>3</sub> ;	NaF;	Na <sub>2</sub> SO <sub>4</sub> ** , NaF
KF, KCl, KBr, KJ;	KF, K <sub>2</sub> SO <sub>4</sub> ;	KF
	CsCl;	CsCl
CaCl <sub>2</sub> ;	CaCl <sub>2</sub> ;	CaCl <sub>2</sub> **
Ba(NO <sub>3</sub> ) <sub>2</sub> ;		BaCl <sub>2</sub>
MnCl <sub>2</sub>	MnSO <sub>4</sub>	
<b>Solvents in ternary and multicomponent systems [5, 7]</b>		
	LiF–LiCl;	
	LiF–NaF, LiF–NaCl;	LiF–NaF
	LiF–KF, LiF–KCl;	
	LiCl–KF, LiCl–KCl;	
	LiCl–CaCl <sub>2</sub> ;	
NaF–NaCl;	NaF–KF;	NaF–NaCl, NaF–NaCl–Ca(OH) <sub>2</sub> *;
NaCl–KCl;		NaCl–CaCl <sub>2</sub> , NaCl–CaCl <sub>2</sub> –Ca(OH) <sub>2</sub> *
KCl–CaCl <sub>2</sub> ;	KF–KCl;	
	CaCl <sub>2</sub> –Ca(OH) <sub>2</sub> *	

**Notes:** (a) *One asterisk*: first publication. (b) *Two asterisks*: habit changes as {111} + {100} → {100} with increase of supersaturation. (c) Authors and years of publications: 1 – Scheerer and Drechsel 1873, 2 – Wells 1946a, 3 – Shushkanov 1969, Becqerel 1874, 4 – Chizhov et al. 1973, 5 – Glikin 1981, 6 – Kiryanova et al. 1984, 7 – Kiryanova and Glikin 1986.

position, and, especially, due to influence of supersaturation, which, in most cases, has not been taken into account.

The complexity mentioned above can be illustrated by the example of thoroughly investigated CaF<sub>2</sub>–NaCl–NaF–CaCl<sub>2</sub> system (Fig. 7.10m) (Kiryanova and Glikin 1986). Isotherms and habit isolines are characterized by profound lack of coincidence. The cubic habit becomes more pronounced with decrease of temperature and deviation of the melt composition from the stoichiometric ratios both toward the excess of Ca and toward the excess of F. The above results do not agree with simplified speculative notions (Wells 1946a, b, c; Shafranovskii 1957). Also, the cubic habit becomes more pronounced with decrease of supersaturation, except for the binary CaF<sub>2</sub>–CaCl<sub>2</sub> subsystem having the opposite tendency. It is interesting to point out a contraction and inflection of the habit isolines in neighborhood of eutectic (662°C) and peritectic (605°C) nonvariant points.

The data obtained in hydrothermal, aqueous low-temperature, and dry flux systems, along with some peculiar cases are presented and discussed in the following section (Sect. 7.4), where they are considered from the point of view of the structure-chemical model.



**Fig. 7.10** Fluorite morphodromes in dry flux systems (Glikin 1981; Kiryanova and Glikin 1986): (a-l) distribution of octahedral and cubic habits in phase equilibrium diagrams, (m) detailed morphodromes and isolines of similar habits in CaF<sub>2</sub>-NaCl-NaF-CaCl<sub>2</sub> system (figures at isolines: upper figure shows averaged habit characteristics indicating increasing development of the octahedron with increase of the figure, the lower figure shows the tendency of the habit to change with decrease of supersaturation)

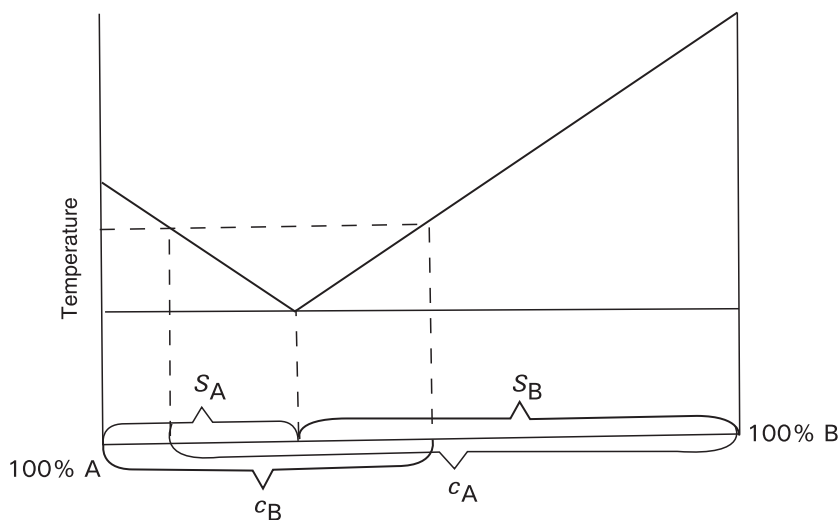
## 7.4 Structure-Chemical Model of Crystal Faceting

Structure-chemical model of crystal faceting (Glikin 1978, 1981; Glikin and Glazov 1979; Kiryanova and Glikin 1986; Glikin et al. 2002) extends the adsorption concept of morphogenesis (see Sect. 7.1), and, for the most part, its chemical aspect.

Formation of an adsorption film is influenced by chemical interactions between solution and crystal; in this aspect, they are similar to topochemical (metasomatic) interactions. The difference is that an absorbed substance does not form a new phase. The results of metasomatic reactions can be predicted using phase diagrams (Glikin 1996; and Chapter 4 of the present monograph), so, in this case, the phase diagrams are also supposed to contain information about composition of the adsorption layers.

Adsorption film structure can be represented as follows.

The first layer consists of a substance formed in the interaction between the dissolved matter and crystal components, which, according to Paneth's rule, has the lowest solubility in the system (Paneth 1914; Laemmlein 1948, 1973; Buckley 1951). The author (Glikin 1981) suggested that the relative solubility of each component should be estimated in accordance with the size of a compound stability region depicted in the phase diagrams: the larger the region, the lower is the substance solubility. Figure 7.11 illustrates this proportion in a binary system; nevertheless, it is likely to be held true for multicomponent systems as well. Such a tendency should be observed when the liquidus surfaces have similar angles of inclination in the diagram, which seems to be true for a majority of systems.



**Fig. 7.11** Correlation between solubilities ( $c$ ) of components A and B in a binary eutectic system and dimensions of their stability regions ( $S$ )

The second and the following layers mainly consist of a substance with corresponding region in the phase diagram situated in the closest proximity to the figurative point of the crystallizing solution. It is clear that this substance should possess the highest metastability. If a structural similarity exists between the substance and the substrate, it can facilitate prolonged lifetime period for adsorbed pre-nucleation centers. Formation of metastable polymorphous modifications due to the film inheriting the structural pattern of the substrate is an acknowledged phenomenon observed in a series of epitaxial growth processes.

Epitaxial adsorbate–adsorbent compatibility is taken for a criterion of the adsorption film strength (Bunn 1933; Laemmlein 1948, 1973; Petrov 1964). At present, there has not been developed a universal quantitative method for estimation of epitaxial compatibility of structures having arbitrary type of symmetry. The author (e.g., Glikin 1978) has mentioned that parameter compatibility of the flat nets having different symmetry patterns can be estimated according to their area elements having similar geometry features, while energy compatibility between the adsorbate and adsorbent particles can be estimated in accordance with statistic data defining extent of their isomorphism in various compounds. This approach could allow introducing some quantitative criteria for the two most important attributes of epitaxial compatibility, which, at present state of knowledge, cannot be used to create a unified numerical characteristic.

Substantiation of the structure-chemical model comprises data-defining “morphogenetic effectiveness” of solvent components, alterations of crystal shapes under changing conditions, and some other kinetic effects. Of course, these data are indirect, and thus cannot be unambiguous. Nevertheless, they can provide a solid basis for experimentally justified theoretical conclusions.

The idea of morphogenetic effectiveness of macroimpurities has been introduced, assuming that the impurities have independent “competing” influence upon the faceting. It is supposed that the effects can be estimated by means of comparative analysis of crystal faceting in systems differing in the solvent component combinations. Of course, such supposition greatly simplifies the matter, since it does not take into account interaction of the components, and the effects are estimated on the basis of general predominance of a certain crystal form regardless to faceting variations. Nevertheless, the method yields good results.

We used this method for analyzing fluorite faceting. In dry flux systems (Fig. 7.10) the component influence is as follows:  $KF^{100} > NaCl^{111} = LiCl^{100} > KCl^{111} > CaCl_2^{100} > NaF^{100} > LiF^{111}$  (Glikin 1981), where the upper figures are the indices of the face induced by the presence of a particular impurity. Cubic faceting is typical for all low-temperature aqueous-solution systems having almost neutral pH, and it does not change with alteration of the salt composition of the system. This fact proves the greatest influence of water, i.e., the component common for all systems investigated (Chizhov et al. 1973). Transition to cubic–octahedral faceting occurring at elevated temperatures and at high acidity or alkalinity of the medium is an evidence of increasing effects of the salt components (Kiryanova and Glikin 1986). The identical octahedral faceting of fluorite in either NaCl- or KCl-containing high-temperature hydrothermal and dry systems (Tables 7.4 and 7.6) is in a good agreement

with this conclusion and can be explained by maximal effect of the salt components and their equal influence upon the faceting pattern in these systems.

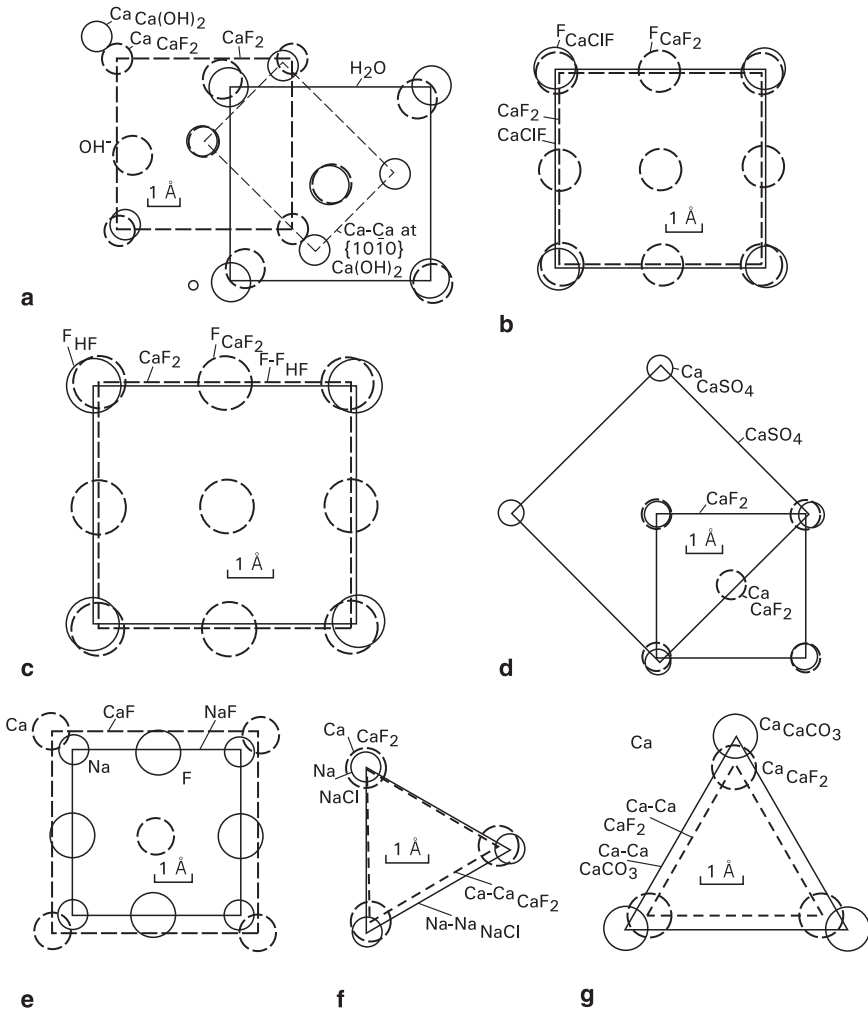
However, this regularity was not displayed by systems containing  $\text{CaCl}_2$  or  $\text{K}_2\text{SO}_4$ . Here, fluorite has octahedral faceting under hydrothermal conditions, while in dry media the faceting is cubic. In general, therefore, molecular complexes responsible for faceting pattern differ in binary and ternary systems, so, the resulting crystal habit is also affected by interdependent action of various impurities in ternary and more complex systems.

Cubic faceting of fluorite in low-temperature aqueous media containing salts and having pH, which is close to neutrality (Fig. 7.9, Table 7.5), is believed to be a result of forming a two-layer adsorption film. The film consists of  $\text{Ca}(\text{OH})_2$  and  $\text{H}_2\text{O}$ , which constitute the first and the following layers, respectively. The size of component stability region for such systems is difficult to estimate; however, we can assume with a high degree of reliability that in the majority of almost neutral systems the least soluble compound, among all the possible structures that can be construed by combining each positive and negative ion present in the solution, is portlandite  $\text{Ca}(\text{OH})_2$ . The portlandite layer connects fluorite with adsorption water film, corresponding to one of the principal stability regions in the system that is most likely to be the closest region to the experimental figurative points.

Indeed, in most cases, addition of an acid results in formation of octahedral faceting that can be explained in our opinion by disruption of  $\text{Ca}(\text{OH})_2$  layer due to elevation of portlandite solubility in acidic media. Appearance of a new undiagnosed phase in association with the octahedral fluorite in acidic medium indicates formation of new stable compounds forming adsorption layers with new composition and structure. Unfortunately, insufficient data prevented identification of these compounds. Formation of the octahedron in alkaline media is evidently associated with a change in the proceeding of adsorption process, which also cannot be detailed at present. Nevertheless, it should be mentioned that cubic faceting of fluorite in alkaline medium is always accompanied by formation of portlandite that is surely to play a certain part in the adsorptive processes. Attention should also be drawn to the fact that diminishing stability of the cubic crystals in acidic media was predicted (Glikin and Glazov 1979) by the proposed structural-chemical model, and then proved by experiments (Kiryanova et al. 1984).

Diminishing stability of cubic faceting at elevated temperatures (Fig. 7.9) can be attributed to increased morphogenetic influence of the solution salt components owing to disruption of the top water adsorption layers due to dehydration of the surface of fluorite and the salt components. Some idea about the processes taking place in the top adsorption layers, which contain compounds represented by the regions located near the figurative point, can be derived from the fact that morphodrome isolines of  $\text{CaF}_2$ - $\text{CaCl}_2$ - $\text{NaCl}$ - $\text{NaF}$  system have pronounced characteristic properties in the vicinity of the eutectic points (Fig. 7.10*m*) that account for the differences in morphogenetic processes characterized by the adjacent regions situated at the both sides of the corresponding eutectic points.

Figure 7.12*a* shows the supposed adsorption structure formed on fluorite, which forms in conformity to epitaxial conditions and can be presented as follows: substrate/first adsorption layer/subsequent adsorption layers. Differences between interatomic



**Fig. 7.12** Suggested structures of some adsorption films formed on fluorite crystals: (a)  $\text{CaF}_2^{100}/\text{Ca}(\text{OH})_2^{1010}/\text{H}_2\text{O}_{1c}^{100}$ , (b)  $-\text{CaF}_2^{100}/\text{CaClF}^{100}$ , (c)  $-\text{CaF}_2^{100}/\text{HF}^{100}$ , (d)  $-\text{CaF}_2^{100}/\text{CaSO}_4^{100}$ , (e)  $-\text{CaF}_2^{100}/\text{NaF}^{100}$ , (f)  $-\text{CaF}_2^{111}/\text{NaF}^{111}/\text{NaCl}^{111}$ , (g)  $-\text{CaF}_2^{111}/\text{CaCO}_3^{0001}$

distances of portlandite  $\{10\bar{1}0\}$  rectangular OH-nets and fluorite  $\{100\}$  square F-nets are 18% for a long side and 10% for a short one. These ions being isomorphic in many compounds and the nets being single-charged favor epitaxial growth. Square O-nets of ice-1c ( $\text{H}_2\text{O}$  cubic modification), differ from portlandite  $\{10\bar{1}0\}$  OH-nets by 6 and 3% at both directions, and 14% difference exists between the O-nets of water and the  $\{100\}$  F-nets of fluorite. All these ions exhibit isomorphic properties in a great number of compounds, with their nets being single-charged. This case makes it necessary to introduce an assumption of formation of metastable ice modification inheriting the substrate structure within the adsorption layer.

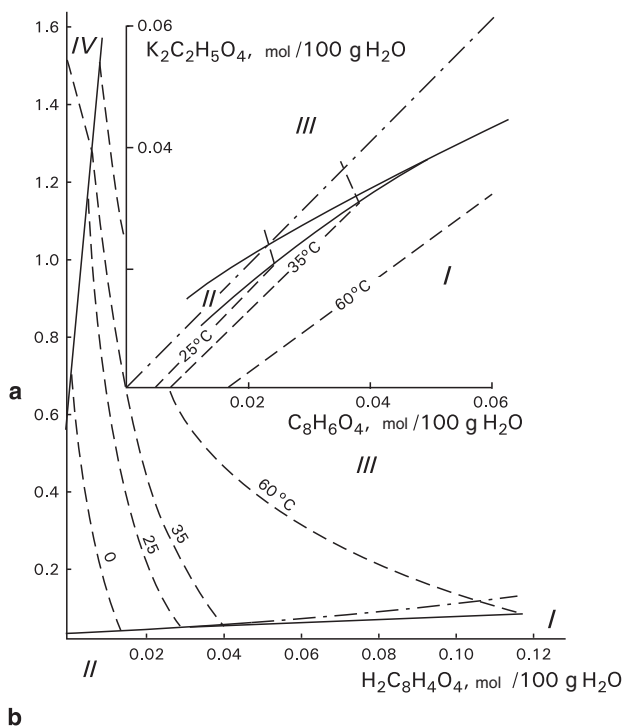
Figures 7.12*b–j* show some other structures of adsorption films drawn on the basis of experimental data on morphogenetically effective components. It is to be noted that some of these structures agree with reported data concerning epitaxial growth (Krastanov and Stranski 1938; Minerals 1963; Kleber et al. 1967):  $\{100\}$  NaF $\parallel\{100\}$ CaF<sub>2</sub> (CaF<sub>2</sub><sup>100</sup>/NaF<sup>100</sup> structure),  $\{111\}$ NaCl $\parallel\{111\}$ CaF<sub>2</sub> (CaF<sub>2</sub><sup>111</sup>/NaF<sup>111</sup>/NaCl<sup>111</sup> structure), and  $\{0001\}$ CaCO<sub>3</sub> $\parallel\{111\}$ CaF<sub>2</sub> (CaF<sub>2</sub><sup>111</sup>/CaCO<sub>3</sub><sup>0001</sup> structure).

The above considerations can provide an interpretation for a well-known morphological phenomenon of widely differing faceting of isostructural compounds: NaNO<sub>3</sub> has only the  $\{11\bar{2}1\}$  *F*-shape, but CaCO<sub>3</sub> forms a “record” number of faceting patterns, and NaNO<sub>3</sub> is made up of ions that form only highly soluble (or essentially soluble) inorganic salts. Therefore, it is unlikely to form solid adsorption complexes, and its faceting is almost unaffected by the presence of impurities. On the contrary, ions making up CaCO<sub>3</sub> generally form insoluble salts and thus determine various adsorption schemes and facilitate formation of a wide diversity of faces (Glikin and Glazov 1979).

Crystallization peculiarities of potassium acidic phthalate KHC<sub>8</sub>H<sub>4</sub>O<sub>4</sub> (Glikin et al. 1979) can also provide, however indirect, substantiation for our structural-chemical model, and, in particular, for definition of the most important adsorption-layer components in the phase diagrams according to the phase region size and the region proximity to figurative points. Regions of stoichiometric solutions, which are normally used to grow this compound, are located in close proximity to the nearest-neighbor region of potassium “superacidic” phthalate K<sub>2</sub>C<sub>8</sub>H<sub>4</sub>O<sub>4</sub>·4C<sub>8</sub>H<sub>6</sub>O<sub>4</sub>·4H<sub>2</sub>O. Moreover, according to decrease in size, the phase regions of the diagram can be arranged in the following order: KHC<sub>8</sub>H<sub>4</sub>O<sub>4</sub> > C<sub>8</sub>H<sub>6</sub>O<sub>4</sub> (phthalic acid) > K<sub>2</sub>C<sub>8</sub>H<sub>4</sub>O<sub>4</sub>·4C<sub>8</sub>H<sub>6</sub>O<sub>4</sub>·4H<sub>2</sub>O > H<sub>2</sub>O (Fig. 7.13). Thus, the composition of the first adsorption layer is determined by phthalic acid molecules, and that of the following layers is defined by molecules of the superacidic salt. Addition of KOH to the solution results in disruption of these components, and finally, in an abrupt change in the relative growth rates of the faces and in variation of the crystal forms. This also leads to preservation of the crystal quality and acceleration of the face growth in five to eight times (Glikin et al. 1974, 1979). It is to be mentioned that these experimental results were theoretically predicted.

## 7.5 Effect of Infrared Radiation on Crystal Growth Kinetics in Solutions

A sensitivity of growth kinetics of water-soluble salts to optical radiation is a direct evidence of the leading role of water structure in the growth mechanism. Original reliable data for influence of a weak light flux upon the crystallization rate were obtained for NaBrO<sub>3</sub> by Kasatkin (1966). We showed that growth of the  $\{100\}$  face in NaClO<sub>3</sub> crystals accelerated when the system was irradiated with infrared light with a wavelength in the range of basic vibrational frequencies of water molecules. The effect was accounted for by weakening of the intermolecular bonds of water due to their resonance activation (Glikin et al. 1976; Glikin 1978).



**Fig. 7.13** Phase diagram of  $K_2C_8H_4O_4$ - $C_8H_6O_4$ - $H_2O$  system (Glikin et al. 1979; plotted after the data of Reference book... 1970); (a) general view (axes scales are different), (b) region of acidic compositions (equal scales). *Dash lines* – isotherms, *solid lines* – eutonic borders, *dash-dot line* – stoichiometric composition for potassium acidic phthalate. *Designation of the regions*: I –  $C_8H_6O_4$  (phthalic acid), II –  $K_2C_8H_4O_4 \cdot 4C_8H_6O_4 \cdot 4H_2O$  (superacid salt), III –  $KC_8H_5O_4$  (potassium acidic phthalate), IV –  $K_2C_8H_4O_4$  (potassium phthalate)

Our experiments consisted in comparing the growth rates of the {100} crystal faces in  $NaClO_3$  defined in ordinary growth experiments and in systems irradiated with weak IR radiation. The rates were measured using the microcrystallization device (Fig. 2.1; Petrov et al. 1969). Crystallization was carried out under controlled stationary conditions ( $\pm 0.01^\circ C$ ) in the temperature range of 37–44°C. Supersaturation state was achieved by lowering the temperature. The experiments used a 20 W incandescent lamp and a system of light filters that allowed illuminating or darkening the crystals and cutting the radiation of various infrared diapasons.

Using a filter with 1.5–3.5  $\mu m$  light transmission interval (maximum at  $\lambda \cong 2.9 \mu m$ ) caused a definite increase of the growth rates; this effect was not observed when filters with maximal transmission at  $\lambda \cong 0.75, 0.9, 1.2,$  and  $1.6 \mu m$  were used (Table 7.7). As the main infrared absorption band of  $OH^-$  group is at 3  $\mu m$ , the corresponding bonds should undergo resonant excitation when exposed to radiation that results in acceleration of diffusion processes in the system.



**Table 7.7** Growth rates for the {100} form of NaClO<sub>3</sub> ( $\mu\text{m}/\text{min}$ ) in the dark ( $v_1$ ) and under IR irradiation ( $v_2$ ) ( $\sigma$  – dispersion,  $\beta$  – validity of rate differences,  $\Delta v$ )

$T, ^\circ\text{C}$	$v_1$	$\sigma v_1$	$v_2$	$\sigma v_2$	$\Delta v$	$\sigma \Delta v$	$\beta$
<b>1.5–3.5<math>\mu\text{m}</math> filter (transparence maximum at 2.9<math>\mu\text{m}</math>)</b>							
37.6	1.02	0.11	1.17	0.25	0.17	0.14	0.98
37.8	0.76	0.08	0.97	0.08	0.23	0.06	0.999
38.0	0.72	0.17	0.86	0.14	0.13	0.11	0.98
40.0	0.89	0.12	0.96	0.14	0.11	0.08	0.98
40.5	1.11	0.15	1.39	0.14	0.24	0.10	0.999
40.5	0.74	0.23	0.87	0.19	0.14	0.09	0.99
40.5	1.62	0.12	1.73	0.19	0.13	0.11	0.98
40.6	0.91	0.14	1.09	0.19	0.13	0.07	0.99
40.6	0.68	0.11	0.85	0.12	0.17	0.09	0.99
40.6	0.87	0.09	1.01	0.55	0.17	0.24	0.90
43.8	2.05	0.29	2.10	0.24	0.11	0.07	0.99
<b>0.7–1.0<math>\mu\text{m}</math> filter (transparence maximum at 0.75<math>\mu\text{m}</math>)</b>							
40.0	1.52	0.23	1.47	0.25	-0.02	0.14	0.2
<b>0.85–3<math>\mu\text{m}</math> filter (transparence maxima at 0.9, 1.2, and 1.6<math>\mu\text{m}</math>)</b>							
40.0	0.83	0.35	0.85	0.35	0.02	0.22	0.1
40.6	0.73	0.21	0.68	0.17	-0.01	0.11	0.1

Presence and absence of the effect when different filters were used, as well as acceleration (not slowing down!) of the growth rate in irradiated systems indicate the absence of systematic errors, in particular, those caused by uncontrolled warming of the system.

Using different heat media to warm the system changes the growth rate that also proves the supposition of different sensitivity of the crystallization process to weak infrared radiation with various spectral compositions (Glikin 1976, 1978). The measurements were carried out following the same procedure, the only difference being in interchanging the heat media differing in spectral characteristics (water and heptane) instead of interchanging the infrared filters. The growth rates of the {100} face in NaClO<sub>3</sub> (Table 7.8) measured when using heptane to warm the system were essentially higher than the rates obtained with aqueous warming. Contamination of the solution eliminates the difference that, as in the previous case, also proves the authenticity of the effect.

We assume this effect to be related to superposition of the solution absorption spectrum and the heating medium radiation spectrum, which triggers various resonance modes of chemical bond excitation within the system.

It is to be noted that the effects described were predicted by structure-chemical concept, which allows considering them as a direct demonstration of the solvent role in a growth process. Nevertheless, the question is which part of the system is responsible for these effects, whether it is an absorption film or a bulk of the solution. The factors discussed (IR radiation from an outer source and a heating medium) present new methodological opportunities for investigation of molecular processes in crystal-solution systems.

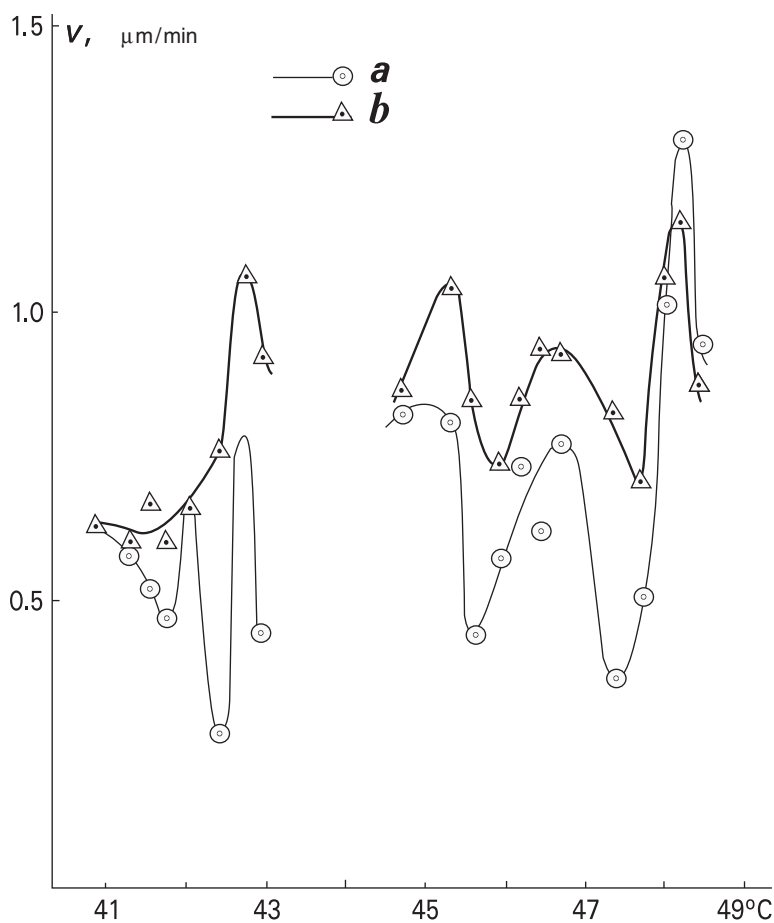
**Table 7.8** Growth rates for the {100} form  $\text{NaClO}_3$  ( $\mu\text{m}/\text{min}$ ) in water ( $v_1$ ) and heptane ( $v_2$ ) used as a heating media ( $\sigma$  — dispersion,  $\beta$  — validity of rate differences,  $\Delta v$ )

$T, ^\circ\text{C}$	$v_1$	$\sigma v_1$	$v_2$	$\sigma v_2$	$\Delta v$	$\sigma \Delta v$	$\beta$
<b>Pure solution</b>							
41.5	0.52	0.15	0.67	0.29	0.13	0.12	0.95
41.7	0.46	0.21	0.60	0.19	0.16	0.07	0.997
42.4	0.25	0.13	0.77	0.32	0.56	0.26	0.99
42.7	0.78	0.52	1.06	0.47	0.34	0.26	0.95
42.9	0.44	0.22	0.92	0.28	0.47	0.26	0.99
45.6	0.43	0.14	0.84	0.26	0.43	0.16	0.999
45.9	0.57	0.11	0.73	0.14	0.16	0.12	0.98
46.15	0.73	0.18	0.85	0.20	0.15	0.12	0.98
46.4	0.62	0.24	0.93	0.39	0.30	0.28	0.95
47.35	0.35	0.26	0.82	0.35	0.42	0.31	0.97
47.7	0.50	0.24	0.71	0.24	0.19	0.16	0.95
<b>Contaminated solution</b>							
40.8	0.63	0.09	0.63	0.09	0.00	0.10	0.0
41.25	0.58	0.07	0.60	0.16	0.02	0.12	0.35
42.0	0.66	0.18	0.66	0.22	0.00	0.14	0.0
44.65	0.82	0.25	0.86	0.39	0.09	0.23	0.68
45.25	0.81	0.28	1.04	0.46	0.21	0.28	0.85
46.65	0.78	0.30	0.92	0.43	0.20	0.42	0.74
48.0	1.02	0.46	1.05	0.33	0.02	0.45	0.1
48.15	1.30	0.32	1.16	0.32	-0.17	0.15	0.94
48.4	0.94	0.21	0.87	0.24	-0.06	0.19	0.54

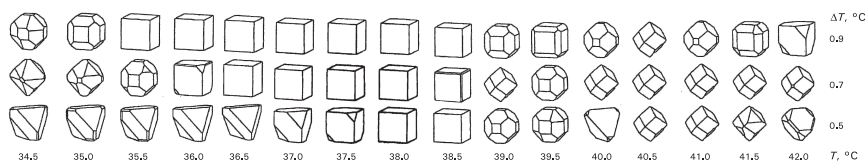
## 7.6 Kinetic Anomalies of Crystal Growth in Solutions

In the context of direct proof of the structure-chemical concept it is necessary to turn to so-called anomalies of crystal growth rates manifesting themselves in pronounced nonmonotonous temperature dependences of growth rates (Fig. 7.14). These anomalies were discovered in 1967 by V. V. Sipyagin and A. A. Chernov in the course of detailed kinetic investigations of crystal growth in aqueous solutions and have been reported by several authors for  $\text{KClO}_3$  and  $\text{NaClO}_3$  (Sipyagin 1967),  $\text{KCl}$  (Punin and Petrov 1972),  $\text{KNO}_3$ ,  $\text{NaNO}_2$ ,  $\text{NaNO}_3$ ,  $\text{NaClO}_4$ ,  $\text{KNaC}_4\text{H}_4\text{O}_6 \cdot 4\text{H}_2\text{O}$  (Sipyagin and Chernov 1972),  $\text{KH}_2\text{PO}_4$  (Kibalczyk and Kolasinski 1977),  $\text{FeCl}_2 \cdot 4\text{H}_2\text{O}$  (Franke 1986), and  $\text{CuSO}_4 \cdot 5\text{H}_2\text{O}$  (Bocharov 2004; Bocharov and Glikin 2008). They are most likely to be typical for all or at least for a great number of substances.

Kinetic anomalies represent a specific essential factor of crystal morphogenesis. They can totally alter the crystal shape in a narrow temperature range (Fig. 7.15; Glikin et al. 2003). Effects of anomalies are especially important in the morphogenetic analysis of the soluble compounds, which crystallize at relatively low temperatures. This is typical, for example, for salt deposits or for some processes in crusts of weathering. However, it should be emphasized that temperature range of about 0–50°C, where the anomalies were discovered, was taken exceptionally due to its availability for a quantitative experiment; the possibility for the anomalies



**Fig. 7.14** Temperature anomalies of crystal growth rate: the {100}  $\text{NaClO}_3$  faces for supercooling  $1.0^\circ\text{C}$  when using water (a) and heptane (b) as a heating medium (Using data obtained by Glikin 1976)



**Fig. 7.15** Change in crystal forms of  $\text{NaClO}_3$  in the temperature anomaly region of growth rate at the following supercooling degrees: 0.5, 0.7, and  $0.9^\circ\text{C}$  (Glikin et al. 2003). The forms were calculated from the precision growth rates measured by Sipyagin in kinetic regime (intensive stirring)

to occur at other temperatures is not restricted so far. Anomalous kinetics and respective variations of crystal habits resulting from structural rearrangements in solution should be expected to exist in hydrothermal and magmatic mineral formations. As to anomalies occurring under hydrothermal conditions, they may be induced by “polymorphic transformations” of water that are reflected in numerous data reporting nonmonotonous character of temperature dependence of water properties (Ovchinnikov and Masalovich 1977). This publication discusses properties of solutions suffering nonmonotonous transformations at temperatures ranging from 4°C to 350°C, the properties including hydrolysis characteristics, electrical conductivity, specific heat, compressibility, solubility, etc. Anomalies of solubility in water have been found for hydrogen, helium, nitrogen, oxygen, methane, gypsum, fluorite, and quartz; the latter has a solubility maximum at 340°C, which corresponds to the estimated temperature of complete disrupting the ice-like water structure.

It is to be noted that in hydrothermal systems, such as  $\text{CaF}_2\text{-NaCl-H}_2\text{O}$ ,  $\text{CaF}_2\text{-CaCl}_2\text{-H}_2\text{O}$ , and  $\text{CaF}_2\text{-KF-H}_2\text{O}$ , relative development of the cubic and octahedral fluorite crystals has nonmonotonous temperature dependence (Fig. 7.9; Kiryanova and Glikin 1986), which is likely to be explained by kinetic anomalies. Anomalous morphology of crystals in dry flux systems was shown by the example of fluorite faceting in  $\text{CaF}_2\text{-NaCl-CaCl}_2\text{-NaF}$  system. It was shown that relationship between cube and octahedron has nonmonotonous temperature dependence at the vicinity of the eutectic and peritectic points, where structural rearrangements of crystallization medium can be expected to occur (Fig. 7.10*m*; Kiryanova and Glikin 1986).

Previously, on the basis of experimental data and theoretical models of crystal morphogenesis, it has been emphasized that various adsorption mechanisms determining crystal faceting in various media make unification of morphogenetic mineral series impossible (Glikin and Petrov 1966; Glikin and Glazov 1979; Glikin 1981; Kiryanova and Glikin 1986, 1999; Glikin et al. 2002). This conclusion becomes even more categorical due to existence of kinetic anomalies of crystal growth. Thus, we come to the conclusion that searching general approaches to mineralogenetic reconstitutions by means of crystal faceting analysis has no future. At the same time, interpretations of particular experimental morphological phenomena remain both possible and desirable. Moreover, those interpretations can be quite successful, as it was shown by the above discussion of stability of fluorite cubic habit and calcite pinacoid faceting under conditions of low-temperature mineral formation via water adsorption on these mineral faces (Kiryanova and Glikin 1986, 1999).

## 7.7 Nature of Kinetic Anomalies and Crystal Growth Mechanisms

Anomalies are accounted for by structural rearrangements occurring either in the adsorption layer formed at the crystal surface (Sipyagin 1967; Sipyagin and Chernov 1972; Chernov and Sipyagin 1976; Sipyagin et al. 1976) or simultaneously in the adsorption layer and bulk of the solution, particularly when the layer

inherits the structural changes of the bulk (Punin and Petrov 1972; Chernov and Sipyagin 1980; Glikin et al. 1982; Bocharov and Glikin 2008).

The first point of view is based upon structural NMR investigations of film layers of  $\text{KClO}_3$  saturated aqueous solutions on crystal faces of this substance (Sipyagin et al. 1976; Chernov and Sipyagin 1980). The measurements showed that proton mobility in the layers has abnormal values at the temperatures, at which the growth rate anomalies occur. An additional direct proof of molecular structuring of the adsorption layers is anisotropy of the proton mobility in directions, which are parallel to the surface of the crystals that also confirms the proposed structural-chemical model.

The second point of view is supported by coincidence of temperatures at which the anomalies occur and changes in some characteristic bulk properties of the solutions, e.g., solubility, partial molal heat of dissolving, partial molar volume (Punin and Petrov 1972), and viscosity (Franke and Punin 1972), as well as by reported abnormal solubility behavior of several salts in water (Kiryanova 2003). These display a connection between the kinetic anomalies and solution bulk structure.

The behavior of kinetic anomaly peaks shows a simultaneous relation of adsorption layer and bulk properties to the anomalies (Glikin et al. 1982). Temperature dependence of peak heights and positions upon supersaturation was analyzed for 32 anomalies belonged to three substances and the following values were found: for  $\text{KCl}$  in combined regime at natural convection, anomalies of the  $\{100\}$  faces were observed at 7, 12, 16, 22, and  $60^\circ\text{C}$  (Punin and Petrov 1972); for  $\text{NaClO}_3$  in combined regime anomalies of the  $\{100\}$  faces – at 36 and  $39.5^\circ\text{C}$  (Glikin's data of 1974); for  $\text{NaClO}_3$  in kinetic regime with intensive stirring (Sipyagin's data of 1967): for  $\{100\}$  – at 7, 23, 36,  $39.5$ , and  $40.5^\circ\text{C}$ , for  $\{110\}$  – at 8, 36.5, and  $39.5^\circ\text{C}$ , for  $\{111\}$  – at 7, 36,  $39.5$ , and  $40.5^\circ\text{C}$ ; and for  $\text{KClO}_3$  in kinetic regime with intensive stirring (Sipyagin's data of 1967) for  $\{110\}$  – at 34, 36, and  $40.5^\circ\text{C}$ , for  $\{011\}$  – at 30 and  $36^\circ\text{C}$ , for  $\{100\}$  – at 17, 34, 37, and  $44^\circ\text{C}$ , for  $\{101\}$  – at 32, 36, and  $42^\circ\text{C}$ . Without going into details, the following is worth being noticed. First, discrepancy in correlation between the peak height and supersaturation observed in kinetic regime for different faces agrees with conclusion about the anomaly arising due to structural rearrangements of the adsorption layer. Second, for various substances relation between the temperature shift of anomalies and change in supersaturation correlates with shapes of temperature solubility curves, which also indicate rearrangement proceeding in the bulk of the solution. Therefore, an investigation of growth-rate anomalies supports the idea about structuring the adsorption film, which determines the growth kinetics, although anomalies themselves are likely to be of dual nature.

It appears that revealing the nature of anomalies can acquire a key significance in understanding the structure of the adsorption layer, which determines numerous phenomena that are functionally related to the crystal growth rate, including faceting and surface relief, inclusions, capturing isomorphous and other impurities, epitaxy, etc., and will ultimately provide the basis for a crystal-genetic theory of solutions. However this approach requires a totally new methodological basis. Usual direct measurements of crystal growth rates in the course of conventional precipitation

from aqueous-salt solutions cannot provide with sufficient information due to the method being too laborious and not allowing principally to plot continuous temperature dependences during maintaining a constant degree of supercooling; this leads to loss of information about precise shapes of kinetic curves.

We tried to find a more productive approach to solve the problem by using an equipotential electrocrystallization method (Glikin et al. 2002; Bocharov and Glikin 2008) that makes it possible to monitor the growth rate by measuring the current density at a changing temperature in solution having a constant concentration, provided the driving force (overvoltage) is constant. Moreover such an approach allows to compare growths of crystals and that of liquid phases (for instance copper, mercury, and their solid and liquid amalgams). Distinction in the nature of crystal and amorphous substrates determines structural differences of the adsorption layers. Thus, significant differences in the nature of anomalies observed during the solid- and liquid-phase transitions are to determine their adsorption nature, while similarity of their characteristic features define their generation within the solution bulk.

In principle, the mechanisms of crystal growth during electrochemical reduction and during conventional salt precipitation are similar and determined by the stages of diffusion transport of ions in a solution, their diffusion in the adsorption layer, and their attachment to the crystal at the edges of steps. The additional stage of electrocrystallization is reduction of a cation to the metallic state but it is fairly short and does not limit the kinetics. Therefore, the main kinetic regularities should be similar for salt crystal growth and for electrochemical growth of a metal crystal. This conclusion can be deduced from the existing experimental data and general concepts (Chernov 1984).

We investigated kinetics of electrochemical reduction of metals in aqueous solutions (Bocharov and Glikin 2008). The temperature dependence of the metal-reduction rate in solutions has not been thoroughly studied. Anomalies in electroreduction of solid and liquid metals have not been compared with salt crystallization from solution, and there are not any reported indications on testing the corresponding techniques in published literature.

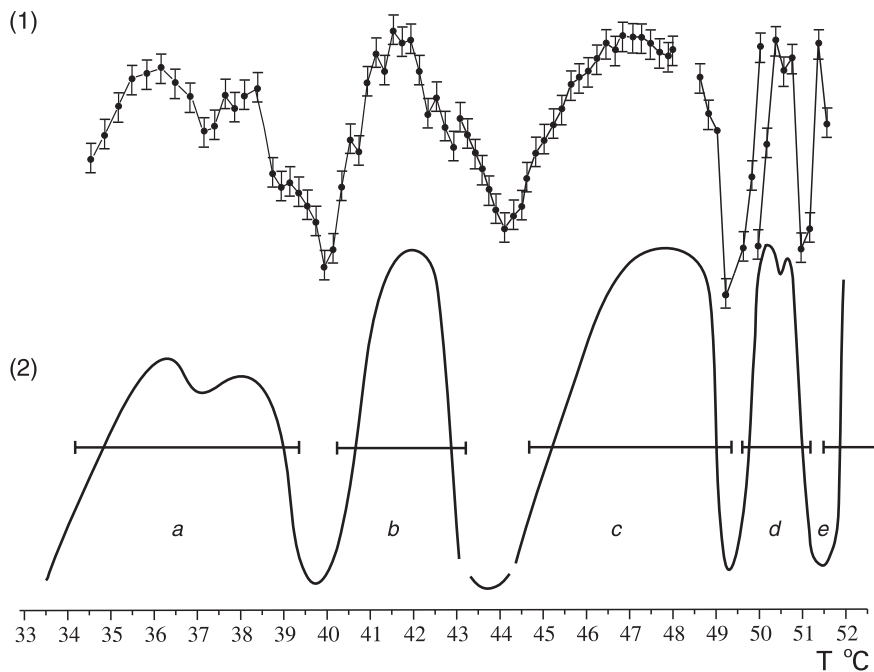
Metallic copper and mercury were reduced from aqueous solutions of their salts. A 40-ml three-electrode cell was used. The main electrode (cathode) and the reference electrode were made of the same material (copper or mercury, depending on the system studied). It was assumed that the potential difference between the main electrode and the reference electrode is zero in the absence of polarization (external current source). The counter electrode (anode) was made of the same material as the cathode (copper system) or inert materials: molybdenum or platinum (mercury system).

A P-5827M potentiostat with a  $\pm 0.5$  mV error of maintaining overvoltage was used. Experiments for both systems were performed at fixed overvoltages: 5, 40, 60, 100, and 150 mV (hereinafter, absolute values of overvoltage and current are indicated; it is to be remembered that direction of current flow from anode to cathode is generally characterized by negative values). The temperature of the system was controlled with an error of  $\pm 0.05^\circ\text{C}$  using an HAAKE DC-10 ultrathermostat. In different experiments, this parameter was increased or decreased with a step

of 0.2–1°C in the range of 30–60°C. After temperature stabilization at each point, the current through the cell was measured. The current measurement time at a fixed temperature varied from 10 to 50 min. To determine the random error, the current strength was measured at constant temperatures of 34.5, 35.0, and 45.0°C (Cu) and 34.5°C (Hg) and overvoltages of 10 and 60 mV for 5 h. The maximum spread of current strengths in these experiments (up to  $\pm 5\%$  for Cu and  $\pm 4\%$  for Hg) was assumed to be the random error in all experiments.

*Copper* was reduced from  $\text{CuSO}_4$  solutions with concentrations of 2.5, 5, 10, 15, and 25 g per 100 g  $\text{H}_2\text{O}$  with addition of 0.1–0.4 ml of  $\text{H}_2\text{SO}_4$  per 100 ml solution to prevent electrode oxidation. The following reactants were used:  $\text{CuSO}_4 \cdot 5\text{H}_2\text{O}$  of analytic grade,  $\text{H}_2\text{SO}_4$  of analytic grade, and  $\text{H}_2\text{O}$  distilled once. The main and reference electrodes were made of a polycrystalline unannealed copper wire having a diameter of 0.5 mm, and the counter electrode was cut out of a copper plate in the shape of a disk with a thickness of 0.5 mm and a diameter of 20 mm.

Independent experiments revealed the presence of kinetic anomalies (Fig. 7.16, curve 1). The results obtained in the adjacent temperature ranges were partially overlapping, and we could combine them into a generalized polytherm (Fig. 7.16, curve 2). The generalized polytherm was plotted on the basis of more than 20 experimental dependencies, which were selected from more than 100 curves, having pronounced



**Fig. 7.16** Kinetic anomalies of Cu reduction in a  $\text{CuSO}_4$  solution: (1) experimental data and (2) generalized curve (Bocharov and Glikin 2008)

nonmonotonic features. Each dependence curve covered a range of about 5°C and contained about 25 points measured with a step of about 0.2°C. The main part of the generalized polytherm was obtained by superposition of four or more individual curves having similar extrema, while in the range from 48°C to 50°C there are more than 10 extrema. The range 43–45°C, however, did not include any superposition of data obtained in different experiments.

The generalized polytherm for Cu (Fig. 7.16, curve 2) is characterized by strong nonmonotonic features showing in the form of differently pronounced five peaks separated by minima: peak *a* in the range of 34–39°C (doublet with a weak minimum at 37.0°C), with a normalized intensity ranging from 1.3 to 1.35 and a full half-width of 4°C; peak *b* in the range of 41.0–43.0°C, with an intensity of 1.4–1.7 and a half-width of about 2.5°C; peak *c* in the range of 45.0–49.0°C, with an intensity of about 1.6 and a half-width of 3°C; peak *d* in the range of 50.0–51.0°C (doublet with a weak minimum at 50.4°C), with an intensity of 1.6–1.7 and full half-width of 0.9°C; and peak *e* (low-temperature wing), apparently with a maximum at about 52°C. The boundaries between the temperature ranges of the peaks can be determined with an error not less than ±0.5°C due to irregular shift of minima from experiment to experiment: 39.0–41.0°C, 43.0–45.0°C (the minimum has not been determined precisely and is plotted on the basis of interpolation of the wings of neighboring anomalies), 49.0–50.0°C, and 51.0–51.5°C. The density of anomalies in the temperature scale is 0.2°C<sup>-1</sup> (doublets are considered as unified maxima).

The extrema are symmetric except for peak *c*, which has a flatter left wing. Such difference in the shape may be caused by such complicating factors as extrema in the left-wing appearing with gradually increasing current strength; their smoothing out results in the asymmetry of the total peak.

*Mercury* was reduced from Hg(NO<sub>3</sub>)<sub>2</sub> solutions having concentrations of 2.5 g per 100 g H<sub>2</sub>O with addition of 1 ml HNO<sub>3</sub> per 100 ml solution (to increase the salt solubility). The following reactants were used: Hg(NO<sub>3</sub>)<sub>2</sub> of analytic grade, HNO<sub>3</sub> of analytic grade, and H<sub>2</sub>O distilled once; mercury was preliminarily purified by sparging through a dilute HNO<sub>3</sub> solution. The main and reference mercury electrodes filled annular grooves in teflon spacers and were connected with the measuring devices by a platinum wire isolated from the solution. A molybdenum or platinum spiral (wire 20-cm long and 0.5 mm in diameter) was used as a counter electrode. About 50 experimental curves were obtained, of which 30 exhibited anomalies in the range of 44–54°C. Figure 7.17 shows the most characteristic examples. The polytherms are almost similar since all the curves contain peaks at 44.5–45°C, 45.5–46.5°C, 47.2–48.0°C, and 50.2–50.6°C and most curves contain peaks in the ranges of 48.0–48.7°C and 49.0–49.8°C. At the same time, the curves differ in the intensities of the extrema, which in some cases can even disappear (e.g., the peak in the range 49.0–49.8°C). Anomalies have a lower intensity (in comparison with those for Cu) versus the background of a large number of random (including small) current strength oscillations. Therefore, extrema were singled out if they had been detected in at least three different experiments. It is of importance that measurements for each polytherm were performed during the same experiment under the same conditions.



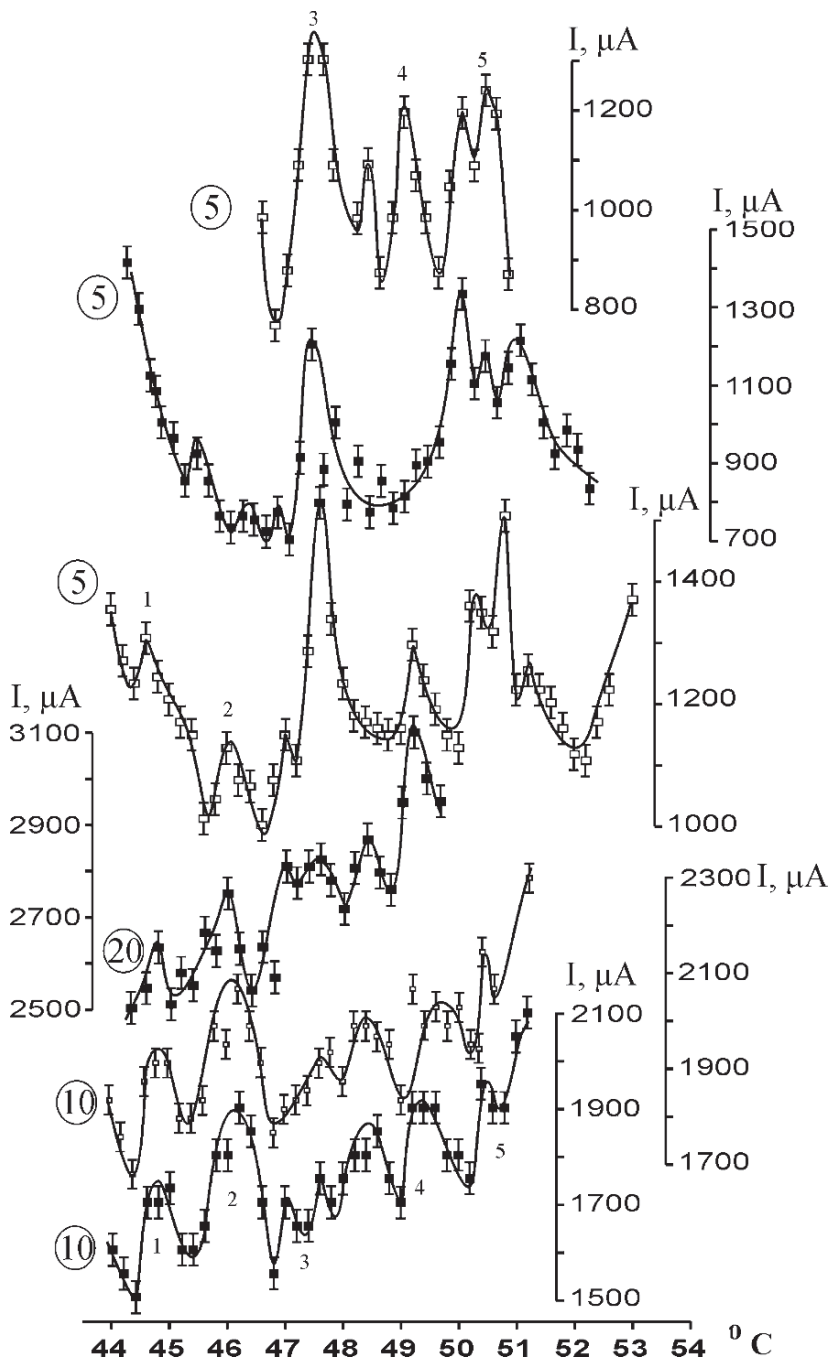


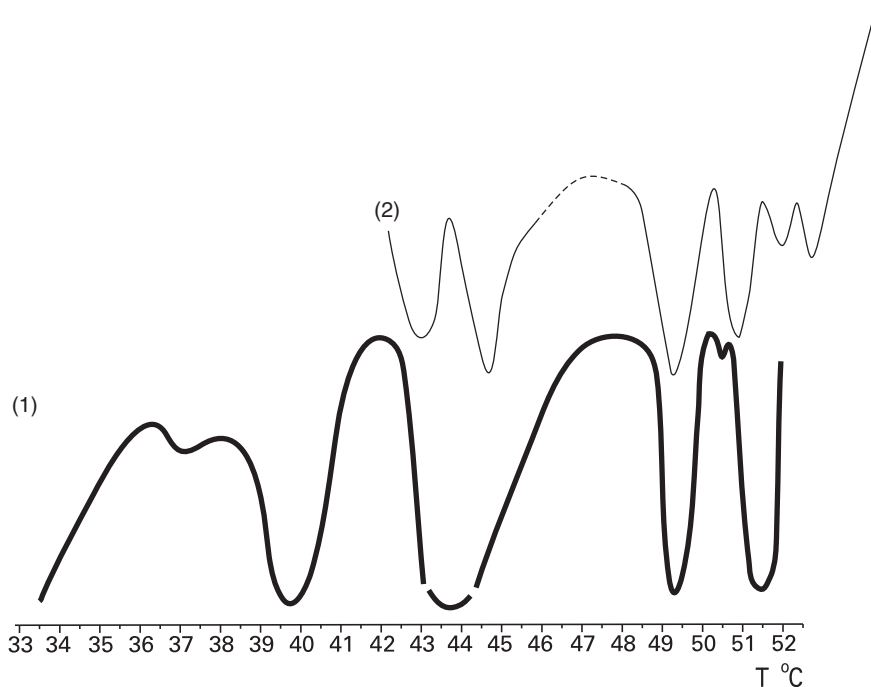
Fig. 7.17 Kinetic anomalies of Hg reduction in a  $\text{Hg}(\text{NO}_3)_2$  solution (the curves correspond to different overvoltages, indicated by encircled numbers) (Bocharov and Glikin 2008)

On the whole, five peaks can be singled out: peak 1 in the range of 44–45°C, with an intensity and half-width that vary in different experimental curves from 1.05 to 1.15°C and from 0.3 to 0.5°C, respectively; peak 2 in the range of 45–46.5°C, with an intensity of 1.1–1.3 and a half-width of 0.5–1.0°C; peak 3 in the range of 47.0–48.0°C, with an intensity of ~1.3 and a half-width of 0.5–1.0°C (this peak is pronounced in all curves and is generally the strongest); peak 4 in the range of 49.0–49.3°C, with an intensity lower than 1.1 (sometimes to 1.2) and a half-width of 0.3–0.7°C; and peak 5 in the range of 50.5–51.5°C (doublet with a minimum in the range of 50.8–51.3°C), with an intensity of 1.15–1.25 and a half-width of about 1.5°C (almost constant). The density of extrema is 0.65°C<sup>-1</sup>, i.e., higher than that for Cu. The shape of almost all extrema for Hg is symmetric, the exception being peak 3, which in some curves can be split at the low-temperature wing; as a result of this splitting, the peak flattens out and becomes asymmetric.

The experiments show that the electrochemical method is a convenient tool allowing to rapidly obtain precise characteristics of anomalies. At the same time, some complexities were revealed that are related to the nonstationary character of this process. For example, it was expected that fine-crystallite copper electrodes would make it possible to minimize the difference in the surface relief for different experiments. However, the change in the structural imperfection of the polycrystalline surface and its faceting elements during experiments turned out to be significant; apparently, this circumstance is responsible for some current instability. The degradation, splitting, and shift of anomalies is likewise related (at least in part) to the change in the crystal faceting since the interrelation between superimposed peaks, belonging to different faces and having different temperature positions, changes with time (the different position of peaks of different faces was likewise observed for most salts studied: Sipyagin 1967; Sipyagin and Chernov 1972; Chernov and Sipyagin 1980). In the case of Hg deposition, it can be also suggested that cyclic change in the curvature and area of the main electrode meniscus significantly affects the random errors.

According to the results shown in Figs. 7.14, 7.16, and 7.17, and the published data cited above, kinetic anomalies have been observed in all the cases of phase deposition under consideration: reduction of solid and liquid metals and salt crystal growth. Despite the evident differences, these processes are similar in comprising the diffusion stages in the bulk of the aqueous salt solution and forming the adsorption layer. Therefore, the kinetic anomalies are determined by the general factors, affecting the kinetics of one or both stages, and the results obtained by us are consistent with the concept of structural alterations in a crystallization medium. Configuration comparison of the anomalies for Cu, Hg, and CuSO<sub>4</sub>·5H<sub>2</sub>O makes it possible to return to discussion on the relationship between the alterations and the processes occurring in the bulk of the solution and/or adsorption processes.

The characteristics of the anomalies for Cu and CuSO<sub>4</sub>·5H<sub>2</sub>O are comparable. Figure 7.18 shows that the sharp peaks for both materials are located in the same temperature ranges and have close half-widths and densities. These crystals grow in the same medium, and the similarity of their anomalies confirms that the latter are generated in the bulk of the solution. It can be stated that manifestation of



**Fig. 7.18** Comparison of the kinetic anomalies of (1) Cu reduction and (2) growth of the  $\{1\ 1\ \bar{1}\}$  face of  $\text{CuSO}_4 \cdot 5\text{H}_2\text{O}$  at supercooling  $3.0^\circ\text{C}$  (Bocharov and Glikin 2008)

anomalies in this pair of systems is not significantly affected by the obviously different type of the surface and, correspondingly, the significant differences in the structure of adsorption layers and surface processes. The anomalies for Cu and Hg (Figs. 7.16 and 7.17) are both similarly pronounced and have similar intensities (to 1.3 and 1.7, respectively); this circumstance also may indicate their similar nature, i.e., generation in the bulk of the solution.

Moreover, the anomalies for different materials have some specificity; this fact can be accounted for by different influence of the adsorption stage. The most radical differences in the structures of the anomalous regions are observed for Cu and Hg. The peak densities are  $0.2^\circ\text{C}^{-1}$  and  $0.65^\circ\text{C}^{-1}$  respectively. The peak half-width for Cu ranges from  $1^\circ\text{C}$  to  $4^\circ\text{C}$ , whereas that for Hg rarely exceeds  $1^\circ\text{C}$ . In the range of  $45\text{--}49^\circ\text{C}$ , Cu and Hg exhibit a wide peak and a triplet, respectively; in the range of  $49\text{--}50^\circ\text{C}$ , a minimum and a wing of peak *d* are observed for Cu and a single peak is observed for Hg. However, it should be noted that the wide anomalies observed for Cu could be split into narrower components in experiments with a higher resolution (similar to that obtained for Hg). The anomalies of the materials studied differ also in intensity. For  $\text{CuSO}_4 \cdot 5\text{H}_2\text{O}$ , the intensities are most significant and reach 10.0, a value that is comparable with reported data for some other salts (it is necessary to point out that we could not estimate the intensity of the strongest peak in the range

of 45–49°C due to a rapid wedging out of the face). For Cu, the maximum intensities are 1.7, whereas for Hg they are somewhat smaller, reaching 1.3.

It is noteworthy that various anomalies of the same material exhibit different variations in intensity. For example, for Hg, with a decrease in overvoltage, the peaks in the range of 44–47°C smooth out, whereas the intensity of the peak observed in the range of 47–48°C sharply increases; in the range of 48–52°C, a change in the ratio of the peak intensities is also observed, although it is not so pronounced. On the contrary, salts exhibit a similar change in the intensities of different anomalies for the same face with a change in supersaturation (Glikin et al. 1982), whereas the relative peak intensities for  $\text{CuSO}_4 \cdot 5\text{H}_2\text{O}$  change only slightly.

Specificity of anomalies of various materials can be accounted for by different types of their surfaces. It is possible that the low intensity of electrochemical anomalies results in the higher rates of boundary processes in comparison with those observed during crystallization from a solution. This concept is in a good agreement with the fact that the anomalies of Hg are less intensive than those of Cu, since the rate of adsorption on an amorphous substrate exceeds that on a crystalline substrate, which has a limited number of growth points.

It is most likely that both the bulk of solution and the adsorption layer are responsible for generation of anomalies. The adsorption layer, in particular, inherits the bulk structural alterations. To separate the roles of the bulk and surface processes, it is necessary to perform measurements with a higher temperature resolution and improved reproducibility of the intensity data.

The results obtained give a new objective evidence for the reality of kinetic anomalies of crystal growth and their relationship with the structural alterations in the crystallization medium.

Mechanisms of crystal growth in solutions are defined by molecular forms of matter, i.e., associations, complexes, clusters, and other elements of the liquid structuring in the solution bulk and adsorption layers. Unfortunately, applications of direct instrumental measurements to the solution structures are extremely limited, and peculiarities of the crystal growth have to be related to the solution structure only via indirect indications. Even a single system includes a wide diversity of structural elements (e.g., see water clusters of Bernal-Fowler's model), which are continuously undergoing deformations, transformations, interchanges, etc., that result in their having indefinite and statistic meaning, which is so unlike to that of the solids. Nevertheless, discussion of matter diffusion migration forms, adsorption layer structure, capture of inclusions, and other molecular processes of crystallization require corresponding pictorial models of associated particles in solutions that are constantly developed to meet this demand. Thus, at the end of the nineteenth century, E. S. Fedorov suggested in-building of three-dimensional blocks formed within the medium (D. I. Mendeleev suggested his main principles of solution structures at about the same time) into the crystal structure and his theory, almost unaltered, has been used till date. Developing the model of so-called quatarons also takes into account dynamics of structural elements (Askhabov 2002, 2004, 2006). However, it should be acknowledged that these models involve a great deal of hypothesizing.

Discovering the kinetic anomalies of the crystal growth is probably one of the most important achievements of crystallogenesis, which has not been fully appreciated yet. In our opinion, revealing the nature of anomalies is to be considered as a key for deciphering molecular mechanisms of crystallization, and available experimental data allow the creation of a model of origin of structural rearrangements and anomalies in solution.

First, it can be assumed that each anomalous peak corresponds to a specific state of the solution; this assumption has been already discussed in connection with supposedly different structural states of the solution corresponding to the regions located on the opposite sides of the peak (Glikin et al. 2002). Abrupt acceleration of the growth can result from a structural disordering of the liquid under the action of certain temperature influence. Such disordering, in turn, can result from an oscillatory resonance created by various structural elements of the solution, i.e., water associates, solvate complexes, clusters, quatarons, ion pairs, free particles, etc. Temperature dependencies of oscillation frequencies of these particles are naturally different. At some temperatures, some of the dependences would coincide, causing the resonance phenomena to occur and the structural properties to alter, the latter involving the rate of crystal growth. A wide diversity of the solution structural components, each of them inevitably having an individual oscillatory spectrum and, consequently, a specific temperature dependence of the spectrum, ensures existence of a wide variety of resonance and, hence, anomalous states.

The following macroscopic phenomena can form a basis for this model:

1. Temperature shifts of pure-water absorption maxima and those of the aqueous solutions are different, while for  $\text{H}_2\text{O}$  and  $\text{NaClO}_3$  similar maxima observed at about 750 nm coincide at 39°C (Ganz 1936, 1937). The same temperature corresponds to a range of anomalous growth rates of the substances in question (Sipyagin 1967; Sipyagin and Chernov 1972; Chernov and Sipyagin 1980). Thus, it can be supposed that the anomalies can be induced by resonance interaction of water components and solvate complexes. Nevertheless, it should be noted that external irradiating of the solution having the temperature in the above diapason did not result in any acceleration of the growth of sodium chlorate crystals (Glikin et al. 1976).
2. Growth rate of sodium chlorate crystals can increase by about 30% (the average value is about 16%) if the solution is irradiated with the IR light of 3,000 nm wavelength (Glikin et al. 1976). This IR range corresponds to the main absorption band of water, i.e., the resonance excitation of aqueous solution components is found to accelerate crystal growth.
3. Heating the system  $\text{NaClO}_3\text{--H}_2\text{O}$  in various heating media (water and heptane) changes the growth rate of the crystals by about 31% (maximum is about 124%; Glikin 1976). This effect can be accounted for by differences in radiation spectral characteristics of different heating media resulting in different selective warming of the chemical bonds of the system constituents due to resonance excitation. Analogous process is also likely to proceed at the cluster level.

Verification of the model can be obtained in the course of studying the anomalies in the experiments of electroreducing the metals accompanied by simultaneous IR irradiation in various wavelength diapasons in the way similar to that described above for  $\text{NaClO}_3$  (Glikin et al. 1976). At the same time, further investigations of anomaly spectra of various substances and systems of various structures, as well as in different solvents seem to be necessary. Such investigations could facilitate interpretation of various anomalous peaks and elucidate the origin of anomalies.

## References

- Abramovich YuM, Nechaev YuA (1960) Autigenous fluorite in Kungur sedimentary rocks of the Perm side of the Urals. *Doklady Acad Sci USSR* 135:2:414-415 (Russ.)
- Aliiev RM, Mirzoeva FR (1971) On the presence and crystallography features of fluorite of the Gushchin deposit. *Doklady Acad Sci Azerbaijan SSR* 27:1:47-49 (Russ.)
- Arkhipchuk RZ (1971) Habit evolution of some minerals in fluorite deposits of the Western Transbaikalia. In: *Mineralogy and Mineralogical Crystallography*. Ed Sverdlovsk Mining Institute, Sverdlovsk (Russ.) Please, change 'Arkhipchuk 1966' to 'Arkhipchuk 1971' in the note 13 to Table 7.3, page 267
- Arkhipchuk RZ, Lokerman AA (1966) New data for the dependence of fluorite crystal habit on the formation conditions. *Miner Collected Papers Lvov Univ* 20:4:602-605 (Russ.)
- Arkhipchuk RZ, Vovk PK (1971) Crystal morphology of fluorite from the Darasun deposit. In: *Mineralogy and Mineralogical Crystallography*. Ed Sverdlovsk Mining Institute, Sverdlovsk (Russ.)
- Artem'ev DN (1914) Method of crystallization of spheres and its application for studying forms and structure of crystalline matter. Petrograd [See also In: Popoff B (ed) *Travaux de la Société Impériale des Naturalistes de Pétersbourg*. Vol. XXXVII, livr. 5. Section de Géologie et de Minéralogie. Birkenfeld, Petrograd 1915] (Russ.)
- Askhabov AM (1979) Regeneration of crystals. Nauka, Leningrad (Russ.)
- Askhabov AM (2002) Clusters of the "hidden phase" (quaterones) and their role in the processes of crystal nucleation and growth. In: Kovalchuk MV (ed) *Problems of modern crystallography: physics of crystallization*. To the G.G. Laemmlein's centenary. Fizmatlit, Moscow (Russ.)
- Askhabov AM (2004) Cluster (quaterone) self-organization of the matter at nanolevel and formation of crystalline and non-crystalline materials. *Zapiski Russ Miner Obsh* 4:108-123 (Russ.)
- Askhabov AM (2006) Cluster (quaterone) mechanism of formation of liquid water. *Zapiski Russ Miner Obsh* 1:123-129 (Russ.)
- Avdonin VN (1968) Fluorite in Carbonian limestones of the East side of the Urals. *Proc Inst Geol Geochem Ural Branch Acad Sci USSR: Miner Collected Papers* 8:71-76 (Russ.)
- Balitskii VS, Ozerova NA, Komova VV (1983) Hydrothermal crystallization and typomorphic features of zinnabar and antimonite. Nedra, Moscow (Russ.)
- Barabanov VF (1959) Fluorite from the Bukuka wolframite deposit (East Transbaikalia). *Zapiski Vsesoyuz Miner Obsh* 88:2:129-136 (Russ.)
- Becquerel M (1874) Dixieme memoire sur la formation de diversis substances cristallises dans les espaces kapillaires. *Compt Rend* 78:1081
- Bienfait M, Boistelle R, Kern R (1964) Théorie des morphodromes; applications aux formes de croissance de NaCl en solution aqueuse en présence d'impuretés. *C. R. Acad. Sci.* 258:3:880-883
- Bocharov SN (2004) Kinetic anomalies of crystal growth as indicators of structure transformations in the solution *Vestn. St. Peter. Univ. Ser. 7 Geol Geogr* 3:16-21
- Bocharov SN, Glikin AE (2008) Kinetic anomalies of crystal growth: development of methodical approaches and interpretations. *Crystallogr Reports* 53:1:147-153

- Bogoyavlenskaya IV, Blyakhman EI (1968) Temperature of fluorite formation of the Irbin deposit. Proc Res Inst Synthesis Mineral Row Materials: Investigation of Mineral Forming Solutions 11:228 (Russ.)
- Bravais A (1866) Etudes cristallographiques. Gauthier-Villars, Paris
- Buckley HE (1951) Crystal growth. New York, London
- Bulakh AG (1981) Graphics of crystals. Nedra, Moscow (Russ.)
- Bunn CW (1933) Adsorption, oriented overgrowth and mixed crystal formation. Proc Roy Soc (London) A141:567–593
- Bushinskii GI (1936) On the fluorite origin in sedimentary rocks. Izvestia Acad Sci USSR, ser geol 5:775–779 (Russ.)
- Bystrom A, Wilhelmi KA (1951) The crystal structure of  $(\text{NH}_4)_2\text{Cr}_2\text{O}_7$ . Acta Chem Scand 5:1003–1010
- Chernov AA (1984) Processes of crystallization. In: Vainshtein BK, Chernov AA, Shuvalou LA (eds) Modern Crystallography III, Crystal Growth. Springer, Berlin
- Chernov AA, Sipyagin VV (1976) Ordering the solution films on the crystal surfaces and growth of crystals. In: GI Distler, Pyu Butyagin (eds) Active surface of solids. Nauka, Moscow (Russ.)
- Chernov AA, Sipyagin VV (1980) Peculiarities in crystal growth from aqueous solutions connected with their structures. In: E. Kaldis (ed) Current topics in materials science, Vol. 5. North-Holland, Amsterdam/New York/Oxford
- Chizhov MK, Petrov TG, Glikin AE (1973) On the possible way of environment influence on the fluorite crystal habits. In: Frank-Kamenetskii VA (ed) Crystallography and crystallochemistry 2. Leningrad State University, Leningrad (Russ.)
- Dalgaard GAP, Hazell AC, Hazell RG (1974) The crystal structure of ammonium dichromate,  $(\text{NH}_4)_2\text{Cr}_2\text{O}_7$ . Acta Chem Scand A28:5:541–545
- Dolivo-Dobrovol'skii VV (1968) On the energy calculations of mineral crystallization sequences. Zapiski Vsesoyuz Miner Obsh 4:508–510 (Russ.)
- Dolivo-Dobrovol'skii VV (1973) On correlation between a so-called structural looseness of minerals and interatomic distances in crystals. Zapiski Vsesoyuz Miner Obsh 6:730–735 (Russ.)
- Donnay JDH, Harker D (1937) A new law of crystal morphology extending the law of Bravais. Amer Miner 22:5:446–467
- Dymkov YuM (1957) Fluorite crystals passed skeleton growth stage. Proc Miner Museum Acad Sci USSR 8:146–150 (Russ.)
- Ermakov NP (1948) Use of defects in fluorite crystals for investigating mineral natural history. Miner Collected Papers Lvov Geol Soc 2:53–74 (Russ.)
- Evzikova NZ (1958) On a question on changing the habit of mineral crystals in the process of their growth. Zapiski Vsesoyuz Miner Obsh 6:647–656. (Russ.)
- Evzikova NZ (1959) Notes to the paper by V.F.Barabanov “Fluorite from the Bukuka volframite deposit (East Transbaikalia)”. Zapiski Vsesoyuz Miner Obsh 88:5:612–614 (Russ.)
- Evzikova NZ (1965) The principles of structural and geometric analysis of crystal faces. Zapiski Vsesoyuz Miner Obsh 2:129–142 (Russ.)
- Evzikova NZ (1983) The problem of mineralogical interpretation of crystal forms. Zapiski Vsesoyuz Miner Obsh 1:112–117 (Russ.)
- Evzikova NZ (1984) Exploratory crystal morphology. Nedra. Moscow.
- Faiziev AR (1973) On the fluorite morphology at the Ak-Jilga deposit (East Pamir). Zapiski Vsesoyuz Miner Obsh 102:6:685 (Russ.)
- Faiziev AR (1978) Crystallomorphology of fluorite from deposits of Central Tajikistan. In: Rundkvist DV, Marin YuB (eds) Minerals and mineral associations. Nauka, Leningrad (Russ.)
- Frank-Kamenetskii VA, Pavlishin VI, Yushkin NP, et al. (1987) Main results and tasks of mineralogical crystallography. Miner Zhurn 9:1:7–15 (Russ.)
- Franke VD (1986) Temperature anomalies of growth rates of  $\text{FeCl}_2 \cdot 4\text{H}_2\text{O}$  crystals in solutions containing hydrochloric acid. In: Frank-Kamenetskii VA (ed) Aspects of genetic and structural crystallography. Leningrad Society of Naturalists, Leningrad (Proc Leningrad Soc Naturalists 79:2:131–138) (Russ.)

- Franke VD, Punin YuO (1972) Investigation of viscosity of potassium chloride solutions in the region of the phase transition in solution In: Frank-Kamenetskii VA (ed) Crystallography and crystallochemistry. Leningrad State University, Leningrad (Russ.)
- Friedel, G. (1904). Etude sur les groupements cristallins. Extrait du Bulletin de la Société de l'Industrie minière, Quatrième série, Tomes III e IV. Saint-Etienne, Société de l'imprimerie Thèolier J. Thomas et C., 485 pp.
- Ganz E (1936) Über dem Absorptionsspektrum von wässrigen Lösungen 0.70–0.90 $\mu$ . Zs Phys Chem (Leipzig) Abt B 33:163–178
- Ganz E (1937) Absorption spectra of aqueous solutions between 0.70 and 0.90 $\mu$  // Zs. Phys. Chem. (Leipzig) Abt B 35:1–10
- Gendelev SSh (1961) Morphological classification of crystal growth striae. Zapiski Vsesoyuz Miner Obsh 6:629–636 (Russ.)
- Gendelev SSh (1963) Face morphology of crystals of yttrium-iron garnet. Kristallografia 3:431–436 (Russ.)
- Glazov AI (1981) Methods of crystal morphometry. Nedra, Leningrad (Russ.)
- Glazov AI, Glikin AE (1981) Necessary comments to the publication Problem of genetic interpretation of crystal habit. Zapiski Vsesoyuz Miner Obsh 2:252–254 (Russ.)
- Glazov AI, Glikin AE (1983) On some methodological aspects of investigations of crystal habits. Zapiski Vsesoyuz Miner Obsh 3:372–376 (Russ.)
- Glikin AE (1976) Composition of a heating medium as a factor of crystallization process. Kristallografiya 21:3:622–623 (Russ.)
- Glikin AE (1978) Development and grounds for a structural-chemical evaluation of influence of the medium components upon the crystal faceting. PhD thesis. Leningrad State University, Leningrad (Russ.)
- Glikin AE (1981) Effect of flux components on CaF<sub>2</sub> crystal habit. J. Cryst. Growth 52:98–103
- Glikin AE (1982) Methods for evaluation of solution supersaturation in examinations of the crystal typomorphism. In: Frank-Kamenetskii (ed) Crystallography and crystallochemistry 4. Leningrad State University, Leningrad (Russ.)
- Glikin AE (1995) Crystallogenesis and geological-mineralogical sciences – coordination problems (by example of metasomatism phenomena). Zapiski Vsesoyuz Miner Obsh 4:116–125 (Russ.)
- Glikin AE (1996) The physicochemical aspect of the unsteady state of metasomatic crystal production. Geochem Intern 33:8:117–128 (Russ.)
- Glikin AE, Glazov AI (1979) Problem of genetic interpretation of the crystal habit. Zapiski Vsesoyuz Miner Obsh 5:536–551 (Russ.)
- Glikin AE, Glazov AI (1983) Rational and discussional in the problem of genetic interpretation of the crystal habits. In: Yushkin NP (ed) New ideas in genetic mineralogy. Nauka, Leningrad (Russ.)
- Glikin AE, Petrov TG (1966) Experimental investigation of growth habits of fluorite crystals in hydrothermal conditions. In: Lasarenko EK (ed) Collected Miner Papers Lvov Geol Soc 20:3:443–446 (Russ.)
- Glikin AE, Nikolaeva VP, Artamonova OI (1974) A method for growing monocrystals of potassium biphthalate. Authorship certificate 421355. Bull Invent 12 (Russ.)
- Glikin AE, Petrov TG, Boldyreva OM (1976) On the influence of light upon crystallization of NaClO<sub>3</sub> from aqueous solutions. Kristallografiya 21:1:225–226 (Russ.)
- Glikin AE, Nikolaeva VP, Petrov TG (1979) Crystallization of potassium biphthalate from neutral and alkaline aqueous solutions. In: Smirnov YuM (ed) Physics of crystallization. Kalinin State University, Kalinin (Russ.)
- Glikin AE, Sipyagin VV, Punin YuO (1982) On the influence of supersaturation upon behavior of anomalies of crystal growth rates. In: Frank-Kamenetskii (ed) Crystallography and crystallochemistry 4. Leningrad State University, Leningrad (Russ.)
- Glikin AE, Franke VD, Marina EYu et al. (1994) Crystallochemical aspects of ammonium dichromate morphology. Vestnik St. Petersburg State Univ (ser 4) 2:11:113–115 (Russ.)
- Glikin AE, Kiryanova EV, Sinai MYu et al. (2002) To the problem of crystal morphogenesis in solutions. In: Kovalchuk MV (ed) Problems of modern crystallography: physics of crystallization. To the G. G. Laemmlein's centenary. Fizmatlit, Moscow (Russ.)



- Glikin AE, Bocharov SN, Kiryanova EV et al. (2003) Growth rate anomalies and faceting of sodium chlorate crystals. *Zapiski Vsesoyuz Miner Obsh* 2:99–107 (Russ.)
- Groth P (1906) *Chemische Kristallographie 1*. Verlag von Wilhelm Engelmann, Leipzig
- Hartman P (1963) Crystal form and crystal structure. In: Fox D et al. (eds) *Physics and chemistry of the organic solid state*, Vol. 1. Interscience, New York.
- Hartman P (1974) On the crystal habit of fluorite. In: Aleksiev, E, Mincheva-Stefanova I, Radonova TG (eds) *Mineral genesis*. Publishing House of the Bulgarian Academy of Science. Sofia.
- Hartman P, Perdok WG (1955a) On the relation between structure and morphology of crystals 1. *Acta Cryst* 8:1:49–52
- Hartman P, Perdok WG (1955b) On the relation between structure and morphology of crystals 2. *Acta Cryst* 8:9:521–529
- Hartman P, Perdok WG (1956) An interpretation of the law of Donnay and Harker. *Amer Miner* 41:5–6
- Häüy RJ (1801) *Traité de mineralogie*. Chez Louis Paris
- Holzgang F (1930) Zur Morphologie von Fluorit, Scheelit und Brookit. *Schweiz Min Petr Mitt* 10:374–476
- Honigman B (1958) *Gleichgewichts- und Wachstumsformen von Kristallen*. Dr. Dietrich Steinkopff Verlag, Darmstadt.
- ICPDF* (1999) *Power Diffraction File International Center for Diffraction Data*, Swarthmore Pennsylvania, USA
- Ikornikova NYu. (1975) Hydrothermal synthesis of crystals in chloride systems. Nauka, Moscow (Russ.)
- Kalb G (1923) Kristalltracht, Vorkommen und Bildungstemperatur der Mineralien. *Cbl. Miner. Geol., Paläontol* 11:23
- Kasatkin AP (1966) Influence of light upon growth of NaBrO<sub>3</sub> crystals. *Kristallografiya* 11:2:328–330 (Russ.)
- Kasatkin IA, Glikin AE, Grunskii OS (1995) Multi-headed (multi-edged) and parallel-block structures of crystals resulting from their growth in non-stationary conditions. In: *Geology* 2. Tikhonov AN (ed) Moscow State University, Moscow (Russ.)
- Kazakov AV, Sokolova EI (1950) Conditions of fluorite formation in sedimentary rocks. *Proc Inst Geol Soc Acad Sci USSR, ser geol* 114:40:22–64 (Russ.)
- Kern R (1968) Croissance cristalline et adsorption. *Bull. Soc. Franc. Mineral. Cristallogr.* 91:3:247–266.
- Kibalczyk W, Kolasinski W (1977) Badanie liniowej prędkości wzrostu kryształów KDP. *Zeszk nauk Politech Łódź* 271:51–62 (Polish)
- Kiryanova EV (2003) New effects of crystal-solution phase equilibria in a model system NaNO<sub>3</sub>-H<sub>2</sub>O. *J Cryst Growth* 253:1–4:452–459
- Kiryanova EV, Glikin AE (1986) Regularities of crystal morphology of synthetic fluorite. *Zapiski Vsesoyuz Miner Obsh* 2:226–234 (Russ.)
- Kiryanova EV, Glikin AE (1999) The laws of fluorite and calcite habit formation in terms of the morphogenetic structural-chemical concept. *J Cryst Growth* 198/199:697–703
- Kiryanova EV, Glikin AE, Kazitsyna OYu (1984) Acid-alkaline influence of a medium upon the fluorite crystal habit (in the course of low-temperature mineral formation). *Zapiski Vsesoyuz Miner Obsh* 5:628–632 (Russ.)
- Kleber W (1955/1956) Über Hypomorphie. *Wiss Zs Humboldt-Univ Berlin, Math-Natur R* 5:1–13
- Kleber W (1960) Hypermorphie. *Neues Jahrb Miner* 94:2
- Kleber W, Ickert L, Ahrens E (1967) Ein Beitrag zur Epitaxie von Alkalihalogeniden auf Calcium und Bariumfluorid. *Krist und Techn* 2:1:47–54
- Korytov FYa (1972) Shape and color of fluorite from Transbaikalia fluorite deposits. In: *Typomorphism of minerals and its practical significance*. Nedra, Moscow (Russ.)
- Kostov I, Kostov RI (1999) *Crystal habit of minerals*. Academy Publishing House & Pensoft Publishing (Bulgarian Academic Monographs 1), Sofia
- Kozlova OG, Kharitonov YuA, Belov NV (1979) Hypomorphy and hyperperomorphy. *Doklady Acad Sci USSR* 247:1:100–106 (Russ.)

- Krastanov L, Stranski I (1938) Über die Kristallisation von Alkalihalogenidkristallen auf Fluorit. *Zs. Krist Bd 99*:5:444–451
- Kukushkina OA, Pleskova MA, Simonova LI (1976) Typomorphism of accessory fluorite from some granite massifs. *Sketches on Genetic Mineralogy*. Nauka, Moscow (Russ.)
- Kunz AF (1974) Typomorphic peculiarities of natural and synthetic crystals of  $\text{CaF}_2$ . In: Fishman MV (ed) *Geology and minerals of the North-East of European part of the USSR*
- Kunz AF (1976) Fluorite crystal growth under hydrothermal conditions and its structural and morphological features. In: Yushkin NP (ed) *Problems of genetic information in minerals*. Komi Branch Acad Sci USSR, Syktyvkar
- Kunz AF (1982) Crystallization of yttrium fluorite under hydrothermal conditions. *Proc Inst Geol Komi Branch Acad Sci USSR, Crystallogenesi* 39:31–41. Ed Acad Sci USSR, Syktyvkar.
- Laemmlin GG (1948) Sectorial structure of crystals. *Academy of Science USSR*. Moscow [see also: Laemmlin GG (1973)] (Russ.)
- Laemmlin GG (1973) *Morphology and genesis of crystals*. Nauka, Moscow (Russ.)
- Lieberts J (1965) Hydrothermal-Untersuchungen an einigen Verbindungen. *Chem Ing Techn* 37:8:830–832
- Mikhailov MA, Sipovskii DP, Glikin AE, et al. (1973) Crystallization of yttrium-iron garnet and orthoferrite under hydrothermal conditions. In: Frank-Kamenetskii VA (ed) *Crystallography and crystallochemistry 2*. Leningrad State University, Leningrad (Russ.)
- Minerals* (1960–2003) Reference book I–V. Nauka, Moscow (Russ.)
- Minerals* 2:1 (1963) Reference book. Nauka, Moscow (Russ.)
- Moskalyuk AA, Zakharchenko AI (1966) Results of investigating gas-liquid inclusions in fluorite and quartz crystals of pegmatites in the Kaib granit massif (Central Kazakhstan). *Proc Res Inst Synthesis Mineral Raw Materials: Investigation of Mineral Forming Solutions* 9:87–92. (Russ.)
- Nikolaeva VP, Petrov TG (1973) Correlations between vicinal formations produced on a face of the alum octahedron and crystal structure defects. In: Frank-Kamenetskii VA (ed) *Crystallography and crystallochemistry 2*. Leningrad State University, Leningrad (Russ.)
- Novgorodova MI (1968) On morphology of chalcopyrite crystals obtained from deposits belonging to various genetic types. *Zapiski Vsesoyuz Miner Obsh* 5:582–593 (Russ.)
- Ovchinnikov LN, Masalovich AM (1977) Polymorphism of water and its role in hydrothermal mineral formation. *Zapiski Vsesoyuz Miner Obsh* 106:2:179–192.
- Paneth F (1914) Über Adsorbierung und Fällung der Radioelemente. *Phys Zs* 15:924–939
- Pleskova MA, Balitskii VS (1966) Typomorphic features and formation conditions of fluorite in pegmatites of Central Kazakhstan. *Miner Collected Papers Lvov Univ* 20:4:519–525 (Russ.)
- Petrov TG (1964) Effect of media upon the growth of potassium nitrate crystals from aqueous solutions. *Kristallografiya* 9:4:541–546 (Russ.)
- Petrov TG (1977) On impossibility of determination of crystallization sequence according to individual characteristics of minerals. *Zapiski Vsesoyuz Miner Obsh* 4:499–502 (Russ.)
- Petrov TG, Treivus EB, Kasatkin AP (1969) Crystal growing from solutions. Academic, New York
- Petrov TG, Treivus EB, Punin YuO, Kasatkin AP (1983) Crystal growing from solutions. Nedra, Moscow (Russ.)
- Petrovskii VA (1983) Growth of crystals in heterogeneous solutions. Nauka, Leningrad (Russ.)
- Pleskova MA, Balitskii VS (1966) Typomorphic features and formation conditions of fluorite in pegmatites of Central Kazakhstan. *Miner Collected Papers Luov Univ* 20:4:519–525 (Russ.)
- Popov VA (1984) Applied crystal morphology of minerals. Academy of Science USSR. Sverdlovsk (Russ.)
- Popov VA, Popova VI (1996) Associations of mineral crystal habits. Academy of Science USSR. Miass (Russ.)
- Pruss E (1981) Flußspat. Skalenoedrische Flußspat-Kristalle von Wölsendorf und Zschopau. *Lapis* 6:1:14
- Punin YuO, Nekhorosheva AG (1987) Decomposition of copper sulfate crystals under non-stationary growth conditions. *Vestnik Leningrad State University. Ser. Geol Geogr* 18:68–72 (Russ.)
- Punin YuO, Petrov TG (1972) Anomalies of growth rates of potassium chloride crystals growing from aqueous solutions. In: Sheftal NN (ed) *Growth of crystals IX*. Nauka, Moscow (Russ.)

- Pupin JR, Turco G (1972) Unetipologie originale du zircon accessorie. *Bull. Soc Franc Miner Crist* 95:348–359
- RyklD, Bauer J (1972) Hydrotermalni syntesa fluoritu. *Sb Vysoká Škola Chemicko-Technologická (VSCT) Praha* 14:13–19 (Czech)
- Scheerer T, Drechsel E (1873) Künstliche Darstellung von Flußspat und Schwerspat. *Zs. prakt. Chem* 7:63
- Shafranovskii II (1957) *Crystals of minerals 1: flat-faced forms*. Leningrad State University, Leningrad (Russ.)
- Shafranovskii II (1968) *Lectures on crystal morphology of minerals*. Vysshaya Shkola, Moscow (Russ.)
- Shafranovskii II (1981) Some notes concerning the problems of genetic interpretation of the crystal habits. *Zapiski Vsesoyuz Miner Obsh* 1:119–124 (Russ.)
- Shubnikov AV (1975) Influence of solution supersaturation degree upon the habits of precipitating alum crystals. In: AV Shubnikov (ed) *Selected works on crystallography*. Nauka, Moscow (Russ.)
- Shushkanov AD (1969) On the hydrothermal synthesis of fluorite. *Proc VII Conf young researchers, Miner Sect 2*. Ed. All-Union Institute for Mineral Row Materials, Moscow (Russ.)
- Shuvalov LA, Urusovskaya AA, Zheludev IS, et al. (1988) Physical properties of crystals. In: Vainshtein BK, Chernov AA, Shuvalov LA (eds) *Modern Crystallography III*. Springer, Berlin.
- Sipovskii DP (1964) First stages of crystal regeneration in solutions (exemplary systems:  $KAl(SO_4)_2 \cdot 12H_2O$ ,  $NaBrO_3$ ,  $NaCl$ ). *Kristallografia* 9:2:242–247 (Russ.)
- Sipyagin VV (1967) Some anomalies of  $NaClO_3$  and  $KClO_3$  face growth rates depending upon the temperature at constant supersaturation. *Kristallografia* 4:678–683 (Russ.)
- Sipyagin VV, Chernov AA (1972) Anomalous temperature dependences of growth rates of  $KNO_3$ ,  $NaNO_3$ ,  $NaNO_2$ ,  $NaClO_4$  and Seignette salt crystal faces when growing from aqueous solutions. *Kristallografiya* 5:1003–1008 (Russ.)
- Sipyagin VV, Chernov AA, Fedin EI, et al. (1976) NMR investigation of solution thin films adsorbed on the crystal faces. *Kristallografia* 2:370–380 (Russ.)
- Solubility* (1961–1970) Reference book 1–3. Nauka, Moscow (Russ.)
- Stroitelev SA (1961) Origin of combination striae in crystals. *Zapiski Vsesoyuz Miner Obsh* 6:709–713 (Russ.)
- Sunagawa I (2005) *Crystals*. Cambridge University Press. Cambridge/New York/Melbourne/Madrid/Cape Town/Singapore/São Paulo
- Tatarskii VB (1965) *Crystal optics and the immersion method*. Nedra, Moscow (Russ.)
- Tatarskii VB (1967) On compositions of the flat nets, which are parallel to various faces of a crystal. *Miner Sborn Lvov Univ* 21:4:386–387 (Russ.)
- Treivus EB (1986) On corresponding forms of mineral crystals. *Zapiski Vsesoyuz Miner Obsh* 3:390–392 (Russ.)
- Treivus EB (1989) Some kinetic aspects of crystal morphology of minerals. *Zapiski Vsesoyuz Miner Obsh* 3:91–100 (Russ.)
- Vasilkova NN, Kukushkina OA, Sidorenko GA, Shushkanov AY (1972) Experimental investigation of fluorite typomorphic features. In: *Typomorphism of minerals and its practical significance*. Nedra, Moscow (Russ.)
- Vasilkova NN, Kukushkina OA (1976) Fluorite crystal morphology by the results of hydrothermal synthesis. In: *Novelties in mineralogical investigations*. Ed: All-Union Institute for Mineral Row Materials, Moscow (Russ.)
- Vasilkova NN, Kulikov IV, Lyapunov SM (1980) Fluorite as an indicator of formation conditions and zoning of sheelite-fluorite ore association of Tyrnyauz. *Miner J* 2:6:45–54 (Russ.)
- Volkova LP (1953) Fluorite in Bashkirian High-Permian sedimentary rocks. *Izvestia Acad Sci USSR, ser geol* 6:117 (Russ.)
- Vovk PK, Melnikov VS (1966) Fluorite crystal morphology from some fluorite deposits of the Khurai group (Western Transbaikalia). *Miner Collected Papers Lvov Univ* 20:4:498–507 (Russ.)
- Voskresenskaya IE, Barsukova ML (1968) Preparation and properties of certain iron-containing and non-iron tourmalins. In: Lobachev AN (ed) *Hydrothermal synthesis of crystals*. Nauka, Moscow 75–191 (Russ.)

- Wells AF (1946a) Crystal habit and internal structure I. *Phil Mag* 37:266:184–199
- Wells AF (1946b) Crystal habit and internal structure II. *Phil Mag* 37:267:217–236
- Wells AF (1946c) Crystal habit and internal structure III. *Phil Mag* 37:272:605–630
- Winchell AN, Winchell H (1964) The microscopical characters of artificial inorganic solid substances: optical properties of artificial minerals. Academic, New York/London
- Wyckoff R (1966) *Crystal structures* 3. Wiley, New York/London/Sydney
- Yaroshevskii AA (1959) To the relations of garnet crystal habit with mineral forming conditions. In: *Proc Miner Museum Acad Sci USSR* 10:137–141 (Russ.)
- Yushkin NP, Romashkin YuN, Markova GA (1983) Ural-New Earth fluorite region. Nauka, Leningrad (Russ.)
- Zatsikha BV (1968) Fluorite formation conditions in pegmatites of the granite massif Stone Graves (Azov region). In: Smirnov VI, Ermakov NP, Dolgov YuA et al. (eds) *Mineralogical Thermometry and Barometry 2 osov* (Russ.)
- Zatsikha BV, Vovk PK, Pavlishin VI, Kurovets MI (1971) Fluorite of chamber pegmatites from Vol. *Doklady Acad Sci Ukrainynian SSR* B10:884–888 (Ukrainian)
- Zemyatchenskii PA (1909) *Crystallogenic sketches I*. Imperial Academy of Science, St. Petersburg (Russ.)
- Zemyatchenskii PA (1911) *Crystallogenic sketches II*. Imperial Academy of Science, St. Petersburg (Russ.)
- Zidarova B, Maleev MN, Kostov I (1978) Crystallogenesis and habit zoning of fluorite from Mikhailovsoe deposit, Central Rodopi. In: *Geochemistry, Mineralogy, and Petrology* 8. Ed: Bulgarian Acad Sci, Sofia (Bulgarian)

# Conclusion

## On Interrelation between Crystallogenesis and Geological and Mineralogical Sciences

The contents of the monograph show that analysis of complex crystallogenic processes involving determination of elementary structural units and elementary processes taking place in these units makes a basis for a clear understanding of crystallogenesis as a whole. Such an approach should take into account four aspects: (1) physicochemical basis of the process defining conditions of growth, dissolution, and equilibrium in various combinations; (2) factors defining the process pathway, the most important of which comprise a number of phases and their compositions, supersaturation, temperature, pressure (hydrostatic and stress), and imperfection of crystals; (3) molecular and macroscopic mechanisms of growth and dissolution including bordering processes of capturing the inclusions and adsorption, volume processes of diffusion and convection in solution, and diffusion and formation of strained areas in crystals; and (4) nature of the substances undergoing the above processes, which can be monocrystals having particular composition, atomic–molecular structure, and imperfection, or aggregates having various degrees of ordering.

Only the first, second, and fourth aspects of the process can be experimentally controlled; some ideas about mechanisms (the third aspect) require additional theorization involving the concepts of crystallogenesis and related sciences. Naturally, completeness of the control and conclusions depend to a great extent upon statement of a problem, methodological scope, and development of the corresponding theories. During investigations of natural objects, only some particular features of the substances, which are products of corresponding processes, which, in turn, had terminated long before the investigations started, can be controlled (the fourth aspect). Conclusions about conditions and mechanisms of the processes (aspects 1–3) can be made on the basis of observations of the substance characteristic features. In such cases completeness of observations and conclusions depends not only upon the statement of a problem and methodological scope, but also upon preservation of the process attributes.

Difficulties stated above gave rise to different approaches to genetic interpretations. Geological approach is based, as a rule, upon regularities naturally following the observations. For example, some well-known definitions of metasomatic process and its examinations make use of phenomenological signs including, e.g., volume ratios, crystal morphology, phase compositions, and distributions and concentrations

of chemical reactants. On the other hand, basis for crystallogenic interpretations and theoretical generalizations consist in reconstruction of the process mechanism. Therefore, in the present monograph consideration of metasomatic process, as well as the other crystallogenic phenomena, e.g., joint growth, capturing admixtures, epitaxy, and faceting involves elucidation of their physicochemical nature, factors, and crystallogenic interpretations.

Inconsistent concept of metasomatism is probably the truest reflection of general state of geological–genetic guideline, which has a long history, full of contradictory theories. This situation became established long ago. Almost 3 decades ago, N. P. Yushkin mentioned “a large proportion of subjectivity in developing genetic schemes,” while A. G. Zhabin pointed out “plain truth – neglect of theoretical problems of our science.” There has been a little change in situation ever since; so, further progress of genetic analysis seems to require a reliable theoretical basis, which has to be developed independently from mineralogical observations.

Crystallogenesis may offer such an opportunity, particularly, its intensively developing branch of crystallogenic simulation of mineral formation processes. This approach can be generalized as follows: a set of basic elements of crystal forms and structures, as well as a set of basic elementary genetic constituents, is relatively small, and only a vast diversity of their combinations determines variety of crystal-forming effects. In principle, all known structural and morphological peculiarities of minerals can be artificially reproduced under corresponding conditions, including low-temperature, hydrothermal, flux (magmatic), or gas-transportation regime. Moreover, majority of phenomena, in particular, including artificial simulating of natural mineral formation, has reliable quantitative or qualitative theoretical interpretations.

Nevertheless, the processes of natural mineral formation are usually simulated without taking into consideration any crystallogenic factors. It can be explained by the following reasons.

Until 1920s crystallogenic investigations had been conducted exclusively on mineralogical basis. Invention of artificial preparation of minerals and formulation of the theory of crystal growth resulted in development of two relatively independent branches, which set forth wholly different tasks. “Physical” branch, which is usually considered to be dealing with “crystal growth,” mostly develops methods and theory mainly involving relatively simple investigations of growing a single crystal in mono-component and, sometimes, binary systems. At present, this branch is being developed by numerous research groups. Mineralogical branch of crystallogenic investigations appeared to be weakened and lagged a way behind the rapidly developing theory. This made incorrect approach for more complex problems of reconstructing conditions and processes of natural crystal formation impossible. Surely enough, a few research crystallogenic groups in geological institutions have not been able to withstand such general tendencies.

Incompleteness of modern crystallogenesis theory weakens its mineralogical aspects. Complete quantitative theories have been developed only for crystallizations in simple gaseous and melt systems. Monomineral crystallization in binary and in some more complex systems is provided with qualitative models. Theoretical

basis of polymineral crystal formation, which is typical for a number of natural and industrial processes, is in its initial stage. Therefore, resultant difficulties in interpreting some phenomena give rise to opposing explanations of natural and experimental process of crystal formation and creation of too simplified inadequate models. Moreover, absence of educational programs for training specialists, who would be able to investigate crystallogenesis of natural and synthetic substances, further aggravates the situation.

Moreover, some crystal formation phenomena comprise processes requiring detailed visual observations, but some of them are impossible to perform due to the absence of reliable physical methods for investigations at molecular level, i.e., sometimes due to lack of necessary facilities results of crystallogenic studies can be stated only with some degree of probability. It should also be pointed out that descriptions of phenomena are not usually obvious enough and the process models are complex and sometimes ambiguous owing to hardly discernible convergence of the phenomena. Construction of models of natural processes by analogy with laboratory objects is even more complicated, as only extremely limited and indirect information on mineral forming conditions is available, and the least available is information about the most significant, i.e., kinetic parameters.

On the contrary, well-developed and widely used experimental methods for determining physical and physicochemical constants (e.g., diffractometry and spectroscopy) ensure obtaining definite and illustrative results, which can be used directly in mineralogy. This can explain usual focusing on crystal properties in a search of cause–effect relationships. The examples of this approach include crystallization series or series of mineral replacements compiled according their structural constants or melting points, series of morphological evolution of minerals, so-called corresponding forms of faceting, thermodynamic influence of intergrain borders, etc.

Relevancy and appropriateness of the above methods have been discussed repeatedly. However, numerous discussions of metasomatism problems and other processes of mineral formation have a surprisingly weak influence upon genetic concepts. Intuitive models appear to be highly resistant toward counterarguments based upon experimental and theoretical concepts of crystallogenesis.

As a result, geological literature turned out to be overloaded with numerous speculative and unrealistic notions, and corresponding scientific and practical problems appear to be extremely intricate and controversial. Therefore, reliable attributes for mineral origin reconstructions are extremely scarce for both relatively simple cases of growth/dissolution of mineral individuals, and more complicated cases of polymineral crystal formation, and of course, for the cases of supreme complexity, namely, transformations in crystalline aggregates. Thus, serious contradictions exist in interpretations of formation of inclusions in minerals; genetic nature of isomorphism and epitaxy has not thoroughly been studied; there are some difficulties in differentiation of primary and secondary attributes of minerals and rocks ... the list is endless. Use of intuitive models is most commonly reasoned by a notion of incomparability of natural and experimental processes of crystallogenesis. It is interesting to note that this reasoning is usually applied to some elements

of morphology and certain types of macrodefects, while comparison of crystallochemical features of natural and artificially obtained products appears, on the contrary, quite usual. It can be said that an opposite point of view also can be postulated without any reasonable grounds.

Thus, extremely simplified mineralogical-genetic models not related or distantly related to the theory of crystallogenesis and experimental results appear to be highly prevailing. These models often have quite perfect logical structure, which, however, is inwardly closed and is not correlated with the concepts of related sciences. This situation, although possible and even desirable for abstract sciences and philosophic theories such as mathematics and theology, is absolutely unacceptable for sciences dealing with material objects. Well-known cases of a deformed development of biology, cybernetics, medicine, sociology, and economics in some societies can serve as illustrations for such a tendency; in this respect, popularity of analogous models of mineral formation is quite alarming.

The contents of the monograph prove diversity and vast variety of factors determining the processes of natural crystallization. On one hand, it to some degree restricts the use of traditional attributes of minerals in genetic reconstructions, as well as shows inappropriateness of ungrounded simplifications. On the other hand, the state of the art does not allow proposing any algorithms for genetic analysis, and the perspectives of their formulation are still unclear. However, the presented multidimensional picture allows false interpretations of some phenomena on the basis of combination of some factors chosen arbitrarily. Only strict selection of assumptions and rigorous analysis of material on their basis can help in avoiding such false interpretations.

Mutual relations between crystallogenesis and geological sciences have been described in a quite few publications. This problem does not seem to be regarded seriously. At present it seems necessary to unite both crystallogenic and crystallochemical approaches in mineralogical models. In some our works – studying isomorphic replacement, epitaxial growth, and forms of crystals – it has been taken into account. Importance of crystal chemistry for mineralogy is universally acknowledged. Both branches of science have common history, objects, and models; improvement of interaction between crystallogenesis and crystal chemistry will promote its interaction with geological and mineralogical sciences. The concept of polymineral-metasomatic crystallogenesis presented in the monograph can form a basis for such interaction. The monograph shows applicability of mineralogical methods to solve genetic tasks and possibility of interpreting known mineralogical data that, in turn, promotes application of nontrivial methodological approaches to the genetic analysis. It seems possible that at least some of traditional concepts of crystal formation prevailing in geology, but involving some elements which contradict theory and practice of crystallogenesis, may be reconsidered on the basis of the presented data. We hope that the present monograph will assist in finding solutions for some mineralogenetic and petrogenetic problems.



# Index

## A

- Aggregate metasomatic transformation
  - monocrystals replacement and growth
    - crystal faceting, 181
    - diffusion field, 177, 189
    - diffusion–infiltration theory, 178
    - KNO<sub>3</sub> solution, 181
    - metasomatic crystallogenesis, 177, 182
    - minerals compositions and spatial distributions, 179
    - Na<sub>2</sub>S<sub>2</sub>O<sub>3</sub>–NaNO<sub>3</sub>–H<sub>2</sub>O system, 181
    - polymineral recrystallization, 182, 195–222
    - volume effect, 178
  - Y-Fe-garnet, 180
  - Y-Fe-perovskite, 180
- polymineral recrystallization
  - activity and passivity 212–216
  - grain size change 219–220
  - natural and experimental products, 195–197
  - regularities and mechanisms, 211–222
  - technique and experimental results, 197–211
  - three-stage 216–219
  - thermooscillatory 199–209, 211–220
  - thermogradient 209–211, 221–222
- rapakivi-type structures formation
  - chain orbiculars, 187
  - characteristic features, 194
  - formation scheme, 188
  - Lisegang rings, 188
  - metasomatism, 183
  - phenocrysts, 183–185, 187–189, 193, 194
  - primary crystal zonality, 194
  - shell orbiculars, 185, 186
  - vermiform quartz, 189
  - volume effect, 193

- Ammonium dichromate
  - habit types, 256
  - morphology, 260, 263, 264
  - schematic cross-section, 263
  - shape peculiarities, 261–262
  - spherical coordinates and face symbols, 255
  - structural constants, 254
  - symmetry, 259
  - temperature variations, 261
- Autoepitaxial excrescences, 16
- Amorphous products
  - dissipated automorphs, 25
  - faceted and blurred pseudomorphs, 24
- Automorphs, 16
  - bag-shaped, 24
  - dissipated, 16, 24
  - localized, 16, 20, 22–24
  - translocated, 16, 46, 47
- C
- Co(NH<sub>4</sub>)<sub>2</sub>(SO<sub>4</sub>)<sub>2</sub> · 7H<sub>2</sub>O–Ni(NH<sub>4</sub>)<sub>2</sub>(SO<sub>4</sub>)<sub>2</sub> · 7H<sub>2</sub>O–H<sub>2</sub>O system, 100
- Crystal faceting
  - crystal growth kinetics
    - growth rate anomalies, 282–294
    - infrared radiation effect, 279–282
  - crystal habit
    - ammonium dichromate, 260–262
    - combined striations, 265
    - crystals morphological evolution, 260
    - metasomatic conditions, 266
    - multi-edged and multiheaded subindividuals, 265
    - supersaturation, 260
  - fluorite regularities
    - CaF<sub>2</sub>–CaCl<sub>2</sub>–H<sub>2</sub>O system, 268, 269
    - CaF<sub>2</sub>–KF–H<sub>2</sub>O system, 268–270

- Crystal faceting (*cont.*)
- CaF<sub>2</sub>-LiCl-H<sub>2</sub>O system, 268, 270
  - CaF<sub>2</sub>-NaCl-H<sub>2</sub>O system, 268, 269
  - CaF<sub>2</sub>-NaCl-NaF-CaCl<sub>2</sub> system, 273, 274
  - counter-diffusion method, 270, 272
  - Donnay-Harker's order, 268
  - dry flux systems, 273
  - experimental data, 270, 271
  - hydrothermal deposit, 266
  - morphodromes, 268, 269, 274
  - morphology, 268
  - structure-chemical morphogenesis model, 266
- stationary forms
- adsorptive influence, 251
  - Bravais Law, 250, 254
  - cleavage orientation and perfection, 254
  - crystal typomorphic property, 251
  - diminution theory, 250
  - face size, 253
  - growth rate, 253
  - hyperomorphy, 259
  - hypomorphy, 259
  - Miller index values, 257
  - morphogenesis, 249
  - pseudosymmetry, 259
  - supercooling degree, 254
  - supersaturation, 252
  - water-soluble ammonium dichromate, 254
  - Y-Fe-garnet crystals, 251, 252
- structure-chemical model
- adsorption film structure, 275, 277, 278
  - binary eutectic system, 275
  - CaF<sub>2</sub>-CaCl<sub>2</sub>-NaCl-NaF system, 277
  - epitaxial adsorbate-adsorbent compatibility, 276
  - morphogenetic effectiveness, 276
  - portlandite, 277, 278
  - potassium acidic phthalate, 279
  - proton mobility anisotropy, 285
  - water influence, 276
- Crystal growth kinetics
- growth rate anomalies
    - CaF<sub>2</sub>-NaCl-CaCl<sub>2</sub>-NaF system, 284
    - copper reduction, 287
    - crystal-genetic theory, 285
    - crystallogenesis, 293
    - current density, 286
    - Cu vs. Cu SO<sub>4</sub>·5H<sub>2</sub>O, 290, 291
    - ice-like water structure, 284
    - KClO<sub>3</sub>, 285
    - macroscopic phenomena, 293
    - mechanisms, 286, 292
    - mercury reduction, 288, 289
    - metal electrochemical reduction, 286
    - morphogenesis, 282
    - NaClO<sub>3</sub>-H<sub>2</sub>O system, 293
    - polymorphic transformations, 284
    - polytherm, 287-289
    - proton mobility, 275
    - random error, 287
    - salt deposit, 282
    - sodium chlorate crystal, 293
    - temperature dependence, 282, 283, 285
  - infrared radiation effect
    - crystallization, 279, 280
    - NaClO<sub>3</sub>, 280-282
- Crystal joint growth
- crystal morphology
    - carnallite grain formation, 66, 67
    - eutonic solutions, 64
    - KCl crystal facets, 64-65
    - texture types, 64, 66
  - KCl-NaCl-MgCl<sub>2</sub>-H<sub>2</sub>O system
    - binary equilibria, 72
    - isoconcentration and isothermal eutonic lines, 75-76
    - isothermal line convergence, 75
    - Schreinemakers phase diagram, 72-74
  - kinetic effects and peculiarities
    - diffusion layer, 78
    - diffusion limitation, crystallization process, 76
    - isolated seed behaviour, 77-78
    - metastable equilibrium, 78
    - NaCl solubility, 81
    - nonmonotonous growth rate characteristics, 79-80
    - phase equilibria, 80
    - physicochemical interpretation, 76-77
    - solution composition and eutonic concentrations, 78-79
    - supersaturation, 79
  - kinetics, supercooled solutions, 66-68
    - binary solutions, 66-68
    - growth rate correlation, 69-71
    - kinematical curves, 69
    - nonmonotonous correlation, 68-69
    - quaternary system, 69-70
    - ternary eutonic solutions, 68
  - supercooled solution technique
    - crystallization methods, 61-62
    - eutonic concentrations, 62
    - microcrystallization device, 62-63
    - Schreinemakers concentration diagrams, 63

- Crystallogensis  
 analysis of, 301  
 factors, 304  
 mineral formation processes, 302  
 physical and physicochemical constants, 303
- Crystal replacement, mineralogical aspects  
 actinolite monocrystalline pseudomorph, 50, 51  
 advancing sites, 48  
 amorphous structure, 46  
 cause–effect relationships, 47  
 classification modification, 48  
 conventional types, 46  
 dissipated automorphs, 46,  
 embossed and faceted pseudomorphs, 46  
 isomorphic replacement, 52  
 localized automorphs, 46,  
 monocrystalline structure, 46  
 natural morphological analogs, 49, 50  
 polycrystalline structure, 46  
 space-time superposition, 47  
 translocated automorphs, 46, 47  
 volume-excess reactions, 53  
 zircon and tourmaline poikilitic crystals, 51  
 zoned topaz crystals, 50
- E**  
 Educt, 7  
 Epimorphs, 8  
 Epitaxy and quasiepitaxy  
 CaCO<sub>3</sub> microcrystals orientation  
 distribution, 240  
 rhombohedron surfaces, 240  
 growing or dissolving substrate  
 crystal orientation and process  
 kinetics, 237  
 epitaxial texture, 230  
 growth rates and dissolution, 235, 236  
 morphology, 235  
 quasiepitaxial texture, 230  
 vertical texture, 231, 236, 238  
 principle phenomena  
 excrescence formation, 230, 231  
 oriented and disoriented accretions, 230  
 precipitating crystals, 231  
 techniques  
 assays, 231  
 calcite substrate, 234  
 cleaved microfragments  
 precipitation, 234  
 crystallochemical matching, 232  
 growth and dissolution rates, 234  
 histograms of orientation distribution, 234  
 KCl–NaCl–(MgCl<sub>2</sub>)–H<sub>2</sub>O system, 232  
 K<sub>2</sub>Cr<sub>2</sub>O<sub>7</sub>–KBr–H<sub>2</sub>O system, 232  
 saturation temperatures, 232  
 sodium nitrate substrate, 234  
 textures formation model  
 adhesion, 240  
 crystal disorientation, 243  
 long-range forces, 244  
 nuclei mechanical turning, 242  
 oriented nucleation, 241
- Eutonic systems, 153
- I**  
 Implanted inclusions, 19  
 Isomorphic/non-isomorphic components  
 equilibrium diagram, 168–169  
 isomorphic replacement processes,  
 169–170  
 volume-deficit monocrystalline  
 replacement, 167–168  
 Isomorphic replacement, 52  
 Isothermal replacement  
 complex systems, 162–164  
 ternary systems  
 alyotropic compounds, 161  
 polymorphic modifications, 160  
 salting-in and salting-out process,  
 157–158
- K**  
 KAl(SO<sub>4</sub>)<sub>2</sub>·12H<sub>2</sub>O–CuSO<sub>4</sub>·5H<sub>2</sub>O, 209  
 KAl(SO<sub>4</sub>)<sub>2</sub>·12H<sub>2</sub>O–NiSO<sub>4</sub>·7H<sub>2</sub>O, 209, 210  
 KCl–KBr–H<sub>2</sub>O system, 98, 100  
 KCl–K<sub>2</sub>Cr<sub>2</sub>O<sub>7</sub>, 209  
 K<sub>2</sub>Cr<sub>2</sub>O<sub>7</sub>–KBr–H<sub>2</sub>O system  
 phase diagram, 233  
 K<sub>2</sub>CrO<sub>4</sub>–K<sub>2</sub>SO<sub>4</sub>–H<sub>2</sub>O system, 98
- M**  
 Metasomatic crystallogensis  
 isothermal replacement  
 complex systems, 162–164  
 ternary systems, 157–160  
 metasomatic reaction, 155–156  
 polythermal processes  
 metasomatic reactions, 166–167  
 varying temperature, 164–165  
 Roseboom diagrams, 154  
 Schreinemakers diagrams, 153–154  
 Treivus diagrams, 154–155

- Metasomatic crystallogenesi*s* (*cont.*)  
 volume effects  
 replacement process, 170–171  
 trajectory calculations, 172–173
- Mixed crystal formation  
 equilibrium, quasi-equilibrium, and non-equilibrium conditions  
 crystallizing phase, 101  
 isomorphous components proportion, 101–102  
 isothermic replacement, 106  
 metasomatic component, 104  
 monocrystalline volume-deficit replacement, 95  
 monocrystalline volume-excess replacement, 95, 102  
 polythermal isomorphous replacement, 104–105  
 precipitation principles, 100  
 quasi-equilibrium trajectory, 102  
 substance dissolution, 103–104  
 supersaturation estimation, 102  
 trajectory divergence, 102–103  
 undersaturation estimation, 103
- heterogeneous metastable equilibrium  
 experimental results, 115  
 isomorphous components, 107  
 isomorphous-mixed crystals, 114  
 meta-equilibrium crystallization, 113  
 metasomatic reactions, 113–114  
 quasi-equilibrium crystallization, 109–112  
 solid phase precipitation, 109  
 spontaneous crystallization, 114  
 supercooling solutions, 107–108  
 thermodynamic equilibrium, 107, 109
- inhomogeneity  
 bulk inhomogeneity, 143  
 cluster texture, 143–144  
 (K,Rb)HC<sub>8</sub>H<sub>4</sub>O<sub>4</sub> protuberance texture, 141–142  
 protuberance faceting degrees, 142–143
- isomorphous component selection  
 mechanism  
 ensemble mechanism, 148–149  
 metasomatic replacement, 148  
 nonselective crystallization, 147  
 statistical mechanism, 149
- isomorphism process characteristics  
 admixture particle incorporation, 85–86  
 crystallogenesi*s* interpretations, 85  
 crystal morphology, 86  
 heterogeneous metastable equilibrium, 87–88  
 liquid phase heteroepitaxy, 87  
 metasomatic component, 88  
 nontrivial phenomena, 86  
 physicochemical analysis, 86–87
- mass precipitation  
 bimodal distribution, 146–147  
 crystal compositions, 146  
 K(Br,Cl) series, 145–146  
 meta-equilibrium states, 147  
 (Pb,Ba)(NO<sub>3</sub>)<sub>2</sub> series, 145
- material balance and replacement  
 mechanism  
 diffusion component interchange, 96  
 heterometry effect, 95  
 KAl(SO<sub>4</sub>)<sub>2</sub>·12H<sub>2</sub>O–KCr(SO<sub>4</sub>)<sub>2</sub>·12H<sub>2</sub>O System  
 chromium ↔ aluminium  
 interchange, 89–91  
 feedback mechanism, 91–92  
 initial alum crystals, 88–89  
 metasomatic transformations, 91  
 monocrystal isomorphous composition, 88  
 potassium interchange, 89, 92  
 water interchange, 89, 91–92
- modified concentration diagrams  
 isocomposites, 96  
 isotherm lines, 96  
 metasomatic crystallogenesi*s* process, 96  
 phase equilibria, 98–99  
 solid phase equilibrium compositions, 97–98  
 thermodynamic equilibria, 98  
 volume-deficit mechanism and volume-excess scenario, 98, 100
- mosaic distribution, 93  
 thermodynamic equilibrium, 95–96  
 volume-deficit replacement, 93–94  
 volume-excess replacement, 94–95
- Monocrystals metasomatic replacement  
 dissipated automorphs, 25  
 faceted and blurred pseudomorphs, 24  
 autoepitaxial excrescences, 17, 41, 51, 52  
 kinetic factors and products shape  
 direct and inverse reactions, 36, 37  
 monocrystalline pseudomorphs, 39  
 nucleation and growth rates, 38  
 protocystal dissolution and new formation, 37  
 translocated automorphs, 39, 40  
 zonal distribution and microimpurities, 40
- mineralogical aspects  
 actinolite monocrystalline pseudomorph, 50, 51  
 advancing sites, 48

- cause–effect relationships, 47
  - classification modification, 48
  - conventional types, 46
  - isomorphic replacement, 52
  - natural morphological analogs, 49, 50
  - space-time superposition, 47
  - translocated automorphs, 46, 47
  - volume-excess reactions, 53
  - zircon and tourmaline poikilitic crystals, 51
  - zoned topaz crystals, 50
  - natural and experimental products
    - conventional genetic schemas, 10
    - low-temperature simulation, 11, 12
    - monocrystalline pseudomorphs, 9
    - morphology-structural analogs, 11
    - phenomenological model and three-zone model, 10
    - polycrystalline pseudomorphs, 7–9
    - volume ratio, 10, 11
  - physicochemical systems and products structure
    - Schreinemakers diagrams, 31, 32
    - synchronized metasomatic replacement, 31
    - types *Ia*, *Ib*, *II*, and *III*
  - protocrystals imperfection
    - BaSO<sub>4</sub> fine-grained aggregates, 42
    - inclusion replacement, 41
    - replacement rates, 45
    - structural-morphological classification, 44, 45
  - retgersite-nickelhexahydrate ( $\alpha$ - $\beta$ -NiSO<sub>4</sub>·6H<sub>2</sub>O)
    - blurred pseudomorph–localized automorph, 27
    - faceted pseudomorphs, 26, 27
    - metasomatic replacement, 26
  - structural-morphological classification, 30
  - technique, terminology, and experimental results
    - blurred pseudomorphs, 17–19, 21, 22
    - dissipated automorphs, 24
    - embossed pseudomorphs, 16–18, 20
    - faceted pseudomorphs, 16–21
    - flat thin sections, 12, 15
    - localized automorphs, 20, 22–24
    - model reactions, 13–14
    - translocated automorphs, 20
    - reaction types, 12, 15
  - volume effects
    - educts and products ratio, 34
    - volume-deficit replacements, 34
    - volume-excess replacements, 35
  - Monocrystals morphology. *See also* Monocrystals metasomatic replacement
    - arcanite-tarapacaite K<sub>2</sub>(S,Cr)O<sub>4</sub> series
    - autoepitaxial excrescences, 138–139
    - divergence, 141
    - experimental results and predictive estimations, 140
    - isothermal interaction, 137
    - saturation temperature, mixed solutions, 139–141
    - volume-deficit replacements, 137–138
    - volume-excess replacement, 137–138
    - zoned structure, 138
  - potassium–rubidium acidic phthalates (K,Rb)HC<sub>8</sub>H<sub>4</sub>O<sub>4</sub> series
    - atomic force microscopy, 132–134
    - flat preparation methods, 128
    - isothermal reactions, 128–131
    - physicochemical interpretation, 134–137
    - thermostatically controlled cell, 131–132
  - Tutton salt series (Co,Ni)(NH<sub>4</sub>)<sub>2</sub>(SO<sub>4</sub>)<sub>2</sub>·6H<sub>2</sub>O
    - flat preparation methods, 115–117
    - isothermal reactions, 117–119
    - physicochemical interpretation, 122–128
    - thermostatically controlled cell, 119–122
- N**
- NaBrO<sub>3</sub>–NaClO<sub>3</sub>–H<sub>2</sub>O system, 100
  - (NH<sub>4</sub>)<sub>2</sub>Cr<sub>2</sub>O<sub>7</sub>. *See* Ammonium dichromate
  - NH<sub>4</sub>H<sub>2</sub>PO<sub>4</sub>–KH<sub>2</sub>PO<sub>4</sub>–H<sub>2</sub>O system, 100
  - (NH<sub>4</sub>)<sub>2</sub>Ni(SO<sub>4</sub>)<sub>2</sub>·6H<sub>2</sub>O–CuSO<sub>4</sub>·5H<sub>2</sub>O, 209
  - Nickelhexahydrate. *See* Retgersite ( $\alpha$ - $\beta$ -NiSO<sub>4</sub>·6H<sub>2</sub>O)
- P**
- Pb(NO<sub>3</sub>)<sub>2</sub>–Ba(NO<sub>3</sub>)<sub>2</sub>–H<sub>2</sub>O system, 98
  - Perimorphs, 8
  - Phenocrysts
    - classification, 187, 188
    - faceted, 185, 188, 192
    - feldspar, 183, 184
    - morphological and chemical peculiarities, 183
    - spheroid, 185, 188, 189, 192–194

- Physicochemical model, mixed crystal formation
- equilibrium, quasi-equilibrium, and non-equilibrium conditions
    - crystallizing phase, 101
    - figurative points, 100–101
    - isomorphic components proportion, 101–102
    - isothermic replacement, 106
    - metasomatic component, 104
    - monocrystalline volume-deficit replacement, 95
    - monocrystalline volume-excess replacement, 102
    - polythermal isomorphic replacement, 104–105
    - precipitation principles, 100
    - quasi-equilibrium trajectory, 102
    - substance dissolution, 103–104
    - trajectory divergence, 102–103
    - undersaturation estimation, 103
  - heterogeneous metastable equilibrium
    - experimental results, 115
    - isomorphic components, 107
    - isomorphic-mixed crystals, 114
    - meta-equilibrium crystallization, 113
    - metasomatic reactions, 113–114
    - quasi-equilibrium crystallization, 109–112
    - solid phase precipitation, 109
    - spontaneous crystallization, 114
    - supercooling solutions, 107–108
    - thermodynamic equilibrium, 107, 109
  - modified concentration diagrams
    - isotherm lines, 96
    - metasomatic crystallogenic process, 96
    - phase equilibria, 98–99
    - solid phase equilibrium compositions, 97–98
    - thermodynamic equilibria, 98
    - volume-deficit mechanism and volume-excess scenario, 98, 100
- Physicochemical model, phase equilibria
- KCl–NaCl–MgCl<sub>2</sub>–H<sub>2</sub>O system
    - binary equilibria, 72
    - isoconcentration and isothermal eutonic lines, 75–76
    - isothermal line convergence, 75
    - Schreinemakers phase diagram, 72–74
  - kinetic effects and peculiarities
    - diffusion layer, 78
    - diffusion limitation, crystallization process, 76
    - isolated seed behaviour, 77–78
    - metastable equilibrium, 78
    - NaCl solubility, 81
    - nonmonotonous growth rate
      - characteristics, 79–80
    - phase equilibria, 80
    - physicochemical interpretation, 76–77
    - process kinetics, 81–82
    - solution composition and eutonic concentrations, 78–79
    - supersaturation, 79
- Physicochemical systems, replacement products
- Schreinemakers diagrams, 31, 32
  - synchronized metasomatic replacement, 31
  - types *Ia*, *Ib*, *II*, and *III*
- Poikilitic crystals formation
- metasomatic formation, 163–164
  - Schreinemakers diagrams, 162–163
- Polymineral aggregates recrystallization
- natural and experimental products
    - aqueous salt systems, 197
    - complex crystallogenic process, 197
    - isomorphic miscibility, 195
    - random spatiotemporal correlations, 197
- regularities and mechanisms
- activity and passivity, 212
  - antisymmetric zonality, 222
  - crystal heterogeneous and nonoptimal spatial distribution, 216
  - eutonic line, 215, 216, 220
  - eutonic points, 212
  - factor analysis, 219
  - feedback efficiency, 214
  - grain coordination, 217
  - grain fragmentation, 220
  - macrocells, 217
  - multimodal granulometric composition, 218
  - phase concentration diagrams, 213
  - physicochemical aspect, 215, 216
  - salting-in and salting-out effect, 212, 213, 215
  - thermogradient columns, 221
  - three-stage sequence, 215, 216
  - zoned structure asymmetry, 221
- technique and experimental results
- comb structures, 204
  - compositional characteristics, 202
  - crystal average size, 201
  - degree of idiomorphism, 203
  - grain size, 208
  - granulometric heterogeneity, 203
  - isometric spotty segregations, 206

- $K_2Cr_2O_7$ – $NaNO_3$ – $H_2O$  system, 198  
 kinetic curves, 203, 205  
 macro and micromorphology, 198  
 matter redistribution phenomena, 209  
 $NaNO_3$ – $K_2Cr_2O_7$ , 199, 200, 206  
 temperature parameters, 198, 199  
 zonal structures, 209
- Polymineral-metasomatic crystallogenesi**  
 classification, 3–5  
 crystal faceting, 2  
 direct growth and dissolution processes,  
 1, 2  
 elementary, subelementary, and  
 overelementary stages, 1, 2, 3  
 stages, 1
- Polythermal processes**  
 metasomatic reactions, 166–167  
 non-isothermal processes, 165–166  
 varying temperature, 164–165
- Potassium–rubidium acidic phthalates**  
 (K,Rb) $HC_8H_4O_4$  series  
 atomic force microscopy, 132–134  
 flat preparation methods, 128  
 isothermal reactions  
   epitaxial texture features, 130–131  
   faceted autoepitaxial excrescences,  
   129–130  
   imperfection zone, 129  
   isomorphic replacement, 128  
   vs. Tutton salt crystals, 131  
 physicochemical interpretation  
   vs. (Co,Ni)( $NH_4$ ) $_2$ ( $SO_4$ ) $_2$ ·6 $H_2O$  series,  
   134–135  
   faceting and subsequent ordering,  
   136–137  
   kinetic effects, 137  
   volume-deficit and volume-excess  
   mechanism, 136  
   volume solubilities, 135–136  
   thermostatically controlled cell, 131–132
- Pre-growth replacement, 120–121
- Protocrystals, replacement product**  
 imperfection  
   BaSO $_4$  fine-grained aggregates, 42  
   inclusion replacement, 41  
   replacement rates, 45  
   structural-morphological classification,  
   44, 45  
 morphological correlations, 28, 29
- Pseudomorphs**  
 asynchronous, 10  
 blurred, 17–19, 21, 22  
 box-like, 8  
 case-like, 8, 22  
 corona, 9  
 coronite, 9  
 displacement, 10,  
 drusite, 9  
 embossed, 16–18, 20  
 faceted, 16–21  
 filling-up, 10  
 hollow, 9, 22  
 homoaxial, 9  
 ion-exchanging, 10  
 monocrystalline, 39  
 negative, 9  
 positive, 15,  
 polycrystalline, 7–9  
 profiled, 8  
 shadow, 9  
 synchronous, 10  
 transformation, 10
- R**  
**Rapakivi-type structures formation**  
 chain orbiculars, 187  
 characteristic features, 194  
 formation scheme, 188  
 Lisegang rings, 188  
 metasomatism, 183  
 phenocrysts  
   classification, 187, 188  
   faceted, 185, 188, 192  
   feldspar, 183, 184  
   morphological and chemical  
   peculiarities, 183  
   spheroid, 185, 188, 189, 192–194  
 primary zonality, 194  
 shell orbiculars, 185, 186  
 vermiform quartz, 189  
 volume effect, 193
- Rb $HC_8H_4O_4$ –K $HC_8H_4O_4$ – $H_2O$  system, 98**
- Retgersite ( $\alpha$ - $\beta$ -NiSO $_4$ ·6 $H_2O$ )**  
 blurred pseudomorph localized, 27  
   automorph, 27  
 faceted pseudomorphs, 26, 27  
 metasomatic replacement, 26
- Roseboom diagrams, 154
- S**  
 Salting-in process, 15, 31, 33, 39  
 Salting-out process, 15, 31, 34, 41  
 Schreinemakers diagrams, 153–154  
   KCl–NaCl–MgCl $_2$ – $H_2O$  system,  
   72–74  
 supercooled solution technique, 63

- Spongy structure, 19
- Structure-chemical model
- adsorption film structure, 275, 277, 278
  - binary eutectic system, 275
  - CaF<sub>2</sub>-CaCl<sub>2</sub>-NaCl-NaF system, 277
  - CaF<sub>2</sub>-CaCl<sub>2</sub>-H<sub>2</sub>O system, 269
  - CaF<sub>2</sub>-KF-H<sub>2</sub>O system, 269
  - CaF<sub>2</sub>-NaCl-H<sub>2</sub>O system, 269
  - epitaxial adsorbate-adsorbent
    - compatibility, 276
  - morphogenetic effectiveness, 276
  - portlandite, 277, 278
  - potassium acidic phthalate, 279
  - proton mobility anisotropy, 285
  - stability, 277
  - water influence, 276
- T**
- Thermogradient recrystallization, 209
- Thermooscillatory recrystallization, 199
- Treivus diagrams, 154-155
- Tutton salt series (Co,Ni)(NH<sub>4</sub>)<sub>2</sub>(SO<sub>4</sub>)<sub>2</sub> · 6H<sub>2</sub>O
- flat preparation methods
    - equilibrium composition, 116
    - kinetic measurements, 117
    - kinetic-morphological phenomena, 115
- isothermal reactions
- autoepitaxial excrescences, 118
  - replacement rate, 119
  - spongy structure, 117
  - volume-deficit replacement, 117-118
  - volume-excess replacement, 118-119
  - zoned structure, 118-119
- physicochemical interpretation
- figurative points, 124
  - kinetic-morphological nonmonotony, 127-128
  - meta-equilibrium supercooling, 127
  - morphological attributes, 124-125
  - prognostic analysis, 126
  - Schreinemakers phase diagram, 122-124
- thermostatically controlled cell
- crystal dissolution, 122
  - crystal surface relief monitoring, 119-120
  - kinetic estimation, 119
  - pre-growth replacement, 120-121
- V**
- Volume effects
- replacement process, 34-36, 170-171
  - trajectory calculations, 172-173